

DISCOVERY AND DEVELOPMENT OF DRUGS FOR NEGLECTED DISEASES: CHAGAS DISEASE, HUMAN AFRICAN TRYPANOSOMIASIS, AND LEISHMANIASIS

EDITED BY: Gildardo Rivera, Navin B. Patel and Debasish Bandyopadhyay
PUBLISHED IN: Frontiers in Chemistry





frontiers

Frontiers eBook Copyright Statement

The copyright in the text of individual articles in this eBook is the property of their respective authors or their respective institutions or funders. The copyright in graphics and images within each article may be subject to copyright of other parties. In both cases this is subject to a license granted to Frontiers.

The compilation of articles constituting this eBook is the property of Frontiers.

Each article within this eBook, and the eBook itself, are published under the most recent version of the Creative Commons CC-BY licence.

The version current at the date of publication of this eBook is CC-BY 4.0. If the CC-BY licence is updated, the licence granted by Frontiers is automatically updated to the new version.

When exercising any right under the CC-BY licence, Frontiers must be attributed as the original publisher of the article or eBook, as applicable.

Authors have the responsibility of ensuring that any graphics or other materials which are the property of others may be included in the CC-BY licence, but this should be checked before relying on the CC-BY licence to reproduce those materials. Any copyright notices relating to those materials must be complied with.

Copyright and source acknowledgement notices may not be removed and must be displayed in any copy, derivative work or partial copy which includes the elements in question.

All copyright, and all rights therein, are protected by national and international copyright laws. The above represents a summary only. For further information please read Frontiers' Conditions for Website Use and Copyright Statement, and the applicable CC-BY licence.

ISSN 1664-8714

ISBN 978-2-88971-792-7

DOI 10.3389/978-2-88971-792-7

About Frontiers

Frontiers is more than just an open-access publisher of scholarly articles: it is a pioneering approach to the world of academia, radically improving the way scholarly research is managed. The grand vision of Frontiers is a world where all people have an equal opportunity to seek, share and generate knowledge. Frontiers provides immediate and permanent online open access to all its publications, but this alone is not enough to realize our grand goals.

Frontiers Journal Series

The Frontiers Journal Series is a multi-tier and interdisciplinary set of open-access, online journals, promising a paradigm shift from the current review, selection and dissemination processes in academic publishing. All Frontiers journals are driven by researchers for researchers; therefore, they constitute a service to the scholarly community. At the same time, the Frontiers Journal Series operates on a revolutionary invention, the tiered publishing system, initially addressing specific communities of scholars, and gradually climbing up to broader public understanding, thus serving the interests of the lay society, too.

Dedication to Quality

Each Frontiers article is a landmark of the highest quality, thanks to genuinely collaborative interactions between authors and review editors, who include some of the world's best academicians. Research must be certified by peers before entering a stream of knowledge that may eventually reach the public - and shape society; therefore, Frontiers only applies the most rigorous and unbiased reviews.

Frontiers revolutionizes research publishing by freely delivering the most outstanding research, evaluated with no bias from both the academic and social point of view. By applying the most advanced information technologies, Frontiers is catapulting scholarly publishing into a new generation.

What are Frontiers Research Topics?

Frontiers Research Topics are very popular trademarks of the Frontiers Journals Series: they are collections of at least ten articles, all centered on a particular subject. With their unique mix of varied contributions from Original Research to Review Articles, Frontiers Research Topics unify the most influential researchers, the latest key findings and historical advances in a hot research area! Find out more on how to host your own Frontiers Research Topic or contribute to one as an author by contacting the Frontiers Editorial Office: frontiersin.org/about/contact

DISCOVERY AND DEVELOPMENT OF DRUGS FOR NEGLECTED DISEASES: CHAGAS DISEASE, HUMAN AFRICAN TRYPANOSOMIASIS, AND LEISHMANIASIS

Topic Editors:

Gildardo Rivera, Instituto Politécnico Nacional (IPN), Mexico

Navin B. Patel, Veer Narmad South Gujarat University, India

Debasish Bandyopadhyay, The University of Texas Rio Grande Valley, United States

Citation: Rivera, G., Patel, N. B., Bandyopadhyay, D., eds. (2021). Discovery and Development of Drugs for Neglected Diseases: Chagas Disease, Human African Trypanosomiasis, and Leishmaniasis. Lausanne: Frontiers Media SA.
doi: 10.3389/978-2-88971-792-7

Table of Contents

- 05 Editorial: Discovery and Development of Drugs for Neglected Diseases: Chagas Disease, Human African Trypanosomiasis, and Leishmaniasis**
Gildardo Rivera, Navin B. Patel and Debasish Bandyopadhyay
- 08 Evaluation of Safety and Antileishmanial Efficacy of Amine Functionalized Carbon-Based Composite Nanoparticle Appended With Amphotericin B: An in vitro and Preclinical Study**
Mallikarjuna Rao Gedda, Prasoon Madhukar, Alok Kumar Vishwakarma, Vimal Verma, Anurag Kumar Kushwaha, Ganesh Yadagiri, Shyam Lal Mudavath, Om Prakash Singh, Onkar Nath Srivastava and Shyam Sundar
- 17 Targeting L-Proline Uptake as New Strategy for Anti-chagas Drug Development**
Lucía Fargnoli, Esteban A. Panozzo-Zénere, Lucas Pagura, María Julia Barisón, Julia A. Cricco, Ariel M. Silber and Guillermo R. Labadie
- 32 Use of Natural Products in Leishmaniasis Chemotherapy: An Overview**
Luiza F. O. Gervazoni, Gabrielle B. Barcellos, Taiana Ferreira-Paes and Elmo E. Almeida-Amaral
- 75 Identification of Chalcone Derivatives as Inhibitors of Leishmania infantum Arginase and Promising Antileishmanial Agents**
Andreza R. Garcia, Danielle M. P. Oliveira, Jessica B. Jesus, Alessandra M. T. Souza, Ana Carolina R. Sodero, Alane B. Vermelho, Ivana C. R. Leal, Rodrigo Octavio M. A. Souza, Leandro S. M. Miranda, Anderson S. Pinheiro and Igor A. Rodrigues
- 85 Discovery of Diaryl Ether Substituted Tetrahydrophthalazinones as TbrPDEB1 Inhibitors Following Structure-Based Virtual Screening**
Erik de Heuvel, Albert J. Kooistra, Ewald Edink, Sjors van Klaveren, Jeffrey Stuijt, Tiffany van der Meer, Payman Sadek, Dorien Mabilie, Guy Caljon, Louis Maes, Marco Siderius, Iwan J. P. de Esch, Geert Jan Sterk and Rob Leurs
- 95 Ubiquitination and the Proteasome as Drug Targets in Trypanosomatid Diseases**
Marie-José Bijlmakers
- 113 An Overview on the Therapeutics of Neglected Infectious Diseases—Leishmaniasis and Chagas Diseases**
Brindha J, Balamurali M. M and Kaushik Chanda
- 132 Structure Activity Relationship of N-Substituted Phenylhydrazolones Against Trypanosoma cruzi Amastigotes**
Maarten Sijm, Louis Maes, Iwan J. P. de Esch, Guy Caljon, Geert Jan Sterk and Rob Leurs

145 Development and Characterization of PLGA Nanoparticles Containing 17-DMAG, an Hsp90 Inhibitor

Kercia P. Cruz, Beatriz F. C. Patricio, Vinícius C. Pires, Marina F. Amorim, Alan G. S. F. Pinho, Helenita C. Quadros, Diana A. S. Dantas, Marcelo H. C. Chaves, Fabio R. Formiga, Helvécio V. A. Rocha and Patrícia S. T. Veras

156 Benzopyrazine-Based Small Molecule Inhibitors As Trypanocidal and Leishmanicidal Agents: Green Synthesis, In Vitro, and In Silico Evaluations

Jonathan Rock, Daniel Garcia, Omar Espino, Shaila A. Shetu, Manuel J. Chan-Bacab, Rosa Moo-Puc, Navin B. Patel, Gildardo Rivera and Debasish Bandyopadhyay



Editorial: Discovery and Development of Drugs for Neglected Diseases: Chagas Disease, Human African Trypanosomiasis, and Leishmaniasis

Gildardo Rivera^{1*}, Navin B. Patel² and Debasish Bandyopadhyay^{3,4*}

¹Laboratorio de Biotecnología Farmacéutica, Centro de Biotecnología Genómica, Instituto Politécnico Nacional, Reynosa, Mexico, ²Department of Chemistry, Veer Narmad South Gujarat University, Surat, India, ³Department of Chemistry, University of Texas Rio Grande Valley, Edinburg, TX, United States, ⁴School of Earth Environment and Marine Sciences (SEEMS), University of Texas Rio Grande Valley, Edinburg, TX, United States

Keywords: trypanocidal, leishmanicidal, trypanosomiasis, neglected tropical diseases, therapeutics, drug development

Editorial on the Research Topic

Discovery and Development of Drugs for Neglected Diseases: Chagas Disease, Human African Trypanosomiasis, and Leishmaniasis

OPEN ACCESS

Edited and reviewed by:

Michael Kassiou,
The University of Sydney, Australia

*Correspondence:

Debasish Bandyopadhyay
debasish.bandyopadhyay@
utrgv.edu
Gildardo Rivera
gildardors@hotmail.com

Specialty section:

This article was submitted to
Medicinal and Pharmaceutical
Chemistry,
a section of the journal
Frontiers in Chemistry

Received: 13 September 2021

Accepted: 20 September 2021

Published: 07 October 2021

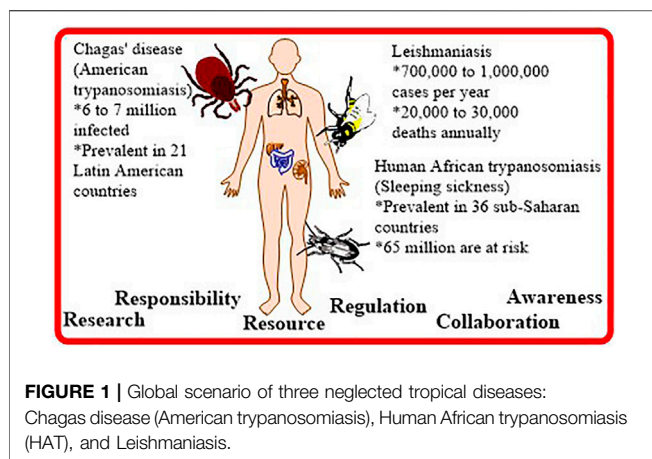
Citation:

Rivera G, Patel NB and
Bandyopadhyay D (2021) Editorial:
Discovery and Development of Drugs
for Neglected Diseases: Chagas
Disease, Human African
Trypanosomiasis, and Leishmaniasis.
Front. Chem. 9:775327.
doi: 10.3389/fchem.2021.775327

Twenty tropical diseases have been listed by the World Health Organization (WHO) as *Neglected Tropical Diseases* (NTDs). These tropical diseases are called “neglected” for three primary reasons: 1) These diseases are widespread worldwide among the economically weaker (neglected?) section of the society; 2) Although the total number of mortality, morbidity, disability, and health disparity caused annually by the NTDs is more than that attributed by the so-called *elite* diseases like cancer, diabetes, human immunodeficiency virus/acquired immunodeficiency syndrome (HIV/AIDS), cardio- or neurological diseases but NTD patients do not receive comparable attention or treatment opportunities either from the governments or healthcare professionals or non-governmental organizations (NGOs); 3) The scope of drug development research in this field is minimal due to insufficient (negligible) funding, and pharma giants are not interested in developing effective drugs for NTDs on time, due to insignificant profit. It is highly challenging to develop new and novel drugs to combat these tropical diseases to upthrust the lifespan and lifestyle of the socioeconomically deprived people affected by NTDs (**Figure 1**). The major goal of this research topic is to shed light on the global scenario (current status of the ailments, treatment options, and recent drug development efforts) of three major NTDs, viz. Chagas disease (American trypanosomiasis), Human African trypanosomiasis (HAT), and Leishmaniasis. This research topic contains three reviews and seven research articles.

Mother Nature can be an excellent source of leishmanicidal compounds. An in-depth review summarizing the leishmanicidal activity of various crude extracts and isolated compounds against promastigote and amastigote (intracellular and axenic) forms has been published (Gervazoni et al.). The leishmanicidal activity of different classes of compounds such as alkaloids, terpenoids, flavonoids, coumarins, quinones, and their respective biosynthetic pathways, published between 2000–2020, has been counted in. Mechanisms of action of various natural compounds (if known) have also been discussed in this review.

Bijlmakers specified the limitation of effective drugs for treating trypanocidal and leishmanicidal infections. In treating trypanosomatid diseases, the author reviewed the protozoal ubiquitin-proteasome system as potential therapeutic targets (primarily UBA1 and ubiquitin-like enzymes). This review discussed the mechanisms of action of a series of ubiquitination inhibitors.



Brindha et al. reviewed the mechanisms of action of the target-based trypanocidal and leishmanicidal pharmaceuticals and druglike molecules. A few significant biomolecular targets such as trypanothione reductase, cathepsin L-cysteine protease (cruzain), CYP51 (sterol 14-ademethylase), kinetoplastid proteasome, heme peroxidation, have been discussed in detail. This review also includes a discussion on nano-formulation of the therapeutics.

The *Leishmania infantum* arginase (LiARG) was considered as a drug target for antileishmanial evaluation, and a series of chalcone derivatives were screened (Garcia et al.). In this study, three chalcone derivatives were identified as LiARG inhibitors. Moreover, three chalcone derivatives demonstrated activity against the promastigote and intracellular amastigote forms of *Leishmania infantum*. The authors proposed the presence of a nitro group at the *para*-position on chalcone "B" ring as an essential factor to induce leishmanicidal activity.

The heat shock protein 90 (Hsp90) inhibitors such as 17-dimethylaminoethylamino-17-demethoxygeldanamycin (17-DMAG) could be a therapeutic option for treating cutaneous leishmaniasis. Cruz et al. reported developing 17-DMAG-containing nanoparticles using poly(lactic-co-glycolic acid) via a double emulsion procedure. The nanoparticles were internalized by macrophages and accumulated in the cell cytoplasm. The authors evaluated the release kinetics of 17-DMAG from the nanoparticle.

Chemical modification of medicinally privileged molecules targeting more potent and/or selective molecules is ongoing in drug discovery research. Sijm et al. successfully conducted chemical modification of one of their previously reported trypanocidal molecules with particular attention to reduce the cLogP values of their newly synthesized molecules with similar potency. It is expected that the newly synthesized *N*-substituted dihydropyrazolone derivatives should demonstrate better drug metabolism and pharmacokinetics (DMPK) properties (Sijm et al.). The authors have studied the qualitative structure-activity relationship (SAR) by diversifying the substituent on the nitrogen atom adjacent to the carbonyl group in the dihydropyrazolone core.

The small molecule TbrPDEB1 inhibitors can play an important role against the protozoan *T. brucei*. Thus, a series of small molecule tetrahydrophthalazinone derivatives have been designed through structure-guided virtual screening (Heuvel et al.). A multi-step

sequence consisting of mesylation-Friedel-Crafts acylation-Diels-Alder reaction-heterocyclization-demesylation was used to synthesize the guaiacol-bearing tetrahydrophthalazinone derivatives. Therefore, the phenolic-OH group was explored to synthesize a series of corresponding diaryl/heteroaryl ether derivatives. The compounds showed selectivity while compared to MRC-5 cell lines.

Cu(II)-mediated 1,3-dipolar alkyne-azide cycloaddition strategy was followed to synthesize 16 triazolyl proline derivatives (Fargnoli et al.). The authors evaluated the end-products as L-proline transport inhibitors against *Trypanosoma cruzi* epimastigotes, and cytotoxicity was measured in VERO cell lines. This study identified the 1, 2, 3-triazole as an appropriate linker for the transport inhibitors and effectively validated L-proline uptake blockers as trypanocidal agents.

Amphotericin B is a natural polyene compound that belongs to the WHO's list of essential medicines. Gedda et al. developed a nanostructure-based method for targeted delivery of Amphotericin B. The f-Comp-AmB nanocomposite demonstrated multi-fold better leishmanicidal activity than two previously reported nanocomposites of the drug and the drug itself against the intracellular amastigotes of *L. donovani* in the J774A.1 cell lines. In addition, the f-Comp-AmB composite showed lower cytotoxicity than two other nanocomposites of Amphotericin B.

Environmental protection is one of the significant criteria in modern drug discovery research. Rock et al. reported an ultrasound-assisted on-water synthesis of benzopyrazines without using any catalyst/support/additive. A series of eleven benzopyrazines were synthesized and evaluated *in vitro*. One benzopyrazine demonstrated comparable trypanocidal and leishmanicidal activities with commercial drugs (Rock et al.). Two other benzopyrazines showed moderate leishmanicidal activity against *L. mexicana* (M378) strain. The authors hypothesized the inhibition of four enzymes as biomolecular targets and validated the hypothesis by *in silico* and *in vitro* evaluations.

In a timely manner, this research topic presents a concise account of the current status and drug discovery approaches related to three neglected tropical diseases: Chagas disease, HAT, and leishmaniasis. Appropriate actions should be taken to protect millions of people worldwide who are struggling with a fatality, disability, disruption of social life, and seclusion.

AUTHOR CONTRIBUTIONS

DB wrote the manuscript, and GR and NP reviewed the manuscript. All authors contributed to the article and approved the submitted version.

ACKNOWLEDGMENTS

The topic editors wish to thank all the contributors, reviewers, handling editors, and the editorial officials of Frontiers in Chemistry for support and guidance. Sincere thanks to the Department of Chemistry and the School of Earth Environment and Marine Sciences (SEEMS) of the University of Texas Rio

Grande Valley for start-up funding and extending facilities for this research topic (to DB). The Department of Chemistry at the University of Texas Rio Grande Valley acknowledges the generous support provided by the Robert A. Welch Foundation (Grant No. BX-0048). GR thankfully acknowledges the support from Secretaría de Investigación y Posgrado-Instituto Politécnico Nacional, grant number (GR: SIP-SIP-20200491 and 20210050).

Conflict of Interest: The authors declare that the research was conducted in the absence of any commercial or financial relationships that could be construed as a potential conflict of interest.

Publisher's Note: All claims expressed in this article are solely those of the authors and do not necessarily represent those of their affiliated organizations, or those of the publisher, the editors and the reviewers. Any product that may be evaluated in this article, or claim that may be made by its manufacturer, is not guaranteed or endorsed by the publisher.

Copyright © 2021 Rivera, Patel and Bandyopadhyay. This is an open-access article distributed under the terms of the Creative Commons Attribution License (CC BY). The use, distribution or reproduction in other forums is permitted, provided the original author(s) and the copyright owner(s) are credited and that the original publication in this journal is cited, in accordance with accepted academic practice. No use, distribution or reproduction is permitted which does not comply with these terms.



Evaluation of Safety and Antileishmanial Efficacy of Amine Functionalized Carbon-Based Composite Nanoparticle Appended With Amphotericin B: An *in vitro* and Preclinical Study

OPEN ACCESS

Edited by:

Gildardo Rivera,
National Polytechnic Institute of
Mexico (IPN), Mexico

Reviewed by:

Saikat Majumder,
University of Pittsburgh, United States
Bruno Mendes Roatt,
Universidade Federal de Ouro
Preto, Brazil

*Correspondence:

Om Prakash Singh
opbhu07@gmail.com
Shyam Sundar
drshyamsundar@hotmail.com

[†]These authors have contributed
equally to this work

Specialty section:

This article was submitted to
Medicinal and Pharmaceutical
Chemistry,
a section of the journal
Frontiers in Chemistry

Received: 31 March 2020

Accepted: 18 May 2020

Published: 03 July 2020

Citation:

Gedda MR, Madhukar P,
Vishwakarma AK, Verma V,
Kushwaha AK, Yadagiri G,
Mudavath SL, Singh OP,
Srivastava ON and Sundar S (2020)
Evaluation of Safety and
Antileishmanial Efficacy of Amine
Functionalized Carbon-Based
Composite Nanoparticle Appended
With Amphotericin B: An *in vitro* and
Preclinical Study. *Front. Chem.* 8:510.
doi: 10.3389/fchem.2020.00510

Mallikarjuna Rao Gedda^{1†}, Prasoon Madhukar^{1†}, Alok Kumar Vishwakarma²,
Vimal Verma¹, Anurag Kumar Kushwaha¹, Ganesh Yadagiri³, Shyam Lal Mudavath³,
Om Prakash Singh^{1,4*}, Onkar Nath Srivastava² and Shyam Sundar^{1*}

¹ Infectious Disease Research Laboratory, Department of Medicine, Institute of Medical Sciences, Banaras Hindu University, Varanasi, India, ² Department of Physics, Institute of Science, Banaras Hindu University, Varanasi, India, ³ Infectious Disease Biology Laboratory, Chemical Biology Unit, Institute of Nano Science and Technology, Habitat Centre, Mohali, India, ⁴ Department of Biochemistry, Institute of Science, Banaras Hindu University, Varanasi, India

Visceral leishmaniasis (VL) has been a major health concern in the developing world, primarily affecting impoverished people. It is caused by a protozoan parasite *Leishmania donovani* and is characterized by immune dysfunction that can lead to deadly secondary infections. Several adverse side effects limit the existing treatment options; hence, the need of the hour is some drug option with high efficacy and no toxicity. To make targeted delivery of Amphotericin B (AmB), we have used amine-functionalized versions of carbon nanostructures, namely f-CNT and f-Graphene (f-Grap). The results with f-Grap-AmB, because of a much larger surface area, were expected to be better. However, the results obtained by us showed only marginal improvement (IC₅₀ f-Grap-AmB; 0.0038 ± 0.00119 μg/mL). This is, in all likelihood, due to the agglomeration effect of f-Grap-AmB, which is invariably obtained with graphene. To resolve this issue, we have synthesized a graphene-CNT composite (graphene 70% and CNT 30% by weight). Because CNT is dispersed in between graphene sheets, the agglomeration effect is avoided, and our study suggests that the f-Composite-AmB (f-Comp-AmB) showed no toxicity against the murine J774A.1 macrophage cell line and did not induce any hepatic or renal toxicity in Swiss albino mice. The f-Comp-AmB also showed a remarkable elevation in the *in vitro* and *in vivo* antileishmanial efficacy in comparison to AmB and f-CNT-AmB or f-Grap-AmB in J774A.1 and Golden Syrian hamsters, respectively. Additionally, we have also observed that the percentage suppression of parasite replication in the spleen of the hamster was significantly higher in the f-Comp-AmB (97.79 ± 0.2375) treated group in comparison with the AmB (85.66 ± 1.164) treated group of hamsters. To conclude, f-Comp-AmB could be a safe and reliable therapeutic option over the other carbon-based nanoparticles (NPs), i.e., f-CNT-AmB, f-Grap-AmB, and conventional AmB.

Keywords: visceral leishmaniasis, cytotoxicity, nanoparticles, graphene-CNT composite, antileishmanial activity

INTRODUCTION

Visceral leishmaniasis (VL) is a fatal protozoan disease caused by the intramacrophagic amastigote form of the *Leishmania donovani* parasite and is transmitted through the bite of the sand fly vector belonging to the genus *Phlebotomus* (Tiwari et al., 2018; Gedda et al., 2019b). The current treatment options are improving, but their clinical promise is limited by adverse side effects, high cost, resistance, storage problems, and cumbersome mode of administration. The side effects include nephrotoxicity, myocarditis, severe vomiting/diarrhea, gastrointestinal and cardiac toxicity, etc. (Gedda et al., 2019b; Singh et al., 2019). Another significant problem with conventional treatment is the likelihood of disease relapse. For instance, following the conventional drug treatment, recurrence of VL or post-kala-azar dermal leishmaniasis (PKDL) can occur, in which patients show macular, papular, or nodular skin lesions often containing heavily parasitized macrophages (Singh et al., 2016). Although a single dose of liposomal amphotericin-B formulation (AmBisome) has minimal toxicity and enhanced efficacy when compared to AmB (Sundar et al., 2010), the high cost of the drug and its subsequent lack of access by the people most commonly affected (from lower economic strata in the endemic regions of the Indian and African subcontinent) has been a major concern (Sinha et al., 2010). Recently, new drugs, such as oxaboroles (DNDI-6148) and nitroimidazole (DNDI-0690) by DNDi, are in the pipeline for preclinical development against VL and CL for an optimized pharmacological profile. Still, their complete clinical trials may take several years (DNDi, 2017). Hence, there is an urgent need to move toward obtaining definitive data for making recommendations on new drug delivery systems as soon as possible. Such novel delivery systems could more accurately target the intramacrophage parasite for the amastigote clearance. Nanomedicine, a promising field for infectious diseases, has retained the hope for better VL drugs in the coming time. Many research groups have employed several NP-based AmB formulations against the infected macrophage both at the *in vitro* and *in vivo* levels for the treatment of experimental leishmaniasis (Khatik et al., 2014; Asthana et al., 2015; Shahnaz et al., 2017).

Graphene and its subordinates are presently at the cutting edge of almost every emerging field of science and design, including biomedical applications that involve therapeutic delivery, advancement in biosensors, bacteriostatic imaging, photothermal therapy, etc. (Hu et al., 2010; Kuila et al., 2011; Robinson et al., 2011; Akhavan et al., 2012; Yang et al., 2013). The entrancing physicochemical properties, ease of synthesis, and adaptable generation combined with characteristic biocompatibility and simple biofunctionalization make graphene an alluring nano scaffold for medicinal purposes, such as in drug delivery in preclinical and clinical conditions (Sanchez et al., 2011; Novoselov et al., 2012; Amrollahi-Sharifabadi et al., 2018). f-Grap has also appeared as a promising nanocarrier for the effective delivery of drugs due to its ability to cross cell membranes and move into the intracellular environment (Mudavath et al., 2014). Graphene has extraordinary application potential, and it enjoys zero band gaps, is inert to reaction, and has a multilayer formation due to graphene sheet π - π stacking.

Additionally, π - π stacking in the graphene sheet surface (area $\sim 2,630 \text{ m}^2/\text{g}$) with delocalized p-electrons can be utilized for effective ultra-high loading of AmB.

Despite the extraordinary application potential, it cannot be ignored that hydrophobic graphene sheets (GS) tend to agglomerate due to Van Der Waals forces, which seems to be the main concern for drug delivery (Rodriguez-Perez et al., 2013). But this can be nullified by the amine functionalization of GS, which acts as a safer alternative to graphene oxide for biomedical applications (Singh et al., 2012). The f-CNTs are no less effective in transporting therapeutic molecules. f-CNTs can covalently link nanotubes and biomolecules, such as peptides, proteins, and nucleic acids, facilitating their easy access through the cell membranes (Karimi et al., 2015). It has also been found that f-CNT doesn't alter the viability of intracellular targets because of their uptake by lymphocytes and macrophages. Our research group has reached these conclusions after exploring a variety of amine-functionalized NPs (f-CNT and f-Grap) appended with AmB (f-CNT-AmB and f-Grap-AmB) against experimental leishmaniasis upon administration through intraperitoneal and oral routes (Prajapati et al., 2011a,b; Mudavath et al., 2014, 2016). With effective results of f-CNT-AmB and f-Grap-AmB as a drug delivery system, we have functionalized and characterized the graphene and CNT composite NP (f-Comp with 70% graphene and 30% CNTs) to prevent the agglomeration of graphene (Patel et al., 2018) for the effective loading of AmB (f-Comp-AmB). This process yielded better antileishmanial activity with relatively less toxicity than AmB, f-CNT-AmB, and f-Grap-AmB.

MATERIALS AND METHODS

Synthesis, Functionalization, and Characterization of f-CNT-AmB, f-Grap-AmB, and f-Comp-AmB

Synthesis of GS

The well-known modified Hummer's method was used to synthesize the GS in which 3 g of highly purified graphite powder was slowly added into the solvent containing a mixture of H_2SO_4 and H_3PO_4 followed by its oxidation with 15 mg of KMnO_4 powder and simultaneous magnetic stirring for 12 h at 50°C to properly mix the contents (Patel et al., 2018). Then, 3 ml of H_2O_2 was added drop-wise into the solution until a yellow-brown color appeared that removes the excess amount of KMnO_4 . The graphite oxide powder thus obtained was washed with dilute HCl until the pH of the solution became 7. The powder was dried at 80°C under a vacuum (10^{-3} torr) for 12 h, followed by the thermal exfoliation of graphite oxide powder (100 mg) at $1,050^\circ\text{C}$ under an inert argon (Ar) atmosphere.

Synthesis of CNT

CNTs were synthesized by a spray-assisted chemical vapor deposition technique (Patel et al., 2018). The precursors used were benzene (C_6H_6) and ferrocene ($\text{C}_{10}\text{H}_{10}\text{Fe}$). An optimum quantity of ferrocene powder was dissolved into a high-purity benzene solution. The solution was sprayed through the nozzle of the pyrolysis set up with the help of Ar gas into the preheated

quartz tube of diameter 1 cm. The hollow carbon cylinder, which consisted of aligned CNTs, was formed onto the inner surface of the quartz tube. The tube whose inner surface contained the deposited CNT configuration was soaked overnight in dilute hydrofluoric acid. The CNTs were collected in powder form. CNTs were stirred into the solutions containing a mixture of H_2SO_4 and HNO_3 (3:1) for 12 h to remove the Fe content.

Synthesis of Composite

Graphene (35 mg) and acid-treated CNTs (15 mg) were dispersed into ethanol solution in different beakers. Both the solutions were sonicated for 3 h, followed by their mixing and followed by sonication for 3 h more to obtain a homogeneous dispersion. The solution so obtained was stirred for 12 h with the help of a magnetic stirrer. The resulting solution was dried at 60°C to obtain the GS-CNT composite material.

Functionalization of GS, CNT, and GS-CNT

For the functionalization of freshly synthesized GS, acid-treated CNTs, and GS-CNT composite, a solution of 0.1 M L-cysteine was prepared in double-distilled water (Talat et al., 2015). Then, 25 mg of GS was added into 250 mL of double distilled water and then sonicated at room temperature for an hour to obtain a homogeneous dispersion. A few drops of L-cysteine solution was added in the GS solution and sonicated for 30 min, followed by stirring for 3 h at room temperature. The solution was thoroughly washed with double-distilled water by centrifugation at 10,000 rpm to remove the unbound L-cysteine. This washing process was repeated five times to ensure the removal of all the unbound L-cysteine. The powder so obtained was dried in an oven at 60°C overnight. The CNTs and GS-CNT composite were subjected to similar treatment for their functionalization. The functionalization with the amine group bearing L-cysteine enables these carbon carriers to bind with the carboxylic group of AmB readily.

Attachment of AmB to f-GS, f-CNTs, and f-GS-CNT

To attach the drug, at first, 50 mg of amine-functionalized GS, CNTs, and GS-CNT were dispersed into 20 mL of double-distilled water in three different beakers. Then, a drug solution was prepared by dissolving 50 mg of AmB into 20 mL of dimethyl sulfoxide (DMSO) followed by sonication for half an hour. Last, 20 mL of drug solution was added drop-wise into three different solutions containing dispersed f-GS, f-CNTs, and f-GS-CNT composite. The obtained solutions were sonicated for 30 h at room temperature. The solution was thoroughly washed with double-distilled water under the centrifugation at 10,000 rpm for 10 min to remove the unbound drug. The drug-attached f-GS (AmB-f-GS), CNTs (AmB-f-CNTs), and Comp (AmB-f-GS-CNT) were collected in powdered form and dried in a hot air oven at 60°C overnight.

Material Characterizations

Structural analysis of the samples was carried out by powder X-ray diffraction (XRD) technique using a PANalytical X'Pert PRO diffractometer with a $\text{Cu K}\alpha$ beam ($\lambda = 1.5415\text{\AA}$) operated at 40 kV and 40 mA. The surface morphologies of the different samples were investigated by scanning electron

microscopy (SEM) using an instrument of FEI quanta 200. In SEM analysis, all the powder samples were mounted on a separate metallic stub with the help of carbon paper. The microstructural studies were done by using transmission electron microscopy (FEI Technai-20 G2; acceleration voltage = 200 kV). Before the application of the electron beam, the powder sample was sonicated in ethanol and then the dispersed sample mounted on a copper grid holder. Attachment of the drug and functionalization was done by Perkin Elmer (Spectrum 100 FT-IR Spectrometer) instrument. First, we have recorded the FTIR spectra of the potassium bromide (KBr) pellet as a background. A small quantity of the prepared sample was mixed with KBr powder with the help of agate mortar and pestle. The mixture was pelletized with the help of hydraulic pressure. The prepared pellet was put into a metallic holder to record the spectrum.

Biological Activity

Macrophage Cell Culture

Murine J774A.1 macrophage cell lines (derived from reticulosarcoma) were procured from the National Centre for Cell Sciences (NCCS) and were used as a cellular host. Cell lines were cultured in RPMI 1640 liquid medium containing 50 mg/L gentamicin and 10% heat-inactivated fetal bovine serum (Thermo Fisher Scientific) in CO_2 incubator with 5% CO_2 and 95% humidity. After the confluency of the J774.A1 macrophage cell lines, they were scrapped from the culture flask and transferred to 50-ml tubes. Tubes were centrifuged at 2,500 rpm for 10 min at 4°C and then washed with 1X PBS twice and suspended in 1 ml complete RPMI 1640 medium, and finally, the number of cells was counted using a hemocytometer.

Culture of Parasite

Leishmania donovani LEM 138 (MHOM/IN/00/DEVI) parasite was cultured *in vitro* in liquid medium (M199) supplemented with 10% heat-inactivated FBS and antibiotics in a BOD incubator. After the growth of the parasite, it was transferred to 50-ml tubes. Tubes were then centrifuged at 2,000 rpm for 10 min at 4°C and then washed with 1X PBS twice and suspended in 1 mL complete M199 medium, and the number of parasites was counted using a hemocytometer.

Animals

Male Swiss albino mice, *Mus musculus* (30–40 g), were purchased from the Central Animal Facility, Institute of Medical Sciences (IMS), Banaras Hindu University (BHU), Varanasi, India for *in vivo* toxicity assay and male Syrian golden hamsters, *Mesocricetus auratus* (50–60 g) were purchased from the Central Drug Research Institute (CDRI) animal house facility, Lucknow, India for *in vivo* antileishmanial activity. Both studies were performed using procedures accepted by the Central Animal Ethics Committee (CAEC), IMS, BHU (CAEC number Dean/2014/CAEC/615). The guidelines of the Council for the Purpose of Control and Supervision of Experiments on Animals (CPCSEA), Ministry of Environment and Forests, Government of India were strictly followed.

In vitro Assessment of Cytotoxicity

The different treatment groups, AmB, f-CNTs, f-CNT-AmB, f-Grp, f-Grp-AmB, f-Comp, and f-Comp-AmB, were assessed for their cytotoxic effects. For this purpose, nearly 5×10^4 J774A.1 macrophages were aliquoted into 96-well plates and incubated in triplicate with AmB (0.005–0.64 $\mu\text{g/mL}$), f-CNTs (0.0625–8 $\mu\text{g/mL}$), f-CNT-AmB (0.005–0.64 $\mu\text{g/mL}$), f-Grp (0.0625–8 $\mu\text{g/mL}$), f-Grp-AmB (0.005–0.64 $\mu\text{g/mL}$), f-Comp (0.0625–8 $\mu\text{g/mL}$), or f-Comp-AmB (0.005–0.64 $\mu\text{g/mL}$) for 72 h at physiological temperature, 5% CO_2 , and analyzed using a 3-(4,5-dimethylthiazol-2-yl)-2,5-diphenyl tetrazolium bromide (MTT) assay. The untreated cells served as controls, and their optical density (OD) is taken as a measure of 100% survival. This experiment was performed twice to ensure the validity of the finding and reproducibility, and the concentration required to kill 50% of the cells (CC_{50}) was calculated from the graph of ODs plotted against varying drug concentrations.

In vitro Antileishmanial Activity Against Intracellular Amastigotes

The J774A.1 macrophages were seeded on eight-chamber Lab Tek tissue culture slides (USA Scientific, Inc., Ocala, FL, USA) at a density of 5×10^4 cells/well and allowed to adhere for 2 h inside a CO_2 incubator with 5% CO_2 at 37°C . The nonadherent macrophages were removed by washing the wells twice with serum-free RPMI 1640 medium. The adherent macrophages were then infected with the metacyclic stage of *L. donovani*, maintaining a *Leishmania*:macrophage ratio of 10:1 in a 200- μL final solution of a complete RPMI 1640 medium overnight. Then, 24 h postincubation, free promastigotes were washed with serum-free RPMI 1640 medium, and infected macrophages were incubated with AmB (0.04–0.00125 $\mu\text{g/mL}$), f-CNT (0.04–0.00125 $\mu\text{g/mL}$), f-CNT-AmB (0.04–0.00125 $\mu\text{g/mL}$), f-Grp (0.04–0.00125 $\mu\text{g/mL}$), f-Grp-AmB (0.04–0.00125 $\mu\text{g/mL}$), f-Comp (0.04–0.00125 $\mu\text{g/mL}$), and f-Comp-AmB (0.04–0.00125 $\mu\text{g/mL}$) and in duplicate for 72 h with 5% CO_2 at 37°C except in the control well, followed by methanol fixing for a minute and staining with Giemsa (Qualigens, Mumbai, India). In each well, at least 100 macrophage nuclei were counted for estimating the percentage of infected macrophages, and the number of amastigotes per 100 macrophages and the IC_{50} (concentration of drug that inhibits 50% of *L. donovani* amastigotes) of each drug was calculated (Manandhar et al., 2008).

In vivo Toxicity Assay

The *in vivo* toxicity of AmB, f-CNT, f-CNT-AmB, f-Grp, f-Grp-AmB, f-Comp, and f-Comp-AmB was assessed in 84 Swiss albino mice (25 ± 5 weeks of age) with a 5-day course of daily intraperitoneal injection using 5, 10, and 20 mg/kg dose regimens in 12 mice with four mice for each concentration. The control groups, comprising four mice each, were injected with PBS. After the 5-day course, mice were euthanized, blood was drawn, and serum was separated by centrifugation. Serums were used to assess hepatic and renal function by quantifying the levels of biomarkers, such as aspartate transaminase (AST), alanine aminotransferase (ALT), urea, and creatinine to

evaluate hepatotoxicity and nephrotoxicity, respectively, using commercially available kits (Autozyme GPT; Accurex Biomedical Pvt. Ltd., Mumbai, India. Enzopak SGOT; Reckon Diagnostics Pvt. Ltd., Gujarat, India. Lyphozyme Urea Berthelot; Beacon Diagnostics Pvt. Ltd., Gujarat, India. Autozyme creatinine; Accurex Biomedical Pvt. Ltd., Mumbai, India).

In vivo Antileishmanial Efficacy

Hamsters are an outstanding model of *L. donovani* infection as they share several common medical and immunopathological aspects with human VL and can endure regular spleen biopsies while being tested for the parasite burden. Eighty-eight male hamsters (4–6 weeks of age) were infected by intracardiac injection of 1×10^7 promastigotes of *L. donovani* LEM138. Eight hamsters were randomly selected, collectively from all the groups, and sacrificed to isolate the spleen for confirmation of the infection by Giemsa staining of the splenic smears. There were seven treatment groups, each with three subgroups, along with one positive and one negative control, consisting of four animals each. AmB, f-CNT, f-CNT-AmB, f-Grp, f-Grp-AmB, f-Comp, and f-Comp-AmB were reconstituted for *in vivo* administration in 1X PBS at a concentration of 5, 10, and 20 mg/kg body weight. The first, second, and third subgroups were treated with 5, 10, and 20 mg/kg of AmB; the fourth, fifth, and sixth groups were provided with 5, 10, and 20 mg/kg of f-CNT; the seventh, eighth, and ninth groups with 5, 10, and 20 mg/kg of f-CNT-AmB; the 10th, 11th, and 12th groups with 5, 10, and 20 mg/kg of f-Grp; the 13th, 14th, and 15th groups with 5, 10, and 20 mg/kg of f-Grp-AmB; the 16th, 17th, and 18th groups with 5, 10, and 20 mg/kg off-Comp; and the 19th, 20th, and 21st groups were treated with 5, 10, and 20 mg/kg off-Comp-AmB intraperitoneally for five consecutive days while the control group received an equal volume of 1X PBS (vehicle). Autopsies were conducted on the seventh day, and the spleen was surgically removed for further examination. Postautopsy, the weight and length of the spleen were measured immediately, and dabbing was done to get imprints on the glass slides. The slides were then examined for the estimation of parasite burden, percentage of inhibition of parasite load, and percentage of suppression of parasite replication (Manandhar et al., 2008). This experiment was repeated for reproducibility.

Statistical Analysis

The CC_{50} and IC_{50} values were calculated by the latest version of GraphPad Prism software, and a one-way ANOVA test was applied to determine the cytotoxicity and antileishmanial activity with $p < 0.05$ as the significant value.

RESULTS

Structural Studies

To unravel the structural and microstructural details, the as-synthesized GS, CNT, and GC73 (GS-CNT composite) were characterized by the XRD technique, which is shown in **Figure 1**. **Figure 1A** shows typical XRD patterns of GS. The weak and broad peak corresponding to the plane (00.2) at 2θ value 23.86° indicates the formation of thermally exfoliated GS. **Figure 1B**

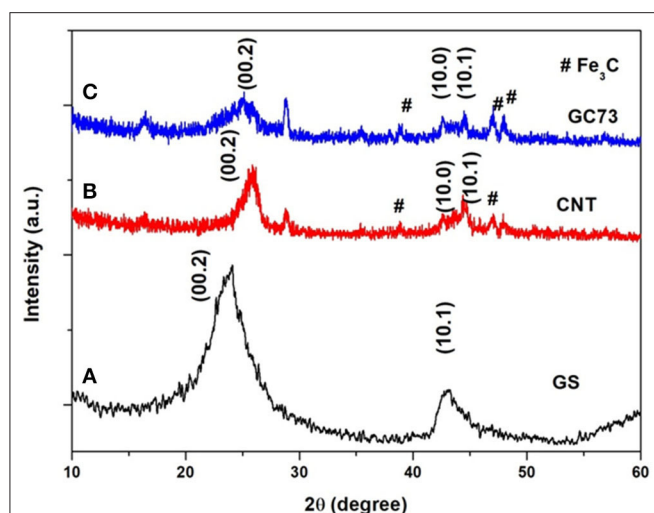


FIGURE 1 | X-ray powder diffraction patterns of the (A) graphene sheet (GS) (B) carbon nanotube (CNT), and (C) composite (graphene-CNT). The composite with 70% graphene and 30% CNT has shown structural quality and stability with fewer chances for agglomeration.

shows the XRD patterns of the prepared randomly oriented CNTs. The peak corresponding to the plane (00.2), which is relatively sharp, indicates the formation of CNTs. XRD patterns of GS and CNT composite are shown in **Figure 1C**, which suggests that the peak corresponding to the plane (00.2) shifts toward the lower angle side ($2\theta = 24.995$) and becomes broad, which is due to the combined size effects of GS and CNT.

Morphological Studies of GS, CNT, and GS-CNT Composite

The scanning electron microscopy (SEM) technique was employed to observe the surface morphology of the as-synthesized material. **Figure 2** shows representative SEM micrographs of as-prepared materials. **Figure 2a** shows the planar sheets with wrinkles, which indicates the formation of GS. **Figure 2b** reveals the formation of randomly oriented CNTs. **Figure 2c** shows the surface morphology of the GS and CNT composite (GC73). It is clear from **Figure 2c** that the presence of CNT prevents the agglomeration of GS. It may be mentioned that, for CNT, the carbons are in mixed sp^2 and sp^3 states, and in graphene, the carbon is in purely the $2S$ state.

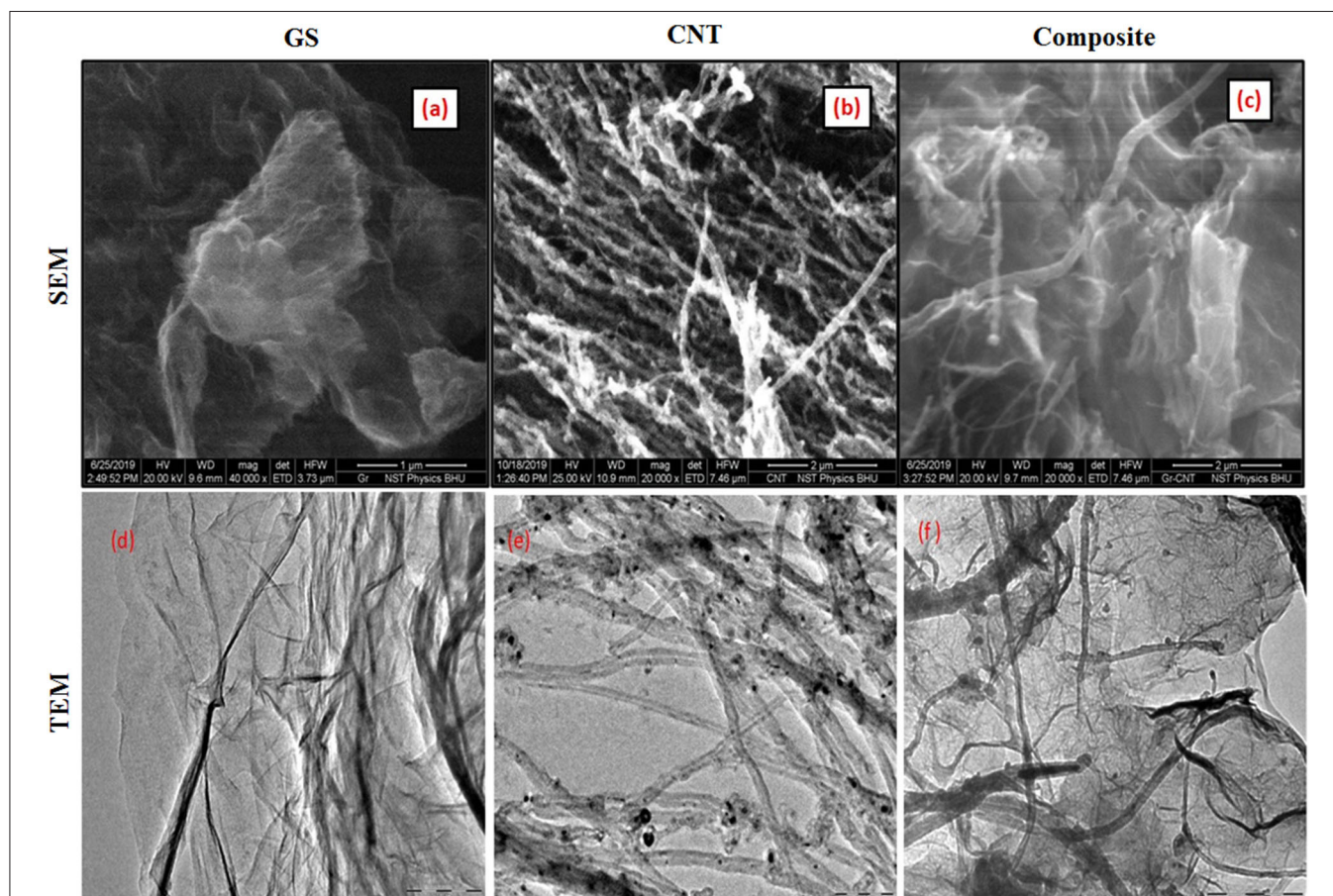


FIGURE 2 | Scanning electron microscopy (SEM) shows the surface topology of the (a) graphene sheet (GS), (b) carbon nanotube (CNT), and (c) composite (graphene-CNT). The TEM image shows the presence of the (d) graphene sheet (GS), (e) carbon nanotube (CNT), and (f) composite (graphene-CNT).

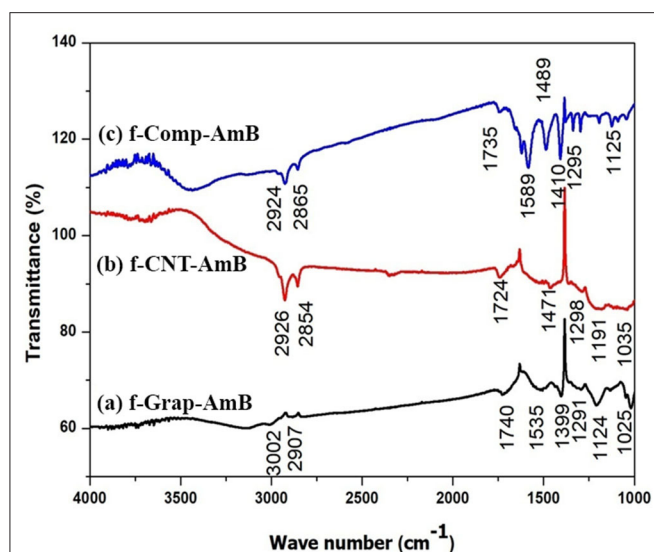


FIGURE 3 | Fourier-transform infrared spectroscopy (FTIR) spectrum of (A) f-CNT-AmB, (B) f-Grap-AmB, and (C) f-Comp-AmB, which shows the data of characterization of functionalized NP with a peak at $1,637\text{ cm}^{-1}$ that represents the carbon skeleton and peaks at $2,930$ and $3,492\text{ cm}^{-1}$ that reveal the C-H bond of CH_2 and the N-H bond of NH_2 , confirming the amine attachment in CNTs, graphene, and composites. The peaks at $1,750$ and $1,150\text{ cm}^{-1}$ represent C=O and C-O bonds of the ester group, and the peak at $1,050\text{ cm}^{-1}$ confirms the C-O-H bond present in AmB attached to f-CNTs, f-graphene, and f-composites.

Microstructural Studies of GS, CNT, and GS-CNT Composite

We have used the transmission electron microscopy (TEM) technique to investigate the microstructure of the as-prepared carbon nano variants (GS, CNT, and GS-CNT composite). **Figure 2d** exhibits the TEM image of GS. The transparent sheets with the presence of wrinkles indicate the formation of graphene. **Figure 2e** shows the TEM image of a randomly oriented carbon nanotube. **Figure 2f** represents the TEM image of the GS-CNT composite, which indicates the dispersion of CNTs inside the GS. The presence of CNTs inside the GS prevents the agglomeration of graphene.

FTIR Studies of f-GS, f-CNT, and f-GS-CNT-AmB

To investigate the functionalization of carbon nano variants (f-GS, f-CNT, and f-GS-CNT) with AmB, we have performed FTIR measurements, which are shown in **Figure 3**. **Figure 3A** shows the FTIR spectrum of the drug attached with amine-functionalized GS. The peak corresponds to $3,003\text{ cm}^{-1}$, and $2,907\text{ cm}^{-1}$ is due to C-H stretching. The peak at $1,535\text{ cm}^{-1}$ is due to the stretching mode of the C=C, which is present in GS. The peak corresponding to $1,291\text{ cm}^{-1}$ is due to the stretching of C-N, which confirms the GS functionalized with an amine. The peak at $1,124\text{ cm}^{-1}$ is due to the presence of the C-O bond, and the peak corresponding to $1,740\text{ cm}^{-1}$ is due to the carbonyl C=O stretching, which is present in

AmB. These observations confirm that the drug was attached with amine-functionalized GS. **Figure 3B** shows the FTIR of three drug attached with amine-functionalized CNT. The peaks present at $2,926$ and $2,854\text{ cm}^{-1}$ are due to C-H stretching. The peak at $1,471\text{ cm}^{-1}$ is due to the stretching mode of the C=C. The peak corresponding to $1,298\text{ cm}^{-1}$ is due to the stretching of C-N, which confirms the CNT functionalized with an amine. The peak at $1,191\text{ cm}^{-1}$ is due to the presence of the C-O bond. The peak corresponding to $1,724\text{ cm}^{-1}$ is due to the carbonyl C=O stretching, which is present in AmB, which confirms that the drug was attached with functionalized CNT. **Figure 3C** indicates the FTIR of the drug attached with amine-functionalized f-GS-CNT. The peaks at $2,924$ and $2,865\text{ cm}^{-1}$ indicate the C-H stretching. The peak at $1,489\text{ cm}^{-1}$ is due to the stretching mode of the C=C. The peak corresponding to $1,295\text{ cm}^{-1}$ is due to the stretching of C-N, which confirms the f-GS-CNT functionalized with an amine. The peak at $1,295\text{ cm}^{-1}$ is due to the presence of the C-O bond. The peak corresponding to $1,735\text{ cm}^{-1}$ is due to the carbonyl C=O, which confirms that the drug was attached with f-GS-CNT. The quantity of loading of AmB for the carbon nano variants (f-GS, f-CNT, and f-GS-CNT) as checked from the FTIR peaks was found to be similar.

In vitro Toxicity

Our present toxicity study on these NPs showed that CC_{50} of the compounds against the J774A.1 cell line were f-Grap-AmB ($0.57 \pm 0.125\text{ }\mu\text{g/mL}$), f-Comp-AmB ($0.604 \pm 0.171\text{ }\mu\text{g/mL}$), AmB ($0.63 \pm 0.157\text{ }\mu\text{g/mL}$), f-CNT-AmB ($0.63 \pm 0.179\text{ }\mu\text{g/mL}$), f-Comp ($7.12 \pm 0.897\text{ }\mu\text{g/mL}$), f-Grap ($7.84 \pm 2.6\text{ }\mu\text{g/mL}$), and f-CNTs ($8 \pm 1.05\text{ }\mu\text{g/mL}$).

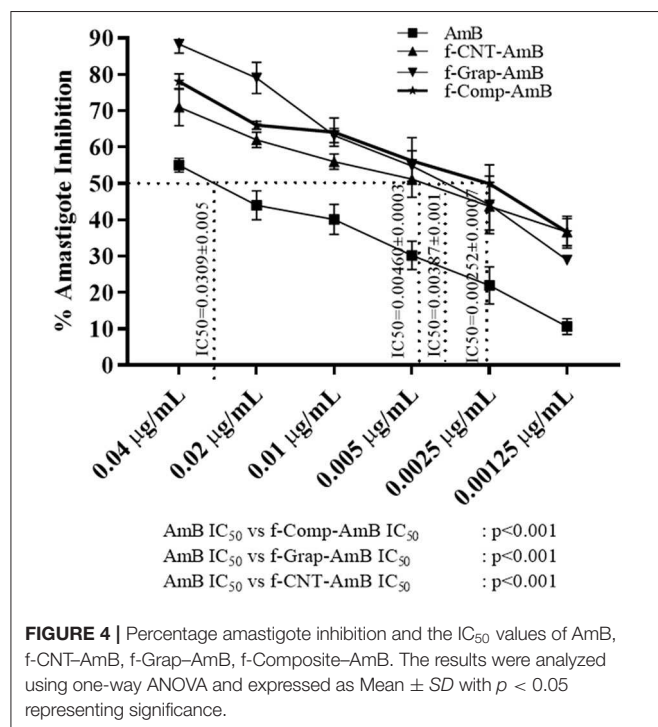
In vitro Antileishmanial Activity

Amastigotes, the infective form of *Leishmania*, reside and replicate in the macrophages. Reduction in the number of intracellular amastigotes of infected macrophages is indicative of the better antileishmanial activity of a drug formulation. The antileishmanial activity of the compounds was AmB, $\text{IC}_{50} = 0.0309 \pm 0.00501\text{ }\mu\text{g/mL}$; f-CNT-AmB, $\text{IC}_{50} = 0.00460 \pm 0.00038\text{ }\mu\text{g/mL}$; f-Gr-AmB, $\text{IC}_{50} = 0.00387 \pm 0.00119\text{ }\mu\text{g/mL}$; f-Comp-AmB, $\text{IC}_{50} = 0.00252 \pm 0.00078\text{ }\mu\text{g/mL}$ as shown in **Figure 4**. The potency of the drugs in inhibiting the intramacrophage parasites is 6.7, 7.98, and 12.22 times more than AmB for f-CNT-AmB, f-Gr-AmB, and f-Comp-AmB, respectively ($p < 0.001$). This gives substance to the conclusion that f-Comp-AmB is a better antileishmanial formulation compared to conventional AmB in comparison with the conventional f-CNT-AmB and f-Gr-AmB.

f-Comp-AmB Did Not Induce Hepatorenal Toxicity in Swiss Albino Mice

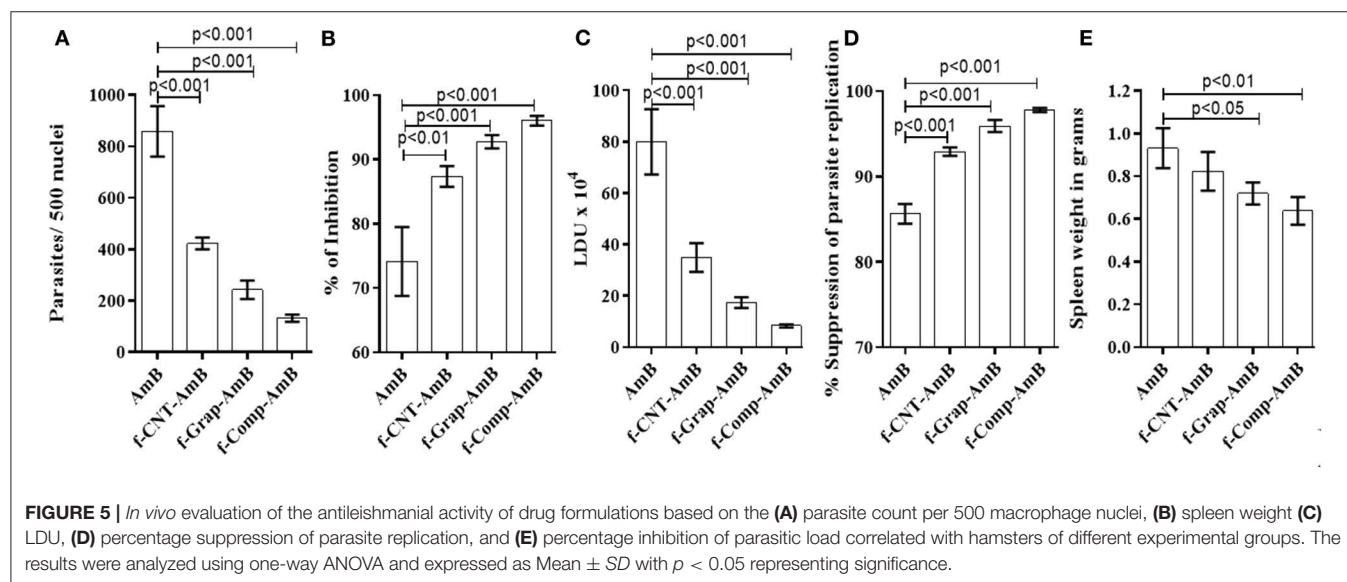
Toxicity is one of the major concerns associated with drug formulations. So, we tried to find out the potential *in vivo* toxicity of the formulations in Swiss albino mice. There were no evident indications of toxic effects for AmB, f-CNT, f-CNT-AmB, f-Grap, f-Grap-AmB, f-Comp, and f-Comp-AmB injected mice at a dose of up to 20 mg/kg within 5 days.

There was no significant difference in the body weights of the treatment group when compared with the control groups, and none of the groups showed mortality. The blood serum biochemistry of the renal and hepatic enzymes, urea (14.75–18.75 mg/dL), creatinine (0.3225–0.4850 mg/dL), AST (35.75–51 IU/L), or ALT (40.25–51.25 IU/L) showed no observable difference between the control and treatment groups at all doses, and all were within the normal reference range (Supplementary Table 1).



f-Comp-AmB Showed Improved Antileishmanial Activity in the Hamster Model of VL

The effects of both sets of *in vivo* studies were conflated to produce a mean value for evaluation. There was no significant difference in the weight of hamsters in the control and treatment groups. f-Comp-AmB showed remarkable improvement in the antileishmanial activity in comparison to AmB, which is evident from the side-by-side bar patterns of parasite count per 500 macrophage nuclei (Figure 5A and Supplementary Figure 1), Leishman Donovan units (LDU) (Figure 5C), percentage suppression of parasite replication (Figure 5D), and percentage inhibition of the parasite load (Figure 5B). These results are corroborated by the weight of the spleen in different treatment groups (Figure 5E). The percentage inhibition of parasites in the spleens of f-Comp-AmB treated *Leishmania* infected hamsters (96.04 ± 0.7526) was higher when compared with conventional AmB treated *Leishmania*-infected hamsters (74.13 ± 5.338) ($p < 0.001$, Supplementary Table 2). f-Comp-AmB also showed a more significant reduction in the parasite burden ($8.351 \pm 0.633 \times 10^4$ LDU) than in AmB treated groups (79.97 ± 12.72 LDU) ($p < 0.001$, Supplementary Table 2). Even the percentage suppression of parasite replication was higher for f-Comp-AmB (97.79 ± 0.2375) when compared with AmB-treated *Leishmania*-infected hamsters (85.66 ± 1.164) ($p < 0.001$, Supplementary Table 2). The percentage inhibition of parasites and percentage suppression of parasite replication by f-CNT-AmB and f-Grap-AmB were found to be 87.36 ± 1.613 ($p < 0.01$), 92.92 ± 0.4802 ($p < 0.001$) and 92.77 ± 1.039 ($p < 0.001$), 95.92 ± 0.7118 ($p < 0.001$), respectively, which are slightly higher than the conventional AmB treated groups while lower than that of f-comp-AmB. Above this, a significant reduction was observed in the spleen size of f-Comp-AmB-treated hamsters (3.167 ± 0.30 cm) in comparison with the infected hamsters (4.73 ± 0.40 cm) (Supplementary Figure 2) ($p = 0.005$), suggesting a decline in the parasite burden.



DISCUSSION

The present work explores the *in vitro* and *in vivo* toxicity and antileishmanial efficacy of a novel treatment approach for VL: amine-functionalized AmB attached composite NP (70% f-Grap and 30% f-CNT) against f-Grap attached AmB, f-CNT attached AmB, and solely conventional AmB. The amine functionalization enables the composite to attach with the carboxylic group of AmB, forming a stable f-Comp-AmB conjugate, and the bond being covalent prevents the dissociation of AmB during drug delivery. Other carbon nanomaterials have also been extensively explored for drug delivery (De Jong and Borm, 2008).

The f-Comp-AmB showed significantly enhanced antileishmanial activity against the intracellular amastigotes of *L. donovani* in the J774A.1 cell lines with 12.2-fold improvement in IC₅₀ values in comparison with conventional AmB. Although the other functionalized carbon nanomaterials, i.e., f-Grap-AmB and f-CNT-AmB, have shown only 7.98- and 6.71-fold improvement in the *in vitro* antileishmanial activity over the conventional AmB, which has been in corroboration with our previous *in vitro* results (Prajapati et al., 2011a,b; Mudavath et al., 2014). The enhanced uptake of f-Comp-AmB by macrophages present superior *in vitro* antileishmanial efficacy than the other nanoformulations, i.e., f-Grap-AmB, and f-CNT-AmB, and hence, it can be a better drug-delivery system of AmB for the intramacrophagic amastigotes. These results are in agreement with the outcomes of an *in vivo* experiment involving hamster models of *L. donovani* infection. The f-Comp-AmB showed a remarkable decline in parasite load and enhanced intracellular delivery and effectiveness of AmB when administered to the infected hamsters in comparison to other alternatives, such as AmB, f-CNT-AmB, and f-Grap-AmB.

The toxicity and high cost of the AmB treatment in VL raise concerns that can be potentially addressed by amine functionalization of carbon-based NPs although, in recent years, several safer formulations of AmB (AmBisome, Fungizone, Amphotec, and Abelcet) have been made commercialized at a significantly increased rate. The use of carbon-based NPs for AmB drug delivery is considerably cost-effective (Sanchez et al., 2011) although cytotoxicity has played a substantial role in limiting several harnessed NPs for the drug-delivery applications. Also, both CNT and graphene oxide have shown serious concerns due to their cytotoxicity and absence of hemocompatibility (Singh et al., 2011; Gedda et al., 2019a). But the amine functionalization of carbon-based NPs, i.e., CNT and graphene, was shown to be a safe alternative (Prajapati et al., 2011a; Mudavath et al., 2014), and hence, this study has utilized their amine-functionalized composite variant. The IC₅₀ values are much lower than CC₅₀ values of their respective f-NP drugs, which means that these functionalized NP drugs are nontoxic to macrophages, and they show inhibition of the intramacrophage parasite at very low concentrations. Additionally, the mice *in vivo* toxicity parameters through hepatic and renal biochemical assays through the AST, ALT, creatine, and urea results have also confirmed the nontoxic nature of f-Comp-AmB, which has been in agreement with our previous studies with f-Grap-AmB (Mudavath et al., 2014) and f-CNT-AmB (Prajapati et al., 2011a,b).

In conclusion, the carbon-based f-Comp-AmB made from two different components does not correspond to a new compound; rather it displays a synergy between the best effects of the two. The composites are least toxic with better antileishmanial activity in comparison with classical AmB, f-CNT-AmB, and f-Grap-AmB. These preliminary *in vitro* and preclinical studies provide a stepping-stone for generating better treatment options for visceral leishmaniasis.

DATA AVAILABILITY STATEMENT

The raw data supporting the conclusions of this article will be made available by the authors, without undue reservation.

ETHICS STATEMENT

The animal study was reviewed and approved by the Central Animal Ethics Committee (CAEC), Banaras Hindu University (CAEC number Dean/2014/CAEC/615).

AUTHOR CONTRIBUTIONS

MG, OPS, ONS, and SS: conceptualization of the project. MG, PM, and AV: data curation. MG, PM, and OPS: data analysis and validation. MG, PM, AV, VV, AK, GY, and SM: laboratory investigation. OPS, ONS, and SS: project administration. ONS and SS: funding resources. MG, PM, AV, and OPS: visualization. MRG, PM, AV, OPS, ONS, and SS: writing original draft. MG, PM, AV, VV, AK, GY, SM, OPS, ONS, and SS: writing—review and editing. All authors contributed to the article and approved the submitted version.

FUNDING

This work was supported by the Department of Science & Technology (SR/NM/NS-57/2016), New Delhi (Under nano-mission), and in part by the Extramural Program of the National Institute of Allergy and Infectious Diseases, National Institutes of Health (TMRC grant number U19AI074321). SM acknowledges the Government of India for funding under the DST-SERB Early Career Research Award (ECR/2016/000977). The funders had no role in the design, decision to publish, or preparation of the report.

SUPPLEMENTARY MATERIAL

The Supplementary Material for this article can be found online at: <https://www.frontiersin.org/articles/10.3389/fchem.2020.00510/full#supplementary-material>

Supplementary Figure 1 | Giemsa-stained dabbled smears of *L. donovani*-infected hamster spleen tissue at 100X. White arrows indicate *L. donovani* amastigotes in untreated, AmB, and f-Comp-AmB groups.

Supplementary Figure 2 | Spleen sizes of different experimental groups in hamsters.

Supplementary Table 1 | *In vivo* biochemical parameters for hepatic and renal functions in Swiss albino mice. *n*, number of mice; ALT, Alanine aminotransferase; AST, Aspartate transaminase; AmB, Amphotericin B; f-CNT, Amine-modified

carbon nanotubes; f-CNT-AmB, AmB conjugated with CNT; f-Grp, Amine-modified graphene; f-Grp-AmB, AmB conjugated with f-Grp; f-Comp, Amine-modified composite; f-Comp-AmB, AmB conjugated with f-composite. The results were represented as Mean \pm SD.

REFERENCES

- Akhavan, O., Ghaderi, E., and Rahighi, R. (2012). Toward single-DNA electrochemical biosensing by graphene nanowalls. *ACS Nano* 6, 2904–2916. doi: 10.1021/nn300261t
- Amrollahi-Sharifabadi, M., Koohi, M. K., Zayerzadeh, E., Hablolvarid, M. H., Hassan, J., and Seifalian, A. M., et al. (2018). *In vivo* toxicological evaluation of graphene oxide nanoplatelets for clinical application. *Int. J. Nanomed.* 13, 4757. doi: 10.2147/IJN.S168731
- Asthana, S., Gupta, P. K., Jaiswal, A. K., Dube, A., and Chourasia, M. K. (2015). Targeted chemotherapy of visceral leishmaniasis by lactoferrin-appended amphotericin B-loaded nanoreservoir: *in vitro* and *in vivo* studies. *Nanomedicine* 10, 1093–1109. doi: 10.2217/nnm.14.182
- De Jong, W. H., and Borm, P. J. (2008). Drug delivery and nanoparticles: applications and hazards. *Int. J. Nanomed.* 3:133. doi: 10.2147/IJN.S596
- DNDi (2017). *New Hope for Novel Drugs for Leishmaniasis: Update of DNDi's Leishmaniasis R&D Pipeline*. Geneva: Drugs for Neglected Disease initiative. Available online at: <http://www.dndi.org/>
- Gedda, M. R., Babele, P. K., Zahra, K., and Madhukar, P. (2019a). Epigenetic aspects of engineered nanomaterials: is the collateral damage inevitable? *Front. Bioeng. Biotechnol.* 7:228. doi: 10.3389/fbioe.2019.00228
- Gedda, M. R., Singh, O. P., Srivastava, O. N., and Sundar, S. (2019b). Therapeutic leishmaniasis: recent advancement and developments in nanomedicines. *Nanotechnol. Mod. Anim. Biotechnol.* 1, 195–220. doi: 10.1007/978-981-13-6004-6_6
- Hu, W., Peng, C., Luo, W., Lv, M., Li, X., Li, D., et al. (2010). Graphene-based antibacterial paper. *ACS Nano* 4, 4317–4323. doi: 10.1021/nn101097v
- Karimi, M., Solati, N., Ghasemi, A., Estiar, M. A., Hashemkhani, M., Kiani, P., et al. (2015). Carbon nanotubes part II: a remarkable carrier for drug and gene delivery. *Exp. Opin. Drug Deliv.* 12, 1089–1105. doi: 10.1517/17425247.2015.1004309
- Khatik, R., Dwivedi, P., Khare, P., Kansal, S., Dube, A., Mishra, P. R., et al. (2014). Development of targeted 1, 2-diacyl-sn-glycero-3-phospho-l-serine-coated gelatin nanoparticles loaded with amphotericin B for improved *in vitro* and *in vivo* effect in leishmaniasis. *Exp. Opin. Drug Deliv.* 11, 633–646. doi: 10.1517/17425247.2014.889678
- Kuila, T., Bose, S., Khanra, P., Mishra, A. K., Kim, N. H., Lee, J. H., et al. (2011). Recent advances in graphene-based biosensors. *Biosensors Bioelectron.* 26, 4637–4648. doi: 10.1016/j.bios.2011.05.039
- Manandhar, K. D., Yadav, T. P., Prajapati, V. K., Kumar, S., Rai, M., Dube, A., et al. (2008). Antileishmanial activity of nano-amphotericin B deoxycholate. *J. Antimicrob. Chemother.* 62, 376–380. doi: 10.1093/jac/dkn189
- Mudavath, S. L., Talat, M., Rai, M., Srivastava, O. N., and Sundar, S. (2014). Characterization and evaluation of amine-modified graphene amphotericin B for the treatment of visceral leishmaniasis: *in vivo* and *in vitro* studies. *Drug Design Dev. Ther.* 8:1235. doi: 10.2147/DDDT.S63994
- Mudavath, S. L., Talat, M., Rai, M., Srivastava, O. N., and Sundar, S. (2016). An oral formulation of Amphotericin B for the treatment of visceral Leishmaniasis: f-Gr-AmB. *Int. J. Infect. Dis.* 45:367. doi: 10.1016/j.ijid.2016.02.790
- Novoselov, K. S., Fal, V., Colombo, L., Gellert, P., Schwab, M., Kim, K., et al. (2012). A roadmap for graphene. *Nature* 490:192. doi: 10.1038/nature11458
- Patel, C., Tripathi, P., Vishwakarma, A. K., Talat, M., Soni, P. K., Yadav, T., et al. (2018). Enhanced hydrogen generation by water electrolysis employing carbon nano-structure composites. *Int. J. Hydrog. Energy* 43, 3180–3189. doi: 10.1016/j.ijhydene.2017.12.142
- Prajapati, V. K., Awasthi, K., Gautam, S., Yadav, T. P., Rai, M., Srivastava, O. N., et al. (2011a). Targeted killing of Leishmania donovani *in vivo* and *in vitro* with amphotericin B attached to functionalized carbon nanotubes. *J. Antimicrob. Chemother.* 66, 874–879. doi: 10.1093/jac/dkr002
- Supplementary Table 2 |** *In vivo* efficacy studies in Syrian Golden hamsters using AmB, f-CNT, f-Grp, f-Comp, f-CNT-AmB, f-Grp-AmB, and f-Comp-AmB against experimental leishmaniasis. The results were analyzed using one-way ANOVA and expressed as Mean \pm SD with $p < 0.05$ representing significance.
- Prajapati, V. K., Awasthi, K., Yadav, T. P., Rai, M., Srivastava, O. N., Sundar, S., et al. (2011b). An oral formulation of amphotericin B attached to functionalized carbon nanotubes is an effective treatment for experimental visceral leishmaniasis. *J. Infect. Dis.* 205, 333–336. doi: 10.1093/infdis/jir735
- Robinson, J. T., Tabakman, S. M., Liang, Y., Wang, H., Sanchez Casalongue, H., Vinh, D., et al. (2011). Ultrasmall reduced graphene oxide with high near-infrared absorbance for photothermal therapy. *J. Am. Chem. Soc.* 133, 6825–6831. doi: 10.1021/ja2010175
- Rodriguez-Perez, L., Herranz, M. Á., and Martín, N. (2013). The chemistry of pristine graphene. *Chem. Commun.* 49, 3721–3735. doi: 10.1039/c3cc38950b
- Sanchez, V. C., Jachak, A., Hurt, R. H., and Kane, A. B. (2011). Biological interactions of graphene-family nanomaterials: an interdisciplinary review. *Chem. Res. Toxicol.* 25, 15–34. doi: 10.1021/tx200339h
- Shahnaz, G., Edagwa, B. J., McMillan, J., Akhtar, S., Raza, A., Qureshi, N. A., et al. (2017). Development of mannose-anchored thiolated amphotericin B nanocarriers for treatment of visceral leishmaniasis. *Nanomedicine* 12, 99–115. doi: 10.2217/nnm-2016-0325
- Singh, O. P., Gedda, M. R., Mudavath, S. L., Srivastava, O. N., and Sundar, S. (2019). Envisioning the innovations in nanomedicine to combat visceral leishmaniasis: for future theranostic application. *Nanomedicine* 14, 1911–1927. doi: 10.2217/nnm-2018-0448
- Singh, O. P., Singh, B., Chakravarty, J., and Sundar, S. (2016). Current challenges in treatment options for visceral leishmaniasis in India: a public health perspective. *Infect. Dis. Poverty* 5:8. doi: 10.1186/s40249-016-0112-2
- Singh, S. K., Singh, M. K., Kulkarni, P. P., Sonkar, V. K., Grácio, J. J., Dash, D., et al. (2012). Amine-modified graphene: thrombo-protective safer alternative to graphene oxide for biomedical applications. *ACS Nano* 6, 2731–2740. doi: 10.1021/nn300172t
- Singh, S. K., Singh, M. K., Nayak, M. K., Kumari, S., Shrivastava, S., Grácio, J. J., et al. (2011). Thrombus inducing property of atomically thin graphene oxide sheets. *ACS Nano* 5, 4987–4996. doi: 10.1021/nn201092p
- Sinha, P. K., Roddy, P., Palma, P. P., Kociejowski, A., Lima, M. A., Das, V. N. R., et al. (2010). Effectiveness and safety of liposomal amphotericin B for visceral leishmaniasis under routine program conditions in Bihar, India. *Am. J. Trop. Med. Hyg.* 83, 357–364. doi: 10.4269/ajtmh.2010.10-0156
- Sundar, S., Chakravarty, J., Agarwal, D., Rai, M., and Murray, H. W. (2010). Single-dose liposomal amphotericin B for visceral leishmaniasis in India. *N. Engl. J. Med.* 362, 504–512. doi: 10.1056/NEJMoa0903627
- Talat, M., Awasthi, K., Sundar, S., and Srivastava, N. O. (2015). Functionalization of carbon nanomaterials (eg carbon nanotubes and graphene) using L-cysteine. *Innovat. Corros. Mater. Sci.* 5, 105–112. doi: 10.2174/235209490502151106194945
- Tiwari, N., Gedda, M. R., Tiwari, V. K., Singh, S. P., and Singh, R. K. (2018). Limitations of current therapeutic options, possible drug targets and scope of natural products in control of leishmaniasis. *Mini Rev. Med. Chem.* 18, 26–41. doi: 10.2174/1389557517666170425105129
- Yang, M., Yao, J., and Duan, Y. (2013). Graphene and its derivatives for cell biotechnology. *Analyst* 138, 72–86. doi: 10.1039/C2AN35744E

Conflict of Interest: The authors declare that the research was conducted in the absence of any commercial or financial relationships that could be construed as a potential conflict of interest.

Copyright © 2020 Gedda, Madhukar, Vishwakarma, Verma, Kushwaha, Yadagiri, Mudavath, Singh, Srivastava and Sundar. This is an open-access article distributed under the terms of the Creative Commons Attribution License (CC BY). The use, distribution or reproduction in other forums is permitted, provided the original author(s) and the copyright owner(s) are credited and that the original publication in this journal is cited, in accordance with accepted academic practice. No use, distribution or reproduction is permitted which does not comply with these terms.



Targeting L-Proline Uptake as New Strategy for Anti-chagas Drug Development

Lucía Fargnoli¹, Esteban A. Panozzo-Zénere¹, Lucas Pagura², María Julia Barisón³, Julia A. Cricco², Ariel M. Silber³ and Guillermo R. Labadie^{1,4*}

¹ Facultad de Ciencias Bioquímicas y Farmacéuticas, Instituto de Química de Rosario (IQUIR), Universidad Nacional de Rosario, Rosario, Argentina, ² Instituto de Biología Molecular y Celular de Rosario (IBR), Consejo Nacional de Investigaciones Científicas y Técnicas CONICET-Facultad de Ciencias Bioquímicas y Farmacéuticas, Universidad Nacional de Rosario, Rosario, Argentina, ³ Laboratory of Biochemistry of Tryps-LaBTryps, Departamento de Parasitología, Instituto de Ciências Biomédicas, Universidade de São Paulo, Cidade Universitária, São Paulo, Brazil, ⁴ Departamento de Química Orgánica, Facultad de Ciencias Bioquímicas y Farmacéuticas, Universidad Nacional de Rosario, Rosario, Argentina

OPEN ACCESS

Edited by:

Gildardo Rivera,
National Polytechnic Institute of
Mexico (IPN), Mexico

Reviewed by:

Claudia Masini d'Avila-Levy,
Oswaldo Cruz Foundation
(Fiocruz), Brazil
Juan Diego Maya,
University of Chile, Chile

*Correspondence:

Guillermo R. Labadie
labadie@iquir-conicet.gov.ar

Specialty section:

This article was submitted to
Medicinal and Pharmaceutical
Chemistry,
a section of the journal
Frontiers in Chemistry

Received: 02 April 2020

Accepted: 06 July 2020

Published: 25 August 2020

Citation:

Fargnoli L, Panozzo-Zénere EA,
Pagura L, Barisón MJ, Cricco JA,
Silber AM and Labadie GR (2020)
Targeting L-Proline Uptake as New
Strategy for Anti-chagas Drug
Development. *Front. Chem.* 8:696.
doi: 10.3389/fchem.2020.00696

L-Proline is an important amino acid for the pathogenic protists belonging to *Trypanosoma* and *Leishmania* genera. In *Trypanosoma cruzi*, the etiological agent of Chagas disease, this amino acid is involved in fundamental biological processes such as ATP production, differentiation of the insect and intracellular stages, the host cell infection and the resistance to a variety of stresses. In this study, we explore the L-Proline uptake as a chemotherapeutic target for *T. cruzi*. Novel inhibitors have been proposed containing the amino acid with a linker and a variable region able to block the transporter. A series of sixteen 1,2,3-triazolyl-proline derivatives have been prepared for *in vitro* screening against *T. cruzi* epimastigotes and proline uptake assays. We successfully obtained inhibitors that interfere with the amino acid internalization, which validated our design targeting the metabolite's transport. The presented structures are one of few examples of amino acid transporter inhibitors. The unprecedented application of this strategy on the development of new chemotherapy against Chagas disease, opens a new horizon on antiparasitic drug development against parasitic diseases and other pathologies.

Keywords: Chagas disease, proline uptake, *T. cruzi* epimastigotes, cytotoxicity, target validation

INTRODUCTION

Chagas disease is one of the most neglected infectious disease. It is endemic in the Americas, with 8–10 million people infected and 25 million people at risk (Nunes et al., 2013). The disease is divided in the acute and the chronic phase. The first have a noticeable parasitemia, the absence of humoral response and is largely asymptomatic. The chronic phase has a non-evident parasitemia and a robust IgG response being asymptomatic in 60–70% of the cases (Pérez-Molina and Molina, 2018). The chemotherapy against Chagas disease relies mainly on two drugs introduced more than 40 years ago: Nifurtimox (Nf) and Benznidazole (Bz) (Urbina, 2010). Both drugs are efficient on the acute phase, but in the chronic phase is controversial (Morillo et al., 2015). In addition, severe side effects due to toxicity and the emergence of resistance calls for urgent development of new drugs (Guedes et al., 2011).

Trypanosoma cruzi is a hemoflagellated parasite that causes Chagas disease. This parasite presents a complex life cycle among two kinds of hosts: mammals and reduviid insects,

which transmit the infection. Along its life-cycle at least four stages were clearly identified, epimastigotes (replicative stage) and metacyclic trypomastigotes (infective, non-replicative stage) in the insect and blood stream trypomastigotes and amastigotes (intracellular replicative stage). Also, during its life-cycle the parasite faces different environments and it must adjust its “life-style” including its metabolism to changes in nutrients availability, temperature, together other environmental variables.

Among many other important metabolites, amino acids are particularly relevant for the biology of *T. cruzi*, besides protein synthesis (Marchese et al., 2018), playing fundamental roles in energy management (Pereira et al., 2000) and nitrogen metabolism (Crispim et al., 2018; Girard et al., 2018). When epimastigotes proliferation arrests, there is a metabolic switch from a carbohydrates to an amino acids based metabolism, with a consequent change in the protein expression profile (Barisón et al., 2017; Avila et al., 2018). In fact, it has been demonstrated that amino acids such as proline (Paes et al., 2013), histidine (Barison et al., 2016), and even alanine (Girard et al., 2018), as well as the proline oxidation product P5C (Mantilla et al., 2015), can fuel electrons to the respiratory chain, powering the mitochondrial ATP synthesis (Sylvester and Krassner, 1976; Martins et al., 2009; Paes et al., 2013; Barison et al., 2016). Some neutral amino acids can also function as osmolytes, serving to counteract volume perturbations following a shift in extracellular osmolarity (Rohloff et al., 2003; Silber et al., 2005; Avila et al., 2018).

Particularly, proline is involved in energization of the host-cells invasion by metacyclic trypomastigotes (Martins et al., 2009), as well as growth and differentiation of the insect (Contreras Vt et al., 1988; Tonelli et al., 2004; Silber et al., 2009) and the intracellular stages (Tonelli et al., 2004). Additionally, its accumulation in the parasite cytoplasm provides resistance to oxidative and thermal stress (Tonelli et al., 2004; Magdaleno et al., 2009; Paes et al., 2013; Sayé et al., 2014). The proline availability is mediated by an interplay of the biosynthesis degradation and uptake process (Sylvester and Krassner, 1976; Silber et al., 2002; Magdaleno et al., 2009; Paes et al., 2013; Sayé et al., 2014; Mantilla et al., 2017). In particular, the inhibition of proline uptake by competitive transporter interrupters, diminished the parasites ability to tolerate oxidative imbalance, nutritional stress and to complete the infection cycle (Magdaleno et al., 2009).

Taking the proline uptake as a novel drug target we decided to develop new transporter inhibitors and evaluate their antiproliferative activity against *Trypanosoma cruzi*. These new compounds were initially evaluated on *T. cruzi* epimastigotes, validating their action mechanism by proline transport experiments. A comprehensive analysis of the structure-activity relationship allowed a rational pipeline to design selective metabolite transporter inhibitors.

MATERIALS AND METHODS

Chemistry

General Remarks

Chemical reagents were purchased from commercial suppliers and used without further purification, unless otherwise noted.

Dry, deoxygenated diethyl ether (Et_2O), tetrahydrofuran (THF), and dichloromethane (DCM) were obtained bypassing commercially available pre-dried, oxygen-free solvents through activated alumina columns. DMF was distilled from BaO. Reactions were monitored by thin-layer chromatography (TLC) performed on 0.2 mm Merck silica gel aluminum plates (60F-254) and visualized using ultraviolet light (254 nm) and by potassium permanganate and heat as developing reagents. All reactions were performed under an atmosphere of nitrogen using oven-dried glassware and standard syringe/septa techniques. Column chromatography was performed with silica gel 60 (230–400 mesh). Yields were calculated for material judged homogeneous by thin layer chromatography (TLC) and nuclear magnetic resonance (^1H NMR).

^1H and ^{13}C NMR spectra were acquired on a Bruker Avance II 300 MHz (75.13 MHz) using CDCl_3 as solvent. Chemical shifts (δ) were reported in ppm downfield from tetramethylsilane and coupling constants are in hertz (Hz). NMR spectra were obtained at 298 K unless otherwise stated and samples run as a dilute solution of the stated solvent. All NMR spectra were referenced to the residual undeuterated solvent as an internal reference. The following abbreviations were used to explain the multiplicities: s = singlet, d = doublet, t = triplet, q = quartet, m = multiplet, br = broad. Assignment of proton resonances was confirmed by correlated spectroscopy. Electrospray ionization high-resolution mass spectra (ESI-HRMS) were recorded on a Bruker MicroTOF II. IR spectra were obtained using an FT-IR Shimadzu spectrometer and only partial spectral data are listed. Melting points were measured on an Electrothermal 9100 apparatus and are uncorrected.

Experimental Procedures and Spectroscopic Data

Synthesis of N-Propargyl Methyl Prolinate (2)

To a solution of methyl prolinate (200 mg, 1.22 mmol) in 10 mL of $\text{Et}_2\text{O}_{(\text{anh})}$, NEt_3 (439 mg, 4.3 mmol) and 80 % propargyl bromide in toluene (263 μL , 2.45 mmol) were added in this order and the reaction mixture was stirred at room temperature for 12 h. The solvent was evaporated, and the crude product was purified by column chromatography in silica gel with increasing ethyl acetate/hexane gradient to yield the expected product as a yellow oil (129 mg, 72 %).

^1H NMR (300 MHz, CDCl_3): δ 3.72 (s, 3H, OCH_3), 3.61–3.55 (m, 2H, C5-H, C2-H), 3.45–3.39 (m, 1H, C6-H), 3.07–3.01 (m, 1H, C6-H), 2.75–2.67 (m, 1H, C5-H), 2.20–2.06 (m, 2H, C7-H and C3-H), 2.08–1.76 (m, 3H, C3-H, C4-H). ^{13}C NMR (75 MHz, CDCl_3): δ 173.9 (COO), 78.2 (C), 73.2 (CH), 62.4 (CH), 52.1 (CH_2), 51.9 (OCH_3), 41.1 (CH_2), 29.5 (CH_2), 23.2 (CH_2).

General Procedure for the Cu(I) Mediated 1,3-Dipolar Cycloaddition

N-Propargyl methyl prolinate (1 eq) and the azide (1.1 eq) were suspended in 10 mL/eq of $t\text{BuOH}:\text{H}_2\text{O}$ (1:1) and then 1M CuSO_4 solution (0.05 eq) and finally 1M sodium ascorbate solution (0.2 eq) and the mixture stirred overnight at room temperature. Brine was added, and the solution was extracted with dichloromethane. Combined organic extracts

were dried over sodium sulfate and evaporated. Products were purified by column chromatography in silica gel with increasing hexanes/ethyl acetate/methanol gradients.

Methyl ((1-(2-Ethoxy-2-Oxoethyl)-1H-1,2,3-Triazol-4-yl)Methyl)-L-Proline (3a)

Compound **3a** was prepared from 45 mg (0.27 mmol) of N-propargyl methyl proline **1**, following the general procedure for the 1,3-dipolar cycloaddition, affording 66 mg of a yellowish oil in 80 % yield. ¹H NMR (300 MHz, CDCl₃): δ 7.62 (s, 1H, C7-H), 5.09 (d, *J* = 2.6 Hz, 2H, C8-H), 4.20 (q, *J* = 7.5 Hz, 2H, CH₂CH₃), 4.01 (d, *J* = 13.8 Hz, 1H, C6-H), 3.82 (d, *J* = 13.8 Hz, 1H, C6-H), 3.64 (s, 3H, OMe), 3.29 (dd, *J* = 8.7, 6.1 Hz, 1H, C2-H), 3.10–3.04 (m, 1H, C5-H), 2.50 (dt, *J* = 8.4 Hz, *J* = 8.2 Hz, 1H, C5-H), 2.07–1.74 (m, 4H, C3-H and C4-H), 1.23 (t, *J* = 7.5 Hz, 3H, CH₂CH₃). ¹³C NMR (75 MHz, CDCl₃): δ 174.1 (COO), 166.3 (COO), 144.5 (C6'), 124.4 (C7), 64.4 (C2), 62.4 (CH₂), 53.0 (C5), 52.0 (OCH₃), 50.8 (C8), 48.2 (C6), 29.3 (C3), 23.0 (C4), 14.0 (CH₃). IR (film): ν_{max} 3458, 3439, 2954, 2357, 1732, 1643, 1444, 1217, 1051, 1024, 875, 798, 756 cm⁻¹. ESI-HRMS *m/z* [M+K]⁺ calcd for C₁₃H₂₀KN₄O₄ 335.1116, found 335.1113.

Methyl ((1-(5-Ethoxy-5-Oxopentyl)-1H-1,2,3-Triazol-4-yl)Methyl)-L-Proline (3b)

Compound **3b** was prepared from 45 mg (0.27 mmol) of N-propargyl methyl proline **1**, following the general procedure for the 1,3-dipolar cycloaddition, affording 63 mg of a yellowish oil in 69 % yield. ¹H NMR (300 MHz, CDCl₃): δ 7.50 (s, 1H, C7-H), 4.38 (d, *J* = 2.6 Hz, 2H, C8-H), 4.09 (q, *J* = 7.5 Hz, 2H, CH₂CH₃), 3.97 (d, *J* = 13.8 Hz, 1H, C6-H), 3.79 (d, *J* = 13.8 Hz, 1H, C6-H), 3.65 (3H, OMe), 3.28 (dd, *J* = 8.7, 6.1 Hz, 1H, C2-H), 3.12–3.07 (m, 1H, C5-H), 2.53–2.45 (m, 1H, C5-H), 2.32–2.08 (m, 6H, CH₂), 1.91–1.76 (m, 4H, C3-H and C4-H), 1.20 (t, *J* = 7.5 Hz, 3H, CH₂CH₃). ¹³C NMR (75 MHz, CDCl₃): δ 174.4 (C=O), 172.3 (COO), 144.5 (C6'), 122.8 (C7), 64.6 (C2), 60.6 (CH₂CH₃), 53.3 (C5), 51.8 (OCH₃), 49.1 (C8), 48.5 (C6), 30.6 (CH₂), 29.6 (CH₂), 29.3 (C3), 25.4 (C4), 23.0 (CH₂), 14.1 (CH₂CH₃). IR (film): ν_{max} 3437, 3138, 2954, 2358, 1730, 1633, 1444, 1377, 1348, 1274, 1199, 1047, 1028, 854, 802 cm⁻¹. ESI-HRMS *m/z* [M+H]⁺ calcd for C₁₆H₂₇N₄O₄ 339.2027, found 339.2029.

Methyl ((1-Benzyl-1H-1,2,3-Triazol-4-yl)Methyl)-L-Proline (3c)

Compound **3c** was prepared from 45 mg (0.27 mmol) of N-propargyl methyl proline **1**, following the general procedure for the 1,3-dipolar cycloaddition, affording 66 mg of a yellowish oil in 80 % yield. ¹H NMR (300 MHz, CDCl₃): δ 7.42 (s, 1H, C7-H), 7.36–7.30 (m, 3H, Ph), 7.27–7.21 (m, 2H, Ph), 5.48 (d, *J* = 2.6 Hz, 2H, C8-H), 3.95 (d, *J* = 13.8 Hz, 1H, C6-H), 3.78 (d, *J* = 13.8 Hz, 1H, C6-H), 3.60 (s, 3H, OMe), 3.27 (dd, *J* = 8.7, 6.1 Hz, 1H, C2-H), 3.09 (m, 1H, C5-H), 2.48 (dt, *J* = 8.4, 8.2 Hz, 1H, C5-H), 2.18–1.66 (m, 4H, C3-H and C4-H). ¹³C NMR (75 MHz, CDCl₃): δ 174.6 (COO), 145.1 (C6'), 134.8 (Ph, C), 129.2 (Ph, CH), 128.8 (Ph, CH), 128.3 (Ph, CH), 122.8 (C7), 64.9 (C2), 54.2 (C5), 53.5 (C8), 51.9 (OCH₃), 48.9 (C6), 29.5 (C3), 23.2 (C4). IR (film): ν_{max} 3493, 3140, 2951, 2850, 2359, 1745, 1732, 1556, 1496, 1454, 1359,

1284, 1049, 769, 725 cm⁻¹. ESI-HRMS *m/z* [M+Na]⁺ calcd for C₁₆H₂₀N₄NaO₂ 323.1478, found 323.1474.

Methyl ((1-Cyclohexyl-1H-1,2,3-Triazol-4-yl)Methyl)-L-Proline (3d)

Compound **3d** was prepared from 45 mg (0.27 mmol) of N-propargyl methyl proline **1**, following the general procedure for the 1,3-dipolar cycloaddition, affording 31 mg of a yellowish oil in 39% yield. ¹H NMR (300 MHz, CDCl₃): δ 7.51 (s, 1H, C7-H), 4.44 (d, *J* = 2.6 Hz, 2H, C8-H), 3.97 (d, *J* = 13.8 Hz, 1H, C6-H), 3.79 (d, *J* = 13.8 Hz, 1H, C6-H), 3.66 (s, 3H, OMe), 3.29 (dd, *J* = 8.7, 6.1 Hz, 1H, C2-H), 3.16–3.10 (m, 1H, C5-H), 2.46 (dt, *J* = 8.4, 8.2 Hz, 1H, C5-H), 2.20–1.63 (m, 12H, C3-H and cyclohexyl), 1.51–1.21 (m, 3H, C4-H and cyclohexyl). ¹³C NMR (75 MHz, CDCl₃): δ 174.5 (COO), 144.0 (C6'), 120.3 (C7), 64.8 (C2), 59.7 (C5), 53.4 (C8), 51.85 (OCH₃), 48.9 (C6), 33.5 (CH₂), 32.4 (C3), 29.4 (CH₂), 25.2 (CH₂), 23.0 (C4). IR (film): ν_{max} 3417, 3142, 2935, 2856, 2362, 1737, 1732, 1633, 1450, 1371, 1276, 1201, 1049, 997, 894, 823, 777 cm⁻¹. ESI-HRMS *m/z* [M+H]⁺ calcd for C₁₅H₂₅N₄O₂ 293.1972, found 293.1970.

Methyl ((1-(3-Phenylpropyl)-1H-1,2,3-Triazol-4-yl)Methyl)-L-Proline (3e)

Compound **3e** was prepared from 45 mg (0.27 mmol) of N-propargyl methyl proline **1**, following the general procedure for the 1,3-dipolar cycloaddition, affording 73 mg of a yellowish oil in 82% yield. ¹H NMR (300 MHz, CDCl₃): δ 7.43 (s, 1H, C7-H), 7.24–7.19 (m, 2H, Ph), 7.18–7.08 (m, 3H, Ph), 4.21 (d, *J* = 2.6 Hz, 2H, C8-H), 3.93 (d, *J* = 13.8 Hz, 1H, C6-H), 3.76 (d, *J* = 13.8 Hz, 1H, C6-H), 3.60 (s, 3H, OMe), 3.24 (dd, *J* = 8.7, 6.1 Hz, 1H, C2-H), 3.06 (m, 1H, C5-H), 2.53–2.44 (m, 5H), 2.23–1.61 (m, 4H, C3-H and C4-H). ¹³C NMR (75 MHz, CDCl₃): δ 174.5 (COO), 144.6 (C6'), 140.3 (Ph), 128.7 (Ph), 128.5 (Ph), 126.4 (Ph), 122.8 (C7), 64.7 (C2), 53.4 (C5), 51.9 (OCH₃), 49.5 (C8), 48.7 (C6), 32.5 (CH₂), 31.7 (C3), 29.5 (CH₂), 23.5 (C4). IR (film): ν_{max} 3626, 3458, 3138, 2949, 2854, 2358, 1732, 1602, 1496, 1444, 1354, 1278, 1172, 1085, 1049, 1004, 785, 748, 702 cm⁻¹. ESI-HRMS *m/z* [M+Na]⁺ calcd for C₁₈H₂₄N₄NaO₂ 351.1791, found 351.1790.

Methyl ((1-Cinnamyl-1H-1,2,3-Triazol-4-yl)Methyl)-L-Proline (3f)

Compound **3f** was prepared from 45 mg (0.27 mmol) of N-propargyl methyl proline **1**, following the general procedure for the 1,3-dipolar cycloaddition, affording 53 mg of a yellowish oil in 60% yield. ¹H NMR (300 MHz, CDCl₃): δ 7.58 (s, 1H, C7-H), 7.43–7.21 (m, 5H, Ph), 6.65 (d, *J* = 15.8 Hz, 1H, C9-H), 6.33 (m, 1H, C10-H), 5.11 (d, *J* = 2.6 Hz, 2H, C8-H), 4.00 (d, *J* = 13.8 Hz, 1H, C6-H), 3.82 (d, *J* = 13.8 Hz, 1H, C6-H), 3.66 (s, 3H, OMe), 3.31 (dd, *J* = 8.7, 6.1 Hz, 1H, C2-H), 3.14 (m, 1H, C5-H), 2.52 (dt, *J* = 8.4, 8.2 Hz, 1H, C5-H), 2.20–2.04 (m, 1H, C3-H), 2.00–1.71 (m, 3H, C3-H, C4-H₂). ¹³C NMR (75 MHz, CDCl₃): δ 174.5 (COO), 144.9 (C6'), 135.3 (Ph), 135.3 (C9-H), 128.7 (Ph), 128.5 (CH), 126.7 (Ph), 122.5 (C10-H), 121.9 (C7), 64.7 (C2), 53.4 (C5), 52.3 (OCH₃), 51.8 (C8), 48.7 (C6), 29.4 (C3), 23.0 (C4). IR (film): ν_{max} 3541, 3138, 2951, 2845, 2358, 1741, 1732, 1552,

1448, 1359, 1278, 1203, 1174, 1128, 1047, 970, 756, 694 cm^{-1} . ESI-HRMS m/z $[M+Na]^+$ calcd for $C_{18}H_{22}N_4NaO_2$ 349.1635, found 349.1625.

Methyl ((1-(Naphthalen-2-ylmethyl)-1H-1,2,3-Triazol-4-yl)Methyl)-L-Proline (3g)

Compound **3g** was prepared from 20 mg (0.12 mmol) of N-propargyl methyl proline **1**, following the general procedure for the 1,3-dipolar cycloaddition, affording 34 mg of a light orange solid in 81% yield. M.p. 64.0–64.9 °C. ^1H NMR (300 MHz, CDCl_3): δ 7.85–7.82 (m, 3H, naphthyl), 7.74 (s, 1H, C-H), 7.52–7.49 (m, 2H, naphthyl), 7.46 (s, 1H, C7-H), 7.37–7.33 (m, 1H, naphthyl), 5.66 (d, $J = 3.6$ Hz, 2H, C8-H), 3.97 (d, $J = 13.9$ Hz, 1H, C6-H), 3.80 (d, $J = 13.9$ Hz, 1H, C6-H), 3.60 (s, 3H, OMe), 3.26 (dd, $J = 8.7, 6.1$ Hz, 1H, C2-H), 3.06 (m, 1H, C5-H), 2.46 (dt, $J = 8.4, 8.2$ Hz, 1H, C5-H), 2.15–1.65 (m, 4H, C3-H and C4-H). ^{13}C NMR (75 MHz, CDCl_3): δ 174.4 (COO), 145.1 (C6'), 133.2 (C), 133.1 (C), 131.9 (C), 129.1 (CH), 127.9 (CH), 127.7 (CH), 127.4 (CH), 126.7 (CH), 125.3 (C7), 122.7 (CH), 122.7 (CH), 64.7 (C2), 54.3 (C5), 53.4 (C8), 51.8 (OCH₃), 43.7 (C6), 29.4 (C3), 23.0 (C4). IR (KBr): ν_{max} 3500, 3132, 2949, 2818, 2358, 1732, 1600, 1548, 1508, 1435, 1338, 1273, 1203, 1172, 1126, 1047, 891, 771 cm^{-1} . ESI-HRMS m/z $[M+H]^+$ calcd for $C_{20}H_{23}N_4O_2$ 351.1815, found 351.1826.

Methyl ((1-Octyl-1H-1,2,3-Triazol-4-yl)Methyl)-L-Proline (3h)

Compound **3h** was prepared from 20 mg (0.12 mmol) of N-propargyl methyl proline **1**, following the general procedure for the 1,3-dipolar cycloaddition, affording 31 mg of a yellow oil in 81% yield. ^1H NMR (300 MHz, CDCl_3): δ 7.44 (s, 1H, C7-H), 4.24 (t, $J = 7.2$ Hz, 2H, C8-H), 3.93 (d, $J = 13.8$ Hz, 1H, C6-H), 3.75 (d, $J = 13.8$ Hz, 1H, C6-H), 3.61 (s, 3H, OMe), 3.23 (dd, $J = 8.6, 6.0$ Hz, 1H, C2-H), 3.08–3.02 (m, 1H, C5-H), 2.49–2.41 (dt, 1H, $J = 8.4, 8.1$ Hz, C5-H), 2.03–1.71 (m, 5H), 1.22–1.17 (m, 11H), 0.79 (t, $J = 6.5$ Hz, 3H, CH₃). ^{13}C NMR (75 MHz, CDCl_3): δ 174.4 (COO), 144.4 (C6'), 122.5 (C7), 64.6 (C2), 53.2 (C5), 51.8 (OCH₃), 50.2 (C8), 48.6 (C6), 31.6 (CH₂), 30.2 (CH₂), 29.4 (C3), 29.0 (CH₂), 28.9 (CH₂), 26.4 (CH₂), 23.0 (C4), 22.5 (CH₂), 14.0 (CH₃). IR (film): ν_{max} 3604, 3458, 3136, 2926, 2357, 1345, 1645, 1444, 1354, 1172, 1047, 771 cm^{-1} . ESI-HRMS m/z $[M+Na]^+$ calcd for $C_{17}H_{30}N_4NaO_2$ 345.2261, found 345.2261.

Methyl

((1-Decyl-1H-1,2,3-Triazol-4-yl)Methyl)-L-Proline (3i)

Compound **3i** was prepared from 20 mg (0.12 mmol) of N-propargyl methyl proline **1**, following the general procedure for the 1,3-dipolar cycloaddition, affording 32 mg of a yellow oil in 75% yield. ^1H NMR (300 MHz, CDCl_3): δ 7.49 (s, 1H, C7-H), 4.32 (t, $J = 7.2$ Hz, 2H, C8-H), 4.02 (d, $J = 13.8$ Hz, 1H, C6-H), 3.83 (d, $J = 13.8$ Hz, 1H, C6-H), 3.66 (s, 3H, OMe), 3.33 (dd, $J = 8.7, 6.1$ Hz, 1H, C2-H), 3.17–3.08 (m, 1H, C5-H), 2.58–2.50 (dt, $J = 8.4, 8.2$ Hz, 1H, C5-H), 2.11–1.77 (m, 4H, C3-H and C4-H), 1.27–1.21 (m, 16H), 0.84 (t, $J = 6.6$ Hz, 3H, CH₃). ^{13}C NMR (75 MHz, CDCl_3): δ 174.5 (COO), 144.4 (C6'), 122.7 (C7), 64.7

(C2), 53.4 (C5), 51.9 (OCH₃), 50.4 (C8), 48.7 (C6), 31.9 (CH₂), 30.4 (CH₂), 29.5 (C3), 29.5 (CH₂), 29.3 (CH₂), 29.1 (CH₂), 29.1 (CH₂), 26.5 (CH₂), 23.1 (C4), 22.7 (CH₂), 14.2 (CH₃). IR (film): ν_{max} 3458, 2926, 2854, 2358, 1745, 1732, 1651, 1444, 1373, 1278, 1199, 1172, 1047, 891, 783, 721 cm^{-1} . ESI-HRMS m/z $[M+H]^+$ calcd for $C_{19}H_{35}N_4O_2$ 351.2754, found 351.2746.

Methyl ((1-Hexadecyl-1H-1,2,3-Triazol-4-yl)Methyl)-L-Proline (3j)

Compound **3j** was prepared from 20 mg (0.12 mmol) of N-propargyl methyl proline **1**, following the general procedure for the 1,3-dipolar cycloaddition, affording 22 mg of a white solid in 42 % yield. M.p. 60–60.9 °C. ^1H NMR (300 MHz, CDCl_3): δ 7.47 (s, 1H, C7-H), 4.29 (t, $J = 7.2$ Hz, 2H, C8-H), 3.99 (d, $J = 13.8$ Hz, 1H, C6-H), 3.80 (d, $J = 13.8$ Hz, 1H, C6-H), 3.67 (s, 3H, OMe), 3.30 (dd, $J = 8.7, 6.1$ Hz, 1H, C2-H), 3.16–3.11 (m, 1H, C5-H), 2.57–2.48 (dt, $J = 8.9, 7.8$ Hz, 1H, C5-H), 1.91–1.84 (m, 4H), 1.28–1.23 (m, 28H), 0.85 (t, $J = 6.6$ Hz, 3H, CH₃). ^{13}C NMR (75 MHz, CDCl_3): δ 174.7 (COO), 144.7 (C6'), 122.6 (C7), 64.6 (C2), 53.2 (C5), 52.0 (OCH₃), 50.5 (C8), 48.9 (C6), 32.1 (CH₂), 30.5 (CH₂), 29.9 (CH₂), 29.8 (CH₂), 29.8 (CH₂), 29.7 (CH₂), 29.6 (CH₂), 29.6 (CH₂), 29.6 (CH₂), 29.4 (C3), 29.3 (CH₂), 29.2 (CH₂), 28.9 (CH₂), 26.4 (CH₂), 23.0 (C4), 22.6 (CH₂), 14.0 (CH₃). IR (KBr): ν_{max} 3124, 2914, 2357, 1745, 1728, 1556, 1444, 1336, 1269, 1197, 1053, 848, 790, 719 cm^{-1} . ESI-HRMS m/z $[M+Na]^+$ calcd for $C_{25}H_{46}N_4NaO_2$ 457.3513, found 457.3512.

Methyl (Z)-((1-(Octadec-9-en-1-yl)-1H-1,2,3-Triazol-4-yl)Methyl)-L-Proline (3k)

Compound **3k** was prepared from 20 mg (0.12 mmol) of N-propargyl methyl proline **1**, following the general procedure for the 1,3-dipolar cycloaddition, affording 33 mg of a light-yellow oil in 59 % yield. ^1H NMR (300 MHz, CDCl_3): δ 7.49 (s, 1H, C7-H), 5.35–5.31 (m, CH=CH, 2H), 4.30 (t, $J = 7.2$ Hz, 2H, C8-H), 4.00 (d, $J = 13.8$ Hz, 1H, C6-H), 3.81 (d, $J = 13.8$ Hz, 1H, C6-H), 3.68 (s, 3H, OMe), 3.30 (dd, $J = 8.8, 6.1$ Hz, 1H, C2-H), 3.15–3.10 (m, 1H, C5-H), 2.56–2.48 (dt, $J = 8.5, 8.1$ Hz, 1H, C5-H), 2.16–1.79 (m, 6H), 1.27–1.25 (m, 26H), 0.87 (t, $J = 6.7$ Hz, 3H, CH₃). ^{13}C NMR (75 MHz, CDCl_3): δ 174.4 (COO), 144.4 (C6'), 130.0 (CH=), 129.7 (CH=), 122.5 (C7), 64.7 (C2), 53.3 (C5), 51.8 (OCH₃), 50.3 (C8), 48.6 (C6), 31.9 (CH₂), 30.3 (CH₂), 29.7 (CH₂), 29.7 (CH₂), 29.5 (C3), 29.4 (CH₂), 29.4 (CH₂), 29.3 (CH₂), 29.1 (CH₂), 29.0 (CH₂), 29.0 (CH₂), 27.2 (CH₂), 27.1 (CH₂), 26.5 (CH₂), 23.0 (C4), 22.6 (CH₂), 14.1 (CH₃). IR (film): ν_{max} 3564, 3477, 3136, 2924, 2852, 2358, 2096, 1745, 1556, 1444, 1373, 1276, 1199, 1172, 1047, 968, 891, 775, 723 cm^{-1} . ESI-HRMS m/z $[M+K]^+$ calcd for $C_{27}H_{48}KN_4O_2$ 499.3408, found 499.3412.

Methyl

((1-Icosyl-1H-1,2,3-Triazol-4-yl)Methyl)-L-Proline (3l)

Compound **3l** was prepared from 20 mg (0.12 mmol) of N-propargyl methyl proline **1**, following the general procedure for the 1,3-dipolar cycloaddition, affording 34 mg of a white solid in 58 % yield. M.p. 72.7–73.7 °C. ^1H NMR (300 MHz,

CDCl₃): δ 7.49 (s, 1H, C7-H), 4.31 (t, J = 7.2 Hz, 2H, C8-H), 4.01 (d, J = 13.8 Hz, 1H, C6-H), 3.82 (d, J = 13.8 Hz, 1H, C6-H), 3.69 (s, 3H, OMe), 3.30 (dd, J = 8.5, 5.7 Hz, 1H, C2-H), 3.14–3.1 (m, 1H, C5-H), 2.54–2.46 (dt, J = 8.5, 7.9 Hz, 1H, C5-H), 1.91–1.84 (m, 4H), 1.28–1.23 (m, 36H), 0.87 (t, J = 6.7 Hz, 3H, CH₃). ¹³C NMR (75 MHz, CDCl₃): δ 174.5 (COO), 144.4 (C6'), 122.4 (C7), 64.7 (C2), 53.3 (C5), 51.8 (OMe), 50.2 (C8), 48.6 (CH₂), 31.9 (CH₂), 30.2 (CH₂), 29.6 (CH₂), 29.5 (CH₂), 29.3 (CH₂), 29.0 (CH₂), 26.4 (CH₂), 23.0 (CH₂), 22.6 (CH₂), 14.1 (CH₃). IR (KBr): ν_{\max} 3649, 3124, 3076, 2916, 2846, 2358, 1743, 1462, 1338, 1271, 1211, 1055, 1037, 852, 771, 719 cm⁻¹. ESI-HRMS m/z [M+Na]⁺ calcd for C₂₉H₅₄NaN₄O₂ 513.4139, found 513.4125.

Methyl ((1-(3,7-Dimethylocta-2,6-Dien-1-yl)-1H-1,2,3-Triazol-4-yl)Methyl)-L-Proline (3m)

Compound **3m** was prepared from 30 mg (0.18 mmol) of N-propargyl methyl proline **1**, following the general procedure for the 1,3-dipolar cycloaddition, affording 47 mg of a yellow oil in 87 % yield. ¹H NMR (300 MHz, CDCl₃): δ 7.46 (s, 1H, C7-H), 5.41 (t, J = 7.2 Hz, 1H, C9-H), 5.08–5.01 (m, 1H, C13-H), 4.90 (t, J = 7.2 Hz, 2H, C8-H), 4.01 (d, J = 13.6 Hz, 1H, C6-H), 3.82 (d, J = 13.6 Hz, 1H, C6-H), 3.66 (s, 3H, OMe), 3.30 (dd, J = 8.1, 6.0 Hz, 1H, C2-H), 3.12–3.1 (m, 1H, C5-H), 2.54–2.46 (dt, J = 8.4, 8.2 Hz, 2H, C5-H), 1.7 (m, 6H, C3-H and C4-H), 1.65 (s, 3H, CH₃), 1.63 (m, 6H, CH₃), 1.55 (m, 3H, CH₃). ¹³C NMR (75 MHz, CDCl₃): δ 174.5 (COO), 144.4 (C6'), 122.7 (C7), 64.7 (C2), 53.4 (C5), 51.9 (OCH₃), 50.4 (C8), 48.7 (C6), 31.9 (CH₂), 30.4 (CH₂), 29.5 (C3), 29.3 (CH₂), 29.1 (CH₂), 26.5 (CH₂), 23.1 (C4), 22.7 (CH₂), 17.6 (CH₃), 16.5 (CH₃), 16.0 (CH₃). IR (film): ν_{\max} 3564, 3140, 2926, 2358, 1867, 1747, 1732, 1506, 1435, 1373, 1217, 1174, 1124, 1047, 844, 771 cm⁻¹. ESI-HRMS m/z [M+H]⁺ calcd for C₁₉H₃₅N₄O₂ 351.2754, found 351.2746.

Methyl

((1-((2E,6E)-3,7,11-Trimethyldodeca-2,6,10-Trien-1-yl)-1H-1,2,3-Triazol-4-yl)Methyl)-L-Proline (3n) and Methyl

((1-((2E,6Z)-3,7,11-Trimethyldodeca-2,6,10-Trien-1-yl)-1H-1,2,3-Triazol-4-yl)Methyl)-L-Proline (3o)

Compound **3n** and **3o** were prepared from 50 mg (0.30 mmol) of N-propargyl methyl proline **1**, following the general procedure for the 1,3-dipolar cycloaddition, affording 53 mg of **3n** and 28 mg of **3o** as yellowish oils in 43 % and 23 % yield, respectively.

3n: ¹H NMR (300 MHz, CDCl₃): δ 7.47 (s, 1H, C7-H), 5.42 (t, J = 7.2 Hz, 1H, C9-H), 5.08–5.06 (m, 2H, C13-H and C16-H), 4.95 (t, J = 7.2 Hz, 2H, C8-H), 4.00 (d, J = 13.7 Hz, 1H, C6-H), 3.80 (d, J = 13.7 Hz, 1H, C6-H), 3.69 (s, 3H, OMe), 3.31 (dd, J = 8.7, 6.1 Hz, 1H, C2-H), 3.16–3.10 (m, 1H, C5-H), 2.61–2.48 (dt, J = 8.4, 8.2 Hz, 1H, C5-H), 1.70 (m, 4H, C3-H and C4-H), 2.12–1.91 (m, 8H), 1.78 (s, 3H, CH₃), 1.65 (s, 3H, CH₃), 1.63 (m, 3H, CH₃), 1.55 (m, 3H, CH₃). ¹³C NMR (75 MHz, CDCl₃): δ 174.4 (COO), 144.4 (C6'), 143.1 (C), 135.7 (C), 131.3 (C), 124.2 (CH), 123.3 (CH), 122.0 (C7-H), 116.9 (CH), 64.7 (C2), 53.2 (C5), 51.8

(OCH₃), 48.6 (C8), 47.8 (C6), 39.6 (CH₂), 39.4 (CH₂), 29.3 (C3), 26.6 (CH₂), 26.1 (CH₂), 25.6 (CH₂), 22.9 (CH₃), 17.6 (CH₃), 16.5 (CH₃), 16.0 (CH₃). IR (film): ν_{\max} 3417, 3124, 2992, 2358, 1867, 1747, 1732, 1539, 1456, 1317, 1271, 1122, 1047, 773 cm⁻¹. ESI-HRMS m/z [M+H]⁺ calcd for C₂₄H₃₉N₄O₂ 415.3067, found 415.3067.

3o: ¹H NMR (300 MHz, CDCl₃): δ 7.47 (s, 1H, C7-H), 5.42 (t, J = 7.2 Hz, 1H, C9-H), 5.08–5.06 (m, 2H, C13-H and C16-H), 4.95 (t, J = 7.2 Hz, 2H, C8-H), 4.00 (d, J = 13.7 Hz, 1H, C6-H), 3.80 (d, J = 13.7 Hz, 1H, C6-H), 3.69 (s, 3H, OMe), 3.31 (dd, J = 8.7, 6.1 Hz, 1H, C2-H), 3.16–3.10 (m, 1H, C5-H), 2.61–2.48 (dt, J = 8.4, 8.2 Hz, 1H, C5-H), 1.7 (m, 4H, C3-H and C4-H), 2.12–1.91 (m, 8H), 1.78 (s, 3H, CH₃), 1.65 (s, 3H, CH₃), 1.63 (m, 3H, CH₃), 1.55 (m, 3H, CH₃). ¹³C NMR (75 MHz, CDCl₃): δ 174.4 (COO), 144.4 (C6'), 143.1 (C), 135.7 (C), 131.3 (C), 124.2 (CH), 123.3 (CH), 122.0 (C7-H), 116.9 (CH), 64.7 (C2), 53.2 (C5), 51.8 (OCH₃), 48.6 (C8), 47.8 (C6), 39.6 (CH₂), 39.4 (CH₂), 29.3 (C3), 26.6 (CH₂), 26.1 (CH₂), 25.6 (CH₂), 22.9 (CH₃), 17.6 (CH₃), 16.5 (CH₃), 16.0 (CH₃). IR (film): ν_{\max} 3417, 3124, 2962, 2924, 2341, 1745, 1732, 1625, 1446, 1435, 1377, 1215, 1172, 1047, 775 cm⁻¹. ESI-HRMS m/z [M+H]⁺ calcd for C₂₄H₃₉N₄O₂ 415.3067, found 415.3067.

Methyl ((1-((E)-3,7,11,15-Tetramethylhexadec-2-en-1-yl)-1H-1,2,3-Triazol-4-yl)Methyl)-L-Proline (3p) and Methyl ((1-(3,7,11,15-Tetramethylhexadec-2-en-1-yl)-1H-1,2,3-Triazol-4-yl)Methyl)-L-Proline (3q)

Compound **3p** and **3q** were prepared from 50 mg (0.30 mmol) of N-propargyl methyl proline **1**, following the general procedure for the 1,3-dipolar cycloaddition, affording 22 mg of **3p** (*E*-isomer) and 23 mg of **3q** (mixture *E:Z*) as yellowish oils in 38 % and 39 % yield, respectively.

3p: ¹H NMR (300 MHz, CDCl₃): δ 7.47 (s, 1H, C7-H), 5.39 (t, J = 7.2 Hz, 1H, C9-H), 4.91 (t, J = 7.2 Hz, 2H, C8-H), 3.98 (d, J = 13.7 Hz, 1H, C6-H), 3.78 (d, J = 13.7 Hz, 1H, C6-H), 3.68 (s, 3H, OMe), 3.29 (dd, J = 8.7, 6.1 Hz, 1H, C2-H), 3.14–3.09 (m, 1H, C5-H), 2.54–2.46 (dt, J = 8.4, 8.2 Hz, 1H, C5-H), 2.11 (s, 3H, C10-CH₃), 2.02–1.84 (m, 4H, C3-H and C4-H), 1.77–1.75 (m, 3H), 1.36–1.06 (m, 18H), 0.86–0.81 (m, 12H, CH₃). ¹³C NMR (75 MHz, CDCl₃): δ 174.4 (COO), 144.4 (C6'), 143.7 (C10), 122.1 (C7), 117.4 (C9), 64.8 (C2), 53.7 (C5), 51.9 (OCH₃), 48.7 (C6), 39.8 (C8), 39.4 (CH₂), 37.4 (CH₂), 37.3 (CH₂), 37.0 (CH₂), 36.9 (CH₂), 36.7 (CH₂), 32.7 (CH₂), 32.3 (CH₂), 29.7 (C3), 29.4 (C4), 28.0 (CH₂), 25.5 (CH₂), 25.0 (CH₂), 24.8 (CH₂), 24.5 (CH₃), 23.4 (CH₃), 23.0 (CH₃), 22.7 (CH₃), 22.6 (CH₃). IR (film): ν_{\max} 3500, 3140, 2926, 2358, 1747, 1506, 1456, 1377, 1172, 1047, 933, 862, 775 cm⁻¹. ESI-HRMS: mass calculated for C₂₉H₅₂N₄NaO₂ (M+Na)⁺, 511.3982, found 511.3970.

3q: ¹H NMR (300 MHz, CDCl₃): δ 7.47 (s, 1H, C7-H), 5.39 (t, J = 7.2 Hz, 1H, CH), 4.91 (t, J = 7.2 Hz, 2H, C8-H), 3.98 (d, J = 13.7 Hz, 1H, C6-H), 3.78 (d, J = 13.7 Hz, 1H, C6-H), 3.68 (s, 3H, OMe), 3.29 (dd, J = 8.7, 6.1 Hz, 1H, C2-H), 3.14–3.09 (m, 1H, C5-H), 2.54–2.46 (dt, J = 8.4 Hz, J =

8.2 Hz, 1H, C5-H), 2.11 (s, 3H, CH₃), 2.02–1.84 (m, 4H, C3-H and C4-H), 1.77–1.75 (m, 3H), 1.36–1.06 (m, 18H), 0.86–0.81 (m, 12H, CH₃). ¹³C NMR (75 MHz, CDCl₃): δ 174.4 (COO), 144.4 (C6'), 143.7 (C10), 122.1 (C7), 117.4 (C9), 64.8 (C2), 53.7 (C5), 51.9 (OCH₃), 48.7 (C6), 39.8 (C8), 39.4 (CH₂), 37.4 (CH₂), 37.3 (CH₂), 37.0 (CH₂), 36.9 (CH₂), 36.7 (CH₂), 32.7 (CH₂), 32.3 (CH₂), 29.7 (C3), 29.4 (C4), 28.0 (CH₂), 25.5 (CH₂), 25.0 (CH₂), 24.8 (CH₂), 24.5 (CH₃), 23.4 (CH₃), 23.0 (CH₃), 22.7 (CH₃), 22.6 (CH₃). IR (film): ν_{max} 3500, 3140, 2926, 2358, 1747, 1506, 1456, 1377, 1172, 1047, 933, 862, 775 cm⁻¹. ESI-HRMS *m/z* [M+Na]⁺ calcd for C₂₉H₅₂N₄NaO₂ 511.3982, found 511.3970.

BIOLOGY

Reagents

All reagents were purchased from Sigma-Aldrich (St. Louis, MO, USA). Culture medium and fetal calf serum (FCS) were purchased from Cultilab (Campinas, SP, Brazil).

Cells and Parasites

T. cruzi CL strain clone 14 epimastigotes (Brener and Chiari, 1965) were maintained in the exponential growth phase by subculturing every 48 h in Liver Infusion Tryptose (LIT) medium supplemented with 10% FCS (Vitrocell, Campinas, São Paulo, Brazil) at 28 °C.

Growth Inhibition Assays

T. cruzi epimastigotes in the exponential growth phase (5.0–6.0 × 10⁷ cells mL⁻¹) were cultured in fresh LIT medium. The cells were treated with different concentrations of drugs or not treated (negative control). A combination of Rotenone (60 μM) and Antimycin (0.5 μM) was used as a positive control for inhibition as previously described. (Magdaleno et al., 2009) The cells (2.5 × 10⁶ mL⁻¹) were transferred to 96-well culture plates and incubated at 28 °C. Cell proliferation was quantified by reading the optical density (OD) at 620 nm for 8 days. The OD was converted to cell density values (cells per mL) using a linear regression equation previously obtained under the same conditions. The concentration of compounds that inhibited 50% of parasite proliferation (IC₅₀) was determined during the exponential growth phase (4 days) by fitting the data to a typical sigmoidal dose-response curve using OriginPro8. The compounds were evaluated in quadruplicate in each experiment. The results shown here correspond to three independent experiments. As a cell growth inhibition control, growth curves in which 200 mM rotenone and 0.5 mM antimycin were added to the culture medium were run in parallel for all experiments.

Cytotoxicity Assay

To evaluate the analogs toxicity, Vero cells previously plated on 96 multi-well plate in DMEM 2% FBS and incubated for 48 h at 37 °C in a humid atmosphere containing 5% CO₂, were incubated with 700 μL of DMEM 2% FBS supplemented with each analog for 48 h. The concentration (μM) was different with each analog:

- **3i**: 20 μM, 40 μM, 60 μM, 80 μM, 100 μM and 120 μM.
- **3k**: 5 μM, 10 μM, 15 μM, 20 μM, 25 μM and 30 μM.
- **3n**: 5 μM, 10 μM, 15 μM, 20 μM, 25 μM and 30 μM.
- DMSO: 5 μM, 25 μM, 50 μM and 100 μM.
- Benznidazole: 10 μM, 100 μM, 200 μM and 300 μM.

The viability of cells was measured by MTT dye (3-(4,5-Dimethylthiazol-2-yl)-2,5-diphenyltriazolium bromide, Sigma-Aldrich) colorimetric method. Benznidazole and DMSO were used as positive and negative controls, respectively. Data are expressed as means ± SD of the results of three independent assays of each condition.

L-Proline Transport Inhibition Assay

Parasites in exponential growth phase were washed three times by centrifugation and resuspended in phosphate buffered saline (PBS), pH 7.4. Cells were counted in a Neubauer chamber, adjusted with the same buffer to a final density of 200 × 10⁶ cells/mL and distributed in aliquots of 100 μL (containing 20 × 10⁶ cells each). Transport assays were initiated by the addition to the assay tubes of 100 μL of the desired dilution of L-proline in PBS in the presence of 0.5 mCi of L-[3H] proline. Unless otherwise specified, V₀ was measured at 28 °C for 30 s by incorporation of 0.75 and 3 mM L-proline traced with 1 μCi of U-¹⁴C-L-Pro (Perkin Elmer). In all cases, proline transport was stopped by addition of 800 μL of cold 50 mM proline in PBS (pH 7.4), and rapid washing by centrifugation at 10,000x g for 2 min. Background values in each experiment were measured by simultaneous addition of radiolabeled L-proline and stop solution as previously described (Silber et al., 2002).

Competition Assay

For the competition assays, the transport experiments were performed as described above using the L-Pro concentration corresponding to the K_m (0.31 mM). Those conditions were chosen considering an inhibitory activity by structurally related compounds should be competitive, and so, should be evidenced by a change in the V_{max} at L-Pro concentrations close to the K_m. Non-competitive inhibitors, if any, should diminish V_{max}, which is measured at 10 × K_m L-Pro (3.1 mM) (Silber et al., 2002).

Statistical Analysis

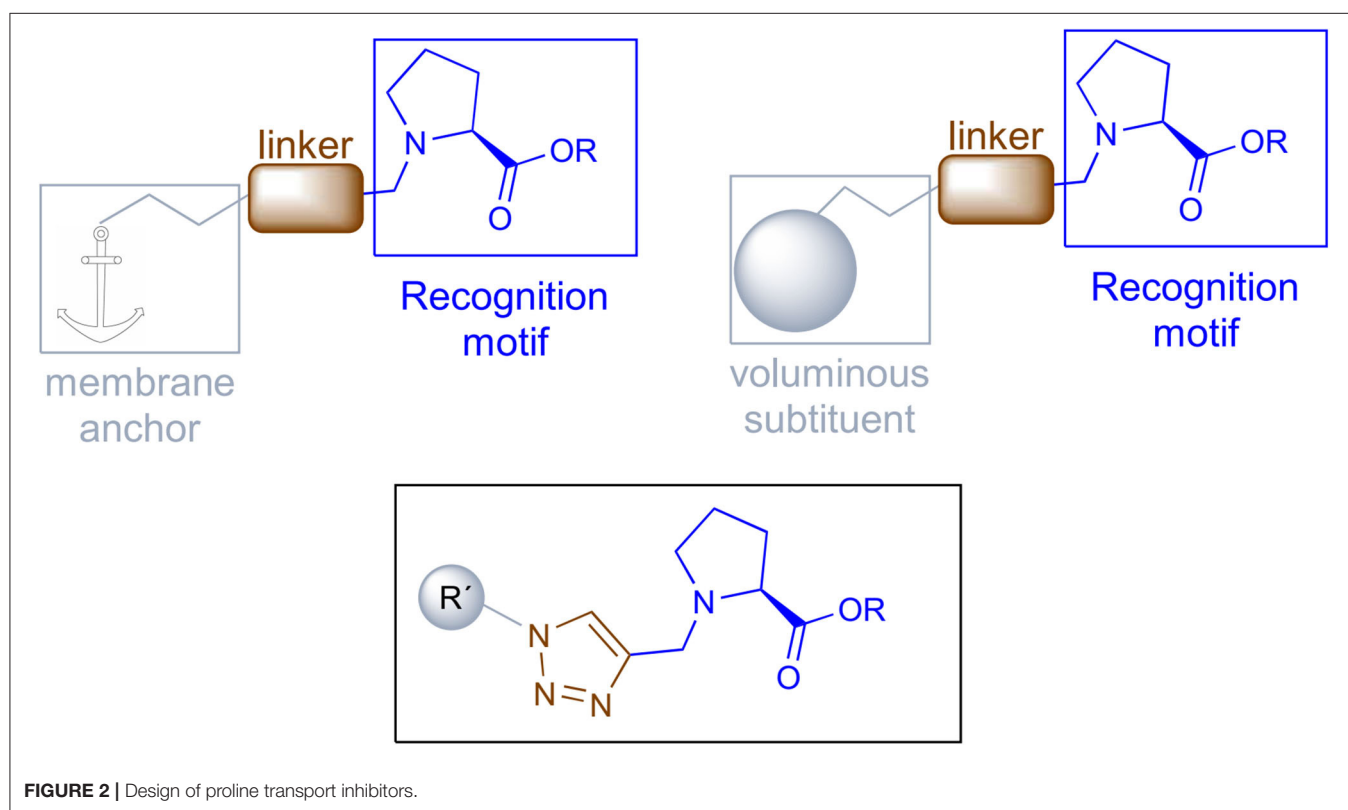
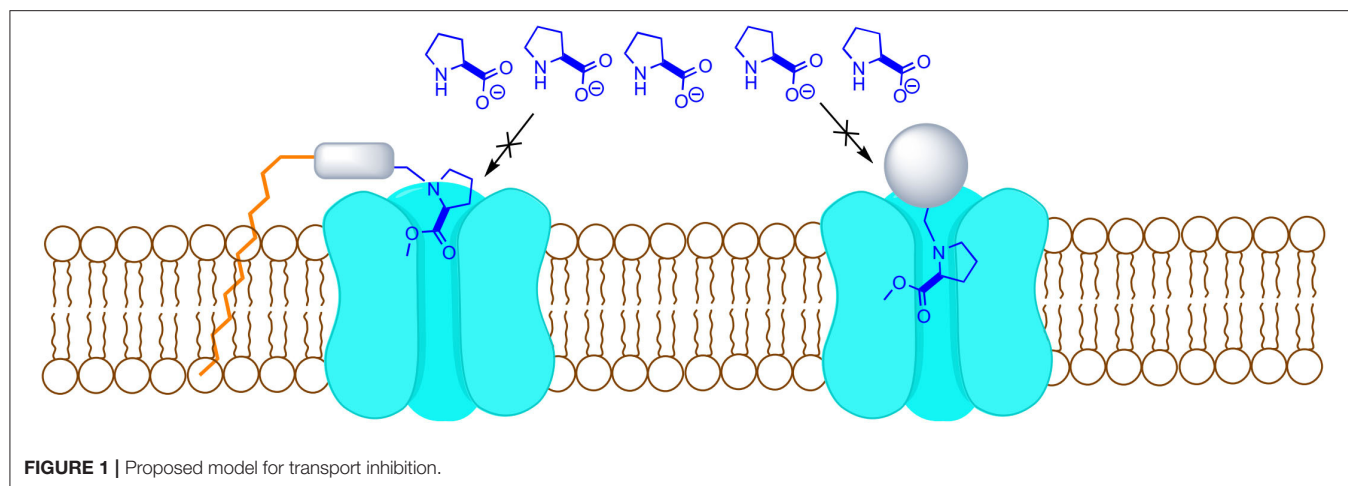
One-way ANOVA followed by the Tukey test was used for statistical analysis. The T-test was used to analyze differences between groups. P < 0.05 was considered statistically significant.

RESULTS

Synthesis of L-Proline Transport Inhibitors

A proper uptake blocker needs to be recognized by the transporter, but not being able to go through, by adding a bulky substituent or a membrane interacting portion that prevents its transport (Figure 1).

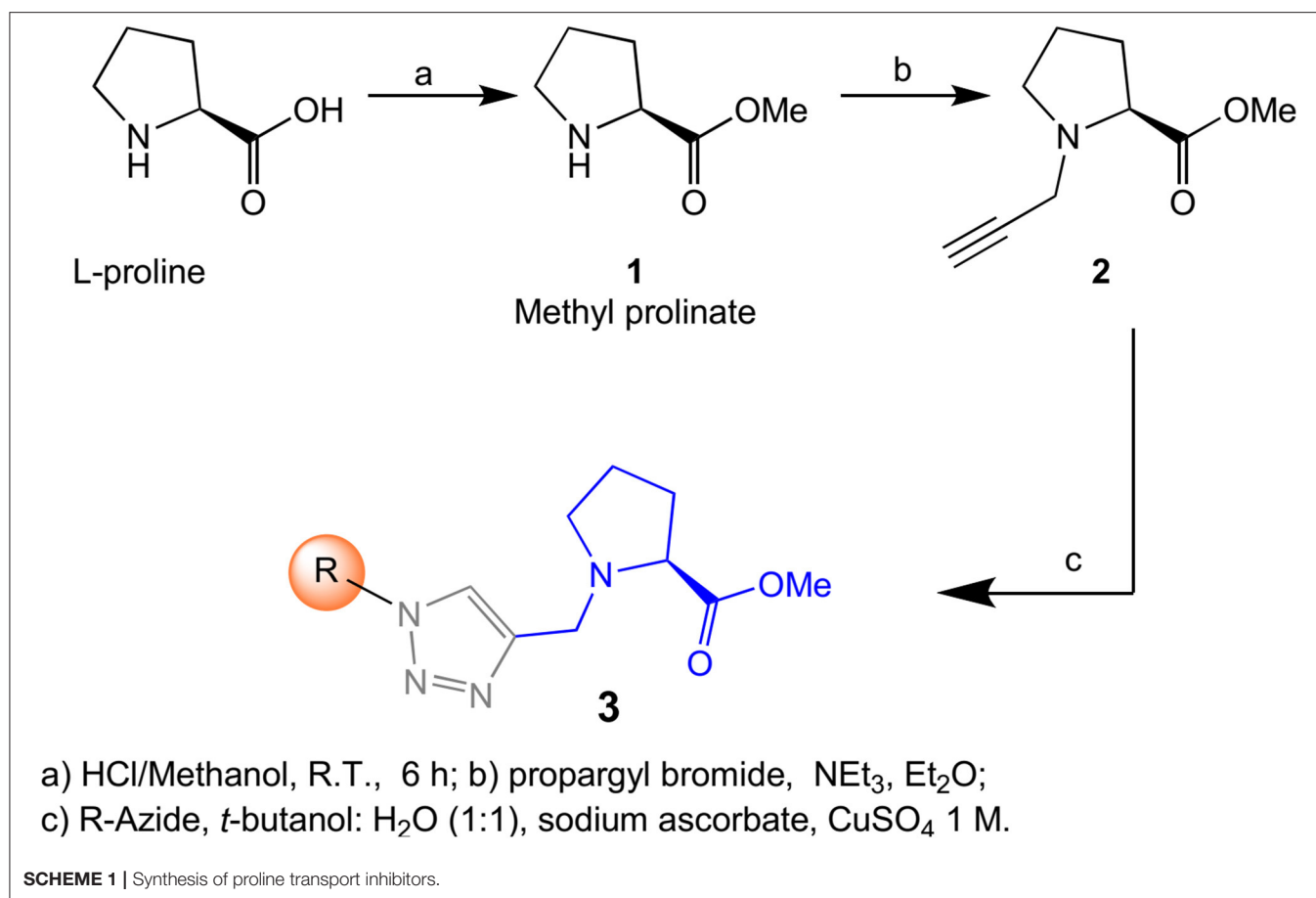
This model will require a compound holding a recognition motif, a linker and a membrane anchor or a voluminous substituent to block the L-proline incorporation. The recognition portion will have L-proline to specifically interact with the



transporter, the membrane anchor should be a non-polar group and both parts will be connected by a 1,2,3-triazole (**Figure 2**).

To validate the proposed model, we proceeded to make a small library following the synthetic strategy shown on **Scheme 1**. The synthesis started from commercial L-proline, preparing the key intermediate in two steps, including an esterification to produce the methyl proline **1** followed by an N-alkylation with propargyl bromide. Once the required key propargyl methyl proline **2** intermediate was prepared, a pool of different azides covering a variety of steric moieties including, aryl, alkyl and isoprenyl substituents was selected to explore their

capacity to interact with the membrane. Azides were prepared by direct substitution of bromide with sodium azide on DMF except for geranyl-, farnesyl-, and phytolazides, which were synthesized from geraniol, farnesol and phytol, respectively, using diphenylphosphoryl azide (DPPA) following Thompson's procedure (Thompson et al., 1993). Phytolazide was found to be a mixture of three chemical entities in equilibrium: tertiary azide, *E* and *Z* isomers of the primary azide, following the same behavior previously observed on geranyl-, and farnesylazide (Porta et al., 2014). Allylic azides can be obtained as a mixture, because they exist as equilibrating mixtures of regioisomers due to



the [3,3] sigmatropic rearrangement (Winstein rearrangement) (Gagneuz et al., 1969). That was the case of geranyl, farnesyl and phytolazide, a mixture of primary:tertiary (8:1), being the primary as 1.6:1 (*E:Z*) ratio (Porta et al., 2017b).

Having prepared the pool of azides, we continued with the synthesis of a focused library of inhibitors through click chemistry. Reactions were conducted in a parallel solution synthesis setup under copper (II) sulfate catalytic conditions in water:*t*-BuOH (1:1), using sodium ascorbate as a reductant (Rostovtsev et al., 2002; Labadie et al., 2011; Porta et al., 2017a). In general, reactions needed an excess of azides for completion and a reaction time was 18 h. All the products have 1,4-substitution on the 1,2,3-triazole as expected, based on the original description of this methodology and our previous work (Porta et al., 2014, 2017a). Reactions with aliphatic and benzylic azides produced a single product, with yields that are slightly better for the last ones. The reaction with the mixture of geranyl azides generated **3i**, which was identified as an inseparable mixture of *E* and *Z* isomers (¹H NMR, 1.5:1), in accordance with our previous results (Porta et al., 2017a). When farnesyl azide was used, a mixture of regioisomers was also obtained with the same ratio, but in this case they were separable (Figure 3). When phytolazide was used the same regioisomers were isolated after the reaction with N-propargyl methyl proline **1**, presenting a higher *E:Z* ratio (1.8:1). Extensive purification work allowed only the isolation of

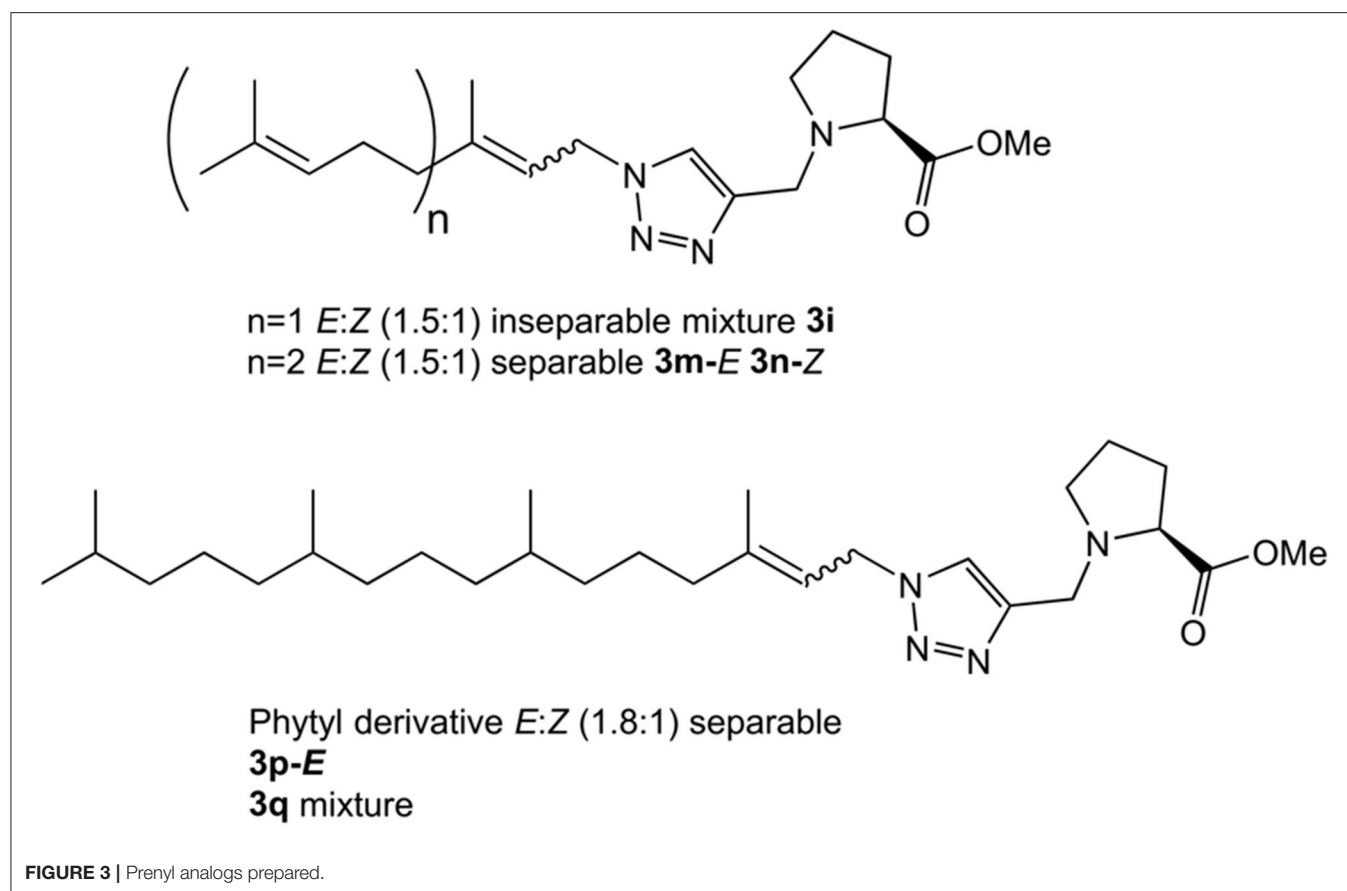
the *E*-isomer of a pure compound (**3p-E**, Figure 3), leaving the remaining product **3q** as a mixture *E:Z*.

Final products **3a-3q**, presented in Table 1, were obtained with an average 67 % yield after purification and were completely characterized by 1D and 2D NMR and ESI-HRMS.

In order to evaluate the biological activity of the prepared collection we decided to initially determine the activity on *T. cruzi* epimastigotes. Then, to validate the L-proline transporter as the molecular target, the intracellular concentration of the amino acid was measured in competition assays with compounds that shown the best antiparasitic activity. Finally, the cytotoxicity of the selected candidates was evaluated in African green monkey kidney epithelial (VERO) cells to estimate the selectivity toward the parasite.

In vitro Activity Against *T. cruzi* Epimastigotes

The compounds collection was assayed against *T. cruzi* epimastigotes (CL strain clone 14) (Brenner and Chiari, 1965) at a maximum concentration of 100 μM. Eight compounds of the total list did not affect the parasite growth at that concentration (**3a**, **3b**, **3c**, **3d**, **3e**, **3f**, **3h**, **3m**), being considered inactive. (Table 1) The naphthyl derivative **3g** and the eicosanyl analog **3l** have an IC₅₀ of 100 μM. A second group of active members of the collection includes the remaining prenyl derivatives **3n**, **3o**,



3p and **3p** with IC_{50} s 48.32, 58.60, 69.75, 48.27 μ M, respectively. (Table 1) The remaining group contains the aliphatic derivatives **3i**, **3j** and **3k**. Those compounds have IC_{50} s below 40 μ M, being the most active members the collection. The decyl and the oleyl derivatives **3i** and **3k** have similar activity (IC_{50} of 38.97 and 35.06 μ M, respectively), while the cetyl analog **3j** has a IC_{50} of 24.07 μ M, considerably slower than the other two (Table 1).

In vitro Cytotoxicity Assay on Vero Cells

Vero cells are well established model to test cytotoxicity *in vitro* because it is an aneuploid and a continuous cell lineage. Initially the library was screened at a fix concentration of 4.75 μ g/mL and none of the analogs showed cytotoxic activity. The most active analogs of the series, compounds **3i**, **3j**, **3k**, and **3n**, were submitted to a further analysis to determine their IC_{50} . Compound **3j** was not soluble at 50 μ M which made not possible to calculate its IC_{50} . Analogs **3i**, **3k**, and **3n** were soluble in a concentration range allowing to perform the assay, showing IC_{50} of 43 μ M, 17 μ M and 14 μ M, respectively.

Proline Transport Assay

In order to obtain a deeper insight into the molecular mechanism of the most active compounds, we performed a proline transport competition assay. The compounds with an IC_{50} lower than 50 μ M (**3i**, **3j**, **3k**, and **3n**) were selected to perform the proline uptake assay aiming to determine the transport inhibition

(Magdaleno et al., 2009). The analogs were assayed on *T. cruzi* epimastigotes incubated with proline at the transporter K_m concentration (0.31 mM), and the analogs were assayed at concentration 10-fold higher (3.1 mM). Surprisingly, we observed that the compounds with higher activity on *T. cruzi* epimastigotes (lower IC_{50} values) showed inhibition but they were not strong enough when compared to analogs with lower antiparasitic activity (higher IC_{50} values). As can be seen on Figure 4, compounds **3i** (*T. cruzi* epimastigotes IC_{50} = 38 μ M) and **3n** (*T. cruzi* epimastigotes IC_{50} = 49 μ M) showed a proline transport inhibition higher than 75% being more active than the analog **3j** that only produced an inhibition of 20%. The oleyl derivate (**3k**), with an unsaturated fatty tail, has a similar IC_{50} on *T. cruzi* epimastigotes compared to the cetyl analog (**3j**) showing no inhibition in terms of proline uptake (Table 2).

DISCUSSION

The selective inhibition of transporters has been proposed as a valuable target to develop new medications against different pathologies including neurological disorders (Qosa et al., 2016) and parasitic diseases (Sayé et al., 2019). The specific inhibition of neuronal glycine, alanine, serine, and cysteine transporters have been studied as molecular targets for new treatment of schizophrenia (Pinard et al., 2010; Schneider et al., 2012;

TABLE 1 | Anti-*T. cruzi* activity of the proline derivatives.

Compound	R	Yield (%)	<i>T. cruzi</i> ^a IC ₅₀ [μM]
3a	CH ₂ COOEt	80	>100
3b	(CH ₂) ₄ COOEt	69	>100
3c	Bn	80	>100
3d	Cyclohexyl	39	>100
3e	Ph-CH ₂ CH ₂ CH ₂	82	>100
3f	Cinnamyl	60	>100
3g	CH ₂ -naphthyl	81	100
3h	Octyl	81	>100
3i	Decyl	75	38.97 ± 1.37
3j	Cetyl	42	24.07 ± 0.66
3k	Oleyl	59	35.06 ± 6.96
3l	Eicosanyl	58	100
3m	Geranyl	87	>100
3n	<i>E</i> -Farnesyl	43	48.32 ± 1.29
3o	<i>Z</i> -Farnesyl	23	58.60 ± 1.37
3p	<i>E</i> -Phytyl	38	69.75 ± 2.17
3q	Phytyl-Mixture	39	48.27 ± 5.81
Benznidazole			7.00 [57]

^aEpimastigotes CL14, results shown are means (SD) from the three independent experiments.

Carland et al., 2014). A high-affinity transporter for proline has been identified, providing an important evidence for proline as a neurotransmitter (Hauptmann et al., 1983). A high throughput screening campaign for high affinity proline transporter inhibitors resulted in the identification of the selective inhibitor LP-403812 (Yu et al., 2009). Summarizing, the participation of metabolites uptake in critical processes in health and diseases has been well demonstrated.

A systematic design pipeline for molecules targeting molecular transporters has not been properly explored. The discovery of most of transporters inhibitors happened by chance or through large HTS campaigns. Burns et al. (2009) pioneered a work in this sense proposing a polyamine-fatty acid conjugate as a polyamine transporter inhibitor. In their rational, the polyamine portion is recognized by the transporter and the fatty acid interacts with the membrane, blocking the polyamine entrance. The newly designed inhibitors (L-Lyz(C18-Acyl-spermine) combined with DMFO display selective antitumoral activity. All the inhibitors mentioned before contained an amino acid portion, or an amino acid mimic, that is recognized by the transporter as a common feature (Figure 5).

With those precedents in mind, we proposed/presented here a general model for aminoacid transporter inhibitors. Our model

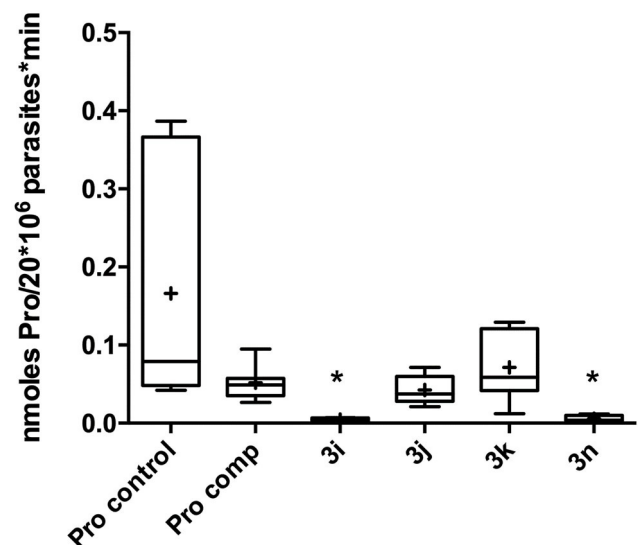
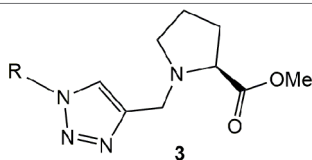


FIGURE 4 | Proline uptake assay. Pro control = Proline control, Pro comp = L-Proline as competitor. **3i-k** and **3n** = proline level incubated (**p* < 0.05) with selected analogs. Pro control (0.31 mM L-proline, [³H] proline, PBS). Pro Comp (3.1 mM L-proline, [³H] proline, PBS). Compounds **3i-k** and **3n** (0.31 mM L-proline, 3.1 mM analog **3x**, [³H] proline, PBS). Stop solution: 50 mM L-proline added after 30 s.

TABLE 2 | Proline uptake inhibition of selected analogs.

Compound	R	<i>T. cruzi</i> IC ₅₀ [μM]	% of Proline inh.
3i	Decyl	38.97 ± 1.37	87
3j	Cetyl	24.07 ± 0.66	18 [#]
3k	Oleyl	35.06 ± 6.96	0
3n	<i>E</i> -Farnesyl	48.32 ± 1.29	99

[#]Precipitation was observed over the experiment.

included an aminoacid portion for recognition, linked to a variable region with different lipophilic and bulk substituents.

We identified the 1,2,3-triazole as a proper linker for our transport inhibitors. The neutral nature of this heterocycle has properly suited the requirements for bioconjugation, protein labeling and immobilization (Gauchet et al., 2006; McKay and Finn, 2014) and for combining different pharmacophores to make hybrid compounds or chimeras. The Cu(I) azide-alkyne reaction, the quintessence of click chemistry, had a strong impact in many research areas including Medicinal Chemistry (Tron et al., 2008; Agalave et al., 2011). The easy reaction conditions has made this methodology very useful to rapidly prepare libraries of compounds, including antiparasitic drug candidates (Carvalho et al., 2010; Hamann et al., 2014; Porta et al., 2017a).

Using 1,2,3-triazole as linker, we prepared products introducing substituents with proper membrane anchor properties. Fatty acids and isoprenyl chains are selectively introduced in proteins by post translational modifications and served as a mediator for membrane association increasing

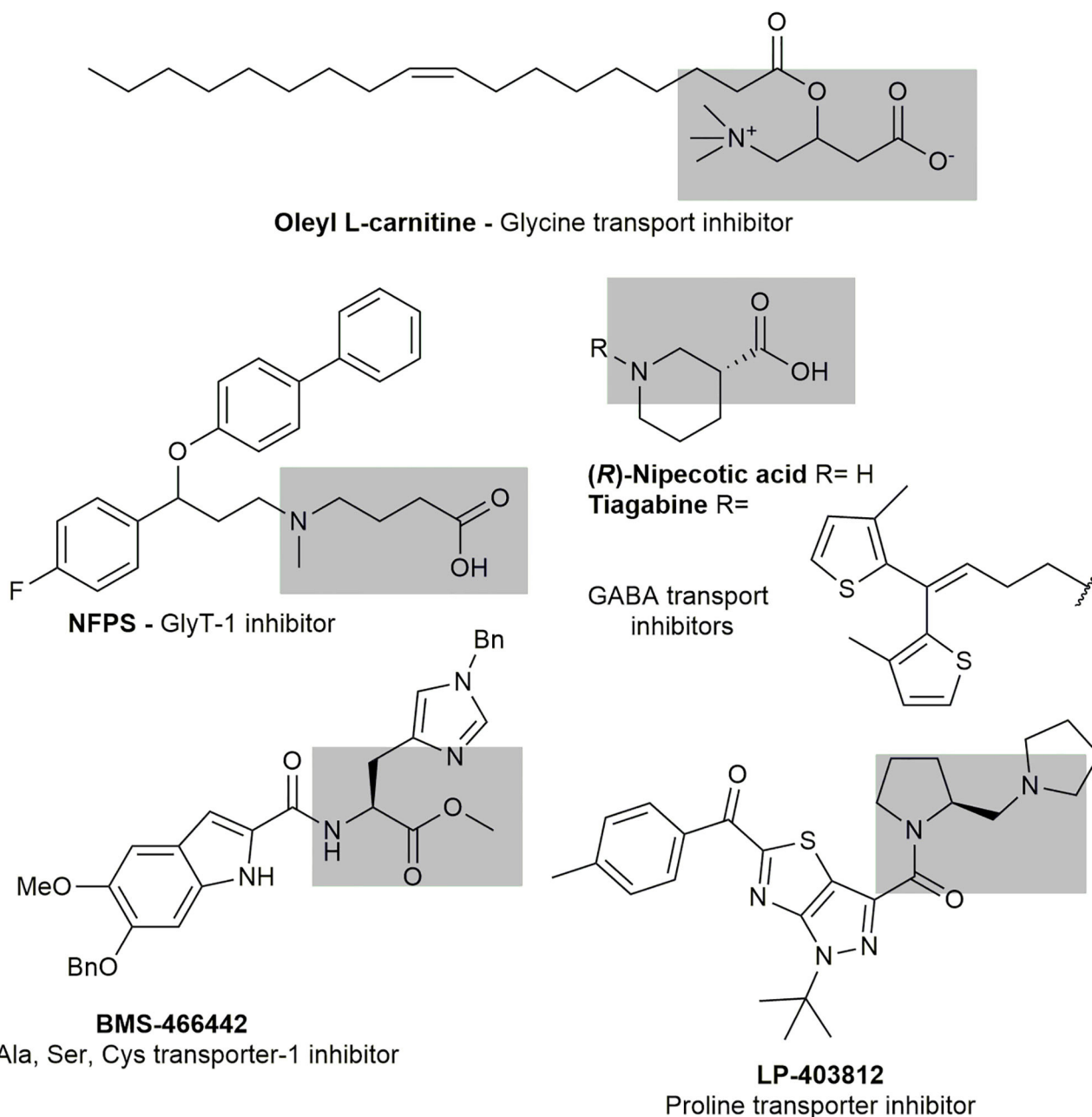
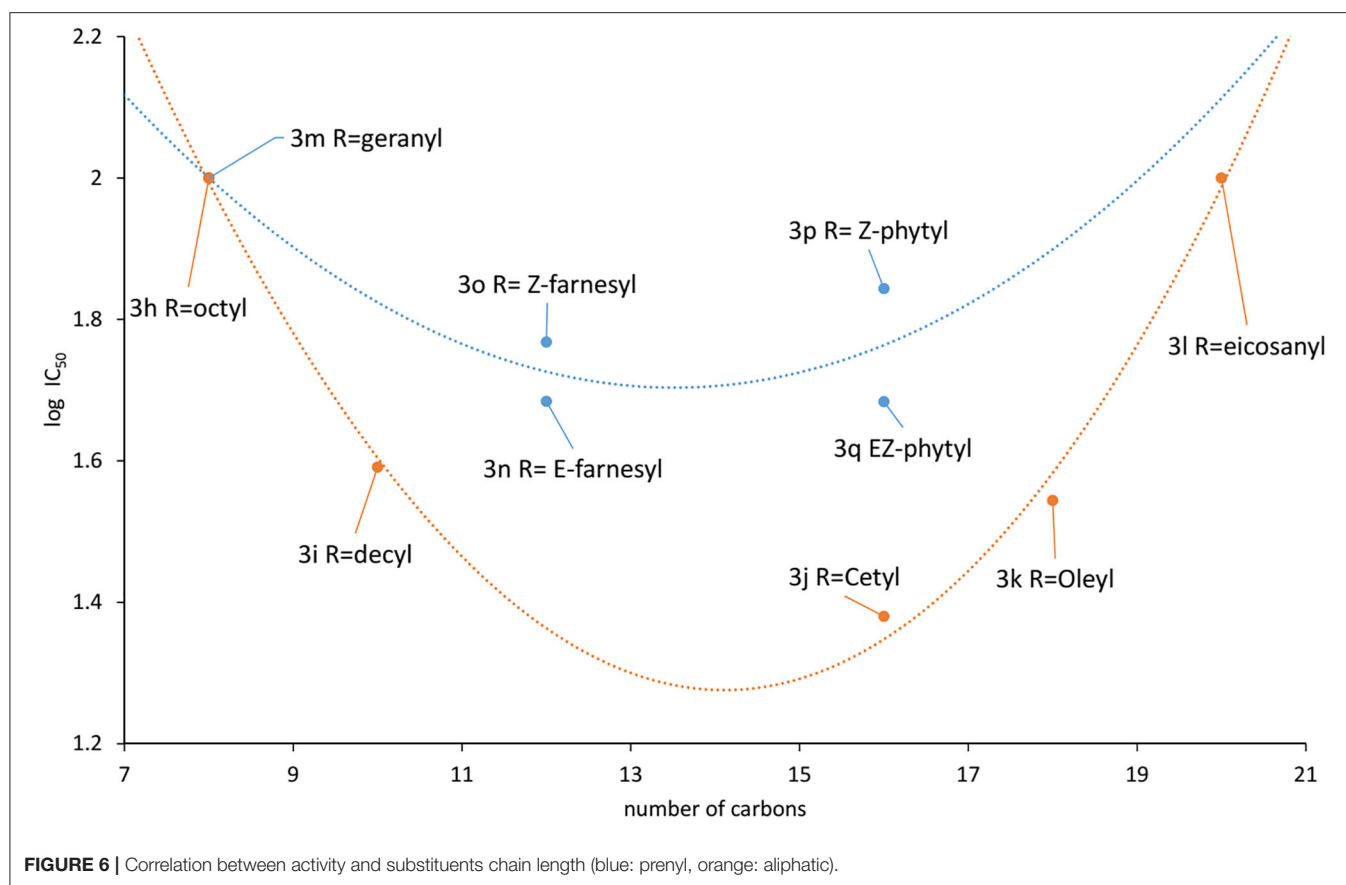


FIGURE 5 | Known amino acid transport inhibitors.

their molecular hydrophobicity (Hannoush and Sun, 2010). Looking to produce similar anchoring properties, isoprenyl and linear long alkyl chain were selected as some of the 1,2,3-triazole substituents, introduced as azide on the heterocycle. Additionally, azides with bulky substituent were also used looking to obstruct the transporter. A library of 17 compounds was finally prepared including two alkyl ester, five alicyclic and aryl, five alkyl and five prenyl derivatives.

The proline uptake systems have similar biochemical characteristics in epimastigotes and the mammalian *T. cruzi*

stages (Silber et al., 2002; Tonelli et al., 2004). It has been demonstrated that these stages are sensitive to proline availability (Tonelli et al., 2004) and uptake (Magdaleno et al., 2009). With those precedents in mind, we decided to evaluate the activity on epimastigotes. The results of the inhibition on *T. cruzi* epimastigotes shown that half of the compounds prepared did not show activity at the maximum concentration tested of 100 μ M. Between the inactive analogs, **3a** and **3b** holds the shortest substituents of the library and have esters on the side-chain. Being the most polar substituent of the series and



susceptible to hydrolysis, seems to be a possible explanation for the lack of activity. Analogs **3c**, **3d**, **3e**, and **3f**, contain non-polar cyclic substituents either aryl or alicyclic, were also inactive. Interestingly, the naphthyl derivative **3g**, the bulkier member of the collection, has an IC_{50} of $100 \mu M$. Together those results shown that polycyclic bulky substituents could be required to improve the activity. Nevertheless, the fact that the aromatic analogs were inactive discouraged the idea that π -stacking interactions are involved on the binding to the molecular target.

As was mentioned before, fatty acids and isoprenyl chains contribute as mediators for protein membrane anchoring, therefore, ten analogs were included with those substituents. The hypothesis that this kind of substituents contribute to improve the activity, seems to be validated because only the analogs holding the shorter substituents, **3h** (R=octyl) and **3m** (R=geranyl) were inactive. A detailed look at the aliphatic derivatives' activities did not show a direct correlation between the IC_{50} and the chain length. The activity increases from octyl **3i** to decyl **3h** derivative ($IC_{50} > 100$ and 38.27 mM, respectively), being the cetyl analog **3j**, the most active (IC_{50} 24.54 mM). Then, the activity decreases to 35.06 mM for the oleyl derivative **3k** and 100 mM for the eicosanyl analog **3l**. A similar behavior is observed for the prenyl derivatives, but in this case the difference is less pronounced. Moving from the geranyl derivative **3h** to the farnesyl analogs the activity increase to 48.32 mM for the *E*-isomer **3n** that is slightly more active than the *Z*-isomer **3o** (59.60 mM). Then, as happened with the alkylated analogs, the

activity decreases for the longer member of the family, the phytyl derivatives **3p** (*E*-isomer) and **3q** (*E/Z* mixture), with IC_{50} s 69.75 and 48.27 mM, respectively.

A tendency can be visualized when the $\log IC_{50}$ was plotted against the carbon chain length and the aliphatic and the prenylated are separately correlated (**Figure 6**). One interesting outcome of this chart is that both curves have their minimum around 14 carbon atoms, that appears to be the optimal chain length for the activity.

These comparisons of the compounds have shown that most of them are considerable more active than L-thiazolidine-4-carboxylic acid (T4C), the only reported antichagasic proline derivative, with an IC_{50} of $890 \mu M$ on *T. cruzi* epimastigotes (Magdaleno et al., 2009). Analogs **3j**, **3i**, **3k**, **3n** were 36, 23, 22, and 18 times more active than T4C. That marked difference on the activity highlight the importance of the proline ring decoration on the antiparasitic activity.

The cytotoxicity of most active compounds (analogs **3i**, **3k**, and **3n**) were tested in cultured monkey kidney Vero cells to estimate the selectivity toward the parasite. The IC_{50} were $43 \mu M$, $17 \mu M$ and $14 \mu M$, respectively, being an adequate concentration window for future studies in intracellular stages. The selectivity index, (calculated as IC_{50} Vero cells / IC_{50} *T. cruzi* epimastigotes) were 1.13, 0.43 and 0.25 for compounds **3i**, **3k**, and **3n**, respectively. This numbers shown a similar susceptibility to the mentioned compounds. The toxicity displayed may be linked to the proline transport inhibition, but that hypothesis must be

validated. These results are not promising at this point to propose that compounds of our collection could be good candidates for anti-chagasic drug development. Nevertheless, the applied strategy settles the basis to design inhibitors against *T. cruzi* biological targets in both, the insect, and the mammalian stages.

Finally, to validate the L-proline transporter as the molecular target, the intracellular concentration of the amino acid was measured in competition assays with compounds that shown the best antiparasitic activity. Analogs **3i**, **3k**, and **3n** were assayed. Interestingly, the proline uptake inhibition of those compounds did not follow the antiparasitic activity. The first hypothesis to explain that behavior was based on the presence of unsaturations on fatty tail. The difference between **3i** and **3k** relay on the unsaturation on the oleyl chain of the last. The structure of **3k** shows a twisted conformation produced by the C9–double bond that also restricts the rotation around the neighbor bonds. Furthermore, the tail length of **3i** and **3k** differ in 6 carbon and the most active is the decyl analog (**3i**) in terms of transport inhibition, matching the behavior displayed in **Figure 6**. The *E*-farnesyl derivative **3n** has a trimethyl substituted side-chain that is twelve carbon long, with three double bonds. Interestingly, this analog produced a complete inhibition of the proline uptake but is the less active of this series against *T. cruzi*. (**Table 2**) The fact that this analog was a superior inhibitor of the transporter could be the result of a better binding. Also, it could be attributed to the markedly different conformation of the analog due to the restricted rotation of the isoprenyl chain. Those restrictions should contribute to block the transporter once the proline region is recognized (Sayé et al., 2017). The inhibition of proline uptake by analogs **3i** and **3n**, resulted considerably more active than that inhibition by T4C (Magdaleno et al., 2009). Those differences were clearly related with the N1-allylated-1,2,3-triazolyl chain introduced on the proline.

CONCLUSIONS

In the present study, a strategy to design amino acids transport inhibitors was proposed. The uptake blocker is composed by a recognition motif, a linker and a bulky substituent or a membrane interacting portion. A set of seventeen 1,5-substituted-1,2,3-triazole derivatives of methyl proline were prepared to validate the design. They were initially assayed against *T. cruzi* epimastigotes showing comparable potency than the control drug benznidazole. The antiparasitic activity profile of the series allowed us to establish a well-defined structural-activity relationship were the nature of the side-chain play a critical role. In order to validate the design, the inhibition of the proline uptake was studied with the analogs **3i**, **3j**, **3k**, and **3n** that displayed the best antiparasitic activity. The analogs with **3i** (R=decyl) and **3n** (R=*E*-farnesyl) produced a markedly reduction of the internalized proline. Those studies are strong evidence to validate our design of the transporter inhibitor that also linked the antiparasitic activity with the proline uptake.

The proline uptake has been explored as target for Chagas disease by drug repurposing. Using that approach, crystal violet has been identified as an interesting candidate (Sayé et al., 2020).

Our approach is the first report of new compounds that have been design, prepared and validated as proline uptake blockers with antiparasitic activity. Unfortunately, the most active products displayed low selectivity toward the parasite, not being good candidates for future development as antichagasic drugs. Nevertheless, a complete study on the other *T. cruzi* life cycle stages could confirm or discard that hypothesis. The validated design of aminoacid transport inhibitor should open new applications on the study of physiological role of amino acid transporters in the central nervous system.

DATA AVAILABILITY STATEMENT

The raw data supporting the conclusions of this article will be made available by the authors, without undue reservation.

AUTHOR CONTRIBUTIONS

LF and EP-Z were responsible for the synthesis, purification and structural characterization of all the products. LF and MB performed the antiproliferative assays against *Trypanosoma cruzi*, carried out the proline transport inhibition assays, and interpreted the results. LF and LP performed the cytotoxicity assays on Vero cells. GL wrote most of the manuscript and supervised the study. GL, AS, and JC were the project leaders organizing and guiding experiments. All authors contributed to refining the manuscript and approved the final manuscript.

FUNDING

The authors wish to express their gratitude to UNR (Universidad Nacional de Rosario, Bio503), Agencia Nacional de Promoción Científica y Tecnológica (ANPCyT PICT- 2017-2096 awarded to GL) and Fundação de Amparo à Pesquisa do Estado de São Paulo grants 2016/06034-2 (awarded to AS) and Conselho Nacional de Pesquisas Científicas e Tecnológicas (CNPq) grants 404769/2018-7 and 308351/2013-4 (awarded to AS). The research leading to these results has, in part, received funding from the UK Research and Innovation via the Global Challenges Research Fund under grant agreement A Global Network for Neglected Tropical Diseases grant number MR/P027989/1. GL and JC are members of the Research Career of the Consejo Nacional de Investigaciones Científicas y Técnicas de Argentina (CONICET). LF, EP-Z, and LP thanks CONICET for the award of a Fellowship.

ACKNOWLEDGMENTS

This manuscript has been released as a pre-print at ChemRxiv (Fargnoli et al., 2019).

SUPPLEMENTARY MATERIAL

The Supplementary Material for this article can be found online at: <https://www.frontiersin.org/articles/10.3389/fchem.2020.00696/full#supplementary-material>

REFERENCES

- Agalave, S. G., Maujan, S. R., and Pore, V. S. (2011). Click Chemistry: 1,2,3-Triazoles as Pharmacophores. *Chem. Asian J.* 6, 2696–2718. doi: 10.1002/asia.201100432
- Avila, C. C., Mule, S. N., Rosa-Fernandes, L., Viner, R., Barison, M. J., Costa-Martins, A. G., et al. (2018). Proteome-wide analysis of *Trypanosoma cruzi* exponential and stationary growth phases reveals a subcellular compartment-specific regulation. *Genes* 9:413. doi: 10.3390/genes9080413
- Barison, M. J., Damasceno, F. S., Mantilla, B. S., and Silber, A. M. (2016). The active transport of histidine and its role in ATP production in *Trypanosoma cruzi*. *J. Bioenerg. Biomembr.* 48, 437–449. doi: 10.1007/s10863-016-9665-9
- Barisón, M. J., Rapado, L. N., Merino, E. F., Pral, E. M. F., Mantilla, B. S., Marchese, L., et al. (2017). Metabolomics profiling reveals a finely tuned, starvation-induced metabolic switch in *Trypanosoma cruzi* epimastigotes. *J. Biol. Chem.* 292, 8964–8977. doi: 10.1074/jbc.M117.778522
- Brener, Z., and Chiari, E. (1965). Aspects of early growth of different *Trypanosoma cruzi* strains in culture medium. *J. Parasitol.* 51, 922–926. doi: 10.2307/3275869
- Burns, M. R., Graminski, G. F., Weeks, R. S., Chen, Y., and O'Brien, T. G. (2009). Lipophilic lysine–spermine conjugates are potent polyamine transport inhibitors for use in combination with a polyamine biosynthesis inhibitor. *J. Med. Chem.* 52, 1983–1993. doi: 10.1021/jm801580w
- Carland, J. E., Handford, C. A., Ryan, R. M., and Vandenberg, R. J. (2014). Lipid inhibitors of high affinity glycine transporters: Identification of a novel class of analgesics. *Neurochem. Int.* 73, 211–216. doi: 10.1016/j.neuint.2013.08.012
- Carvalho, I., Andrade, P., Campo, V. L., Guedes, P. M., Sesti-Costa, R., Silva, J. S., et al. (2010). 'Click chemistry' synthesis of a library of 1,2,3-triazole-substituted galactose derivatives and their evaluation against *Trypanosoma cruzi* and its cell surface trans-sialidase. *Bioorg. Med. Chem.* 18, 2412–2427. doi: 10.1016/j.bmc.2010.02.053
- Contreras Vt, A.-J. T., Bonaldo, M. C., Thomaz, N., Barbosa, H. S., Meirelles Mde, N., and Goldenberg, S. (1988). Biological aspects of the Dm 28c clone of *Trypanosoma cruzi* after metacyclogenesis in chemically defined media. *Mem. Inst. Oswaldo Cruz.* 83, 123–133. doi: 10.1590/S0074-02761988000100016
- Crispim, M., Damasceno, F. S., Hernández, A., Barisón, M. J., Pretto Sauter, I., Souza Pavani, R., et al. (2018). The glutamine synthetase of *Trypanosoma cruzi* is required for its resistance to ammonium accumulation and evasion of the parasitophorous vacuole during host-cell infection. *PLoS Negl. Trop. Dis.* 12:e0006170. doi: 10.1371/journal.pntd.0006170
- Fargnoli, L., Panozzo-Zénere, E. A., Pagura, L., Barisón, M. J., Cricco, J. A., Silber, A. M., et al. (2019). New L-proline uptake inhibitors with anti-*Trypanosoma cruzi* activity. *ChemRxiv*. doi: 10.26434/chemrxiv.7564991. [Epub ahead of print].
- Gagneuz, A., Winstein, S., and Young, W. G. (1969). Rearrangement of allyl azides. *J. Org. Chem.* 1, 5956–5957. doi: 10.1021/ja01507a045
- Gauchet, C., Labadie, G. R., and Poulter, C. D. (2006). Regio- and chemoselective covalent immobilization of proteins through unnatural amino acids. *J. Am. Chem. Soc.* 128, 9274–9275. doi: 10.1021/ja061131o
- Girard, R. M. B. M., Crispim, M., Alencar, M. B., and Silber, A. M. (2018). Uptake of L-Alanine and Its Distinct Roles in the Bioenergetics of *Trypanosoma cruzi*. *mSphere* 3, e00338–e00318. doi: 10.1128/mSphereDirect.00338-18
- Guedes, P. M. M., Silva, G. K., Gutierrez, F. R. S., and Silva, J. S. (2011). Current status of Chagas disease chemotherapy. *Expert Rev. Anti Infect. Ther.* 9, 609–620. doi: 10.1586/eri.11.31
- Hamann, A. R., De Kock, C., Smith, P. J., Van Otterlo, W. A., and Blackie, M. A. (2014). Synthesis of novel triazole-linked mefloquine derivatives: biological evaluation against *Plasmodium falciparum*. *Bioorg. Med. Chem. Lett.* 24, 5466–5469. doi: 10.1016/j.bmcl.2014.10.015
- Hannoush, R. N., and Sun, J. (2010). The chemical toolbox for monitoring protein fatty acylation and prenylation. *Nat. Chem. Biol.* 6, 498–506. doi: 10.1038/nchembio.388
- Hauptmann, M., Wilson, D. F., and Erecinska, M. (1983). High affinity proline uptake in rat brain synaptosomes. *FEBS Lett.* 161, 301–305. doi: 10.1016/0014-5793(83)81029-1
- Labadie, G. R., De La Iglesia, A., and Morbidoni, H. R. (2011). Targeting tuberculosis through a small focused library of 1,2,3-triazoles. *Mol. Divers.* 15, 1017–1024. doi: 10.1007/s11030-011-9319-0
- Magdaleno, A., Ahn, I. Y., Paes, L. S., and Silber, A. M. (2009). Actions of a proline analogue, L-thiazolidine-4-carboxylic acid (T4C), on *Trypanosoma cruzi*. *PLoS ONE* 4:e4534. doi: 10.1371/journal.pone.0004534
- Mantilla, B. S., Marchese, L., Casas-Sánchez, A., Dyer, N. A., Ejeh, N., Biran, M., et al. (2017). Proline metabolism is essential for *trypanosoma brucei* survival in the tsetse vector. *PLoS Path.* 13:e1006158. doi: 10.1371/journal.ppat.1006158
- Mantilla, B. S., Paes, L. S., Pral, E. M. F., Martil, D. E., Thiemann, O. H., Fernández-Silva, P., et al. (2015). Role of Δ 1-Pyrroline-5-carboxylate dehydrogenase supports mitochondrial metabolism and host-cell invasion of *Trypanosoma cruzi*. *J. Biol. Chem.* 290, 7767–7790. doi: 10.1074/jbc.M114.574525
- Marchese, L., Nascimento, J., Damasceno, F., Bringaud, F., Michels, P., and Silber, A. (2018). The uptake and metabolism of amino acids, and their unique role in the biology of pathogenic trypanosomatids. *Pathogens* 7:36. doi: 10.3390/pathogens7020036
- Martins, R. M., Covarrubias, C., Rojas, R. G., Silber, A. M., and Yoshida, N. (2009). Use of L-proline and ATP production by *Trypanosoma cruzi* metacyclic forms as requirements for host cell invasion. *Infect. Immun.* 77, 3023–3032. doi: 10.1128/IAI.00138-09
- Mckay, C. S., and Finn, M. G. (2014). Click chemistry in complex mixtures: bioorthogonal bioconjugation. *Chem. Biol.* 21, 1075–1101. doi: 10.1016/j.chembiol.2014.09.002
- Morillo, C. A., Marin-Neto, J. A., Avezum, A., Sosa-Estani, S., Rassi, A. Jr., Rosas, F., et al. (2015). Randomized trial of benznidazole for chronic chagas' cardiomyopathy. *New Engl. J. Med.* 373, 1295–1306. doi: 10.1056/NEJMoa1507574
- Nunes, M. C. P., Dones, W., Morillo, C. A., Encina, J. J., and Ribeiro, A. L. (2013). Chagas disease: an overview of clinical and epidemiological aspects. *J. Am. Coll. Cardiol.* 62, 767–776. doi: 10.1016/j.jacc.2013.05.046
- Paes, L. S., Suárez Mantilla, B., Zimbres, F. M., Pral, E. M. F., Diogo De Melo, P., Tahara, E. B., et al. (2013). Proline dehydrogenase regulates redox state and respiratory metabolism in *Trypanosoma cruzi*. *PLoS ONE* 8:e69419. doi: 10.1371/journal.pone.0069419
- Pereira, C. A., Alonso, G. D., Paveto, M. C., Iribarren, A., Cabanas, M. L., Torres, H. N., et al. (2000). *Trypanosoma cruzi* arginine kinase characterization and cloning: a novel energetic pathway in protozoan parasites. *J. Biol. Chem.* 275, 1495–1501. doi: 10.1074/jbc.275.2.1495
- Pérez-Molina, J. A., and Molina, I. (2018). Chagas disease. *Lancet* 391, 82–94. doi: 10.1016/S0140-6736(17)31612-4
- Pinard, E., Alanine, A., Alberati, D., Bender, M., Borroni, E., Bourdeaux, P., et al. (2010). Selective GlyT1 inhibitors: discovery of [4-(3-Fluoro-2-trifluoromethylpyridin-2-yl)piperazin-1-yl][5-methanesulfonyl-2-((S)-2,2,2-trifluoro-1-methylethoxy)phenyl]methanone (RG1678), a promising novel medicine to treat schizophrenia. *J. Med. Chem.* 53, 4603–4614. doi: 10.1021/jm100210p
- Porta, E. O., Carvalho, P. B., Avery, M. A., Tekwani, B. L., and Labadie, G. R. (2014). Click chemistry decoration of amino sterols as promising strategy to developed new leishmanicidal drugs. *Steroids* 79, 28–36. doi: 10.1016/j.steroids.2013.10.010
- Porta, E. O. J., Jäger, S. N., Nocito, I., Lepesheva, G. I., Serra, E. C., Tekwani, B. L., et al. (2017a). Antitrypanosomal and antileishmanial activity of prenyl-1,2,3-triazoles. *Med. Chem. Comm.* 8, 1015–1021. doi: 10.1039/C7MD00008A
- Porta, E. O. J., Vallejos, M. M., Bracca, A. B. J., and Labadie, G. R. (2017b). Experimental and theoretical studies of the [3,3]-sigmatropic rearrangement of prenyl azides. *RSC Adv.* 7, 47527–47538. doi: 10.1039/C7RA09759J
- Qosa, H., Mohamed, L. A., Alqahtani, S., Abuasal, B. S., Hill, R. A., and Kaddoumi, A. (2016). Transporters as drug targets in neurological diseases. *Clin. Pharmacol. Ther.* 100, 441–453. doi: 10.1002/cpt.435
- Rohloff, P., Rodrigues, C. O., and Docampo, R. (2003). Regulatory volume decrease in *Trypanosoma cruzi* involves amino acid efflux and changes in intracellular calcium. *Mol. Biochem. Parasitol.* 126, 219–230. doi: 10.1016/S0166-6851(02)00277-3
- Rostovtsev, V. V., Green, L. G., Fokin, V. V., and Sharpless, K. B. (2002). A stepwise huisgen cycloaddition process: copper(I)-catalyzed regioselective "ligation" of azides and terminal alkynes. *Angew. Chem. Int. Ed. Engl.* 41,

- 2596–2599. doi: 10.1002/1521-3773(20020715)41:14<2596::AID-ANIE2596>3.0.CO;2-4
- Sayé, M., Fargnoli, L., Reigada, C., Labadie, G. R., and Pereira, C. A. (2017). Evaluation of proline analogs as trypanocidal agents through the inhibition of a *Trypanosoma cruzi* proline transporter. *Biochim. Biophys. Acta-Gen. Subj.* 1861, 2913–2921. doi: 10.1016/j.bbagen.2017.08.015
- Sayé, M., Gauna, L., Valera-Vera, E., Reigada, C., Miranda, M. R., and Pereira, C. A. (2020). Crystal violet structural analogues identified by in silico drug repositioning present anti-*Trypanosoma cruzi* activity through inhibition of proline transporter TcAAP069. *PLoS Negl. Trop. Dis.* 14:e0007481. doi: 10.1371/journal.pntd.0007481
- Sayé, M., Miranda, M. R., Di Girolamo, F., De Los Milagros Cámara, M., and Pereira, C. A. (2014). Proline modulates the trypanosoma cruzi resistance to reactive oxygen species and drugs through a novel D, L-proline transporter. *PLoS ONE* 9:e92028. doi: 10.1371/journal.pone.0092028
- Sayé, M., Reigada, C., Gauna, L., Valera-Vera, E. A., Pereira, C. A., and Miranda, M. R. (2019). Amino acid and polyamine membrane transporters in *Trypanosoma cruzi*: biological function and evaluation as drug targets. *Curr. Med. Chem.* 26, 6636–6651. doi: 10.2174/0929867326666190620094710
- Schneider, C. A., Rasband, W. S., and Eliceiri, K. W. (2012). NIH image to imageJ: 25 years of image analysis. *Nat. Methods* 9, 671–675. doi: 10.1038/nmeth.2089
- Silber, A. M., Colli, W., Ulrich, H., Alves, M. J., and Pereira, C. A. (2005). Amino acid metabolic routes in *Trypanosoma cruzi*: possible therapeutic targets against Chagas' disease. *Curr. Drug Targets Infect. Disord.* 5, 53–64. doi: 10.2174/1568005053174636
- Silber, A. M., Tonelli, R. R., Lopes, C. G., Cunha-E-Silva, N., Torrecilhas, A. C. T., Schumacher, R. I., et al. (2009). Glucose uptake in the mammalian stages of *Trypanosoma cruzi*. *Mol. Biochem. Parasitol.* 168, 102–108. doi: 10.1016/j.molbiopara.2009.07.006
- Silber, A. M., Tonelli, R. R., Martinelli, M., Colli, W., and Alves, M. J. M. (2002). Active transport of L-proline in trypanosoma cruzi. *J. Eukaryot. Microbiol.* 49, 441–446. doi: 10.1111/j.1550-7408.2002.tb00225.x
- Sylvester, D., and Krassner, S. M. (1976). Proline metabolism in *Trypanosoma cruzi* epimastigotes. *Comp. Biochem. Physiol. B: Biochem. Mol. Biol.* 55, 443–447. doi: 10.1016/0305-0491(76)90318-7
- Thompson, A. S., Humphrey, G. R., Demarco, A. M., Mathre, D. J., and Grabowski, E. J. J. (1993). Direct conversion of activated alcohols to azides using diphenyl phosphorazidate. A practical alternative to Mitsunobu conditions. *J. Org. Chem.* 58, 5886–5888. doi: 10.1021/jo00074a008
- Tonelli, R. R., Silber, A. M., Almeida-De-Faria, M., Hirata, I. Y., Colli, W., and Alves, M. J. M. (2004). L-Proline is essential for the intracellular differentiation of *Trypanosoma cruzi*. *Cell. Microbiol.* 6, 733–741. doi: 10.1111/j.1462-5822.2004.00397.x
- Tron, G. C., Pirali, T., Billington, R. A., Canonico, P. L., Sorba, G., and Genazzani, A. A. (2008). Click chemistry reactions in medicinal chemistry: applications of the 1,3-dipolar cycloaddition between azides and alkynes. *Med. Res. Rev.* 28, 278–308. doi: 10.1002/med.20107
- Urbina, J. A. (2010). Specific chemotherapy of Chagas disease: Relevance, current limitations and new approaches. *Acta Trop.* 115, 55–68. doi: 10.1016/j.actatropica.2009.10.023
- Yu, X.-C., Zhang, W., Oldham, A., Buxton, E., Patel, S., Nghi, N., et al. (2009). Discovery and characterization of potent small molecule inhibitors of the high affinity proline transporter. *Neurosci. Lett.* 451, 212–216. doi: 10.1016/j.neulet.2009.01.018

Conflict of Interest: The authors declare that the research was conducted in the absence of any commercial or financial relationships that could be construed as a potential conflict of interest.

Copyright © 2020 Fargnoli, Panozzo-Zénere, Pagura, Barisón, Cricco, Silber and Labadie. This is an open-access article distributed under the terms of the Creative Commons Attribution License (CC BY). The use, distribution or reproduction in other forums is permitted, provided the original author(s) and the copyright owner(s) are credited and that the original publication in this journal is cited, in accordance with accepted academic practice. No use, distribution or reproduction is permitted which does not comply with these terms.



Use of Natural Products in Leishmaniasis Chemotherapy: An Overview

Luiza F. O. Gervazoni[†], Gabrielle B. Barcellos[†], Taiana Ferreira-Paes and Elmo E. Almeida-Amaral^{*}

Laboratório de Bioquímica de Tripanosomatídeos, Instituto Oswaldo Cruz, Fundação Oswaldo Cruz, Rio de Janeiro, Brazil

OPEN ACCESS

Edited by:

Gildardo Rivera,
National Polytechnic Institute of
Mexico (IPN), Mexico

Reviewed by:

Marcus Scotti,
Federal University of Paraíba, Brazil
Edson Roberto Silva,
University of São Paulo, Brazil

*Correspondence:

Elmo E. Almeida-Amaral
elmo@ioc.fiocruz.br

[†]These authors have contributed
equally to this work

Specialty section:

This article was submitted to
Medicinal and Pharmaceutical
Chemistry,
a section of the journal
Frontiers in Chemistry

Received: 03 July 2020

Accepted: 07 October 2020

Published: 23 November 2020

Citation:

Gervazoni LFO, Barcellos GB,
Ferreira-Paes T and
Almeida-Amaral EE (2020) Use of
Natural Products in Leishmaniasis
Chemotherapy: An Overview.
Front. Chem. 8:579891.
doi: 10.3389/fchem.2020.579891

Leishmaniasis is an infectious parasitic disease that is caused by protozoa of the genus *Leishmania*, a member of the Trypanosomatidae family. Leishmaniasis is classified by the World Health Organization as a neglected tropical disease that is responsible for millions of deaths worldwide. Although there are many possible treatments for leishmaniasis, these treatments remain mostly ineffective, expensive, and long treatment, as well as causing side effects and leading to the development of resistance. For novel and effective treatments to combat leishmaniasis, many research groups have sought to utilize natural products. In addition to exhibiting potential as therapeutic compounds, natural products may also contribute to the development of new drugs based on their chemical structures. This review presents the most promising natural products, including crude extracts and isolated compounds, employed against *Leishmania* spp.

Keywords: natural product, Leishmaniasis, chemotherapy, *in vivo*, *in vitro*, intracellular amastigotes

INTRODUCTION

Caused by protozoa of the genus *Leishmania*, which is a member of the Trypanosomatidae family, leishmaniasis is an infectious parasitic disease. This disease has a wide variety of clinical manifestations, ranging from the cutaneous form to the visceral form. Visceral leishmaniasis, the form that can cause death, affects the organs and viscera of mammalian hosts; conversely, cutaneous leishmaniasis, which can be divided into different manifestations, affects the skin and mucous membranes of mammalian hosts. Classified as a neglected disease by the World Health Organization (WHO, 2016), leishmaniasis affects over 300 million people across all continents.

The current treatment for leishmaniasis is based on pentavalent antimonials, which are drugs that were developed over decades (Vianna, 1912; Burza et al., 2018) with a long-established administration profile in the hospital environment. These drugs are becoming increasingly ineffective due to resistance. Amphotericin B emerged as an alternative treatment; however, its long-standing treatment and dose-dependent side effects led to the development of a liposomal formulation to significantly reduce the side effects and duration of treatment; nevertheless, this formulation is expensive. Paromomycin is already registered in India, but the effectiveness of this treatment has not been determined to date in Africa. As the most promising treatment discovered in recent decades and the first oral drug for leishmaniasis, miltefosine is registered in India and a small number of other countries and has recently been registered by the FDA (IMPAVIDO) for the treatment of visceral and cutaneous leishmaniasis. Miltefosine is effective but expensive and teratogenic (DNDi, 2016).

Although there are many possibilities for leishmaniasis treatment, these treatments remain mostly ineffective, expensive and old, as well as causing side effects and leading to the development of resistance. For novel and effective treatments to combat leishmaniasis, many research groups have investigated natural products.

Natural products are secondary metabolites present in the roots, stalks, leaves, fruits, seeds, vegetables, and other parts of plants with a wide structural variety that mediates interactions between plants and their environment. These metabolites are usually observed around the world in diets as main foods or teas, spices, and sauces. A considerable number of metabolites have anti-protozoal activity (Winkel, 2006; Schmidt et al., 2012a).

Natural products are known in pharmacology for having potential applications as therapeutic drugs, which have been described since ancient times, in addition to contributing to the discovery and development of new drugs based on the chemical structures of these products with specific modifications (Viegas et al., 2006; Ioset, 2008).

In this review, we present the most promising crude extracts and isolated compounds derived from the four major plant metabolic pathways; these products were recently studied to determine their effectiveness as chemotherapy agents for treating leishmaniasis.

All crude extracts and compounds that have defined IC₅₀ values are represented in tables at the end of each section.

MATERIALS AND METHODS

This review aims to update and summarize information concerning the early drug discovery process based on crude extracts, fractions, and isolated compounds obtained from natural products, specifically herbal-derived compounds, to treat leishmaniasis. The keywords employed in this study included leishmaniasis, natural products, chemotherapy, *in vivo*, *in vitro*, and intracellular amastigote using the current databases: PubMed, Web of Science, Science Direct, and Google Scholar. Our search covered English-language articles published in international scientific journals, indexed over the period 2000–2020. The choice criteria were articles that investigated the leishmanicidal activity of natural products against promastigote,

axenic amastigote, and intracellular amastigote forms, the mechanism of action and/or the use of advanced techniques to search for alternative treatments for leishmaniasis. Selected articles describing the use of novel natural products with leishmanicidal activity against promastigotes of *Leishmania* spp. were considered. All crude extracts and compounds that have defined IC₅₀ values are represented in Tables 1–7.

CRUDE EXTRACTS AND FRACTIONS (LEAVES, ROOTS, SEEDS, FRUITS, AND STALKS)

It is well-known that crude extracts have been employed as medicinal drugs since the times of ancient civilizations. In those eras, the simple action of grinding the leaves of certain plants was considered to be medicine. With the growth of technology and knowledge, extracts from leaves, seeds, and other parts of the plant have been tested against several diseases, and some of these extracts have been highly successful (Viegas et al., 2006).

Four plants from different families, namely, *Asparagus gracilis* from the *Asparagaceae* family, *Stellaria media* from the *Caryophyllaceae* family, *Sida cordata* from the *Malvaceae* family and *Jurinea dolomiaea* (*J. dolomiaea*) from the *Asteraceae* family, were tested against a strain of *Leishmania tropica* isolated from a patient from Pakistan. All four plants were prepared as methanol extracts or n-hexane, chloroform, ethyl acetate, n-butanol and water fractions. The most potent methanol extract was from *J. dolomiaea*, which exhibited an IC₅₀ value of 10.9 µg/mL, but the highest antileishmanial activity was obtained from the ethyl acetate fraction from *J. dolomiaea* with an IC₅₀ value of 5.3 µg/mL. All of the extracts and fractions were not toxic, exhibiting IC₅₀ values greater than 100 µg/mL and potent extracts with selectivity indices greater than 10 (Shah et al., 2014).

A series of 16 Brazilian medicinal plants were investigated *in vitro* to determine their efficacy against *L. amazonensis*. Among the 44 extracts and fractions, the most potent were the hexanic fraction of *Dipteryx alata* (*D. alata*) with an IC₅₀ value of 0.08 µg/mL, the ethanolic fraction of *Hymenaea stignocarpa* with an IC₅₀ value of 4.70 µg/mL, and both the chloroformic and ethanolic fractions of *Jacaranda cuspidifolia* (*J. cuspidifolia*), which exhibited IC₅₀ values of 7.4 and 10.96 µg/mL, respectively (Ribeiro et al., 2014).

Physalis angulata, which is from the *Solanaceae* family, is a well-known medicinal plant (Mahalakshmi and Nidavani, 2014). For leishmaniasis, Nogueira et al. (2013) tested the ethanolic extract of this plant against two species of *Leishmania*. In an antipromastigote assay, EEPa (ethanolic extract of *Physalis angulata*) exhibited IC₅₀ values of 5.35 and 4.50 g/mL for *Leishmania amazonensis* and *Leishmania braziliensis*, respectively. The antiamastigote assay using *L. amazonensis* demonstrated an IC₅₀ value of 1.23 g/mL with a selectivity index of 5.

Tetradenia riparia, a plant from the *Lamiaceae* family, is commonly employed as a traditional medicine in Africa for infectious parasitic diseases, such as malaria, cryptococcosis, and candidiasis. Against an *L. amazonensis* promastigote, the

Abbreviations: 2HF, 2'-Hydroxyflavanone; ABC, ATP-binding cassette; AEPA, Aqueous extract of *Physalis angulata* root; AP-1, Activator protein 1; ATP, Adenosine triphosphate; BPQ, Buparvaquone; C, Carbon; CC₅₀, Concentration that promotes 50% cytotoxicity; DHDE, Dehydrodieugiol; DNA, Deoxyribonucleic acid; DNDi, Drugs for Neglected Diseases Initiative; ED₅₀, Median effective dose; EEPa, Ethanolic extract of *Physalis angulata*; EGCG, (–)-Epigallocatechin 3-O-gallate; FDA, Food and Drug Administration; GFP, Green fluorescent protein; HPLC, High-performance liquid chromatography; IC₅₀, Half maximal inhibitory concentration; iNOS, Nitric oxide synthase inducible; LD₅₀, Median lethal dose; MFI, Mean fluorescence intensity; mRNA, Messenger ribonucleic acid; MuEO, *Myracrodruon urundeuva* essential oil; NF-κB, Nuclear factor kappa-light-chain-enhancer of activated B cells; NO, Nitric oxide; PBS, Phosphate saline buffer; ROS, Reactive oxygen species; Sb^v, Pentavalent antimony; SI, Selectivity index; ΣFIC, Fractional inhibitory concentration sum; Th1, Helper T cell 1; Th2, Helper T cell 2; TIC, Total ion chromatogram; TrEO, *Tetradenia riparia* essential oil; TrROY, 6,7-Dehydroroyleanone; WHO, World Health Organization.

TABLE 1 | Leishmanicidal activities of crude extracts and fractions.

Class	Plant	Part	Extract/fraction	<i>Leishmania</i> species	Assay	Values	References
Crude extracts and fractions	<i>Jurinea dolomiæa</i>	Roots	Methanol extract	<i>Leishmania tropica</i>	<i>In vitro</i>	Promastigotes: IC ₅₀ : 10.9 µg/mL	Shah et al., 2014
					<i>In vivo</i> toxicity assay	Brine shrimp test: CC ₅₀ : 733.0 µg/mL	
			n-Hexane fraction		<i>In vitro</i>	Promastigotes: IC ₅₀ : 7.2 µg/mL	
					<i>In vivo</i> toxicity assay	Brine shrimp test: CC ₅₀ : 982.5 µg/mL	
			Chloroform fraction		<i>In vitro</i>	Promastigotes: IC ₅₀ : 47.7 µg/mL	
					<i>In vivo</i> toxicity assay	Brine shrimp test: CC ₅₀ : 834.5 µg/mL	
			Ethyl acetate fraction		<i>In vitro</i>	Promastigotes: IC ₅₀ : 5.3 µg/mL	
					<i>In vivo</i> toxicity assay	Brine shrimp test: CC ₅₀ : 569.5 µg/mL	
			n-Butanol fraction		<i>In vitro</i>	Promastigotes: IC ₅₀ : 21.8 µg/mL	
					<i>In vivo</i> toxicity assay	Brine shrimp test: CC ₅₀ : 958.3 µg/mL	
			Water fraction		<i>In vitro</i>	Promastigotes: IC ₅₀ : 6.0 µg/mL	
					<i>In vivo</i> toxicity assay	Brine shrimp test: CC ₅₀ : 1593.0 µg/mL	
Crude extracts and fractions	<i>Asparagus gracilis</i>	Aerial	Methanol extract	<i>Leishmania tropica</i>	<i>In vitro</i>	Promastigotes: IC ₅₀ : 33.9 µg/mL	Shah et al., 2014
					<i>In vivo</i> toxicity assay	Brine shrimp test: CC ₅₀ : 321.5 µg/mL	
			n-Hexane fraction		<i>In vitro</i>	Promastigotes: IC ₅₀ : 36.6 µg/mL	
					<i>In vivo</i> toxicity assay	Brine shrimp test: CC ₅₀ : 280.6 µg/mL	
			Chloroform fraction		<i>In vitro</i>	Promastigotes: IC ₅₀ : 28.3 µg/mL	
					<i>In vivo</i> toxicity assay	Brine shrimp test: CC ₅₀ : 383.5 µg/mL	
			Ethyl acetate fraction		<i>In vitro</i>	Promastigotes: IC ₅₀ : 13.5 µg/mL	
					<i>In vivo</i> toxicity assay	Brine shrimp test: CC ₅₀ : 211.9 µg/mL	
			n-Butanol fraction		<i>In vitro</i>	Promastigotes: IC ₅₀ : 18.9 µg/mL	
					<i>In vivo</i> toxicity assay	Brine shrimp test: CC ₅₀ : 588.6 µg/mL	
			Water fraction		<i>In vitro</i>	Promastigotes: IC ₅₀ : 12.6 µg/mL	
					<i>In vivo</i> toxicity assay	Brine shrimp test: CC ₅₀ : 460.0 µg/mL	
Crude extracts and fractions	<i>Sida cordata</i>	Whole plant	Methanol extract	<i>Leishmania tropica</i>	<i>In vitro</i>	Promastigotes: IC ₅₀ : 41.8 µg/mL	Shah et al., 2014

(Continued)

TABLE 1 | Continued

Class	Plant	Part	Extract/fraction	Leishmania species	Assay	Values	References
Crude extracts and fractions	Stellaria media	Whole plant	n-Hexane fraction	Leishmania tropica	In vivo toxicity assay	Brine shrimp test: CC ₅₀ : 125.7 μg/mL	Shah et al., 2014
					In vitro	Promastigotes: IC ₅₀ : 9.2 μg/mL	
			Chloroform fraction		In vivo toxicity assay	Brine shrimp test: CC ₅₀ : 879.5 μg/mL	
					In vitro	Promastigotes: IC ₅₀ : 125.5 μg/mL	
			Ethyl acetate fraction		In vivo toxicity assay	Brine shrimp test: CC ₅₀ : 802.8 μg/mL	
					In vitro	Promastigotes: IC ₅₀ : 56.8 μg/mL	
			n-Butanol fraction		In vivo toxicity assay	Brine shrimp test: CC ₅₀ : 309.9 μg/mL	
					In vitro	Promastigotes: IC ₅₀ : 228.5 μg/mL	
			Water fraction		In vivo toxicity assay	Brine shrimp test: CC ₅₀ : 882.4 μg/mL	
					In vitro	Promastigotes: IC ₅₀ : 259.1 μg/mL	
			In vivo toxicity assay		Brine shrimp test: CC ₅₀ : 211.9 μg/mL		
			Crude extracts and fractions		Bowdichia virgiloides Kunth. Campomanesia lineatifolia Ruiz & Pav	Leaves Leaves	
In vivo toxicity assay	Brine shrimp test: CC ₅₀ : 436.7 μg/mL						
n-Hexane fraction	In vitro	Promastigotes: IC ₅₀ : 170.4 μg/mL					
	In vivo toxicity assay	Brine shrimp test: CC ₅₀ : 542.5 μg/mL					
Chloroform fraction	In vitro	Promastigotes: IC ₅₀ : 155.5 μg/mL					
	In vivo toxicity assay	Brine shrimp test: CC ₅₀ : 600.0 μg/mL					
Ethyl acetate fraction	In vitro	Promastigotes: IC ₅₀ : 36.4 μg/mL					
	In vivo toxicity assay	Brine shrimp test: CC ₅₀ : 789.3 μg/mL					
n-Butanol fraction	In vitro	Promastigotes: IC ₅₀ : 49.5 μg/mL					
	In vivo toxicity assay	Brine shrimp test: CC ₅₀ : 760.2 μg/mL					
Water fraction	In vitro	Promastigotes: IC ₅₀ : 184.8 μg/mL					
	In vivo toxicity assay	Brine shrimp test: CC ₅₀ : 660.7 μg/mL					
Crude extracts and fractions	Bowdichia virgiloides Kunth.	Leaves	Ethanollic	In vitro	NA	Ribeiro et al., 2014	
			Hexanic		NA		
Crude extracts and fractions	Campomanesia lineatifolia Ruiz & Pav	Leaves	Ethanollic		Promastigotes: IC ₅₀ : 103.3 μg/mL		

(Continued)

TABLE 1 | Continued

Class	Plant	Part	Extract/fraction	Leishmania species	Assay	Values	References
Crude extracts and fractions	<i>Cecropia pachystachya</i> Trécul	Leaves	Buthanolic fraction	<i>L. amazonensis</i>	<i>In vitro</i>	Promastigotes: IC ₅₀ : 62.3 µg/mL	Ribeiro et al., 2014
			Dichloromethane fraction			NA	
			Ethyl acetate fraction			Promastigotes: IC ₅₀ : 96.1 µg/mL	
			Hexanic fraction			Promastigotes: IC ₅₀ : 147.7 µg/mL	
		Ethanollic	NA				
		Leaves	Hexanic			NA	
			Ethanollic			Promastigotes: IC ₅₀ : 61.5 µg/mL	
			Hexanic			Promastigotes: IC ₅₀ : 62.3 µg/mL	
			Buthanolic fraction			Promastigotes: IC ₅₀ : 61.2 µg/mL	
			Dichloromethane fraction			Promastigotes: IC ₅₀ : 91.6 µg/mL	
	Ethyl acetate fraction		Promastigotes: IC ₅₀ : 77.3 µg/mL				
	<i>Diospyros hispida</i> D.C.	Leaves	Hexanic			NA	
			Ethanollic			Promastigotes: IC ₅₀ : 51.5 µg/mL	
			Hexanic			Promastigotes: IC ₅₀ : 0.08 µg/mL Intracellular amastigotes: 0.08 µg/mL	
		Leaves	Hexanic			Promastigotes: IC ₅₀ : 31.6 µg/mL	
			Hexanic			NA	
			Ethanollic			Promastigotes: IC ₅₀ : 44.1 µg/mL	
		Leaves	Hexanic			Promastigotes: IC ₅₀ : 35.8 µg/mL	
			Ethanollic			Promastigotes: IC ₅₀ : 4.7 µg/mL	
			Hexanic			Promastigotes: IC ₅₀ : 199.4 µg/mL	
			Ethanollic			Promastigotes: IC ₅₀ : 13.2 µg/mL	
Hexanic			NA				
<i>Jacaranda caroba</i> Vell.	Leaves	Ethanollic	NA				
		Ethanollic	NA				
		Ethanollic	NA				
<i>Jacaranda cuspidifolia</i> Mart.	Roots	Ethanollic	NA	Ribeiro et al., 2014			
		Ethanollic	NA				
		Ethanollic	NA				

(Continued)

TABLE 1 | Continued

Class	Plant	Part	Extract/fraction	Leishmania species	Assay	Values	References	
Crude extracts and fractions	<i>Jacaranda ulei</i> Bureau & K. Schum.	Stem bark	Ethanolic	<i>L. amazonensis</i>	<i>In vitro</i>	Promastigotes: IC ₅₀ : 10.96 μg/mL	Nogueira et al., 2013	
			Hexanic			Intracellular amastigotes: 5 μg/mL		
			Chloroformic fraction			NA		
			Leaves			Ethanolic		Promastigotes: IC ₅₀ : 7.4 μg/mL
								Intracellular amastigotes: 5 μg/mL
								NA
		<i>Vernonia phosphorea</i> Vell.	Stem bark			Ethanolic		NA
						Hexanic		NA
						Hexanic		Promastigotes: IC ₅₀ : 160.9 μg/mL
			Roots			Ethanolic		Promastigotes: IC ₅₀ : 92.7 μg/mL
						Hexanic		NA
								NA
	<i>Physalis angulate</i> (EPPa)	Stem	Ethanolic extract	<i>L. amazonensis</i>	Promastigotes: IC ₅₀ : 5.4 μg/mL	Nogueira et al., 2013		
					Intracellular amastigotes: IC ₅₀ : 1.2 μg/mL			
					Promastigotes: IC ₅₀ : 4.5 μg/mL			
<i>Tetradenia riparia</i> (TrEO)	Leaves	Essential oil		<i>L. amazonensis</i>	<i>In vitro</i>	Promastigotes: IC ₅₀ : 0.03 μg/mL	Demarchi et al., 2015	
						Intracellular amastigotes: IC ₅₀ : 0.03 μg/mL		

NA, no activity ($IC_{50} > 200 \mu g/mL$).

essential oil of *Tetradenia riparia* (TrEO), which contains a mixture of terpenoids, exhibited an IC₅₀ value of 0.03 µg/mL after 24 h. Cytotoxicity in human erythrocytes was tested, and at a concentration of 5 µg/mL, TrEO was determined not to be toxic (Demarchi et al., 2015). Alterations in promastigote morphology were observed. TrEO was able to induce cytoplasmic vacuolization, and membranous profiles and lipid vesicles appeared in the organelle along with membrane blebbing, nuclear fragmentation and chromatin condensation, which are events that are associated with autophagy. Against the intracellular amastigote form, TrEO showed an IC₅₀ value of 0.03 µg/mL and a selectivity index of 5.6. TrEO was also capable of increasing the mRNA expression of iNOS in murine peritoneal macrophages; however, alterations in nitrite production were not observed.

Crude extracts and fraction presented in this section are summarized in **Table 1**.

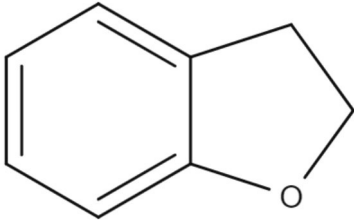
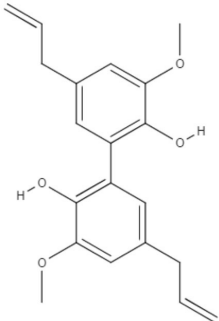
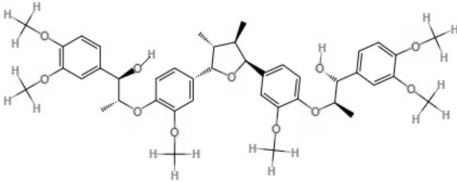
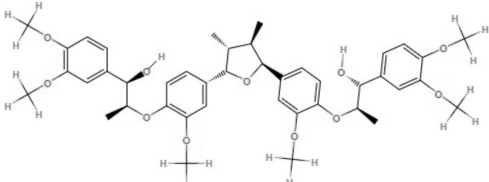
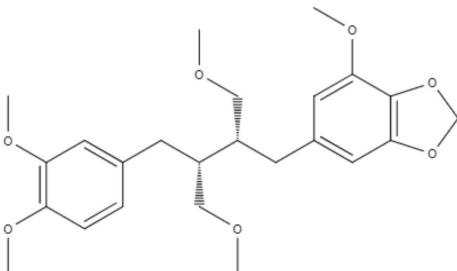
METABOLITES OF THE SHIKIMATE PATHWAY

Lignans and Neolignans

Lignans and neolignans are metabolites that can be found in approximately 60 vascular plant families (Winkel, 2006). Lignans are dimeric phenylpropanoids, and neolignans are small molecules with two phenylpropanoid units. The diversity in this class consists of the distribution of aromatic rings and the nature of the propyl fragments (Rye and Barker, 2013). Several groups have chosen to investigate lignans and neolignans because they have properties favorable to drug development and for their anti-inflammatory and antioxidant activity, which may minimize the effects of the inflammatory response (Maia et al., 2020).

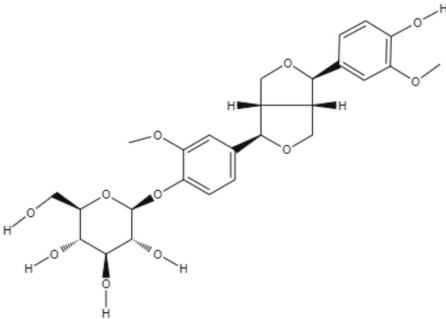
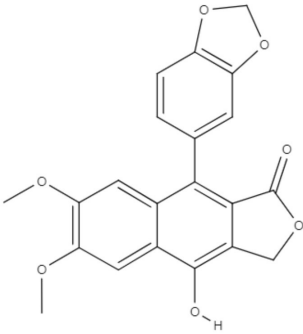
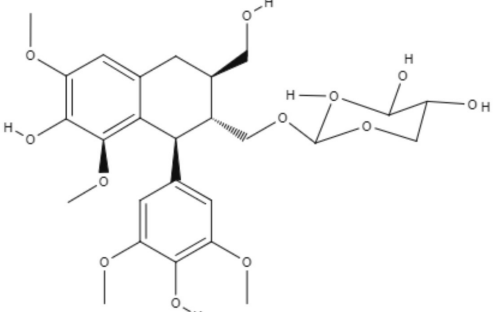
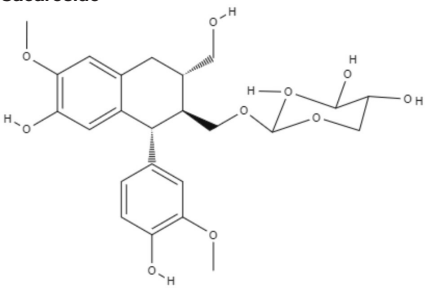
Notably, several studies have focused on the search for natural compounds with potential leishmanicidal activity directly using

TABLE 2 | Chemical structure and leishmanicidal activities of lignans and neolignans.

Class	Subclass	Compound name and chemical structure	<i>Leishmania</i> species	Assay	Values	References
Neolignanes	Benzofuran	2,3-Dihydrobenzofuran 	<i>L. amazonensis</i>	<i>In vitro</i>	Promastigotes: IC ₅₀ : 1.04 μM Intracellular amastigotes: IC ₅₀ : 1.4 μM	De Castro Oliveira et al., 2017
	Ortho-biphenyl	Dehydrodieugiol (DHDE) 	<i>L. amazonensis</i>	<i>In vitro</i>	Promastigotes: IC ₅₀ : 42.4 μg/mL	Rodrigues et al., 2016
Neolignanes	Tetrahydrofuran dineolignans	Threo,threo-manassatin A  Erythro-manassatin A 	<i>L. amazonensis</i>	<i>In vitro</i>	Promastigotes: IC ₅₀ : 35.4 μM Intracellular amastigotes: IC ₅₀ : 20.4 μM Promastigotes: IC ₅₀ : 17.6 μM Intracellular amastigotes: IC ₅₀ : 16.0 μM	Brito et al., 2019
Lignans	Dibenzylbutanes	Niranthin 	<i>L. donovani</i>	<i>In vitro</i>	Intracellular amastigotes: IC ₅₀ : 1.26 μM Antimony-resistant intracellular amastigotes: IC ₅₀ : 1.68 μM	Chowdhury et al., 2012

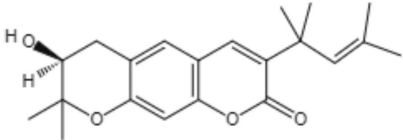
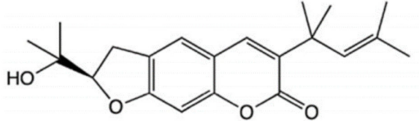
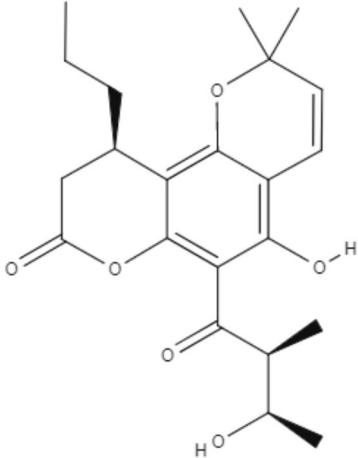
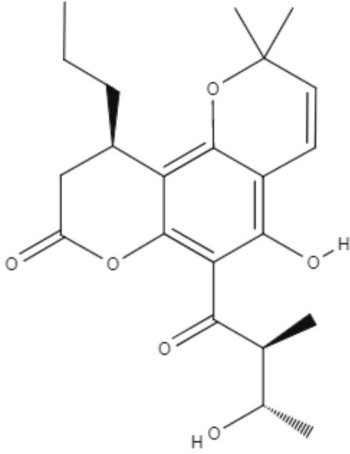
(Continued)

TABLE 2 | Continued

Class	Subclass	Compound name and chemical structure	<i>Leishmania</i> species	Assay	Values	References
				<i>In vivo</i>	ND	
	Furofuran	Epipinoresinol-4-O-β-D-glucopyranoside 	<i>L. major</i>	<i>In vitro</i>	Promastigotes: IC ₅₀ : 36.5 μ M	Maia et al., 2020
			<i>L. braziliensis</i>		Promastigotes: IC ₅₀ : 5.4 μ M	
Lignan	Xanthine	Diphyllin 	<i>L. infantum</i>	<i>In vitro</i>	Promastigotes: IC ₅₀ : 14.4 μ M Intracellular amastigotes: IC ₅₀ : 0.2 μ M	Di Giorgio et al., 2005
	Aryltetralin lignans	Lyoniside 	<i>L. donovani</i>	<i>In vitro</i>	Intracellular amastigotes: IC ₅₀ : 0.79 μ M	Saha et al., 2013
Lignan	Aryltetralin lignans	Sacaroside 	<i>L. donovani</i>	<i>In vivo</i> <i>In vitro</i>	ND Intracellular amastigotes: IC ₅₀ : 0.82 μ M	Saha et al., 2013
				<i>In vivo</i>	ND	

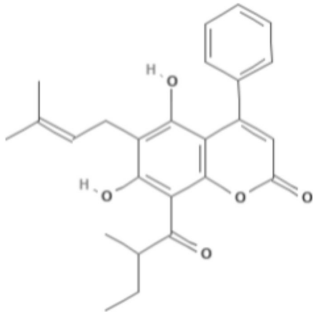
ND, Not determined.

TABLE 3 | Chemical structure and leishmanicidal activities of coumarins.

Class	Subclass	Compound name and chemical structure	Leishmania species	Assay	Values	References
Coumarin	Dihydropyranocoumarins	(+)-3-(1'-dimethylallyl)-decursinol 	<i>L. amazonensis</i>	<i>In vitro</i>	Promastigotes: IC ₅₀ : 35.8 μM	Ferreira et al., 2010
		(-)-heliectin 		<i>In vivo</i>	ND	
				<i>In vitro</i>	Promastigotes: IC ₅₀ : 18.5 μM	
				<i>In vivo</i>	ND	
Coumarin	Tricyclic pyranocoumarins	Calanolide E1 	<i>L. major</i>	<i>In vitro</i>	Promastigotes: IC ₅₀ : 36.5 μM	Silva et al., 2020
		Calanolide E2 			Promastigotes: IC ₅₀ : 29.1 μM	

(Continued)

TABLE 3 | Continued

Class	Subclass	Compound name and chemical structure	Leishmania species	Assay	Values	References
Coumarin	Coumarin-type mammea	Mammae A/BB	<i>L. amazonensis</i>	<i>In vitro</i>	Promastigotes: IC ₅₀ : 3.0 µg/mL IC ₉₀ : 5 µg/mL Axenic amastigotes: IC ₅₀ : 0.88 µg/mL IC ₉₀ : 2.3 µg/mL	Brenzan et al., 2007
					Promastigotes: IC ₅₀ : 7.4 ± 0.3 µM Intracellular amastigotes: IC ₅₀ : 14.3 ± 2.2 µM	Breza et al., 2008
				<i>In vivo</i>	ND	Tiuman et al., 2012

ND, Not determined.

biological screening through phenotypic methods to assess the potential of lignans and neolignans against *Leishmania* species. The efficacy of a lignin found in garlic (*Allium sativum*) against *L. amazonensis* promastigotes was investigated. Dehydrodieuginol (DHDE), an ortho-biphenyl neolignan, showed an IC₅₀ value of 42.2 µg/mL (Rodrigues et al., 2016).

The efficacy of 2,3-dihydrobenzofuran, a neolignan used to treat liver diseases and vascular diseases of the brain and found in propolis and other plants, against *L. amazonensis* was studied. This compound showed IC₅₀ values of 1.04 and 1.4 µM for promastigotes and intracellular amastigotes, respectively. The intracellular amastigote activity may be mediated by the activation of macrophages, as *L. amazonensis*-infected BALB/c macrophages treated with 2,3-dihydrobenzofuran exhibited an increase in nitric oxide production, lysosomal volume, and macrophage phagocytic ability (De Castro Oliveira et al., 2017).

Saracoside and lyoniside, two lignans isolated from *Saraca indica*, were able to interact with *L. donovani* DNA, inducing apoptosis-like cell death. The IC₅₀ values of lyoniside and saracoside against the intracellular amastigote were 0.79 and 0.82 µM, respectively. BALB/c mice infected with *L. donovani* were treated intraperitoneally with both lignans (lyoniside and saracoside) at doses of 2.5 and 5 mg/kg/day. Both doses of lyoniside and saracoside were capable of significantly decreasing the parasite loads in the spleen and liver (Saha et al., 2013).

Dyphylin, an aryl-naphthalene lignin isolated from *Haplophyllum bucharicum*, is known to have activity against viruses and cancers. In promastigotes of *L. infantum*, dyphylin exhibited an IC₅₀ value of 14.4 µM. Furthermore, dyphylin was not determined to be cytotoxic for macrophages exhibiting a CC₅₀ value of 32.2 µM. In the intracellular amastigote of *L.*

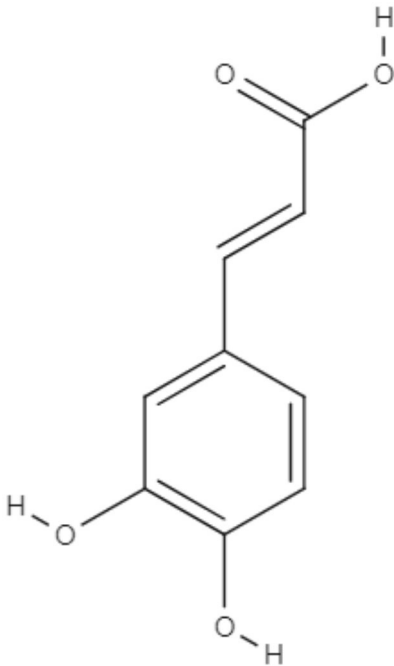
infantum, dyphylin exhibited an IC₅₀ value of 0.2 µM, reaching a selectivity index of 178. As a possible mechanism of action, dyphylin may interfere with the cell cycle and protein synthesis and increases intracellular lipid accumulation. However, dyphylin did not increase nitric oxide (NO) production (Di Giorgio et al., 2005).

Niranthin, a lignan from *Phyllanthus amarus*, was evaluated against *L. donovani*. The compound was able to inhibit *L. donovani* promastigote proliferation and exhibited good activity against intracellular amastigote with an IC₅₀ value of 1.26 µM; this lignan was not observed to be toxic to macrophages. The effects of niranthin were also tested against an antimony-resistant strain of *L. donovani*. Niranthin exhibited an IC₅₀ value of 1.68 µM, indicating that the compound is able to inhibit resistant amastigotes. It is essential for the drug discovery process to determine how natural compounds interfere in the host-parasite relationship, since the ideal compound should not be as toxic to the host as it is to the parasite. Niranthin was determined to have the ability to induce apoptosis (Chowdhury et al., 2012).

To verify the effect of niranthin *in vivo*, BALB/c mice were infected intracardially with *L. donovani* and treated with niranthin for 3 weeks at intraperitoneal or intramuscular doses of 5 and 10 mg/kg/day. Splenic and hepatic parasitic loads were almost completely eliminated at the dose of 10 mg/kg/day. Immunological analyses were performed, indicating the ability of niranthin to increase NO levels and switch from a Th2 response to a Th1 response (Chowdhury et al., 2012).

To optimize the choice of lignans and neolignans with potential effects against *Leishmania* species and to prevent possible failures from being detected only in preclinical tests, several computational tools can contribute strongly to database creation

TABLE 4 | Chemical structure and leishmanicidal activities of caffeic acid.

Class	Compound name and chemical structure	<i>Leishmania</i> species	Assay	Values	References
Caffeic acid		<i>L. amazonensis</i>	<i>In vitro</i>	Promastigotes: IC ₅₀ : 5.2 μM Intracellular amastigotes: IC ₅₀ : 16.0 μM	Montrieux et al., 2014
			<i>In vivo</i>	ND	
		<i>L. infantum</i>	<i>In vitro</i>	Promastigotes: IC ₅₀ : 12.5 μg/mL	Bortoleti et al., 2019
			<i>In vivo</i>	ND	
			<i>In vitro</i>	Intracellular amastigotes: IC ₅₀ : 21.9 μM	Garcia et al., 2019

ND, Not determined.

by predicting protein functions, modeling protein structures, simulating metabolic pathway kinetics, predicting biological activities, predicting toxicity, and predicting the affinities and flexibilities between receptors and ligands, which can facilitate the development and identification of drugs with the potential to treat various diseases and promote the development of efficacious drugs with reduced toxicity (Maia et al., 2020).

The design and synthesis of analogs of natural compounds is a strategy extensively used to identify effective new treatments against leishmaniasis. Design analogs enable the enhancement of many biological and chemical characteristics of compounds to afford new hits, such as bioactivity, selectivity, water solubility, and lipophilicity (Meanwell, 2011).

Along with the approach of advanced technologies for the design of new biologically more potent drugs, it is essential to understand the biology of the parasite to direct these studies.

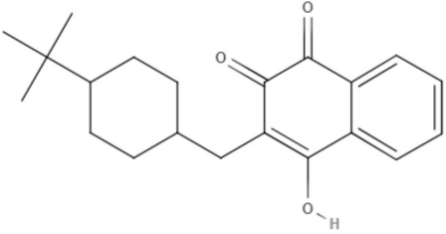
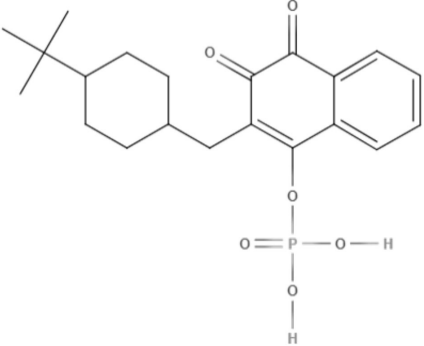
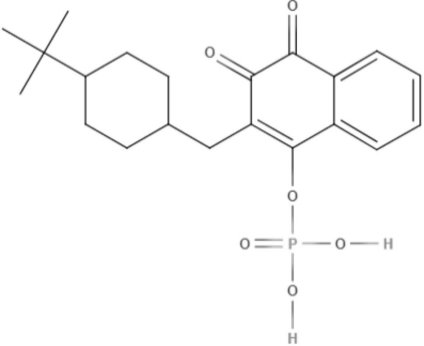
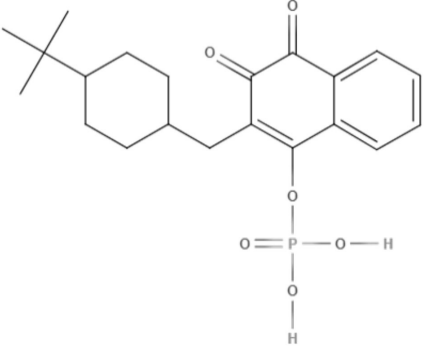
Two neolignans, threo, threo-manassantin A and threo, erythro-manassantin A, isolated from *Saururus cernuus* exhibited activity against promastigotes (IC₅₀ of 35.4 and 17.6 μM, respectively) and intracellular amastigotes (IC₅₀ of 20.4 and

16.0 μM, respectively) of *Leishmania amazonensis*. Regardless of the mode of action, these compounds seem to act directly on parasites, since host cells did not show signs of cell activation. Both molecules were determined to be able to interact with the parasite plasmatic membrane and to interfere with the parasite nucleus (Brito et al., 2019).

Virtual screening and experimental validation have been utilized to identify lignans with leishmanicidal potential, low toxicity, and selective activity against several *Leishmania* targets. A set of 160 lignans (i.e., 14 furans, 10 furofurans, 14 dibenzylbutyrolactols, 22 dibenzylbutanes, 21 dibenzocycloocyadienes, 17 aryltetralins, 3 aryl-naphthalenes, 8 neolignan alkyl aryl ethers, 16 neolignan benzofurans, and 9 neolignan benzodiones) were selected using predictive models that were built using data for *L. major* and *L. braziliensis* (Maia et al., 2020).

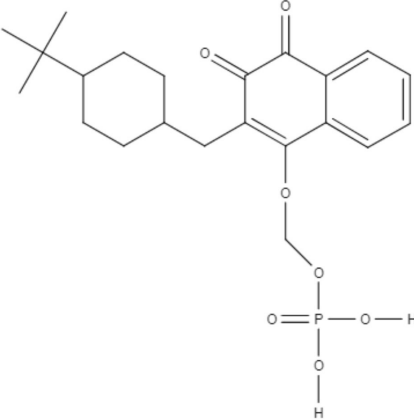
In brief, the workflow consisted of predicting the ADMET properties of these lignans. Through this tool, 42 compounds have good lipophilicity, water solubility, pharmacokinetic action and low or no predicted risk for the development of mutagenicity,

TABLE 5 | Chemical structure and leishmanicidal activities of quinones.

Class	Subclass	Compound name and chemical structure	Leishmania species	Assay	Values	References
Quinones	Hydroxynaphthoquinones		<i>L. donovani</i>	<i>In vitro</i>	Promastigotes: IC ₅₀ : 0.006 μM	Mäntylä et al., 2004
			<i>L. aethiopica</i>		Intracellular amastigotes: IC ₅₀ : 0.04 μM	
			<i>L. major</i>		Promastigotes: IC ₅₀ : 0.013 μM	
					Intracellular amastigotes: IC ₅₀ : 3.6 μM	
			<i>L. amazonensis</i>		Promastigotes: IC ₅₀ : 0.001 μM	
					Intracellular amastigotes: IC ₅₀ : 1.8 μM	
Quinones	Hydroxynaphthoquinones		<i>L. donovani</i>	<i>In vitro</i>	Promastigotes: IC ₅₀ : 0.004 μM	Mäntylä et al., 2004
					Intracellular amastigotes: IC ₅₀ : 5.5 μM	
			<i>L. mexicana</i>		Promastigotes: IC ₅₀ : 0.004 μM	
					Intracellular amastigotes: IC ₅₀ : 1.3 μM	
			<i>L. panamensis</i>		Promastigotes: IC ₅₀ : 0.04 μM	
					Intracellular amastigotes: IC ₅₀ : 0.9 μM	
Quinones	Hydroxynaphthoquinones		<i>L. donovani</i>	<i>In vitro</i>	Promastigotes: IC ₅₀ : 0.009 μM	Mäntylä et al., 2004
					Intracellular amastigotes: IC ₅₀ : 4.3 μM	
			<i>L. aethiopica</i>		Promastigotes: IC ₅₀ : 0.1 μM	
					Intracellular amastigotes: IC ₅₀ : 7.4 μM	
			<i>L. major</i>		Promastigotes: IC ₅₀ : 0.06 μM	
					Intracellular amastigotes: IC ₅₀ : 6.3 μM	
Quinones	Hydroxynaphthoquinones		<i>L. amazonensis</i>		Promastigotes: IC ₅₀ : 0.02 μM	
					Intracellular amastigotes: IC ₅₀ : 15.7 μM	

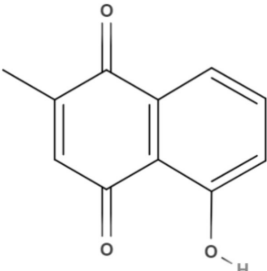
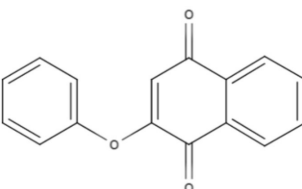
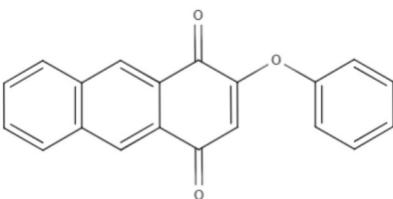
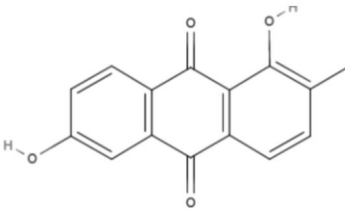
(Continued)

TABLE 5 | Continued

Class	Subclass	Compound name and chemical structure	Leishmania species	Assay	Values	References
Quinones	Hydroxynaphthoquinones	3-phosphonooxymethyl-buparvaquone (3-POM-BPQ) 	<i>L. mexicana</i>		Promastigotes: IC ₅₀ : 0.04 μM Intracellular amastigotes: IC ₅₀ : 4.0 μM	
			<i>L. panamensis</i>		Promastigotes: IC ₅₀ : 0.1 μM Intracellular amastigotes: IC ₅₀ : 2.1 μM	
			<i>L. donovani</i>	<i>In vitro</i>	Promastigotes: IC ₅₀ : 0.003 μM Intracellular amastigotes: IC ₅₀ : 0.1 μM	Mäntylä et al., 2004
			<i>L. aethiopica</i>		Promastigotes: IC ₅₀ : 0.06 μM Intracellular amastigotes: IC ₅₀ : 3.99 μM	
			<i>L. major</i>		Promastigotes: IC ₅₀ : 0.012 μM Intracellular amastigotes: IC ₅₀ : 1.9 1 μM	
			<i>L. amazonensis</i>		Promastigotes: IC ₅₀ : 0.007 μM Intracellular amastigotes: IC ₅₀ : 8.8 μM	
			<i>L. mexicana</i>		Promastigotes: IC ₅₀ : 0.01 μM Intracellular amastigotes: IC ₅₀ : 2.5 μM	
			<i>L. panamensis</i>		Promastigotes: IC ₅₀ : 0.12 μM Intracellular amastigotes: IC ₅₀ : 1.2 μM	
		BPQ BPQ-3-PHOS 3-POM-BPQ	<i>L. major</i>	<i>In vivo</i>	ND	Garnier et al., 2007
		BPQ-SNEDDS^a	<i>L. donovani</i> <i>L. infantum</i>	<i>In vitro</i> <i>In vivo</i>	Promastigotes: IC ₅₀ : 3.3 μg/mL Intracellular amastigotes: IC ₅₀ : 0.09 μg/mL	Smith et al., 2018

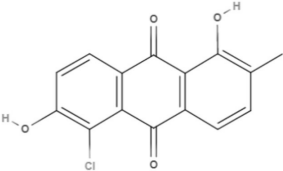
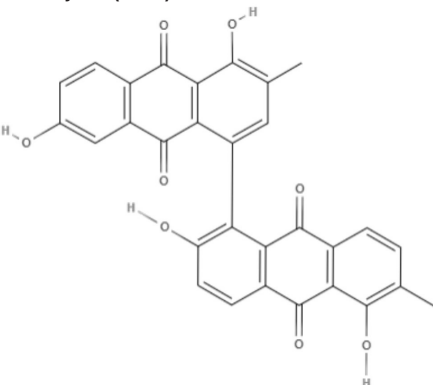
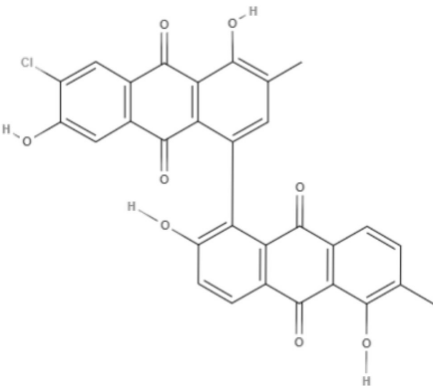
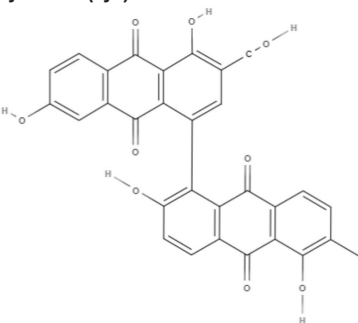
(Continued)

TABLE 5 | Continued

Class	Subclass	Compound name and chemical structure	Leishmania species	Assay	Values	References
Quinones	Naphthoquinones	BPQ solid SNEDDS ^b	<i>L. infantum</i>	<i>In vitro</i>	Promastigotes: IC ₅₀ : < 0.012 µg/mL Intracellular amastigotes: IC ₅₀ : < 0.005 µg/mL	Smith et al., 2018
		BPQ-NLC ^c	<i>L. infantum</i>	<i>In vivo</i> <i>In vitro</i>	Intracellular amastigotes: IC ₅₀ : 229.0 nM	Monteiro et al., 2019
		BPQ-NLC-PB-[A ⁻] ^d			Intracellular amastigotes: IC ₅₀ : 145.7 nM	
		BPQ-NLC-PB-[C ⁺] ^e			Intracellular amastigotes: IC ₅₀ : 150.5 nM	
	Anthraquinones	Plumbagin 	<i>L. donovani</i>	<i>In vitro</i>	Promastigotes: IC ₅₀ : 0.34 µM Axenic amastigotes: IC ₅₀ : 0.21 µM	Sharma et al., 2012
		2-phenoxy-naphthoquinone 	<i>L. donovani</i>	<i>In vitro</i>	Promastigotes: IC ₅₀ : 0.74 µM Axenic amastigotes: IC ₅₀ : 1.26 µM	Lizzi et al., 2012
	Anthraquinones	2-phenoxy-anthraquinone 	<i>L. donovani</i>	<i>In vitro</i>	Promastigotes: IC ₅₀ : 2.8 µM Axenic amastigotes: IC ₅₀ : 0.34 µM	Lizzi et al., 2012
Quinones	Anthraquinones	Soranjidiol (Sor) 	<i>L. amazonensis</i>	<i>In vitro</i>	Promastigotes: LD ₅₀ : 16.3 J/cm ² LD ₉₀ : 22.1 J/cm ²	Dimmer et al., 2019

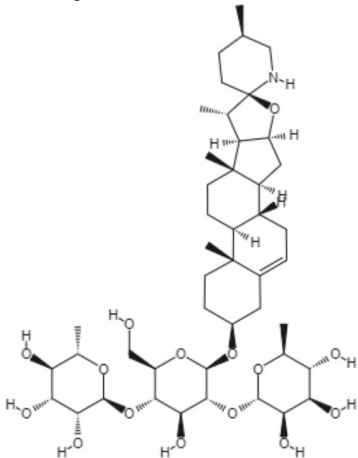
(Continued)

TABLE 5 | Continued

Class	Subclass	Compound name and chemical structure	<i>Leishmania</i> species	Assay	Values	References
Quinones	Anthraquinones	5-Chlorosoranjidiol (5-ClSor) 	<i>L. amazonensis</i>	<i>In vitro</i>	Promastigotes: LD ₅₀ : 13.8 J/cm ² LD ₉₀ : 22.2 J/cm ²	Dimmer et al., 2019
		Bisoranjidiol (Bisor) 	<i>L. amazonensis</i>	<i>In vitro</i>	Promastigotes: LD ₅₀ : 15.2 J/cm ² LD ₉₀ : 19.3 J/cm ²	Dimmer et al., 2019
		7-chlorobisoranjidiol (7-ClBisor) 	<i>L. amazonensis</i>	<i>In vitro</i>	ND	Dimmer et al., 2019
		Lycionine (Lyc) 	<i>L. amazonensis</i>	<i>In vitro</i>	ND	Dimmer et al., 2019

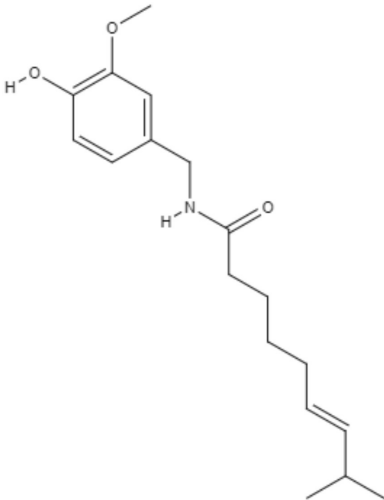
^aBuparvaquone (BPQ) loaded self-nanoemulsifying drug delivery system (SNEDDS).^bBPQ loaded self-nanoemulsifying drug delivery system compressed into tablet.^cBPQ delivered by nanostructured lipid carrier (NLC).^dBPQ co-delivered by nanostructured lipid carrier (NLC) and polymyxin B (PB)–anionic formulation.^eBPQ co-delivered by nanostructured lipid carrier and polymyxin B–cationic formulation.ND, Not demonstrated; LD₅₀, Light Dose that cause 50% of promastigote lethality; LD₉₀, Light Dose that cause 90% of promastigote lethality.

TABLE 6 | Chemical structure and leishmanicidal activities of alkaloids.

Class	Subclass	Compound name and chemical structure	<i>Leishmania</i> species	Assay	Values	References
Alkaloids	Glicoalkaloids	Solamargine	<i>L. mexicana</i>	<i>In vitro</i>	<ul style="list-style-type: none"> • Promastigotes: IC₅₀: 35.1 μM • Amastigotes (inside BMDM): IC₅₀: 13.4 μM • Amastigotes (inside BMDDC): IC₅₀: 6.03 μM 	Lezama-Dávila et al., 2016
		 Solasonine		<i>In vivo</i> <i>In vitro</i>	<ul style="list-style-type: none"> • Promastigotes: IC₅₀: 36.5 μM • Amastigotes (inside BMDM): IC₅₀: 9.3 μM • Amastigotes (inside BMDDC): IC₅₀: 5.9 μM 	
Alkaloids	Piperidines	Piperine (PIP)	<i>L. infantum</i>	<i>In vivo</i> <i>In vitro</i>	<ul style="list-style-type: none"> • Promastigotes: IC₅₀: 3.03 μg/mL • Axenic amastigotes: IC₅₀: 23.98 μg/mL • Combination with meglumine antimoniate (compound : meglumine antimoniate): • Promastigotes: IC₅₀: 2.1 μg/mL (50% : 50%) • IC₅₀: 4.3 μg/mL (25% : 75%) • IC₅₀: 4.5 μg/mL (12.5% : 87.5%) • IC₅₀: 4.7 μg/mL (6.25% : 93.75%) 	Vieira-Araújo et al., 2018

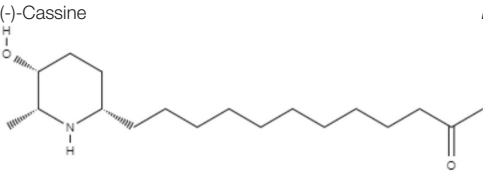
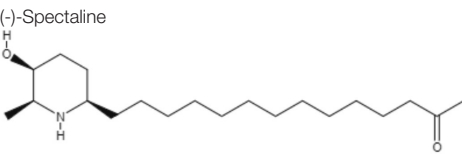
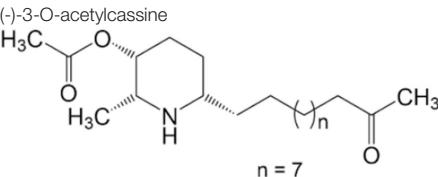
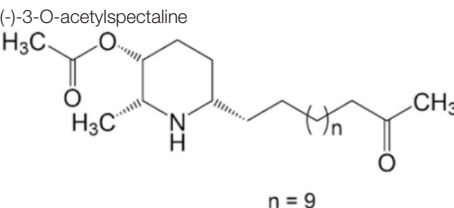
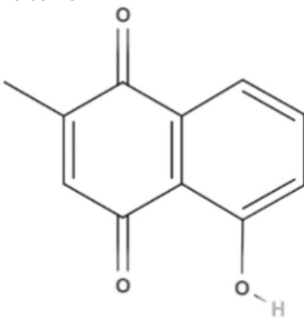
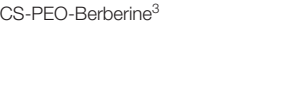
(Continued)

TABLE 6 | Continued

Class	Subclass	Compound name and chemical structure	Leishmania species	Assay	Values	References
Alkaloids	Piperidines	Capsaicin (CAP)	<i>L. infantum</i>	<i>In vitro</i>	Axenic amastigotes: IC ₅₀ : 18.7 μg/mL (50% : 50%) <ul style="list-style-type: none">• IC₅₀: 7.3 μg/mL (25% : 75%)• IC₅₀: 16.6 μg/mL (12.5% : 87.5%)IC₅₀: 19.1 μg/mL (6.25% : 93.75%)	Vieira-Araújo et al., 2018
					Promastigotes: IC ₅₀ : 5.01 μg/mL	
Alkaloids	Piperidines	HDGG-AmB-Pip-NPs ¹	<i>L. donovani</i>	<i>In vitro</i>	Combination with meglumine antimoniate (compound : meglumine antimoniate): <ul style="list-style-type: none">• Promastigotes: IC₅₀: 2.9 μg/mL (50% : 50%)• IC₅₀: 5.6 μg/mL (25% : 75%)• IC₅₀: 5.5 μg/mL (12.5% : 87.5%)• IC₅₀: 18.4 μg/mL (6.25% : 93.75%)	Ray et al., 2020
		Eu-HDGG-AmB-Pip-NPs ²		<i>In vivo</i>	Axenic amastigotes: IC ₅₀ : 22.3 μg/mL (50% : 50%)	
			<i>L. donovani</i>	<i>In vitro</i>	<ul style="list-style-type: none">• IC₅₀: 23.9 μg/mL (25% : 75%)• IC₅₀: 28.3 μg/mL (12.5% : 87.5%)• IC₅₀: 27.5 μg/mL (6.25% : 93.75%)	Ray et al., 2020
				<i>In vivo</i>	Promastigotes: IC ₅₀ : 21.9 ng/mL	
					Intracellular amastigotes: IC ₅₀ : 4.9 ng/mL	
					Promastigotes: IC ₅₀ : 24.0 ng/mL	
					Intracellular amastigotes: IC ₅₀ : 18.3 ng/mL	

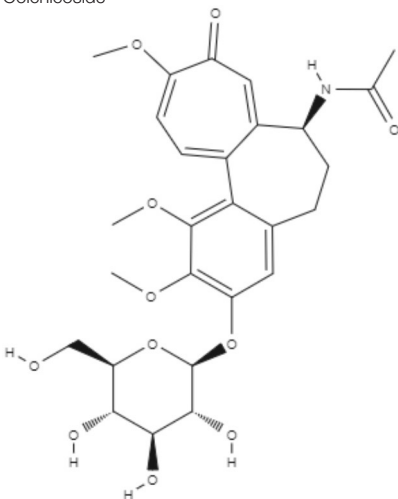
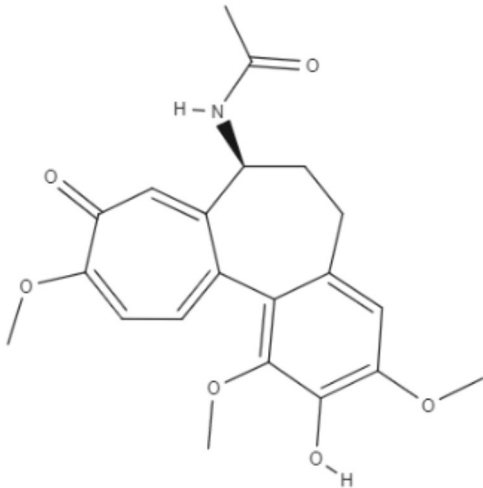
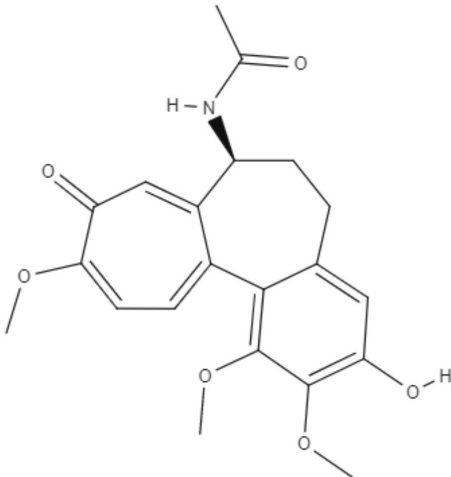
(Continued)

TABLE 6 | Continued

Class	Subclass	Compound name and chemical structure	<i>Leishmania</i> species	Assay	Values	References
Alkaloids	Piperidines	(-)-Cassine 	<i>L. amazonensis</i>	<i>In vitro</i>	Promastigotes: IC ₅₀ : 25.2 µg/mL	Lacerda et al., 2018
		(-)-Spectaline 			Promastigotes: IC ₅₀ : 15.8 µg/mL	
		(-)-3-O-acetylcassine 	<i>L. amazonensis</i>	<i>In vitro</i>	Promastigotes: IC ₅₀ : 30.3 µg/mL	Lacerda et al., 2018
		(-)-3-O-acetylspectaline 			Promastigotes: IC ₅₀ : 25.9 µg/mL	
	Isoquinolines	Berberine 	<i>Leishmania donovani</i> UR6	<i>In vitro</i>	<ul style="list-style-type: none"> • Promastigotes: IC₅₀: 4.8 µM • IC₉₀: 50.0 µM 	De Sarkar et al., 2018
		CS-PEO-Berberine ³ 	<i>L. major</i>	<i>In vitro</i>	<ul style="list-style-type: none"> • Promastigotes: IC₅₀: 0.2 µg/mL • Amastigotes: IC₅₀: 0.9 µg/mL 	Rahimi et al., 2020

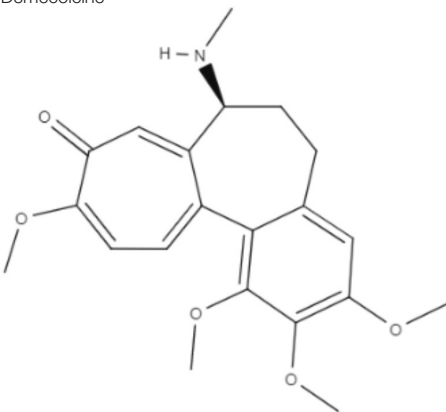
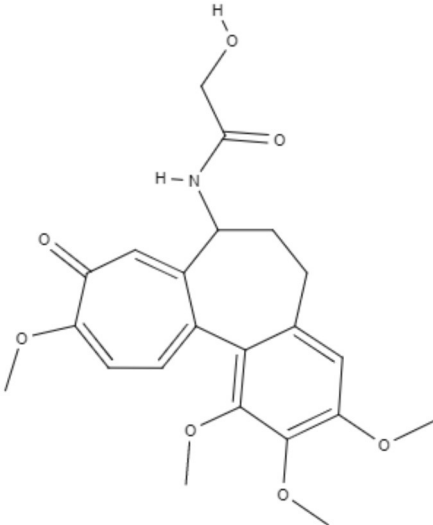
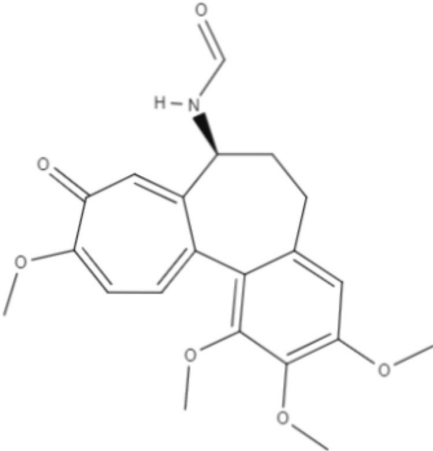
(Continued)

TABLE 6 | Continued

Class	Subclass	Compound name and chemical structure	Leishmania species	Assay	Values	References
Alkaloids	Tropolones	Colchicoside	<i>L. major</i>	<i>In vitro</i>	<ul style="list-style-type: none"> • Promastigotes: IC₅₀: 0.2 µg/mL • Amastigote: IC₅₀: 4.0 µg/mL 	Azadbakht et al., 2020
				<i>In vivo</i> toxicity assay	<ul style="list-style-type: none"> • Brine shrimp test: LD₅₀: 452.8 µg/mL • LD₉₀: 1782.7 µg/mL • Acute toxicity in mice: LD₅₀: 9.1 µg/mL 	
		2-Demethyl colchicine		<i>In vitro</i>	<ul style="list-style-type: none"> • Promastigotes: IC₅₀: 0.5 µg/mL • Amastigotes: IC₅₀: 10.2 µg/mL 	
Alkaloids	Tropolones		<i>L. major</i>	<i>In vivo</i> toxicity assay	<ul style="list-style-type: none"> • Brine shrimp test: LD₅₀: 518.9 µg/mL • LD₉₀: 1852.5 µg/mL • Acute toxicity in mice: LD₅₀: 8.3 µg/mL 	Azadbakht et al., 2020
		3-Demethyl colchicine		<i>In vitro</i>	<ul style="list-style-type: none"> • Promastigotes: IC₅₀: 0.4 µg/mL • Amastigotes: IC₅₀: 11.1 µg/mL 	
Alkaloids	Tropolones		<i>L. major</i>	<i>In vivo</i> toxicity assay	<ul style="list-style-type: none"> • Brine shrimp test: LD₅₀: 568.5 µg/mL • LD₉₀: 1982.8 µg/mL • Acute toxicity in mice: LD₅₀: 9.0 µg/mL 	Azadbakht et al., 2020

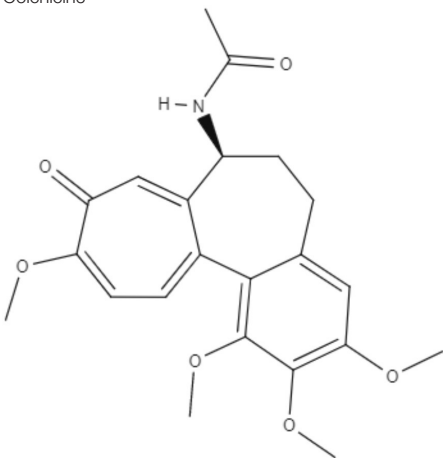
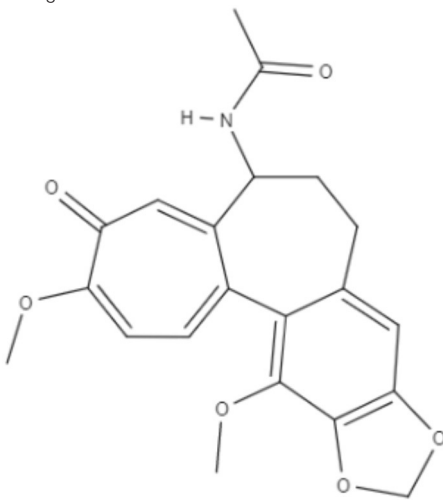
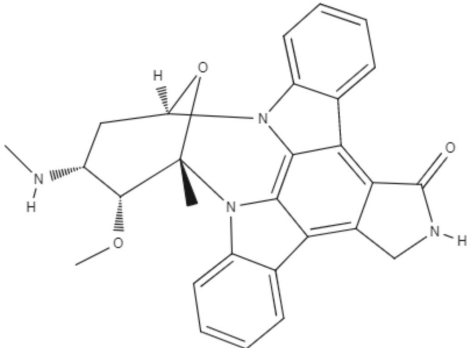
(Continued)

TABLE 6 | Continued

Class	Subclass	Compound name and chemical structure	Leishmania species	Assay	Values	References
		Demecolcine 		<i>In vitro</i> <i>In vivo</i> toxicity assay	<ul style="list-style-type: none"> • Promastigotes: IC₅₀: 0.7 µg/mL • Amastigotes: IC₅₀: 14.8 µg/mL • Brine shrimp test: LD₅₀: 542.4 µg/mL • LD₉₀: 1693.0 µg/mL • Acute toxicity in mice: LD₅₀: 9.7 µg/mL 	
Alkaloids	Tropolones	Colchifoline 	<i>L. major</i>	<i>In vitro</i> <i>In vivo</i> toxicity assay	<ul style="list-style-type: none"> • Promastigotes: IC₅₀: 0.7 µg/mL • Amastigotes: IC₅₀: 14.0 µg/mL • Brine shrimp test: LD₅₀: 528.5 µg/mL • LD₉₀: 1734.5 µg/mL • Acute toxicity in mice: LD₅₀: 9.1 µg/mL 	Azadbakht et al., 2020
		N-deacetyl-N-formyl colchicine 		<i>In vitro</i> <i>In vivo</i> toxicity assay	<ul style="list-style-type: none"> • Promastigotes: IC₅₀: 0.5 µg/mL • Amastigotes: IC₅₀: 10.2 µg/mL • Brine shrimp test: LD₅₀: 542.8 µg/mL • LD₉₀: 1846.9 µg/mL • Acute toxicity in mice: LD₅₀: 7.9 µg/mL 	

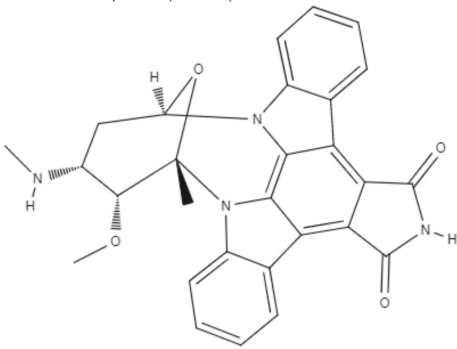
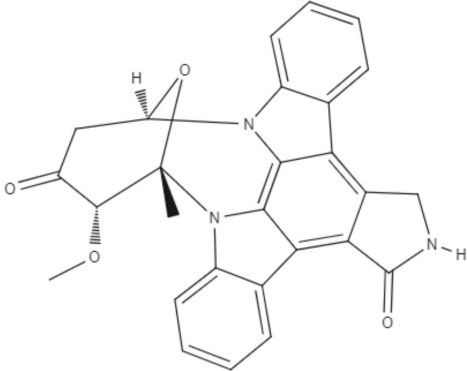
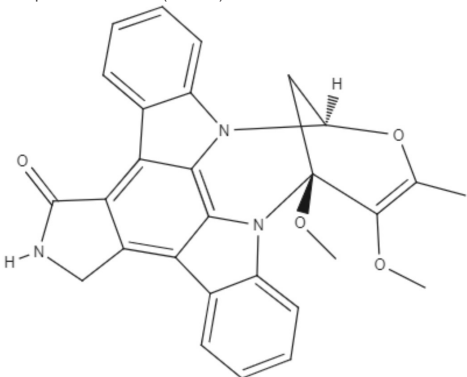
(Continued)

TABLE 6 | Continued

Class	Subclass	Compound name and chemical structure	<i>Leishmania</i> species	Assay	Values	References
Alkaloids	Tropolones	Colchicine	<i>L. major</i>	<i>In vitro</i>	<ul style="list-style-type: none"> • Promastigotes: IC₅₀: 0.4 µg/mL • Amastigotes: IC₅₀: 8.7 µg/mL 	Azadbakht et al., 2020
				<i>In vivo</i> toxicity assay	<ul style="list-style-type: none"> • Brine shrimp test: LD₅₀: 585.2 µg/mL • LD₉₀: 1952.5 µg/mL • Acute toxicity in mice: LD₅₀: 6.1 µg/mL 	
		Cornigerine		<i>In vitro</i>	<ul style="list-style-type: none"> • Promastigotes: IC₅₀: 0.8 µg/mL • Amastigotes: IC₅₀: 11.9 µg/mL 	
				<i>In vivo</i> toxicity assay	<ul style="list-style-type: none"> • Brine shrimp test: LD₅₀: 538.8 µg/mL • LD₉₀: 1889.0 µg/mL • Acute toxicity in mice: LD₅₀: 7.8 µg/mL 	
Alkaloids	Indolocarbazoles	Staurosporine (STS)	<i>L. amazonensis</i>	• <i>In vitro</i>	<ul style="list-style-type: none"> • Promastigotes: IC₅₀: 0.08 µM • Intracellular amastigotes: IC₅₀: 10.0 µM 	Cartuche et al., 2020
			<i>L. donovani</i>		Promastigotes: IC ₅₀ : 2.1 µM	

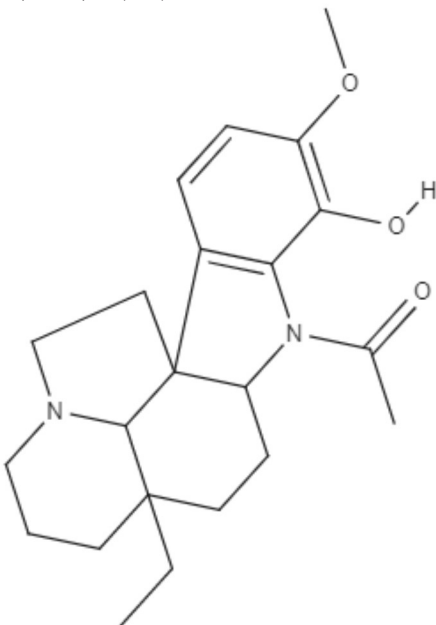
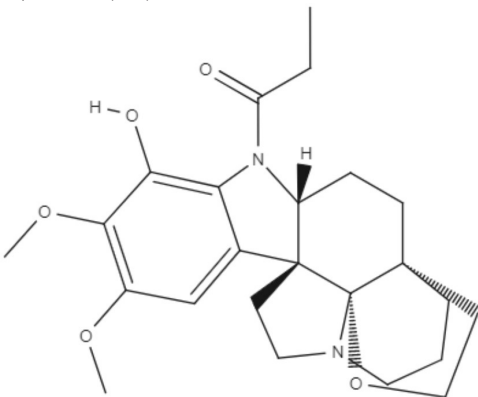
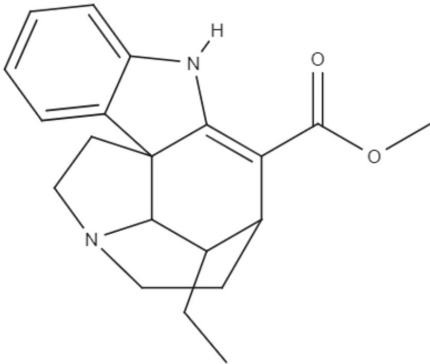
(Continued)

TABLE 6 | Continued

Class	Subclass	Compound name and chemical structure	Leishmania species	Assay	Values	References
		7-Oxostaurosporine (7OSTS) 	<i>L. amazonensis</i> <i>L. donovani</i>		<ul style="list-style-type: none"> • Promastigotes: IC₅₀: 3.6 μM • Intracellular amastigotes: IC₅₀: 0.1 μM Promastigotes: IC ₅₀ : 0.6 μM	
Alkaloids	Indolocarbazoles	4'-Demethylamine-4'-oxostaurosporine (4'D4'OSTS) 	<i>L. amazonensis</i> <i>L. donovani</i>	<i>In vitro</i>	<ul style="list-style-type: none"> • Promastigotes: IC₅₀: 17.1 μM • Intracellular amastigotes: IC₅₀: 2.0 μM Promastigotes: IC ₅₀ : > 40 μM	Cartuche et al., 2020
		Streptocarbazole B (SCZ B) 	<i>L. amazonensis</i> <i>L. donovani</i>		<ul style="list-style-type: none"> • Promastigotes: IC₅₀: 10.4 μM • Intracellular amastigotes: IC₅₀: 2.5 μM Promastigotes: IC ₅₀ : > 40 μM	

(Continued)

TABLE 6 | Continued

Class	Subclass	Compound name and chemical structure	<i>Leishmania</i> species	Assay	Values	References
Alkaloids	Indoles	<p>Aspidocarpine (APC)</p>  <p>Aspidoalbine (APA)</p> 	<ul style="list-style-type: none"> • <i>L. amazonensis</i> • <i>L. braziliensis</i> • <i>L. panamensis</i> • <i>L. mexicana</i> 	<ul style="list-style-type: none"> • <i>In silico</i> • Docking studies 	ND	Morales-Jadán et al., 2020
Alkaloids	Indoles	<p>Tubotaiwine (TBT)</p> 	<ul style="list-style-type: none"> • <i>L. amazonensis</i> • <i>L. braziliensis</i> • <i>L. panamensis</i> • <i>L. mexicana</i> 	<ul style="list-style-type: none"> • <i>In silico</i> • Docking studies 	ND	Morales-Jadán et al., 2020

^aAmphotericin B (AmB) and piperine (Pip) entrapped in guar gum (HDGG) nanoparticles (NPs).

^bEudragit L30D-coated AmB and Pip-loaded guar gum nanoparticles.

^cChitosan (CS)-polyethylene oxide (PEO) nanofibers containing berberine.

ND, Not demonstrated; BMDM, Bone marrow derived macrophage; BMDDC, Bone marrow derived dendritic cell.

tumorigenesis, negative effects on the reproductive system, or irritability. Next, ligand-based virtual screening was performed to evaluate the potential antileishmanial activity of these compounds using the random forest (RF) algorithm with the parameters of specificity, sensitivity, accuracy, positive predicted value (PPV), and negative predicted value (NPV) for performance and robustness. This model was able to select 11 compounds with active potential, with probabilities ranging from 50 to 75%, for *L. major*, and 21 potentially active compounds against *L. braziliensis* were selected and exhibited the same probabilities.

To choose the potential targets in both *L. major* and *L. braziliensis*, sequence alignment was employed to verify the similarities and identities of the enzymes selected in this study across different species. In addition, differences and structural similarities could be identified that might contribute to rational drug planning. After sequence alignment and homology modeling were performed, three enzymes were chosen for both species: GPDH (glycerol-3-phosphate dehydrogenase), PTR1 (pteridine reductase 1), and TR (trypanothione reductase).

After all these virtual screenings, four lignans (secoisolaricresinol, pinoresinol-4-O- β -D-glucopyranoside, epipinoresinol-4-O- β -D-glucopyranoside, and pinoresinol-4-O- β -D-apiofuranosyl-(1 \rightarrow 2)- β -D-glucopyranoside) were selected, and their potential to inhibit the growth of promastigote forms of *L. major* and *L. braziliensis* was tested. Epipinoresinol-4-O- β -D-glucopyranoside was the only compound that exhibited activity against both species tested, presenting IC₅₀ values for *L. major* and *L. braziliensis* of 36.5 and 5.4 μ M, respectively (Maia et al., 2020).

Lignans that have a defined IC₅₀ are summarized in Table 2.

Coumarins

Coumarins are derivatives that have a hydroxyl group, which differs in their biological properties. Many enzymes are related to coumarin biosynthesis; therefore, this group has various classes, such as simple coumarin, dimeric coumarin, furanocoumarin, and pyranocoumarin (Jain and Joshi, 2012). The diversity of structures within the coumarin group enables them to exhibit many biological activities, including anti-*Leishmania* activity. Various studies have described not only the *in vitro* activity of these compounds against *Leishmania* but also their mechanism of action and performance in preclinical studies. Mammaea A/BB, which were extracted from *Calophyllum brasiliense*, showed IC₅₀ values of 7.4 μ M against promastigotes and 14.3 μ M against intracellular amastigotes of *Leishmania amazonensis* (Brezan et al., 2008). Regarding the mechanism of action, mammaea A/BB was able to induce mitochondrial membrane damage and cause changes in ultrastructure in *L. amazonensis* promastigotes (Brenzan et al., 2012). However, only when topically and intramuscularly administered did mammaea A/BB reduce the lesion sizes in mice infected with *L. amazonensis* compared to mice treated with meglumine antimoniate (Tiuman et al., 2012).

Helietta apiculata Benth is a native plant of Paraguay, Brazil, and Argentina and is popularly known as “cana-de-vado” in Brazil. (+)-3-(1'-dimethylallyl)-Decursinol and (-)-heliettin, two coumarins extracted from *Helietta apiculata* Benth, were tested against *L. amazonensis* *in vitro* and *in vivo*. In *L. amazonensis* promastigotes, the IC₅₀ values were 35.8 μ M and 18.5 μ M for (+)-3-(1'-dimethylallyl)-decursinol and (-)-heliettin, respectively (Table 3). In the *in vivo* study, BALB/c mice infected with *L. amazonensis* were injected intraperitoneally with 10 mg/kg/day (+)-3-(1'-dimethylallyl)-decursinol or (-)-heliettin for 14 days. Both coumarins were capable of decreasing parasite loads similar to those observed when the reference drug, meglumine antimoniate, was used (Ferreira et al., 2010).

Part of their life cycle of *Leishmania* parasites occurs in the sand fly. Since these parasites develop entirely in the digestive system of the vector, interacting with digestive enzymes and other structures from the intestinal tract of the vector, little is known concerning the effect of plant-derived secondary metabolites during the interaction between parasites and vector or even on basic sand fly digestive physiology. Additionally, vector control is one of the key strategies for reducing the number of leishmaniasis cases, and it needs more research and development (Ferreira et al., 2018).

Based on this concept, Ferreira et al. (2010) tested the effect of two coumarins, esculin and esculetin, on sand flies infected with *L. infantum* and *L. mexicana*. These molecules were added to the sugar meal of *Lutzomyia longipalpis*. Interestingly, esculetin significantly reduced the viability of *L. infantum* and *L. mexicana* in a concentration-dependent manner. Esculin also might block the transmission of leishmaniasis with no repellent effects or reduction in the amount of sugar ingested. In this way, these compounds may represent promising tools for starting the development of antiparasitic sugar baits with less selective pressure for resistance in vector populations (Ferreira et al., 2010). This work demonstrates that coumarin is a promising natural compound that can act on two fronts: as a treatment for leishmaniasis and as a tool to control leishmaniasis vectors.

Two coumarins obtained from stem bark of *Calophyllum brasiliense* demonstrated activity against amastigotes of *Leishmania infantum*. Calanolides E1 (1) and E2 (2) presented IC₅₀ values of 37.1 and 29.1 μ M, respectively (Table 3). The structure-activity relationship between compounds 1 and 2 was determined. Compound 2, corresponding to anti stereochemistry between carbons C-20 and C-30, showed higher activity against amastigote forms of *L. infantum*, suggesting that the configuration of C-30 plays an important role in the interaction of this derivative and the tested parasites (Silva et al., 2020).

Moreover, compounds 1 and 2 were subjected to substructure filtering to evaluate their PAINS characteristics. This analysis is crucial to the development of new lead compounds, since some physical/chemical properties of the studied compounds could be associated with their reactivity (non-covalent binding) or non-specific interactions with therapeutic targets of parasites (Silva et al., 2020). Both compounds did not contain any PAINS substructures; in other words, there is a reduced probability that

their biological activities are artifacts caused by reactivity or colloidal aggregation. These data suggest that coumarins 1 and 2 may serve as scaffolds in the design of novel drug candidates for leishmaniasis (Silva et al., 2020).

Coumarins that have a defined IC_{50} are summarized in Table 3.

Caffeic Acid

Generally observed in carbohydrate derivatives, such as glycosides, starches, esters and sugar esters, caffeic acids are the most representative hydroxycinnamic acids. Structural modifications, such as amides or esters, may increase the diversity of biological properties of new analogs. Radicals exhibiting 3,4-dihydroxy-substitution patterns have shown inhibitory properties and have attracted interest with respect to being used as drugs (Touaibia et al., 2012).

Computer tools have been used as a preview screening of compounds to evaluate whether the compounds have the chemical characteristics of an oral drug. Before bioguided assays of caffeic acid against *Leishmania* sp. were conducted, an *in silico* test of caffeic acid was performed to assess its potential as an oral drug. Molinspiration property calculation software (www.molinspiration.com) was used to calculate the parameters related to oral bioavailability according to Lipinski's rule of five. Lipinski's rule of five describes important molecular properties for a drug's pharmacokinetics in the human body with a high probability of human intestinal absorption and oral bioavailability. Caffeic acid satisfied Lipinski's rule of five with no violation, demonstrating that it is a good drug candidate for oral administration. After the *in silico* evaluation, bioguide assays were developed. Caffeic acid showed IC_{50} values of 12.5 $\mu\text{g/mL}$ against promastigotes (Bortoleti et al., 2019), 16.0 μM against intracellular amastigotes of *Leishmania amazonensis* (Montrieux et al., 2014) and 21.9 μM for intracellular amastigotes of *L. infantum* (Garcia et al., 2019) (Table 4). Regarding these promising *in vitro* results, the effects of caffeic acid in an *in vivo* model of infection were examined. A preclinical trial of caffeic acid in BALB/c mice infected with *L. amazonensis* promastigotes was conducted. The caffeic acid treatment was administered by the intralésional route every 4 days for 30 days of the experiment. The treatment was able to reduce lesion sizes and parasitic loads in treated animals compared to untreated animals and animals treated with vehicle (Montrieux et al., 2014).

As a mechanism of action, caffeic acid was able to alter promastigote cell morphology and cell volume accompanied by loss of mitochondrial integrity, increase in reactive oxygen species (ROS) production, phosphatidylserine exposure, and loss of plasma membrane integrity, suggesting an apoptosis-like process. Caffeic acid also increased TNF- α , ROS, and NO and reduced IL-10 levels, as well as iron availability (Bortoleti et al., 2019; Garcia et al., 2019). Through these results, it is possible to conclude that caffeic acid has leishmanicidal effects with a mechanism of action that triggers multiple targets that affect the viability of the parasite.

Although caffeic acid has properties that make it a good candidate for oral drugs, its distribution in biological systems is limited due to its hydrophobic nature (Durak et al., 2020).

However, it is important to note that no studies were identified that employed advanced technologies in the investigation of caffeic acid or its derivatives in *Leishmania* spp. or evaluated the pharmacokinetics of this substance. One hypothesis for this scarcity of published research is that although caffeic acid has had its biological effects characterized, its limitations in relation to bioavailability, such as its hydrophobic nature, make the synthesis of this compound difficult (Durak et al., 2020).

Quinones

Based on their aromatic carbon skeletons, quinones can be classified as benzoquinones, anthraquinones and naphthoquinones. The benzoquinones comprise ubiquinone and plastoquinone, which differ in their substitution patterns and exhibit different levels of unsaturation on their side chain. Ubiquinones are involved in respiratory chain reactions. Anthraquinones are the oldest known compounds that are used as colorants. Naphthalene is the most natural naphthoquinone and is important in medicinal chemistry because it exerts biological effects on various pathogens, such as *Leishmania* (Schmidt et al., 2012b).

Plumbagin, a naphthoquinone extracted from *Pera benensis*, was tested against *L. donovani* and exhibited an excellent IC_{50} value of 0.34 and 0.21 μM for promastigotes and axenic amastigotes, respectively. It has been shown that the possible mechanism of action of this compound involves the non-competitive inhibition of trypanothione reductase, a key enzyme in *Leishmania* redox homeostasis, leading to an increase in reactive oxygen species and changing the redox balance (Sharma et al., 2012).

Buparvaquone (BPQ) and its phosphate prodrugs (BPQ-3-PHOS and 3-POM-BPQ) are hydroxynaphthoquinone, which were tested against several species of *Leishmania* (*L. major*, *L. amazonensis*, *L. aethiopica*, *L. mexicana*, and *L. panamensis*) *in vitro*. BPQ, BPQ-3-PHOS, and 3-POM-BPQ demonstrated low IC_{50} values against promastigotes and amastigotes of all *Leishmania* species tested, exhibiting better activity than amphotericin B and pentostan (Mäntylä et al., 2004). The IC_{50} values of BPQ, BPQ-3-PHOS, and 3-POM-BPQ for each *Leishmania* species are described in Table 5.

BPQ, BPQ-3-PHOS, and 3-POM-BPQ were also tested *in vivo* with different topical formulations as a hydrous gel, an anhydrous gel and an emulsion, targeting *Leishmania major*-infected BALB/c mice (Garnier et al., 2007). The hydrous gel formulation produced the best results. This formulation inhibited the infiltration of infected cells and decreased parasitic load by approximately 50%. These formulations were additionally tested against *L. donovani*-infected BALB/c mice. BPQ-3-PHOS was demonstrated to be the most active compound, with a decrease of approximately two-thirds in the liver parasite burden compared to the untreated control (Garnier et al., 2007).

It has previously been described that BPQ is poorly soluble in water with a lower *in vivo* activity (Croft et al., 1992). To overcome this limitation, a novel BPQ-loaded self-nanoemulsifying drug delivery system (BPQ-SNEDDS and BPQ solid SNEDDS) was developed. These formulations demonstrated activity against *L. infantum* promastigote and intracellular amastigote forms that was superior to miltefosine (Smith et al., 2018). An oral pharmacokinetic assay in mice was performed, and the BPQ-SNEDDS showed good bioavailability, increasing the AUC_{0–24} by 55%. During *in vivo* infection, BPQ-SNEDDS and BPQ solid SNEDDS were able to inhibit parasite replication in the spleen and liver of infected mice. These formulations are promising and may be able to overcome the limitations found in the use of BPQ, and further studies are warranted to provide more information regarding their effects (Smith et al., 2018).

In a similar approach, three different nanostructured formulations (BPQ-NLC, BPQ-NLC-PB-[A[−]] and BPQ-NLC-PB-[C⁺]) were developed and employed against *L. infantum*. All formulations showed lower IC₅₀ values (229.0 nM, 145.7 nM, 150.5 nM for BPQ-NLC, BPQ-NLC-PB-[A[−]] and BPQ-NLC-PB-[C⁺], respectively) than did free BPQ, thereby improving the anti-amastigote activity of this compound (Monteiro et al., 2019).

Over the years, natural product libraries and collections have been successfully established, enabling investigators to link chemical classes to biological activities. In recent years, quinone activity has been exploited, and a library of quinone-polyamine conjugates has been constructed. These conjugates were tested against three species known to cause human parasitic diseases, including *L. donovani*. Some derivatives were determined to inhibit the activity of trypanothione reductase. All compounds presented good IC₅₀ against *L. donovani*, with emphasis being placed on compounds 2-phenoxy-anthraquinone and 2-phenoxy-naphthoquinone, which demonstrated the best IC₅₀ values against the axenic amastigotes (0.34 and 1.26 μM, respectively) and promastigotes (2.8 and 0.74 μM, respectively) of *L. donovani* (Lizzi et al., 2012).

Using a different approach to topical treatment of cutaneous leishmaniasis, Dimmer et al. (2019) tested the antiparasitic photodynamic inactivation of soranjidiol (Sor) and its derivatives 5-chlorosoranjidiol (5-ClSor), bisoranjidiol (Bisor), 7-chlorobisoranjidiol (7-ClBisor), and lycionine (Lyc). Sor and its derivatives are anthraquinones isolated from *Heterophyllaea pustulata* Hook f. Photodynamic inactivation (PDI) is a methodology that combines photosensitive drugs with light to kill parasites. Light excites photosensitive molecules that generate ROS in the presence of oxygen. Soranjidiol, 5-chlorosoranjidiol and bisoranjidiol combined with violet-blue light caused a decrease in parasite viability of *L. amazonensis* promastigotes. Bisoranjidiol-mediated PDI induced significant alterations in the size and shape of promastigotes. Furthermore, soranjidiol is the most efficient anthraquinone to combat leishmaniasis, causing fewer toxic effects in fibroblast cells (Dimmer et al., 2019).

The quinones that were presented along with their leishmanicidal activities (IC₅₀) are summarized in **Table 5**.

COMPOUNDS FROM AMINO ACID PATHWAYS

Alkaloids

Alkaloids are nitrogenous compounds with alkaline character. However, there are some exceptions, with certain compounds containing amino or amido atoms. Alkaloids are classified based on the presence and activity of specific amino acids, which form a fundamental component of the alkaloid skeleton. For example, the amino acid lysine produces piperidine, quinolizidine and indolizidine alkaloids, and the amino acid ornithine produces pyrrolidine and tropane alkaloids. The amino acid tyrosine gives rise to phenylethylamines and tetrahydroisoquinoline alkaloids. Tyrosine also produces other alkaloids in which phenolic oxidative links play a fundamental role (Kurek, 2019).

All alkaloids possessing amino acid precursors are true alkaloids or protoalkaloids. True alkaloids share a common heterocyclic ring with one nitrogen atom, while the main characteristic of protoalkaloids is a nitrogen atom that does not belong to the heterocyclic ring, such as cocaine. However, many alkaloids do not originate from amino acids but from the amination of other substrates, such as steroids, terpenoids, acetates and phenylalanine. Some authors have classified alkaloids that do not originate from amino acids as pseudoalkaloids. Finally, alkaloids that are produced via pathways resembling those by which purine nucleic acids are produced are classified as purine alkaloids (Dewick, 2009).

Many types of alkaloids have been described as having biological activities against trypanosomatids, such as *Leishmania* spp. Two heterocyclic steroids were isolated from *Solanum lycocarpum*, and their *in vitro* and *in vivo* activities were tested. Against *L. mexicana*, intracellular amastigote forms, solamargine, and solasonine showed IC₅₀ values of 6.03 and 5.9 μM, respectively. These IC₅₀ values were superior to the IC₅₀ observed with sodium stibogluconate (Lezama-Dávila et al., 2016).

Interestingly, solamargine and solasonine induced different immunochemical pathways in macrophages and dendritic cells. *L. mexicana* was eliminated more efficiently by dendritic cells when incubated with solamargine and solasonine at a concentration of 10 μM. Additionally, both compounds were capable of enhancing the expression levels of transcription factors, such as NFκB/AP-1, also at a concentration of 10 μM. Nitric oxide levels decreased in both macrophages and dendritic cells only after treatment with solamargine, indicating that its mechanism of action is dependent on nitric oxide (Lezama-Dávila et al., 2016).

The *in vivo* study was performed using C57BL/6 mice infected with *L. mexicana*. Treatment with topical formulations of 10 μM solamargine and solasonine significantly reduced parasite loads and lesion sizes in the ear (Lezama-Dávila et al., 2016).

Combination therapy has been employed as a strategy for improving the treatment of leishmaniasis. The combination of piperine and its analog capsaicin with meglumine antimoniate has been tested. Against *L. infantum*, both alkaloids alone showed better antipromastigote activity than meglumine antimoniate with IC₅₀ values of 5.01 μg/mL for capsaicin and 3.03 μg/mL

for piperine. The combinations of piperine or capsaicin with meglumine antimoniate (50% + 50%) were the most effective against promastigotes, exhibiting IC₅₀ values of 2.1 and 2.9 µg/mL, respectively. The best anti-amastigote activity occurred in the combination of piperine with meglumine antimoniate (25% + 75%), presenting a synergistic effect with an IC₅₀ value of 7.3 µg/mL (Vieira-Araújo et al., 2018).

It has already been described that piperine has a bioavailability enhancing effect (Randhawa et al., 2011). To explore this property and improve the bioavailability of amphotericin B, nanoformulations of piperine (PIP), and amphotericin B (AmB) coated with nanoparticles (HDGG-AmB-Pip-NPs and Eu-HDGG-AmB-Pip-NPs) were developed, and their leishmanicidal effects were evaluated. Both formulations showed good IC₅₀ against promastigotes (21.9 and 24 ng/mL, respectively) and intracellular amastigotes (4.9 and 18.3 ng/mL, respectively) of *L. donovani*. When formulations were administered in *L. donovani*-infected golden hamsters by the intraperitoneal route, HDGG-AmB-Pip-NPs and Eu-HDGG-AmB-Pip-NPs reduced parasite load by 95 and 96%, respectively, compared to the untreated control and were more effective than amphotericin B treatment (Ray et al., 2020).

Pharmacokinetics analysis showed that Eu-HDGG-AmB-Pip-NPs improved the plasma concentration-time profile of amphotericin B compared to amphotericin B treatment. The tissue distribution was evaluated, and Eu-HDGG-AmB-Pip-NPs showed the highest amphotericin B accumulation in the liver and spleen. This compound was also detected in the kidney, but at the lowest concentration, it was detected in the liver and spleen. Furthermore, Eu-HDGG-AmB-Pip-NPs cause changes in serum levels. The use of piperine in association with reference drugs for the treatment of leishmaniasis in nanoformulations shows promising results that should be further explored (Ray et al., 2020).

Senna spectabilis is a tree of the family Fabaceae, and piperidine alkaloids, such as (-)-cassine, (-)-spectaline, (-)-3-O-acetylcassine and (-)-3-O-acetylspectaline, can be extracted from it. These alkaloids were tested against *L. amazonensis* promastigotes, and all of them presented leishmanicidal effects, with compound (-)-spectaline being more effective (IC₅₀ = 15.8 µg/mL). However, the IC₅₀ value of this compound was higher than that of amphotericin B. In addition, all piperidine alkaloids showed less toxicity than amphotericin B. In a more modern approach, *in silico* analysis using molecular docking was performed to evaluate how these piperidine alkaloids bound to the enzyme arginase. The alkaloid (-)-spectaline showed a stronger interaction with arginase than other alkaloids, suggesting arginase as a possible target for the (-)-spectaline (Lacerda et al., 2018).

Berberine is an isoquinoline alkaloid and is extracted from *Berberis vulgaris*. Previous studies have shown that berberine has leishmanicidal activity and can induce a redox imbalance following the enhanced generation of ROS (Saha et al., 2009). Since *Leishmania* has only one mitochondrion, which is the major ROS product, the effects of berberine on the mitochondria of non-pathogenic *Leishmania donovani* UR6 were tested. This alkaloid showed a reduction in

the viability of promastigotes in a concentration-dependent manner with an IC₅₀ value of 4.8 µM and stimulated the generation of ROS in these cells. Berberine was also able to increase the levels of mitochondrial superoxide of promastigotes and induced depolarization of mitochondrial transmembrane potential. Concentration-dependent inhibition of complex I-III and II-III activities was observed in promastigotes, as well as a decrease in ATP levels. Although berberine has been tested on non-pathogenic parasites, these data provide support for future studies to search for a possible mechanism of action for this promising alkaloid (De Sarkar et al., 2018).

In the search for a new approach to improve the treatment of cutaneous leishmaniasis, the leishmanicidal effects of chitosan (CS)-polyethylene oxide (PEO) nanofibers containing berberine were tested. CS-PEO-Berberine showed an IC₅₀ of 0.2 and 0.9 µg/mL against promastigotes and in intracellular amastigotes of *L. major*, respectively, indicating that this formulation can be provided as a good alternative topical treatment for cutaneous leishmaniasis (Rahimi et al., 2020).

Colchicine, demecolcine, and thiocolchicoside are tropolone alkaloids extracted from *Colchicum kuurdicum* (Bornm.) Stef., a perennial monocotyledon plant. Eight tropolones (colchicoside, 2-demethyl colchicine, 3-demethyl colchicine, demecolcine, colchifoline, N-deacetyl-N-formyl colchicine and cornigerine) were isolated from *Colchicum kuurdicum* and tested against *L. major*. All tropolones showed good IC₅₀ and leishmanicidal effects. Colchicoside and colchicine were the most effective, exhibiting IC₅₀ values of 4.0 and 8.7 µg/mL against intracellular amastigote forms. All tropolones presented *in vitro* iron chelating activity between 19 and 25%, with colchicine showing the highest activity. Tropolones also demonstrated significant anti-inflammatory effects, with anti-denaturation effects of between 50 and 80%. Additionally, these compounds caused only 5% hemolysis, demonstrating safety for systemic usages. To analyze toxicity, a brine shrimp toxicity test and an acute toxicity test in mice were performed. All tropolones showed higher LD₅₀ and LD₉₀, and the median lethal dose of these compounds was between 6 and 10 mg/kg. To evaluate a possible mechanism of action of these tropolones, molecular docking was performed targeting tubulin protein. Based on dock scores, colchicoside and demecolcine presented the highest and the lowest affinity to tubulin, respectively. The best isomers of antitubulin were colchicoside, colchicine and N-deacetyl-N-formyl colchicine. These findings demonstrate that these tropolone alkaloids are promising compounds, especially colchicoside alkaloids, which showed strong results in leishmanicidal effects and docking studies (Azadbakht et al., 2020).

Staurosporine (STS) is an indolocarbazole isolated from *Streptomyces sanyensis*. To evaluate the antileishmania activity and to elucidate a possible mechanism of induced cell death, natural staurosporines (STS, 7OSTS, 4'D4'OSTS, and SCZ B) and its commercial analogs rebeccamycin, K252a, K252b, K252c, and arcyriaflavin A were tested against *L. amazonensis*, *L. donovani* and *T. cruzi*. The compounds STS and 7OSTS showed the lowest IC₅₀ values against promastigotes of *L. amazonensis* (0.08 and 3.6 µM, respectively) and *L. donovani* (2.1 and 0.1 µM, respectively), while 4'D4'OSTS and SCZ B

were not active against *L. donovani*, and rebeccamycin K252c and arcylflavin were inactive in both parasites. Compound 7OSTS was more active against *L. amazonensis* amastigotes (IC_{50} of $0.1 \mu M$) than was miltefosine. This indolocarbazole induced mitochondrial damage in *L. amazonensis* but not in *L. donovani*, as determined using the IC_{90} . However, cytoplasmic membrane permeability in *L. donovani* was induced by 7OSTS but not in *L. amazonensis*. Despite the differences in activity observed during the tests against *L. amazonensis* and *L. donovani*, the natural indolocarbazole 7OSTS exhibited promise (Cartuche et al., 2020).

Aspidosperma spruceanum Benth. ex Müll. Arg is a tree of the Apocynaceae family that has medicinal properties and has been used for leishmaniasis treatment in Amazonian regions (Morales-Jadán et al., 2020). Using bioinformatic tools, a new approach to predict new compounds capable of fighting diseases, three indole alkaloids (from *Aspidosperma spruceanum*) were investigated against *Leishmania* targets. The chosen indole alkaloids were aspidocarpine (APC), aspidalbine (APA) and tubotaiwine (TBT), and *in silico* tests showed that all of them fulfilled Lipinski's rule. Four *Leishmania* species cause leishmaniasis in the region where *Aspidosperma spruceanum* is used: *L. braziliensis*, *L. panamensis*, *L. amazonensis*, and *L. mexicana*. Five targets of *Leishmania* common to all these species were modeled, and 3D structures were determined for the targets, which were dihydrofolate reductase-thymidylate synthase (DHFR-TS), pteridine reductase 1 (PTR1), pyruvate kinase (PK), hypoxanthine-guanine phosphoribosyltransferase (HGPRT), and squalene synthase (SQS) (Morales-Jadán et al., 2020).

Docking simulations showed that all three indole alkaloids can interact strongly with the *Leishmania* targets. Aspidalbine had more affinity for the active site of PTR1 and against *L. panamensis*, it is able to inhibit some of the functional aspects. The alkaloids demonstrated more affinity to *Leishmania* proteins than to human homologs. These results may be useful for guiding future analyses of the leishmanicidal effects of these compounds *in vivo* and elucidating their possible mechanisms of action (Morales-Jadán et al., 2020).

Alkaloids that were presented along with their leishmanicidal activities (IC_{50}) are summarized in (Table 6).

Flavonoids

Flavonoids can be defined as a group of metabolites originating from the combination of the skimate and acetate pathways biosynthesized from cinnamic acid, which has a C6-C3-C6 basic structure and phenylbenzopyran functionality. The product of the first cyclization is chalcone, a precursor of most groups of flavonoids. These natural compounds are divided according to the linkage between the aromatic rings to the benzopyran portion in phenylbenzopyran flavonoids, isoflavonoids and neoflavonoids. Phenylbenzopyrans flavonoids (2-phenylbenzopyrans) are classified as flavan, flavanone, flavone, flavonol, dihydroflavonol, flavan-3-ol, flavan-4-ol and flavan-3,4-diol according to both oxidation and saturation of the heterocyclic C-ring. Isoflavonoids (3-benzopyrans) have a 3-phenylchroman structure with a wide range that can be classified as isoflavan, isoflavone, isoflavanone, isoflav-3-ene, isoflavanol,

rotenoid, coumestane, 3-arylcoumarin, coumaronochromene, and pterocarpin. Neoflavonoids (4-benzopyrans) have a structure similar to flavonoids and isoflavonoids and are divided into 4-arylcoumarins, 3,4-dihydro-4-arylcoumarins and neoflavones. These groups have a variety of biological activities, including against trypanosomes (Winkel, 2006; Schmidt et al., 2012b).

Quercetin, a flavonol extracted from *Kalanchoe pinnata*, demonstrated activity against promastigotes of *L. amazonensis* (IC_{50} value of $31.4 \mu M$ after 48 h). This compound increased reactive oxygen species levels, causing mitochondrial damage and leading to the death of the parasite (Fonseca-Silva et al., 2013). Against *L. amazonensis* intracellular amastigotes, quercetin exhibited an IC_{50} value of $3.4 \mu M$ and a selectivity index of 16.8 (Fonseca-Silva et al., 2013).

Quercetin was also capable of inhibiting arginase, an important enzyme in leishmanial infections, as a possible target for leishmaniasis chemotherapy (Manjolin et al., 2013). Despite these studies, the mechanism of action of quercetin is still unknown. This compound was also tested *in vivo* in *L. amazonensis*-infected mice, a murine model of cutaneous leishmaniasis. Quercetin was orally administered and reduced lesion size and parasite burden in the infected ear at a dose of 16 mg/kg/day (Muzitano et al., 2009).

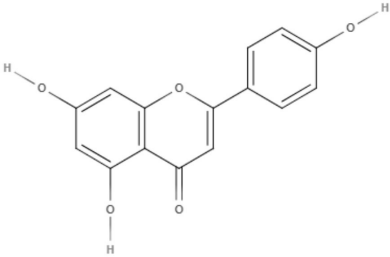
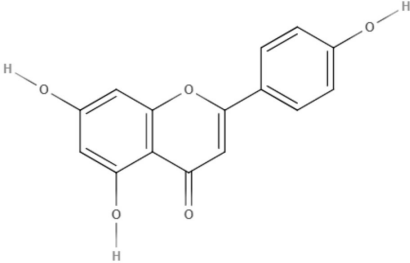
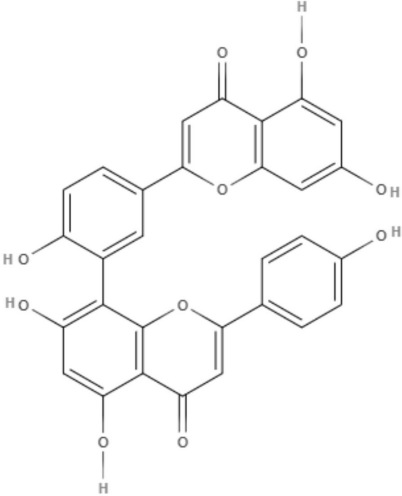
Apigenin, an important flavone tested in the last decade (Kashyap et al., 2018), showed IC_{50} values of $23.7 \mu M$ and $4.3 \mu M$ for promastigotes and the intracellular amastigote form of *L. amazonensis*, respectively. The inhibition of intracellular amastigote growth reached 71% after 72 h at the highest dose tested ($12 \mu M$) (Fonseca-Silva et al., 2015).

Apigenin was also tested *in vivo* in the cutaneous form of leishmaniasis. This compound was able to reduce the lesion size and parasitic load compared to the control and the reference (meglumine antimoniate), presenting ED_{50} and ED_{90} values of 0.73 and 1.2 mg/kg, respectively (Fonseca-Silva et al., 2016).

As a possible mechanism of action, it was demonstrated that *L. amazonensis*-infected macrophages treated with apigenin showed an increase in the intracellular reactive oxygen species (ROS) and in the number of double-membrane vesicles and myelin-like membrane inclusions, which are characteristics of the autophagic pathway. Furthermore, fusion between autophagosome-like structures and parasitophorous vacuoles was observed (Fonseca-Silva et al., 2016).

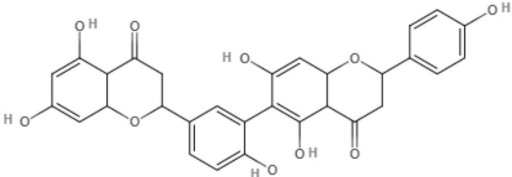
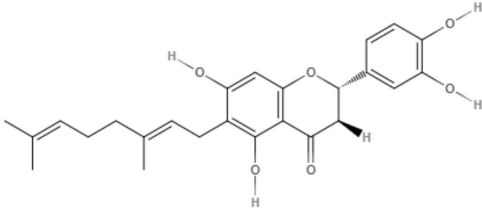
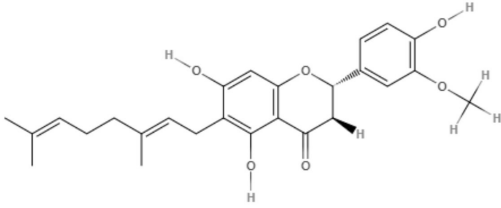
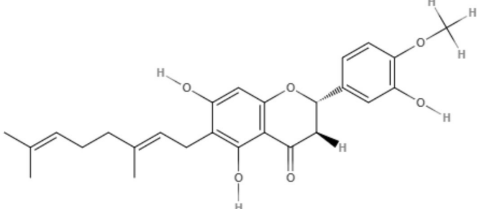
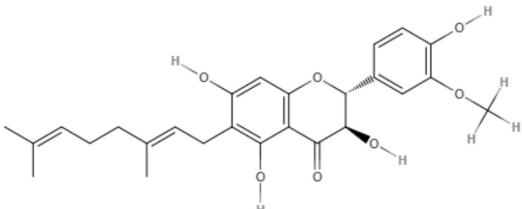
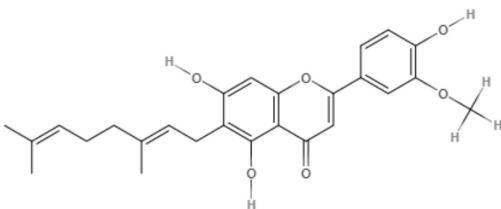
Following new chemotherapy perspectives for leishmaniasis, Emiliano and Almeida-Amaral (2018) tested apigenin in a combination model with miltefosine, which is the first oral drug for leishmaniasis. This association was first tested *in vitro* in THP-1-derived macrophages infected with *L. amazonensis* promastigotes. The ΣFIC (fractional inhibitory concentration sum) was 1.61, showing an additive effect. The *in vivo* efficacy of this combination was assessed in a cutaneous murine model with BALB/c mice infected with *L. amazonensis*. Apigenin and miltefosine were tested alone (2 and 8 mg/kg/day, respectively) or in combination, using half of the original doses (1 mg/kg/day + 4 mg/kg/day, respectively). Both compounds alone exhibited their expected effects in reducing lesion size and parasite load. The combination scheme was also able to significantly reduce the

TABLE 7 | Chemical structure and leishmanicidal activities of flavonoids.

Class	Subclass	Compound name and chemical structure	<i>Leishmania</i> species	Assay	Values	References
Flavonoids	Flavonol	Quercetin 	<i>L. amazonensis</i>	<i>In vitro</i>	Promastigotes: IC_{50} : 31.4 μ M Intracellular amastigotes: IC_{50} : 3.4 μ M	Fonseca-Silva et al., 2013
				<i>In vivo</i>	ND	Muzitano et al., 2009
			<i>L. tropica</i>	<i>In vitro</i>	Promastigotes: IC_{50} : 182.3 μ g/mL Intracellular amastigotes: IC_{50} : 137.4 μ g/mL	Mehwish et al., 2019
	Flavone	Apigenin 	<i>L. amazonensis</i>	<i>In vitro</i>	Promastigotes: IC_{50} : 23.7 μ M Intracellular amastigotes: IC_{50} : 4.3 μ M	Fonseca-Silva et al., 2015
				<i>In vivo</i>	ND	Fonseca-Silva et al., 2016; Emiliano and Almeida-Amaral, 2018
Flavonoids	Flavone	Amentoflavone 	<i>L. amazonensis</i>	<i>In vitro</i>	Intracellular amastigotes: IC_{50} : 0.2 μ M	Rizk et al., 2014

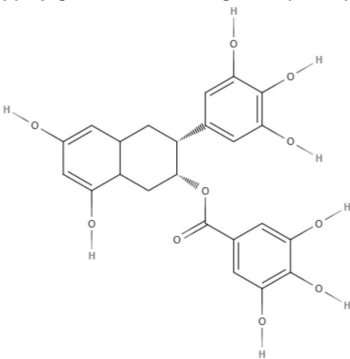
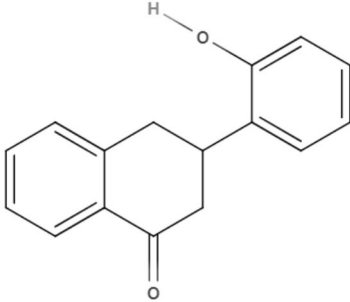
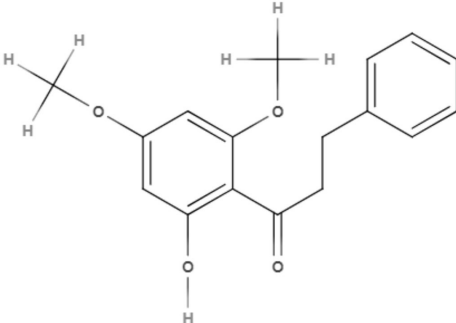
(Continued)

TABLE 7 | Continued

Class	Subclass	Compound name and chemical structure	<i>Leishmania</i> species	Assay	Values	References
Flavonoids	Flavone	Robustoflavone 			Intracellular amastigotes: IC ₅₀ : 5.3 μM	
		Diplacone 	<i>L. donovani</i>	<i>In vitro</i>	Axenic amastigotes: IC ₅₀ : 4.8 μg/mL	Salem et al., 2011
		3'-O-methyldiplacone 			Axenic amastigotes: IC ₅₀ : 7.5 μg/mL	
		4'-O-methyldiplacona 			Axenic amastigotes: IC ₅₀ : 7.5 μg/mL	
		3'-O-methyldiplacol 	<i>L. donovani</i>	<i>In vitro</i>	Axenic amastigotes: IC ₅₀ : 7.2 μg/mL	Salem et al., 2011
		Cannflavin A 			Axenic amastigotes: IC ₅₀ : 14.6 μg/mL	

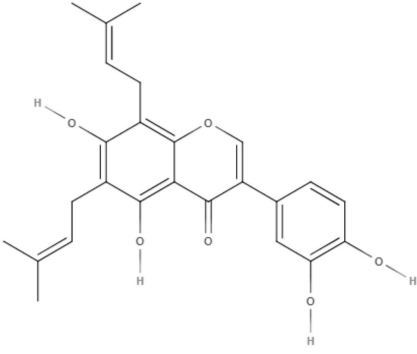
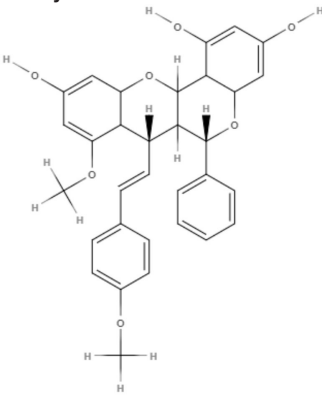
(Continued)

TABLE 7 | Continued

Class	Subclass	Compound name and chemical structure	Leishmania species	Assay	Values	References
Flavonoids	Flavanol	(-)-Epigallocatechin 3-O-gallate (EGCG) 	<i>L. amazonensis</i>	<i>In vitro</i>	Intracellular amastigotes: IC ₅₀ : 1.6 μM	Inacio et al., 2013
			<i>L. braziliensis</i>	<i>In vivo</i>	ND	
			<i>L. braziliensis</i>	<i>In vitro</i>	Promastigotes: IC ₅₀ : 278.8 μM Intracellular amastigotes: IC ₅₀ : 3.4 μM	Inacio et al., 2014
			<i>L. infantum</i>	<i>In vivo</i>	ND	
			<i>L. infantum</i>	<i>In vitro</i>	Intracellular amastigotes: IC ₅₀ : 2.6 μM <i>In vivo</i> ED ₅₀ : 12.4 mg/kg ED ₉₀ : 21.5 mg/kg	Inacio et al., 2019
	Flavanone	2'-hydroxyflavanone 	<i>L. amazonensis</i>	<i>In vitro</i>	Promastigotes: IC ₅₀ : 20.51 μM Intracellular amastigotes: IC ₅₀ : 3.09 μM Antimony-resistant L. amazonensis IC ₅₀ : 3.36 μM	Gervazoni et al., 2018
				<i>In vivo</i>	ND	
Flavonoids	Chalcone	Flavokavain B 	<i>L. amazonensis</i>	<i>In vitro</i>	Promastigotes: IC ₅₀ : 11.2 μM	Flores et al., 2007
				<i>In vivo</i>	ND	

(Continued)

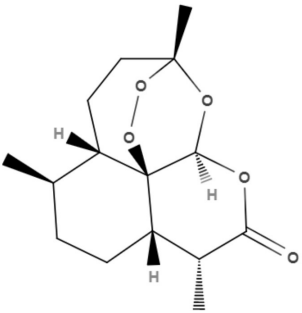
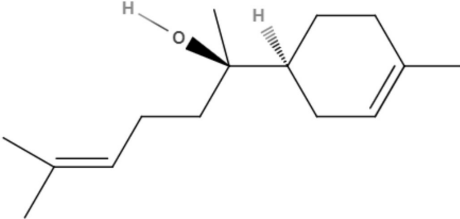
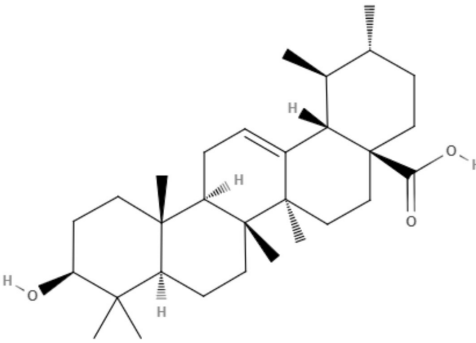
TABLE 7 | Continued

Class	Subclass	Compound name and chemical structure	<i>Leishmania</i> species	Assay	Values	References
Isoflavone		5,7,3',4'-tetrahydroxy-6,8-diprenylisoflavone (CMT) 	<i>L. braziliensis</i>	<i>In vitro</i>	Promastigotes: IC ₅₀ : 11.2 μM	Pereira et al., 2020
			<i>L. donovani</i>	<i>In vitro</i>	Promastigotes: IC ₅₀ : 11.2 μM	
			<i>L. amazonensis</i>	<i>In vitro</i>	Promastigotes: IC ₅₀ : 2.7 μg/mL Axenic amastigotes: IC ₅₀ : 1.1 μg/mL	
Flavonoids	Biflavonoid	CMT-Mic^a Brachydin B 	<i>L. infantum</i>	<i>In vitro</i>	Promastigotes: IC ₅₀ : 6.4 μg/mL Axenic amastigotes: IC ₅₀ : 2.5 μg/mL ND	Rocha et al., 2018
			<i>L. infantum</i>	<i>In vivo</i>	ND	
			<i>L. braziliensis</i>	<i>In vitro</i>	Promastigotes: IC ₅₀ : 7.05 μM	
			<i>L. amazonensis</i>	<i>In vitro</i>	Promastigotes: IC ₅₀ : 9.16 μM Intracellular amastigotes: IC ₅₀ : 2.2 μM ND	
			<i>L. braziliensis</i>	<i>In vitro</i>	Promastigotes: IC ₅₀ : 8.8 μM	
			<i>L. amazonensis</i>	<i>In vitro</i>	Promastigotes: IC ₅₀ : 10.0 μM Intracellular amastigotes: IC ₅₀ : 6.25 μM	

ND, Not determined.

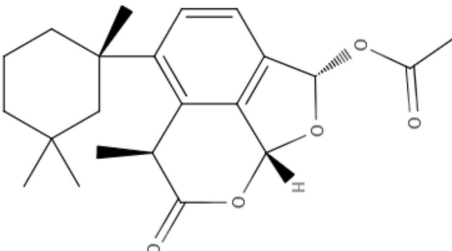
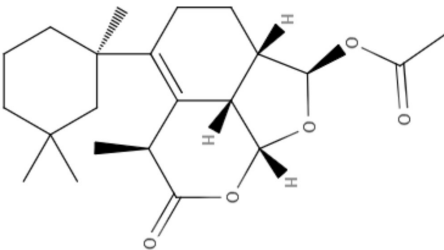
^a5,7,3',4'-tetrahydroxy-6,8-diprenylisoflavone-containing micelles.

TABLE 8 | Chemical structure and leishmanicidal activities of terpenoids.

Class	Subclass	Compound name and chemical structure	Leishmania species	Assay	Values	Reference
Terpenoids	Sesquiterpene	Artemisinin 	<i>L. major</i>	<i>In vitro</i>	Promastigotes: IC ₅₀ : 0.75 μM Intracellular amastigotes: IC ₅₀ : 3 μM	Yang and Liew, 1993
			<i>L. donovani</i>	<i>In vitro</i>	Promastigotes: IC ₅₀ : 160.0 μM Intracellular amastigotes: IC ₅₀ : 22.0 μM	Sen et al., 2007
				<i>In vivo</i>	ND	Sen et al., 2010
	Sesquiterpene	(-)-α-Bisabolol 	<i>L. donovani</i>	<i>In vitro</i>	Intracellular amastigotes: IC ₅₀ : 39.4 μM	Corpas-López et al., 2015
			<i>L. infantum</i>	<i>In vitro</i>	Intracellular amastigotes: IC ₅₀ : 56.9 μM	Corpas-López et al., 2016a
				<i>In vivo</i>	ND	
			<i>L. major</i>	<i>In vitro</i>	Intracellular amastigotes: IC ₅₀ : 33.7 μM	
			<i>L. tropica</i>	<i>In vitro</i>	Intracellular amastigotes: IC ₅₀ : 25.2 μM	Corpas-López et al., 2016b
				<i>In vivo</i>	ND	
			<i>L. amazonensis</i>	<i>In vitro</i>	Promastigotes: IC ₅₀ : 6.2 μg/mL Intracellular amastigotes: ND	Yamamoto et al., 2015
Terpenoids	Triterpenoids	Ursolic acid 				
			<i>L. infantum</i>	<i>In vivo</i>	ND	Jesus et al., 2017

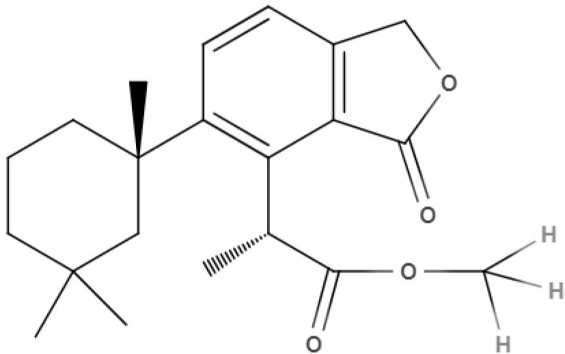
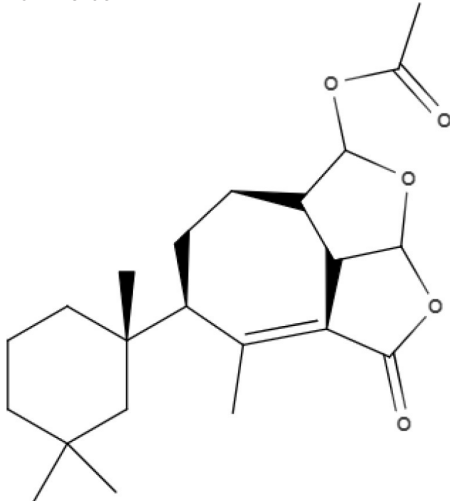
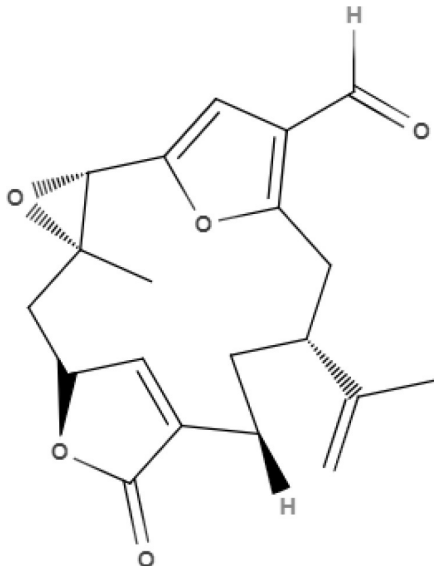
(Continued)

TABLE 8 | Continued

Class	Subclass	Compound name and chemical structure	Leishmania species	Assay	Values	Reference
Terpenoids	Triterpenoids	UA – NLC ^a	<i>L. donovani</i>	<i>In vitro</i>	Axenic amastigotes: IC ₅₀ : 1.8 μM	Das et al., 2017
					Intracellular amastigotes: IC ₅₀ : 1.1 μM	
				<i>In vivo</i>	ND	
			<i>L. donovani</i> - SSGR	<i>In vitro</i>	Axenic amastigotes: IC ₅₀ : 16.2 μM	
					Intracellular amastigotes: IC ₅₀ : 11.5 μM	
				<i>In vivo</i>	ND	
			<i>L. donovani</i> - PMMR	<i>In vitro</i>	Axenic amastigotes: IC ₅₀ : 36 μM	
					Intracellular amastigotes: IC ₅₀ : 24.5 μM	
				<i>In vivo</i>	ND	
			<i>L. donovani</i>	<i>In vitro</i>	Axenic amastigotes: IC ₅₀ : 0.12 μM	Das et al., 2017
					Intracellular amastigotes: IC ₅₀ : 0.09 μM	
				<i>In vivo</i>	ND	
			<i>L. donovani</i> - SSGR	<i>In vitro</i>	Axenic amastigotes: IC ₅₀ : 1.1 μM	
					Intracellular amastigotes: IC ₅₀ : 2.9 μM	
				<i>In vivo</i>	ND	
			<i>L. donovani</i> - PMMR	<i>In vitro</i>	Axenic amastigotes: IC ₅₀ : 3.5 μM	
					Intracellular amastigotes: IC ₅₀ : 5.6 μM	
				<i>In vivo</i>	ND	
Terpenoids	Diterpenes	Aplysulphurin 	<i>L. donovani</i>	<i>In vitro</i>	Intracellular amastigotes: IC ₅₀ : 3.1 μM	Shilling et al., 2020
		Tetrahydroaplysulphurin-1 			Intracellular amastigotes: IC ₅₀ : 3.5 μM	

(Continued)

TABLE 8 | Continued

Class	Subclass	Compound name and chemical structure	<i>Leishmania</i> species	Assay	Values	Reference
Terpenoids	Diterpenes	Membranolide  Darwinolide 	<i>L. donovani</i>	<i>In vitro</i>	Intracellular amastigotes: IC ₅₀ : 9.7 μ M	Shilling et al., 2020
Terpenoids	Diterpenes	Pukalide aldehyde 	<i>L. donovani</i>	<i>In vitro</i>	Intracellular amastigotes: 1.9 μ M	Thomas et al., 2018

^aUrsolic acid loaded N-octyl-chitosan surface decorated nanostructured lipid carrier system.

ND, Not demonstrated; SSGR, Sodium stibogluconate *L. donovani* resistant cells; PMMR, Paromomycin *L. donovani* resistant cells.

lesion size and parasite load compared to the control, achieving reductions of 75 and 95%, respectively. Serological toxicological markers were measured, indicating possible hepatotoxicity of miltefosine alone (8 mg/kg/day). However, the combination of these compounds did not show any renal or hepatic toxicity, indicating the combination scheme as a new favorable model for leishmaniasis treatment since it is effective and less toxic (Emiliano and Almeida-Amaral, 2018).

The effects of (–)-epigallocatechin 3-O-gallate (EGCG), the most abundant flavanol constituent of green tea (*Camellia sinensis* (L.) Kuntze; Theaceae) has been tested in a murine model of cutaneous leishmaniasis against promastigotes and intracellular amastigotes of *L. amazonensis* and *L. braziliensis*. Against *L. amazonensis* intracellular amastigotes, EGCG demonstrated an IC₅₀ value of 1.6 μM with a selectivity index of 129.4 (Inacio et al., 2013). When tested against *L. braziliensis*, EGCG demonstrated an IC₅₀ value of 278.8 μM for promastigotes and 3.4 μM for amastigotes with a selectivity index of 149.5 (Inacio et al., 2014). As a possible mechanism of action, EGCG increased the ROS levels, which led to a decrease in the mitochondrial membrane potential and a decrease in the ATP levels. EGCG was also tested against *L. infantum*-infected macrophages that exhibited an EC₅₀ of 2.6 μM (Inacio et al., 2019).

In vivo, EGCG was tested against a murine model of cutaneous leishmaniasis using *L. amazonensis* (Inacio et al., 2013) and *L. braziliensis* (Inacio et al., 2014) and a murine model of visceral leishmaniasis using *L. infantum* (Inacio et al., 2019). In cutaneous leishmaniasis, EGCG was able to reduce the lesion size and the parasitic load without serological toxicology. A similar effect was shown in visceral leishmaniasis; EGCG was capable of reducing the liver parasite load, presenting ED₅₀ and ED₉₀ values of 12.4 and 21.5 mg/kg/day, respectively.

It is well-known that antimonial resistance is a current problem in leishmaniasis chemotherapy. In an attempt to promote a new strategy for an old problem, flavonoids have been tested as a possible alternative for the treatment of antimonial-resistant leishmaniasis. 2'-Hydroxyflavanone (2HF), a flavanone commonly found in citric fruits, was able to reduce the infection index in BALB/c macrophages infected with wild-type or antimony-resistant *L. amazonensis* promastigotes with IC₅₀ values of 3.09 and 3.36 μM, respectively. After *in silico* analysis suggested that 2HF was a safe oral compound, the *in vivo* assay was performed. BALB/c mice were infected with wild-type or antimony-resistant *L. amazonensis* promastigotes and treated with 2HF (50 mg/kg/day). 2HF was capable of reducing the lesion size and parasite load compared to untreated and meglumine antimoniate-treated groups in both wild-type and antimony-resistant infections with no hematological or toxicological alterations (Gervazoni et al., 2018).

Several compounds isolated from leaves of *Piper rusbyi* were tested against three species of *Leishmania*. Among all the compounds tested, Flavokavain B, a chalcone, demonstrated good results against *Leishmania*. The IC₅₀ value was 11.2 μM against *L. amazonensis*, *L. donovani*, and *L. braziliensis*, which was more effective than pentamidine. Flavokavain B was also

tested *in vivo* against *L. amazonensis* infection in the footpads of BALB/c mice. With a 5 mg/kg/day subcutaneous dose, flavokavain B exhibited the best results among those tested, reducing the lesion size and being effective *in vivo* (Flores et al., 2007).

The potential activity of two biflavonoids isolated from *Selaginella sellowii*, amentoflavone and robustoflavone, was investigated against the intracellular amastigote of *L. amazonensis*. The IC₅₀ values of amentoflavone and robustoflavone were 0.2 and 5.3 μM, respectively. In addition, the production of NO decreased in the *L. amazonensis*-infected peritoneal macrophages treated with amentoflavone, while treatment with robustoflavone increased the production of NO (Rizk et al., 2014).

The genus *Mimulus* is native to California in North America. Four C-geranyl flavones (diplocone, 3'-O-methyldiplocone, yellow oil, and 3'-O-methyldiplocone) and one geranylated flavone (cannflavin A) were isolated from *Mimulus bigelovii*. The IC₅₀ value was determined to be 7.5 μg/mL for both 3'-O-methyldiplocone and yellow oil against axenic amastigotes. 3'-O-Methyldiplocone obtained an IC₅₀ value of 7.2 μg/mL, and cannflavin A obtained an IC₅₀ value of 14.6 μg/mL, both of which were also tested against axenic amastigotes (Salem et al., 2011).

Maclura tinctoria from the *Moraceae* family is a plant found in tropical countries worldwide, and its extracts are rich in flavonoids. 5,7,3',4'-Tetrahydroxy-6,8-diprenylisoflavone (CMt), an isolated flavonoid from *M. tinctoria* leaf extract, was tested against promastigotes and axenic amastigotes from *L. amazonensis* and *L. infantum*. CMt demonstrated IC₅₀ values of 2.7, 6.4, 1.1, and 2.5 μg/mL for promastigote and axenic amastigotes of *L. amazonensis* and *L. infantum*, respectively. For both *Leishmania* species, 5,7,3',4'-tetrahydroxy-6,8-diprenylisoflavone presented a selectivity index over 180. As a possible mechanism of action, CMt caused disturbances in membrane integrity and membrane potential, including increases in ROS production. In the *in vivo* model for visceral leishmaniasis, 5,7,3',4'-tetrahydroxy-6,8-diprenylisoflavone and a new formulation, such as 5,7,3',4'-tetrahydroxy-6,8-diprenylisoflavone-containing micelles (CMt/Mic), were able to reduce the parasite load in selected organs (liver, spleen, lymph node, and bone marrow) compared to the control groups and miltefosine-treated group. Cytokine analysis indicated a Th1-type response for 5,7,3',4'-tetrahydroxy-6,8-diprenylisoflavone and CMt/Mic treatment as most promising (Pereira et al., 2020).

Brachyidin A, brachyidin B, and brachyidin C, three dimeric flavonoids from *Arrabidaea brachypoda*, were evaluated against *L. amazonensis*, *L. braziliensis*, and *L. infantum* promastigotes. The most promising results were obtained for brachyidin B and brachyidin C, showing IC₅₀ values of 7.05 and 8.8 μM for *L. braziliensis* and IC₅₀ values of 9.16 and 10 μM for *L. amazonensis*. *L. amazonensis* was chosen for the anti-amastigote assay, and only brachyidin B and brachyidin C were tested, exhibiting IC₅₀ values of 2.2 and 6.25 μM, respectively. It is interesting to highlight the only structural difference between brachyidin A, brachyidin B, and brachyidin C as substitutes for the C-ring as a methoxyl group for brachyidin B and a hydroxyl group for brachyidin A. Methoxyl is

known to improve membrane permeability, which can explain the best results observed with bradydin B (Rocha et al., 2018).

To investigate possible macrophage and amastigote alterations induced by bradydin B, transmission electron microscopy was performed. Bradydin B did not generate macrophage toxicity, even at higher concentrations (20 and 50 μ M). However, for amastigotes, bradydin B induced enlargement of the Golgi apparatus, vesicle accumulation and cytoplasmic disorganization with consequent cell death (Rocha et al., 2018).

Bradydin B was administered *in vivo* in *L. amazonensis*-infected mice using two different routes: topical treatment (1% bradydin B) and oral treatment (25 and 50 mg/kg/day). The topical treatment, as well as oral treatment at 25 mg/kg/day, were not able to reduce lesion size compared to the control group. Oral treatment with 50 mg/kg/day reduced the lesion size 1 week after the start of treatment but showed no significant difference between the control group at the end of the treatment (Rocha et al., 2018).

Tryparedoxin peroxidase (Txnpx) and Trypanothione reductase (TryR) are two essential proteins for leishmania survival for their role in parasite redox metabolism. Therefore, these proteins have been considered good targets for the development of new leishmaniasis treatments (Kumar et al., 2017).

Molecular docking analysis was performed for several compounds, including such flavonoids as taxifolin, kaempferol, quercetin, and epigallocatechin-3-gallate. Quercetin and taxifolin demonstrated the highest binding energy with Txnpx. The molecular docking study also indicated that the Lys136 residue is an essential ligand that is critical for the interactions (Gundampati et al., 2014; Kumar et al., 2017).

Molecular docking was also performed using gp63, a metalloprotease found on both promastigote and amastigote surfaces, which is essential for parasite virulence and pathogenesis. This enzyme is considered a good target for leishmaniasis new treatment development. Lanaroflavone, podocarpusflavone A, amentoflavone, and podocarpusflavone B, which are known biflavonoids, had the most significant interactions in a molecular docking study performed for *L. major* and *L. panamensis* gp63. These four flavonoids demonstrated the same pattern of interactions for both *Leishmania* species. Lanaroflavone was the most promising compound of all considering binding affinity (Mercado-Camargo et al., 2020).

The flavonoids present in this section with a defined IC₅₀ are summarized in the **Table 7**.

COMPOUNDS FROM THE MEVALONATE PATHWAY

Terpenoids

Terpenoids are natural compounds derived from C5 isoprene (or isoprenoid) units. The characteristic chemical structure of these compounds contains a skeleton with 5 carbons in a head-to-tail linkage. These compounds are classified as hemiterpenes (C5), monoterpenes (C10), sesquiterpenes (C15), diterpenes (C20),

sesterterpenes (C25), triterpenes (C30), and tetraterpenes (C40). The diversity of terpenoids increases their biological activity spectrum, including several species of *Leishmania*, such as *L. major*, *L. donovani*, *L. infantum*, *L. amazonensis*, *L. braziliensis*, *L. Mexicana*, and *L. panamensis* (Yamamoto et al., 2015).

Artemisinin extracted from *Artemisia annua* and its derivatives were tested against promastigotes of *L. major*, demonstrating an IC₅₀ value of 0.75 μ M. Against intracellular amastigotes, artemisinin presented an IC₅₀ value of 3 μ M and was not toxic to the macrophages (Yang and Liew, 1993).

Artemisinin was also evaluated against *L. donovani*. The IC₅₀ value was 160 μ M against promastigotes and 22 μ M against intracellular amastigotes. Artemisinin induced apoptosis, depolarization of the mitochondrial membrane potential and DNA fragmentation. *In vivo*, using BALB/c mice infected with *L. donovani*, artemisinin was administered at 5 and 10 mg/kg/day to reduce the parasite burden in the spleen (Sen et al., 2007, 2010).

The activity of the monocyclic sesquiterpene alcohol (-)- α -bisabolol, utilized in fragrances and extracted from *Matricaria chamomilla* L., was tested against intracellular amastigotes of *L. infantum* and *L. donovani*, presenting IC₅₀ values of 56.9 and 39.4 μ M, respectively. In addition to the *in vitro* investigation, this compound was also evaluated in a visceral leishmaniasis model, and it was determined to be non-toxic when administered orally, showed no mutagenic activity, was equally distributed across the tissues and reduced the parasite load in the spleen (71.6%) and in the liver (89.2%) (Corpas-López et al., 2015).

The effect of (-)- α -bisabolol was also analyzed in *L. tropica* and *L. major*. Against intracellular amastigotes, the compound demonstrated IC₅₀ values of 25.2 μ M for *L. tropica* and 33.7 μ M for *L. major* with selectivity indices of 46 and 34, respectively. As a mechanism of action, (-)- α -bisabolol was able to increase ROS levels and decrease the mitochondrial membrane potential and phosphatidylserine exposure. In addition, in an ultrastructural analysis, the compound was capable of inducing mitochondrial disruption and chromatin condensation, indicating apoptosis (Corpas-López et al., 2016a). This mechanism of action was also observed in *L. amazonensis* and *L. infantum*. (-)- α -Bisabolol induced phosphatidylserine externalization and caused plasmatic membrane damage, both of which are apoptosis indicators. The compound also decreased ATP levels and disrupted the mitochondrial membrane potential (Hajaji et al., 2018), supporting the hypothesis that the possible mechanism of action for (-)- α -bisabolol is inducing programmed cell death.

(-)- α -Bisabolol was also analyzed *in vivo* against a murine model of cutaneous leishmaniasis using *L. tropica*. Topical formulation was capable of reducing the lesion size and parasite burden (Corpas-López et al., 2016b). (-)- α -Bisabolol was employed in a different approach in a preclinical trial for a canine leishmaniasis model using naturally infected dogs. The dogs were divided into two groups, treated with meglumine antimoniate (100 mg/kg/day) subcutaneously or (-)- α -bisabolol (30 mg/kg/day) orally. The sesquiterpene reduced the parasite load in analyzed tissues, increasing INF- γ levels without any toxicity. An evaluation of cytokines and antibodies suggests a Th1 response induced by the compound, indicating an anti-inflammatory pathway (Corpas-López et al., 2018).

Oleanolic acid and its isomer, ursolic acid (triterpenoids), were studied in promastigotes and intracellular amastigotes of *L. amazonensis*. Oleanolic acid did not demonstrate activity against promastigotes, but when its isomer was tested against promastigotes, an IC_{50} value of 6.2 $\mu\text{g/mL}$ was obtained. Ursolic acid in promastigotes of *L. amazonensis* induced programmed cell death independent of caspase 3/7 but dependent on mitochondria. When the *in vivo* assay was performed for cutaneous leishmaniasis, the compound reduced the lesion size and parasite load (Yamamoto et al., 2015).

To evaluate the effects of ursolic acid in the *in vivo* model of visceral leishmaniasis, female golden hamsters were infected with *Leishmania infantum* promastigotes. Two different doses of ursolic acid were employed, that is, 1 and 2 mg/kg/day, injected intraperitoneally for 15 days. Both doses were able to reduce the parasite load in the liver (over 96% reduction) and spleen (over 92% reduction). Histopathological analysis of the spleen indicated fewer parasites compared to the infected untreated control, and both white and red pulp were conserved by ursolic acid treatment, which was corroborated by INF- γ , IL-4, and IL-10 gene expression and splenic cell proliferation. Ursolic acid did not affect toxicological parameters (Jesus et al., 2017).

Toxicity, high cost, resistance, and reduced bioavailability are current challenges facing leishmaniasis chemotherapy. Nanotechnology has been reported as a promising alternative (Shah and Gupta, 2019). To improve ursolic acid (UA) use for leishmaniasis, a UA-loaded N-octyl-chitosan surface-decorated nanostructured lipid carrier system (UA-NLC) was tested against wild-type *L. donovani* and sodium stibogluconate (SSG-R) and paromomycin (PMM-R) *L. donovani*-resistant axenic amastigotes. UA-NLC exhibited IC_{50} values of 0.12, 1.07, and 3.51 μM for wild-type parasites, SSG-R and PMM-R, respectively, which were lower than those of regular ursolic acid (IC_{50} = 1.82, 16.15, and 36 μM , respectively). Against intracellular amastigotes, UA-NLC exhibited an IC_{50} of 0.09, 2.87, and 5.57 μM , and UA demonstrated an IC_{50} of 1.08, 11.54, and 24.46 μM for wild type, SSG-R and PMM-R, respectively (Das et al., 2017).

In the cytotoxicity evaluation, UA showed a selectivity index of 227.78, and UA-NLC showed an SI of 9111.11, almost 40 times higher. The effect of UA-NLC and regular UA *in vivo*, both administered orally at 10 mg/kg, was assessed. Spleen amastigote suppression was evaluated for wild-type, SSG-R- and PMM-R-infected mice. UA exhibited a percentage of suppression of 68.14, 64.69, and 59.55%, respectively, while UA-NLC achieved better results with 98.75, 88.4, and 90.37%, respectively. All these results suggest that UA-NLC and nanodelivery systems are a promising approach for leishmaniasis chemotherapy (Das et al., 2017).

The Antarctic sponge *Dendrilla membranosa* and other similar species have been a rich source for chemical studies. *Dendrilla antarctica* sponges, as named by Shilling et al. (2020), exhibit a variety of diterpenes in their composition, such as aplysulphurin (1), tetrahydroaplysulphurin-1 (2), membranolid (3), and darwinolid (4). These compounds were evaluated against *Leishmania donovani*-infected macrophages and J774 cells for cytotoxicity assays. Compounds 1 and 2 had the most promising IC_{50} values, 3.1 and 3.5 μM , respectively, while 3 and

4 exhibited values above 10 μM . However, the selective index for compound 1 was less than 10, while for compounds 2, 3, and 4, it was higher than 30 (Shilling et al., 2020).

Plumarella delicatissima is an octocoral specimen of the Southern Ocean known as a source of bioactive terpenoids. Seven terpenoids, (keikipukalide A-E, pukalide aldehyde, and ineleganolide), were isolated from *Plumarella* sp. and analyzed against *L. donovani* amastigote. Pukalide aldehyde was the most promising compound, exhibiting an IC_{50} value of 1.9 μM . X-ray crystallography of all isolated terpenoids indicates the differences between *Pulmarella* sp. terpenoid chemical structure, which is an important first step in structure-activity studies that should be conducted in further research (Thomas et al., 2018).

Using a novel and different approach, Ogungbe and Setzer (2013) studied potential *in silico* targets for terpenoids in *Leishmania*. Unlike *in vitro* and *in vivo* approaches, *in silico* approaches are able to predict different aspects of a potential bioactive compound, such as its possible targets, best radicals or chemical structure, for better antileishmanial activity. Molecular docking analysis was performed for several known antiparasitic plant-derived terpenoids. Each terpenoid class studied was docked with each chosen *Leishmania* species (*L. infantum*, *L. Mexicana*, *L. major*, and *L. donovani*). The most promising targets were nicotinamidase (*L. infantum*), uridine diphosphate-glucose pyrophosphorylase, methionyl t-RNA synthetase and dihydroorotate dehydrogenase (*L. major*), glycerol-3-phosphate dehydrogenase (*L. mexicana*) for the matching terpenoid classes. Furthermore, these results may help to guide new research on the development of new potent antileishmanial terpenoids (Ogungbe and Setzer, 2013).

The terpenoids present in this section with a defined IC_{50} are summarized in the **Table 8**.

DISCUSSION

Although leishmaniasis are a group of diseases that have drug-based treatments, it remains a major challenger to research fields, since the currently available drug arsenal is reduced relative to the number of species that cause these diseases. Moreover, the chemotherapy that is utilized demands patient hospitalization and has been administered for many years, which can cause the occurrence of resistance and therapeutic failure. Therefore, research on new drugs for the treatment of these diseases is necessary.

The drug discovery process includes many steps to choose a new drug to treat a specific disease, and this process is expensive and time-consuming. Therefore, many strategies have been developed to optimize time and money.

There are 3 strategies more widely used in the drug discovery process:

- (1) Fragment drug discovery based on molecules built for purpose. In this type of approach, automated techniques are used to trial compounds (i.e., high-throughput crystallography) to identify and optimize small molecules that bind to their target proteins with a variety of binding affinities (i.e., surface plasmon

resonance). Hydrogen/deuterium exchange coupled with mass spectrometry (HDX-MS) and fragment libraries are techniques that play essential roles in this strategy. HDX-MS is a well-suited approach for investigating the alterations in protein conformation induced by small molecule ligand binding (Marciano et al., 2014). The fragment libraries identify smaller compounds, the “fragments,” which bind to different parts of a biological target. The primary rationale is that the identified hits provide access to a broader chemical space while screening a limited number of compounds (Schulz et al., 2011).

- (2) Target direct screening is a biochemical approach based on repurposing or modifying existing molecules. In this approach, gene family platforms, compound libraries, computational models/informatics, structural biology and cellular and biochemical assays are extensively used to assess whether an existing molecule can be redirected as a treatment for the disease of interest (Lage et al., 2018). Some disadvantages of target direct screening, such as drug discovery and biochemical approach fragments for trypanosomatids, are the scarcity of fully validated drug targets and the need for additional screening to avoid off-target effects (Lage et al., 2018).
- (3) Phenotypic drug discovery is a ‘physiologically relevant’ biological system or cellular signaling pathway that is directly investigated by chemical approaches to identify biologically active compounds. In contrast to the target-based strategies, these methods do not rely on knowledge of the identity of a specific drug target or a hypothesis about its role in disease. In this type of screening, advanced methodologies are able to answer many questions about a specific organic system, such as high content imaging, advanced informatics, advanced cellular assays, stem cells, SCORE, *in vivo* imaging, and the use of zebrafish models (Moffat et al., 2017).

The most widely employed methods for drug discovery against kinetoplastids are phenotypic, which is entirely justified, since the parasites have complex life cycles (the same parasite has different hosts and different forms in response to different temperatures and pH). The action of a compound on the parasite depends on its stage of life. As the drug discovery process can be developed at any stage of the parasite’s life, the results may vary widely. Generally, in the case of trypanosomatids, the infective form of the parasite in the mammalian host is chosen to perform the drug discovery process; in the case of *Leishmania* sp., it is the intracellular amastigote (Lage et al., 2018).

In this review, the extensive models utilized for the drug discovery process employ dye-based indicators of parasite viability, such as resazourin, which is used for testing the drug susceptibilities of parasites. To evaluate the mechanism of action, methodologies are generally used to measure the levels of reactive oxygen species and the type of cell death triggered by the test compound.

Recent advances in automated microscopy have the capacity to increase throughput by replacing laborious manual microscopic observations with high-content imaging, and this technique is being successfully utilized in *in vitro*

whole-organism screening against live kinetoplastid parasites (Siqueira-Neto et al., 2012). Bioinformatic tools that predict the potential of the compound as a drug, such as Linpinki’s rules, along with other tools that predict the interaction of this compound with proteins (docking assays), provide robust data to assist in choosing cell-based assays to perform and enable the exclusion of certain compounds if they do not exhibit good results *in silico*.

Despite all the advantages of automated microscopy, it is important to note that there are some limitations that still need to be overcome; for example, the complex life cycles of trypanosomatids are challenging to reproduce in the laboratory, and effectiveness in one parasitic stage does not guarantee a strong *in vivo* effect (Lage et al., 2018).

Most drug discovery screenings for anti-kinetoplastid drugs are performed with synthetic compound libraries to search for active compounds, but such synthetic libraries are often limited in structural diversity and novelty (Fox et al., 2006). Natural products may be a solution to this problem, because as was extensively discussed throughout this review, in addition to having several biological activities, they have underexplored chemical entities that may be employed as templates for the synthesis of new drugs.

Research on natural products has been increasingly conducted over the years, as these products may represent an alternative treatment of leishmaniasis and may be considered potential chemotherapy agents, since they demonstrate promising results against *Leishmania* spp. All plant metabolic pathways described in this review showed strong activity against several species of *Leishmania in vitro*, and most importantly, some compounds showed activity *in vivo* using visceral and cutaneous leishmaniasis models of infection, which were often better than the results presented by the reference drugs.

Concerning the mechanism of action of these natural products, several compounds are capable of altering the mitochondrial membrane potential, causing an increase in intracellular ROS levels and a decrease in ATP concentration and leading to programmed cell death. Furthermore, using molecular docking approaches, some molecules were capable of interacting with important enzymes for the redox homeostasis of *Leishmania*, such as trypanothione reductase and trypanothione synthetase; however, it is important to demonstrate the inhibition of these activities by the selected molecules using recombinant enzymes. *In vivo*, some natural compounds were observed to reduce the parasite load and to act as immunomodulators.

In this scenario, it is possible that these compounds may be employed as a source of new treatments for leishmaniasis in the future, adding to the treatments already administered in the clinic.

AUTHOR CONTRIBUTIONS

All authors listed have made a substantial, direct and intellectual contribution to the work, and approved it for publication.

FUNDING

This work was supported by Fundação Carlos Chagas Filho de Amparo a Pesquisa do Estado do Rio de Janeiro (FAPERJ), Conselho Nacional de Desenvolvimento Científico e Tecnológico (CNPq), Coordenação de Aperfeiçoamento de

Pessoal de Nível Superior (CAPES), Programa Estratégico de Apoio a Pesquisa em Saúde (PAPES/FIOCRUZ), and the Fundação Oswaldo Cruz (FIOCRUZ). EA-A was the recipient of a research scholarship from Conselho Nacional de Desenvolvimento Científico e Tecnológico (CNPq).

REFERENCES

- Azadbakht, M., Davoodi, A., Hosseini-mehr, S. J., Keighobadi, M., Fakhar, M., Valadan, R., et al. (2020). Tropolone alkaloids from *Colchicum kurdicum* (Bornm.) Stef. (Colchicaceae) as the potent novel antileishmanial compounds; purification, structure elucidation, antileishmanial activities and molecular docking studies. *Exp. Parasitol.* 213:107902. doi: 10.1016/j.exppara.2020.107902
- Bortoleti, B. T. D. S., Tomiotto-Pellissiera, F., Gonçalves, M. D., Miranda-Sapla, M. M., Assolini, J. P., Carlotto, A. C., et al. (2019). Caffeic acid has antipromastigote activity by apoptosis-like process; and anti-amastigote by TNF- α /ROS/NO production and decreased of iron availability. *Phytomedicine* 57, 262–270. doi: 10.1016/j.phymed.2018.12.035
- Brenzan, M. A., Nakamura, C. V., Prado Dias Filho, B., Ueda-Nakamura, T., Young, M. C., and Aparício Garcia Cortez, D. (2007). Antileishmanial activity of crude extract and coumarin from *Calophyllum brasiliense* leaves against *Leishmania amazonensis*. *Parasitol. Res.* 101, 715–722. doi: 10.1007/s00436-007-0542-7
- Brenzan, M. A., Santos, A. O., Nakamura, C. V., Filho, B. P., Ueda-Nakamura, T., Young, M. C., et al. (2012). Effects of (-) mamea A/BB isolated from *Calophyllum brasiliense* leaves and derivatives on mitochondrial membrane of *Leishmania amazonensis*. *Phytomedicine* 19, 223–230. doi: 10.1016/j.phymed.2011.10.008
- Brezan, M. A., Nakamura, C. V., Filho, B. P. D., Ueda-Nakamura, T., Young, M. C., Corrêa, A. G., et al. (2008). Structure-activity relationship of (-) mamea A/BB derivatives against *Leishmania amazonensis*. *Biomed. Pharmacother.* 62, 651–658. doi: 10.1016/j.biopha.2008.08.024
- Brito, J. R., Passero, L. F. D., Bezerra-Souza, A., Laurenti, M. D., Romoff, P., Barbosa, H., et al. (2019). Antileishmanial activity and ultrastructural changes of related tetrahydrofuran dineolignans isolated from *Saururus cernuus* L. (Saururaceae). *J. Pharm. Pharmacol.* 12, 1871–1878. doi: 10.1111/jph.13171
- Burza, S., Croft, S. L., and Boelaert, M. (2018). Leishmaniasis. *Lancet* 392, 951–970. doi: 10.1016/S0140-6736(18)31204-2
- Cartuche, L., Sifaoui, I., López-Arencibia, A., Bethencourt-Estrella, C. J., San Nicolás-Hernández, D., Lorenzo-Morales, J., et al. (2020). Antikinetoplastid activity of indolocarbazoles from *Streptomyces sanyensis*. *Biomolecules* 10:657. doi: 10.3390/biom10040657
- Chowdhury, S., Mukherjee, T., Mukhopadhyay, R., Mukherjee, B., Sengupta, S., Chattopadhyay, S., et al. (2012). The lignan niranthin poisons *Leishmania donovani* topoisomerase IB and favours a Th1 immune response in mice. *EMBO Mol. Med.* 4, 1126–1143. doi: 10.1002/emmm.201201316
- Corpas-López, V., Merino-Espinosa, G., Acedo-Sánchez, C., Díaz-Sáez, V., Navarro-Moll, M. C., Morillas-Márquez, F., et al. (2018). Effectiveness of the sesquiterpene (-)- α -bisabolol in dogs with naturally acquired canine leishmaniasis: an exploratory clinical trial. *Vet. Res. Commun.* 42, 121–130. doi: 10.1007/s11259-018-9714-4
- Corpas-López, V., Merino-Espinosa, G., Díaz-Sáez, V., Morillas-Márquez, F., Navarro-Moll, M. C., and Martín-Sánchez, J. (2016a). The sesquiterpene (-)- α -bisabolol is active against the causative agents of Old World cutaneous leishmaniasis through the induction of mitochondrial-dependent apoptosis. *Apoptosis* 21, 1071–1081. doi: 10.1007/s10495-016-1282-x
- Corpas-López, V., Merino-Espinosa, G., López-Viota, M., Gijón-Robles, P., Morillas-Mancilla, M. J., López-Viota, J., et al. (2016b). Topical treatment of *Leishmania tropica* infection using (-)- α -bisabolol ointment in a hamster model: effectiveness and safety assessment. *J. Nat. Prod.* 79, 2403–2407. doi: 10.1021/acs.jnatprod.6b00740
- Corpas-López, V., Morillas-Márquez, F., Navarro-Moll, M. C., Merino-Espinosa, G., Díaz-Sáez, V., and Martín-Sánchez, J. (2015). (-)- α -bisabolol, a promising oral compound for the treatment of visceral leishmaniasis. *J. Nat. Prod.* 78, 1202–1207. doi: 10.1021/np5008697
- Croft, S. L., Hogg, J., Gutteridge, W. E., Hudson, A. T., and Randall, A. W. (1992). The activity of hydroxynaphthoquinones against *Leishmania donovani*. *J. Antimicrob. Chemother.* 30, 827–832. doi: 10.1093/jac/30.6.827
- Das, S., Ghosh, S., De, A. K., and Bera, T. (2017). Oral delivery of ursolic acid-loaded nanostructured lipid carrier coated with chitosan oligosaccharides: development, characterization, *in vitro* and *in vivo* assessment for the therapy of leishmaniasis. *Int. J. Biol. Macromol.* 102, 996–1008. doi: 10.1016/j.ijbiomac.2017.04.098
- De Castro Oliveira, L. G., Brito, L. M., de Moraes Alves, M. M., Amorim, L. V., Sobrinho-Júnior, E. P., de Carvalho, C. E., et al. (2017). *In vitro* effects of the neolignan 2,3-dihydrobenzofuran against *Leishmania amazonensis*. *Basic Clin. Pharmacol. Toxicol.* 120, 52–58. doi: 10.1111/bcpt.12639
- De Sarkar, S., Sarkar, D., Sarkar, A., Dighal, A., Staniek, K., Gille, L., et al. (2018). Berberine chloride mediates its antileishmanial activity by inhibiting *Leishmania* mitochondria. *Parasitol. Res.* 118, 335–345. doi: 10.1007/s00436-018-6157-3
- Demarchi, I. G., Thomazella, M. V., de Souza Terron, M., Lopes, L., Gazim, Z. C., Cortez, D. A., et al. (2015). Antileishmanial activity of essential oil and 6,7-dehydroroyleanone isolated from *Tetradenia riparia*. *Exp. Parasitol.* 157:128–137. doi: 10.1016/j.exppara.2015.06.014
- Dewick, P. M. (ed.). (2009). “The shikimate pathway: aromatic amino acids and phenylpropanoids,” in *Medicinal Natural Products*. New Jersey: John Wiley & Sons, 137–186. doi: 10.1002/9780470742761.ch4
- Di Giorgio, C., Delmas, F., Akhmedjanova, V., Ollivier, E., Bessonova, I., Riad, E., et al. (2005). *In vitro* antileishmanial activity of diphyllin isolated from *Haplophyllum bucharicum*. *Planta Med.* 71, 366–369. doi: 10.1055/s-2005-864106
- Dimmer, J., Cabral, F. V., Sabino, C. P., Silva, C. R., Núñez-Montoya, S. C., Cabrera, J. L., et al. (2019). Natural anthraquinones as novel photosensitizers for antiparasitic photodynamic inactivation. *Phytomedicine* 61:152894. doi: 10.1016/j.phymed.2019.152894
- DNDi (2016). Available online at: <https://www.dndi.org/diseases-projects/leishmaniasis/> (accessed December, 2016).
- Durak, S., Arasoglu, T., Ates, S. C., and Derman, S. (2020). Enhanced antibacterial and antiparasitic activity of multifunctional 2 polymeric nanoparticles. *Nanotechnology* 31:5705. doi: 10.1088/1361-6528/ab6ab9
- Emiliano, Y. S. S., and Almeida-Amaral, E. E. (2018). Efficacy of apigenin and miltefosine combination therapy against experimental cutaneous leishmaniasis. *J. Nat. Prod.* 81, 1910–1913. doi: 10.1021/acs.jnatprod.8b00356
- Ferreira, M. E., Rojas de Arias, A., Yaluff, G., de Bilbao, N. V., Nakayama, H., Torres, S., et al. (2010). Antileishmanial activity of furoquinolines and coumarins from *Helietta apiculata*. *Phytomedicine* 17, 375–378. doi: 10.1016/j.phymed.2009.09.009
- Ferreira, T. N., Pita-Pereira, D., Costa, S. G., Brazil, R. P., Moraes, C. S., Diaz-Albiter, H. M., et al. (2018). Transmission blocking sugar baits for the control of *Leishmania* development inside sand flies using environmentally friendly beta-glycosides and their aglycones. *Parasit. Vectors* 11:614. doi: 10.1186/s13071-018-3122-z
- Flores, N., Cabrera, G., Jiménez, I. A., Piñero, J., Giménez, A., Bourdy, G., et al. (2007). Leishmanicidal constituents from the leaves of *Piper rusbyi*. *Planta Med.* 73, 206–211. doi: 10.1055/s-2007-967123
- Fonseca-Silva, F., Canto-Cavaleiro, M. M., Menna-Barreto, R. F. S., and Almeida-Amaral, E. E. (2015). Effect of apigenin on *Leishmania amazonensis* is associated with reactive oxygen species production followed by mitochondrial dysfunction. *J. Nat. Prod.* 78, 880–884. doi: 10.1021/acs.jnatprod.5b00011

- Fonseca-Silva, F., Inacio, J. D. F., Canto-Cavalheiro, M. M., and Almeida-Amaral, E. E. (2013). Reactive oxygen species production by quercetin causes the death of *Leishmania amazonensis* intracellular amastigotes. *J. Nat. Prod.* 76, 1505–1508. doi: 10.1021/np400193m
- Fonseca-Silva, F., Inacio, J. D. F., Canto-Cavalheiro, M. M., Menna-Barreto, R. F., and Almeida-Amaral, E. E. (2016). Oral efficacy of apigenin against cutaneous leishmaniasis: involvement of reactive oxygen species and autophagy as a mechanism of action. *PLoS Negl. Trop. Dis.* 10:e0004442. doi: 10.1371/journal.pntd.0004442
- Fox, S., Farr-Jones, S., Sopchak, L., Boggs, A., Nicely, H. W., Khoury, R., et al. (2006). High-throughput screening: update on practices and success. *J. Biomol. Screen* 11, 864–869. doi: 10.1177/1087057106292473
- Garcia, A. R., Oliveira, D. M. P., Amaral, A. C. F., Jesus, J. B., Rennó Sodero, A. C., Souza, A. M. T., et al. (2019). *Leishmania infantum* arginase: biochemical characterization and inhibition by naturally occurring phenolic substances. *J. Enzyme Inhib. Med. Chem.* 34, 1100–1109. doi: 10.1080/14753666.2019.1616182
- Garnier, T., Mäntylä, A., Järvinen, T., Lawrence, J., Brown, M., and Croft, S. (2007). *In vivo* studies on the antileishmanial activity of buparvaquone and its prodrugs. *J. Antimicrob. Chemother.* 60, 802–810. doi: 10.1093/jac/dkm303
- Gervazoni, L. F. O., Gonçalves-Ozório, G., and Almeida-Amaral, E. E. (2018). 2'-Hydroxyflavanone activity in vitro and in vivo against wild-type and antimony-resistant *Leishmania amazonensis*. *PLoS Negl. Trop. Dis.* 12: e0006930. doi: 10.1371/journal.pntd.0006930
- Gundampati, R. K., Sahu, S., Shukla, A., Pandey, R. K., Patel, M., Banik, R. M., et al. (2014). Tryparedoxin peroxidase of *Leishmania braziliensis*: homology modeling and inhibitory effects of flavonoids for anti-leishmanial activity. *Bioinformation* 10, 353–357. doi: 10.6026/97320630010353
- Hajaji, S., Sifaoui, I., López-Arencibia, A., Reyes-Battle, M., Jiménez, I. A., Bazzocchi, I. L., et al. (2018). Leishmanicidal activity of α -bisabolol from Tunisian chamomile essential oil. *Parasitol. Res.* 117, 2855–2867. doi: 10.1007/s00436-018-5975-7
- Inacio, J. D. F., Canto-Cavalheiro, M. M., and Almeida-Amaral, E. E. (2013). *In vitro* and *in vivo* effects of (-)-epigallocatechin 3-O-gallate on *Leishmania amazonensis*. *J. Nat. Prod.* 76, 1993–1996. doi: 10.1021/np400624d
- Inacio, J. D. F., Fonseca, M. S., and Almeida-Amaral, E. E. (2019). (-)-Epigallocatechin 3-O-gallate as a new approach for the treatment of visceral leishmaniasis. *J. Nat. Prod.* 82, 2664–2667. doi: 10.1021/acs.jnatprod.9b00632
- Inacio, J. D. F., Gervazoni, L., Canto-Cavalheiro, M. M., and Almeida-Amaral, E. E. (2014). The effect of (-)-Epigallocatechin 3-O-gallate *in vitro* and *in vivo* in *Leishmania braziliensis*: involvement of reactive oxygen species as a mechanism of action. *PLoS Negl. Trop. Dis.* 8:e3093. doi: 10.1371/journal.pntd.0003093
- Ioset, J.-R. (2008). Natural products for neglected diseases: a review. *Curr. Org. Chem.* 12, 643–666. doi: 10.2174/138527208784577394
- Jain, P. K., and Joshi, H. (2012). Coumarin: chemical and pharmacological profile. *J. Appl. Pharm. Sci.* 2, 236–240. doi: 10.7324/JAPS.2012.2643
- Jesus, J. A., Fragoso, T. N., Yamamoto, E. S., Laurenti, M. D., Silva, M. S., Ferreira, A. F., et al. (2017). Therapeutic effect of ursolic acid in experimental visceral leishmaniasis. *Int. J. Parasitol. Drugs Drug Resist.* 7, 1–11. doi: 10.1016/j.ijddr.2016.12.002
- Kashyap, D., Sharma, A., Tuli, H. S., Sak, K., Garg, V. K., Buttar, H. S., et al. (2018). Apigenin: a natural bioactive flavone-type molecule with promising therapeutic function. *J. Funct. Foods* 48, 457–471. doi: 10.1016/j.jff.2018.07.037
- Kumar, A., Saha, B., and Singh, S. (2017). Dataset generated for dissection of mechanisms of trypanothione reductase and tryparedoxin peroxidase through dynamic network analysis and simulations in leishmaniasis. *Data Brief.* 15, 757–769. doi: 10.1016/j.dib.2017.10.031
- Kurek, J. (ed.). (2019). *Introductory Chapter: Alkaloids - Their Importance in Nature and for Human Life, Alkaloids - Their Importance in Nature and Human Life*. IntechOpen. Available online at: <https://www.intechopen.com/books/alkaloids-their-importance-in-nature-and-for-human-life/introductory-chapter-alkaloids-their-importance-in-nature-and-for-human-life>
- Lacerda, R. B. M., Freitas, T. R., Martins, M. M., Teixeira, T. L., da Silva, C. V., Candido, P. A., et al. (2018). Isolation, leishmanicidal evaluation and molecular docking simulations of piperidine alkaloids from *Senna spectabilis*. *Bioorg. Med. Chem.* 26, 5816–5823. doi: 10.1016/j.bmc.2018.10.032
- Lage, O. M., Ramos, M. C., Calisto, R., Almeida, E., Vasconcelos, V., and Vicente, F. (2018). Current screening methodologies in drug discovery for selected human diseases. *Mar. Drugs* 16:279. doi: 10.3390/md16080279
- Lezama-Dávila, C. M., McChesney, J. D., Bastos, J. K., Miranda, M. A., Tiossi, R. F., da Costa J. C., et al. (2016). A new antileishmanial preparation of combined solamargine and solasonine heals cutaneous leishmaniasis through different immunochemical pathways. *Antimicrob. Agents Chemother.* 60, 2732–2738. doi: 10.1128/AAC.02804-15
- Lizzi, F., Veronesi, G., Belluti, F., Bergamini, C., López-Sánchez, A., Kaiser, M., et al. (2012). Conjugation of quinones with natural polyamines: toward an expanded antitrypanosomatid profile. *J. Med. Chem.* 55, 10490–10500. doi: 10.1021/jm301112z
- Mahalakshmi, A. M., and Nidavani, R. B. (2014). *Physalis angulata* L.: an ethnopharmacological review. *Indo Am. J. Pharm. Res.* 4, 1479–1486. doi: 10.1044/1980-iajpr.14337
- Maia, M. S., Silva, J. P. R., Nunes, T. L., Sousa, J. M. S., Rodrigues, G. C. S., Monteiro, A. F. M., et al. (2020). Virtual screening and the *in vitro* assessment of the antileishmanial activity of lignans. *Molecules* 25:2281. doi: 10.3390/molecules25102281
- Manjolin, L. C., dos Reis, M. B., do Maquiaveli, C. C., Santos-Filho, O. A., and da Silva, E. R. (2013). Dietary flavonoids fisetin, luteolin and their derived compounds inhibit arginase, a central enzyme in *Leishmania (Leishmania) amazonensis* infection. *Food Chem.* 141, 2253–2262. doi: 10.1016/j.foodchem.2013.05.025
- Mäntylä, A., Garnier, T., Rautio, J., Nevalainen, T., Vepsäläinen, J., Koskinen, A., et al. (2004). Synthesis, *in vitro* evaluation, and antileishmanial activity of water-soluble prodrugs of buparvaquone. *J. Med. Chem.* 47, 188–195. doi: 10.1021/jm030868a
- Marciano, D. P., Dharmarajan, V., and Griffin, P. R. (2014). HDX-MS guided drug discovery: small molecules and biopharmaceuticals. *Curr. Opin. Struct. Biol.* 28, 105–111. doi: 10.1016/j.sbi.2014.08.007
- Meanwell, N. A. (2011). Improving drug candidates by design: a focus on physicochemical properties as a means of improving compound disposition and safety. *Chem. Res. Toxicol.* 24, 1420–1456. doi: 10.1021/tx200211v
- Mehwish, S., Khan, H., Rehman, A. U., Khan, A. U., Khan, M. A., Hayat, O., et al. (2019). Natural compounds from plants controlling leishmanial growth via DNA damage and inhibiting trypanothione reductase and trypanothione synthetase: an *in vitro* and *in silico* approach. *3 Biotech* 9:303. doi: 10.1007/s13205-019-1826-1
- Mercado-Camargo, J., Cervantes-Ceballos, L., Vivas-Reyes, R., Pedretti, A., Serrano-García, M. L., and Gómez-Estrada, H. (2020). Homology modeling of leishmanolysin (gp63) from *Leishmania panamensis* and molecular docking of flavonoids. *ACS Omega* 5, 14741–14749. doi: 10.1021/acsomega.0c01584
- Moffat, J., Vincent, F., Lee, J., Eder, J., and Prunotto, M. (2017). Opportunities and challenges in phenotypic drug discovery: an industry perspective. *Nat. Rev. Drug Discov.* 16, 531–543. doi: 10.1038/nrd.2017.111
- Monteiro, L. M., Löbenberg, R., Fotaki, N., de Araújo, G. L. B., Cotrim, P. C., and Bou-Chacra, N. (2019). Co-delivery of buparvaquone and polymyxin B in a nanostructured lipid carrier for leishmaniasis treatment. *J. Glob. Antimicrob. Resist.* 8, 279–283. doi: 10.1016/j.jgar.2019.06.006
- Montrieux, E., Perera, W. H., García, M., Maes, L., Cos, P., and Monzote, L. (2014). *In vitro* and *in vivo* activity of major constituents from *Pluchea carolinensis* against *Leishmania amazonensis*. *Parasitol. Res.* 113, 2925–2932. doi: 10.1007/s00436-014-3954-1
- Morales-Jadán, D., Blanco-Salas, J., Ruiz-Téllez, T., and Centeno, F. (2020). Three alkaloids from an apocynaceae species, *Aspidosperma spruceanum* as antileishmaniasis agents by *in silico* demo-case studies. *Plants* 9:E983. doi: 10.3390/plants9080983
- Muzitano, M. F., Falcão, C. A. B., Cruz, E. A., Bergonzi, M. C., Bilia, A. R., Vincieri, F. F., et al. (2009). Oral metabolism and efficacy of *Kalanchoe pinnata* flavonoids in a murine model of cutaneous

- leishmaniasis. *Planta Med.* 75, 307–311. doi: 10.1055/s-0028-1088382
- Nogueira, R. C., Rocha, V. P. C., Nonato, F. R., Tomassini, T. C., Ribeiro, I. M., dos Santos, R. R., et al. (2013). Genotoxicity and antileishmanial activity evaluation of *Physalis angulata* concentrated ethanolic extract. *Environ. Toxicol. Pharmacol.* 36, 1304–1311. doi: 10.1016/j.etap.2013.10.013
- Ogungbe, I. V., and Setzer, W. N. (2013). *In-silico* Leishmania target selectivity of antiparasitic terpenoids. *Molecules* 18, 7761–7847. doi: 10.3390/molecules18077761
- Pereira, I., Mendonça, D., Tavares, G., Lage, D. P., Ramos, F. F., and Oliveira-da-Silva, J. A., et al. (2020). Parasitological and immunological evaluation of a novel chemotherapeutic agent against visceral leishmaniasis. *Parasite Immunol.* e12784. doi: 10.1111/pim.12784. [Epub ahead of print].
- Rahimi, M., Seyyed Tabaei, S. J., Ziai, S. A., and Sadri, M. (2020). Anti-leishmanial effects of chitosan-polyethylene oxide nanofibers containing berberine: an applied model for leishmania wound dressing. *Iran. J. Med. Sci.* 45, 286–297. doi: 10.30476/IJMS.2019.45784
- Randhawa, G. K., and Kullar, J. S., Rajkumar (2011). Bioenhancers from mother nature and their applicability in modern medicine. *Int. J. Appl. Basic Med. Res.* 1, 5–10. doi: 10.4103/2229-516X.81972
- Ray, L., Karthik, R., Srivastava, V., Singh, S. P., Pant, A. B., Goyal, N., et al. (2020). Efficient antileishmanial activity of amphotericin B and piperine entrapped in enteric coated guar gum nanoparticles. *Drug Deliv. Transl. Res.* doi: 10.1007/s13346-020-00712-9
- Ribeiro, T. G., Chávez-Fumagalli, M. A., Valadares, D. G., Franca, J. R., Lage, P. S., Duarte, M. C., et al. (2014). Antileishmanial activity and cytotoxicity of Brazilian plants. *Exp. Parasitol.* 143, 60–68. doi: 10.1016/j.exppara.2014.05.004
- Rizk, Y. S., Fischer, A., Cunha M de, C., Rodrigues, P. O., Marques, M. C., Matos, M. F., et al. (2014). *In vitro* activity of the hydroethanolic extract and biflavonoids isolated from *Selaginella sellowii* on Leishmania (Leishmania) amazonensis. *Mem. Inst. Oswaldo Cruz* 109, 1050–1056. doi: 10.1590/0074-0276140312
- Rocha, V. P. C., Quintino da Rocha, C., Ferreira Queiroz, E., Marcourt, L., Vilegas, W., and Grimaldi, G. B., et al. (2018). Antileishmanial activity of dimeric flavonoids isolated from *Arrabidaea brachypoda*. *Molecules* 24:1. doi: 10.3390/molecules24010001
- Rodrigues, L. C., Barbosa-Filho, J. M., de Oliveira, M. R., do Nascimento Nêris, P. L., Borges, F. V., and Mioso, R. (2016). Synthesis and antileishmanial activity of natural dehydriedeugenol and its mono- and dimethyl ethers. *Chem. Biodivers.* 13, 870–874. doi: 10.1002/cbdv.201500280
- Rye, C. E., and Barker, D. (2013). Asymmetric synthesis and anti-protozoal activity of the 8,40-oxynolignans virolin, surinamensin and analogues. *Eur. J. Med. Chem.* 60, 240–248. doi: 10.1016/j.ejmech.2012.12.013
- Saha, P., Sen, R., Hariharan, C., Kumar, D., Das, P., and Chatterjee, M. (2009). Berberine chloride causes a caspase-independent, apoptotic-like death in *Leishmania donovani* promastigotes. *Free Radic. Res.* 43, 1101–1110. doi: 10.1080/10715760903186124
- Saha, S., Mukherjee, T., Chowdhury, S., Mishra, A., Chowdhury, S. R., Jaisankar, P., et al. (2013). The lignan glycosides lyoniside and saracoside poison the unusual type IB topoisomerase of *Leishmania donovani* and kill the parasite both *in vitro* and *in vivo*. *Biochem. Pharmacol.* 86, 1673–1687. doi: 10.1016/j.bcp.2013.10.004
- Salem, M. M., Capers, J., Rito, S., and Werbovetz, K. A. (2011). Antiparasitic activity of C-geranyl flavonoids from *Mimulus bigelovii*. *Phyther. Res.* 25, 1246–1249. doi: 10.1002/ptr.3404
- Schmidt, T. J., Khalid, S. A., Romanha, A. J., Alves, T. M., Biavatti, M. W., Brun, R., et al. (2012a). The potential of secondary metabolites from plants as drugs or leads against protozoan neglected diseases - Part I. *Curr. Med. Chem.* 19, 2128–2175. doi: 10.2174/092986712800229023
- Schmidt, T. J., Khalid, S. A., Romanha, A. J., Alves, T. M., Biavatti, M. W., Brun, R., et al. (2012b). The potential of secondary metabolites from plants as drugs or leads against protozoan neglected diseases - Part II. *Curr. Med. Chem.* 19, 2176–2228. doi: 10.2174/092986712800229087
- Schulz, M. N., Landstro, J. M., Bright, B., and Hubbard, R. E. (2011). Design of a Fragment Library that maximally represents available chemical space. *J. Comput. Aided Mol. Des.* 25, 611–620. doi: 10.1007/s10822-011-9461-x
- Sen, R., Bandyopadhyay, S., Dutta, A., Mandal, G., Ganguly, S., Saha, P., et al. (2007). Artemisinin triggers induction of cell-cycle arrest and apoptosis in *Leishmania donovani* promastigotes. *J. Med. Microbiol.* 56, 1213–1218. doi: 10.1099/jmm.0.47364-0
- Sen, R., Ganguly, S., Saha, P., and Chatterjee, M. (2010). Efficacy of artemisinin in experimental visceral leishmaniasis. *Int. J. Antimicrob. Agents* 36, 43–49. doi: 10.1016/j.ijantimicag.2010.03.008
- Shah, A., and Gupta, S. S. (2019). Anti-leishmanial nanotherapeutics: a current perspective. *Curr. Drug Metab.* 20, 473–482. doi: 10.2174/1389200219666181022163424
- Shah, N. A., Khan, M. R., and Nadhman, A. (2014). Antileishmanial, toxicity, and phytochemical evaluation of medicinal plants collected from Pakistan. *Biomed. Res. Int.* 2014:384204. doi: 10.1155/2014/384204
- Sharma, N., Shukla, A. K., Das, M., and Dubey, V. K. (2012). Evaluation of plumbagin and its derivative as potential modulators of redox thiol metabolism of Leishmania parasite. *Parasitol. Res.* 110, 341–348. doi: 10.1007/s00436-011-2498-x
- Shilling, A. J., Witowski, C. G., Maschek, J. A., Azhari, A., Vesely, B. A., Kyle, D. E., et al. (2020). Spongian diterpenoids derived from the antarctic sponge dendrilla antarctica are potent inhibitors of the leishmania parasite. *J. Nat. Prod.* 83, 1553–1562. doi: 10.1021/acs.jnatprod.0c00025
- Silva, L. G., Gomes, K. S., Costa-Silva, T. A., Romanelli, M. M., Tempone, A. G., Sartorelli, P., et al. (2020). Calanolides E1 and E2, two related coumarins from *Calophyllum brasiliense* Cambess. (Clusiaceae), displayed *in vitro* activity against amastigote forms of *Trypanosoma cruzi* and *Leishmania infantum*. *Nat. Prod. Res.* 1478–6419. doi: 10.1080/14786419.2020.1765347. [Epub ahead of print]
- Siqueira-Neto, J. L., Moon, S., Jang, J., Yang, G., Lee, C., Moon, H. K., et al. (2012). An image-based high-content screening assay for compounds targeting intracellular *Leishmania donovani* amastigotes in human macrophages. *PLoS Negl. Trop. Dis.* 6:e1671. doi: 10.1371/journal.pntd.0001671
- Smith, L., Serrano, D. R., Mauger, M., Bolás-Fernández, F., Dea-Ayuela, M. A., and Lalatsa, A. (2018). Orally bioavailable and effective buparvaquone lipid-based nanomedicines for visceral leishmaniasis. *Mol. Pharm.* 15, 2570–2583. doi: 10.1021/acs.molpharmaceut.8b00097
- Thomas, S. A. L., von Salm, J. L., Clark, S., Ferlita, S., Nemani, P., and Azhari, A., et al. (2018). Keikipikalides, furanocembrane diterpenes from the antarctic deep sea octocoral *Plumarella delicatissima*. *J. Nat. Prod.* 81, 117–123. doi: 10.1021/acs.jnatprod.7b00732
- Tiuman, T. S., Brenzan, M. A., Ueda-Nakamura, T., Filho, B. P., Cortez, D. A., and Nakamura, C. V. (2012). Intramuscular and topical treatment of cutaneous leishmaniasis lesions in mice infected with *Leishmania amazonensis* using coumarin (-) mamea A/BB. *Phytomedicine* 19, 1196–1199. doi: 10.1016/j.phymed.2012.08.001
- Touaibia, M., Jean-Francois, J., and Doiron, J. (2012). Caffeic acid, a versatile pharmacophore: an overview. *Mini Rev. Med. Chem.* 11, 695–713. doi: 10.2174/138955711796268750
- Vianna, G. (1912). Comunicação à Sessão de 24 de abril de 1912 da Sociedade Brasileira de Dermatologia. *Arch. Bras. Med.* 1, 36–38.
- Viegas, C., Da Silva Bolzani, V., and Barreiro, E. J. (2006). OS produtos naturais e a química medicinal moderna. *Quim. Nova* 29, 326–337. doi: 10.1590/S0100-40422006000200025
- Vieira-Araújo, F. M., Macedo Rondon, F. C., Pinto Vieira, Í. G., Pereira Mendes, F. N., Carneiro de Freitas, J. C., and Maia de Moraes, S. (2018). Sinergism between alkaloids piperine and capsaicin with meglumine antimoniate against *Leishmania infantum*. *Exp. Parasitol.* 188, 79–82. doi: 10.1016/j.exppara.2018.04.001
- WHO (2016). *Global Health Observatory Data Repository*. World Health Organization. [Internet]. Available online at: <http://apps.who.int/> (accessed July 15, 2016).

- Winkel, B. S. J. (2006). "The biosynthesis of flavonoids," in *The Science of Flavonoids*, ed E. Grotewold (Columbus, Ohio: Springer), 71–96.
- Yamamoto, E. S., Campos, B. L. S., Jesus, J. A., Laurenti, M. D., Ribeiro, S. P., and Kallás, E. G., et al. (2015). The effect of ursolic acid on leishmania (*Leishmania*) amazonensis is related to programmed cell death and presents therapeutic potential in experimental cutaneous leishmaniasis. *PLoS ONE* 10:e0144946. doi: 10.1371/journal.pone.0144946
- Yang, D. M., and Liew, F. Y. (1993). Effects of qinghaosu (artemisinin) and its derivatives on experimental cutaneous leishmaniasis. *Parasitology* 106, 7–11. doi: 10.1017/S0031182000074758

Conflict of Interest: The authors declare that the research was conducted in the absence of any commercial or financial relationships that could be construed as a potential conflict of interest.

Copyright © 2020 Gervazoni, Barcellos, Ferreira-Paes and Almeida-Amaral. This is an open-access article distributed under the terms of the Creative Commons Attribution License (CC BY). The use, distribution or reproduction in other forums is permitted, provided the original author(s) and the copyright owner(s) are credited and that the original publication in this journal is cited, in accordance with accepted academic practice. No use, distribution or reproduction is permitted which does not comply with these terms.



Identification of Chalcone Derivatives as Inhibitors of *Leishmania infantum* Arginase and Promising Antileishmanial Agents

Andreza R. Garcia¹, Danielle M. P. Oliveira², Jessica B. Jesus^{1,3}, Alessandra M. T. Souza³, Ana Carolina R. Sodero³, Alane B. Vermelho⁴, Ivana C. R. Leal⁵, Rodrigo Octavio M. A. Souza⁶, Leandro S. M. Miranda⁶, Anderson S. Pinheiro^{2*} and Igor A. Rodrigues^{1,5*}

OPEN ACCESS

Edited by:

Gildardo Rivera,
Instituto Politécnico Nacional
(IPN), Mexico

Reviewed by:

Chiranjib Pal,
West Bengal State University, India
Somaditya Dey,
Government of West Bengal, India
Debarati Mukherjee,
West Bengal State University, India

*Correspondence:

Anderson S. Pinheiro
pinheiro@iq.ufrj.br
Igor A. Rodrigues
igor@pharma.ufrj.br

Specialty section:

This article was submitted to
Medicinal and Pharmaceutical
Chemistry,
a section of the journal
Frontiers in Chemistry

Received: 31 October 2020

Accepted: 14 December 2020

Published: 14 January 2021

Citation:

Garcia AR, Oliveira DMP, Jesus JB, Souza AMT, Sodero ACR, Vermelho AB, Leal ICR, Souza ROMA, Miranda LSM, Pinheiro AS and Rodrigues IA (2021) Identification of Chalcone Derivatives as Inhibitors of *Leishmania infantum* Arginase and Promising Antileishmanial Agents. *Front. Chem.* 8:624678. doi: 10.3389/fchem.2020.624678

¹ Graduate Program in Pharmaceutical Sciences, School of Pharmacy, Federal University of Rio de Janeiro, Rio de Janeiro, Brazil, ² Department of Biochemistry, Institute of Chemistry, Federal University of Rio de Janeiro, Rio de Janeiro, Brazil, ³ Department of Drugs and Medicines, School of Pharmacy, Federal University of Rio de Janeiro, Rio de Janeiro, Brazil, ⁴ Department of General Microbiology, Institute of Microbiology Paulo de Goes, Federal University of Rio de Janeiro, Rio de Janeiro, Brazil, ⁵ Department of Natural Products and Food, School of Pharmacy, Federal University of Rio de Janeiro, Rio de Janeiro, Brazil, ⁶ Department of Organic Chemistry, Institute of Chemistry, Federal University of Rio de Janeiro, Rio de Janeiro, Brazil

Arginase catalyzes the hydrolysis of L-arginine into L-ornithine and urea, acting as a key enzyme in the biosynthesis of polyamines. *Leishmania* growth and survival is dependent on polyamine biosynthesis; therefore, inhibition of *Leishmania* arginase may be a promising therapeutic strategy. Here, we evaluated a series of thirty-six chalcone derivatives as potential inhibitors of *Leishmania infantum* arginase (LiARG). In addition, the activity of selected inhibitors against *L. infantum* parasites was assessed *in vitro*. Seven compounds exhibited LiARG inhibition above 50% at 100 μ M. Among them, compounds LC41, LC39, and LC32 displayed the greatest inhibition values ($72.3 \pm 0.3\%$, $71.9 \pm 11.6\%$, and $69.5 \pm 7.9\%$, respectively). Molecular docking studies predicted hydrogen bonds and hydrophobic interactions between the most active chalcones (LC32, LC39, and LC41) and specific residues from LiARG's active site, such as His140, Asn153, His155, and Ala193. Compound LC32 showed the highest activity against *L. infantum* promastigotes (IC_{50} of $74.1 \pm 10.0 \mu$ M), whereas compounds LC39 and LC41 displayed the best results against intracellular amastigotes (IC_{50} of 55.2 ± 3.8 and $70.4 \pm 9.6 \mu$ M, respectively). Moreover, compound LC39 showed more selectivity against parasites than host cells (macrophages), with a selectivity index (SI) of 107.1, even greater than that of the reference drug Fungizone[®]. Computational pharmacokinetic and toxicological evaluations showed high oral bioavailability and low toxicity for the most active compounds. The results presented here support the use of substituted chalcone skeletons as promising LiARG inhibitors and antileishmanial drug candidates.

Keywords: *Leishmania infantum*, arginase, inhibition, chalcone, antileishmanial activity

INTRODUCTION

Leishmania infantum is the etiological agent of visceral leishmaniasis (VL), a lethal infectious disease that afflicts neglected populations mainly distributed in Africa, Asia and Latin America. Recently, the World Health Organization estimated that 30,000 new cases of VL occur worldwide (World Health Organization, 2020). Despite the global effort to develop effective vaccines and new leishmanicidal drugs, the control of this disease remains a challenge, especially as other clinical forms of leishmaniasis have emerged. Among the drug discovery strategies, the search for specific inhibitors of *Leishmania* essential enzymes has shown promising results (das Neves et al., 2019; Reguera et al., 2019).

Arginase plays a pivotal role for the survival of *Leishmania*. This enzyme acts as a binuclear manganese metalloprotease responsible for L-arginine bioconversion into ornithine, which represents the first step of the polyamine pathway. In the past few years, *Leishmania* arginase (ARG) has been proposed as a potential target for new drug candidates of natural (Girard-Thernier et al., 2015; Glisic et al., 2016; da Silva et al., 2019) or synthetic origin (Crizanto de Lima et al., 2019). Indeed, ARG inhibition affects not only the polyamine pathway and, consequently, parasite growth, but also the thiol pathway since spermidine, the final product of the polyamine pathway, is converted into trypanothione. The thiol pathway is essential for the elimination of reactive oxygen species (ROS) generated by the macrophage oxidative burst and establishment of infection (Ilari et al., 2017; Pessenda and da Silva, 2020). Previously, Muleme et al. (2009) demonstrated that *Leishmania major* ARG null mutants showed phenotypes of diminished proliferation *in vitro* (macrophage infection) and *in vivo* (Balb/C mouse infection) contexts; this finding reinforces that ARG is essential for *Leishmania* pathophysiology and is therefore an intriguing target for new therapeutics.

Chalcones, or 1,3-diaryl-2-propen-1-ones, are naturally occurring compounds belonging to the flavonoid family. They are characterized by a simple scaffold of two phenolic rings connected by a three-carbon α,β unsaturated carbonyl bridge (Rosa et al., 2019). Compounds with chalcone structures exhibit diverse biological activities and, consequently, they have attracted researchers' attention as a curious starting point for the synthesis of molecular entities with potential pharmacological properties (Gomes et al., 2017b). Indeed, antitumor, anti-inflammatory, antioxidant (Venturelli et al., 2016), and antimicrobial (Noreljaleel et al., 2018) activities have been described for natural chalcones (and derivatives thereof). Moreover, chalcone-based compounds exhibited inhibitory effects against trypanosomatids, including *Trypanosoma cruzi* and *Leishmania* (Espinoza-Hicks et al., 2019).

Previously, our group described the inhibition of *L. infantum* recombinant arginase (LiARG) by naturally occurring phenolic substances (Garcia et al., 2019). Here, we report on a new possible mechanism of action of chalcone derivatives against *L. infantum* by showing that these chemical entities inhibit LiARG. We screened a library of thirty-six synthetic chalcone derivatives against LiARG. We showed by molecular docking

that the most active inhibitors interact directly with essential residues at the enzyme's active site. Moreover, we investigated the antileishmanial effect of chalcone derivatives against the promastigote and intracellular amastigote forms of *L. infantum*, as well as their cytotoxicity, in order to determine their selectivity. Furthermore, preliminary pharmacokinetic and toxicological evaluations were performed using *in silico* approach. Finally, we evaluated the ability of chalcone derivatives to modulate the host immune response.

MATERIALS AND METHODS

Leishmania infantum Arginase (LiARG) Expression and Purification

LiARG expression and purification was performed as described previously (Garcia et al., 2019). *Escherichia coli* BL21 (DE3) cells were transformed with RP1B-LiARG. Cells were grown at 37°C until mid-exponential phase ($A_{600} \sim 0.6$). Protein expression was induced with 1 mM IPTG and cells were grown for 16 h at 30°C. Cells were harvested by centrifugation, resuspended in lysis buffer [50 mM Tris-HCl (pH 8.0), 500 mM NaCl, 5 mM imidazol, 0.1% Triton-X 100, 250 μ M PMSF, 10 mM β -mercaptoethanol] and lysed by sonication (15 cycles 60 s on and 60 s off, 100 W). The cell lysate was centrifuged (8,000 X g, 40 min, 4°C), and the clarified supernatant was loaded onto a His-Trap HP column (GE Healthcare, USA). A wash step with 100 mM manganese chloride was carried out for enzyme activation. LiARG was eluted with an imidazole gradient ranging from 5 to 500 mM. Fractions containing LiARG were pooled and dialyzed in the presence of His₆-TEV protease for removal of the N-terminal His₆ tag. A second nickel-affinity chromatography step was used to remove the His₆ tag and His₆-TEV. Finally, purified LiARG was dialyzed against [50 mM CHES (pH 9.5), 100 mM NaCl, 5 mM DTT, 250 μ M PMSF], concentrated and stored at -80°C.

Enzyme Inhibition Assay

LiARG activity was measured using the UREA CE kit (Labtest, Brazil). Urea concentration was determined spectrophotometrically (SpectraMax M5, Molecular Devices, CA) by hydrolyzing urea into ammonia and then converting ammonia into indophenol blue, which absorbs light at 600 nm (Fawcett and Scott, 1960). Enzyme activity was measured with 0.2 μ g/mL LiARG incubated with 50 mM L-arginine in 50 mM CHES (pH 9.5) at 37°C for 5 min. A set of thirty-six synthetic substituted chalcones was used to screen for potential LiARG inhibitors. Synthesis of chalcone derivatives were described previously by Ventura et al. (2015). In addition, the purity of the chalcone derivatives was determined by 200 MHz ¹H- and 50 MHz ¹³C-NMR as well as mass spectrometry (Ventura et al., 2015). For inhibitor screening, the concentration of chalcone derivatives was kept fixed at 100 μ M. Quercetin (100 μ M) was used as a reference arginase inhibitor (da Silva et al., 2012). Inhibitors were first dissolved in DMSO at 50 mM. Percentages of inhibition were calculated considering enzyme activity of the control (absence of inhibitor) as 100%. Control reactions were performed in the presence of the same amount of DMSO (0.1%). All measurements were performed in triplicates, at least twice

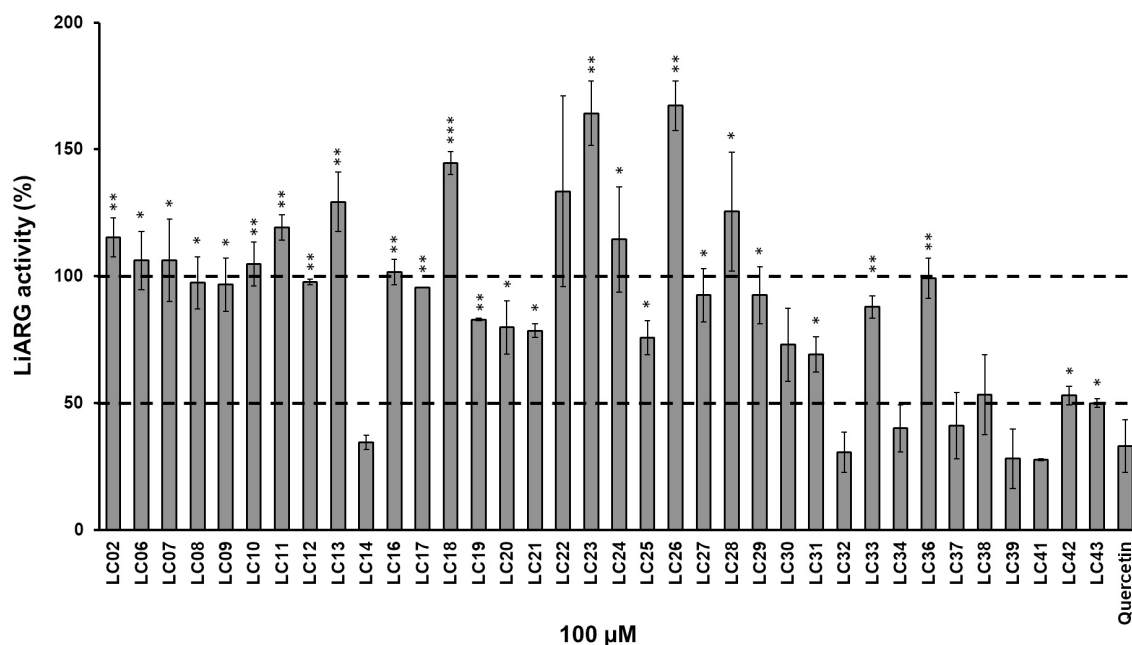


FIGURE 1 | Inhibition of LiARG by chalcone derivatives. LiARG ability to catalyze the conversion of L-arginine into urea was measured in the presence of thirty-six different chalcone derivatives at 100 μ M concentration. Quercetin (100 μ M) was used as a reference LiARG inhibitor. The control reaction was performed in the absence of any inhibitor. The results are expressed as percentage of LiARG activity taking the enzymatic activity of the control as 100%. A statistical analysis using Student's *t*-test was performed comparing each chalcone derivative to quercetin (control). *P*-values < 0.05 (one asterisk), <0.005 (two asterisks) and <0.0005 (three asterisks) were considered significantly different from the control. The dashed lines represent 100% (control) and 50% LiARG activity, which is the cutoff used for selection of the best inhibitors.

independently. The chalcone derivatives that showed inhibitory activity against LiARG > 50% were selected for the biological assays (Figure 1).

Molecular Docking

To perform the molecular docking of the selected chalcone derivatives (LC32, LC39, and LC41) into the active site of LiARG, we used LiARG three-dimensional model and docking parameters from our previous work (Garcia et al., 2019). The three-dimensional structures of compounds LC32, LC39, and LC41 were constructed using the Spartan'10 software (Wavefunction Inc, CA). The enzyme:inhibitor complexes generated by molecular docking were analyzed by AutoDockTools 1.5.6 (Morris et al., 2009) and PyMOL (The PyMOL Molecular Graphics System, Version 1.4.1 Schrödinger, LLC.).

Computational Physicochemical Pharmacokinetic and Toxicological Predictions

The two-dimensional structures were drawn with ACD/ChemSketch (Osterberg and Norinder, 2001). Pharmacokinetic properties and toxicological endpoints were evaluated using qualitative and quantitative models implemented in ADMET Predictor™ software version 9.5 (Simulations Plus, Inc., Lancaster, CA, USA) (Tiwari et al., 2018; Abreu et al., 2020). Using this software, we evaluated the theoretical oral

bioavailability based on the Lipinski “rule of five” (Lipinski, 2004). In addition, the metabolic profile of the most active chalcone derivatives (LC32, LC39, and LC41) was evaluated by predicting if the derivatives could act as substrates or inhibitors of nine cytochrome P450 isoforms (CYP1A2, 2A6, 2B6, 2C8, 2C9, 2C19, 2D6, 2E1, and 3A4). The toxicological endpoints evaluated were hepatotoxicity, mutagenicity, carcinogenicity, acute toxicity, and cardiotoxicity (Pinheiro et al., 2017; Tiwari et al., 2018). Hepatotoxicity parameters were specifically studied using five relevant biomarkers, ALP, SGOT, SGPT, GGT, and LDH enzymes. Cardiac toxicity was predicted by the likelihood that a compound will block the hERG K⁺ channel. In addition, mutagenicity was predicted based on Ames Test, while carcinogenicity predicted the capability of the chalcone derivative to develop tumors in rat or mouse. Lastly, the acute toxicity prediction was based on the amount of orally administered chemical (in mg/kg body weight) required to kill 50% of the rats tested.

Cytotoxicity Assay

RAW 264.7 macrophages were cultured in DMEM medium (Sigma-Aldrich, USA) supplemented with 10% fetal bovine serum at 37°C in 5% CO₂ atmosphere. Cells were plated on 96-well microplates at a density of 10⁵ cells/well and incubated at 37°C in 5% CO₂ for 2 h. After this period, increasing concentrations of inhibitors (0.9–4,307 μ M) were added and the cultures were incubated at 37°C in 5%

CO₂ for 48 h. Subsequently, cell viability was measured by a colorimetric assay using 3-(4,5-dimethylthiazol-2-yl)-2,5-diphenyl tetrazolium bromide (MTT) (Sigma-Aldrich, USA). MTT was added to the culture medium at a final concentration of 1.0 mg/mL, and cultures were incubated at 37°C in 5% CO₂ for 3 h. MTT was transformed by the living cells in formazan crystals that were dissolved in DMSO. The concentration of formazan was measured spectrophotometrically at 570 nm (SpectraMax M5, Molecular Devices, CA). The 50% cytotoxic concentration (CC₅₀) values were determined by the nonlinear regression fits of the dose-response curves using GraphPad Prism 8.0. All measurements were performed in triplicates, twice independently.

Activity Against *Leishmania infantum* Promastigotes

Promastigotes of *Leishmania infantum* strain MHOM/BR/1974/PP75 were cultured in Schneider's medium supplemented with 10% fetal bovine serum at 26°C. First, the selected LiARG inhibitors were diluted in culture medium at concentrations ranging from 2.9 to 1,723.0 µM. Then, late-exponential phase (after 96 h growth) *L. infantum* promastigotes, at a final density of 10⁵ parasites/mL, were incubated with previously diluted inhibitors at 26°C for 96 h. Subsequently, parasite viability was determined by a colorimetric assay using resazurin (Sigma-Aldrich, USA). Resazurin was added to the culture medium at a final concentration of 0.001% (w/v), and cultures were further incubated at 26°C for 4 h (Rólon

et al., 2006). Resazurin is reduced to resorufin by living cells, and the relative concentration of resorufin/resazurin was measured spectrophotometrically at 570/600 nm (SpectraMax M5, Molecular Devices, CA), respectively. Fungizone[®] (2.0–650.0 nM) was used as the reference drug. The 50% inhibitory concentration (IC₅₀) values were determined by the nonlinear regression fits of the dose-response curves using GraphPad Prism 8.0. All measurements were performed in triplicates, twice independently.

Activity Against *Leishmania infantum* Amastigotes

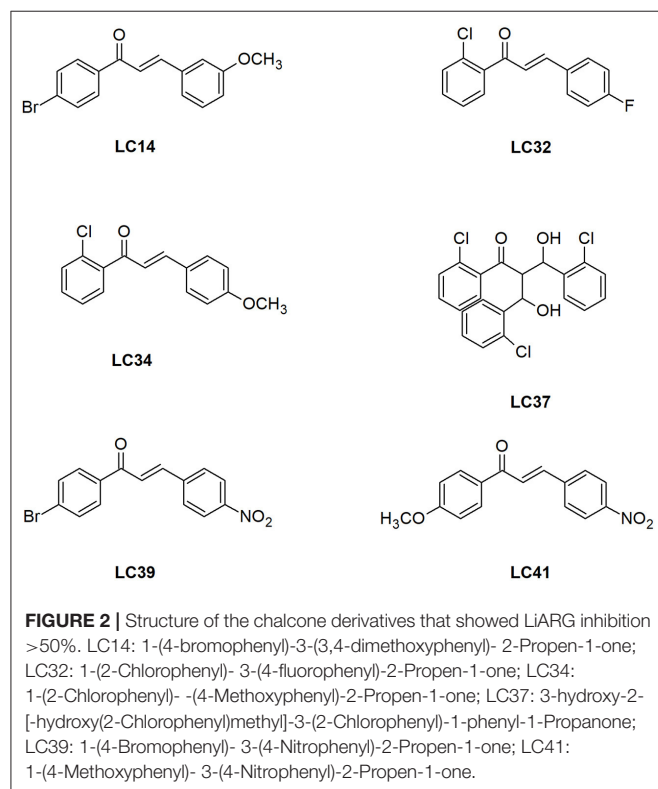
Intracellular anti-amastigote activity was determined using the promastigote recovery assay with minor modifications (Ferreira et al., 2017). RAW 264.7 macrophages were plated on 96-well microplates at a density of 10⁵ cells/well and incubated at 37°C in 5% CO₂ for 2 h. After this period, adherent cells were washed twice with phosphate buffered saline (PBS, pH 7.2) and infected with stationary-phase *L. infantum* promastigotes at a 10:1 parasite/macrophage ratio. After 4 h of infection at 37°C in 5% CO₂, free parasites were removed by a wash step with PBS and infected macrophages were incubated for an additional 24 h to allow parasite differentiation into amastigotes. Then, infected cells were treated with increasing concentrations of selected LiARG inhibitors (11.0–54.0 µM) for 48 h. After this period, the culture supernatant was collected for the evaluation of NO production by the Griess reaction (Misko et al., 1993), and cells were washed with PBS. Subsequently, PBHIL medium supplemented with 5% fetal bovine serum was added and the cultures were incubated at 26°C for 72 h to recover *L. infantum* promastigotes. Only viable amastigotes can differentiate into promastigotes. Then, parasite viability was determined by a colorimetric assay using MTT (1.0 mg/mL) (Sigma-Aldrich, USA), as described earlier. Fungizone[®] (130–540 nM) was used as the reference drug. Results were expressed as percentages of viability in relation to the control (100% viability). The 50% inhibitory concentration (IC₅₀) values were determined by the nonlinear regression fits of the dose-response curves using GraphPad Prism 8.0. All measurements were performed in triplicates, twice independently.

Selectivity Index

The selectivity index for promastigotes and intracellular amastigotes of *L. infantum* was calculated by taking the ratio between the CC₅₀ obtained for the host cell and the IC₅₀ obtained for the parasite. Inhibitors displaying selectivity index > 10 were considered low cytotoxic (Katsuno et al., 2015).

Statistical Analysis

Statistical analysis was determined based on Student *t*-test and one-way ANOVA with Tukey's comparison post-test using the GraphPad Prism 8.0 software, considering *p* < 0.05 as significant.



RESULTS AND DISCUSSION

LiARG Inhibition by Chalcone Derivatives

First, we investigated the inhibitory activity of a set of thirty-six chalcone derivatives, containing different substituents on rings A and B (Ventura et al., 2015), against purified recombinant LiARG. All compounds were tested at a final concentration of 100 μ M. **Figure 1** shows the percentages of inhibition exhibited by the thirty-six chalcone derivatives tested against LiARG. The previously known arginase inhibitor quercetin was used as a positive control (da Silva et al., 2012). A total of 16 chalcones showed inhibitory activity against LiARG. We highlight the compounds that displayed percentages of inhibition > 50%: LC14, LC32, LC34, LC37, LC39, and LC41. Chalcones LC41, LC39, and LC32 inhibited $72.3 \pm 0.3\%$, $71.9 \pm 11.6\%$, and $69.5 \pm 7.9\%$ of LiARG activity, respectively, presenting an inhibitory potential greater than that of the reference inhibitor quercetin ($67.1 \pm 10.3\%$). In addition, LC14 exhibited an inhibitory activity of $65.4 \pm 2.8\%$, while LC34 and LC37 inhibited 59.9 ± 9.2 and $58.9 \pm 9.2\%$ of LiARG activity, respectively (**Figure 1**).

Chen et al. (2001) showed that licochalcone A was able to inhibit *L. major* and *L. donovani* fumarate reductase, an enzyme that acts in the respiratory chain of the parasites. In addition, this compound also inhibited NADH dehydrogenase and succinate dehydrogenase of *L. major*. Moreover, the compound 2',4'-dihydroxychalcone was reported as a potent inhibitor of glycerol-3-phosphate dehydrogenase from *L. amazonensis* (Passalacqua et al., 2015). The compounds 2',4,4'-trihydroxy-3,3'-diprenylchalcone (bipinnatone A) and 2',4,4'-trihydroxy-3',5'-iprenylchalcone (bipinnatone B) proved to be potential inhibitors of the same enzyme in an *in silico* study (Ogungbe et al., 2014). Recently, da Silva et al. (2019) demonstrated that flavonoids structurally related to quercetin inhibit *Leishmania amazonensis* arginase (LaARG). Among the flavonoids tested, taxifolin showed the most effective inhibition result (88%) at 100 μ M. Although chalcones and chalcone-based compounds have been described as inhibitors of other *Leishmania* enzymes, to the best of our knowledge, this is the first report on the inhibition of *Leishmania* arginase by this class of flavonoids.

Previously, a synthetic chalcone [(E)-1-(2-methoxy-4-((3-methylbut-2-en-1-yl)oxy)phenyl)-3-(4-nitrophenyl)prop-2-en-1-one] with a prenyloxy group in ring A and a nitro group in ring B demonstrated a potent inhibitory activity against *Leishmania* trypanothione reductase (Ortalli et al., 2018). Here, all chalcone derivatives containing a nitro group at position 4 of ring B were able to inhibit LiARG, especially LC39 and LC41. Indeed, the presence of a nitro group in ring B was previously correlated with a strong antileishmanial activity and selectivity (de Mello et al., 2018).

Structural Characterization of Chalcone Derivatives Interaction With LiARG

To gain further insights into the mechanism of inhibition, the three most active chalcone derivatives, those with percentages of inhibition greater than that of quercetin (LC32, LC39, and LC41) (**Figure 2**), were docked into the active site of LiARG. For the molecular docking studies, we used the three-dimensional model

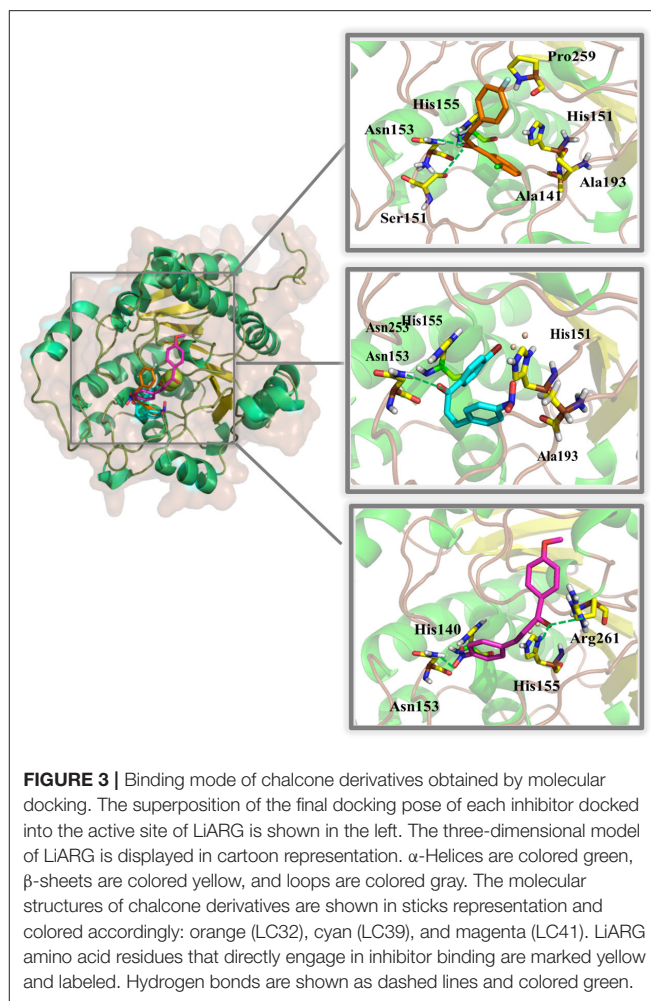


FIGURE 3 | Binding mode of chalcone derivatives obtained by molecular docking. The superposition of the final docking pose of each inhibitor docked into the active site of LiARG is shown in the left. The three-dimensional model of LiARG is displayed in cartoon representation. α -Helices are colored green, β -sheets are colored yellow, and loops are colored gray. The molecular structures of chalcone derivatives are shown in sticks representation and colored accordingly: orange (LC32), cyan (LC39), and magenta (LC41). LiARG amino acid residues that directly engage in inhibitor binding are marked yellow and labeled. Hydrogen bonds are shown as dashed lines and colored green.

of LiARG previously constructed by our group using comparative modeling (Garcia et al., 2019).

The binding modes of LC32, LC39, and LC41 showed estimated binding energy values of -4.42 , -6.91 , and -3.80 kcal/mol, respectively (**Figure 3**). The docking results suggested that LC32 interacts with the active site of LiARG through three possible hydrogen bonds between the oxygen atom of the compound's carbonyl group and the polar side chains of residues Ser151 (OH—O distance of 2.8Å), Asn153 (NH—O distance of 1.9Å) and His155 (NH—O distance of 2.1Å). Moreover, the 2-chlorophenyl group makes van der Waals and hydrophobic interactions with His140, Ala 141, Ser151, Ala193, and Pro259 (**Figure 3**). In contrast, LC39 makes one hydrogen bond between its carbonyl group and the nitrogen atom of Asn153 side chain (NH—O distance of 1.9Å). In addition, LC39 interacted mainly by van der Waals and hydrophobic contacts with residues His140, His155, and Ala193 (**Figure 3**). It is worth noting that His140, Asn153, and His155 are conserved among all arginases and have been described as key residues for ligand binding with *L. mexicana* arginase (Ash, 2004; D'Antonio et al., 2013). Lastly, three hydrogen

bonds were observed for the LC41:LiARG complex. Two of them are between the compound's carbonyl group and the oxygen atom of the side chains of His155 (NH—O distance of 2.1Å) and Arg261 (NH—O distance of 2.5Å), while the third occurs between the hydroxy-imino-λ1-oxidanyl-phenyl group and the amidic nitrogen of Asn153 side chain (NH—O distance of 1.9Å). LC41 also has van der Waals interactions with His140 (**Figure 3**). Interestingly, residues Ala141, Ser151, and Ala193 occupy the same positions as Ala140, Ser150, and Ala192, respectively, in *L. mexicana* arginase, where they interact with the nor-NOHA, ABH, and BEC competitive inhibitors (da Silva et al., 2012; D'Antonio et al., 2013; Hai and Christianson, 2016). Moreover, the observed interaction between LC32 and Ala141 was also described for the rosmarinic acid:LiARG complex by molecular docking (Garcia et al., 2019). Remarkably, the chalcone derivatives exhibited more van der Waals and hydrophobic contacts with LiARG than rosmarinic acid. Glisic et al. (2016) prospected 5667 flavonoids

in the MetIDB database using an EIIP/AQVN filter and 3D QSAR. Ten compounds were selected for docking into the *Leishmania* arginase model structure, and compound 39 was selected as the best inhibitor. This compound displayed interactions with Ser150(H), Asn143(H), Asp194(H), Ala192(A), Thr257(A) residues (Glisic et al., 2016). Taken together, the results suggested that flavonoid scaffolds may be starting points for drug design aiming Leishmania ARG inhibition and disease control.

Computational Pharmacokinetic and Toxicological Evaluations of Chalcone Derivatives

In the drug design context, pharmacokinetic and toxicological properties are crucial aspects to achieve good oral bioavailability and safe drugs. Thus, the ADMET computational evaluations were carried out to compare the three chalcone derivatives

TABLE 1 | *In silico* pharmacokinetic and toxicological properties of the most active chalcones derivatives against LiARG (LC32, LC39, and LC41) and miltefosine.

Drug/Chalcones	ADMET predictor							
	Pharmacokinetic properties			Toxicological endpoints				
	CYP inhibition	CYP substrate	Rule of 5	hERG inhibitor	Hepatotoxic	Mutagenic	Carcinogenic	Acute toxicity in rats
LC32	1A2, 2C19 3A4	1A2, 2A6, 2B6, 2C8, 2C9, 2C19, 2D6, 3A4	Yes	Yes	No	No	No ^{R,M}	726.79
LC39	1A2, 2C19, 3A4-	1A2, 2A6, 2B6, 2C9, 2C19, 2D6, 2E1. 3A4	Yes	No	No	Yes	No ^{R,M}	1,568.17
LC41	1A2,3A4	1A2,2A6, 2B6, 2C9, 2D6, 2E1, 3A4	Yes	No	No	Yes	No ^{R,M}	2,374.28
Miltefosine	–	–	Yes	No	No	No	No ^{R,M}	855.10

R: rats; M: mice.

TABLE 2 | LiARG inhibition, anti-*L. infantum* activity and cytotoxicity of chalcone derivatives.

Chalcone	ARGLi inhibition (%) (100 μM)	RAW 264.7	Promastigotes	Amastigotes	Selectivity Index	
		CC ₅₀ ± SE (μM)	IC ₅₀ ± SE (μM)	IC ₅₀ ± SE (μM)	PRO	AMA
LC14	65.4 ± 2.8	75.1 ± 8.9	283.4 ± 14.2	n.d.	<1	n.d
LC32	69.5 ± 7.9	479.1 ± 19.5	74.1 ± 10.9	111.5 ± 19.8	6.5	4.3
LC34	59.9 ± 9.2	3,010.9 ± 88.0	747.2 ± 22.3	65.4 ± 10.9	4.0	46.0
LC37	58.9 ± 9.2	>4,000	>1,500	n.d.	n.d.	n.d
LC39	71.9 ± 11.6	4531.0 ± 212.0	398.0 ± 44.2	42.3 ± 17.1	11.4	107.1
LC41	72.3 ± 0.3	1,146.8 ± 58.8	319.1 ± 14.3	43.7 ± 13.7	3.6	26.2
Fungizone®	n.d	11.9 ± 0.2	0.024 ± 0.0007	0.138 ± 0.01	503.2	86.9

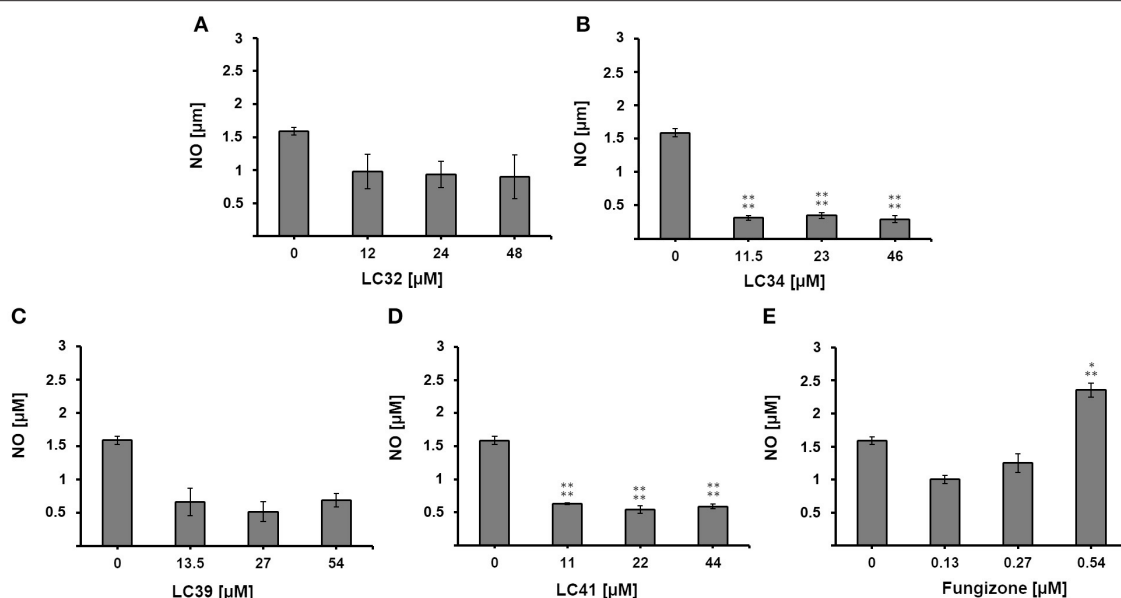


FIGURE 4 | Effect of chalcone derivatives on the production of nitric oxide by *L. infantum*-infected macrophages. *L. infantum*-infected macrophages were treated with increasing concentrations of (A–D) chalcone derivatives (11–54 μM) or (E) the reference drug fungizone (0.13–0.54 μM) and nitrite concentration was measured by the Griess reaction. Control represents the amount of nitric oxide produced by *L. infantum*-infected macrophages in the absence of any treatment. Statistical analysis of the differences between mean values obtained for the experimental groups was done by ANOVA with Tukey's *post hoc* test. P -value < 0.0005 (three asterisks), p < 0.0001 (four asterisks) were considered significantly different from the control.

with the greatest inhibitory activity against LiARG (LC32, LC39, and LC41) (Figure 2) with miltefosine, the only oral treatment available for leishmaniasis. Our results suggest that these derivatives exhibit good oral bioavailability, based on the Lipinski rule of 5 (Lipinski, 2004). In addition, LC32, LC39, and LC41 showed inhibitory potency against CYP1A2 and 3A4 and a potential to be substrates for CYP1A2, CYP2B6, CYP2C9, CYP2D6, CYP2E1, and CYP3A4 isoforms. CYP3A4 is one of the main isoforms of cytochrome P450, responsible for xenobiotic metabolism. Overall, its inhibition may cause drug-drug interactions (Tirona and Kim, 2017) (Table 1).

Concerning the toxicity endpoints evaluated, only LC32 showed potential to act as a hERG inhibitor, and thus we predicted cardiotoxicity. Fortunately, LC32, LC39, LC41, and miltefosine displayed no risks of hepatotoxicity, carcinogenicity and acute rat toxicity (Table 1). These *in silico* results support the findings of de Mello et al. (2018) that chalcones with activity against *Leishmania* generally show good pharmacokinetic and low toxicity profiles (de Mello et al., 2018). Therefore, the chalcone derivatives LC32, LC39, and LC41 may support the research and development of more effective and less toxic LiARG inhibitors.

Antileishmanial and Cytotoxic Activities of Chalcone Derivatives

After this first screening, the chalcone derivatives exhibiting more than 50% LiARG inhibition (LC14, LC32, LC34, LC37, LC39, and LC41) (Figure 2) were selected for the investigation

of their activity against the promastigote forms of *L. infantum*. Fungizone[®] was used as a reference drug control. The results demonstrated in Table 2 reveal that all selected chalcone derivatives displayed antileishmanial activity, albeit with IC_{50} values higher than that of Fungizone[®] (IC_{50} of 23.8 ± 0.7 nM). LC32 exhibited the greatest effect against *L. infantum* promastigotes with an IC_{50} of 74.1 ± 10.9 μM . Then, chalcones LC14, LC41, and LC39 showed similar IC_{50} values of 283.4 ± 14.2 , 319.1 ± 14.3 , and 398.0 ± 44.2 μM , respectively. Lastly, LC34 showed an IC_{50} of 747.2 ± 22.3 μM , and LC37 was the only chalcone derivative that did not display *in vitro* activity against *L. infantum* promastigotes at the highest concentration tested.

Next, we evaluated the cytotoxicity of the selected chalcone derivatives against RAW 264.7 macrophages, enabling us to determine their selectivity against parasite cells. LC39 showed a CC_{50} of $4,531.0 \pm 212.0$ μM and thus a SI of 11.4, proving to be more than 10 times selective against *L. infantum* promastigotes. In contrast, LC14 displayed a CC_{50} of 75.1 ± 8.9 μM (SI < 1), being more toxic to the host cell than the parasite. The chalcone derivatives LC34, LC41, and LC32 showed CC_{50} values of $3,010.9 \pm 88.0$ (SI of 4.0), $1,146.8 \pm 58.8$ (SI of 2.6), and 479.1 ± 19.5 μM (SI of 6.5), respectively. Indeed, the replacement of a bromide at position 4 of ring A of LC39 by a methoxy group in LC41 may play an important role in the cytotoxicity for macrophages. In addition, LC37, which did not show anti-*L. infantum* promastigote activity, also did not inhibit the growth of RAW 264.7 macrophages at the highest concentration tested.

Considering their anti-*L. infantum* promastigote activity and selectivity against parasite cells ($SI > 1.0$), the chalcone derivatives LC32, LC34, LC39, and LC41 were selected for the analysis of their activity against *L. infantum* intracellular amastigotes. Fungizone[®] was again used as a reference drug control. *L. infantum*-infected peritoneal macrophages were treated with the selected chalcone derivatives and the viability of promastigotes recovered from infected macrophages was measured. All chalcone derivatives were able to reduce the parasite load when compared to untreated control cells, displaying IC_{50} values of 42.3 ± 17.1 (LC39), 43.7 ± 13.7 (LC41), 65.4 ± 10.9 (LC34), and $111.5 \pm 19.8 \mu M$ (LC32) (Table 2). Maquiaveli et al. (2017) demonstrated that ARG inhibitors can interact with their target in infected macrophages. The authors reported that verbascoside, a naturally occurring caffeoyl phenylethanoid glycoside, decreased the number of intracellular amastigote forms of *L. amazonensis* by arginase inhibition. Indeed, they observed that the anti-amastigote activity of verbascoside was reversed by the addition of L-ornithin, suggesting that inhibition of parasite ARG is the most likely mode of action. Here, we provide important evidence that compounds LC32, LC34, LC39, and LC41 hamper parasite burden in macrophages by ARG inhibition. However, further investigation is still necessary in order to confirm ARG as a target in the cellular model.

Chalcone LC39 showed the lowest IC_{50} value against intracellular amastigotes, resulting in a SI of 107.1, even greater than that of the reference drug Fungizone[®] (IC_{50} of $0.138 \pm 0.01 \mu M$; SI of 86.9). It is noteworthy that a SI over 10 is considered ideal according to the hit and lead criteria in drug discovery for infectious diseases previously established by Katsuno et al. (2015). Indeed, the presence of a nitro group in ring B seems to influence the antileishmanial activity, as suggested by Gomes et al. (2017a). The authors showed that the presence of a 5-nitrofuran group in ring B enhanced the bioactivity against *L. infantum*. In this study, the elevated SI value indicates LC39 as a promising antileishmanial agent, as selectivity is a highly desired feature in leishmanicidal drugs.

The relationship between the chalcone's structure and its antileishmanial activity was recently reviewed by Tajuddeen et al. (2018). The authors reported that aryl rings, which constitute the core pharmacophores of chalcones, are essential for the bioactivity. In fact, the presence of bulky substituents at positions 2' and 3' of ring B seems to increase chalcone activity, while the same substituents at position 4' leads to a decrease in the antileishmanial effect. However, alpha propane chain α - β unsaturated seems to have low influence on the antileishmanial activity of chalcones. Interestingly, LC37, which presents substitutions in the propane chain, inhibited LiARG but displayed neither antileishmanial nor cytotoxic effects against macrophages at the highest concentrations tested.

To further investigate the nature of the antileishmanial activity, we evaluated whether treatment with the selected chalcone derivatives (LC32, LC34, LC39, and LC41) increased NO production by *L. infantum*-infected macrophages. For

this, the supernatant of infected and treated macrophages was analyzed by the Griess reaction. *In vitro* treatment with LC32 and LC41 significantly decreased the production of NO by *L. infantum*-infected macrophages when compared to the untreated control cells. In addition, LC34 and LC39 showed no significant difference to the untreated control (Figure 4). The results presented here corroborates those reported by Ventura et al. (2015), which showed the inhibition of NO production by RAW 264.7 macrophages after treatment with LC14 and LC41 (IC_{50} for NO of 58.9 ± 6.8 and $13.5 \pm 5.5 \mu M$, respectively). Indeed, previous studies have already connected the anti-inflammatory effect of chalcones to the inhibition of NO production (Ban et al., 2004; Park et al., 2009a,b; Reddy et al., 2011; Kim et al., 2013). Our results suggest that the chalcone derivatives were unable to modulate the host immune response and thus their antileishmanial activity may occur in a nitrosative stress-independent fashion, most likely directly on the parasite by inhibiting *Leishmania* arginase. ARG inhibition may lead to polyamine depletion, which may consequently affect parasite metabolism and proliferation. In addition, the enzyme inhibition could compromise the parasite redox balance, since the lack of spermidine impairs trypanothione production (Muxel et al., 2018). As a result, parasites would be more susceptible to oxygen reactive species generated by the host cell defense. Interestingly, other consequences of arginase inhibition have been suggested. Recently, transcriptomic data comparing *Leishmania amazonensis arg*⁻ to parasite wild-type (WT) revealed that arginase downregulates several virulence factors, including LPG, PPG, GP63, and amastin (Aoki et al., 2019).

CONCLUSION

We report for the first time on the ability of chalcones to inhibit *L. infantum* arginase. Among the chalcone derivatives tested against LiARG, three (LC32, LC39, and LC41) showed inhibitory potential greater than the reference inhibitor quercetin. *In silico* studies indicated the direct interaction of chalcone derivatives with LiARG's active site residues as well as their low toxicity and good oral bioavailability. In addition, the chalcone derivatives LC34, LC39, and LC41 were effective against the promastigote and intracellular amastigote forms of *L. infantum*. Remarkably, LC39 stood out for being highly selective to the parasite, even more so than the reference drug Fungizone[®]. Interestingly, our results point at the nitro group substituent in ring B as an important factor for the antileishmanial effect of chalcones, corroborating previous findings. Taken together, the results presented here bring new perspectives for *Leishmania* arginase inhibitors and the development of chalcone-based drug candidates against visceral leishmaniasis.

DATA AVAILABILITY STATEMENT

The raw data supporting the conclusions of this article will be made available by the authors, without undue reservation.

AUTHOR CONTRIBUTIONS

AV, AP, and IR designed the work. AG, JJ, AP, and IR wrote the manuscript. AG and DO performed the enzymatic assays and data analysis. AMTS, and ARS performed the *in silico* analysis. IL, RS, and LM synthesized the chalcone derivatives. AG performed the biological assays. All authors contributed to the article and approved the submitted version.

REFERENCES

- Abreu, L. C. L., Abraham-Vieira, B. A., Souza, A. M. T., Pinto, E. C., Gonçalves, M. D. S., Simon, A., et al. (2020). Forced degradation studies of norepinephrine and epinephrine from dental anesthetics: development of stability-indicating HPLC method and *in silico* toxicity evaluation. *Biomed. Chromatogr.* 34:e4832. doi: 10.1002/bmc.4832
- Aoki, J. I., Laranjeira-Silva, M. F., Muxel, S. M., and Floeter-Winter, L. M. (2019). The impact of arginase activity on virulence factors of *Leishmania amazonensis*. *Curr. Opin. Microbiol.* 52, 110–115. doi: 10.1016/j.mib.2019.06.003
- Ash, D. E. (2004). Structure and function of arginases. *J. Nutr.* 134, 760S–764S. doi: 10.1093/jn/134.10.2760S
- Ban, H. S., Suzuki, K., Lim, S. S., Jung, S. H., Lee, S., Ji, J., et al. (2004). Inhibition of lipopolysaccharide-induced expression of inducible nitric oxide synthase and tumor necrosis factor- α by 2'-hydroxychalcone derivatives in RAW 264.7 cells. *Biochem. Pharmacol.* 67, 1549–1557. doi: 10.1016/j.bcp.2003.12.016
- Chen, M., Zhai, L., Christensen, S. B., Theander, T. G., and Kharazmi, A. (2001). Inhibition of fumarate reductase in *Leishmania major* and *L. donovani* by chalcones. *Antimicrob. Agents Chemother.* 45, 2023–2029. doi: 10.1128/AAC.45.7.2023-2029.2001
- Crizanto de Lima, E., Castelo-Branco, F. S., Maquiaveli, C. C., Farias, A. B., Rennó, M. N., Boechat, N., et al. (2019). Phenylhydrazides as inhibitors of *Leishmania amazonensis* arginase and antileishmanial activity. *Bioorg. Med. Chem.* 27, 3853–3859. doi: 10.1016/j.bmc.2019.07.022
- da Silva, E. R., Brogi, S., Lucon-Júnior, J. F., Campiani, G., Gemma, S., and Maquiaveli, C. D. C. (2019). Dietary polyphenols rutin, taxifolin and quercetin related compounds target *Leishmania amazonensis* arginase. *Food Funct.* 10, 3172–3180. doi: 10.1039/C9FO00265K
- da Silva, E. R., Maquiaveli, C. D. C., and Magalhães, P. P. (2012). The leishmanicidal flavonols quercetin and quercitrin target *Leishmania (Leishmania) amazonensis* arginase. *Exp. Parasitol.* 130, 183–188. doi: 10.1016/j.exppara.2012.01.015
- D'Antonio, E. L., Ullman, B., Roberts S. C., Dixit, U. G., Wilson, M. E., Hai, Y., et al. (2013). Crystal structure of arginase from *Leishmania mexicana* and implications for the inhibition of polyamine biosynthesis in parasitic infections. *Arch. Biochem. Biophys.* 535, 163–176. doi: 10.1016/j.abb.2013.03.015
- das Neves, G. M., Kagami, L. P., Gonçalves, I. L., and Eifler-Lima, V. L. (2019). Targeting pteridine reductase 1 and dihydrofolate reductase: the old is a new trend for leishmaniasis drug discovery. *Future Med. Chem.* 11, 2107–2130. doi: 10.4155/fmc-2018-0512
- de Mello, M. V. P., Abraham-Vieira, B. A., Domingos, T. F. S., de Jesus, B., de Sousa, A. C. C., Rodrigues, C. R., et al. (2018). A comprehensive review of chalcone derivatives as antileishmanial agents. *Eur. J. Med. Chem.* 150, 920–929. doi: 10.1016/j.ejmech.2018.03.047
- Espinoza-Hicks, J. C., Chacón-Vargas, K. F., Hernández-Rivera, J. L., Nogueira-Torres, B., Tamariz, J., Sánchez-Torres, L. E., et al. (2019). Novel prenyloxy chalcones as potential leishmanicidal and trypanocidal agents: design, synthesis and evaluation. *Eur. J. Med. Chem.* 167, 402–413. doi: 10.1016/j.ejmech.2019.02.028
- Fawcett, J. W., and Scott, J. E. (1960). A rapid and precise method for the determination of urea. *J. Clin. Pathol.* 13, 156–159. doi: 10.1136/jcp.13.2.156
- Ferreira, C., Passos, C. L., Soares, D. C., Costa, K. P., Rezende, M. J., Lobão, A. Q., et al. (2017). Leishmanicidal activity of the alkaloid-rich fraction from *Gutierrezia latifolia*. *Exp. Parasitol.* 172, 51–60. doi: 10.1016/j.exppara.2016.12.014

FUNDING

This work was supported by a grant from Fundação Carlos Chagas Filho de Amparo à Pesquisa do Estado do Rio de Janeiro (FAPERJ), number E-26/202.752/2018. AG is recipient of a Fundação Carlos Chagas Filho de Amparo à Pesquisa do Estado do Rio de Janeiro (FAPERJ) graduate fellowship.

- Garcia, A. R., Oliveira, D. M., Claudia, F., Amaral, A., Jesus, J. B., Rennó Sodero, A. C., et al. (2019). *Leishmania infantum* arginase: biochemical characterization and inhibition by naturally occurring phenolic substances. *J. Enzyme Inhib. Med. Chem.* 34, 1100–1109. doi: 10.1080/14756366.2019.1616182
- Girard-Thernier, C., Pham, T. N., and Demougeot, C. (2015). The promise of plant-derived substances as inhibitors of arginase. *Mini Rev. Med. Chem.* 15, 798–808. doi: 10.2174/1389557515666150511153852
- Glisic, S., Sencanski, M., Perovic, V., Stevanovic, S., and García-Sosa, A. T. (2016). Arginase flavonoid anti-leishmanial *in silico* inhibitors flagged against anti-targets. *Molecules* 21:589. doi: 10.3390/molecules21050589
- Gomes, M. N., Alcântara, L. M., Neves, B. J., Melo-Filho, C. C., Freitas-Junior, L. H., Moraes, C. B., et al. (2017a). Computer-aided discovery of two novel chalcone-like compounds active and selective against *Leishmania infantum*. *Bioorg. Med. Chem. Lett.* 27, 2459–2464. doi: 10.1016/j.bmcl.2017.04.010
- Gomes, M. N., Muratov, E. N., Pereira, M., Peixoto, J. C., Rosseto, L. P., Cravo, P. V., et al. (2017b). Chalcone derivatives: promising starting points for drug design. *Molecules* 22:1210. doi: 10.3390/molecules22081210
- Hai, Y., and Christianson, D. W. (2016). Crystal structures of *Leishmania mexicana* arginase complexed with α,α -disubstituted boronic amino-acid inhibitors. *Acta Crystallogr. F Struct. Biol. Commun.* 72, 300–306. doi: 10.1107/S2053230X16003630
- Ilari, A., Fiorillo, A., Genovese, I., and Colotti, G. (2017). Polyamine-trypanothione pathway: an update. *Future Med. Chem.* 9, 61–77. doi: 10.4155/fmc-2016-0180
- Katsuno, K., Burrows, J. N., Duncan, K., van Huijsduijn, R. H., Takushi, K., and Kita, K. (2015). Hit and lead criteria in drug discovery for infectious diseases of the developing world. *Nat. Rev. Drug Discov.* 14, 751–758. doi: 10.1038/nrd4683
- Kim, S. J., Kim, C. G., Yun, S. R., Kim, J. K., and Jun, J. G. (2013). Synthesis of licochalcone analogues with increased anti-inflammatory activity. *Bioorg. Med. Chem. Lett.* 24, 181–185. doi: 10.1016/j.bmcl.2013.11.044
- Lipinski, C. A. (2004). Lead- and drug-like compounds: the rule-of-five revolution. *Drug Discov. Today Tech.* 1, 337–341. doi: 10.1016/j.ddtec.2004.11.007
- Maquiaveli, C. D. C., Rochetti, A. L., Fukumasu, H., Vieira, P. C., and da Silva, E. R. (2017). Antileishmanial activity of verbascoside: selective arginase inhibition of intracellular amastigotes of *Leishmania (Leishmania) amazonensis* with resistance induced by LPS plus IFN- γ . *Biochem. Pharmacol.* 127, 28–33. doi: 10.1016/j.bcp.2016.12.018
- Misko, T. P., Schilling, R. J., Salvemini, D., Moore, W. M., and Currie, M. G. (1993). A fluorometric assay for the measurement of nitrite in biological samples. *Anal. Biochem.* 214, 11–16. doi: 10.1006/abio.1993.1449
- Morris, G. M., Huey, R., Lindstrom, W., Sanner, M. F., Belew, R. K., Goodsell, D. S., et al. (2009). Autodock4 and AutoDockTools4: automated docking with selective receptor flexibility. *J. Comput. Chem.* 30, 2785–2789. doi: 10.1002/jcc.21256
- Muleme, H. M., Reguera, R. M., Berard, A., Azinwi, R., Jia, P., Okwor, I. B., et al. (2009). Infection with arginase-deficient *Leishmania major* reveals a parasite number-dependent and cytokine-independent regulation of host cellular arginase activity and disease pathogenesis. *J. Immunol.* 183, 8068–8076. doi: 10.4049/jimmunol.08.03979
- Muxel, S. M., Aoki, J. I., Fernandes, J. C. R., Laranjeira-Silva, M. F., Zampieri, R. A., Acuña, S. M., et al. (2018). Arginine and polyamines fate in *Leishmania* infection. *Front. Microbiol.* 8:2682. doi: 10.3389/fmicb.2017.02682
- Norel-Jaleel, A. E. M., Wilhelm, A., Bonnet, S. L., and van der Westhuizen, J. H. (2018). Synthesis and bioactivity of reduced chalcones containing sulfonamide side chains. *J. Nat. Prod.* 81, 41–48. doi: 10.1021/acs.jnatprod.7b00570

- Ogungbe, I. V., Erwin, W. R., and Setzer, W. N. (2014). Antileishmanial phytochemical phenolics: molecular docking to potential protein targets. *J. Mol. Graph. Model.* 48, 105–117. doi: 10.1016/j.jmgm.2013.12.010
- Ortalli, M., Ilari, A., Colotti, G., De Ionna, I., Battista, T., Bisi, A., et al. (2018). Identification of chalcone-based antileishmanial agents targeting trypanothione reductase. *Eur. J. Med. Chem.* 152, 527–541. doi: 10.1016/j.ejmech.2018.04.057
- Osterberg, T., and Norinder, U. (2001). Prediction of drug transport processes using simple parameters and PLS statistics—the use of ACD/logP and ACD/ChemSketch descriptors. *Eur. J. Pharm. Sci.* 12, 327–337. doi: 10.1016/S0928-0987(00)00189-5
- Park, P. H., Kim, H. S., Hur, J., Jin, X. Y., Jin, Y. L., and Sohn, D. H. (2009a). YL-I-108, a synthetic chalcone derivative, inhibits lipopolysaccharide-stimulated nitric oxide production in RAW 264.7 murine macrophages: involvement of heme oxygenase-1 induction and blockade of activator protein-1. *Arch. Pharm. Res.* 32, 79–89. doi: 10.1007/s12272-009-1121-5
- Park, P. H., Kim, H. S., Jin, X. Y., Jin, F., Hur, J., Ko, G., et al. (2009b). KB-34, a newly synthesized chalcone derivative, inhibits lipopolysaccharide-stimulated nitric oxide production in RAW 264.7 macrophages via heme oxygenase-1 induction and blockade of activator protein-1. *Eur. J. Pharmacol.* 606, 215–224. doi: 10.1016/j.ejphar.2008.12.034
- Passalacqua, T. G., Torres, F. A. E., Nogueira, C. T., de Almeida, L., Del Cistia, M. L., dos Santos, M. B., et al. (2015). The 2',4'-dihydroxychalcone could be explored to develop new inhibitors against the glycerol-3-phosphate dehydrogenase from *Leishmania* species. *Bioorg. Med. Chem. Lett.* 25, 3564–3568. doi: 10.1016/j.bmcl.2015.06.085
- Pessenda, G., and da Silva, J. S. (2020). Arginase and its mechanisms in *Leishmania* persistence. *Parasite Immunol.* 42:e12722. doi: 10.1111/pim.12722
- Pinheiro, M. S., Viana, G. M., Vieira, B. D. A. A., de Souza, A. M. T., Rodrigues, C. R., Rita de Cássia, E. E., et al. (2017). Identification, characterization and *in silico* ADMET prediction of Roflumilast degradation products. *J. Pharm. Biomed. Anal.* 138, 126–133. doi: 10.1016/j.jpba.2017.02.012
- Reddy, M. V., Hwang, T. L., Leu, Y. L., Chiou, W. F., and Wu, T. S. (2011). Inhibitory effects of Mannich bases of heterocyclic chalcones on NO production by activated RAW 264.7 macrophages and superoxide anion generation and elastase release by activated human neutrophils. *Bioorg. Med. Chem.* 19, 2751–2756. doi: 10.1016/j.bmc.2011.02.038
- Reguera, R. M., Elmahallawy, E. K., García-Estrada, C., Carbajo-Andrés, R., and Balaña-Fouce, R. (2019). DNA topoisomerases of *Leishmania* parasites: druggable targets for drug discovery. *Curr. Med. Chem.* 26, 5900–5923. doi: 10.2174/0929867325666180518074959
- Rólon, M., Vega, C., Escario, J. A., and Gémez-Barrio, A. (2006). Development of resazurin microtiter assay for drug sensibility testing of *Trypanosoma cruzi* epimastigotes. *J. Parasitol. Res.* 99, 103–107. doi: 10.1007/s00436-006-0126-y
- Rosa, G. P., Seca, A. M., Barreto, M. D. C., Silva, A., and Pinto, D. C. (2019). Chalcones and flavanones bearing hydroxyl and/or methoxyl groups: synthesis and biological assessments. *Appl. Sci.* 9:2846. doi: 10.3390/app9142846
- Tajuddeen, N., Isah, M. B., Suleiman, M. A., van Heerden, F. R., and Ibrahim, M. A. (2018). The chemotherapeutic potential of chalcones against leishmaniasis: a review. *Int. J. Antimicrob. Agents* 51, 311–318. doi: 10.1016/j.ijantimicag.2017.06.010
- Tirona, R. G., and Kim, R. B. (2017). Introduction to clinical pharmacology. *Clin. Trans. Sci.* (Academic Press), 365–388. doi: 10.1016/B978-0-12-802101-9.00020-X
- Tiwari, S. K., Singh, D. K., Ladumor, M. K., Chakraborti, A. K., and Singh, S. (2018). Study of degradation behaviour of montelukast sodium and its marketed formulation in oxidative and accelerated test conditions and prediction of physicochemical and ADMET properties of its degradation products using ADMET Predictor™. *J. Pharm. Biomed. Anal.* 158, 106–118. doi: 10.1016/j.jpba.2018.05.040
- Ventura, T. L., Calixto, S. D., de Azevedo Abraham-Vieira, B., de Souza, A. M., Mello, V. M., Rodrigues, C. R., et al. (2015). Antimycobacterial and anti-inflammatory activities of substituted chalcones focusing on an anti-tuberculosis dual treatment approach. *Molecules* 20, 8072–8093. doi: 10.3390/molecules20058072
- Venturelli, S., Burkard, M., Biendl, M., Lauer, U. M., Frank, J., and Busch, C. (2016). Prenylated chalcones and flavonoids for the prevention and treatment of cancer. *Nutrition* 32, 1171–1178. doi: 10.1016/j.nut.2016.03.020
- World Health Organization (2020). Leishmaniasis. Available online at <https://www.who.int/news-room/fact-sheets/detail/leishmaniasis> (accessed October 26, 2020).

Conflict of Interest: The authors declare that the research was conducted in the absence of any commercial or financial relationships that could be construed as a potential conflict of interest.

Copyright © 2021 Garcia, Oliveira, Jesus, Souza, Sodero, Vermelho, Leal, Souza, Miranda, Pinheiro and Rodrigues. This is an open-access article distributed under the terms of the Creative Commons Attribution License (CC BY). The use, distribution or reproduction in other forums is permitted, provided the original author(s) and the copyright owner(s) are credited and that the original publication in this journal is cited, in accordance with accepted academic practice. No use, distribution or reproduction is permitted which does not comply with these terms.



Discovery of Diaryl Ether Substituted Tetrahydrophthalazinones as TbrPDEB1 Inhibitors Following Structure-Based Virtual Screening

Erik de Heuvel¹, Albert J. Kooistra¹, Ewald Edink¹, Sjors van Klaveren¹, Jeffrey Stuijt¹, Tiffany van der Meer¹, Payman Sadek¹, Dorien Mabilie², Guy Caljon², Louis Maes², Marco Siderius¹, Iwan J. P. de Esch¹, Geert Jan Sterk¹ and Rob Leurs^{1*}

¹ Division of Medicinal Chemistry, Amsterdam Institute of Molecular and Life Sciences, Vrije Universiteit Amsterdam, Amsterdam, Netherlands, ² Laboratory of Microbiology, Parasitology and Hygiene, University of Antwerp, Wilrijk, Belgium

OPEN ACCESS

Edited by:

Gildardo Rivera,
Instituto Politécnico Nacional
(IPN), Mexico

Reviewed by:

Maria Paola Costi,
University of Modena and Reggio
Emilia, Italy
Marcelo Silva,
Universidade NOVA de
Lisboa, Portugal

*Correspondence:

Rob Leurs
r.leurs@vu.nl

Specialty section:

This article was submitted to
Medicinal and Pharmaceutical
Chemistry,
a section of the journal
Frontiers in Chemistry

Received: 18 September 2020

Accepted: 16 December 2020

Published: 21 January 2021

Citation:

de Heuvel E, Kooistra AJ, Edink E,
van Klaveren S, Stuijt J, van der
Meer T, Sadek P, Mabilie D, Caljon G,
Maes L, Siderius M, de Esch IJP,
Sterk GJ and Leurs R (2021)
Discovery of Diaryl Ether Substituted
Tetrahydrophthalazinones as
TbrPDEB1 Inhibitors Following
Structure-Based Virtual Screening.
Front. Chem. 8:608030.
doi: 10.3389/fchem.2020.608030

Several members of the 3',5'-cyclic nucleotide phosphodiesterase (PDE) family play an essential role in cellular processes, which has labeled them as interesting targets for various diseases. The parasitic protozoan *Trypanosoma brucei*, causative agent of human African trypanosomiasis, contains several cyclic AMP specific PDEs from which TbrPDEB1 is validated as a drug target. The recent discovery of selective TbrPDEB1 inhibitors has increased their potential for a novel treatment for this disease. Compounds characterized by a rigid biphenyl tetrahydrophthalazinone core structure were used as starting point for the exploration of novel TbrPDEB1 inhibitors. Using a virtual screening campaign and structure-guided design, diaryl ether substituted phthalazinones were identified as novel TbrPDEB1 inhibitors with IC₅₀ values around 1 μ M against *T. brucei*. This study provides important structure-activity relationship (SAR) information for the future design of effective parasite-specific PDE inhibitors.

Keywords: virtual screening, phosphodiesterase TbrPDEB1, trypanosomiasis, cAMP, tetrahydrophthalazinones, medicinal chemistry

INTRODUCTION

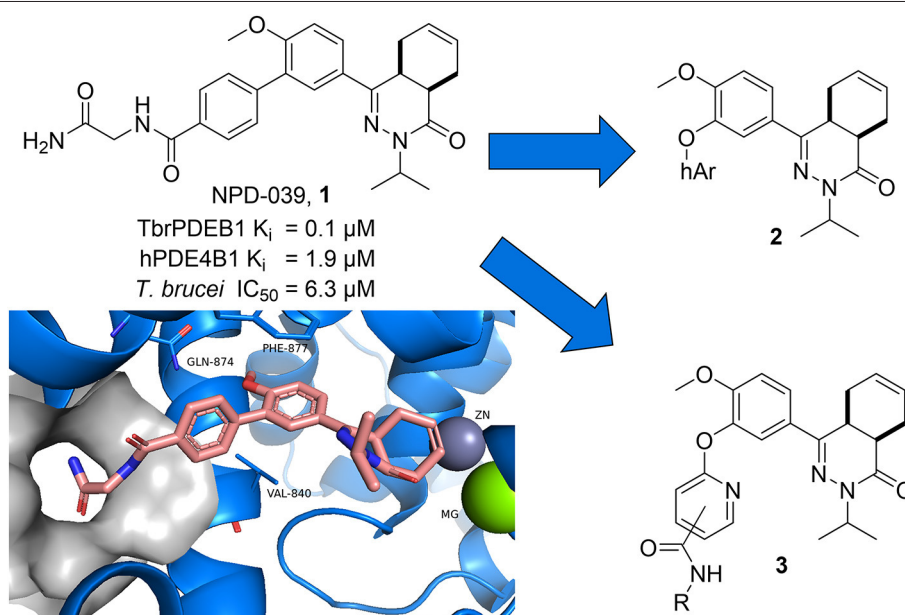
Human African trypanosomiasis, also known as African sleeping sickness, is one of the neglected tropical diseases (NTDs) listed by the WHO and is caused by the protozoan *Trypanosoma brucei* (T.b.) *rhodesiense* and *T.b. gambiense* (Büscher et al., 2017). The majority of drugs that are currently on the market for HAT have been discovered over 30 years ago and have several major disadvantages including severe toxicity, subspecies selectivity, complex administration protocols, and limited clinical efficacy (Babokhov et al., 2013; Eperon et al., 2014; Baker and Welburn, 2018). The first oral drug fexinidazole has recently been approved for HAT and will significantly improve the status of the disease (Deeks, 2019). This new therapy benefits greatly from the ease of administration, but still has some drawbacks including potential relapse and a lower efficacy for late-stage patients compared to the commonly used NECT treatment (De Morais-Teixeira et al., 2019; Pelfrene et al., 2019). In addition, the reported increasing drug resistance could have a detrimental effect on the already limited arsenal of antiprotozoal drugs (Munday et al., 2015; De Koning, 2017). The number of reported cases is slowly decreasing as a result of active screening in endemic regions, still an estimated 65 million people are at risk of infection

(World Health Organization, 2020). HAT has a history that is characterized by reoccurring epidemics and new control strategies and safer drugs are therefore still a necessity to eradicate this fatal disease (Brun et al., 2010; Büscher et al., 2017; Baker and Welburn, 2018).

The family of 3',5'-cyclic nucleotide phosphodiesterases (PDEs) are involved in various essential regulatory processes in many different organisms making them interesting drug targets. The human 3',5'-cyclic nucleotide phosphodiesterases (hPDE) have been extensively studied as drug targets for a broad range of diseases, including COPD, heart failure, and erectile dysfunction (Packer et al., 1991; Boolell et al., 1996; Hatzelmann and Schudt, 2001; Calverley et al., 2009). The *T. brucei* 3',5'-cyclic nucleotide phosphodiesterases B1 (TbrPDEB1) and TbrPDEB2 have previously been identified as potential new targets for the treatment of HAT as, in contrast to the other TbrPDE enzymes, they are essential for parasite virulence (Oberholzer et al., 2007). Simultaneous reduction in expression of TbrPDEB1 and TbrPDEB2 with siRNA resulted in distortions of the cell cycle and eventually cell death (Kunz et al., 2006; Oberholzer et al., 2007). The potential of TbrPDEB1 and TbrPDEB2 as drug targets against HAT was further demonstrated *in vivo* as siRNA-mediated gene silencing in mice prevented parasitemia and finally resulted in animal survival after parasite infection (Oberholzer et al., 2007). Simultaneous inhibition of both isoforms by small molecule inhibitors is conceived possible because of high structural similarity between both paralogues (88% structural identity of the catalytic domain), resulting in a high degree of equipotency as reported for NPD-001 (IC₅₀ TbrPDEB1: 12.0 nM; IC₅₀ TbrPDEB2: 12.4 nM) (De Koning et al., 2012; Orrling et al., 2012; Veerman et al., 2016).

Recently, a first series of molecules with selectivity for TbrPDEB1 over hPDE4 was reported by repurposing a tetrahydrophthalazinone scaffold that was originally developed as hPDE4 inhibitor (Van Der Mey et al., 2001a,b; Blaazer et al., 2018). Potency and selectivity over hPDE4 was obtained by addressing a parasite-specific pocket (P-pocket) in the substrate-binding site of TbrPDEB1 with a rigid biphenyl glycinamide installed on the tetrahydrophthalazinone (NPD-039, shown in **Figure 1**) (Jansen et al., 2013; Blaazer et al., 2018). NPD-039 (**1**) displays high nanomolar potency for TbrPDEB1 ($K_i = 0.1 \mu\text{M}$) with more than 10-fold selectivity over hPDE4 ($K_i = 1.9 \mu\text{M}$) with the glycinamide tail occupying the P-pocket in the crystal structure of **1** in the catalytic domain of TbrPDEB1 (Blaazer et al., 2018). Unfortunately, **1** shows a reduced efficacy against *T. brucei* *in vitro* (IC₅₀ = 6.3 μM) and its development as trypanocidal was therefore halted (Blaazer et al., 2018).

In the present study, we describe one of our efforts to improve on **1** by introducing flexibility into the vector that directs to the P-pocket using a diaryl ether function. Two different design strategies were applied in parallel. Firstly, computer-aided drug design using the structure of NPD-039 co-crystallized in TbrPDEB1 (**Figure 1**, PDB: 5L8C) and commercially available heteroaromatic moieties (hAr, **2**) provided a selection of virtual hits for synthesis to explore accessibility of various aromatic structures in the active site of TbrPDEB1. Secondly, the pyrimidyl group in **3** was decorated with a selection of amide functionalities based on observations in previously reported studies to explore the directionality toward the P-pocket (Blaazer et al., 2018; De Heuvel et al., 2019b). Both compound classes were synthesized and tested to explore the interaction with TbrPDEB1 and their *in vitro* efficacy against *T. brucei*.



MATERIALS AND METHODS

Phosphodiesterase Activity Assays

The TbrPDEB1 catalytic domain phosphodiesterase activity assays were conducted based on a method reported by Sijm et al. (2019) with minor adaptations (Sijm et al., 2019). The PDELight™ HTS cAMP phosphodiesterase Kit (Lonza, Walkersville, USA) was performed at 25°C in non-binding, low volume 384-well plates (Corning, Kennebunk, ME, USA). PDE activity measurements (TbrPDEB1_CD; K_m 3.45 μ M, hPDE4B_CD; K_m 13.89 μ M) were made in “stimulation buffer” (50 mM Hepes, 100 mM NaCl, 10 mM MgCl₂, 0.5 mM EDTA, 0.05 mg/mL BSA, pH 7.5). Single concentration measurements were made at 10 μ M inhibitor concentration (triplo measurements/assay, $n = 2$). Dose-response curves were made in the range 100 μ M–10 pM (triplo measurements/assay, $n = 3$). Compounds were diluted in DMSO (final in-test concentration 1%). Inhibitor dilutions (2.5 μ L) were transferred to the 384-well plates, 2.5 μ L of PDE in stimulation buffer was added and mixed, 5 μ L of cAMP (at $2 \times K_m$ up to 20 μ M) added and the assay mixture was incubated for 20 min at 300 rpm. The reaction was terminated by the addition of 5 μ L of Lonza Stop Buffer supplemented with 10 μ M of NPD-001. Then, 5 μ L of Lonza Detection reagent (diluted to 80% with reaction buffer) was added and the reaction incubated for 10 min at 300 rpm. Luminescence was read with a Victor3 luminometer using a 0.1 s/well program.

RLUs were measured in comparison to the DMSO-only control, NPD-001 always was taken along as positive control as a PDE inhibitor. The K_i values of the inhibitors analyzed are represented as the mean of at least three independent experiments with the associated standard error of the mean (S.E.M.). Due to solubility issues, we were not able to determine full dose-response curves for all compounds; K_i values for such inhibitors were obtained by curve fitting (Graphpad Prism 7.0) and the assumption of full inhibition to a level of inhibition by NPD-001.

Phenotypic Cellular Assays

The phenotypic cellular assays were conducted as previously reported by Blaazer et al. (Blaazer et al., 2018). For the cellular assays, reference drugs as positive controls were suramin (Sigma-Aldrich, Germany) for *T. brucei* ($IC_{50} = 0.04 \pm 0.02 \mu$ M, $n = 5$) and tamoxifen (Sigma-Aldrich, Germany) for MRC-5 cells ($CC_{50} = 10 \pm 2.1 \mu$ M, $n = 5$). All compounds were tested at five concentrations (64, 16, 4, 1, and 0.25 μ M) to establish a full dose-titration and determination of the IC_{50} and CC_{50} , data are represented as the mean of duplicate experiments \pm S.E.M. The final in-test concentration of DMSO did not exceed 0.5%.

For the antitrypanosomal assay, *T.b. brucei* Squib-427 strain (suramin-sensitive) was cultured at 37°C and 5% CO₂ in HMI-9 medium supplemented with 10% fetal calf serum (FCS). Approximately 1.5×10^4 trypomastigotes were added to each well and parasite growth was assessed after 72 h at 37°C by adding resazurin. Viability was assessed fluorimetrically 24 h after addition of resazurin. Fluorescence was measured (excitation

550 nm, emission 590 nm) and the results were expressed as percentage reduction in viability compared to control.

For the cellular cytotoxicity assay, MRC-5 SV2 cells, originally from a human diploid lung cell line, were cultivated in MEM supplemented with L-glutamine (20 mM), 16.5 mM sodium hydrogen carbonate and 5% FCS. For the assay, 10^4 MRC-5 cells/well were seeded onto the test plates containing the pre-diluted sample and incubated at 37°C and 5% CO₂ for 72 h. Cell viability was assessed fluorimetrically 4 h after the addition of resazurin. Fluorescence was measured (excitation 550 nm, emission 590 nm) and the results were expressed as percentage reduction in cell viability compared to controls.

Chemistry

All reagents and solvents were obtained from commercial suppliers and were used as received. All reactions were magnetically stirred and carried out under an inert atmosphere. Reaction progress was monitored using thin-layer chromatography (TLC) and LC-MS analysis. LC-MS analysis was performed on a Shimadzu LC-20AD liquid chromatograph pump system, equipped with an Xbridge (C18) 5 μ m column (50, 4.6 mm), connected to a Shimadzu SPD-M20A diode array detector, and MS detection using a Shimadzu LC-MS-2010EV mass spectrometer. The LC-MS conditions were as follows: solvent A (water with 0.1% formic acid) and solvent B (MeCN with 0.1% formic acid), flow rate of 1.0 mL/min, start 5% B, linear gradient to 90% B in 4.5 min, then 1.5 min at 90% B, then linear gradient to 5% B in 0.5 min, then 1.5 min at 5% B; total run time of 8 min. Silica gel column chromatography was carried out with automatic purification systems using the indicated eluent. Reversed phase column purification was performed on the Grace Davison iES system with C18 cartridges (60 Å, 40 μ m) using the indicated eluent. Nuclear magnetic resonance (NMR) spectra were recorded as indicated on a Bruker Avance 500 (500 MHz for ¹H and 125.8 MHz for ¹³C) instrument equipped with a Bruker CryoPlatform, or on a Bruker DMX300 (300 MHz for ¹H) or a Bruker Biospin (400 MHz for ¹H). Chemical shifts (δ in ppm) and coupling constants (J in Hz) are reported with residual solvent as internal standard (δ ¹H-NMR: CDCl₃ 7.26; DMSO-*d*₆ 2.50; δ ¹³C-NMR: CDCl₃ 77.16; DMSO-*d*₆ 39.52). Abbreviations used for ¹H-NMR descriptions are as follows: s = singlet, d = doublet, t = triplet, q = quartet, hept = heptet, dd = doublet of doublets, dt = doublet of triplets, tt = triplet of triplets, m = multiplet, app d = apparent doublet, br = broad signal. Exact mass measurements (HRMS) were performed on a Bruker micrOTOF-Q instrument with electrospray ionization (ESI): in positive ion mode and a capillary potential of 4,500 V. Microwave reactions were carried out in a Biotage Initiator⁺ using sealed microwave vials. Systematic names for molecules were generated with the ChemBioDraw Ultra 14.0.0.117 (PerkinElmer, Inc.). The reported yields refer to isolated pure products and are not optimized. The purity, reported as the LC peak area % at 254 nm, of all final compounds was $\geq 95\%$ based on LC-MS. All compounds are isolated as a racemic mixture of *cis*-enantiomers. A detailed overview of the synthetic procedures can be found in the Supplementary Information (SI) in **Supplementary Material**.

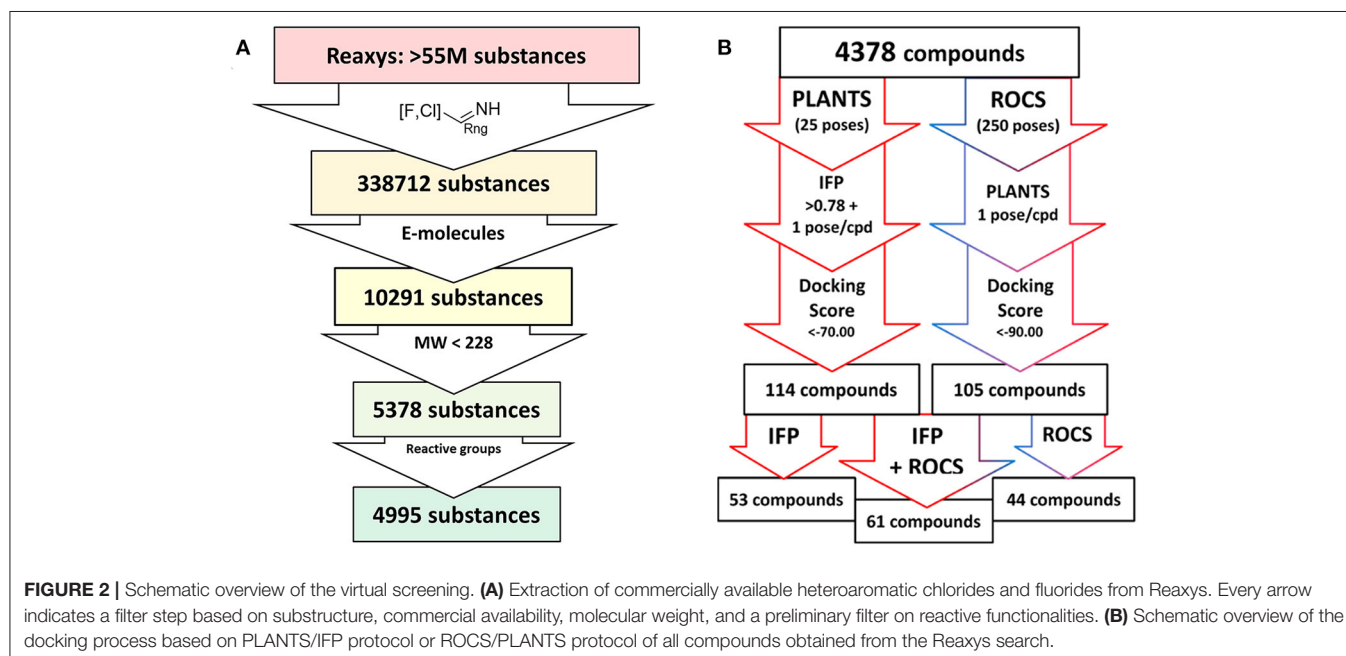
RESULTS AND DISCUSSION

Virtual Screening

The compound dataset for the virtual screening was based on commercially available heteroaryl chlorides which were combined with the core phenyltetrahydrophthalazinone scaffold using the MOE Combinatorial Library module (Figure 2). Reaxys was used to search for commercially available building blocks to use in a straightforward nucleophilic aromatic substitution reaction with a phenol tetrahydrophthalazinone. The Reaxys search was focused on commercially available (via E-molecules) heteroaromatic chlorides with a molecular weight <228 Da to design a library of compounds with a maximum molecular weight of 500 Da. The combinatorial library consisted of almost 5,000 compounds which were docked in the crystal structure of NPD-039 (1, PDB: 5L8C) using two different methods. Firstly, all compounds were docked using PLANTS and scored based on the similarity of the interaction fingerprint (IFP) compared with NPD-039. A high IFP similarity with NPD-039 suggests a similar binding mode and a higher probability of having similar affinity. All compounds were also scored using the overall docking score. Using a combination of scoring criteria (an IFP similarity >0.78 and a docking score <70) resulted in 114 selected compounds. In a second virtual screening approach, all computation library compounds were compared to the binding pose of NPD-039 in TbrPDEB1 using ROCS. The best scoring pose per compound was docked in the crystal structure of TbrPDEB1 using PLANTS and the compounds with a docking score <90 were selected, resulting in 105 compounds.

Combining the hit sets from both virtual screening strategies (ROCS and PLANTS) resulted in 158 unique compounds that were visually inspected for their synthetic feasibility and binding mode in the crystal structure, resulting in a selection

of 45 compounds (see SI). The compounds were divided into four clusters: 5-membered ring structures, 6-membered ring structures, and fused 5- and 6-membered ring structures (5-ring linked or 6-ring linked). Several representatives from every cluster were selected for synthesis to assure the presence of every ring size in the final set of compounds (Figure 3). For some of the hits, reagents turned out to be more difficult to obtain or expensive; in those cases a more readily available building block to represent the same cluster was used. However, the replacement often resulted in the selection of simplified and rigid building blocks that lack flexible substituents that can penetrate the P-pocket as observed for 1 (Figure 1). It was hypothesized that favorable binding to TbrPDEB1 could be obtained by introducing rigid aromatic systems, as previously observed for the biphenyl series (Blaazer et al., 2018). The docking pose of these more rigid compounds (2a, 2j-q, and to lesser extent conjugated esters 2b, 2d, and amide 2e) showed good directionality toward the P-pocket, as illustrated by the docking pose of 2d (Figure 4A), but did not address or interact with residues in the P-pocket. Nevertheless, the docking pose of these compounds provide essential information for possible future modifications sites. The docked hits containing a flexible substituent (2c, 2f-i, 2q) showed good occupation of the P-pocket, as illustrated by the docking pose of 2h (Figure 4B). The introduction of the ether bond between the aromatic functionalities causes a slight rotation of the anisole in the core scaffold. In most cases, the ether bond is rotated toward the phenylalanine of the hydrophobic clamp, while for several of the larger fused 5- and 6-membered rings (2j, 2l, 2m, and 2n) the ether linker is rotated toward the valine (Figure 4C). Although the spatial filling of the linker is divergent from the phenyl linker of 1 (Figure 4D), the occupancy of substituents is similar to the of the glycineamide tail of 1. A detailed overview of the individual docking poses of 2a-r can be found in the supporting information.



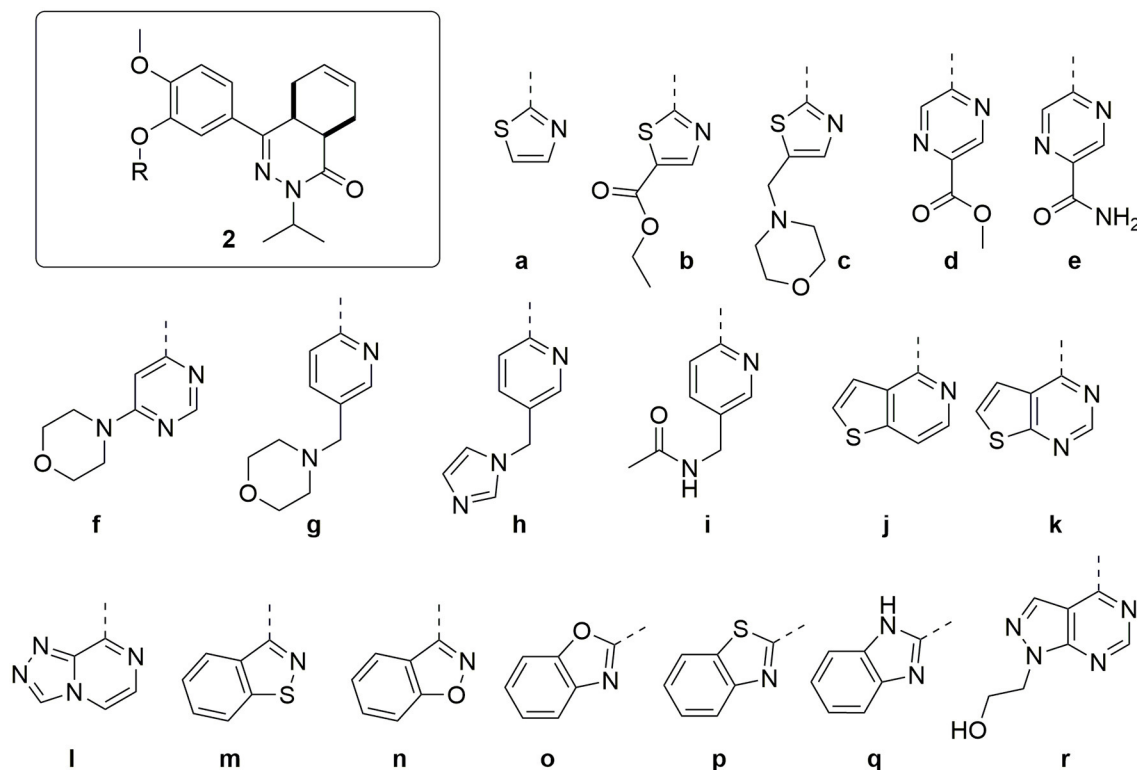


FIGURE 3 | Structures of the selected hits from the virtual screening.

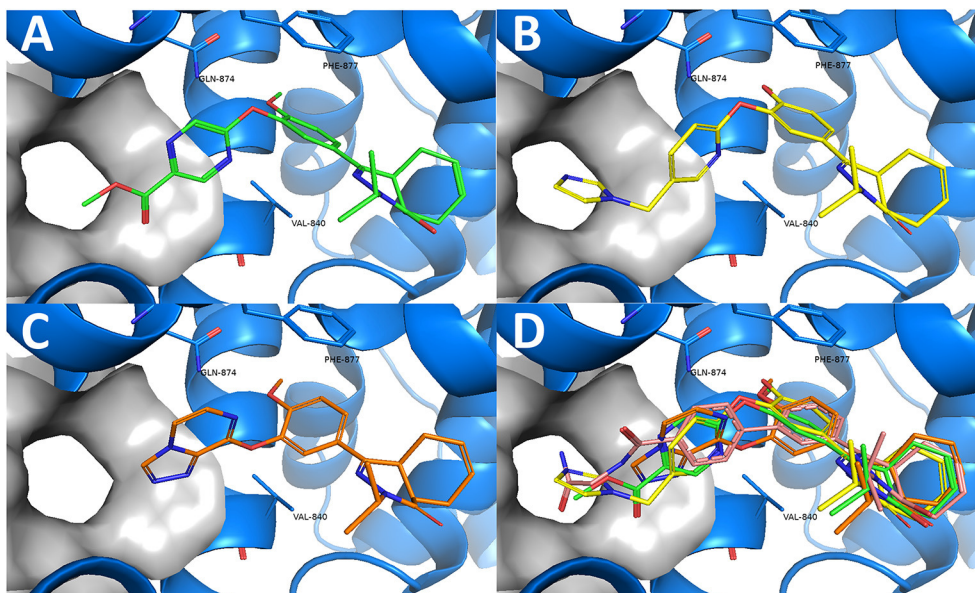


FIGURE 4 | Examples of docked structures in the co-crystal structure of 1 in TbrPDEB1 (PDB: 5L8C). The P-pocket is indicated by the gray surface. **(A)** The docking pose of pyrazine 2d (green). **(B)** The docking pose of 2h (yellow). **(C)** The docking pose of 2l (orange). **(D)** Overlay of the different docking poses of 2d, 2h, and 2l with reference compound 1 (salmon).

Chemistry

The synthesis of the compounds started with mesylation of guaiacol using mesyl chloride (**Scheme 1**). Mesylate **4** was used in a Friedel-Crafts acylation with maleic anhydride to obtain carboxylic acid **5**. Full isomerization toward the *E*-isomer was observed during the reaction. The *trans*-cyclohexene moiety of carboxylic acid **6** was installed using a Diels-Alder reaction with 1,3-butadiene, which was then used in a condensation reaction with isopropyl hydrazine to obtain tetrahydrophthalazinone **7**. The mesylate group was partially removed during the condensation reaction due to the basic conditions and a mixture of products was obtained. The mesylate group was completely removed by subjecting the mixture to a solution of NaOH in MeOH/THF. As shown for similar phenyl tetrahydrophthalazinones, *trans*-cyclohexene isomerizes to the *cis*-cyclohexene under basic conditions (De Heuvel et al., 2019a). The *cis*-conformation was confirmed by a strong NOE-coupling between the two bridgehead protons of tetrahydrophthalazinone **8**. The obtained phenol tetrahydrophthalazinone **8** was used as a building block for the synthesis of the various target compounds.

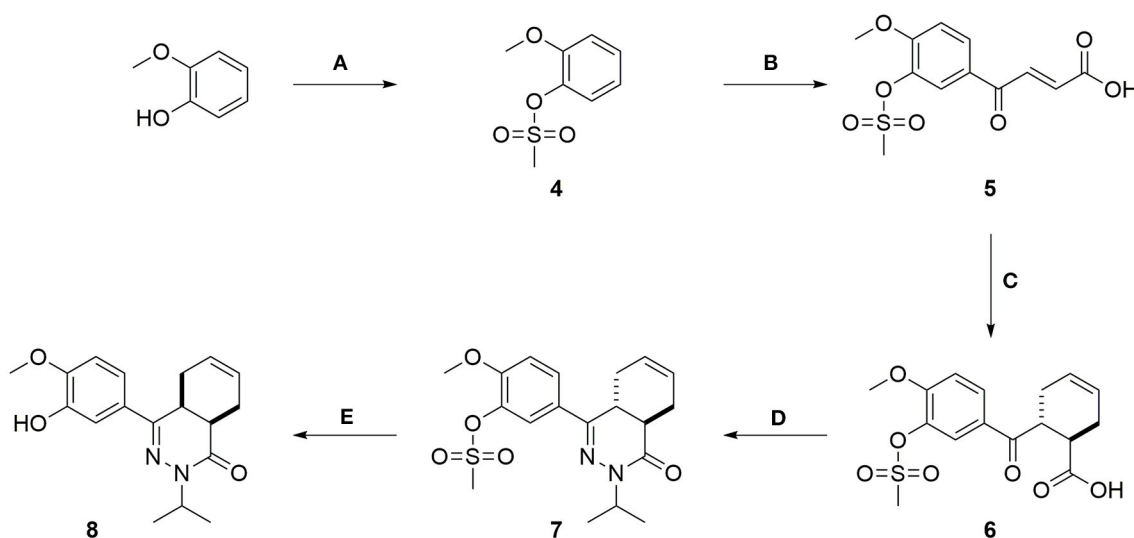
The heteroaromatic ring systems were installed in the tetrahydrophthalazinone core structure using a nucleophilic aromatic substitution reaction at higher temperatures (**Scheme 2**). The reactivity of the various aromatic chlorides differed significantly, leading to varying reaction times and yields. Unfortunately, the synthesis of **2g**, **2i**, **2m-o**, **2q** was unsuccessful due to observed side reactions or instability of the starting material under the reaction conditions. The synthesis of 4- and 6-methyl ester functionalized chloropyridines did not provide the desired intermediates. Therefore, the methyl ester was replaced by a nitrile (**3b** and **3d**) to provide a handle for further modifications. Both methyl esters (**3a** and **3c**) and nitriles (**3b** and **3d**) were successfully hydrolyzed with NaOH

to obtain carboxylic acids **3e-h**. Furthermore, the nitriles were used in a Radziszewski reaction to quickly and efficiently obtain the carboxamides **3j** and **3l**. All other tail groups (**3i**, **3k**, and **3m-w**) were installed in an amide coupling using EDC/HOBt. Unfortunately, the synthesis and functionalization of the 3-position on the pyridine using glycnamide was troublesome and unsuccessful.

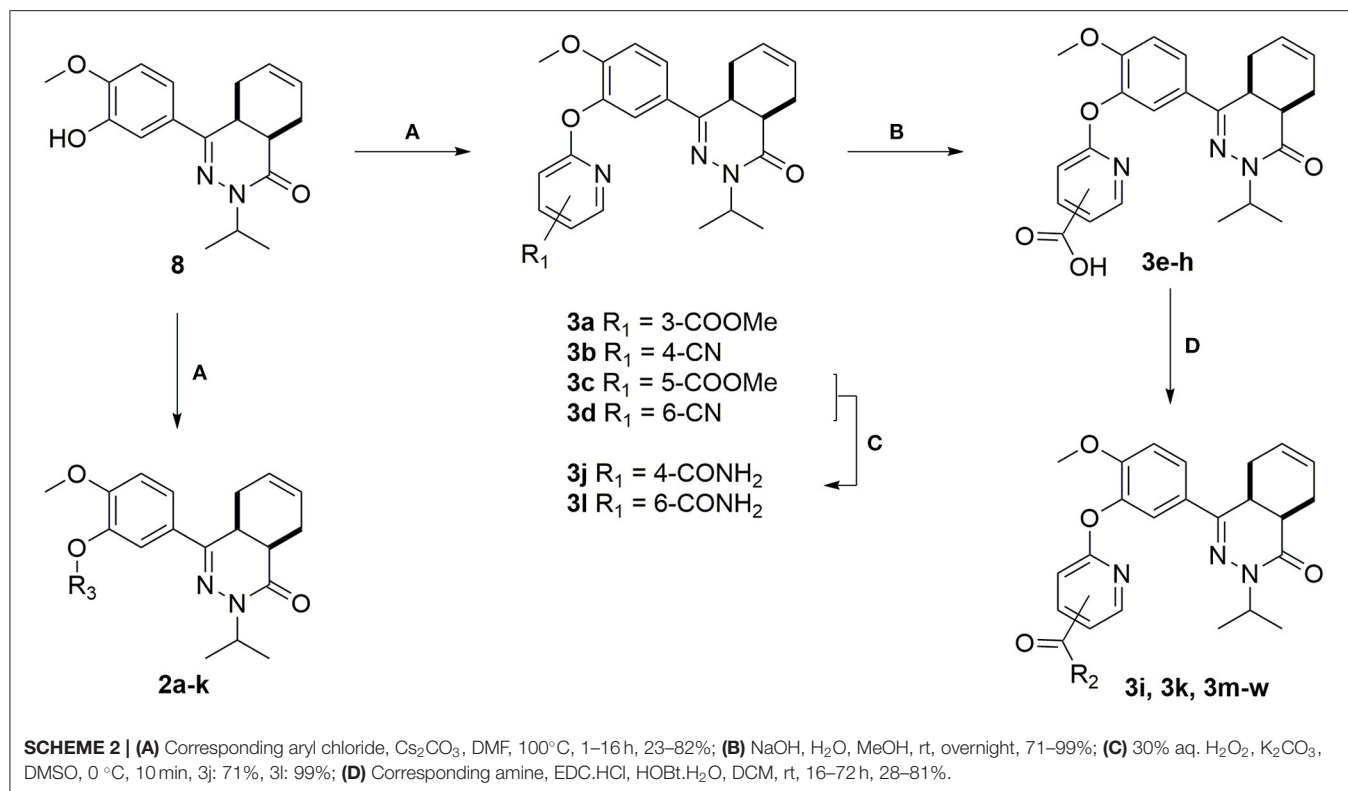
Biochemical Activity

All compounds were initially tested for their biochemical activity against TbrPDEB1 in a single point assay at 10 μ M. All of the 5-membered and 6-membered rings (**2a-f** and **2h**) from the virtual screening hits showed low to moderate inhibition of TbrPDEB1 at this concentration (**Table 1**), but the larger fused 5- and 6-membered rings (**2j-l** and **2p**) showed no inhibition at 10 μ M. The observation of deviant binding poses for this cluster in the virtual screening and the absence of activity suggests that these linkers are too bulky to fit in the limited space toward the P-pocket. The best results were observed for pyrazine **2d** and pyridine **2h**, both having about 50% inhibition at 10 μ M.

The computer-aided design of the pyridines on the different positions gave only a few active compounds (**Table 2**). With exception of **3m**, all substitutions on the 3- and 4-position of the pyridine ring resulted in no inhibition of TbrPDEB1 at 10 μ M. A methyl ester substitution on the 5-position of the pyridine ring (**3c**) resulted in a moderate inhibition, while larger groups or a carboxylic acid were not tolerated on this position. The best results were obtained for substitutions on the 6-position next to the pyridine nitrogen (**3d**, **3h**, **3l**, **3o**, **3s**, and **3w**). With exception of the carboxylic acid functionality, all substitutions on this position resulted in a moderate inhibitory effect, suggesting that this is the ideal vector to fit the side groups into the active site. Although we observed relatively small differences between the different analogs, the best activities



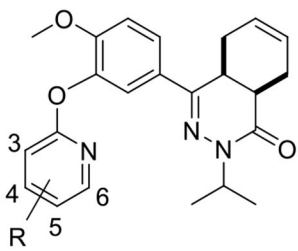
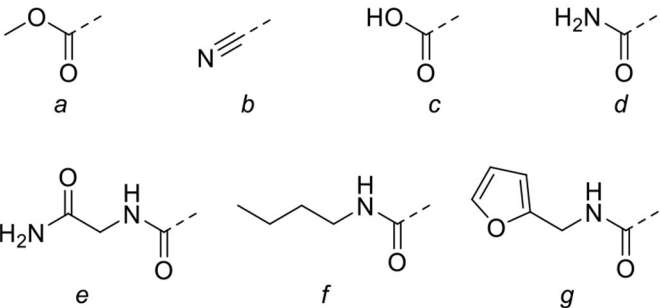
SCHEME 1 | (A) Mesyl chloride, Et₃N, DCM, rt, 1 h, 78%; (B) Maleic anhydride, AlCl₃, DCM, rt, 5 h, 40%; (C) Buta-1,3-diene, THF, 140°C, MW, 1.5 h, 92%; (D) Isopropylhydrazine.HCl, Cs₂CO₃, EtOH, 100°C, MW, 6 h, 75%; (E) NaOH, H₂O, THF, MeOH, 50°C, 2 h, 64%.

**TABLE 1 |** Single point activities of the virtual screening hits against TbrPDEB1 at $10\ \mu\text{M}$.

<p>2</p>					
		a	b	d	e
				d	e
		f	h	j	k
				l	p

#	NPD-	TbrPDEB1 (% inh.)	#	NPD-	TbrPDEB1 (% inh.)
2a	1162	12 ± 3	2h	1,164	49 ± 2
2b	1315	11 ± 0	2j	1,157	No inhibition
2c	1163	40 ± 4	2k	1,160	No inhibition
2d	1337	69 ± 1	2l	1,158	No inhibition
2e	3162	18 ± 9	2p	1,161	No inhibition
2f	1159	11 ± 8			

TABLE 2 | Single point activities of structure guided diaryl ether phthalazinones against TbrPDEB1 at 10 μ M.

									
#	NPD	R	Pos.	TbrPDEB1 (% inh)	#	NPD	R	Pos.	TbrPDEB1 (% inh)
3a	1338	a	3	No inhibition	3m	1,400	e	4	27 \pm 0
3b	1340	b	4	No inhibition	3n	1,392	e	5	5 \pm 1
3c	1339	a	5	50 \pm 1	3o	1,397	e	6	40 \pm 1
3d	1341	b	6	36 \pm 6	3p	1,389	f	3	No inhibition
3e	1342	c	3	No inhibition	3q	3,167	f	4	No inhibition
3f	1394	c	4	No inhibition	3r	1,390	f	5	No inhibition
3g	1343	c	5	11 \pm 6	3s	1,395	f	6	53 \pm 3
3h	1393	c	6	No inhibition	3t	1,344	g	3	No inhibition
3i	1345	d	3	No inhibition	3u	1,444	g	4	No inhibition
3j	1398	d	4	No inhibition	3v	1,391	g	5	No inhibition
3k	3165	d	5	No inhibition	3w	1,396	g	6	51 \pm 9
3l	1399	d	6	48 \pm 10					

were obtained for *n*-butyl and furfuryl substituted diaryl ethers **3s** and **3w**, which both showed slightly more than 50% inhibition at 10 μ M.

All compounds (**2d**, **2h**, **3c**, **3l**, **3s**, and **3w**) showing about 50% inhibition or higher at 10 μ M in the single point assay were selected for a TbrPDEB1 full dose-response assay, their *in vitro* activity against *T. brucei* parasites and *in vitro* cytotoxicity for MRC-5 cells. In line with the results in the 10 μ M assay, all selected diaryl ethers showed interesting inhibitory activity against TbrPDEB1 with pK_i values between 5.9 and 6.2 (Table 3). In the phenotypic assays, this set of compounds, except **3s**, showed an activity comparable to **1** with *T. brucei* IC₅₀ values in the range of 7.9–25 μ M. All compounds, with exception of **2h**, did not show cytotoxicity at the highest measured concentration (CC₅₀ > 64 μ M), resulting in an acceptable cytotoxicity profile for **2d**, **3c**, **3l**, and **3w**. These results suggest that the introduction of the ether functionality has no effect on the cellular activity when compared to **1**.

CONCLUSION

The computer-aided design of novel diaryl substituted tetrahydrophthalazinones resulted in the identification of several compounds with activities in the low micromolar range against TbrPDEB1 and devoid of cytotoxicity against MRC-5

TABLE 3 | *In vitro* activity of selected phthalazinones against TbrPDEB1, *T. brucei* parasites, and MRC-5 cells.

#	TbrPDEB1 K _i (μ M)	<i>T. brucei</i> IC ₅₀ (μ M)	MRC-5 CC ₅₀ (μ M)
1	0.1 ^a	6.3 ^a	35 ^a
2d	0.6 \pm 0.2	16 \pm 10	>64
2h	1.3 \pm 0.2	7.9 \pm 8	31 \pm 8
3c	0.8 \pm 0.2	7.9 \pm 8	>64
3l	0.8 \pm 0.2	16 \pm 10	>64
3s	1.3 \pm 0.3	>64	>64
3w	1.0 \pm 0.2	25 \pm 20	>64

^aReported by Blaazer et al. (2018).

cells. The results suggest a favorable position of modification for *para*-substituted 6-membered heteroaromatics (**2d**, **2h**, and **3c**) or 2,6-substituted pyridines (**3l**, **3s**, **3o**, and **3w**). The current set of compounds provides additional insight in the SAR for development of new selective TbrPDEB1 inhibitors. These results are important in the design of TbrPDEB1 selective inhibitors with adequate selectivity (>30-fold over human PDE4) and efficacy (IC₅₀ < 1 μ M) against this parasite.

DATA AVAILABILITY STATEMENT

The original contributions presented in the study are included in the article/**Supplementary Material**, further inquiries can be directed to the corresponding author.

AUTHOR CONTRIBUTIONS

EH, SK, JS, GS, and IE were involved in compound design, synthesis, and analysis. EH and AK were involved in virtual screening and docking. TM, PS, and MS were involved in the biochemical assays. DM, GC, and LM were involved in the phenotypic cellular assays. LM, GS, IE, and RL supervised the experiments and conceived the project. EH, GS, and RL integrated all data and wrote the manuscript. All authors contributed to the article and approved the submitted version.

REFERENCES

- Babokhov, P., Sanyaolu, A. O., Oyibo, W. A., Fagbenro-Beyioku, A. F., and Iriemenam, N. C. (2013). A current analysis of chemotherapy strategies for the treatment of human African trypanosomiasis. *Pathog. Glob. Health* 107, 242–252. doi: 10.1179/2047773213Y.0000000105
- Baker, C. H., and Welburn, S. C. (2018). The long wait for a new drug for human African trypanosomiasis. *Trends Parasitol.* 34, 818–827. doi: 10.1016/j.pt.2018.08.006
- Blaazer, A. R., Singh, A. K., De Heuvel, E., Edink, E., Orrling, K. M., Veerman, J. J. N., et al. (2018). Targeting a subpocket in *Trypanosoma brucei* phosphodiesterase B1 (TbrPDEB1) enables the structure-based discovery of selective inhibitors with trypanocidal activity. *J. Med. Chem.* 61, 3870–3888. doi: 10.1021/acs.jmedchem.7b01670
- Boolell, M., Allen, M. J., Ballard, S. A., Gepi-Attee, S., Muirhead, G. J., Naylor, A. M., et al. (1996). Sildenafil: an orally active type 5 cyclic GMP-specific phosphodiesterase inhibitor for the treatment of penile erectile dysfunction. *Int. J. Impot. Res.* 8, 47–52.
- Brun, R., Blum, J., Chappuis, F., and Burri, C. (2010). Human african trypanosomiasis. *Lancet* 375, 148–159. doi: 10.1016/S0140-6736(09)60829-1
- Büscher, P., Cecchi, G., Jamonneau, V., and Priotto, G. (2017). Human African trypanosomiasis. *Lancet* 390, 2397–2409. doi: 10.1016/S0140-6736(17)31510-6
- Calverley, P. M. A., Rabe, K. F., Goehring, U.-M., Kristiansen, S., Fabbri, L. M., and Martinez, F. J. (2009). Roflumilast in symptomatic chronic obstructive pulmonary disease: two randomised clinical trials. *Lancet* 374, 685–694. doi: 10.1016/S0140-6736(09)61255-1
- De Heuvel, E., Singh, A. K., Boronat, P., Kooistra, A. J., Van Der Meer, T., Sadek, P., et al. (2019a). Alkynamide phthalazinones as a new class of TbrPDEB1 inhibitors (Part 2). *Bioorg. Med. Chem.* 27, 4013–4029. doi: 10.1016/j.bmc.2019.06.026
- De Heuvel, E., Singh, A. K., Edink, E., Van Der Meer, T., Van Der Woude, M., Sadek, P., et al. (2019b). Alkynamide phthalazinones as a new class of TbrPDEB1 inhibitors. *Bioorg. Med. Chem.* 27, 3998–4012. doi: 10.1016/j.bmc.2019.06.027
- De Koning, H. P. (2017). Drug resistance in protozoan parasites. *Emerg. Topics Life Sci.* 1:627. doi: 10.1042/ETLS20170113
- De Koning, H. P., Gould, M. K., Sterk, G. J., Tenor, H., Kunz, S., Luginbuehl, E., et al. (2012). Pharmacological validation of *Trypanosoma brucei* phosphodiesterases as novel drug targets. *J. Infect. Dis.* 206, 229–237. doi: 10.1093/infdis/jir857
- De Moraes-Teixeira, E., Rabello, A., and Aguiar, M. M. G. (2019). *In vitro* activity and *in vivo* efficacy of fexinidazole against new world leishmania species. *J. Antimicrob. Chemother.* 74, 2318–2325. doi: 10.1093/jac/dkz172

FUNDING

This work was supported by the European Commission 7th Framework Programme FP7-HEALTH-2013-INNOVATION-1 under project reference 602666 Parasite-specific cyclic nucleotide phosphodiesterase inhibitors to target Neglected Parasitic Diseases (PDE4NPD).

ACKNOWLEDGMENTS

We thank F.G.J. Custers (Vrije Universiteit Amsterdam) for the analytical support.

SUPPLEMENTARY MATERIAL

The Supplementary Material for this article can be found online at: <https://www.frontiersin.org/articles/10.3389/fchem.2020.608030/full#supplementary-material>

- Deeks, E. D. (2019). Fexinidazole: first global approval. *Drugs* 79, 215–220. doi: 10.1007/s40265-019-1051-6
- Eperon, G., Balasegaram, M., Potet, J., Mowbray, C., Valverde, O., and Chappuis, F. (2014). Treatment options for second-stage gambiense human African trypanosomiasis. *Expert Rev. Anti Infect. Ther.* 12, 1407–1417. doi: 10.1586/14787210.2014.959496
- Hatzelmann, A., and Schudt, C. (2001). Anti-inflammatory and immunomodulatory potential of the novel PDE4 inhibitor roflumilast *in vitro*. *J. Pharmacol. Exp. Ther.* 297, 267–279.
- Jansen, C., Wang, H., Kooistra, A. J., De Graaf, C., Orrling, K. M., Tenor, H., et al. (2013). Discovery of novel *Trypanosoma brucei* phosphodiesterase B1 inhibitors by virtual screening against the unliganded TbrPDEB1 crystal structure. *J. Med. Chem.* 56, 2087–2096. doi: 10.1021/jm3017877
- Kunz, S., Beavo, J. A., D'angelo, M. A., Flawia, M. M., Francis, S. H., Johnner, A., et al. (2006). Cyclic nucleotide specific phosphodiesterases of the kinetoplastida: a unified nomenclature. *Mol. Biochem. Parasitol.* 145, 133–135. doi: 10.1016/j.molbiopara.2005.09.018
- Munday, J. C., Settimo, L., and De Koning, H. P. (2015). Transport proteins determine drug sensitivity and resistance in a protozoan parasite, *Trypanosoma brucei*. *Front. Pharmacol.* 6:32. doi: 10.3389/fphar.2015.00032
- Oberholzer, M., Marti, G., Baresic, M., Kunz, S., Hemphill, A., and Seebeck, T. (2007). The *Trypanosoma brucei* cAMP phosphodiesterases TbrPDEB1 and TbrPDEB2: flagellar enzymes that are essential for parasite virulence. *FASEB J.* 21, 720–731. doi: 10.1096/fj.06-6818com
- Orrling, K. M., Jansen, C., Vu, X. L., Balmer, V., Bregy, P., Shanmugham, A., et al. (2012). Catechol pyrazolinones as trypanocidals: fragment-based design, synthesis, and pharmacological evaluation of nanomolar inhibitors of trypanosomal phosphodiesterase B1. *J. Med. Chem.* 55, 8745–8756. doi: 10.1021/jm301059b
- Packer, M., Carver, J. R., Rodeheffer, R. J., Ivanhoe, R. J., Dibianco, R., Zeldis, S. M., et al. (1991). Effect of oral milrinone on mortality in severe chronic heart failure. *N. Eng. J. Med.* 325, 1468–1475. doi: 10.1056/NEJM199111213252103
- Pelfrene, E., Harvey Allchurch, M., Ntamabyaliro, N., Nambasa, V., Ventura, F. V., Nagercoil, N., et al. (2019). The European medicines agency's scientific opinion on oral fexinidazole for human African trypanosomiasis. *PLoS Negl. Trop. Dis.* 13: e0007381. doi: 10.1371/journal.pntd.0007381
- Sijm, M., Siciliano De Araújo, J., Kunz, S., Schroeder, S., Edink, E., Orrling, K. M., et al. (2019). Phenylidihydropyrazolones as novel lead compounds against *Trypanosoma cruzi*. *ACS Omega* 4, 6585–6596. doi: 10.1021/acsomega.8b02847

- Van Der Mey, M., Hatzelmann, A., Van Der Laan, I. J., Sterk, G. J., Thibaut, U., and Timmerman, H. (2001a). Novel selective PDE4 inhibitors. 1. Synthesis, structure-activity relationships, and molecular modeling of 4-(3, 4-dimethoxyphenyl)-2 H-phthalazin-1-ones and Analogues. *J. Med. Chem.* 44, 2511–2522. doi: 10.1021/jm010837k
- Van Der Mey, M., Hatzelmann, A., Van Klink, G. P. M., Van Der Laan, I. J., Sterk, G. J., Thibaut, U., et al. (2001b). Novel Selective PDE4 Inhibitors. 2. Synthesis and structure-activity relationships of 4-aryl-substituted cis-tetra- and cis-hexahydrophthalazinones. *J. Med. Chem.* 44, 2523–2535. doi: 10.1021/jm010838c
- Veerman, J., Van Den Bergh, T., Orrling, K. M., Jansen, C., Cos, P., Maes, L., et al. (2016). Synthesis and evaluation of analogs of the phenylpyridazinone NPD-001 as potent trypanosomal TbrPDEB1 phosphodiesterase inhibitors and *in vitro* trypanocidals. *Bioorg. Med. Chem.* 24, 1573–1581. doi: 10.1016/j.bmc.2016.02.032
- World Health Organization (2020). *Trypanosomiasis, Human African (Sleeping Sickness)*. Available online at: [https://www.who.int/news-room/fact-sheets/detail/trypanosomiasis-human-african-\(sleeping-sickness\)](https://www.who.int/news-room/fact-sheets/detail/trypanosomiasis-human-african-(sleeping-sickness)) (accessed October 25, 2020).
- Conflict of Interest:** The authors declare that the research was conducted in the absence of any commercial or financial relationships that could be construed as a potential conflict of interest.
- Copyright © 2021 de Heuvel, Kooistra, Edink, van Klaveren, Stuijt, van der Meer, Sadek, Mabille, Caljon, Maes, Siderius, de Esch, Sterk and Leurs. This is an open-access article distributed under the terms of the Creative Commons Attribution License (CC BY). The use, distribution or reproduction in other forums is permitted, provided the original author(s) and the copyright owner(s) are credited and that the original publication in this journal is cited, in accordance with accepted academic practice. No use, distribution or reproduction is permitted which does not comply with these terms.



Ubiquitination and the Proteasome as Drug Targets in Trypanosomatid Diseases

Marie-José Bijlmakers*

Other, Cambridge, United Kingdom

OPEN ACCESS

Edited by:

Debasish Bandyopadhyay,
The University of Texas Rio Grande
Valley, United States

Reviewed by:

Marta Helena Branquinho,
Federal University of Rio de Janeiro,
Brazil
Edson Roberto Silva,
University of São Paulo, Brazil

*Correspondence:

Marie-José Bijlmakers
mariebijlmakers@gmail.com

Specialty section:

This article was submitted to
Medicinal and Pharmaceutical
Chemistry,
a section of the journal
Frontiers in Chemistry

Received: 18 November 2020

Accepted: 29 December 2020

Published: 28 January 2021

Citation:

Bijlmakers M-J (2021) Ubiquitination
and the Proteasome as Drug Targets in
Trypanosomatid Diseases.
Front. Chem. 8:630888.
doi: 10.3389/fchem.2020.630888

The eukaryotic pathogens *Trypanosoma brucei*, *Trypanosoma cruzi* and *Leishmania* are responsible for debilitating diseases that affect millions of people worldwide. The numbers of drugs available to treat these diseases, Human African Trypanosomiasis, Chagas' disease and Leishmaniasis are very limited and existing treatments have substantial shortcomings in delivery method, efficacy and safety. The identification and validation of novel drug targets opens up new opportunities for the discovery of therapeutic drugs with better efficacy and safety profiles. Here, the potential of targeting the ubiquitin-proteasome system in these parasites is reviewed. Ubiquitination is the posttranslational attachment of one or more ubiquitin proteins to substrates, an essential eukaryotic mechanism that regulates a wide variety of cellular processes in many different ways. The best studied of these is the delivery of ubiquitinated substrates for degradation to the proteasome, the major cellular protease. However, ubiquitination can also regulate substrates in proteasome-independent ways, and proteasomes can degrade proteins to some extent in ubiquitin-independent ways. Because of these widespread roles, both ubiquitination and proteasomal degradation are essential for the viability of eukaryotes and the proteins that mediate these processes are therefore attractive drug targets in trypanosomatids. Here, the current understanding of these processes in trypanosomatids is reviewed. Furthermore, significant recent progress in the development of trypanosomatid-selective proteasome inhibitors that cure mouse models of trypanosomatid infections is presented. In addition, the targeting of the key enzyme in ubiquitination, the ubiquitin E1 UBA1, is discussed as an alternative strategy. Important differences between human and trypanosomatid UBA1s in susceptibility to inhibitors predicts that the selective targeting of these enzymes in trypanosomatids may also be feasible. Finally, it is proposed that activating enzymes of the ubiquitin-like proteins SUMO and NEDD8 may represent drug targets in these trypanosomatids as well.

Keywords: trypanosoma, leishmania, ubiquitination, proteasome, drug target

INTRODUCTION

Trypanosoma brucei, *Trypanosoma cruzi* and *Leishmania* sp are the major disease-causing trypanosomatids in humans that continue to pose a major risk to the health of millions of people worldwide, especially among the poorest in rural regions of tropical countries. These eukaryotic parasites are characterized by a single flagellum and a kinetoplast, a DNA containing

region that is part of a single mitochondrion (Stuart et al., 2008). They all have an invertebrate and vertebrate host, but there are differences in their distribution, transmission and life cycle. *T. brucei*, the causative agent of Human African Trypanosomiasis (HAT), is transmitted by the tsetse fly and only found in Africa. Two different species, *T. brucei gambiense* and *T. brucei rhodesiense*, cause a slow (98% of cases) and rapidly progressing form of HAT, respectively, both of which are lethal if not treated. The *T. brucei* parasites live exclusively extracellularly in the host, during the early mild stage of the disease in the blood, lymph and interstitial spaces, and during the second stage in the central nervous system leading to severe neurological symptoms. *T. cruzi* is transmitted by blood feeding triatominae and endemic in Latin America. This trypanosomatid alternates between non-replicating trypomastigotes that circulate in the blood and dividing amastigotes, a form with only a very short flagellum, in the cytoplasm of mammalian cells after escape from a lysosomal compartment. Whereas the initial symptoms of a *T. cruzi* infection are often mild and undetected, a lifelong infection is established that in 30% of cases leads to a chronic phase of disease with severe damage to the heart and digestive system. Leishmaniasis is caused by more than twenty species of *Leishmania* that are found widespread throughout the world with the majority of disease cases occurring in Asia, Africa, and Latin America. Leishmania parasites are transmitted by the bite of a sandfly that injects the promastigote metacyclic form, which after being taken up by phagocytic cells, transforms into amastigotes that replicate inside the phagolysosome. Leishmaniasis consists of a spectrum of human diseases with symptoms varying from self-limiting ulcers to the destruction of mucocutaneous surfaces, to the deadly visceral leishmaniasis.

With the exception of *T. brucei gambiense* that mainly infects humans, these pathogenic trypanosomatids have animal reservoirs that include small and domestic animals, which makes the control of their transmission very difficult. Early diagnosis and effective medication are therefore of the utmost importance, but only a handful of drugs is available, most of which have been in use for many decades and have severe shortcomings in delivery, toxicity and efficacy (Bilbe, 2015; Rao et al., 2018). However, the past 15 years have seen various important initiatives that have increased the visibility of these neglected tropical diseases, enabled collaborations between industry, academia and the public sector for drug development on a not-for-profit basis, and increased the availability of research funding. This has resulted in significant successes particularly in the treatment of *T. gambiense* HAT for which a safe oral treatment has now become available (Dickie et al., 2020; Neu et al., 2020). More clinical trials are ongoing, also for Chagas' disease and Leishmaniasis treatments, but failures of clinical trials have also been reported. Given the general low success rate of drug development, its low predictability and long duration plus the added anticipation of future drug resistance, multiple parallel efforts in research, drug discovery and development are required to generate a considerable pipeline of anti-trypanosomiasis drug candidates.

New combinations of existing medication as well as the optimization of dosing regimes have already resulted in rapid

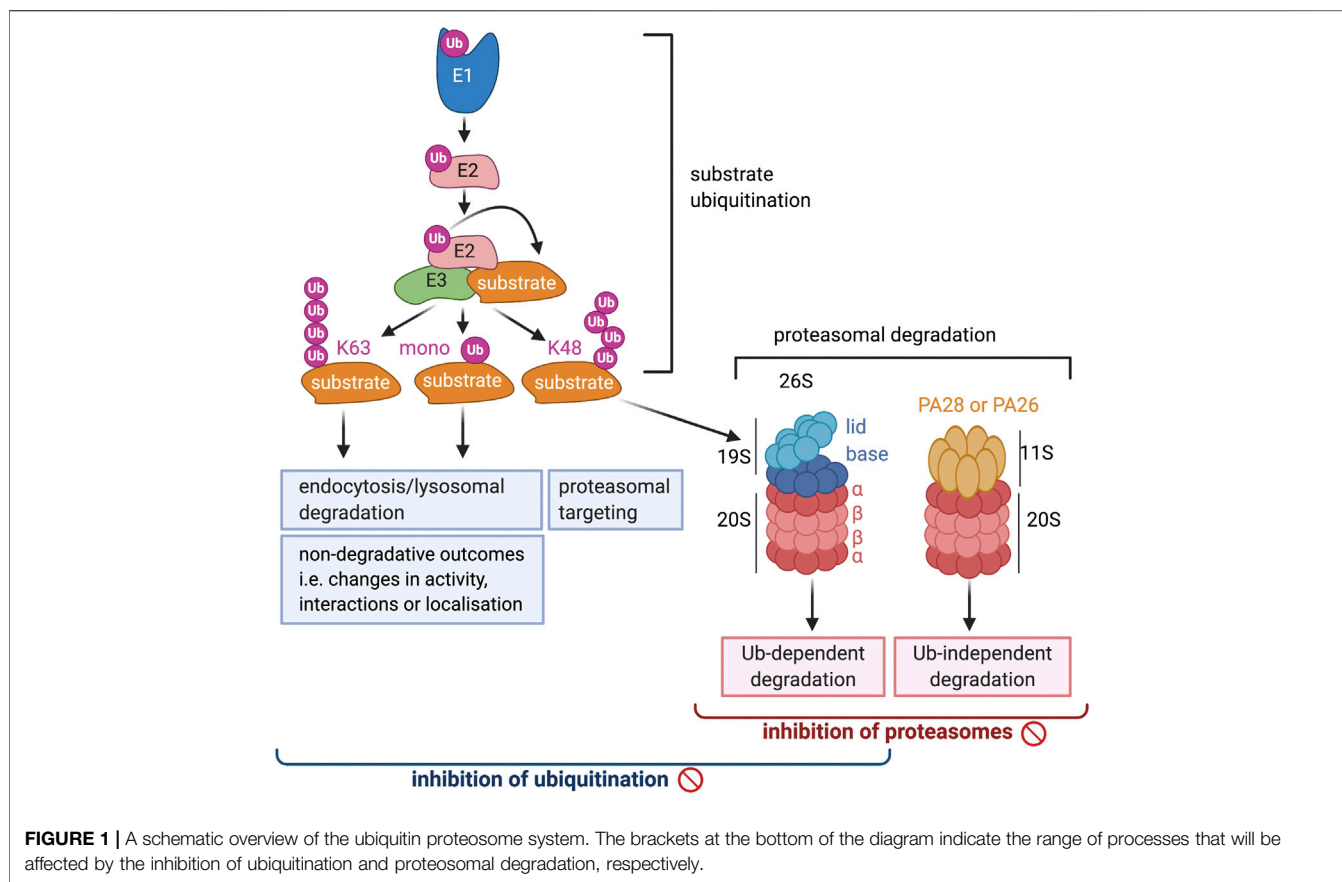
improvements in treatments. Furthermore, the revisiting of compounds with proven anti-trypanosome activity, research into which was abandoned due to a lack of commercial interest, has resulted in the approval and testing of new drugs (Neu et al., 2020). However, advances in analysis and screening techniques, a better knowledge of genomes, proteomes and biological pathways have also opened up many new opportunities that are currently being explored. One approach is to use phenotypic screens as a starting point for the identification of compounds with anti-trypanosomal activity. Alternatively, a target-based approach can be used in which targets are selected based on being indispensable for parasite survival, absent in humans, or sufficiently different from human orthologues, and amenable to enzymatic inhibition. Targets can then be used in high-throughput screens with compound libraries, or existing knowledge on the structure and inhibition of mammalian orthologues can be used for the design of parasite-selective inhibitors to speed up the process of drug discovery. In this review, the ubiquitin-proteasome system will be discussed as a promising source of drug targets for trypanosomal diseases. Both the proteasome and the ubiquitination machinery, which function together as well as separately, are essential for the survival of eukaryotes including trypanosomatids. Inhibitors against both processes have been identified and selective inhibition without affecting mammalian counterparts has been demonstrated for the trypanosomal proteasome and strongly suggested for the trypanosomal ubiquitin activating enzyme.

THE UBIQUITIN-PROTEASOME SYSTEM

Ubiquitination, an Omnipresent and Versatile Protein Modification

Ubiquitination is a post-translational protein modification in eukaryotes that involves the attachment of the small protein ubiquitin to substrates which results in the degradation of substrates or in an alteration of their activity, interaction or localization (Pickart and Eddins, 2004; Komander and Rape, 2012). This reversible modification plays a crucial role in the regulation of almost every cellular process including cell cycle progression, transcriptional control, DNA repair, autophagy, protein trafficking and the removal of misfolded, damaged or old proteins.

The widespread and diverse roles of ubiquitination is reflected in the many different forms that this modification can take, the range of which is still expanding (Yau and Rape, 2016). Ubiquitin is primarily attached to a lysine on the substrate, but other residues such as threonine, serine and cysteine, as well as the N-terminal amino group can be modified as well. Two main types of ubiquitination are distinguished: mono-ubiquitination, when only a single ubiquitin is attached to a substrate residue, or poly-ubiquitination, when the attached ubiquitin itself undergoes sequential rounds of ubiquitination and a poly-ubiquitin chain is formed (Figure 1). Ubiquitin contains seven lysines and a free N-terminus that can all be ubiquitinated so that poly-ubiquitin chains of many different architectures can be formed, including straight Met1-linked chains as well as branched chains in which



one ubiquitin molecule binds two other ubiquitins at different lysines. The most frequently occurring and best studied poly-ubiquitin chains are those linked via K48 or K63 (Swatek and Komander, 2016). K48-linked chains make up >50% of all ubiquitination and are well known to target substrates to the proteasome for degradation (Figure 1), which has now also been shown for K48/K11 branched chains and multiple mono-ubiquitination. K63-linked chains, on the other hand, are not involved in proteasomal degradation, but like single mono-ubiquitination, play a role in lysosomal targeting and degradation of plasma membrane proteins (Figure 1). Additionally, the presence of K63- and Met-linked chains, or mono-ubiquitination, can induce non-proteolytic outcomes and change the interactions, activity or localization of substrates. The roles of ubiquitin chains linked via other lysines are still emerging, but it is clear that these also contribute to degradative as well as non-degradative processes. The demonstration that attached ubiquitin can also be modified by phosphorylation and acetylation adds another level of complexity to the regulatory capacity of this modification (Herhaus and Dikic, 2015).

Ubiquitination can be reversed by de-ubiquitinating proteins (DUBs), a large and diverse group of enzymes that plays a crucial role in the regulation of ubiquitin-controlled processes (Clague et al., 2013). There is further a critical role for ubiquitin-binding domains (UBD), short protein motifs of a multitude of different signatures. These occur on many different proteins and help to

translate the ubiquitin code into specific outcomes (Husnjak and Dikic, 2012).

Ubiquitination Enzymes in *T. brucei*, *T. cruzi* and *Leishmania*

The attachment of ubiquitin to substrates is a multistep process that requires the sequential activity of three classes of proteins (Figure 1). The first step is mediated by the ubiquitin activating enzyme (UBA1), or ubiquitin E1 (Schulman and Harper, 2009). This large multi-domain protein first adenylates ubiquitin at the C-terminus, which then reacts with a catalytic cysteine, resulting in the formation of a high energy thioester ubiquitin ~ E1 conjugate. After binding of a second ubiquitin, the E1 can transfer the thioester bound ubiquitin to a ubiquitin conjugating enzyme or E2, where again a ubiquitin-thioester bond is formed (Stewart et al., 2016). The E2 subsequently interacts with an E3, or ubiquitin ligase, a protein that selects substrates and mediates the transfer of ubiquitin to the substrate. E3 proteins are highly diverse, characterized by an E2-binding domain that is most frequently a RING, HECT or U-box domain (Deshaies and Joazeiro, 2009). Mechanistically, these proteins can be divided into two groups: a small group that includes the HECT and RING-in-between-RING (RBR) proteins forms a covalent intermediate with ubiquitin before transferring it to substrates. A very large group that contains the majority of RING and U box proteins mediates the transfer of ubiquitin to substrates from the

E2 without binding ubiquitin themselves first. E3s proteins can either function on their own or as part of large multi-protein complexes.

Going down the ubiquitination cascade, the number of proteins involved in the separate steps increases vastly (Schulman and Harper, 2009). From yeast to mammals, there is only one E1 that exclusively activates ubiquitin, UBA1 (or UBE1). In vertebrates and sea urchin UBA6, the E1 for the ubiquitin-like protein FAT10, can activate ubiquitin as well, but UBA1 is responsible for more than 90% of all ubiquitination (Pelzer et al., 2007; Liu et al., 2017). At the next level down in mammalian genomes, approximately 40 ubiquitin E2 conjugating proteins can be found. Collectively, these E2s interact with more than 600 ubiquitin E3s, which each recruit sets of substrates that number from a few to several hundreds.

Consistent with this hierarchy, UBA1 is an essential protein. This has been demonstrated by gene ablation studies in yeast and *C. elegans* where UBA1 is the only ubiquitin E1 (McGrath et al., 1991; Kulkarni and Smith, 2008), but also in various human cancer cell lines (Xu et al., 2010) where UBA6 is apparently not able to compensate for the loss of UBA1. This vital role is further illustrated by the cytotoxic effect of UBA1 inhibitors on mammalian cells (Barghout and Schimmer, 2021).

In *T. brucei*, *T. cruzi* and *Leishmania*, ubiquitination has not yet been extensively investigated, but it is clear from genome-wide RNAi screens, genome analysis, and reports on specific cellular processes that also in these parasites this modification plays an essential and widespread role. Genome-wide analysis shows that genes encoding for orthologues of ubiquitin E1, E2 and E3 proteins are all present in these species, as are enzymes involved in de-ubiquitination (Gupta et al., 2018). Ubiquitin E1 proteins can be identified by the presence of two ThiF/MoeB motifs and a C-terminal ubiquitin fold domain (UFD) (Schulman and Harper, 2009). Surprisingly, there are two orthologues of UBA1 in trypanosomatids, called TbUBA1a and TbUBA1b in *T. brucei* (Chung et al., 2008; Boer and Bijlmakers, 2019). Of these two, TbUBA1a is the most closely related to human UBA1 (hUBA1): it is similar in length and 36% identical at the amino acid level. TbUBA1b on the other hand, has an N-terminal extension, several insertions of multiple amino acids and is only 28% identical to hUBA1. The 2 *T. brucei* UBA1s are also only 24% identical to each other, suggesting that they may have arisen from an early gene duplication. In agreement with this, orthologues of both proteins are present in all other kinetoplastids sequenced so far, but no TbUBA1b equivalents are found outside this taxus. *T. cruzi* and *Leishmania* have orthologues that are, respectively, 70% and 55% identical to TbUBA1a, and orthologues that are 68% and 59% identical to TbUBA1b (Boer and Bijlmakers, 2019). TbUBA1b does not show any extensive similarity to the other two E1 proteins with two ThiF domains, UBA6 and UBA7.

Consistent with a function as a ubiquitin E1, TbUBA1b RNAi knockdown in the blood stream form (BSF) of *T. brucei* results in an overall reduction in ubiquitination (Chung et al., 2008). Furthermore, like TbUBA1a, TbUBA1b can activate ubiquitin *in vitro*, which was measured by the transfer of ubiquitin to an E2 (Boer and Bijlmakers, 2019). Both

TbUBA1a and TbUBA1b are expressed in the procyclic insect form as well as in the blood stream form of *T. brucei* (Siegel et al., 2010) (<https://tritrypdb.org/>). While the significance of this expression of two different UBA1s is not yet clear, data from a genome-wide gene ablation screen show that both proteins are essential for *T. brucei* survival (<https://tritrypdb.org/>). In this screen, in which ~10,000 individual genes were targeted by tetracyclin-inducible RNAi, TbUBA1b ranks among the 1% of genes with the severest growth defect upon knockdown (Alsford et al., 2011). Targeting of TbUBA1b led to an 88% reduction in viability after three days of induced RNAi, while targeting of TbUBA1a resulted in a 55% reduction at this time.

The E2 proteins of these parasites have not yet been studied, but approximately 15 E2 genes can be identified in their genomes based on the presence of a UQ-con motif (Gupta et al., 2018). E2s of *T. brucei* are between 26.5–74.3% identical to their human orthologues and based on sequence similarities functions may be attributed to some. For instance, the protein with the highest sequence identity to human E2s, Tb927.5.1000, is an orthologue of the proteins of the UBE2D (UbcH5) family, which are the most versatile E2s with roles in many processes (Brzovic and Klevit, 2006). In the whole-genome RNAi screen, the knockdown of Tb927.5.1000 decreases viability by 77% (Alsford et al., 2011), suggesting that the encoded E2 also has a widespread role in *T. brucei*. Along similar lines, *T. brucei* contains genes for orthologues of UBE2N (Ubc13) and UBE2V1, two E2s that specifically function in the formation of K63-linked poly-ubiquitin chains. The Ubc13 orthologue in *T. brucei* is 66% identical to the human protein, and its knockdown results in a 87% reduction in viability (Alsford et al., 2011), strongly suggesting that K63-linked ubiquitination plays an important role in *T. brucei*.

Based on the presence of RING, HECT or U-box domains, approximately 60 E3 ligases have been identified in the genomes of each individual trypanosomatid (Gupta et al., 2018). The group of RING domain proteins is by far the largest and shows the predicted heterogeneity in architectures as seen in other eukaryotes. Additionally, cullins and F-box proteins that constitute subunits of large E3 complexes are present. The trypanosomatid E3s have not yet been studied in any detail with the exception of a few. A cullin-RING CRL4^{WDRI} was identified in *T. brucei* that controls the levels of Polo-like kinase (TbPLK), a protein with several essential roles in cell division. The impediment of TbPLK ubiquitination by CRL4^{WDRI} was shown to severely affect its function (Hu et al., 2017). An intriguing finding is the identification of SPRING, a RING E3 ligase that is unique to *T. cruzi* (Hashimoto et al., 2010). This protein is secreted by *T. cruzi* and localizes to the nucleus of host cells where it may ubiquitinate proteins. So far SPRING has been demonstrated to have *in vitro* E3 activity, but its significance for *T. cruzi* infection has not yet been shown.

Processes Controlled by Ubiquitination in *T. brucei*, *T. cruzi* and *Leishmania*

The list of processes in which ubiquitination plays a role is still expanding. For a long time ubiquitination has been known to target damaged and old proteins to the proteasome and thus to be

important for protein homeostasis. This is now understood to extend to newly synthesized proteins that have failed to fold properly including those that are synthesized in the ER (Wu and Rapoport, 2018). In the latter case, proteins are translocated out of the ER and ubiquitinated by an ER-associated E2/E3 couple, Ubc6 (UBE2J)/Hrd1, a process known as ER-associated degradation (ERAD). Failure of ERAD induces ER stress, which induces a response mechanism that leads to programmed cell death. A functional ERAD pathway has been shown to be operational in *T. brucei* (Field et al., 2010; Tiengwe et al., 2016; Tiengwe et al., 2018), and orthologues of Ubc6, Hrd1 and other critical components are present. Also in *T. cruzi*, the retrotranslocation of proteins out of the ER has been demonstrated (Labriola et al., 2010). Based on genome analysis it has been proposed that in these parasites a minimal ERAD pathway with little redundancy exists. The resulting higher dependence on individual proteins has been proposed to make this crucial process an attractive drug target (Harbut et al., 2012).

In addition to essential housekeeping roles, ubiquitin-dependent proteasome degradation regulates processes that require the dynamic control of protein levels. Examples of these are the degradation of specific cyclins at different stages of the cell cycle which is essential for cell cycle progression, or the degradation of proteins in cell signaling. Both genomic and functional data show that, like in other eukaryotes, ubiquitination plays an important role in cell cycle progression of trypanosomatids. The large E3 protein complex SCFC (Skp1-CUL1-F-box complex) degrades cell cycle regulators and contains among its fixed components the E2 CDC34 (UBE2R1). Orthologues of Skp1, CULLIN1, RBX1 and CDC34 are all present in *T. brucei*, and the depletion of TbCDC34 results in cell death (Rojas et al., 2017). Further evidence comes from the presence of cyclins with short half-lives, which has been shown for both *T. brucei* and *T. cruzi*. In the presence of proteasome inhibitors, the half-lives of these proteins significantly increase and poly-ubiquitinated forms accumulate (Hellemond and Mottram, 2000; Renzo et al., 2016). The Anaphase promoting complex/cyclosome, APC/C, is another large E3 complex required for cell cycle regulation. Ten APC/C subunits were identified in *T. brucei* and the RNAi knockdown of one of these, AP2, resulted in cell cycle arrest and accumulation of poly-ubiquitinated cyclin B (Bessat et al., 2013). In *Leishmania*, the cell cycle dependent degradation of a kinesin also suggests the involvement of the ubiquitin-proteasome system (Dubessay et al., 2006). Furthermore, in this parasite the ubiquitin mediated degradation of the enzyme methionine adenosyl transferase has been reported. This degradation is believed to be important to control the levels of this metabolically important protein (Pérez-Pertejo et al., 2011).

Non-proteasome dependent outcomes of ubiquitination are also numerous and required for many essential cellular functions that includes a role in regulating the expression of cell surface transmembrane proteins. This has also been shown to be important in *T. brucei* for two abundant transmembrane proteins, ISG65 and ISG75. The mono-ubiquitination of these proteins at the C-terminal domain provides a signal for internalization and targeting to an endosomal/lysosomal

compartment for proteasome-independent degradation (Chung et al., 2008; Leung et al., 2011), which occurs in both the BSF and insect form of *T. brucei*. Furthermore, the knockdown of two de-ubiquitinating proteins, TbUsp7 and TbVdu1, was demonstrated to alter the abundance not only of ISG65 and ISG75 but also of several other proteins at the plasma membrane. The ESCRT machinery, large protein complexes that are required for ubiquitination, internalization and sorting of cell surface proteins, are believed to be present in trypanosomatids (Leung et al., 2011; Silverman et al., 2013) although no orthologues of the E3 ligases known to be associated with this complex have been found.

Thus, it is clear that ubiquitination is involved in many essential processes in trypanosomatids. There is evidence for K48-linked, K63-linked and mono-ubiquitination, and for proteasome-dependent as well as proteasome-independent outcomes. The importance of ubiquitination in these parasites is most succinctly illustrated by the severe impairment of viability upon knockdown of the TbUBA1s.

The Proteasome, the Major Cellular Protease

Structure and Function of the Proteasome

The 26 proteasome is a large structure in the cytoplasm and nucleus that is composed of a proteolytic 20 S core particle capped on either or both sides by a regulatory 19 S particle (Bard et al., 2018) (**Figure 1**). The core particle is barrel-shaped and consists of four rings of seven proteins each, the two outer rings containing α subunits and the two inner rings β subunits. Three of the β subunits, $\beta 1$, $\beta 2$ and $\beta 5$, have proteolytic activity and cleave after negatively charged (caspase-like activity), positively charged (trypsin-like activity) or large hydrophobic amino acids (chymotrypsin-like activity), respectively. The six catalytic sites are located in the hollow of the barrel through which substrates pass resulting in their cleavage into peptides of 15–20 amino acids. All three proteolytic activities are needed for efficient protein degradation although the relative contribution of each may vary for different substrates.

The proteolytic β subunits are N-terminal threonine proteases that are synthesized as proproteins and undergo autolytic cleavage during proteasome assembly which exposes their catalytic N-terminal threonine. The hydroxyl group of the threonine side chain acts as the nucleophile after its deprotonation and attacks the carbonyl carbon atom of the bond to be cleaved, forming a covalent acyl-enzyme tetrahedral intermediate and releasing the first product (Fenteany et al., 1995; Marques et al., 2009). Subsequent hydrolysis of the intermediate releases the second product and reconstitutes the active site of the protease. The deprotonation of the threonine hydroxyl group was reported to be enhanced by the free N-terminal amino group although a Lys at position 33 has more recently been shown to be involved in this (Huber et al., 2016).

One of the functions of the 19 S regulatory particle is to open the channel of the core particle which otherwise remains closed to prevent unwanted proteolytic degradation (Bard et al., 2018). The

19 S regulator is composed of two parts, a base and a lid. The base makes direct contact with the α subunits of the 20 S core particle and contains a ring of six Rpt subunits with ATPase activity that are required for the unfolding and translocation of substrates. This ring associates with three non-ATPase Rpn subunits, Rpn1, Rpn2 and Rpn13 that have structural (Rpn2) and ubiquitin-binding functions (Rpn1 and 13). The lid, which sits on top of the base but also makes direct contact with the core particle, is composed of another nine subunits whereas the subunit Rpn10, another ubiquitin-binding protein, cross-bridges the base and lid. The majority of subunits of the lid have structural functions, while Rpn11 is a de-ubiquitinase (Bard 2018 review). In addition, there are two more de-ubiquitinating enzymes stably associated with the proteasome, Usp14 and Uch37. Apart from the ubiquitin-binding subunits of the 19S, cytoplasmic shuttle factors play a role in delivering poly-ubiquitinated substrates to the proteasome.

The majority of proteins that are degraded by the proteasome are ubiquitinated, but ubiquitin-independent degradation takes place as well (Vigneron and Eynde, 2014). Examples include the degradation of proteins with intrinsically disordered regions and proteins damaged by oxidation. Such degradation can involve the 20 S core particle alone, or the 20 S particle associated with an alternative regulatory particle, 11 S or PA28. PA28 is a heptameric ring structure without ATPase activity that stimulates the activity of the 20 S core particle by opening the gate occupied by the loops of the α subunits (Figure 1) (Rechsteiner and Hill, 2005). The mammalian 11 S regulator can occur in two different forms either composed of a mix of PA28 α and PA28 β subunits, or composed of a single subunit, PA28 γ . PA28 $\alpha\beta$ is induced by interferon- γ and plays a role in antigen presentation by MHC I proteins in the adaptive immune response, PA28 γ is not induced by IFN- γ and is exclusively found in the nucleus. The 20 S associated with an 11 S regulator does not function in general proteolysis but rather has specific functions such as the degradation of peptides, disordered or oxidized proteins.

The proteasome is responsible for 80–90% of protein degradation and is thus the most important protease in the cell. The essential role of the proteasome is clear from the cytotoxic effect of proteasome inhibitors on eukaryotic cells.

Proteasomes of Trypanosomatids

The proteasomes of trypanosomatids resemble those of other eukaryotes but distinguishing features have been reported as well (Muñoz et al., 2015). The most extensively studied is the proteasome of *T. brucei*. Early purification studies failed to detect an association between the 20 and 19 S particle of *T. brucei* (Shao-bing et al., 1996) but this was found to result from an unusual instability of the 26 S proteasome during cell lysis (Li et al., 2002). In this respect, the *T. brucei* 26 S proteasome differs from that of other species including human, but also *T. cruzi* (Diego et al., 2001) and *Leishmania* (Robertson, 1999).

Another surprising observation was that a large fraction of the *T. brucei* 20 S core particle was isolated in a highly active form (To and Wang, 1997). This is the result of an association with an 11 S regulator, PA26, which is a heptameric ring of a single subunit

without ATPase activity that associates with the α subunits of the 20 S particle, thereby opening its gate (Yao et al., 1999; Whitby et al., 2000). Whereas PA26 resembles in structure and activity PA28, it is exclusively expressed in trypanosomatids and does not have extensive sequence similarity to PA28 subunits (Yao et al., 1999). PA26 can activate the 20 S proteasomes of mammals, but vice versa, mammalian PA28 can not activate the *T. brucei* 20 S proteasome (Yao et al., 1999). This again suggests that there are structural differences between the *T. brucei* and mammalian proteasomes. Like PA28, PA26 is involved in ubiquitin-independent degradation of peptides rather than proteins (Yao et al., 1999; Hill et al., 2002), but its physiological role is not yet clear. Both PA26 and the 19 S regulator are present in *T. cruzi* and locate to the cytoplasm, nucleus and kinetoplastid (Cardoso et al., 2011). The exposure of *T. cruzi* to gamma irradiation leads to an upregulation of PA26, suggesting that it may be important under stress conditions (Cerqueira et al., 2017). However, despite its abundance in *T. brucei*, ablation of PA26 did not affect the viability of the procyclic insect form of this parasite (Li et al., 2002).

The composition of the 19 and 20 S particles of trypanosomatids is the same as in other eukaryotes (Huang et al., 2001; Li et al., 2002; Wang et al., 2003; Muñoz et al., 2015). Thus, the 20 S core particle contains seven distinct α and seven distinct β subunits with three catalytic β subunits, but there are no equivalents of the additional three IFN- γ inducible β subunits that are found in vertebrates. The overall sequence identity of the *T. brucei* α subunits with human orthologues ranges between 37–54% and for β subunits between 33–50%. The depletion of either individual α or β subunit by RNAi in *T. brucei* leads to an accumulation of ubiquitinated proteins and a lack of cell growth (Li et al., 2002). Among the 19 S subunits, the six Rpt ATPases show the highest level of sequence conservation with 54–69% identity to human counterparts, whereas the Rpn subunits are between 20–46% identical. The loss of expression of all individual Rpt and Rpn proteins by RNAi results in an increase in ubiquitinated proteins, cell cycle arrest and subsequent cell death (Li et al., 2002; Li and Wang, 2002). This illustrates well the importance of ubiquitin-dependent proteasome degradation for the survival of *T. brucei*.

The proteolytic activity of the *T. brucei* 20 S proteasome displays several unique features. Initial experiments reported an unusual high trypsin-like activity, in contrast to the dominant chymotrypsin-like activity of mammalian proteasomes (Shao-bing et al., 1996). This was based on differences in relative activities of *T. brucei* and rat proteasomes against a limited set of peptides with different amino acids at P1, the site of amide bond lysis. An analysis with large peptide libraries in which also the amino acid requirements at the P2, P3 and P4 positions were taken into account, showed that *T. brucei* proteasomes preferably cleave after hydrophobic residues and therefore also have a dominant chymotrypsin-like activity (Wang et al., 2003). Nevertheless, differences between *T. brucei* and human proteasomes were also obvious in these experiments. Whereas both proteasomes prefer hydrophobic residues at the P2, P3 and P4 positions, only human proteasomes can recognize peptides with His, Lys, Asp

and Glu at these locations. In contrast, only the *T. brucei* 20S proteasome efficiently cleaved peptides with Gln at P1 (Wang et al., 2003). Overall it was concluded from the analysis of the peptide library experiments that the substrate specificity of the *T. brucei* $\beta 5$ subunit is very broad while that of $\beta 2$ is very limited.

Other differences between human and *T. brucei* proteasomes were observed in labeling experiments with the general probe ^{125}I -TyrLeu3-VS, a peptide vinylsulfone, that irreversibly binds to the active site of all three mammalian proteolytic β subunits (Bogyo et al., 1998). Strikingly, the *T. brucei* $\beta 1$ subunit does not react with this probe (Wang et al., 2003), and a similar result was found with a related fluorescently labeled probe, Me4BodipyFL-Ahx3Leu3VS (Wyllie et al., 2019). Furthermore, there was an absence of cleavage at acidic residues in the peptide library experiments (Wang et al., 2003). In the presence of PA26, when a drastic broadening of substrate selectivity was seen and also cleavage at acidic amino acids occurred, labeling of $\beta 1$ with the ^{125}I -TyrLeu3-VS probe was still not detected. This suggests that the $\beta 1$ subunit of *T. brucei* may be inactive or have unknown substrate selectivity. Further differences in substrate selectivity of the $\beta 2$ and $\beta 5$ subunits with the human proteins were also observed. The vinylsulfone ^{125}I -NP-L2N-VS, labels exclusively the $\beta 2$ subunit of *T. brucei*, but both $\beta 2$ and $\beta 5$ of human origin (Wang et al., 2003). Furthermore, the peptide suc-Leu-Leu-Val-Tyr-AMC is cleaved exclusively by $\beta 5$ in human proteasomes, but by $\beta 5$ and $\beta 1$ or $\beta 2$ in the *T. brucei* proteasome (Zmuda et al., 2019).

The proteasome activity of *T. cruzi* has not been as extensively studied, but for this parasite all three proteolytic activities were readily detected, including the caspases-like activity assigned to $\beta 1$ (González et al., 1996). For *Leishmania*, where the analysis is even more preliminary, differences between two different species were detected. The proteasomes of *L. chagasi* showed a three times higher trypsin- than chymotrypsin-like activity (Chagasi) (Silva-Jardim et al., 2004), but this was not the case for *L. mexicana* (Robertson, 1999). The activity of $\beta 1$ was not studied for either. More detailed analyses are required to map the substrate selectivity of the *T. cruzi* and *Leishmania* proteasomes.

INHIBITION OF UBIQUITINATION

UBA1 Inhibitors

An overall inhibition of ubiquitination disrupts proteasomal degradation, lysosomal degradation as well as non-degradative ubiquitin-regulated processes (Figure 1), and thus affects a wide range of vital eukaryotic processes.

UBA1 is by far the preferred drug target of the ubiquitinating enzymes because of its position at the apex of the ubiquitination cascade (Barghout and Schimmer, 2021). Moreover, UBA1 has two catalytic domains, of which the ATP-binding adenylation domain is amenable to inhibition by nucleotide mimetics, a well explored strategy of inhibition. The catalytic cysteine domain can be targeted as well, but thiol reactive molecules often suffer from a general high reactivity and therefore a limited selectivity. A similar problem exists for the targeting of E2 proteins that

also have an active site cysteine. Finally, the possibility of generally targeting E3 proteins is limited because these proteins are highly diverse and the majority do not possess catalytic activity. Instead, they function by optimally placing the E2-bound ubiquitin for attack by lysines of the substrate. Nevertheless, very few UBA1 inhibitors have been developed so far, but this is changing because of the success of proteasome inhibitors in the clinic. The inhibition of ubiquitination is now seen as a possible alternative or complementary approach to proteasome inhibition in cancer treatment.

The activation of ubiquitin by UBA1 starts with the adenylation of the C-terminus of ubiquitin in the presence of ATP, thus forming a ubiquitin~AMP adduct and releasing PPi (Schulman and Harper, 2009) (Figure 2). This takes place at the adenylation domain (AAD) and is followed by a conformational change that brings the catalytic cysteine domain (CCD) closer, so that a UBA~ubiquitin thioester bond is formed and AMP is released. After adenylation of a second ubiquitin, the thioester-bound ubiquitin is primed for transfer to an E2 via a transthioesterification reaction. The E2s are recruited to UBA1 by its UFD.

The first indication that UBA1 inhibition can be achieved, came from the synthesis of an ubiquitin-conjugate, adenosylphospho-ubiquitinol (APU), that mimics the ubiquitin-adenyl intermediate but is not hydrolyzable and inhibits UBA1 in an ATP-competitive manner (Wilkinson et al., 1990). Although this inhibitor is very effective in cell free assays it is unable to enter cells. The same is true for two other ubiquitin conjugate inhibitors Ub-AMSN and Ub-AVSN (Lu et al., 2010).

The first cell-permeable inhibitor is the small molecule PYR-41, which was identified in a screen for E3 inhibitors but showed a more potent effect against UBA1 (Yang et al., 2007). The furan ring of this molecule is essential for its inhibitory activity, but the precise binding of PYR-41 to UBA1 has not yet been established. This compound inhibits the formation of the ubiquitin-thioester bond without affecting the ubiquitin-adenylation step (Ungermannova et al., 2011). When added to cells, PYR-41 inhibits both proteasome-dependent degradation of cyclins and lysosomal degradation of EGFR, as expected from an UBA1 inhibitor (Yang et al., 2007). Transformed cells were found to be more susceptible to killing by PYR-41 than non-transformed cells. However, this molecule also induces covalent protein cross-linking in cells and is therefore not a selective UBA1 inhibitor (Kapur et al., 2011). The molecule PYZD4409 is structurally related to PYR-41 and was found in a small-scale screen for UBA1 inhibitors focused on pyrazolidines (Xu et al., 2010). In cells, this molecule inhibits the degradation of short-lived molecules such as p53 and cyclin D3, but it is expected to display the same off-target effects as PYR-41.

Two molecules, the natural product largazole and NSC624206 were isolated in cell-based screens for inhibitors of the degradation of the cell cycle inhibitor p27 (Ungermannova et al., 2011; Ungermannova et al., 2012). Largazole inhibits UBA1 at the adenylation step *in vitro* but its cellular toxicity may primarily be attributed to HDAC inhibition (Ying et al., 2008; Barghout and Schimmer, 2021). NSC624206 inhibits UBA1 at the thioester formation step (Ungermannova et al., 2011).

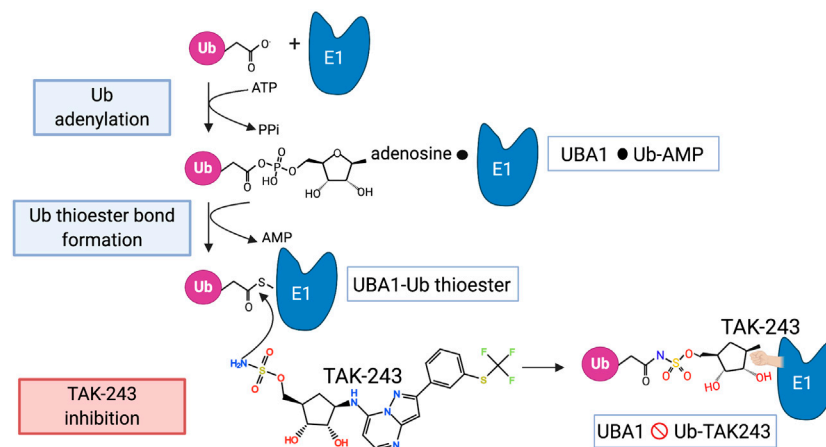


FIGURE 2 | The mechanism of UBA1 inhibition by TAK-243. The steps involved in the activation of ubiquitin by UBA1 are shown as well as the mode of action of TAK-243 as described in the main text. The black circle indicates a non-covalent association.

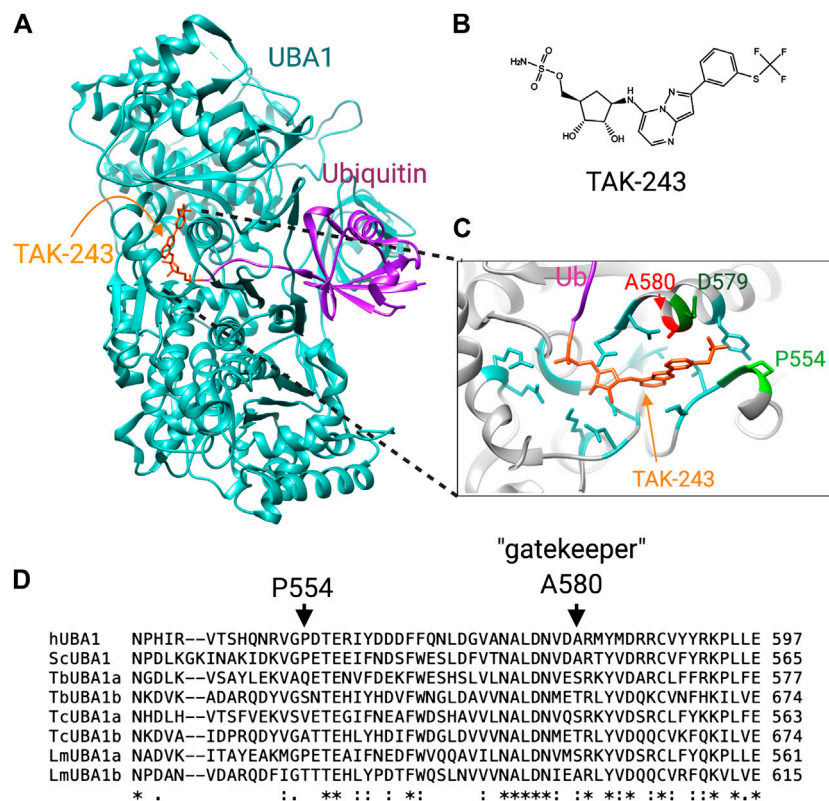


FIGURE 3 | Differences at the TAK-243 binding site between human and trypanosomatid UBA1s. **(A)** The crystal structure of *S. cerevisiae* UBA1 complexed with a TAK-243-ubiquitin adduct (PDB: 5L6J). **(B)** chemical structure of TAK-243. **(C)** Detailed view of the TAK-243 binding site in which the crucial differences with the *T. brucei* TbUBA1s are labeled. **(D)** Amino acid sequence comparison of human, yeast and trypanosomatid UBA1s. The residues that contribute to the resistance of TbUBA1a and TbUBA1b to TAK-243 are indicated with arrows.

NSC624206 was co-crystallized with *S. pombe* UBA1, but its orientation in this structure was not related to its inhibitory activity so its mechanism is not yet clear (Lv et al., 2017).

A great advance in UBA1 targeting came with the development of TAK-243 (previously called MLN7243), a potent selective UBA1 inhibitor with a well-established mode

of action (Hyer et al., 2018) (**Figure 2**). TAK-243 belongs to the same class of molecules as MLN4924 (pevonedistat) that selectively inhibits UBA3 (Soucy et al., 2009), the E1 for the ubiquitin-like protein Nedd8. MLN4924 is currently tested in phase 1 and 2 clinical trials of various malignancies because of the importance of cullin E3 neddylation in cell cycle progression. TAK-243 and MLN4924 are adenosyl sulfamates that act as AMP mimetics and inhibit E1s in a unique manner that has been termed substrate-assisted inhibition since it requires the activity of the E1 in adenylation and thioester bond formation of ubiquitin (or Nedd8) (Brownell et al., 2010; Barghout and Schimmer, 2021). Thus, the mechanism of TAK-243 involves its binding to the ATP binding site of UBA1, from where its sulfamate NH_2 attacks the UBA1~ubiquitin thioester bond. The result is a stable TAK243~ubiquitin adduct that cannot be released from the enzyme and inhibits all further ubiquitin activation (Hyer et al., 2018) (**Figure 2**). In crystal structures TAK-243 can be seen to occupy the site normally taken by AMP where it is bound to ubiquitin (Misra et al., 2017) (**Figure 3**). TAK-243 inhibits cell free UBA1 with an IC_{50} that is respectively 6, 28 and 850x lower than that for UBA6, UBA3 and UBA2 (SUMO E1), and $>5,000 \times$ lower than that for UBA7 (ISG15 E1) and ATG7 (E1 involved in autophagy) (Hyer et al., 2018). In agreement with UBA1 as the main target, TAK243 inhibits the degradation of short-lived molecules in cells, induces ER stress and alters DNA repair. It also arrests cells at the G1 and G2/M phase of the cell cycle and kills a wide variety of tumor cells at EC_{50} s between 0.006 and $1.31 \mu\text{M}$. TAK-243 inhibits the proliferation of xenograft tumors in mice and the presence of TAK-243~ubiquitin adducts can be detected in tumor tissues (Hyer et al., 2018).

Targeting Trypanosomatid UBA1s

The inhibition of *T. brucei* UBA1s by TAK-243 has been investigated by *in vitro* transthiolation assays and showed that both UBA1s are virtually resistant to TAK-243 (Boer and Bijlmakers, 2019). The inhibition of TbUBA1a required >500 -fold higher concentrations than that of hUBA1, and the inhibition of TbUBA1b required >100 -fold higher concentrations. The explanation for this resistance comes from important differences with the human protein at the TAK-243 binding pocket. This shows promise for the design of inhibitors with the opposite property of inhibiting the parasite, but not human UBA1.

The mode of TAK-243 binding has been demonstrated in crystal structures of humanized yeast UBA1 with bound TAK-243-ubiquitin. This revealed that this molecule protrudes further into the AAD domain than AMP (Misra et al., 2017; Hyer et al., 2018). Specifically, the molecule extends into a pocket where the trifluoromethyl-thiophenyl group adopts the shape of a hook (Misra et al., 2017). The resistance of the TbUBA1s to TAK-243 was found to stem from amino acid differences with hUBA1 at this pocket: of the four residues that make tight contacts with the trifluoromethyl-thiophenyl in the humanized yeast UBA1, three are different in both TbUBA1a and TbUBA1b (Boer and Bijlmakers, 2019). The most striking difference is that of the gatekeeper residue, A580 in hUBA1 (**Figure 3**). This alanine is

highly conserved throughout evolution and is found at equivalent positions in other E1s as well. This residue plays a key role in the binding of adenosyl sulfamate inhibitors, which was first demonstrated for UBA3 by the induction of MLN4924 resistance in tumor cells and xenografts (Milhollen et al., 2012; Toth et al., 2012). In two thirds of MLN4924 resistant cells, the UBA3 equivalent of the gatekeeper, A171, was replaced by a bulkier amino acid, such as a threonine or aspartic acid.

In UBA1, a similar role for this residue was demonstrated by the reduced sensitivity of a A580T mutant to inhibition by TAK-243 (Misra et al., 2017). Moreover, an A580S mutation was detected in an AML cell line with evolved resistance to TAK243 (Barghout et al., 2019). However, despite the high evolutionary conservation of this alanine, TbUBA1a contains a serine at the equivalent position (S560) and TbUBA1b a threonine (T657) (Boer and Bijlmakers, 2019) (**Figure 3**). Consistent with an important role in TAK243 resistance, the substitution of these residues to an alanine significantly increased sensitivity to TAK243. This was particularly striking for TbUBA1b where an T657A mutation increased sensitivity to TAK243 ~ 100 times. The second important difference at the “trifluoromethyl-thiophenyl” pocket is the presence of a glutamine (Q534) in TbUBA1a and a serine (S631) in TbUBA1b at the equivalent position of P554 in hUBA1. Substitution of these residues by a proline further increased the sensitivity to TAK-243 of the TbUBA1s, with the greatest effect on TbUBA1a. The difference at the third residue at this pocket, which is an aspartic acid in hUBA1 (D579) and a glutamic acid in TbUBA1a and TbUBA1b, contributes little to TAK-243 resistance consistent with its more conserved nature. Overall, the humanizing mutations increased TAK-243 sensitivity of TbUBA1a ~ 25 x and that of TbUBA1b > 100 x, illustrating the importance of these residues in the distinct susceptibility to TAK-243 inhibition of the *T. brucei* UBA1s compared to the human protein (Boer and Bijlmakers, 2019).

The presence of a threonine at the gatekeeper position of UBA3 has been predicted to clash with the indane group of MLN4924, based on structural modeling (Milhollen et al., 2012). Similarly, the serine and threonine at this position in TbUBA1a and TbUBA1b respectively, are predicted to clash with the thiophenyl group of TAK243 (**Figure 3**). Additionally, structural modeling predicts that the “trifluoromethyl-thiophenyl” pocket is considerably larger in both TbUBA1a and TbUBA1b than in hUBA1 (Boer and Bijlmakers, 2019). Furthermore, the rigidity that comes from P554 at the “far end” of this pocket may put constraints on the hUBA1 pocket that are not present in the *T. brucei* UBA1s (**Figure 3**). These important differences predict that parasite-selective inhibitors can be generated, for which the replacement of the trifluoromethyl group of TAK243 by bulkier groups may be a good starting point. Additionally, the TbUBA1 proteins can be used in high throughput enzymatic assays to screen for novel inhibitors.

Interestingly, the *T. cruzi* UBA1s, TcUBA1a and TcUBA1b, differ at the gatekeeper and the P554 equivalent as well (**Figure 3**). Like TbUBA1a, TcUBA1a has a serine at the gatekeeper position and like TbUBA1b, TcUBA1b has a threonine at this location. In

L. major, LmUBA1a has a serine at the gatekeeper as well, but LmUBA1b contains the conserved alanine (Figure 3). On the other hand, LmUBA1a does not differ from hUBA1 at the P554 equivalent, whereas LmUBA1b does. Nevertheless, the LmUBA1a protein is also more than 100-fold less sensitive to TAK-243 compared to hUBA1, consistent with the importance of the difference at the gatekeeper residue (Boer and Bijlmakers, 2019). It remains to be determined whether the generation of a pan-trypanosomatid UBA1 inhibitor will be possible, or whether the differences between the trypanosomatids require inhibitors to be optimized for each species. It is also not yet known whether both UBAs would need to be targeted in these trypanosomatids. The severity of the TbUBA1b knockdown argues that the sole inhibition of this protein would be sufficient for *T. brucei*, but such data are not available for *T. cruzi* and *Leishmania*. Importantly, a precedent for the targeting of UBA1 in parasites was recently set by the demonstration that TAK243 inhibits the growth and development of *Plasmodium* (Green et al., 2020). Treatment with TAK-243 was found to result in an absence of viable parasites released from red blood cells. An induced knockdown of UBA1 resulted in the same phenotype as TAK243 inhibition, also showing the power of targeting UBA1. The UBA1 of *Plasmodium* does not differ from hUBA1 at the gatekeeper position, and consistently, the recombinant protein was found to be inhibited by TAK-243 at similar IC50s as recombinant hUBA1.

Targeting E1s of Ubiquitin-like Proteins

In addition to UBA1, the trypanosomatids contain genes for five other E1s, namely UBA2, UBA3, UBA5, MOCS3 and ATG7 (Boer and Bijlmakers, 2019). These are involved in the activation of ubiquitin-like proteins and work in cascades with E2 and E3 proteins similar to that of ubiquitination. UBA2 and UBA3 are the E1s for SUMO and Nedd8, respectively, the attachment of which also leads to changes in the activity of substrates. In contrast to UBA1, the E1s for SUMO and Nedd8 are heterodimers. The SUMO E1 is composed of the catalytic UBA2 in which the active adenylation domain, catalytic cysteine domain and the UFD are located, and the structurally important AOS1. A similar division of labor is found in the SUMO E3 that consists of the catalytic UBA3 and the structural APPBP1.

SUMOylation plays crucial roles in many cellular processes including gene expression, DNA repair, protein transport and cell cycle progression (Gareau and Lima, 2010). In accordance with this, sumoylation is essential for eukaryote survival. Trypanosomatids express only one SUMO protein, whereas there are four in humans. The RNAi knockdown of SUMO in *T. brucei* has been shown to be lethal in both the insect and blood stream form (Liao et al., 2010), showing that sumoylation plays an essential role in this parasite as well. Furthermore, data from a genome-wide RNAi screen in *T. brucei* show that knockdown of UBA2 and AOS1 reduce viability by 40 and 75%, respectively (Alsford et al., 2011).

The UBA2/AOS1 and the E2 dedicated to SUMOylation, Ubc9, of *T. brucei* have been purified and shown to have *in vitro* sumoylation activity (Ye et al., 2015). Some substrates

have been identified in *T. brucei*, such as TbAUK1, an orthologue of Aurora B kinase that plays crucial roles in mitosis and cytokinesis. A mutation at the sumoylation site of this protein was shown to interfere with its function (Hu et al., 2014). Sumoylation has further been shown to positively regulate the expression of VSG, the variant surface protein of *T. brucei* that is key to its escape from the immune system (López-Farfán et al., 2014; Saura et al., 2019). Sumoylation of the transcription factor SNF2PH is essential for its presence at the VSG-ES (expression site) promoter and thus for transcription from this site. A proteomics approach with an affinity tagged SUMO identified 45 SUMOylated proteins in *T. brucei* with predominantly roles in the nucleus (Iribarren et al., 2015). In *T. cruzi*, a mass spectrometry-based approach detected more than 200 sumoylation substrates (Bayona et al., 2011). Parasite specific processes may also be regulated by SUMOylation in *T. cruzi* since this modification was not only detected in the nucleus but also on the flagellum. Here, the flagellar rod protein PFR1 was identified to be a SUMOylation substrate (Annoura et al., 2012).

Given the essential role of SUMOylation, inhibition of UBA2 is expected to be lethal and therefore provides another drug targeting possibility. Also for this protein there are indications that parasite selectivity may be achieved. ML-792 is an inhibitor that is selective for UBA2 and has the same mechanism of action as TAK-243 (He et al., 2017). This compound has been shown to be cytotoxic for human cells where it induces mitotic disruption. Mutations in UBA2 that cause a resistance to ML-792 have been identified and contained a substitution at S95 as well as M97, S95N/M97T. Significantly, the UBA2s of all three trypanosomatids do not contain a serine nor a methionine at the S95 and M97 equivalents, respectively. Moreover, the *T. brucei* and *Leishmania* UBA2s contain the resistance inducing asparagine at the corresponding position of S95. This indicates that also for this protein there are considerable differences in inhibitor binding properties between the human and the trypanosomatid form. This may represent another opportunity for the design of parasite-selective inhibitors with cytotoxic effects.

Finally, the knockdown of Nedd8 by RNAi has also been shown to be lethal in *T. brucei* (Liao et al., 2017). A major role of Nedd8 is the activation of cullin CRL-type ubiquitin ligases that play important roles in cell cycle progression. In agreement with this, Nedd8 deficient *T. brucei* showed a reduction in overall ubiquitination, mitotic defects and cell death. Moreover, six cullins were shown to be neddylated in *T. brucei* and a further 70 substrates were identified by affinity purification followed by mass spectrometry. The deficiency in Nedd8 was further found to lead to a detachment of the flagella. Thus, given these essential roles of Nedd8 the trypanosomatid UBA3 may be regarded as a drug target as well.

INHIBITION OF THE PROTEASOME

Proteasome Inhibitors

Proteasome inhibitors have been used extensively in research and were instrumental in obtaining functional and mechanistic

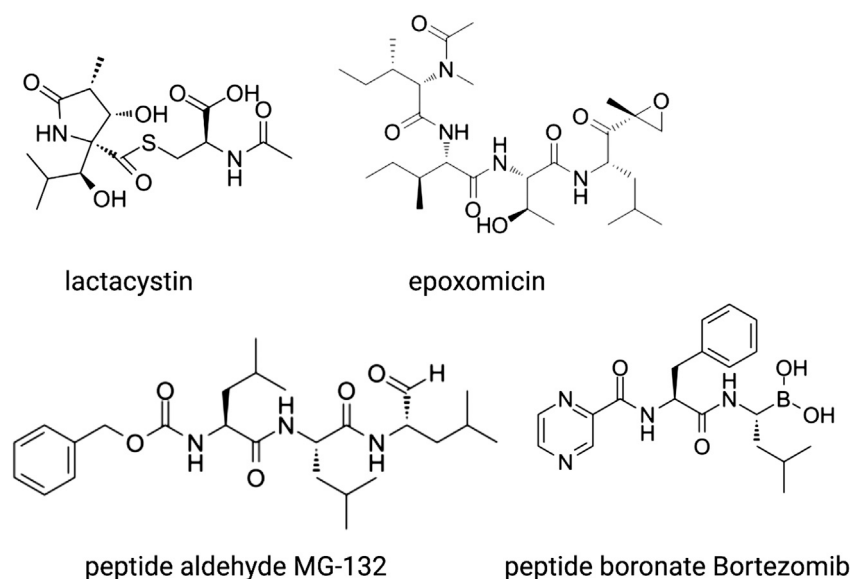


FIGURE 4 | The main classes of proteasome inhibitors that target the proteolytic sites.

insights into proteasome activity (Fenteany et al., 1995; Lee and Goldberg, 1998; Groll and Potts, 2011). More recently they have entered the clinic as anti-cancer drugs. They have also been used in studies of trypanosomatids to determine the role of the proteasomes in the growth and differentiation of these parasites.

Proteasome inhibitors fall into several chemical categories and have been isolated from micro-organisms as well as rationally designed based on pre-existing knowledge of protease inhibition (**Figure 4**). One of the first molecules identified is lactacystin, a natural compound that was isolated from the soil-dwelling bacteria *Streptomyces lactacystinaeus* (Ōmura and Crump, 2019). Lactacystin is a lactam, or cyclic amide, that in aqueous solutions spontaneously converts into the active inhibitor clasto-lactacystin- β -lactone (Dick et al., 1996). This compound binds irreversibly to the catalytic amino-terminal threonine of the β 5 and β 2 subunit where it forms an ester adduct, and reversibly to that of β 1, blocking all proteasome activity (Fenteany et al., 1995). Another naturally occurring γ -lactam- β -lactone is Salinosporamide A, a product of the marine bacteria *Salinospora*, which has a similar mode of action but is > 30x more potent than lactacystin (Feling et al., 2003).

Another natural compound, the linear peptide epoxyketone epoxomicin (**Figure 4**), was isolated from an Actinomycetes strain of bacteria. The selectivity of this inhibitor for the proteasome is even higher than that of lactacystin, which also inhibits the lysosomal protease Cathepsin A (Meng et al., 1999). Epoxomicin undergoes two subsequent rounds of nucleophilic attacks, first by the side chain hydroxyl of the N-terminal threonine and next by the free amine group, which results in an irreversible six-membered morpholino bond. Epoxomicin inhibits all three subunits, but by far the strongest effect is on β 5. Other natural products with anti-proteasomal activity have been isolated from micro-organisms as well, such as the β -lactone

belactasin A, the aldehyde fellutamide B and the syrbactins that have yet another mode of action.

MG-132 was the first synthetic proteasome inhibitor to be generated (Lee and Goldberg, 1998). This compound belongs to the class of peptide aldehydes that were previously characterized as inhibitors of serine and cysteine proteases. The peptide part of MG-132 acts as a substrate analogue whereas the aldehyde is the pharmacophore that reacts reversibly with the hydroxyl group of the catalytic N-terminal threonine. MG-132 inhibits lysosomal cysteine proteases and calpains as well but at higher concentrations than required for proteasome inhibition. Peptide vinyl sulfones were designed as irreversible proteasome inhibitors and have been used as labelling probes to obtain insights into the proteolytic mechanisms and sequence preferences of the catalytic subunits as described above (Bogyo et al., 1997).

Since their first discovery, lactacystin and epoxomicin have been shown to inhibit cell cycle progression. Cancer cell lines and xenograft tumors in mice are considerably more sensitive to these inhibitors than non-transformed cells because of a higher dependence on protein quality control mechanisms that comes with their rapid proliferation rate and, in some hematological malignancies, because of ER stress coming from the production of large amounts of antibodies. Therefore, proteasome inhibitors were explored as anti-cancer drugs, which resulted in the development of bortezomib (**Figure 4**), a boronated dipeptide that is much more potent and selective than MG-132 and has good bioavailability (Adams, 2001). The boronate forms an adduct with the active site of the β subunits, which is stabilized by a hydrogen bond between the free N-terminal amino group and one of the hydroxyl groups of the boronate. This explains its selectivity for N-terminal threonine proteases over other proteases. Bortezomib is now used in the clinic as first-

line treatment for multiple myeloma and mantle cell lymphoma and is being considered for solid tumors. Novel proteasome inhibitors are being developed because of the occurrence of pre-existing or induced resistance to bortezomib and severe adverse effects. These include the epoxomicin-related carfilzomib, the naturally occurring β -lactam marizomib (Salinosporamide), and the orally available boronated dipeptide ixazomib.

Effects of Proteasome Inhibitors on Growth and Differentiation of Trypanosomatids

Proteasome inhibitors have also been shown to cause cell cycle arrest and cell death in trypanosomatids. Treatment of *T. brucei* blood stream form with lactacystin, for instance, causes an arrest in G1 and G2 and cell death by apoptosis after 24 h (Mutomba et al., 1997). Similar results were obtained with the MG-132 related tripeptide aldehyde inhibitor LLnV. Both lactacystin and LLnV were also toxic against the insect form of *T. brucei* although this arrest was at the G2/M phase and required 5–10 x higher concentrations and longer incubations than for the blood stream form. In contrast, the differentiation of the insect form into the blood stream form, a process that does not involve the crossing of cell cycle stage boundaries, was not inhibited by proteasome inhibitors (Mutomba and Wang, 1998).

However, lactacystin does inhibit the differentiation of *T. cruzi*. This parasite infects mammalian cells in the non-cycling trypomastigote form, which subsequently differentiates into amastigotes that replicate in the cytoplasm of the host cells. This differentiation can be mimicked under cell-free conditions, which was found to be strongly inhibited by lactacystin (González et al., 1996). It was further observed that the pretreatment of trypomastigotes with lactacystin did not prevent infection of cells, but resulted in a ~75% reduction in intracellular parasites at 72 h after infection (González et al., 1996). This indicates that also intracellular differentiation was affected and perhaps amastigote proliferation as well. In the absence of inhibitor, amastigotes in the host cell undergo several days of cell division before differentiating into trypomastigotes that leave the cells. When established intracellular amastigote infections were treated with lactacystin, a ~10-fold reduction in released trypomastigotes was observed together with a continued presence of intracellular amastigotes (González et al., 1996). This demonstrated that also the amastigote to trypomastigote differentiation is affected by proteasome inhibition. Another important process in the complicated life cycle of *T. cruzi* is metacyclogenesis, which takes place inside the triatominae and involves the differentiation of the non-infectious proliferating epimastigote into the infectious non-proliferating trypomastigote form. Lactacystin was found to inhibit both the growth of epimastigotes in culture (Cardoso et al., 2008) and metacyclogenesis (Cardoso et al., 2011). Similar results on differentiation were reported for *L. chagasi*, which alternates between the flagellated insect form, the promastigote, that infects human cells and the intracellular non-flagellated amastigote that replicates inside the phagolysosomes of the

host cells. The proliferation of promastigotes in culture was inhibited by lactacystin but their ability to infect cells was not. However, pretreatment of promastigotes with lactacystin severely reduced the survival of the parasite inside host cells (Silva-Jardim et al., 2004).

Thus, although different effects on differentiation have been reported, proteasome inhibition is toxic for all three parasites.

Trypanocidal Proteasome Inhibitors

The toxicity of proteasome inhibitors, together with the differences in substrate selection between trypanosomatid and mammalian proteasomes suggests that selective inhibition of parasite proteasomes can be achieved (Nkemgu-Njinkeng et al., 2002). In addition to the ones described above, a wide range of other proteasome inhibitors of different chemical classes have been shown to kill cultures of *T. brucei* blood stream forms, sometimes at lower EC50s than mammalian cells. These include various peptide aldehydes, epoxomicin and its derivatives, peptidyl vinyl sulfones, peptidyl vinyl esters, and several natural γ -lactam- β -lactones (Glenn et al., 2004; Steverding et al., 2005; Steverding et al., 2011a; Steverding et al., 2011b). Several studies have shown differences in the relative inhibition of β 5 and β 2 subunits between trypanosoma and human proteasomes, again indicative of the parasite proteasome possessing distinct catalytic activities (Nkemgu-Njinkeng et al., 2002; Wang et al., 2003; Zmuda et al., 2019). However, the design or selection of trypanosomatid-selective inhibitors based on these proteolytic differences has not yet been possible (Steverding et al., 2018). Nevertheless, in recent years impressive progress in the development of trypanosomatid-selective proteasome inhibitors with a promise for the clinic has been made. This progress has come from large phenotypic screens in which proteasome inhibitors with an unpredicted mode of action were identified.

The first breakthrough came from a screen of 3,000,000 compounds for cytotoxic effects on *T. brucei*, *T. cruzi* and *L. donovani* (Khare et al., 2016). A candidate molecule was selected based on potency, activity against all three parasites, and limited effects on mammalian cells. This molecule was modified to obtain GNF6702 (Figure 5) with better bioavailability and enhanced potency against intramacrophage *Leishmania*. In mouse models, GNF6702 given via oral gavage was found to be at least as effective as existing drugs against visceral leishmaniasis (*L. donovani* infection), cutaneous leishmaniasis (*L. major* infection), Chagas' disease (chronic *T. cruzi* infection) and stage II HAT (meningoencephalic *T. brucei* infection) (Khare et al., 2016). GNF6702 reduced the number of *L. donovani* by 90% in all five treated mice, cleared *T. cruzi* from all but one out of eight mice, and cured *T. brucei* infection up to 94 days of monitoring in all six mice. In the latter case the compound had to be given at a 10-fold higher concentration (100 mg/kg) because of poor brain accessibility.

The mechanism of GNF6702 was determined by evolving drug-resistant *T. cruzi* strains, which identified the non-proteolytic β 4 subunit of the proteasome as a target (Khare et al., 2016). Overexpression of a β 4 protein carrying the mutations detected in the resistant strains, F24L and I29M,

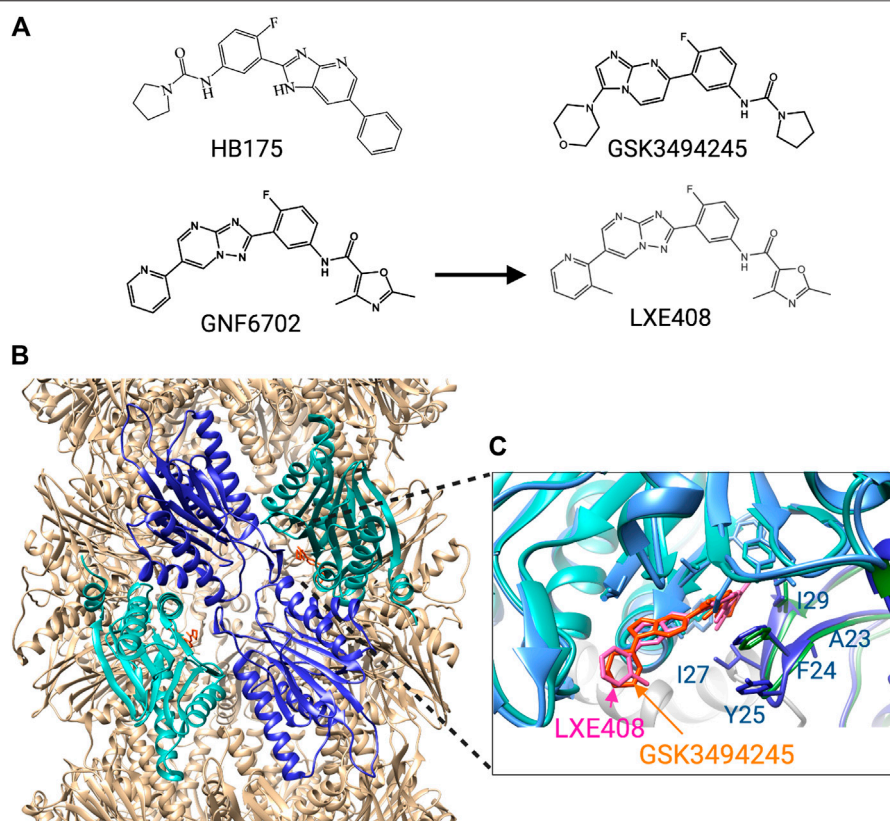


FIGURE 5 | Trypanosomatid selective proteasome inhibitors. **(A)** structures of the inhibitors. **(B)** Cryo-EM structure of *L. tarantulae* proteasome complexed with GNF6702 (PDB 6QM7). The $\beta 5$ subunits are in cyan, and the $\beta 4$ subunits in blue. The inhibitor GNF6702 is in orange. **(C)** Detailed view of the inhibitor binding site located between the $\beta 4$ and $\beta 5$ subunits. The structure of the *L. tarantulae* proteasome with GNF6702 was overlayed with that of the *L. tarantulae* proteasome complexed with LXE408 (PDB6TCZ), showing the similar position of the two inhibitors. The residues of $\beta 4$ that differ in human $\beta 4$ are labeled.

rendered *T. cruzi* and *T. brucei* resistant to GNF6702 but not to bortezomib or MG-132. This is consistent with an alternative mode of inhibition that does not affect the active site of the catalytic proteasome subunits. GNF6702 was further shown to inhibit the chymotrypsin-like activity of the $\beta 5$ subunit, but not the trypsin- and caspase-like activity of the other proteolytic subunits. This, together with the location of the resistance-inducing mutations suggested an allosteric inhibitory mechanism in which the molecule binds in a pocket between the $\beta 4$ and $\beta 5$ subunit.

Insights into such an allosteric inhibition came from the synthesis of GSK3494245 (**Figure 5**), based on a hit from another phenotypic screen (Wyllie et al., 2019). GSK3494245 reduces parasite load by 95% after 10 days in a mouse model of visceral leishmaniasis, similar to treatment with the current drug miltefosine. GSK3494245 is an imidazopyrimidine and thus related in structure to the triazolopyrimidine GNF6702. Therefore, its effect on the proteasome was investigated which demonstrated that like GNF6702, GSK3494245 inhibits the chymotrypsin- but not the trypsin- and caspase-like activity. Importantly, GSK3494245 was > 100-fold less active against human proteasomes. Consistent with a mechanism that involves the proteasome, *Leishmania* strains with evolved

GSK3494245 resistance were found to have mutations at T30 of $\beta 4$ and G197 of $\beta 5$, both of which are located at the $\beta 4$ - $\beta 5$ interface (Wyllie et al., 2019).

The binding mode of GSK3494245 was conclusively determined by cryo-EM using *L. tarantulae* proteasomes (Wyllie et al., 2019). This showed that GSK3494245 binds between the $\beta 4$ and the $\beta 5$ subunit but, unexpectedly, protrudes mostly into the $\beta 5$ subunit (**Figure 5**). Only the pyrrolidine carboxamide group binds in a narrow hydrophobic pocket of $\beta 4$ where it makes contact with six $\beta 4$ residues in addition to three from $\beta 5$. Significantly, the majority of the human $\beta 4$ residues at equivalent positions (**Figure 5**) are different and the corresponding cavity in the human protein is more open, shallow and solvent exposed. This provides a plausible explanation for the lack of GSK3494245 activity against human proteasomes. The G197 residue of $\beta 5$ identified in GSK3494245-resistant *Leishmania*, makes direct contact with the inhibitor, whereas the similarly identified T30 of $\beta 4$ is likely to be important for access to the $\beta 4$ pocket. Also $\beta 4$ residues F24 and I29 that were mutated in the GNF6702-resistant cells, make contact with GSK3494245 (**Figure 5**).

Treatment of *L. donovani* cultures with GSK3494245 resulted in an accumulation of ubiquitinated proteins, swelling of the

parasite and the presence of vesicles indicative of proteotoxic stress, and an arrest at G2/M, all consistent with a targeting of the proteasome (Wyllie et al., 2019).

Yet another large phenotypic screen identified an oxalopyridine with cytotoxic effects on *T. brucei*, which led to the generation of an imidazopyridine referred to as compound 64 (Tatipaka et al., 2014), later called HB175 (Figure 5). This molecule was shown to cure acute hemolympathic HAT in a mouse model. Based on the resistance of a *T. brucei* strain with a $\beta 4$ mutation at F24 to HB175, it was concluded that this molecule is also a proteasome inhibitor (Nagendar et al., 2018). A comparative study analyzed the effects of HB175 and 16 new imidazopyridines alongside GNF6702 and 12 new triazolopyrimidines, which showed that compounds of both classes kill *T. brucei* and intracellular *T. cruzi* at EC50s below 100 nM (Nagendar et al., 2018). While the imidazopyridines were on average slightly more potent, they also showed greater toxicity against a human lymphocytic cell line. Another more favorable characteristic of the triazolopyrimidines was their greater stability in the presence of mouse liver microsomes, which corresponded to a higher blood exposure in mice. The brain penetration of the triazolopyrimidines was also higher than that of the imidazopyridines although this was still not higher than 12% for the triazolopyrimidine GNF6702. In this study, the triazolopyrimidines were therefore only tested against *T. cruzi* and not against *T. brucei* infections. GNF6702 was found to be more potent than two of the novel triazolopyrimidines in a mouse model of acute *T. cruzi* infection, in which mice are infected with a parasite dose that kills 95% within 20 days of infection. Treatment of mice on days 7–11 after infection with GNF6702 resulted in the absence of detectable parasites for 42 days, whereas this was only 13 days for the current drug benznidazole.

In another study, GNF6702 was investigated against *T. brucei* infection together with two related triazolopyrimidines, GNF3849 and NITD689 (Rao et al., 2020). All three compounds were able to cure hemolympathic HAT when given orally three days after infection for four days and mice stayed free of *T. brucei* up to 30 days of monitoring. In a stage II HAT model, mice treated with GNF6702 became parasite free and remained so for 94 days at a dose that was $\sim 3\times$ lower than in the first report on this compound (30 mg/kg instead of 100 mg/kg). Of the three compounds, GNF6702 had the most desirable characteristics since both GNF3849 and NITD689 showed limited *in vivo* availability, GNF3849 because of high protein binding properties and NITD689 because of low stability.

Although GNF6702 showed promising results, its solubility was too limited to make an oral formulation possible (Nagle et al., 2020). The insolubility was predicted to come from the planar shape of the molecule that leads to a crystallizing tendency. To force the molecule out of plane, groups were attached to the pyridine ring which resulted in a more soluble molecule, LXE408 (Figure 3), that retained good anti-proteasomal activity. Crucially, oral administration of LXE408 had greater efficacy in a visceral leishmaniasis model than miltefosine, the only oral medication available, and was as effective as the most potent drug amphotericin B in cutaneous leishmaniasis (Nagle et al., 2020).

The cryo-EM structure of LXE408 bound to *L. tarantulae* proteasomes showed that this molecule binds in a way analogous

to that of GSK3494245 (Nagle et al., 2020) (Figure 5). Thus, most of the molecule protrudes into the $\beta 5$ subunit and only the dimethyl-oxazole packs against $\beta 4$ residues that include F24 and I29. A structure of proteasomes with both LXE408 and bortezomib showed that bortezomib adopts a novel conformation in the presence of LXE408, which explains why the two inhibitors do not compete although their binding sites partially overlap.

LXE408 has a desirable safety profile and is now being tested in phase I clinical trials (Nagle et al., 2020). GSK3494245 also showed reasonable bioavailability and a good safety margin in rat and is being tested in phase I trials as well (Wyllie et al., 2019; Zmuda et al., 2019).

Thus, there are now two candidates of proteasome inhibitors with good efficacy, desirable safety profiles and the promise of short oral treatments. However, more molecules are needed to increase the pipeline given the low success rates of clinical trials. To identify these, target-based screens will also play important roles. To this end, a luminescence-based assay for chymotrypsin-like activity was optimized for high throughput screening with *T. cruzi* proteasomes (Zmuda et al., 2019). The assay was validated with peptide aldehyde (MG132, MG115), peptide boronate (bortezomib, ixazomib) and peptide epoxyketone inhibitors (epoxomicin, oprozomib). Following this, a screen with 18,039 compounds was performed that after a counter screen for technology interfering compounds resulted in 39 hits. Details of the identified molecules have not yet been reported. In addition, a novel tool for the selective screening of proteasome inhibitors in live *T. brucei* has been developed. This involves a modified *T. brucei* strain that expresses a GFP-tagged mutant ubiquitin molecule that cannot be hydrolyzed by deubiquitinating enzymes (Moura et al., 2018). Proof of principle experiments showed that treatment with lactacystin and MG-132 led to an accumulation of GFP-ubiquitin.

CONCLUDING REMARKS

The ubiquitin-proteasome system represents a good theoretical drug target in trypanosomatids because of its essential functions. However, there is now also substantial data demonstrating that selectively targeting this system in these parasites is indeed feasible. This is clearly proven by the development of trypanosomatid selective proteasome inhibitors that target this protein complex in a way not previously envisioned. The current inhibitors are promising, but general success rates of clinical trials are low and so further drug candidates are required. Moreover, there are additional challenges unique for these diseases such as the need for cheap, orally available compounds that can cure during a short treatment. Challenging cellular and tissue distribution criteria need to be met as well, such as the delivery to phagolysosomes for leishmaniasis and the ability to cross the blood-brain barrier for stage II HAT. For these reasons, it will be valuable to continue drug discovery programs including target-based high throughput screening of proteasomes either in purified form or in live trypanosomas modified for this purpose. Additionally, it will be important to explore the alternative, complementary strategy of inhibiting UBA1 enzymes. Trypanosomatid-selective inhibitors of this protein are not yet

available, but there is a good basis to predict that these can be obtained. Using TAK-243 as a starting point may be an effective way to achieve this, but also high throughput assays can be used to enquire additional chemical space. Since the consequences of ubiquitination are more widespread than that of proteasome inhibition, the inhibition of UBA1 may have more potent effects than the inhibition of the proteasome. It can also be envisaged that the complementary effects of proteasome and UBA1 inhibitors may be combined in drug treatment. Finally, further promise lies in the targeting of UBA2 and UBA3 that stand at the helm of essential processes as well and have not been explored for this purpose yet.

REFERENCES

- Adams, J. (2001). Proteasome inhibition in cancer: development of PS-341. *Semin. Oncol.* 28, 613–619. doi:10.1053/sonc.2001.28609
- Alsford, S., Turner, D. J., Obado, S. O., Sanchez-Flores, A., Glover, L., Berriman, M., et al. (2011). High-throughput phenotyping using parallel sequencing of RNA interference targets in the African trypanosome. *Genome Res.* 21, 915–924. doi:10.1101/gr.115089.110
- Annoura, T., Makiuchi, T., Sario, I., Aoki, T., and Nara, T. (2012). SUMOylation of paraflagellar rod protein, PFR1, and its stage-specific localization in trypanosoma cruzi. *PLoS One* 7, e37183. doi:10.1371/journal.pone.0037183
- Bard, J. A. M., Goodall, E. A., Greene, E. R., Jonsson, E., Dong, K. C., and Martin, A. (2018). Structure and function of the 26S proteasome. *Annu. Rev. Biochem.* 87, 1–28. doi:10.1146/annurev-biochem-062917-011931
- Barghout, S. H., Patel, P. S., Wang, X., Xu, G. W., Kavanagh, S., Halgas, O., et al. (2019). Preclinical evaluation of the selective small-molecule UBA1 inhibitor, TAK-243, in acute myeloid leukemia. *Leukemia* 33, 37–51. doi:10.1038/s41375-018-0167-0
- Barghout, S. H., and Schimmer, A. D. (2021). E1 enzymes as therapeutic targets in cancer. *Pharmacol. Rev.* 73, 1–56. doi:10.1124/pharmrev.120.000053
- Bayona, J. C., Nakayasu, E. S., Laverrière, M., Aguilar, C., Sobreira, T. J. P., Choi, H., et al. (2011). SUMOylation pathway in trypanosoma cruzi: functional characterization and proteomic analysis of target proteins. *Mol. Cell. Proteomics* 10, M110007369. doi:10.1074/mcp.m110.007369
- Bessat, M., Knudsen, G., Burlingame, A. L., and Wang, C. C. (2013). A minimal Anaphase promoting complex/cyclosome (APC/C) in trypanosoma brucei. *PLoS One* 8, e59258. doi:10.1371/journal.pone.0059258
- Bilbe, G. (2015). Overcoming neglect of kinetoplast diseases. *Science* 348, 974–976. doi:10.1126/science.aaa3683
- Boer, D. R., and Bijlmakers, M.-J. (2019). Differential inhibition of human and trypanosoma ubiquitin E1S by TAK-243 offers possibilities for parasite selective inhibitors. *Sci Rep.* 9, 16195. doi:10.1038/s41598-019-52618-3
- Bogyo, M., McMaster, J. S., Gaczynska, M., Tortorella, D., Goldberg, A. L., and Ploegh, H. (1997). Covalent modification of the active site threonine of proteasomal β subunits and the *Escherichia coli* homolog HslV by a new class of inhibitors. *Proc. Natl. Acad. Sci. Unit. States Am.* 94, 6629–6634. doi:10.1073/pnas.94.13.6629
- Bogyo, M., Shin, S., McMaster, J. S., and Ploegh, H. L. (1998). Substrate binding and sequence preference of the proteasome revealed by active-site-directed affinity probes. *Chem. Biol.* 5, 307–320. doi:10.1016/s1074-5521(98)90169-7
- Brownell, J. E., Sintchak, M. D., Gavin, J. M., Liao, H., Bruzzese, F. J., Bump, N. J., et al. (2010). Substrate-assisted inhibition of ubiquitin-like protein-activating enzymes: the NEDD8 E1 inhibitor MLN4924 forms a NEDD8-AMP mimetic in situ. *Mol. Cell.* 37, 102–111. doi:10.1016/j.molcel.2009.12.024
- Brzovic, P. S., and Klevit, R. E. (2006). Ubiquitin transfer from the E2 perspective: why is UbcH5 so promiscuous? *Cell Cycle* 5, 2867–2873. doi:10.4161/cc.5.24.3592
- Cardoso, J., Lima, C. D. P., Leal, T., Gradia, D. F., Fragoso, S. P., Goldenberg, S., et al. (2011). Analysis of proteasomal proteolysis during the in vitro metacyclogenesis of trypanosoma cruzi. *PLoS One* 6, e21027. doi:10.1371/journal.pone.0021027
- Cardoso, J., Soares, M. J., Menna-Barreto, R. F. S., Bloas, R. L., Sotomaior, V., Goldenberg, S., et al. (2008). Inhibition of proteasome activity blocks Trypanosoma cruzi growth and metacyclogenesis. *Parasitol. Res.* 103, 941. doi:10.1007/s00436-008-1081-6
- Cerqueira, P. G., Passos-Silva, D. G., Vieira-da-Rocha, J. P., Mendes, I. C., Oliveira, K. A. de, Oliveira, C. F. B., et al. (2017). Effect of ionizing radiation exposure on Trypanosoma cruzi ubiquitin-proteasome system. *Mol. Biochem. Parasitol.* 212, 55–67. doi:10.1016/j.molbiopara.2017.01.005
- Chung, W., Leung, K. F., Carrington, M., and Field, M. C. (2008). Ubiquitylation is required for degradation of transmembrane surface proteins in trypanosomes. *Traffic* 9, 1681–1697. doi:10.1111/j.1600-0854.2008.00785.x
- Clague, M. J., Barsukov, I., Coulson, J. M., Liu, H., Rigden, D. J., and Urbé, S. (2013). Deubiquitylases from genes to organism. *Physiol. Rev.* 93, 1289–1315. doi:10.1152/physrev.00002.2013
- Deshais, R. J., and Joazeiro, C. A. P. (2009). RING domain E3 ubiquitin ligases. *Annu. Rev. Biochem.* 78, 399–434. doi:10.1146/annurev-biochem.78.101807.093809
- Dick, L. R., Cruikshank, A. A., Grenier, L., Melandri, F. D., Nunes, S. L., and Stein, R. L. (1996). Mechanistic studies on the inactivation of the proteasome by lactacystin A central role for clasto-LACTACYSTIN β -LACTONE. *J. Biol. Chem.* 271, 7273–7276. doi:10.1074/jbc.271.13.7273
- Dickie, E. A., Giordani, F., Gould, M. K., Mäser, P., Burri, C., Mottram, J. C., et al. (2020). New drugs for human african trypanosomiasis: a twenty first century success story. *Tropical Med. Infect. Dis.* 5, 29. doi:10.3390/tropicalmed5010029
- Diego, J. L., Katz, J. M., Marshall, P., Gutiérrez, B., Manning, J. E., Nussenzweig, V., et al. (2001). The Ubiquitin-Proteasome pathway plays an essential role in proteolysis during trypanosoma cruzi remodeling. *Biochemistry* 40, 1053–1062. doi:10.1021/bi001659k
- Dubessay, P., Blaineau, C., Bastien, P., Tasse, L., Dijk, J. V., Crobu, L., et al. (2006). Cell cycle-dependent expression regulation by the proteasome pathway and characterization of the nuclear targeting signal of a Leishmania major Kin-13 kinesin. *Mol. Microbiol.* 59, 1162–1174. doi:10.1111/j.1365-2958.2005.05013.x
- Feling, R. H., Buchanan, G. O., Mincer, T. J., Kauffman, C. A., Jensen, P. R., and Renical, W. (2003). Salinosporamide A: a highly cytotoxic proteasome inhibitor from a novel microbial source, a marine bacterium of the new genus Salinospora. *Angew. Chem.* 115, 369–371. doi:10.1002/ange.200390083
- Fenteany, G., Standaert, R., Lane, W., Choi, S., Corey, E., and Schreiber, S. (1995). Inhibition of proteasome activities and subunit-specific amino-terminal threonine modification by lactacystin. *Science* 268, 726–731. doi:10.1126/science.7732382
- Field, M. C., Sergeenko, T., Wang, Y.-N., Böhm, S., and Carrington, M. (2010). Chaperone requirements for biosynthesis of the trypanosome variant surface glycoprotein. *PLoS One* 5, e8468. doi:10.1371/journal.pone.0008468
- Gareau, J. R., and Lima, C. D. (2010). The SUMO pathway: emerging mechanisms that shape specificity, conjugation and recognition. *Nat. Rev. Mol. Cell Biol.* 11, 861–871. doi:10.1038/nrm3011
- Glenn, R. J., Pemberton, A. J., Royle, H. J., Spackman, R. W., Smith, E., Rivett, A. J., et al. (2004). Trypanocidal effect of α , β -epoxyketones indicates that trypanosomes are particularly sensitive to inhibitors of proteasome trypsin-like activity. *Int. J. Antimicrob. Agents* 24, 286–289. doi:10.1016/j.ijantimicag.2004.02.023
- González, J., Ramalho-Pinto, F. J., Frevert, U., Ghiso, J., Tomlinson, S., Scharfstein, J., et al. (1996). Proteasome activity is required for the stage-specific

AUTHOR CONTRIBUTIONS

M-JB confirms being the sole contributor of this work and has approved it for publication.

ACKNOWLEDGMENTS

Figures were created with BioRender.com. Analysis of structures and the generation of images were performed using UCSF Chimera (Pettersen et al., 2004).

- transformation of a protozoan parasite. *J. Exp. Med.* 184, 1909–1918. doi:10.1084/jem.184.5.1909
- Green, J. L., Wu, Y., Encheva, V., Lasonder, E., Prommaban, A., Kunzelmann, S., et al. (2020). Ubiquitin activation is essential for schizont maturation in *Plasmodium falciparum* blood-stage development. *PLoS Pathog.* 16, e1008640. doi:10.1371/journal.ppat.1008640
- Groll, M., and Potts, B. C. (2011). Proteasome structure, function, and lessons learned from beta-lactone inhibitors. *Curr. Top. Med. Chem.* 11, 2850–2878. doi:10.2174/156802611798281320
- Gupta, I., Aggarwal, S., Singh, K., Yadav, A., and Khan, S. (2018). Ubiquitin Proteasome pathway proteins as potential drug targets in parasite *Trypanosoma cruzi*. *Sci. Rep.* 8, 8399. doi:10.1038/s41598-018-26532-z
- Harbut, M. B., Patel, B. A., Yeung, B. K. S., McNamara, C. W., Bright, A. T., Ballard, J., et al. (2012). Targeting the ERAD pathway via inhibition of signal peptide peptidase for antiparasitic therapeutic design. *Proc. Natl. Acad. Sci. Unit. States Am.* 109, 21486–21491. doi:10.1073/pnas.1216016110
- Hashimoto, M., Murata, E., and Aoki, T. (2010). Secretory protein with RING finger domain (SPRING) specific to *Trypanosoma cruzi* is directed, as a ubiquitin ligase related protein, to the nucleus of host cells. *Cell Microbiol.* 12, 19–30. doi:10.1111/j.1462-5822.2009.01375.x
- He, X., Riceberg, J., Soucy, T., Koenig, E., Minissale, J., Gallery, M., et al. (2017). Probing the roles of SUMOylation in cancer cell biology by using a selective SAE inhibitor. *Nat. Chem. Biol.* 13, 1164–1171. doi:10.1038/nchembio.2463
- Hellemond, J. J. V., and Mottram, J. C. (2000). The CYC3 gene of *Trypanosoma brucei* encodes a cyclin with a short half-life. *Mol. Biochem. Parasitol.* 111, 275–282. doi:10.1016/s0166-6851(00)00318-2
- Herhaus, L., and Dikic, I. (2015). Expanding the ubiquitin code through post-translational modification. *EMBO Rep.* 16, 1071–1083. doi:10.15252/embr.201540891
- Hill, C. P., Masters, E. I., and Whitby, F. G. (2002). The proteasome — ubiquitin protein degradation pathway. *Curr. Top. Microbiol.* 268, 73–89. doi:10.1007/978-3-642-59414-4_4
- Hu, H., Yu, Z., Liu, Y., Wang, T., Wei, Y., and Li, Z. (2014). The Aurora B kinase in *Trypanosoma brucei* undergoes post-translational modifications and is targeted to various subcellular locations through binding to TbCPC1. *Mol. Microbiol.* 91, 256–274. doi:10.1111/mmi.12458
- Hu, H., Zhou, Q., Han, X., and Li, Z. (2017). CRL4WDR1 controls polo-like kinase protein abundance to promote bilobe duplication, basal body segregation and flagellum attachment in *trypanosoma brucei*. *PLoS Pathog.* 13, e1006146. doi:10.1371/journal.ppat.1006146
- Huang, L., Jacob, R. J., Pegg, S. C.-H., Baldwin, M. A., Wang, C. C., Burlingame, A. L., et al. (2001). Functional assignment of the 20S proteasome from *trypanosoma brucei* using mass spectrometry and new bioinformatics approaches. *J. Biol. Chem.* 276, 28327–28339. doi:10.1074/jbc.m008342200
- Huber, E. M., Heinemeyer, W., Li, X., Arendt, C. S., Hochstrasser, M., and Groll, M. (2016). A unified mechanism for proteolysis and autocatalytic activation in the 20S proteasome. *Nat. Commun.* 7, 10900. doi:10.1038/ncomms10900
- Husnjak, K., and Dikic, I. (2012). Ubiquitin-binding proteins: decoders of ubiquitin-mediated cellular functions. *Annu. Rev. Biochem.* 81, 291–322. doi:10.1146/annurev-biochem-051810-094654
- Hyer, M. L., Milhollen, M. A., Ciavarrri, J., Fleming, P., Traore, T., Sappal, D., et al. (2018). A small-molecule inhibitor of the ubiquitin activating enzyme for cancer treatment. *Nat. Med.* 24, 186–193. doi:10.1038/nm.4474
- Iribarren, P. A., Berazategui, M. A., Bayona, J. C., Almeida, I. C., Cazzulo, J. J., and Alvarez, V. E. (2015). Different proteomic strategies to identify genuine Small Ubiquitin-like MOdifier targets and their modification sites in *Trypanosoma brucei* procyclic forms. *Cell Microbiol.* 17, 1413–1422. doi:10.1111/cmi.12467
- Kapur, V., Peterson, L. F., Showalter, H. D. H., Kirchhoff, P. D., Talpaz, M., and Donato, N. J. (2011). Protein cross-linking as a novel mechanism of action of a ubiquitin-activating enzyme inhibitor with anti-tumor activity. *Biochem. Pharmacol.* 82, 341–349. doi:10.1016/j.bcp.2011.05.012
- Khare, S., Nagle, A. S., Biggart, A., Lai, Y. H., Liang, F., Davis, L. C., et al. (2016). Proteasome inhibition for treatment of leishmaniasis, Chagas disease and sleeping sickness. *Nature* 537, 229–233. doi:10.1038/nature19339
- Komander, D., and Rape, M. (2012). The ubiquitin code. *Annu. Rev. Biochem.* 81, 203–229. doi:10.1146/annurev-biochem-060310-170328
- Kulkarni, M., and Smith, H. E. (2008). E1 ubiquitin-activating enzyme UBA-1 plays multiple roles throughout *C. elegans* development. *PLoS Genet.* 4, e1000131. doi:10.1371/journal.pgen.1000131
- Labriola, C. A., Conte, I. L., Medus, M. L., Parodi, A. J., and Caramelo, J. J. (2010). Endoplasmic reticulum calcium regulates the retrotranslocation of *trypanosoma cruzi* calreticulin to the cytosol. *PLoS One* 5, e13141. doi:10.1371/journal.pone.0013141
- Lee, D. H., and Goldberg, A. L. (1998). Proteasome inhibitors: valuable new tools for cell biologists. *Trends Cell Biol.* 8, 397–403. doi:10.1016/s0962-8924(98)01346-4
- Leung, K. F., Riley, F. S., Carrington, M., and Field, M. C. (2011). Ubiquitylation and developmental regulation of invariant surface protein expression in trypanosomes. *Eukaryot. Cell* 10, 916–931. doi:10.1128/ec.05012-11
- Li, Z., and Wang, C. C. (2002). Functional characterization of the 11 non-ATPase subunit proteins in the trypanosome 19 S proteasomal regulatory complex. *J. Biol. Chem.* 277, 42686–42693. doi:10.1074/jbc.m207183200
- Li, Z., Zou, C.-B., Yao, Y., Hoyt, M. A., McDonough, S., Mackey, Z. B., et al. (2002). An easily dissociated 26 S proteasome catalyzes an essential ubiquitin-mediated protein degradation pathway in *trypanosoma brucei*. *J. Biol. Chem.* 277, 15486–15498. doi:10.1074/jbc.m109029200
- Liao, S., Hu, H., Wang, T., Tu, X., and Li, Z. (2017). The protein neddylation pathway in *trypanosoma brucei* functional characterization and substrate identification. *J. Biol. Chem.* 292, 1081–1091. doi:10.1074/jbc.m116.766741
- Liao, S., Wang, T., Fan, K., and Tu, X. (2010). The small ubiquitin-like modifier (SUMO) is essential in cell cycle regulation in *Trypanosoma brucei*. *Exp. Cell Res.* 316, 704–715. doi:10.1016/j.yexcr.2009.12.017
- Liu, X., Zhao, B., Sun, L., Bhuripanyo, K., Wang, Y., Bi, Y., et al. (2017). Orthogonal ubiquitin transfer identifies ubiquitination substrates under differential control by the two ubiquitin activating enzymes. *Nat. Commun.* 8, 14286. doi:10.1038/ncomms14286
- López-Farfán, D., Bart, J.-M., Rojas-Barros, D. I., and Navarro, M. (2014). SUMOylation by the E3 ligase TbSIZ1/PIAS1 positively regulates VSG expression in *trypanosoma brucei*. *PLoS Pathog.* 10, e1004545. doi:10.1371/journal.ppat.1004545
- Lu, X., Olsen, S. K., Capili, A. D., Cisar, J. S., Lima, C. D., and Tan, D. S. (2010). Designed semisynthetic protein inhibitors of ub/ubl E1 activating enzymes. *J. Am. Chem. Soc.* 132, 1748–1749. doi:10.1021/ja9088549
- Lv, Z., Yuan, L., Atkinson, J. H., Aldana-Masangkay, G., Chen, Y., and Olsen, S. K. (2017). Domain alternation and active site remodeling are conserved structural features of ubiquitin E1. *J. Biol. Chem.* 292, 12089–12099. doi:10.1074/jbc.m117.787622
- Marques, A. J., Palanimurugan, R., Matias, A. C., Ramos, P. C., and Dohmen, R. J. (2009). Catalytic mechanism and assembly of the proteasome. *Chem. Rev.* 109, 1509–1536. doi:10.1021/cr8004857
- McGrath, J. P., Jentsch, S., and Varshavsky, A. (1991). Uba 1: an essential yeast gene encoding ubiquitin-activating enzyme. *EMBO J.* 10, 227–236. doi:10.1002/j.1460-2075.1991.tb07940.x
- Meng, L., Mohan, R., Kwok, B. H. B., Elofsson, M., Sin, N., and Crews, C. M. (1999). Epoxomicin, a potent and selective proteasome inhibitor, exhibits *in vivo* antiinflammatory activity. *Proc. Natl. Acad. Sci. Unit. States Am.* 96, 10403–10408. doi:10.1073/pnas.96.18.10403
- Milhollen, M. A., Thomas, M. P., Narayanan, U., Traore, T., Riceberg, J., Amidon, B. S., et al. (2012). Treatment-emergent mutations in NAE β confer resistance to the NEDD8-activating enzyme inhibitor MLN4924. *Canc. Cell* 21, 388–401. doi:10.1016/j.ccr.2012.02.009
- Misra, M., Kuhn, M., Löbel, M., An, H., Statsyuk, A. V., Sottriffer, C., et al. (2017). Dissecting the specificity of adenosyl sulfamate inhibitors targeting the ubiquitin-activating enzyme. *Structure* 25, 1120–1129. doi:10.1016/j.str.2017.05.001
- Moura, D. M., Neto, O. P. de M., and Carrington, M. (2018). A new reporter cell line for studies with proteasome inhibitors in *Trypanosoma brucei*. *Mol. Biochem. Parasitol.* 227, 15–18. doi:10.1016/j.molbiopara.2018.11.001
- Muñoz, C., Francisco, J. S., Gutiérrez, B., and González, J. (2015). Role of the ubiquitin-proteasome systems in the biology and virulence of Protozoan parasites. *BioMed Res. Int.* 2015, 141526. doi:10.1155/2015/141526
- Mutomba, M. C., To, W.-Y., Hyun, W. C., and Wang, C. C. (1997). Inhibition of proteasome activity blocks cell cycle progression at specific phase boundaries in

- African trypanosomes. *Mol. Biochem. Parasitol.* 90, 491–504. doi:10.1016/s0166-6851(97)00197-7
- Mutomba, M. C., and Wang, C. C. (1998). The role of proteolysis during differentiation of *Trypanosoma brucei* from the bloodstream to the procyclic form. *Mol. Biochem. Parasitol.* 93, 11–22. doi:10.1016/s0166-6851(98)00012-7
- Nagendar, P., Gillespie, J. R., Herbst, Z. M., Ranade, R. M., Molasky, N. M. R., Faghhi, O., et al. (2018). Triazolopyrimidines and imidazopyridines: structure–activity relationships and *in Vivo* efficacy for trypanosomiasis. *ACS Med. Chem. Lett.* 10, 105–110. doi:10.1021/acsmchemlett.8b00498
- Nagle, A., Biggart, A., Be, C., Srinivas, H., Hein, A., Caridha, D., et al. (2020). Discovery and characterization of clinical candidate LXE408 as a kinetoplastid-selective proteasome inhibitor for the treatment of leishmaniasis. *J. Med. Chem.* 63, 10773–10781. doi:10.1021/acs.jmedchem.0c00499
- Neau, P., Hänel, H., Lameyre, V., Strub-Wourgaft, N., and Kuykens, L. (2020). Innovative partnerships for the elimination of human african trypanosomiasis and the development of fexinidazole. *Tropical Med. Infect. Dis.* 5, 17. doi:10.3390/tropicalmed5010017
- Nkengu-Njinkeng, J., Rosenkranz, V., Wink, M., and Steverding, D. (2002). Antitrypanosomal activities of proteasome inhibitors. *Antimicrob. Agents Chemother.* 46, 2038–2040. doi:10.1128/aac.46.6.2038-2040.2002
- Omura, S., and Crump, A. (2019). Lactacystin: first-in-class proteasome inhibitor still excellent and an exemplar for future antibiotic research. *J. Antibiotics* 72, 189–201. doi:10.1038/s41429-019-0141-8
- Pelzer, C., Kassner, I., Matentzoglou, K., Singh, R. K., Wollscheid, H.-P., Scheffner, M., et al. (2007). UBE1L2, a novel E1 enzyme specific for ubiquitin. *J. Biol. Chem.* 282, 23010–23014. doi:10.1074/jbc.c70011200
- Pérez-Pertejo, Y., Álvarez-Velilla, R., Estrada, C. G., Balana-Fouce, R., and Reguera, R. M. (2011). Leishmania donovani: proteasome-mediated down-regulation of methionine adenosyltransferase. *Parasitology* 138, 1082–1092. doi:10.1017/s0031182011000862
- Pettersen, E. F., Goddard, T. D., Huang, C. C., Couch, G. S., Greenblatt, D. M., Meng, E. C., et al. (2004). UCSF Chimera—a visualization system for exploratory research and analysis. *J. Comput. Chem.* 25, 1605–1612. doi:10.1002/jcc.20084
- Pickart, C. M., and Eddins, M. J. (2004). Ubiquitin: structures, functions, mechanisms. *Biochim. Et Biophys. Acta Bba - Mol. Cell Res.* 1695, 55–72. doi:10.1016/j.bbamcr.2004.09.019
- Rao, S. P. S., Barrett, M. P., Dranoff, G., Faraday, C. J., Gimpelewicz, C. R., Hailu, A., et al. (2018). Drug discovery for kinetoplastid diseases: future directions. *ACS Infect. Dis.* 5, 152–157. doi:10.1021/acsinfectdis.8b00298
- Rao, S. P. S., Lakshminarayana, S. B., Jiricek, J., Kaiser, M., Ritchie, R., Myburgh, E., et al. (2020). Anti-trypanosomal proteasome inhibitors cure hemolymphatic and meningoencephalic murine infection models of african trypanosomiasis. *Tropical Med. Infect. Dis.* 5, 28. doi:10.3390/tropicalmed5010028
- Rechsteiner, M., and Hill, C. P. (2005). Mobilizing the proteolytic machine: cell biological roles of proteasome activators and inhibitors. *Trends Cell Biol.* 15, 27–33. doi:10.1016/j.tcb.2004.11.003
- Renzo, M. A. D., Laverrière, M., Schenkman, S., Wehrendt, D. P., Tellez-Iñón, M. T., and Potenza, M. (2016). Characterization of TcCYC6 from *Trypanosoma cruzi*, a gene with homology to mitotic cyclins. *Parasitol. Int.* 65, 196–204. doi:10.1016/j.parint.2015.12.007
- Robertson, C. D. (1999). The Leishmania mexicana proteasome. *Mol. Biochem. Parasitol.* 103, 49–60. doi:10.1016/s0166-6851(99)00110-3
- Rojas, F., Koszela, J., Búa, J., Llorente, B., Burchmore, R., Auer, M., et al. (2017). The ubiquitin-conjugating enzyme CDC34 is essential for cytokinesis in contrast to putative subunits of a SCF complex in *Trypanosoma brucei*. *PLoS Neglected Trop. Dis.* 11, e0005626. doi:10.1371/journal.pntd.0005626
- Saura, A., Iribarren, P. A., Rojas-Barros, D., Bart, J. M., López-Farfán, D., Andrés-León, E., et al. (2019). SUMOylated SNF2PH promotes variant surface glycoprotein expression in bloodstream trypanosomes. *EMBO Rep.* 20, e48029. doi:10.15252/embr.201948029
- Schulman, B. A., and Harper, J. W. (2009). Ubiquitin-like protein activation by E1 enzymes: the apex for downstream signalling pathways. *Nat. Rev. Mol. Cell Biol.* 10, 319–331. doi:10.1038/nrm2673
- Shao-bing, H., Wah-Yuen, T., Mei-Lie, W., and C. W. C. (1996). Purification and characterization of proteasomes from *Trypanosoma brucei*. *Mol. Biochem. Parasitol.* 78, 33–46. doi:10.1016/s0166-6851(96)02599-6
- Siegel, T. N., Hekstra, D. R., Wang, X., Dewell, S., and Cross, G. A. M. (2010). Genome-wide analysis of mRNA abundance in two life-cycle stages of *Trypanosoma brucei* and identification of splicing and polyadenylation sites. *Nucleic Acids Res.* 38, 4946–4957. doi:10.1093/nar/gkq237
- Silva-Jardim, I., Horta, M. F., and Ramalho-Pinto, F. J. (2004). The Leishmania chagasi proteasome: role in promastigotes growth and amastigote survival within murine macrophages. *Acta Trop.* 91, 121–130. doi:10.1016/j.actatropica.2004.03.007
- Silverman, J. S., Muratore, K. A., and Bangs, J. D. (2013). Characterization of the late endosomal ESCRT machinery in *trypanosoma brucei*. *Traffic* 14, 1078–1090. doi:10.1111/tra.12094
- Soucy, T. A., Smith, P. G., Milhollen, M. A., Berger, A. J., Gavin, J. M., Adhikari, S., et al. (2009). An inhibitor of NEDD8-activating enzyme as a new approach to treat cancer. *Nature* 458, 732–736. doi:10.1038/nature07884
- Steverding, D., Baldisserotto, A., Wang, X., and Marastoni, M. (2011a). Trypanocidal activity of peptidyl vinyl ester derivatives selective for inhibition of mammalian proteasome trypsin-like activity. *Exp. Parasitol.* 128, 444–447. doi:10.1016/j.exppara.2011.03.015
- Steverding, D., Wang, X., Potts, B., and Palladino, M. (2011b). Trypanocidal activity of β -Lactone- γ -Lactam proteasome inhibitors. *Planta Med.* 78, 131–134. doi:10.1055/s-0031-1280315
- Steverding, D., Florea, B. I., and Overkleeft, H. S. (2018). *Trypanosoma brucei*: β 2-selective proteasome inhibitors do not block the proteasomal trypsin-like activity but are trypanocidal. *Mol. Biochem. Parasitol.* 227, 1–4. doi:10.1016/j.molbiopara.2018.11.002
- Steverding, D., Spackman, R. W., Royle, H. J., and Glenn, R. J. (2005). Trypanocidal activities of trileucine methyl vinyl sulfone proteasome inhibitors. *Parasitol. Res.* 95, 73–76. doi:10.1007/s00436-004-1253-y
- Stewart, M. D., Ritterhoff, T., Klevit, R. E., and Brzovic, P. S. (2016). E2 enzymes: more than just middle men. *Cell Res.* 26, 423–440. doi:10.1038/cr.2016.35
- Stuart, K., Brun, R., Croft, S., Fairlamb, A., Gürtler, R. E., McKerrow, J., et al. (2008). Kinetoplastid: related protozoan pathogens, different diseases. *J. Clin. Invest.* 118, 1301–1310. doi:10.1172/jci33945
- Swatek, K. N., and Komander, D. (2016). Ubiquitin modifications. *Cell Res.* 26, 399–422. doi:10.1038/cr.2016.39
- Tatipaka, H. B., Gillespie, J. R., Chatterjee, A. K., Norcross, N. R., Hulverson, M. A., Ranade, R. M., et al. (2014). Substituted 2-phenylimidazopyridines: a new class of drug leads for human african trypanosomiasis. *J. Med. Chem.* 57, 828–835. doi:10.1021/jm401178t
- Tiengwe, C., Koeller, C. M., and Bangs, J. D. (2018). Endoplasmic reticulum-associated degradation and disposal of misfolded GPI-anchored proteins in *Trypanosoma brucei*. *Mol. Biol. Cell* 29, 2397–2409. doi:10.1091/mbc.e18-06-0380
- Tiengwe, C., Muratore, K. A., and Bangs, J. D. (2016). Surface proteins, ERAD and antigenic variation in *Trypanosoma brucei*. *Cell Microbiol.* 18, 1673–1688. doi:10.1111/cmi.12605
- To, W.-Y., and Wang, C. C. (1997). Identification and characterization of an activated 20S proteasome in *Trypanosoma brucei*. *Fed. Eur. Biochem. Soc. Lett.* 404, 253–262. doi:10.1016/s0014-5793(97)00116-6
- Toth, J. I., Yang, L., Dahl, R., and Petroski, M. D. (2012). A gatekeeper residue for NEDD8-activating enzyme inhibition by MLN4924. *Cell Rep.* 1, 309–316. doi:10.1016/j.celrep.2012.02.006
- Ungermannova, D., Parker, S. J., Nasveschuk, C. G., Chapnick, D. A., Phillips, A. J., Kuchta, R. D., et al. (2011). Identification and mechanistic studies of a novel ubiquitin E1 inhibitor. *J. Biomol. Screen* 17, 421–434. doi:10.1177/1087057111433843
- Ungermannova, D., Parker, S. J., Nasveschuk, C. G., Wang, W., Quade, B., Zhang, G., et al. (2012). Largazole and its derivatives selectively inhibit ubiquitin activating enzyme (E1). *PLoS One* 7, e29208. doi:10.1371/journal.pone.0029208
- Vigneron, N., and Eynde, B. J. V. (2014). Proteasome subtypes and regulators in the processing of antigenic peptides presented by class I molecules of the major histocompatibility complex. *Biomolecules* 4, 994–1025. doi:10.3390/biom4040994
- Wang, C. C., Bozdech, Z., Liu, C., Shipway, A., Backes, B. J., Harris, J. L., et al. (2003). Biochemical analysis of the 20 S proteasome of *trypanosoma brucei*. *J. Biol. Chem.* 278, 15800–15808. doi:10.1074/jbc.m300195200

- Whitby, F. G., Masters, E. I., Kramer, L., Knowlton, J. R., Yao, Y., Wang, C. C., et al. (2000). Structural basis for the activation of 20S proteasomes by 11S regulators. *Nature* 408, 115–120. doi:10.1038/35040607
- Wilkinson, K. D., Smith, S. E., O'Connor, L., Sternberg, E., Taggart, J. J., Berges, D. A., et al. (1990). A specific inhibitor of the ubiquitin activating enzyme: synthesis and characterization of adenosyl-phospho-ubiquitinol, a nonhydrolyzable ubiquitin adenylate analog. *Biochemistry* 29, 7373–7380. doi:10.1021/bi00484a004
- Wu, X., and Rapoport, T. A. (2018). Mechanistic insights into ER-associated protein degradation. *Curr. Opin. Cell Biol.* 53, 22–28. doi:10.1016/j.ceb.2018.04.004
- Wyllie, S., Brand, S., Thomas, M., Rycker, M. D., Chung, C., Pena, I., et al. (2019). Preclinical candidate for the treatment of visceral leishmaniasis that acts through proteasome inhibition. *Proc. Natl. Acad. Sci. Unit. States Am.* 116, 201820175. doi:10.1073/pnas.1820175116
- Xu, G. W., Ali, M., Wood, T. E., Wong, D., Maclean, N., Wang, X., et al. (2010). The ubiquitin-activating enzyme E1 as a therapeutic target for the treatment of leukemia and multiple myeloma. *Blood* 115, 2251–2259. doi:10.1182/blood-2009-07-231191
- Yang, Y., Kitagaki, J., Dai, R.-M., Tsai, Y. C., Lorick, K. L., Ludwig, R. L., et al. (2007). Inhibitors of ubiquitin-activating enzyme (E1), a new class of potential cancer therapeutics. *Cancer Res.* 67, 9472–9481. doi:10.1158/0008-5472.can-07-0568
- Yao, Y., Huang, L., Krutchinsky, A., Wong, M.-L., Standing, K. G., Burlingame, A. L., et al. (1999). Structural and functional characterizations of the proteasome-activating protein PA26 from trypanosoma brucei. *J. Biol. Chem.* 274, 33921–33930. doi:10.1074/jbc.274.48.33921
- Yau, R., and Rape, M. (2016). The increasing complexity of the ubiquitin code. *Nat. Cell Biol.* 18, 579–586. doi:10.1038/ncb3358
- Ye, K., Zhang, X., Ni, J., Liao, S., and Tu, X. (2015). Identification of enzymes involved in SUMOylation in Trypanosoma brucei. *Sci Rep.* 5, 10097. doi:10.1038/srep10097
- Ying, Y., Taori, K., Kim, H., Hong, J., and Luesch, H. (2008). Total synthesis and molecular target of largazole, a histone deacetylase inhibitor. *J. Am. Chem. Soc.* 130, 8455–8459. doi:10.1021/ja8013727
- Zmuda, F., Sastry, L., Shepherd, S. M., Jones, D., Scott, A., Craggs, P. D., et al. (2019). Identification of novel trypanosoma cruzi proteasome inhibitors using a luminescence-based high-throughput screening assay. *Antimicrob. Agents Chemother.* 63, e00309–19. doi:10.1128/aac.00309-19
- Conflict of Interest:** The author declares that the research was conducted in the absence of any commercial or financial relationships that could be construed as a potential conflict of interest.

Copyright © 2021 Bijlmakers. This is an open-access article distributed under the terms of the Creative Commons Attribution License (CC BY). The use, distribution or reproduction in other forums is permitted, provided the original author(s) and the copyright owner(s) are credited and that the original publication in this journal is cited, in accordance with accepted academic practice. No use, distribution or reproduction is permitted which does not comply with these terms.



An Overview on the Therapeutics of Neglected Infectious Diseases—Leishmaniasis and Chagas Diseases

Brindha J¹, Balamurali M. M^{1*} and Kaushik Chanda^{2*}

¹Division of Chemistry, School of Advanced Sciences, Vellore Institute of Technology, Chennai, India, ²Department of Chemistry, School of Advanced Sciences, Vellore Institute of Technology, Vellore, India

OPEN ACCESS

Edited by:

Gildardo Rivera,
Instituto Politécnico Nacional (IPN),
Mexico City, Mexico

Reviewed by:

Sara M. Robledo,
University of Antioquia, Medellín,
Colombia
Chiara Borsari,
University of Basel, Basel, Switzerland

*Correspondence:

Balamurali M. M
mmbala@gmail.com
Kaushik Chanda
chandakaushik1@gmail.com

Specialty section:

This article was submitted to
Medicinal and Pharmaceutical
Chemistry,
a section of the journal
Frontiers in Chemistry

Received: 28 October 2020

Accepted: 14 January 2021

Published: 12 March 2021

Citation:

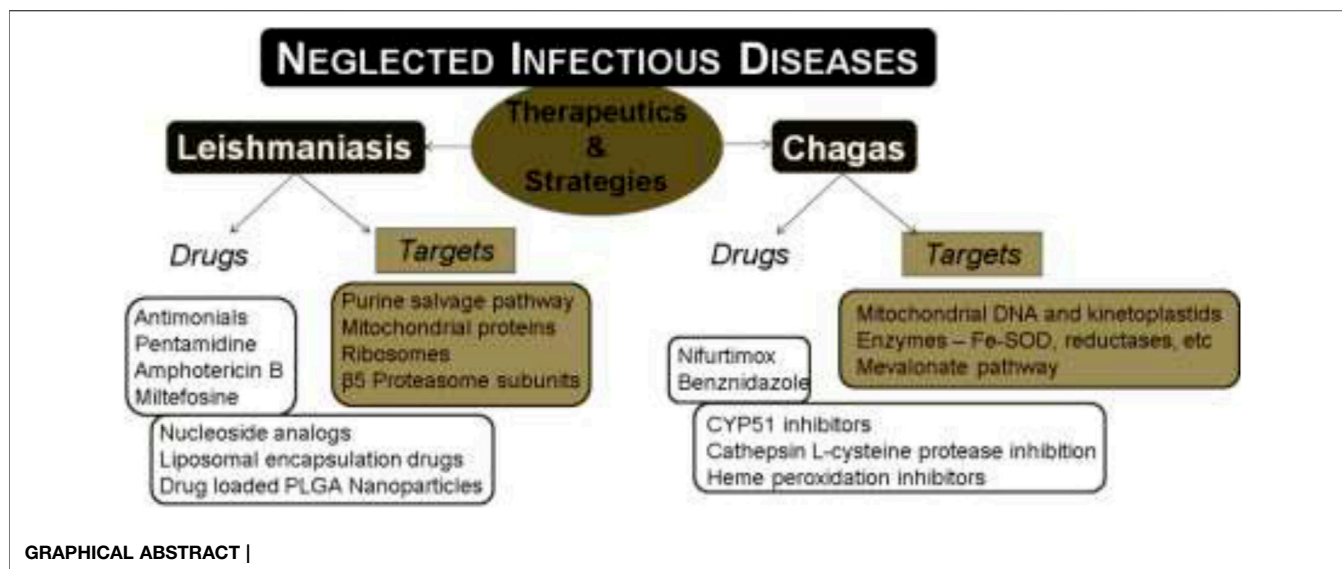
J B, M BM and Chanda K (2021) An
Overview on the Therapeutics
of Neglected Infectious
Diseases—Leishmaniasis
and Chagas Diseases.
Front. Chem. 9:622286.
doi: 10.3389/fchem.2021.622286

Neglected tropical diseases (NTDs) as termed by WHO include twenty different infectious diseases that are caused by bacteria, viruses, and parasites. Among these NTDs, Chagas disease and leishmaniasis are reported to cause high mortality in humans and are further associated with the limitations of existing drugs like severe toxicity and drug resistance. The above hitches have rendered researchers to focus on developing alternatives and novel therapeutics for the treatment of these diseases. In the past decade, several target-based drugs have emerged, which focus on specific biochemical pathways of the causative parasites. For leishmaniasis, the targets such as nucleoside analogs, inhibitors targeting nucleoside phosphate kinases of the parasite's purine salvage pathway, 20S proteasome of *Leishmania*, mitochondria, and the associated proteins are reviewed along with the chemical structures of potential drug candidates. Similarly, in case of therapeutics for Chagas disease, several target-based drug candidates targeting sterol biosynthetic pathway (C14-ademethylase), L-cysteine protease, heme peroxidation, mitochondria, farnesyl pyrophosphate, etc., which are vital and unique to the causative parasite are discussed. Moreover, the use of nano-based formulations towards the therapeutics of the above diseases is also discussed.

Keywords: chagas, leishmaniasis, infectious disease, therapeutics, drugs

INTRODUCTION

Neglected tropical diseases (NTDs) include a group of diverse infectious diseases that are more prevalent in the tropical and subtropical regions of the world. These diseases are more associated with the poverty zones that have limited health facilities. Moreover, these infections are biologically diverse with 20 different diseases under the list of NTDs including Buruli ulcer, Chagas disease, dengue, chikungunya, dracunculiasis (guinea-worm disease), echinococcosis, foodborne trematodiasis, human African trypanosomiasis (sleeping sickness), leishmaniasis, leprosy (Hansen's disease), lymphatic filariasis, mycetoma, chromoblastomycosis and other deep mycoses, onchocerciasis (river blindness), rabies, scabies and other ectoparasites, schistosomiasis, soil-transmitted helminthiasis, snakebite envenoming, taeniasis/cysticercosis, trachoma, and yaws (endemic treponematoses). For the past few decades, many pharmaceutical companies have been supportive towards combating these diseases and thereby a significant portion of the economic burden on developing countries was reduced. There are five different strategies adopted by WHO to manage these NTDs: i) preventive chemotherapy, ii) intensified disease management, iii) vector



control, iv) neglected zoonotic diseases, and v) improved water and sanitation. In the past, several programs to alleviate NTDs were implemented to assist in controlling and eliminating these diseases completely. Many targets proposed in the roadmap of WHO in 2012 have not been achieved to date, though progress is being made to overcome the global impact of NTDs. Recently, the new NTD roadmap for the years 2021–2030 was proposed by WHO (WHO, 2020). WHO has revealed the challenges ahead due to the prevailing COVID-19 pandemic that can hinder the delivery of essential health products for NTDs.

The research on new therapeutic strategies for NTDs focuses on a combination of existing or repurposed drugs, to enhance the efficacy/bioavailability of the available therapeutics; however, the discovery of new drugs also plays a major role in drug discovery for NTDs. Presently available therapies were proved to be toxic and require a longer duration of treatment as compared to the rate of disease progression, along with the development of drug resistance particularly in people infected with NTDs like Chagas disease and leishmaniasis. The above two NTDs are known for the highest mortality rate among others (Hotez et al., 2007).

There are two major ways to identify compounds for these diseases: phenotypic and target-based approaches. The phenotypic approach involves the development of a drug without any knowledge about its target or specific function against the disease (Moffat et al., 2017). In this case, the entire organism, including the pathways/targets, needs to be screened against the drug. The phenotypic approach has been successful in drug discovery and it involves the evaluation of various chemicals against the phenotypes or characteristics observed in an organism (Moffat et al., 2017). But the former lacks understanding of the molecular mechanisms that lead to empirical analysis and delays the progress in obtaining the best drug candidate (Swinney, 2013). The phenotypic approach has the advantage of addressing the problems like cell uptake/efflux and membrane permeability and counterscreening mammalian cells while identifying drug candidates that are active against the whole

cell (Borsari et al., 2019). The high-throughput screening mode has enabled the screening of large libraries of drug candidates against whole-cell parasites. In the target-based approach, the first step involves the identification of possible molecular targets that are significantly involved in the disease (Swinney, 2013). This is followed by designing small molecules that interfere with the potential targets in the causative agent (parasite/bacteria/virus) which are absent/different from those present in the infected host system. This approach is rational and exploits information on the genetics, chemistry, and computational sources, for drug discovery. It also quantitatively measures the drug toxicity/dosages (Capdeville et al., 2002; Durieu et al., 2016). The major drawback in the target-based approach (Lai et al., 2002) is the low productivity caused by poor disease linkages and the molecular complexities that are involved in drug's mode of action (Brown, 2007; Swinney and Anthony, 2011), although in ideal cases, drug discovery can progress through knowledge gained by empirical methods that relate the drug to the molecular mechanisms of action and the involved phenotype to obtain more reliable targets/hypotheses (Garcia-Calvo et al., 2005; Swinney, 2013). There are only a few validated drug targets known against the parasitic diseases and in case of some registered drugs, either the mode of action is poorly understood or it involves various targets (Gilbert, 2013). The correct balance between phenotypic and target-based approaches could possibly lead to successful drug discovery.

Both leishmaniasis and Chagas disease are caused by infectious parasites which are fatal if ignored and untreated. In both cases, the causative parasite shows many unique potential targets in the biochemical machinery. This includes some pathways or targets like the purine/pyrimidine salvage pathways (Bora and Jha, 2020), nucleoside analogs, kinetoplastid proteasomes, mitochondria, etc. There are various potential drug targets available for the treatment of NTDs and intense research is still progressing in this area. The limitations with current therapeutics like toxicity and

TABLE 1 | Standard drugs against leishmaniasis disease.

Standard drug	Mechanism of action	Advantages	Disadvantages	References
Pentavalent antimonials, meglumine antimoniate, and sodium stibogluconate (1a)	Not well known, but two model systems are: Prodrug model—conversion of Sb(V) to toxic Sb(III) and intrinsic Sb(V) activity: By complex formation with ribose/inhibition of type I DNA topoisomerase	Considered as first-line drugs	<ul style="list-style-type: none"> • Daily parenteral administration • Drug resistance • Side effects include nausea, vomiting, weakness and myalgia, abdominal colic, diarrhea, skin rashes, hepatotoxicity, and cardiotoxicity 	(Berman (1997); dos Santos Ferreira et al. (2003); Walker and Saravia (2004); Zhou et al. (2004)
Pentamidine (1c), pentamidine mesylate, and pentamidine isethionate	Not known; drug entry through polyamine/arginine transporters	Second line of defense	Drug resistance which may involve mitochondria/ABC protein PRP1	Basselin et al. (1996); Kandpal and Tekwani (1997); Mukherjee et al. (2006); Coelho et al. (2007)
Amphotericin B (1d)	Channel/pore formation on interaction with membrane sterol	<ul style="list-style-type: none"> • First line of treatment replacing the antimonials against visceral leishmaniasis • Nephrotoxicity overcome by amphotericin B formulations: liposomes, nanoparticles, and emulsions 	Toxic with serious side effects: renal impairment, anemia, fever, malaise, and hypokalaemia	Hartsel and Bolard (1996); Neumann et al. (2009); Cohen (2010); Hamill (2013)
Miltefosine (1e)	Apoptosis like cell death, targeting lipid metabolism, mitochondrial, and immunomodulatory effects	As monotherapy to treat both cutaneous and visceral leishmaniasis	<ul style="list-style-type: none"> • Side effects, mild-to-moderate gastrointestinal problems and mild nephrotoxicity • Long half-life and teratogenicity limit the administration of miltefosine in pregnant women 	Jha et al. (1999); Sundar and Olliaro (2007); Dorlo et al. (2012a); Dorlo et al. (2012b)

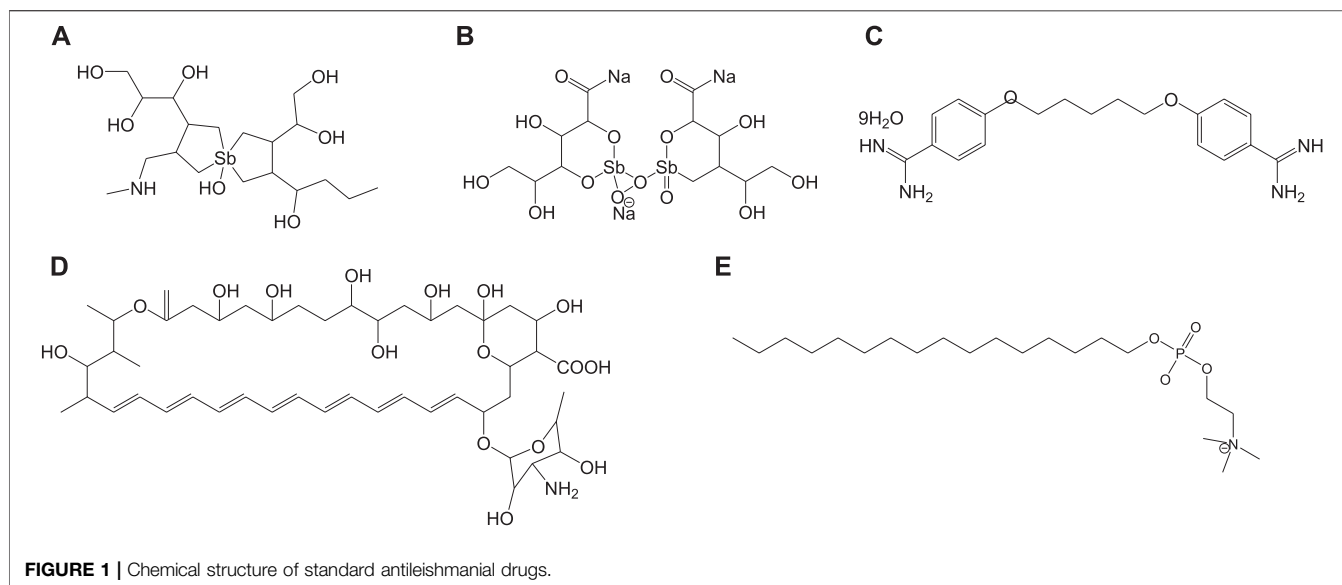
resistance have made the discovery of novel drugs against leishmaniasis and Chagas disease more essential.

In this review, we discuss various available drugs, emerging drug targets, and drug candidates identified by target-based approach against the two NTDs, leishmaniasis and Chagas diseases. We have also summarized the various therapeutic strategies that have been adopted in the past and present for the treatment of these two infectious neglected diseases.

LEISHMANIASIS

Leishmaniasis is one of the infectious NTDs caused by a protozoan parasite vector of genus *Leishmania* that is transmitted to humans through an infected blood-sucking sandfly. There are about 21 reported species of *Leishmania* that causes infections in humans and are endemic in the regions of Asia, Africa, America, and also southern parts of Europe. In leishmaniasis, the causative parasite *Leishmania* species displays a digenetic life cycle, which includes the extracellular motile promastigote, present in the female sandfly vector of the genus *Phlebotomus* (throughout Africa/Asia) or *Lutzomyia* (in America) (Matlashewski, 2001), and intracellular nonmotile amastigote that replicates within the phagolysosomes of host human macrophages. For instance, *P. argentipes* and *P. Salehi* were proven to be the sandfly vectors that causes leishmaniasis in India; *P. celiae*, *P. martini*, *P. saevus*, *P. sergenti*, *P. duboscqi*, *P. longipes*, *P. pedifer*, and *P. sergenti* are some of the sandfly vectors of *Phlebotomus* species that cause leishmaniasis in Ethiopia (Maroli et al., 2013); *Lutzomyia longipalpis* was the major vector in the north and south Americas to cause leishmaniasis infections (Lainson and

Rangel, 2005). Leishmaniasis infections lead to different kinds of diseases based on the species causing the infection (Pearson and Sousa, 1996; Ghedin et al., 1997). In humans, leishmaniasis is reported in three different forms: visceral, mucocutaneous, and cutaneous (Modabber et al., 2007). Visceral leishmaniasis, also called Kala-Azar caused by *Leishmania donovani* or *L. chagasi*, is a serious form of infection, manifested with skin darkening, weight loss, fever, liver/spleen enlargement, and emaciation (Matlashewski, 2001). Visceral leishmaniasis is a chronic infection, associated with high mortality and morbidity. Around 10% of the cured Kala-Azar patients develop post-Kala-Azar dermal leishmaniasis, which is chronic with disfigurement of cutaneous nodules (Adams et al., 2013). Dermal leishmaniasis predominantly occurs as localized cutaneous leishmaniasis along with other aggressive forms like diffused cutaneous leishmaniasis, mucosal leishmaniasis, and cutaneous leishmaniasis. They cause several lesions/disfigurement affecting the psychological well-being of the patients (Alvar et al., 2012). Cutaneous leishmaniasis involves the development of large open sores/lesions from several small lumps at the site of insect bite that eventually heals on its own over an extended period of several months (Matlashewski, 2001; Modabber et al., 2007). Diffused cutaneous leishmaniasis is another form of the disease where lesions are developed over a larger part of the body that resolves only with treatment (Matlashewski, 2001). Mucocutaneous leishmaniasis starts initially as cutaneous leishmaniasis and later spreads to mucous membranes of pharynx, mouth, and nose, depletes the tissues, and causes excessive damage to the face, along with leprosy kind of stigma and impairment of breathing in critical cases (Toledo et al., 2013; Pal et al., 2017; Cruz et al., 2019). Psychiatric disorder is associated with patients with extensive



lesions that are formed due to cutaneous leishmaniasis (Yanik et al., 2004). These patients were found to have a low quality of life with symptoms of depression, high anxiety, and low body image satisfaction (Chahed et al., 2016). The currently available antileishmanial drugs to treat leishmaniasis are associated with several side effects, toxicity, and drug resistance.

Standard Anti-Leishmanial Drugs

Currently used antileishmanial drugs include pentavalent antimonials, pentamidine, amphotericin B, and miltefosine and are known to target different metabolic pathways as discussed in **Table 1**. **Figure 1** depicts the chemical structures of standard drugs reported in the literature to treat leishmaniasis namely: **1a** (meglumine antimoniate or Glucantime®) and **1b** (sodium stibogluconate or Pentostam®), **1c** (pentamidine), **1d** (amphotericin B), and **1e** (miltefosine). To date, the *pentavalent antimonials* are used for the treatment of all the three clinical forms of leishmaniasis. Some examples of pentavalent antimonials include **1a** and **1b** (Goodwin, 1995) (**Figure 1**). During the last century, antimony (III) potassium tartrate (tartar emetic) was used in the treatment of mucocutaneous leishmaniasis, which was then proved to be effective for visceral leishmaniasis in Africa (Cole, 1944), followed by its interruption in clinical usage due to severe side effects. In the 1940s, less toxic pentavalent antimony [Sb(V)] complexes (Berman, 1997) that includes **1a** and **1b** were reported to be more effective (20 mg of Sb/kg/day for 20–30 days). There are two main models that describe the mechanism of action of these pentavalent antimonials in the treatment of leishmaniasis. The first model involves a prodrug concept, in which Sb(V) gets reduced to Sb(III), as observed in several *in vivo* studies (Burguera et al., 1993; Shaked-Mishan et al., 2001), to exhibit antileishmanial activity. Studies have suggested the involvement of thiols like trypanothione, cysteine, and cysteinylglycine or glutathione preferably in the amastigotes (dos Santos Ferreira et al., 2003), along with the involvement of enzymes that are specific to parasites like thiol-dependent reductase/antimoniate reductase (Zhou et al.,

2004). In the second model, Sb(V) itself was shown to possess anti-leishmanial activity, by forming complexes with ribose containing molecules and by inhibiting the type I DNA topoisomerases of *L. donovani* (Chakraborty and Majumder, 1988; Lucumi et al., 1998; Demicheli et al., 2002; Walker and Saravia, 2004). Due to affordability and high cure rate, these pentavalent antimonials have found their use as the first-line therapeutics for leishmaniasis.

Pentamidine (**1c**) was previously available in two forms: pentamidine methanesulfonate and pentamidine isethionate salt (Ghorbani and Farhoudi, 2018). Currently, pentamidine methane sulfonate formulations are not available but pentamidine isethionate is still in use. Treatment of cutaneous leishmaniasis using pentamidine mesylate and pentamidine isethionate is reported with nearly 90% cure rate without relapse of infection (Lai et al., 2002). No serious side effects except for respiratory tract problems were observed in patients treated with pentamidine isethionate. **1c** of dosage, 2 mg/kg every other day for a total of seven injections, was proved to be effective against 80% of patients (in Colombia) for the treatment of cutaneous leishmaniasis (Soto-Mancipe et al., 1993). On comparison of **1c** with **1a** against the treatment of leishmaniasis caused by *L. braziliensis*, **1c** was less effective than **1a** (in Peru) (Andersen et al., 2005). Although its mechanism of action is not well known, the **1c** compounds are found to enter *L. donovani* via the transporters of arginine and polyamine (Kandpal and Tekwani, 1997). This drug was reported to accumulate in the mitochondria (Mukherjee et al., 2006), by decreasing mitochondrial membrane potential and inhibit mitochondrial topoisomerase II (Basselin et al., 1996). The drug resistance in case of **1c** was due to more drug efflux and reduced uptake of the drugs through the involvement of intracellular ABC protein PRP1 (pentamidine resistance protein 1 (Coelho et al., 2007). *Amphotericin B* (**1d**) is another choice of treatment for leishmaniasis in cases where resistance to pentavalent antimonials was observed. **1d** is a polyene antifungal compound (fungizone, C₄₇H₇₃NO₁₇) that targets sterol pathway,

mainly ergosterols present in the cell membrane of the parasite (Purkait et al., 2012). The mechanism of action of **1d** involves the formation of pores or channels on the lipid bilayer membranes of the targeted host cells (Baginski et al., 1997; Neumann et al., 2009). The channels or pores thus created by the membrane active drug **1d** lead to influx of ions/solutes, thereby causing cell death. Membrane sterols are necessary for **1d** to interact and form these channels/pores on the membrane (Hartsel and Bolard, 1996; Cohen, 2010). There are different formulations of **1d**, for instance, amphotericin B lipid complex or ABLC (Abelcet), liposomal amphotericin B or L-AmB (AmBisome), amphotericin B colloidal dispersion, or ABCD (amphocil and amphotec) (Hamill, 2013). ABLC is composed of amphotericin B bound to two lipids, namely, L- α -dimyristoyl phosphatidylcholine (DMPC) and L- α -dimyristoyl phosphatidylglycerol (DMPG), and has a therapeutic dosage of 5 mg/kg/day. ABLC is the largest among these three lipid molecules and was shown to be less effective than the amphotericin B deoxycholate in the stimulation of proinflammatory signaling molecules (Arning et al., 1995; Simitsopoulou et al., 2005). L-AmB was proven to be successful against visceral leishmaniasis, with a dosage level of 3–6 mg/kg/day (Davidson et al., 1991; Boswell et al., 1998). With a single dose of L-AmB, the concentration of the drug in plasma exceeds the concentration achieved by the conventional amphotericin B deoxycholate (Meyerhoff, 1999; Walsh et al., 2001), whereas in case of ABCD (with amphotericin B and cholesteryl sulfate, 3–4 mg/kg/day dosage), the concentration in plasma was less than that maintained by the conventional drug amphotericin B deoxycholate (Herbrecht et al., 1999; Hamill, 2013). Liposomal amphotericin B is an FDA-approved drug for the treatment of visceral leishmaniasis, which is usually administered through intravenous infusion.

Miltefosine (1e) or hexadecylphosphocholine (Impavido[®]) is an alkyl phospholipid and an oral drug that is used for the treatment of all three forms of leishmaniasis. These compounds are phosphocholine analogs used for oral treatment against visceral leishmaniasis disease (Sundar and Oliaro, 2007; Dorlo et al., 2012b). **1e** which works by targeting the cell membrane proteins/signaling pathways of the parasites induces cytotoxicity, ultimately leading to apoptosis. With the intake of 100 mg of miltefosine/day (around 2.5 mg/kg of body weight/day) for a month, high efficacy with 97% cure rate was reported (Jha et al., 1999). However, in the same study, side effects like mild-to-moderate gastrointestinal problems were observed. The mechanism of action of **1e** is not very clear, although different modes of actions have been proposed by several studies. Induced apoptosis-mediated cell death of the parasites (*L. donovani*), based on nuclear DNA condensation and fragmentation, was proposed (Verma and Dey, 2004). **1e** was given as a monotherapy to treat cutaneous or visceral leishmaniasis with a dosage of 2.5 mg/kg/day for a total of 28 days (Dorlo et al., 2012b). **1e**, initially an anticancer drug, was reported to have similar molecular modes of action against both the *Leishmania* spp. and the cancer cells in humans, which is mainly through apoptosis (Paris et al., 2004), lipid metabolism (Rakotomanga et al., 2007), and immunomodulatory effects (Liu et al., 2009; Wadhwa et al., 2009). However, this drug also has the drawback

of renal toxicity and is teratogenic, and not suitable to treat pregnant women. **1e** analogs included two series of ether phospholipids: 1) cyclohexylidene or cyclopentadecylidene substituted ether phospholipids with *N,N,N*-trimethylammonium or *N*-methylpiperidino or *N*-methylmorpholine head groups and 2) rigid head groups in combination with cycloalkylidene moieties in the lipid portion were reported to be 1.5 to 62 times more potent than miltefosine (Calogeropoulou et al., 2008). An alkyl phosphocholine-dinitroaniline hybrid molecule was reported to be effective against promastigotes and intracellular amastigotes form of *L. amazonensis* and more selective than miltefosine (Godinho et al., 2013). Another study showed that a new series of 2-[3-(2-alkyloxy-ethyl)-adamantan-1-yl]-ethoxy substituted ether phospholipids possessed antiparasitic activity with respect to the 2-alkyloxy substituent and were less cytotoxic compared to miltefosine (Papanastasiou et al., 2010).

Emerging Drug Targets and Drugs Against Leishmaniasis

Nucleoside Analogs and Purine Salvage Pathway as Drug Targets

The parasitic protozoan *Leishmania* lacks enzymes that are necessary for *de novo* synthesis of purine nucleotides. Usually, they are compensated by obtaining purine bases from the mammalian host cells *via* purine salvage system. Here, nucleoside transporters play vital roles in translocating purine bases through the cell surface of parasites.

The parasitic transporters are found to be unique compared to the transporters in the mammalian cells, in terms of substrate specificity. There are various pathways for nucleoside uptake with several purine/pyrimidine transporters involved such as LdNT1 and LdNT2, which are well studied (Vasudevan et al., 1998; Carter et al., 2000). Selectively targeting these transporters is difficult but it still remains a potential target, as they can uptake even toxic analogs of nucleosides that inhibit the cell growth of parasites.

Apart from these transporters, there are significant enzymes in the purine salvage pathway that include phosphoribosyl transferases. Purine analogs like allopurinol are known to inhibit phosphoribosyl transferases and are effective against parasites (Martinez and Marr, 1992). Allopurinol is effective against canine leishmaniasis but poses pharmacokinetic safety issues in case of humans (Yasur-Landau et al., 2016). *In vitro* studies have revealed a reduction in intramacrophagic amastigotes of *L. infantum* with the use of nucleoside analogs like immucillins (Freitas et al., 2015a). Immucillins or the synthetic deazapurine nucleoside analogs that include ImmA (IA), ImmH (IH), and SerMe-ImmH (SMIH) and their respective chemical structures are given in **Figure 2** (Freitas et al., 2015b).

Another important enzyme in the purine salvage pathway includes the nucleoside diphosphate kinases (NDKs). An analog of a multitargeted receptor tyrosine kinase (RTK) inhibitor (Chow and Eckhardt, 2007) and a pyrrole-indolinone compound (Vieira et al., 2017) was reported, which binds

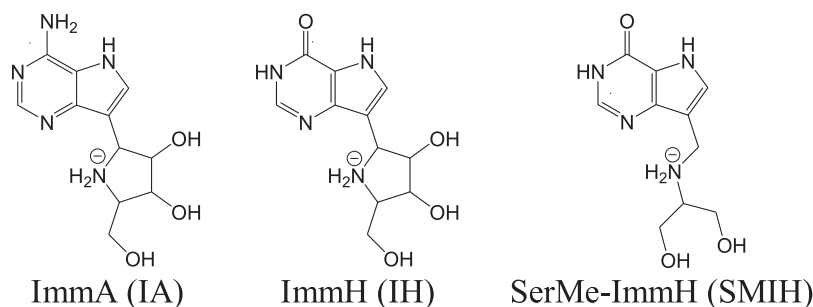


FIGURE 2 | Immucillins, the nucleoside analogs as hit candidates against leishmaniasis.

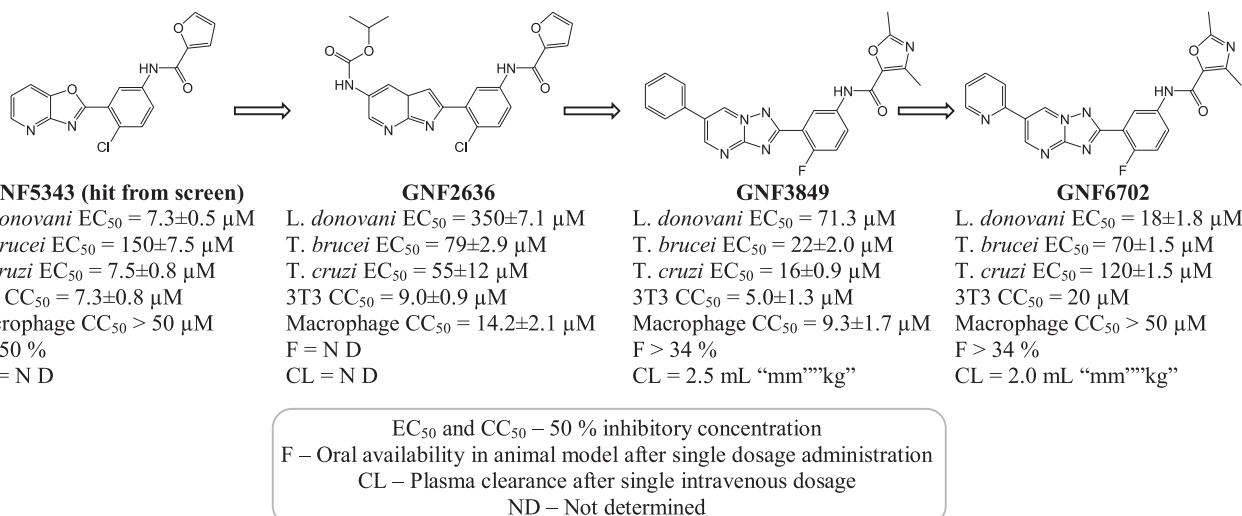


FIGURE 3 | Chemical evolution of proteasome targeting triazolopyrimidine scaffold inhibitors that act by inhibiting the activity of chymotrypsin protease.

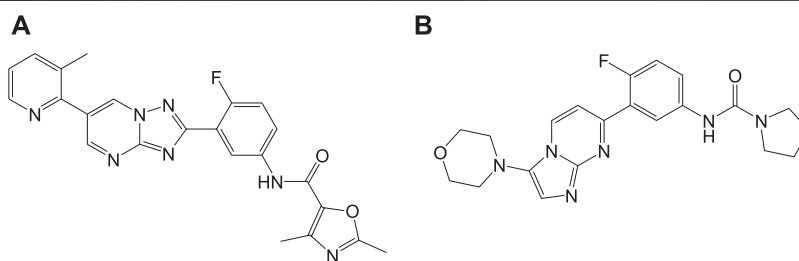
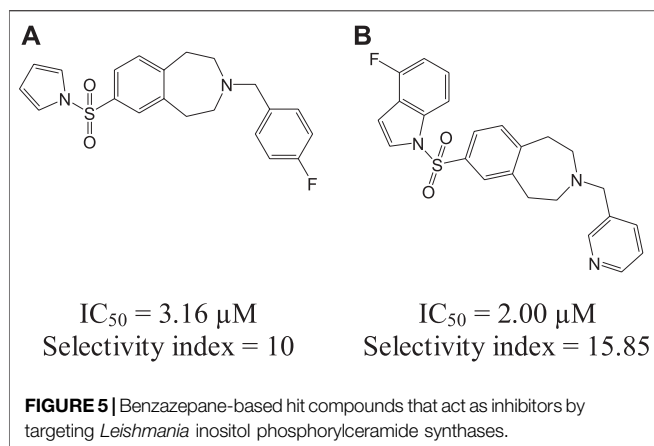


FIGURE 4 | Compounds that inhibit β5 subunits of proteasome.

NDK of *L. major* and exhibits antileishmanial activity *in vitro*. The latter drug was reported to possess potency and efficacy similar to that of the drug amphotericin B. The authors have suggested the use of this compound as a scaffold to develop new inhibitors against NDKs of *Leishmania* spp. (Vieira et al., 2017).

Though pyrimidine is synthesized by both *de novo* and through pyrimidine salvage pathway, enzymes of this pathway

as well as the pyrimidine analogs are regarded as promising drug targets against *Leishmania* (Alzahrani et al., 2017). Recently, *in vitro* studies revealed the use of pyrimidine analogs, cytarabine, and 5-fluorouracil and two purine analogs, azathioprine and 6-mercaptopurine, against the growth of promastigote and amastigote forms of *L. donovani* and *L. infantum* (Azzouz and Lawton, 2017). Out of these four



analogs, cytarabine and 5-fluorouracil were efficient against the promastigote stage of parasites and 5-fluorouracil and azathioprine were effective against the intracellular amastigotes. Here 5-fluorouracil was found to be highly efficient against both stages of parasites by inducing cytoplasmic vacuolization, causing damage to mitochondria, and subsequently damaging the kinetoplast and death of the parasites.

Kinetoplastid Proteasome Inhibition

A selective (20S) proteasome inhibitor GNF6702 (Khare et al., 2016) that has evolved through phenotypic hit has proved proteasomes as a promising target for the treatment of infections by kinetoplastid parasites (Crunkhorn, 2016) including *T. cruzi*, *Leishmania* species, and *T. brucei*. The triazolopyrimidine scaffold of GNF6702 exhibited antiparasitic activity by inhibiting chymotrypsin protease activity. **Figure 3** depicts the evolution of triazolopyrimidine scaffold drugs. The mode of action of this drug was known to occur by noncompetitive mode, without hindering the mammalian proteasomes or cells.

Recently, a structurally related proteasome inhibitor, **4a** (LXE408) which is at present in phase I human clinical trials (Nagle et al., 2020) was reported. A novel mode of noncompetitive binding drug compound **4a** with specific $\beta 5$ proteasome was also reported (**Figure 4**). Oral administration of compound **4a** was reported to have high efficacy in infected mouse models in its preclinical studies and is currently tested for its safety and tolerability in phase I clinical trials.

Another potential antileishmanial compound **4b** (Wyllie et al., 2019) was reported in the literature and its chemical structure is shown in **Figure 4**. The activity of this compound was verified against different clinically significant parasites like *L. donovani*, *L. infantum*, etc. This compound was reported to possess good pharmacokinetics, *in vivo* efficacy in infected mouse models, and comparable efficacy to the only approved oral antileishmanial drug miltefosine. The mechanism of action of this drug involves the profound inhibition of $\beta 5$ subunit of the proteasome *via* chymotrypsin-like activity in parasites. With consistent experimental data and high-resolution cryo-EM studies on this

compound-proteasome complex, a new inhibitor site located between $\beta 4$ and $\beta 5$ proteasome subunits was reported. Due to the positive results in regard to safety and efficacy, this compound is taken further for human trials.

Other Targets and Inhibitors Under Investigation

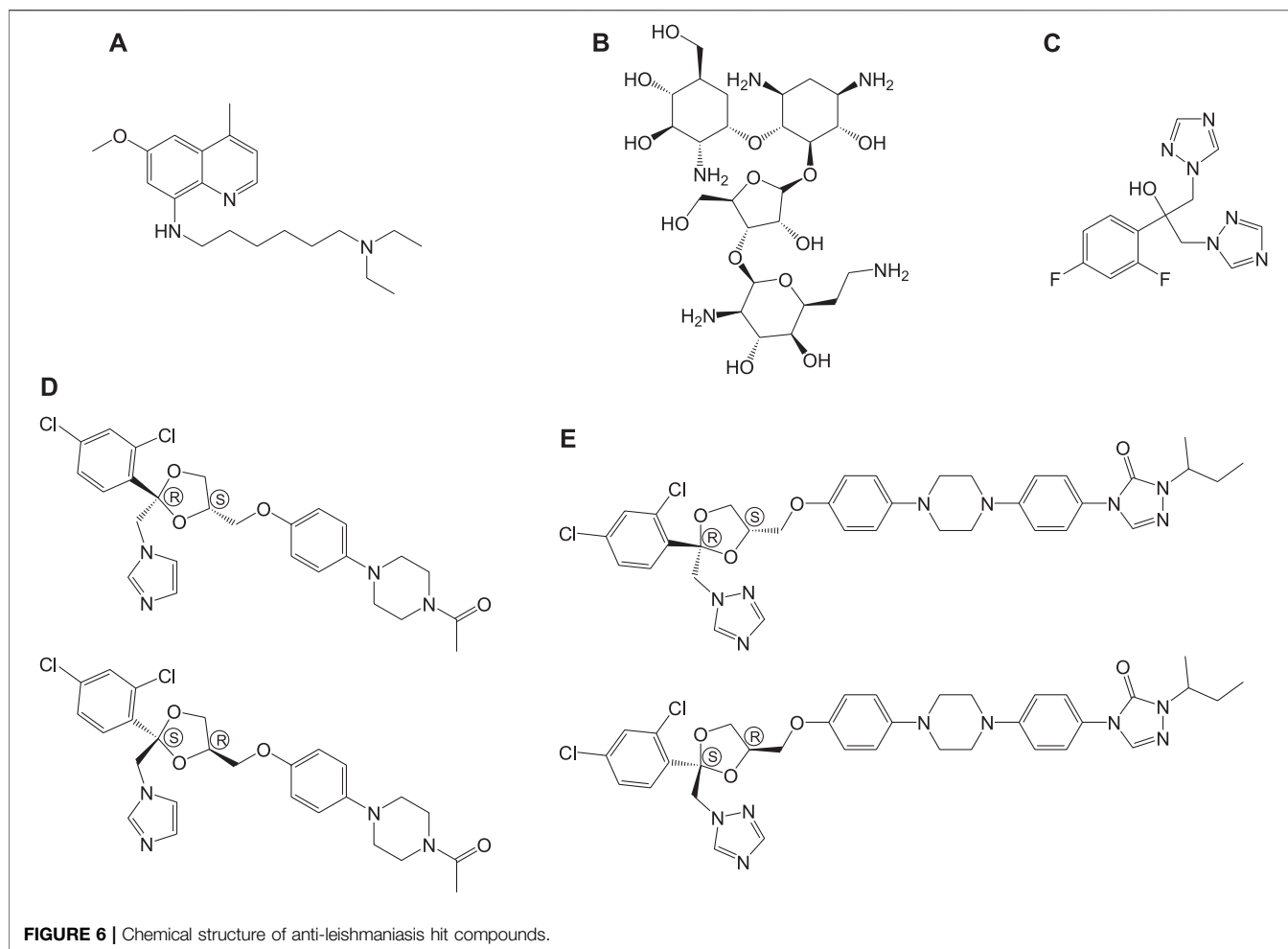
Mitochondria, being one of the most important organelles for parasites, with their unique properties and proteins that differ from mammalian hosts, serve as a potential target for the development of therapeutics against parasitic infections like leishmaniasis (Tasbihi et al., 2019). Currently, the studies on mitochondria of parasites are limited; however, with the available information, chemotherapeutic approaches are being developed against the mitochondria of parasites (Villa-Pulgarín et al., 2017). For instance, chalcones are reported as potential lead compounds against leishmaniasis which target the mitochondrial structure (Zhai et al., 1995; Zhai et al., 1999) and function in the parasites, followed by the inhibition of fumarate reductase (Chen et al., 2001).

Mitochondrial cytochrome bc 1 plays a vital role in electron transport chain and is reported as a potential drug target. Endochin-like quinolones (ELQs) were studied to show toxicity against amastigote forms of *L. donovani* and *L. mexicana* targeting cytochrome bc 1 (Stickles et al., 2015; Ortiz et al., 2016). Hydroxynaphthoquinone buparvaquone has also been reported to be active against cytochrome bc 1, which inhibits electron transport, ATP synthesis, and parasite survival.

The *Leishmania* inositol phosphoryl ceramide (IPC) synthases (Norcliffe et al., 2018) are regarded as one of the potential drug targets. Modeling studies have revealed coumarin derivatives to possess antileishmanial activity, which were further validated by *in vivo* studies (Mandlik et al., 2016; Mandlik and Singh, 2016). *In vitro* studies with a new class of benzazepanes (**5a** and **5b**) are shown in **Figure 5**. Compounds **5a** and **5b** were reported to exhibit anti-*Leishmania* IPC synthase activity (Norcliffe et al., 2018). Similar compounds could be developed and studied to obtain new antileishmanial drugs. Apart from these, kinetoplastid topoisomerases (Das et al., 2008) and nuclear DNA primases (Bhowmik et al., 2020) of *Leishmania* species are suggested as other potential drug targets, for their structural diversity from mammalian hosts as well as their significance in DNA replication in the parasites.

Sitamaquine (**6a**, **Figure 6**) (8-aminoquinolines) (Yeates, 2002) is an antileishmanial oral drug, in which the molecular mechanism of action is yet to be understood. Although sitamaquine is reported to cause visual morphological changes in the parasite (LANGRETH et al., 1983), the specific target is yet to be identified. The interaction of sitamaquine with *L. donovani* revealed that the rapid diffusion of drug through the membrane accumulates in the cytosol by a process independent of energy or sterol in the parasite (Coimbra et al., 2010). Also, the interaction of **6a** with the parasite membrane is transitory (Dueñas-Romero et al., 2007), and its efflux requires energy.

Paromomycin (**6b**, **Figure 6**) in the form of topical formulations was reported for leishmaniasis treatment. Paromomycin (paromomycin sulfate, $C_{23}H_{47}O_{18}S$) drugs are aminoglycoside antibiotics, administered intramuscularly, to



treat leishmaniasis in which mode of action is reported to involve mitochondria (Maarouf et al., 1997) and ribosomes (Maarouf et al., 1995) causing protein inhibition in the parasite. Another group of compounds used for the treatment of leishmaniasis are referred to as the *azoles*, for example, fluconazole (**6c**), ketoconazole (**6d**), and itraconazole (**6e**) as given in **Figure 6** (Prates et al., 2017; Vera et al., 2018; Bisworo et al., 2019). However, the use of azoles was reported to show mixed results (Nagle et al., 2014; Galvao et al., 2017).

The enzymes, bifunctional dihydrofolate reductase-thymidylate synthase, and pteridine reductase 1 in *Leishmania* spp. that are involved in the folate metabolic pathway were studied as targets for leishmaniasis treatment (Docampo et al., 2011). Dihydrofolate reductase enzyme was reported to be unique in the protozoan parasite *Leishmania* relative to that in the human host, thereby considering the enzyme as a promising target for selective drug design (Gilbert, 2002). In addition, pteridine reductase 1 inhibition was found to be essential to avoid the resistance to dihydrofolate reductase inhibitors. Chroman-4-one scaffold was reported to be a promising scaffold for the development of pteridine reductase 1 inhibitors against *Leishmania* spp., with low toxicity (Di Pisa et al., 2017). Structure-based optimization of piperidine-pteridine

derivatives resulted in two compounds, methyl-1-(4-(((2,4-diaminopteridin-6-yl)methyl)(2-ethoxy-2-oxoethyl)amino)benzoyl)piperidine-4-carboxylate and methyl 1-(4-(((2,4-Diaminopteridin-6-yl)methyl)(2-hydroxyethyl)-amino)benzoyl)piperidine-4-carboxylate, with relatively high potency, enhanced binding affinity, and selectivity among other derivatives (Corona et al., 2012). Novel derivative compounds of arylnicotinic acids conjugated with aryl (thio)semicarbazides were also reported to be synthesized based on structure-guided approach targeting the enzyme pteridine reductase 1 (*L. major*) which was also proven to possess enhanced selectivity and antiamastigote activity relative to miltefosine (Eldehna et al., 2019).

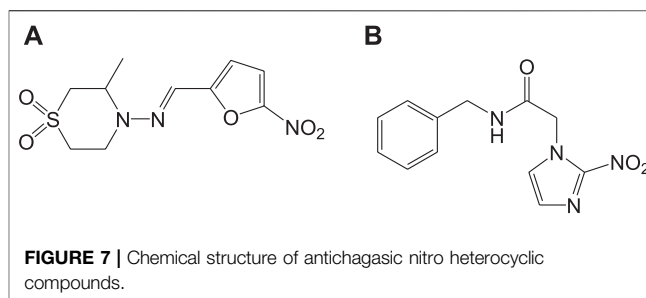
Liposomal Encapsulation and Nanoparticles in Anti-leishmanial Drugs

Nanotechnology-based drug delivery or drug formulations were attempted to improve the efficacy and also to assure safety of drugs. The challenges in oral route of administration of pentamidine drugs were reported to be overcome by means of loading the drug in PLGA nanoparticles (Valle et al., 2019). Here, the nanoparticles were reported to be prepared by double emulsion method and *in vitro/in vivo* studies (infected BALB/c mice) were successful. These drug-loaded PLGA nanoparticles

have shown a new perspective to drug administration with good pharmacological activity. Also, high efficacy has been reported with nanoformulations of amphotericin B (Manandhar et al., 2014), which is more safe and cost-effective and serves as an alternative to the existing conventional drug **1d**. Topical nanoliposomal formulations were prepared to treat cutaneous leishmaniasis, with liposomes containing 0.1, 0.2, and 0.4% **1d** (Lip-AmB), out of which 0.4% Lip-AmB was found to possess longer stability for about 20 months at room temperature (Jaafari et al., 2019). These formulations were effective against the lesions in *L. major*-infected BALB/c mice and also showed inhibition of the promastigotes/amastigotes growth *in vitro*. Fungisome is a liposomal formulation marketed in India (Wijnant et al., 2018), with lipids and formulations different from that of the standard AmBisome. In a study with *L. major*-infected BALB/c murine model (cutaneous leishmaniasis infection), it was reported that fungisome at a dosage of 1 mg/kg revealed toxicity, whereas AmBisome was nontoxic. However, the antileishmanial activity was exhibited with ~5–10 mg/kg of fungisome and also proved to be less efficacious when compared with AmBisome.

Artemisinin and its derivatives are another group of molecules that are reported to be effective for visceral leishmaniasis treatment. These are found to work by generating free radicals leading to apoptosis in parasites (Sen et al., 2010). *In vivo* studies in mice with nanoliposomal formulations of artemisinin were reported to reduce leishmanial intracellular infections (Ghaffarifar et al., 2015). Polymer (PLGA-poly (d,l-lactic-co-glycolic acid))-based nanoparticles were also shown to act as carrier of the drug artemisinin, facilitating sustained release of the drug (*in vitro* studies) along with antileishmanial activity (*ex vivo*). These artemisinin-incorporated PLGA polymeric nanoparticles also exhibited reduction of parasites or antiparasitic activity (Want et al., 2014; Want et al., 2015; Want et al., 2017). The pros of using these drug-loaded nanoparticles include reduction of drug toxicity, enhanced hydrophilicity, and bioavailability. However, these nanoparticles have not attained the level of clinical trials due to the higher cost, lower drug load, and toxicity involved in the preparation stage. Also, the limited availability of reports on nanoparticles with antileishmanial activity necessitated the need for exploration in this field of research that can reach clinical trials.

A recent *in vitro* study involved the use of an FDA-approved drug for malaria treatment (Chavali et al., 2012), halofantrine, for leishmaniasis treatment. By liposomal encapsulation of halofantrine, called halolipo, the issues of hydrophobicity and cardiotoxicity of the halofantrine drug were overcome. Halolipo (~20 nm diameter), on exposure to the protozoan parasite *L. donovani* (promastigotes), led to reduction in viable number of parasites. This could be due to ROS generation and depolarization of mitochondrial membrane of the parasites. Also, *in vitro* studies on the same confirm the selective reduction of viable parasites, dependency on drug concentration, and nontoxicity to mammalian host cells. However, *in vivo* studies ought to be performed with halolipo, so that this drug could be developed as an effective therapeutic for leishmaniasis in near future.



Use of nanosilver has also been tested by several researchers as therapeutics for leishmaniasis. It was reported to possess higher potency as the size becomes smaller (Allahverdiyev et al., 2011a; Allahverdiyev et al., 2011b). Nanosilver is shown to cause DNA damage and generate free radicals in the parasites with increase in immunomodulatory effects in human cell lines (de Menezes et al., 2015). Selenium nanoparticles known to possess antimicrobial, anticancerous, and antioxidant properties were used to develop a novel approach to treat cutaneous lesions and were proven to exhibit antileishmanial activity in both *in vivo* and *in vitro* studies. Also, these nanoparticles exhibited significant potency against *L. tropica* (Shakibaie et al., 2015). Another interesting finding involved silver-doped titanium oxide (TiAg), formulated by green synthesis using essential oil from *Nigella sativa* which showed high antileishmanial activity against *L. tropica* and *L. infantum* (Allahverdiyev et al., 2013). This formulation was proven to be nontoxic with high potency for treatment of cutaneous leishmaniasis. Another nanoformulation based on the combination of the miltefosine drug (Figure 1) with curcumin nanoformulation was reported (Tiwari et al., 2017) to possess enhanced antileishmanial activity both *in vitro* and *in vivo*.

CHAGAS DISEASE

Chagas disease, also called American trypanosomiasis, is one of the NTDs, which is endemic mainly in Latin America and spreads in European countries, Australia, Japan, Canada, and southern parts of the United States. Chagas disease is caused by a parasite named *T. cruzi*, a hemoflagellate protozoan of Kinetoplastida order and Trypanosomatidae family, which can occur in two phases, acute and chronic. This disease was discovered by a physician Carlos Chagas, who had stated during the initial period that there was no specific treatment for this disease, in his publication “Manual of Tropical and Infectious Diseases.” In Chagas disease, the causative protozoan is *Trypanosoma cruzi*, from which the trypomastigote forms are transmitted to humans through insects that belong to the subfamily Triatominae. These infective trypomastigotes are present in the fecal matter of the bug and enter into the tissues of human host through the bitten wound and later develop into an intracellular replicative parasitic form of amastigotes. Other modes of transmission are through infected blood transfusion/organ transplantation and genetic transmission from mother to fetus. Chagas disease occurs

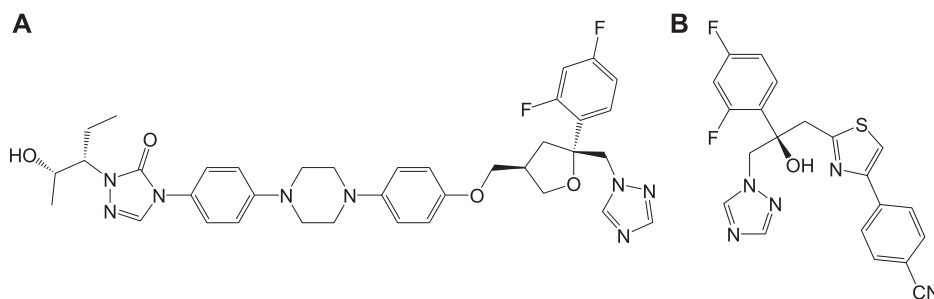


FIGURE 8 | Potent anti-Chagas azole-derived compounds that target sterol biosynthetic pathway.

mainly through two routes, congenital and oral. The congenital Chagas disease occurs throughout the world even in the nonendemic areas. The oral Chagas disease leads to acute disease outbreaks in the areas facing vectorial route interruptions (Sánchez and Ramírez, 2013). Congenital Chagas disease is mostly asymptomatic but includes some nonspecific clinical manifestations like myocarditis, gastrointestinal problems, meningoencephalitis, anemia, low birth weight, jaundice, microcephaly, ocular lesions, etc. (Schijman, 2006; Punukollu et al., 2007). Around 30% of these congenitally affected patients tend to develop symptomatic chronic phase of Chagas disease with cardiac and digestive problems (Rassi et al., 2010; Carlier et al., 2011). These patients possess lower possibility of developing cardiac problems relative to that in patients infected by vectorial route (Bern et al., 2011; Fabbro et al., 2014). In patients with oral Chagas disease infection, high mortality rate is observed in the first two weeks after infection followed by inflammation in the gastric mucosa which extends to proximate mesentery (Hoft et al., 1996). Clinical manifestations like myocarditis, acute heart failure, and meningoencephalitis are observed with orally infected Chagas disease (Punukollu et al., 2007; Shikanai-Yasuda and Carvalho, 2012). In case of acute infections through oral route, clinical features include abdominal pain, gastrointestinal tract bleeding, heart murmurs, palpitations, jaundice, nausea, vomiting, hepatomegaly, enteritis, and chest pain (WHO-Expert-Committee, 2002; Andrade et al., 2014). During the 1960s, the therapeutic activity of nitrofurans in infected murines and humans was discovered but it had a low curative effect which stopped its further development. Moreover, their curative ability differed in geographic areas, potentially due to mutations/variations in genetic strains of the parasites. These drugs were not effective against chronic cases of Chagas disease and include several serious side effects like anorexia, digestive manifestations, hypersensitivity, bone marrow depression, dermatitis with cutaneous eruptions, and peripheral polyneuropathy. The beginning of the 1980s marked the introduction of techniques like immunohistochemistry and PCR, which confirmed the association of parasites and their DNA with the inflammatory reactions resulting in pathological lesions in chronic Chagas disease. Several experimental studies (Morillo et al., 2015; Soy et al., 2015; Fernández et al., 2016) and clinical trials (Andrade et al., 2013; Chatelain, 2017) have been reported to show the

significance of reducing the parasite load in chronic Chagas disease treatment and the associated chronic cardiomyopathy.

Standard Anti-chagasic Drugs

At present, Chagas disease is treated by the two nitro heterocyclic compounds that were discovered in 1960–1970, namely, nifurtimox (**7a**) and benznidazole (**7b**) (Maya Arango et al., 2010), and the chemical structures are shown in Figure 7.

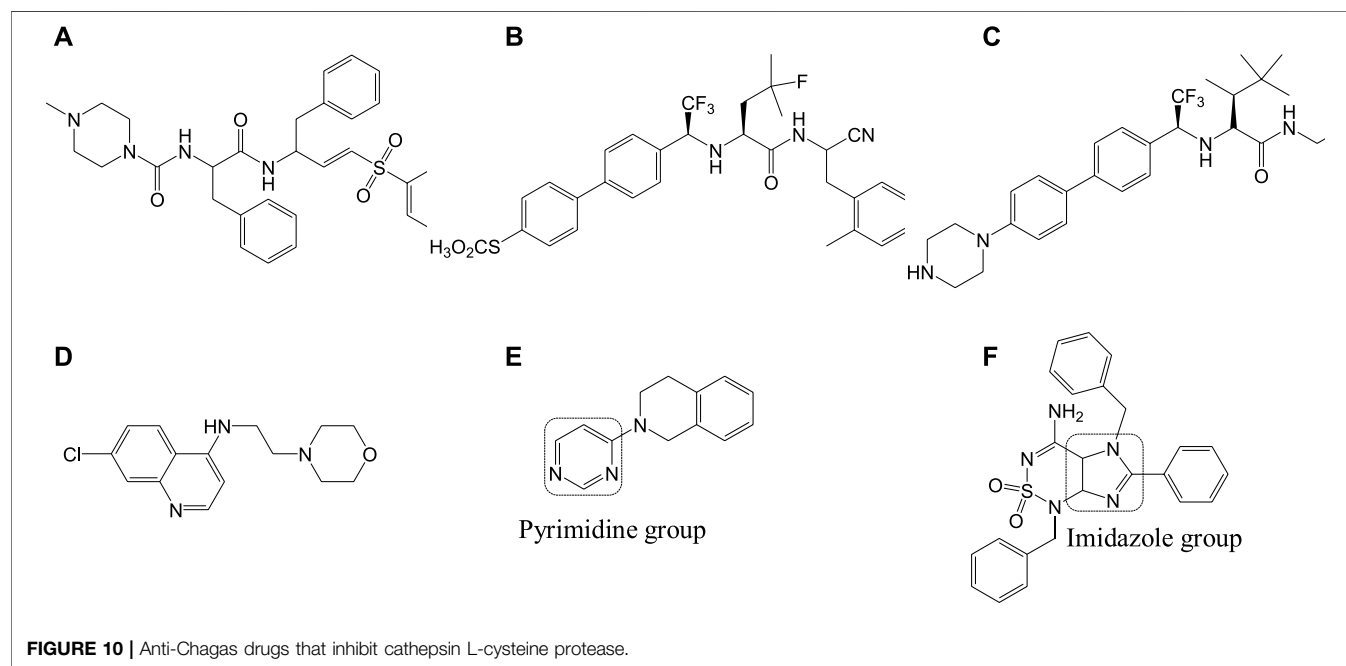
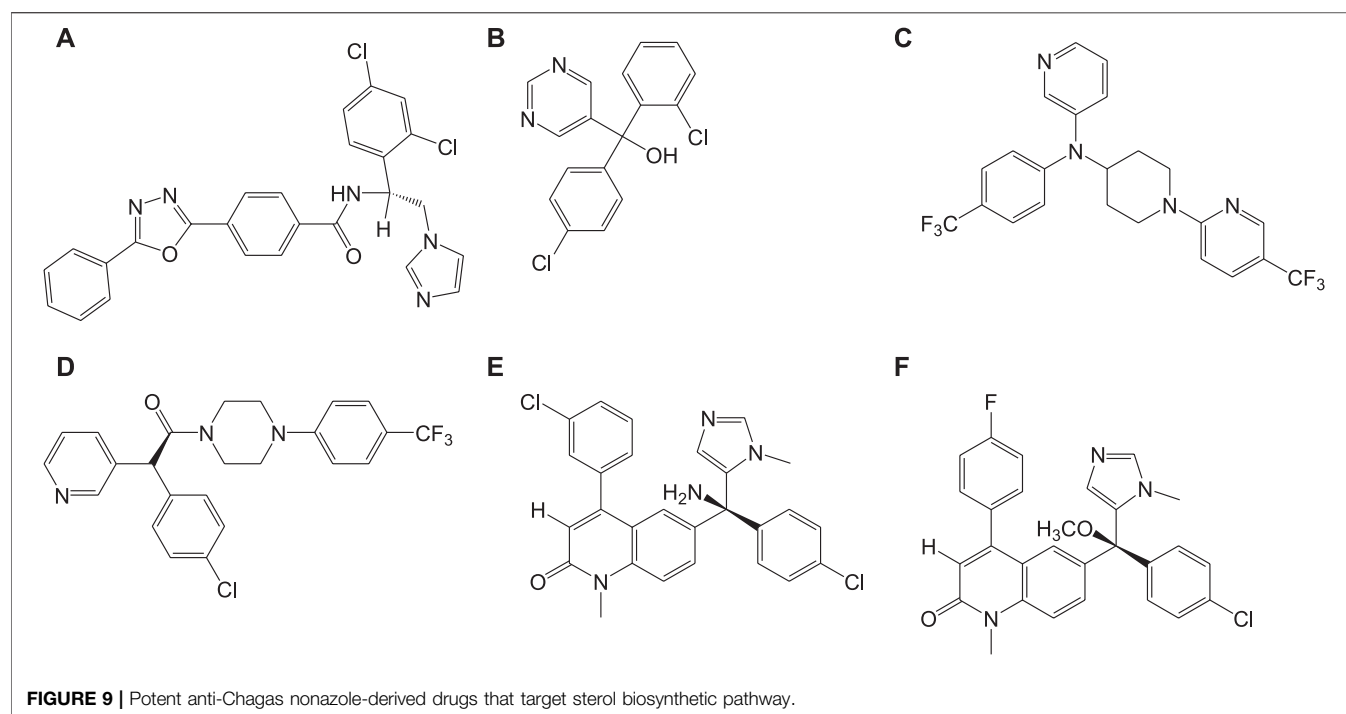
These drugs work by accumulation of free radicals generated by means of the nitro groups, which further resulted in high antioxidant activities in *T. cruzi*, ultimately killing the parasites. As stated before, these drugs are effective only for acute cases of Chagas disease infection along with side effects.

Emerging Drug Targets and Drugs Against Chagas Disease

CYP51 Inhibitors

Inhibitors of sterol biosynthetic pathway have been reported as one of the new drug targets for the treatment of Chagas disease. In particular, C14-ademethylase (CYP51) represents a potential drug target in which various inhibitors like azoles block the ergosterol biosynthesis and sterol C14-demethylase (CYP51) activities in the parasite. *In vivo* studies have revealed that the above compounds possess high potency of antichagasic activity along with good pharmacokinetic properties like longer half-life and large volume of distribution as compared to the previously existing drugs. Phase II clinical trials of the drugs (Figure 8), posaconazole (**8a**), and a prodrug of ravuconazole (**8b**) were reported to ensure safety, without sustained efficacy as single medications, in patients with chronic Chagas disease (Tarleton et al., 2014; Álvarez et al., 2015).

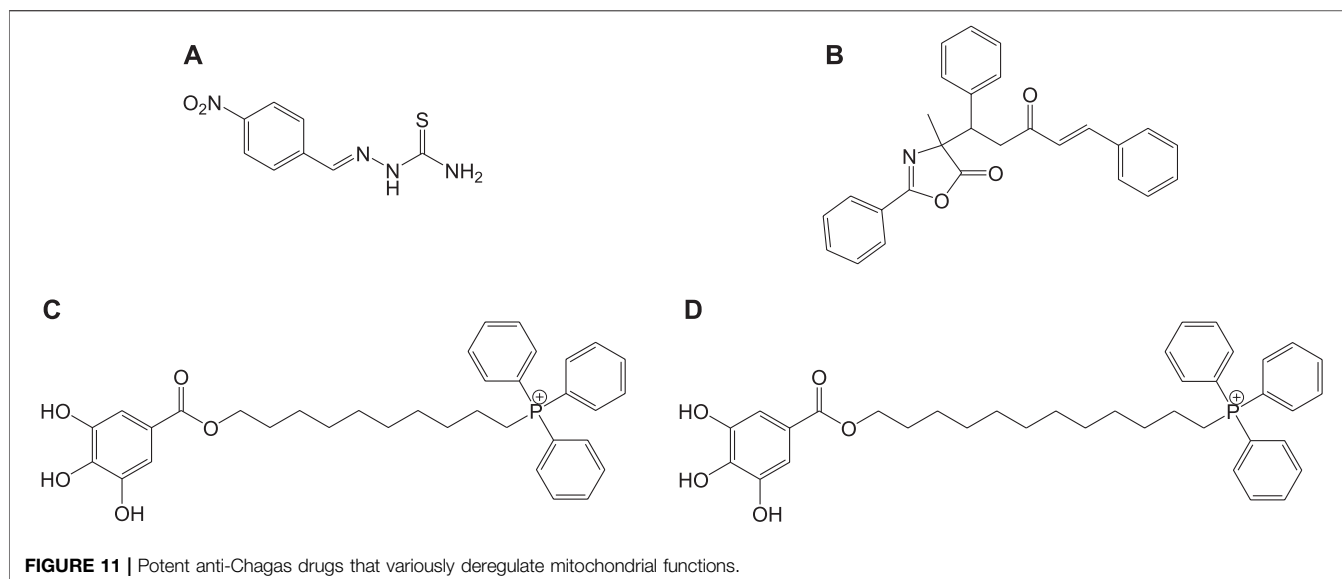
The other strategies involved variation in dosages and combination of drugs to improve the efficacy against Chagas disease. It was also reported that prolonged treatment with azole drugs like **8a** is required for potent antichagasic activity. This idea is also validated by Guedes et al. (da Matta Guedes et al., 2004) in infected dogs with treatment using benznidazole or albaconazole which resulted in complete cure within 60 days of treatment and 90 days of treatment, respectively. This necessitates the consideration of individual dosage regimens, drug concentration, and treatment time for successful treatment. With the high efficacy of azole derivatives, researchers are



currently working on developing rational approaches for antichagasic therapeutics.

In vivo studies with nonazole derivative **9a** for CYP51 inhibition have revealed variations in antichagasic activity with different parasitic strains. With a nonazole CYP51 inhibiting compound, fenarimol (**9b**) as scaffold, two other lead compounds **9c** and **9d** were developed which were reported to possess

antichagasic activity similar to that of **8a** and better than **7b** (Keenan et al., 2013). Buckner et al. developed an analog of tipifarnib (**9e**), anticancer drug, in which farnesyltransferase inhibitory activity was eliminated and CYP51 inhibition was withheld (Buckner et al., 2012). This compound was found to be highly potent with antichagasic activity in mouse models but requires improvement in pharmacokinetic properties. Similarly,



another compound **9f**, an atropisomer evolved from **9e**, was found to possess similar potency against *T. cruzi*. The chemical structures of nonazole-derived drugs that target the sterol biosynthetic pathway are shown in **Figure 9**.

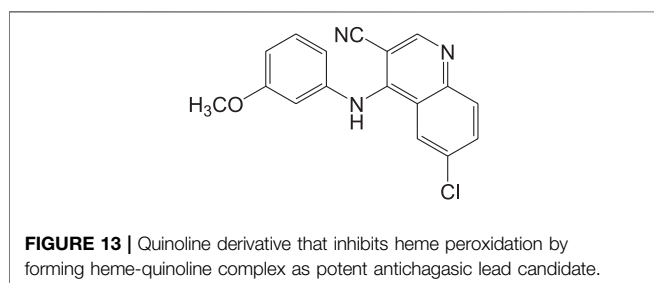
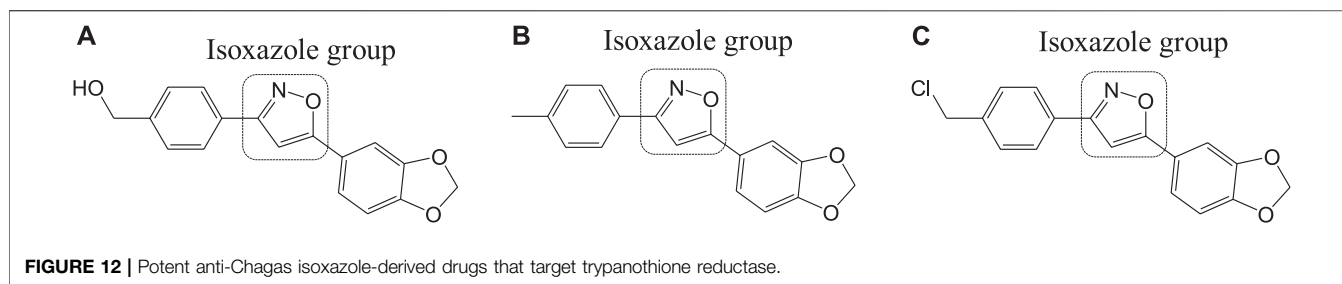
Cruzain Inhibitors

Cruzipain or cruzain denotes cathepsin L-cysteine protease that performs proteolytic activity throughout all stages in the life of *T. cruzi*. Studies have reported the importance of this enzyme in various biological functions including evasion of the immune system and host-parasite interactions (Brak et al., 2010; Bahia et al., 2014). Inhibitors of this protease also serve as significant drug targets in Chagas disease therapeutics. Compound **10a**, a vinyl sulfone, was rationally designed to selectively inhibit this cruzipain protease. This compound was reported to exhibit anti-*T. cruzi* activity in experimental mice models (immunocompetent and immunodeficient) infected with *T. cruzi* (Doyle et al., 2007). However, complete curability was not observed with compound **10a** when tested on acutely infected (*T. cruzi*) dog models, but it was reported to reduce the myocardial damage (Barr et al., 2005). Compound **10a** is currently in its advanced stages of preclinical studies, and also several other cruzipain inhibitor compounds with better potency and selective anti-*T. cruzi* activities are being developed (Brak et al., 2010; Ndao et al., 2014). Recently, two compounds **10b** and **10c** were identified by Ndao et al., which showed curability of 78 and 90%, respectively, in acutely infected murines (Ndao et al., 2014). Several analogs of 8-chloro-N-(3-morpholinopropyl)-5H-pyrimido [5,4-b]indol-4-amine containing indole, pyrimidine, quinoline, aniline, and pyrrole groups were reported to be tested for antichagasic activity. Among the several derivatives, 4-aminoquinoline analogs, in particular compound **10d**, were reported to have anticruzain activity along with antichagasic activity against *T. cruzi* (Tulahuen strain) with lower selectivity. Pyrimidine analog **10e** was found

to be highly active and selective for Chagas disease but lacked anticruzain activity (Schmidt and Krauth-Siegel, 2002). This implicates the need to understand the mechanism of action behind these compounds with *in vivo* studies (Arias et al., 2017; Vázquez et al., 2017). Also, several computational screening studies have revealed the synthesis and biological activities of several imidazole compounds. Among the various compounds identified, compound **10f** (Rodríguez-Poveda et al., 2012) was shown to exhibit high anti-*T. cruzi* activity against three strains including Tulahuen 2, CL-clone B5, and Y. The structures of potent inhibitors that target cathepsin L-cysteine protease are given in **Figure 10**.

Mitochondrial Deregulation Drugs

Mitochondria are vital cell organelles that are involved in ATP synthesis, nutrient oxidation, cellular redox, calcium homeostasis, and apoptosis. It produces hydrogen peroxide as the main oxidative species for cellular signaling in cytosol, and deregulation of mitochondria causes an increase in reactive oxygen species, leading to cytotoxicity and cell death. *T. cruzi* possesses unique mitochondria containing kinetoplasts and compactly packed mitochondrial DNA that accounts for 30% of its entire genome, making mitochondria an important drug target for Chagas disease treatment. An *in vitro* study has investigated the antichagasic activity of 4-nitrobenzaldehyde thiosemicarbazone (**11a**) (**Figure 11**), an S-limonene derivative, which showed potent activity against trypomastigotes and amastigotes of *T. cruzi*. Compound **11b** was reported to deregulate mitochondria of the parasites by cytoplasmic vacuolization, reduction in membrane potential, and increased free radical generation (Britta et al., 2015). Another study evaluated four C-4 functionalized azalactone derivatives for antichagasic activity (de Azeredo et al., 2017). Among these derivatives, one compound **11c** was found to possess three times more anti-*T. cruzi* activity compared to that of the antichagasic drug **7b**. Reduction in mitochondrial



membrane potential and size of epimastigotes was observed by flow cytometry and electron microscopy studies. It is recommended that these compounds could be used as a scaffold in the development of new therapeutic drugs for Chagas disease (de Azeredo et al., 2017). Yet another antichagasic agent was developed using gallic acid derivatives possessing lipophilic groups and triphenylphosphonium moiety that target the mitochondria of *T. cruzi*. Among these derivatives, relatively more potent compounds **11c** and **11d** compared to compound **7a** were reported (Cortes et al., 2015). These compounds were also highly selective and formed pores on mitochondrial membrane by varying the membrane potential. Further new analogs with antichagasic activity can potentially be developed from these derivatives.

Trypanothione Reductase

Trypanothione reductase is another significant therapeutic target for Chagas disease treatment, mainly because of its unique presence in Trypanosomatidae family and not in mammalian cells (Krieger et al., 2000; Khan, 2007; Beig et al., 2015). The reduction of trypanothione disulphide to trypanothione occurs in the presence of NADPH and is catalyzed by the enzyme trypanothione reductase (Fairlamb et al., 1985; Bond et al., 1999; Krieger et al., 2000; Beig et al., 2015).

Different isoxazole analogs were reported to be synthesized by microwave irradiation, with structures based on the natural lignans, veraguensin, and grandisin which exhibited potent activities against *T. cruzi* (Tulahuen strain) trypomastigote forms in the circulating blood and amastigote forms within the cells (da Rosa et al., 2017). Three compounds **12a**, **12b**, and **12c** (Figure 12) were found to be potent against amastigotes at concentrations lower than that reported for benzimidazole derivatives but were inactive against trypomastigotes. By

means of enzymatic assays, isoxazoles were reported to act independently on the enzyme trypanothione reductase. Recent studies have reported computationally screened and evaluated trypanothione reductase inhibitors against Chagas disease, which were obtained from natural products database (da Paixão and da Rocha Pita, 2019).

Heme Peroxidation as Drug Target

In general, heme or ferroprotoporphyrin plays a significant role in various biological processes including energy production, detoxification, respiration, oxygen transport, and antioxidant gene expression. Breakdown of heme is known to generate free radicals, which causes damage to DNA, proteins, lipids, and ultimately the cells. The requirement of heme in *T. cruzi* for multiplication of epimastigote forms by redox mechanism is stated as a potential drug target that can be blocked to possibly inhibit the epimastigotes (de Almeida Nogueira et al., 2011; Nogueira et al., 2017). Quinoline compounds are made of nitrogen heterocyclic groups that form complexes with heme and have been reported to possess activity against plasmodium, *Leishmania*, *T. cruzi*, bacteria, and also cancer (Eswaran et al., 2010; Ganguly et al., 2011; Muscia et al., 2011). Several derivatives of 4-arylaminoquinoline-3-carbonitrile were reported to exhibit anti-*T. cruzi* activity; in particular, compound **13** was found to be more active than compound **7b**, when complexed with hemin (Lechuga et al., 2016). The authors had reported enzymatic conversion of heme to biliverdin favoring oxygenase activity in parasites and also the complex formation of heme-quinoline compound **13** (Figure 13) leading to a reduction in heme levels followed by the generation of reactive oxygen species resulting in the death of parasites.

Other Targets and Formulations for Anti-Chagas Drug Development

T. cruzi depends on inherent sterols including ergosterol and its analogs for survival, where ergosterols play an important part in maintaining the plasma membrane (Urbina et al., 2002; Shang et al., 2014). Ergosterol requires squalene synthase for its biosynthesis, which catalyzes squalene formation by dimerization of two farnesyl pyrophosphate (FPP) molecules (Urbina et al., 2002). Researchers have found that inhibition of the squalene synthase can be a potential drug target for Chagas disease treatment. Inhibitors targeting squalene synthase were developed by several researchers (Chao et al., 2017) and are still in the process of investigation. Similarly, farnesyl diphosphate

synthase (FPPS) in the mevalonate pathway is stated as a potential target for several parasitic diseases (Demoro et al., 2012; Ferrer-Casal et al., 2014). Inhibition of FPPS indirectly blocks the synthesis of farnesyl diphosphate, by blocking the synthesis of farnesyl pyrophosphate and geranylgeranyl pyrophosphate (Aripirala et al., 2012). Several bisphosphonate derivatives are under research against *T. cruzi* by FPPS inhibition, to obtain new therapeutic drugs for Chagas disease (Recher et al., 2013). *T. cruzi* contains four iron superoxide dismutases (Fe-SODs) formed in the mitochondria (TcSODA and C), cytosol (TcSODB1), and glycosomes (TcSODB1-2) (Piacenza et al., 2013), which are unique to these parasites and different from that in humans, thereby serving as potential targets (Mateo et al., 2008). These superoxide dismutases are known to neutralize toxicity generated by oxygen radicals (Temperton et al., 1998). Studies evaluating the antichagasic activity of potential drugs by inhibition of Fe-SOD were also reported; for instance, a series of derivatives of arylaminoketones were tested (Moreno-Viguri et al., 2016) and shown to exert antichagasic activity by means of Fe-SOD inhibition. It is confirmed by analyzing the 1H-Magnetic Nuclear Resonance (¹H NMR) chemical shifts of excreted metabolites from the cultures of epimastigotes of *T. cruzi* *Arequipa* strain that was treated with test compounds.

Nanostructure formulations with trypanocidal activity were developed to lower the toxicity of drugs like **7b**. Nanoparticles including nanostructured lipid carriers, liposomes, quatsomes, solid lipid nanoparticles, and cyclodextrins were evaluated (Scalise et al., 2016; Vinuesa et al., 2017). Cyclodextrins-benznidazole complexes were reported to be relatively lower than that of benznidazole in its free form (Vinuesa et al., 2017).

CONCLUSION

Although the spread of both leishmaniasis and Chagas disease is under control, the threat still exists because of limited therapeutics and increasing incidents of drug resistance. Many drugs that are available to treat these diseases possess serious side effects and existing diversity among the causing parasites. Moreover, many drugs are active only in the acute phase of the disease. Herein, the various therapeutic strategies, drug targets, and drugs for leishmaniasis and Chagas disease were discussed. The significance of these two diseases based on the economic burden and the disability caused by them has opened

new avenues for novel therapeutics and drug targets. The presently employed strategies like novel drug developments and the use of a combination or repurposed drugs have been discussed briefly besides their advantages and future scopes. For leishmaniasis, standard drugs like pentavalent antimonials, pentamidine, amphotericin B, and miltefosine that target various metabolic pathways are discussed with their mechanism of action, advantages over other drugs, and limitations on their use. Various drugs that target the purine salvage pathway, purine and pyrimidine analogs, and their efficiencies at various stages of the pathogens cycle are also reviewed. The role of nanotechnology, various proteasome inhibitors, and enzymes that are under investigation as potential targets for leishmaniasis are also reviewed. With Chagas disease, various standard drugs like nifurtimox and benznidazole and their mechanism of action towards killing the parasites are discussed. Various inhibitors for Chagas disease that target CYP51, cruzain, trypanothione reductase, mitochondrial functions, heme peroxidation, etc. are also discussed. The recently developed nanostructure formulations including nanostructured lipid carriers, liposomes, quatsomes, solid lipid nanoparticles, and cyclodextrins that can reduce the toxic effects of anti-Chagas drugs are detailed.

This review details the advancements towards drug development. In recent years, it has been observed that the sensitivity of the available standard drugs varied in clinical samples over years, due to acquired resistance. Therefore, new therapies and strategies also need to be identified and implemented to prevent the emergence of new drug-resistant strains. Combination therapies and improved diagnosis could play key roles in disease management approaches.

AUTHOR CONTRIBUTIONS

All authors listed have made a substantial, direct, and intellectual contribution to the work and approved it for publication.

ACKNOWLEDGMENTS

The authors gratefully acknowledge Vellore Institute of Technology, Vellore and Chennai campus, for the support and encouragement.

REFERENCES

- Adams, E. R., Versteeg, I., and Leeflang, M. M. (2013). Systematic review into diagnostics for post-Kala-Azar dermal leishmaniasis (PKDL). *J. Trop. Med.* 2013 (8), 150746. doi:10.1155/2013/150746
- Allahverdiyev, A. M., Abamor, E. S., Bagirova, M., Baydar, S. Y., Ates, S. C., Kaya, F., et al. (2013). Investigation of antileishmanial activities of TiO₂@ Ag nanoparticles on biological properties of *L. Tropica* and *L. Infantum* parasites, *in vitro*. *Exp. Parasitol.* 135 (1), 55–63. doi:10.1016/j.exppara.2013.06.001
- Allahverdiyev, A. M., Abamor, E. S., Bagirova, M., and Rafailovich, M. (2011a). Antimicrobial effects of TiO₂ and Ag₂O nanoparticles against drug-resistant bacteria and leishmania parasites. *Future Microbiol.* 6 (8), 933–940. doi:10.2217/fmb.11.78
- Allahverdiyev, A. M., Abamor, E. S., Bagirova, M., Ustundag, C. B., Kaya, C., Kaya, F., et al. (2011b). Antileishmanial effect of silver nanoparticles and their enhanced antiparasitic activity under ultraviolet light. *Int. J. Nanomed.* 6, 2705. doi:10.2147/IJN.S23883
- Alvar, J., Velez, I. D., Bern, C., Herrero, M., Desjeux, P., Cano, J., et al. (2012). Leishmaniasis worldwide and global estimates of its incidence. *PLoS One* 7 (5), e35671. doi:10.1371/journal.pone.0035671
- Álvarez, G., Varela, J., Cruces, E., Fernández, M., Gabay, M., Leal, S. M., et al. (2015). Identification of a new amide-containing thiazole as a drug candidate for treatment of Chagas' disease. *Antimicrob. Agents Chemother.* 59 (3), 1398–1404. doi:10.1128/AAC.03814-14

- Alzahrani, K. J., Ali, J. A., Eze, A. A., Looi, W. L., Tagoe, D. N., Creek, D. J., et al. (2017). Functional and genetic evidence that nucleoside transport is highly conserved in *Leishmania* species: implications for pyrimidine-based chemotherapy. *Int. J. Parasitol. Drugs Drug Resist.* 7 (2), 206–226. doi:10.1016/j.ijpddr.2017.04.003
- Andersen, E. M., Cruz-Saldarriaga, M., Llanos-Cuentas, A., Luz-Cjuno, M., Echevarria, J., Miranda-Verastegui, C., et al. (2005). Comparison of meglumine antimoniate and pentamidine for peruvian cutaneous leishmaniasis. *Am. J. Trop. Med. Hyg.* 72 (2), 133–137. doi:10.4269/ajtmh.2005.72.133
- Andrade, D. V., Gollob, K. J., and Dutra, W. O. (2014). Acute chagas disease: new global challenges for an old neglected disease. *PLoS Negl. Trop. Dis.* 8 (7), e3010. doi:10.1371/journal.pntd.0003010
- Andrade, M. C., Oliveira Mde, F., Nagao-Dias, A. T., Coelho, I. C., Candido Dda, S., Freitas, E. C., et al. (2013). Clinical and serological evolution in chronic Chagas disease patients in a 4-year pharmacotherapy follow-up: a preliminary study. *Rev. Soc. Bras. Med. Trop.* 46 (6), 776–778. doi:10.1590/0037-8682-1646-2013
- Arias, D. G., Herrera, F. E., Garay, A. S., Rodrigues, D., Forastieri, P. S., Luna, L. E., et al. (2017). Rational design of nitrofurantoin derivatives: synthesis and valuation as inhibitors of *Trypanosoma cruzi* trypanothione reductase. *Eur. J. Med. Chem.* 125, 1088–1097. doi:10.1016/j.ejmech.2016.10.055
- Aripalra, S., Szajman, S. H., Jakoncic, J., Rodriguez, J. B., Docampo, R., Gabelli, S. B., et al. (2012). Design, synthesis, calorimetry, and crystallographic analysis of 2-alkylaminoethyl-1, 1-bisphosphonates as inhibitors of *Trypanosoma cruzi* farnesyl diphosphate synthase. *J. Med. Chem.* 55 (14), 6445–6454. doi:10.1021/jm300425y
- Arning, M., Kliche, K., Heer-Sonderhoff, A., and Wehmeier, A. (1995). Infusion-related toxicity of three different amphotericin B formulations and its relation to cytokine plasma levels: infusions-assoziierte toxisität dreier amphotericin B-formulierungen und ihre beziehung zu zytokin-plasmaspiegeln. *Mycoses* 38 (11–12), 459–465. doi:10.1111/j.1439-0507.1995.tb00020.x
- Azzouz, S., and Lawton, P. (2017). *In vitro* effects of purine and pyrimidine analogues on *Leishmania donovani* and *Leishmania infantum* promastigotes and intracellular amastigotes. *Acta Parasitol.* 62 (3), 582–588. doi:10.1515/ap-2017-0070
- Baginski, M., Resat, H., and McCammon, J. A. (1997). Molecular properties of amphotericin B membrane channel: a molecular dynamics simulation. *Mol. Pharmacol.* 52 (4), 560–570. doi:10.1124/mol.52.4.560
- Bahia, M. T., Diniz Lde, F., and Mosqueira, V. C. (2014). Therapeutic approaches under investigation for treatment of Chagas disease. *Expert Opin. Investig. Drugs* 23 (9), 1225–1237. doi:10.1517/13543784.2014.922952
- Barr, S. C., Warner, K. L., Kornreic, B. G., Piscitelli, J., Wolfe, A., Benet, L., et al. (2005). A cysteine protease inhibitor protects dogs from cardiac damage during infection by *Trypanosoma cruzi*. *Antimicrob. Agents Chemother.* 49 (12), 5160–5161. doi:10.1128/AAC.49.12.5160-5161.2005
- Basselin, M., Lawrence, F., and Robert-Gero, M. (1996). Pentamidine uptake in *Leishmania donovani* and *Leishmania amazonensis* promastigotes and axenic amastigotes. *Biochem. J.* W315 (2), 631–634. doi:10.1042/bj3150631
- Beig, M., Oellien, F., Garoff, L., Noack, S., Krauth-Siegel, R. L., and Selzer, P. M. (2015). Trypanothione reductase: a target protein for a combined *in vitro* and *in silico* screening approach. *PLoS Negl. Trop. Dis.* 9 (6), e0003773. doi:10.1371/journal.pntd.0003773
- Berman, J. D. (1997). Human leishmaniasis: clinical, diagnostic, and chemotherapeutic developments in the last 10 years. *Clin. Infect. Dis.* 24 (4), 684–703. doi:10.1093/clind/24.4.684
- Bern, C., Martin, D. L., and Gilman, R. H. (2011). Acute and congenital Chagas disease. *Adv. Parasitol.* 75, 19–47. doi:10.1016/B978-0-12-385863-4.00002-2
- Bhowmik, D., Jagadeesan, R., Rai, P., Nandi, R., Gudan, K., and Kumar, D. (2020). Evaluation of potential drugs against leishmaniasis targeting catalytic subunit of *Leishmania donovani* nuclear DNA primase using ligand based virtual screening, docking and molecular dynamics approaches. *J. Biomol. Struct. Dyn.* 1–15. doi:10.1080/07391102.2020.1739557
- Biswaro, L. S., Garcia, M. P., da Silva, J. R., Neira Fuentes, L. F., Vera, A., Escobar, P., et al. (2019). Itraconazole encapsulated PLGA-nanoparticles covered with mannose as potential candidates against leishmaniasis. *J. Biomed. Mater. Res. B* 107 (3), 680–687. doi:10.1002/jbm.b.34161
- Bond, C. S., Zhang, Y., Berriman, M., Cunningham, M. L., Fairlamb, A. H., and Hunter, W. N. (1999). Crystal structure of *Trypanosoma cruzi* trypanothione reductase in complex with trypanothione, and the structure-based discovery of new natural product inhibitors. *Structure* 7 (1), 81–89. doi:10.1016/s0969-2126(99)80011-2
- Bora, N., and Jha, A. N. (2020). *In silico* metabolic pathway analysis identifying target against leishmaniasis—a kinetic modeling approach. *Front. Genet.* 11, 179. doi:10.3389/fgene.2020.00179
- Borsari, C., Jiménez-Antón, M. D., Eick, J., Bifeld, E., Torrado, J. J., Ollas-Molero, A. I., et al. (2019). Discovery of a benzothioephene-flavonol halting miltefosine and antimonial drug resistance in *Leishmania* parasites through the application of medicinal chemistry, screening and genomics. *Eur. J. Med. Chem.* 183, 111676. doi:10.1016/j.ejmech.2019.111676
- Boswell, G. W., Buell, D., and Bekersky, I. (1998). AmBisome (liposomal amphotericin B): a comparative review. *J. Clin. Pharmacol.* 38 (7), 583–592. doi:10.1002/j.1552-4604.1998.tb04464.x
- Brak, K., Kerr, I. D., Barrett, K. T., Fuchi, N., Debnath, M., Ang, K., et al. (2010). Nonpeptidic tetrafluorophenoxymethyl ketone cruzain inhibitors as promising new leads for Chagas disease chemotherapy. *J. Med. Chem.* 53 (4), 1763–1773. doi:10.1021/jm901633v
- Britta, E. A., Scariot, D. B., Falziroli, H., Da Silva, C. C., Ueda-Nakamura, T., Dias Filho, B. P., et al. (2015). 4-Nitrobenzaldehyde thiosemicarbazone: a new compound derived from S-(+)-limonene that induces mitochondrial alterations in epimastigotes and trypomastigotes of *Trypanosoma cruzi*. *Parasitology* 142 (7), 978–988. doi:10.1017/S0031182015000141
- Brown, D. (2007). Unfinished business: target-based drug discovery. *Drug Discov. Today* 12 (23–24), 1007–1012. doi:10.1016/j.drudis.2007.10.017
- Buckner, F. S., Bahia, M. T., Suryadevara, P. K., White, K. L., Shackelford, D. M., Chennamaneni, N. K., et al. (2012). Pharmacological characterization, structural studies, and *in vivo* activities of anti-Chagas disease lead compounds derived from tipifarnib. *Antimicrob. Agents Chemother.* 56 (9), 4914–4921. doi:10.1128/AAC.06244-11
- Burguera, J., Burguera, M., De Pena, Y., Lugo, A., and Anez, N. (1993). Selective determination of antimony (III) and antimony (V) in serum and urine and of total antimony in skin biopsies of patients with cutaneous leishmaniasis treated with meglumine antimonate. *Trace Elem. Med.* 10 (2), 66–70.
- Calogeropoulou, T., Angelou, P., Detsi, A., Fragiadaki, I., and Scoulica, E. (2008). Design and synthesis of potent antileishmanial cycloalkylidene-substituted ether phospholipid derivatives. *J. Med. Chem.* 51 (4), 897–908. doi:10.1021/jm701166b
- Capdeville, R., Buchdunger, E., Zimmermann, J., and Matter, A. (2002). Glivec (ST1571, imatinib), a rationally developed, targeted anticancer drug. *Nat. Rev. Drug Discov.* 1 (7), 493–502. doi:10.1038/nrd839
- Carlier, Y., Torricio, F., Sosa-Estani, S., Russomando, G., Luquetti, A., Freilich, H., et al. (2011). Congenital Chagas disease: recommendations for diagnosis, treatment and control of newborns, siblings and pregnant women. *PLoS Negl. Trop. Dis.* 5 (10), e1250. doi:10.1371/journal.pntd.0001250
- Carter, N. S., Ben Mamoun, C., Liu, W., Silva, E. O., Landfear, S. M., Goldberg, D. E., et al. (2000). Isolation and functional characterization of the PfNT1 nucleoside transporter gene from *Plasmodium falciparum*. *J. Biol. Chem.* 275 (14), 10683–10691. doi:10.1074/jbc.275.14.10683
- Chahed, M. K., Bellali, H., Ben Jemaa, S., and Bellaj, T. (2016). Psychological and psychosocial consequences of zoonotic cutaneous leishmaniasis among women in Tunisia: preliminary findings from an exploratory study. *PLoS Negl. Trop. Dis.* 10 (10), e0005090. doi:10.1371/journal.pntd.0005090
- Chakraborty, A. K., and Majumder, H. K. (1988). Mode of action of pentavalent antimonials: specific inhibition of type I DNA topoisomerase of *Leishmania donovani*. *Biochem. Biophys. Res. Commun.* 152 (2), 605–611. doi:10.1016/S0006-291X(88)80081-0
- Chao, M. N., Storey, M., Li, C., Rodriguez, M. G., Di Salvo, F., Szajman, S. H., et al. (2017). Selenium-containing analogues of WC-9 are extremely potent inhibitors of *Trypanosoma cruzi* proliferation. *Bioorg. Med. Chem.* 25 (24), 6435–6449. doi:10.1016/j.bmc.2017.10.016
- Chatelain, E. (2017). Chagas disease research and development: is there light at the end of the tunnel? *Comput. Struct. Biotechnol. J.* 15, 98–103. doi:10.1016/j.csbj.2016.12.002
- Chavali, A. K., Blazier, A. S., Tlaxca, J. L., Jensen, P. A., Pearson, R. D., and Papin, J. A. (2012). Metabolic network analysis predicts efficacy of FDA-approved drugs targeting the causative agent of a neglected tropical disease. *BMC Syst. Biol.* 6 (1), 27. doi:10.1186/1752-0509-6-27

- Chen, M., Zhai, L., Christensen, S. B., Theander, T. G., and Kharazmi, A. (2001). Inhibition of fumarate reductase in *Leishmania major* and *L. donovani* by chalcones. *Antimicrob. Agents Chemother.* 45 (7), 2023–2029. doi:10.1128/AAC.45.7.2023-2029.2001
- Chow, L. Q., and Eckhardt, S. G. (2007). Sunitinib: from rational design to clinical efficacy. *J. Clin. Oncol.* 25 (7), 884–896. doi:10.1200/JCO.2006.06.3602
- Coelho, A. C., Messier, N., Ouellette, M., and Cotrim, P. C. (2007). Role of the ABC transporter PRP1 (ABCC7) in pentamidine resistance in *Leishmania amastigotes*. *Antimicrob. Agents Chemother.* 51 (8), 3030–3032. doi:10.1128/AAC.00404-07
- Cohen, B. E. (2010). Amphotericin B membrane action: role for two types of ion channels in eliciting cell survival and lethal effects. *J. Membr. Biol.* 238 (1–3), 1–20. doi:10.1007/s00232-010-9313-y
- Coimbra, E. S., Libong, D., Cojean, S., Saint-Pierre-Chazale, M., Solgadi, A., Le Moyec, L., et al. (2010). Mechanism of interaction of sitamaquine with *Leishmania donovani*. *J. Antimicrob. Chemother.* 65 (12), 2548–2555. doi:10.1093/jac/dkq371
- Cole, A. (1944). Kala-azar in east Africa. *Trans. R. Soc. Trop. Med. Hyg.* 37 (6), 409–435. doi:10.1016/S0035-9203(44)90022-2
- Corona, P., Gibellini, F., Cavalli, A., Saxena, P., Carta, A., Loriga, M., et al. (2012). Structure-based selectivity optimization of piperidine-pteridine derivatives as potent *Leishmania* pteridine reductase inhibitors. *J. Med. Chem.* 55 (19), 8318–8329. doi:10.1021/jm300563f
- Cortes, L. A., Castro, L., Pesce, B., Maya, J. D., Ferreira, J., Castro-Castillo, V., et al. (2015). Novel gallate triphenylphosphonium derivatives with potent antichagasic activity. *PLoS One* 10 (8), e0136852. doi:10.1371/journal.pone.0136852
- Crunkhorn, S. (2016). Antiparasitic drugs: proteasome inhibition combats kinetoplastid infections. *Nat. Rev. Drug Discov.* 15 (10), 676–677. doi:10.1038/nrd.2016.190
- Cruz, I., Albertini, A., Barbeitas, M., Arana, B., Picado, A., Ruiz-Postigo, J. A., et al. (2019). Target product profile for a point-of-care diagnostic test for dermal leishmaniasis. *Parasite Epidemiol. Control* 5, e00103. doi:10.1016/j.parepi.2019.e00103
- da Matta Guedes, P. M., Urbina, J. A., de Lana, M., Afonso, L. C., Veloso, V. M., Tafuri, W. L., et al. (2004). Activity of the new triazole derivative albaconazole against *Trypanosoma (Schizotrypanum) cruzi* in dog hosts. *Antimicrob. Agents Chemother.* 48 (11), 4286–4292. doi:10.1128/AAC.48.11.4286-4292.2004
- da Paixão, V. G., and da Rocha Pita, S. S. (2019). In silico identification and evaluation of new *Trypanosoma cruzi* trypanothione reductase (TcTR) inhibitors obtained from natural products database of the Bahia semi-arid region (NatProDB). *Comput. Biol. Chem.* 79, 36–47. doi:10.1016/j.compbiolchem.2019.01.009
- da Rosa, R., de Moraes, M. H., Zimmermann, L. A., Schenkel, E. P., Steindel, M., and Bernardes, L. S. C. (2017). Design and synthesis of a new series of 3,5-disubstituted isoxazoles active against *Trypanosoma cruzi* and *Leishmania amazonensis*. *Eur. J. Med. Chem.* 128, 25–35. doi:10.1016/j.ejmech.2017.01.029
- Das, B. B., Ganguly, A., and Majumder, H. K. (2008). DNA topoisomerases of *Leishmania*: the potential targets for anti-leishmanial therapy. *Adv. Exp. Med. Biol.* 625, 103–115. doi:10.1007/978-0-387-77570-8_9
- Davidson, R. N., Croft, S. L., Scott, A., Maini, M., Moody, A. H., and Bryceson, A. D. (1991). Liposomal amphotericin B in drug-resistant visceral leishmaniasis. *Lancet* 337 (8749), 1061–1062. doi:10.1016/0140-6736(91)91708-3
- de Almeida Nogueira, N. P., de Souza, C. F., de Souza Saraiva, F. M., Sultano, P. E., Dalmau, S. R., Bruno, R. E., et al. (2011). Heme-induced ROS in *Trypanosoma cruzi* activates CaMKII-like that triggers epimastigote proliferation. One helpful effect of ROS. *PLoS One* 6 (10), e25935. doi:10.1371/journal.pone.0025935
- de Azeredo, C. M., Avila, E. P., Pinheiro, D. L., Amarante, G. W., and Soares, M. J. (2017). Biological activity of the azlactone derivative EPA-35 against *Trypanosoma cruzi*. *FEMS Microbiol. Lett.* 364 (4), fnx020. doi:10.1093/femsle/fnx020
- de Menezes, J. P., Guedes, C. E., Petersen, A. L., Fraga, D. B., and Veras, P. S. (2015). Advances in development of new treatment for leishmaniasis. *Biomed. Res. Int.* 2015, 815023. doi:10.1155/2015/815023
- Demicheli, C., Frezard, F., Lecouvey, M., and Garnier-Suillerot, A. (2002). Antimony(V) complex formation with adenine nucleosides in aqueous solution. *Biochim. Biophys. Acta* 1570 (3), 192–198. doi:10.1016/s0304-4165(02)00198-8
- Demoro, B., Caruso, F., Rossi, M., Benítez, D., González, M., Cerecetto, H., et al. (2012). Bisphosphonate metal complexes as selective inhibitors of *Trypanosoma cruzi* farnesyl diphosphate synthase. *Dalton Trans.* 41 (21), 6468–6476. doi:10.1039/C2DT12179D
- Di Pisa, F., Landi, G., Dello Iacono, L., Pozzi, C., Borsari, C., Ferrari, S., et al. (2017). Chroman-4-One derivatives targeting pteridine reductase 1 and showing anti-parasitic activity. *Molecules* 22 (3), 426. doi:10.3390/molecules22030426
- Docampo, R., Vickers, T. J., and Beverley, S. M. (2011). Folate metabolic pathways in *Leishmania*. *Essays Biochem.* 51, 63–80. doi:10.1042/bse0510063
- Dorlo, T. P., Balasegaram, M., Beijnen, J. H., and de Vries, P. J. (2012a). Miltefosine: a review of its pharmacology and therapeutic efficacy in the treatment of leishmaniasis. *J. Antimicrob. Chemother.* 67 (11), 2576–2597. doi:10.1093/jac/dks275
- Dorlo, T. P., Huitema, A. D., Beijnen, J. H., and de Vries, P. J. (2012b). Optimal dosing of miltefosine in children and adults with visceral leishmaniasis. *Antimicrob. Agents Chemother.* 56 (7), 3864–3872. doi:10.1128/AAC.00292-12
- dos Santos Ferreira, C., Martins, P. S., Demicheli, C., Brochu, C., Ouellette, M., and Frézard, F. (2003). Thiol-induced reduction of antimony (V) into antimony (III): a comparative study with trypanothione, cysteinyl-glycine, cysteine and glutathione. *Biometals* 16 (3), 441–446. doi:10.1023/A:1022823605068
- Doyle, P. S., Zhou, Y. M., Engel, J. C., and McKerrow, J. H. (2007). A cysteine protease inhibitor cures Chagas' disease in an immunodeficient-mouse model of infection. *Antimicrob. Agents Chemother.* 51 (11), 3932–3939. doi:10.1128/AAC.00436-07
- Dueñas-Romero, A. M., Loiseau, P. M., and Saint-Pierre-Chazale, M. (2007). Interaction of sitamaquine with membrane lipids of *Leishmania donovani* promastigotes. *Biochim. Biophys. Acta-Biomembr.* 1768 (2), 246–252. doi:10.1016/j.bbmem.2006.07.003
- Durieu, E., Prina, E., Leclercq, O., Oumata, N., Gaboriaud-Kolar, N., Vougiannopoulou, K., et al. (2016). From drug screening to target deconvolution: a target-based drug discovery pipeline using *Leishmania* casein kinase 1 isoform 2 to identify compounds with antileishmanial activity. *Antimicrob. Agents Chemother.* 60 (5), 2822–2833. doi:10.1128/AAC.00021-16
- Eldehna, W. M., Almahli, H., Ibrahim, T. M., Fares, M., Al-Warhi, T., Boeckler, F. M., et al. (2019). Synthesis, *in vitro* biological evaluation and *in silico* studies of certain aryl nicotinic acids conjugated with aryl (thio) semicarbazides as a novel class of anti-leishmanial agents. *Eur. J. Med. Chem.* 179, 335–346. doi:10.1016/j.ejmech.2019.06.051
- Eswaran, S., Adhikari, A. V., Chowdhury, I. H., Pal, N. K., and Thomas, K. D. (2010). New quinoline derivatives: synthesis and investigation of antibacterial and antituberculosis properties. *Eur. J. Med. Chem.* 45 (8), 3374–3383. doi:10.1016/j.ejmech.2010.04.022
- Fabbro, D. L., Danesi, E., Olivera, V., Codebo, M. O., Denner, S., Heredia, C., et al. (2014). Trypanocide treatment of women infected with *Trypanosoma cruzi* and its effect on preventing congenital Chagas. *PLoS Negl. Trop. Dis.* 8 (11), e3312. doi:10.1371/journal.pntd.0003312
- Fairlamb, A. H., Blackburn, P., Ulrich, P., Chait, B. T., and Cerami, A. (1985). Trypanothione: a novel bis(glutathionyl)spermidine cofactor for glutathione reductase in trypanosomatids. *Science* 227 (4693), 1485–1487. doi:10.1126/science.3883489
- Fernández, M. L., Marson, M. E., Ramirez, J. C., Mastrantonio, G., Schijman, A. G., Altchek, J., et al. (2016). Pharmacokinetic and pharmacodynamic responses in adult patients with Chagas disease treated with a new formulation of benznidazole. *Mem. Inst. Oswaldo Cruz* 111 (3), 218–221. doi:10.1590/0074-02760150401
- Ferrer-Casal, M., Li, C., Galizzi, M., Stortz, C. A., Szajnman, S. H., Docampo, R., et al. (2014). New insights into molecular recognition of 1, 1-bisphosphonic acids by farnesyl diphosphate synthase. *Bioorg. Med. Chem.* 22 (1), 398–405. doi:10.1016/j.bmc.2013.11.010
- Freitas, E. O., Nico, D., Alves-Silva, M. V., Morrot, A., Clinch, K., Evans, G. B., et al. (2015a). Immucillins ImmA and ImmH are effective and non-toxic in the treatment of experimental visceral leishmaniasis. *PLoS Negl. Trop. Dis.* 9 (12), e0004297. doi:10.1371/journal.pntd.0004297
- Freitas, E. O., Nico, D., Guan, R., Meyer-Fernandes, J. R., Clinch, K., Evans, G. B., et al. (2015b). Immucillins impair *Leishmania (L.) infantum* chagasi and

- Leishmania (L.) amazonensis* multiplication *in vitro*. *PLoS One* 10 (4), e0124183. doi:10.1371/journal.pone.0124183
- Galvao, E. L., Rabello, A., and Cota, G. F. (2017). Efficacy of azole therapy for tegumentary leishmaniasis: a systematic review and meta-analysis. *PLoS One* 12 (10), e0186117. doi:10.1371/journal.pone.0186117
- Ganguly, A., Banerjee, K., Chakraborty, P., Das, S., Sarkar, A., Hazra, A., et al. (2011). Overcoming multidrug resistance (MDR) in cancer *in vitro* and *in vivo* by a quinoline derivative. *Biomed. Pharmacother.* 65 (6), 387–394. doi:10.1016/j.biopha.2011.04.024
- Garcia-Calvo, M., Lisnock, J., Bull, H. G., Hawes, B. E., Burnett, D. A., Braun, M. P., et al. (2005). The target of ezetimibe is Niemann-Pick C1-Like 1 (NPC1L1). *Proc. Natl. Acad. Sci. U.S.A.* 102 (23), 8132–8137. doi:10.1073/pnas.0500269102
- Ghaffarifar, F., Esavand Heydari, F., Dalimi, A., Hassan, Z. M., Delavari, M., and Mikaeiloo, H. (2015). Evaluation of apoptotic and antileishmanial activities of artemisinin on promastigotes and BALB/C mice infected with *Leishmania major*. *Iran J. Parasitol.* 10 (2), 258–267.
- Ghedini, E., Zhang, W. W., Charest, H., Sundar, S., Kenney, R. T., and Matlashewski, G. (1997). Antibody response against a *Leishmania donovani* amastigote-stage-specific protein in patients with visceral leishmaniasis. *Clin. Diagn. Lab. Immunol.* 4 (5), 530–535.
- Ghorbani, M., and Farhodi, R. (2018). Leishmaniasis in humans: drug or vaccine therapy? *Drug Des. Devel. Ther.* 12, 25–40. doi:10.2147/DDDT.S146521
- Gilbert, I. H. (2002). Inhibitors of dihydrofolate reductase in *Leishmania* and trypanosomes. *Biochim. Biophys. Acta* 1587 (2–3), 249–257. doi:10.1016/s0925-4439(02)00088-1
- Gilbert, I. H. (2013). Drug discovery for neglected diseases: molecular target-based and phenotypic approaches: minipreview series on phenotypic screening for anti-infective targets. *J. Med. Chem.* 56 (20), 7719–7726. doi:10.1021/jm400362b
- Godinho, J. L., Georgikopoulou, K., Calogropoulou, T., de Souza, W., and Rodrigues, J. C. (2013). A novel alkyl phosphocholine-dinitroaniline hybrid molecule exhibits biological activity *in vitro* against *Leishmania amazonensis*. *Exp. Parasitol.* 135 (1), 153–165. doi:10.1016/j.exppara.2013.06.015
- Goodwin, L. (1995). Pentostam® (sodium stibogluconate): a 50-year personal reminiscence. *Trans. R. Soc. Trop. Med. Hyg.* 89 (3), 339–341. doi:10.1016/0035-9203(95)90572-3
- Hamill, R. J. (2013). Amphotericin B formulations: a comparative review of efficacy and toxicity. *Drugs* 73 (9), 919–934. doi:10.1007/s40265-013-0069-4
- Hartel, S., and Bolard, J. (1996). Amphotericin B: new life for an old drug. *Trends Pharmacol. Sci.* 17 (12), 445–449. doi:10.1016/s0165-6147(96)01012-7
- Herbrecht, R., Letscher, V., Andres, E., and Cavalier, A. (1999). Safety and efficacy of amphotericin B colloidal dispersion. An overview. *Chemotherapy* 45 (Suppl. 1), 67–76. doi:10.1159/000048472
- Hoft, D. F., Farrar, P. L., Kratz-Owens, K., and Shaffer, D. (1996). Gastric invasion by *Trypanosoma cruzi* and induction of protective mucosal immune responses. *Infect. Immun.* 64 (9), 3800–3810. doi:10.1128/IAI.64.9.3800-3810.1996
- Hotez, P. J., Molyneux, D. H., Fenwick, A., Kumaresan, J., Sachs, S. E., Sachs, J. D., et al. (2007). Control of neglected tropical diseases. *N. Engl. J. Med.* 357 (10), 1018–1027. doi:10.1056/NEJMra064142
- Jaafari, M. R., Hatamipour, M., Alavizadeh, S. H., Abbasi, A., Saberi, Z., Rafati, S., et al. (2019). Development of a topical liposomal formulation of amphotericin B for the treatment of cutaneous leishmaniasis. *Int. J. Parasitol. Drugs Drug Resist.* 11, 156–165. doi:10.1016/j.ijpddr.2019.09.004
- Jha, T. K., Sundar, S., Thakur, C. P., Bachmann, P., Karbwang, J., Fischer, C., et al. (1999). Miltefosine, an oral agent, for the treatment of Indian visceral leishmaniasis. *N. Engl. J. Med.* 341 (24), 1795–1800. doi:10.1056/NEJM199912093412403
- Kandpal, M., and Tekwani, B. L. (1997). Polyamine transport systems of *Leishmania donovani* promastigotes. *Life Sci.* 60 (20), 1793–1801. doi:10.1016/s0024-3205(97)00139-2
- Keenan, M., Chaplin, J. H., Alexander, P. W., Abbott, M. J., Best, W. M., Khong, A., et al. (2013). Two analogues of fenarimol show curative activity in an experimental model of Chagas disease. *J. Med. Chem.* 56 (24), 10158–10170. doi:10.1021/jm401610c
- Khan, M. O. (2007). Trypanothione reductase: a viable chemotherapeutic target for antitrypanosomal and antileishmanial drug design. *Drug Target Insights* 2, 129–146. doi:10.1177/117739280700200007
- Khare, S., Nagle, A. S., Biggart, A., Lai, Y. H., Liang, F., Davis, L. C., et al. (2016). Proteasome inhibition for treatment of leishmaniasis, Chagas disease and sleeping sickness. *Nature* 537 (7619), 229–233. doi:10.1038/nature19339
- Krieger, S., Schwarz, W., Ariyanayagam, M., Fairlamb, A., Krauth-Siegel, R., and Clayton, C. (2000). Trypanosomes lacking trypanothione reductase are avirulent and show increased sensitivity to oxidative stress. *Mol. Microbiol.* 35 (3), 542–552. doi:10.1046/j.1365-2958.2000.01721.x
- Lai, A. F. E. J., Vrede, M. A., Soetosenojo, R. M., and Lai, A. F. R. F. (2002). Pentamidine, the drug of choice for the treatment of cutaneous leishmaniasis in Surinam. *Int. J. Dermatol.* 41 (11), 796–800. doi:10.1046/j.1365-4362.2002.01633.x
- Lainson, R., and Rangel, E. F. (2005). *Lutzomyia longipalpis* and the eco-epidemiology of American visceral leishmaniasis, with particular reference to Brazil: a review. *Mem. Inst. Oswaldo Cruz.* 100 (8), 811–827. doi:10.1590/s0074-02762005000800001
- Langreth, S. G., Berman, J. D., Riordan, G. P., and Lee, L. S. (1983). Fine-structural alterations in *Leishmania tropica* within human macrophages exposed to antileishmanial drugs *in vitro* 1. *J. Protozool.* 30 (3), 555–561. doi:10.1111/j.1550-7408.1983.tb01421.x
- Lechuga, G. C., Borges, J. C., Calvet, C. M., de Araújo, H. P., Zuma, A. A., do Nascimento, S. B., et al. (2016). Interactions between 4-aminoquinoline and heme: promising mechanism against *Trypanosoma cruzi*. *Int. J. Parasitol. Drugs Drug Resist.* 6 (3), 154–164. doi:10.1016/j.ijpddr.2016.07.001
- Liu, D., Zhang, T., Marshall, A. J., Okkenhaug, K., Vanhaesebroeck, B., and Uozona, J. E. (2009). The p110δ isoform of phosphatidylinositol 3-kinase controls susceptibility to *Leishmania major* by regulating expansion and tissue homing of regulatory T cells. *J. Immunol.* 183 (3), 1921–1933. doi:10.4049/jimmunol.0901099
- Lucumi, A., Robledo, S., Gama, V., and Saravia, N. G. (1998). Sensitivity of *Leishmania viannia panamensis* to pentavalent antimony is correlated with the formation of cleavable DNA-protein complexes. *Antimicrob. Agents Chemother.* 42 (8), 1990–1995. doi:10.1128/AAC.42.8.1990
- Maarouf, M., de Kouchkovsky, Y., Brown, S., Petit, P. X., and Robert-Gero, M. (1997). *Vivo* Interference of paromomycin with mitochondrial activity of *Leishmania*. *Exp. Cell Res.* 232 (2), 339–348. doi:10.1006/excr.1997.3500
- Maarouf, M., Lawrence, F., Croft, S. L., and Robert-Gero, M. (1995). Ribosomes of *Leishmania* are a target for the aminoglycosides. *Parasitol. Res.* 81 (5), 421–425. doi:10.1007/BF00931504
- Manandhar, K. D., Yadav, T. P., Prajapati, V. K., Basukala, O., Aganja, R. P., Dude, A., et al. (2014). Nanonization increases the antileishmanial efficacy of amphotericin B: an *ex vivo* approach. *Adv. Exp. Med. Biol.* 808, 77–91. doi:10.1007/978-81-322-1774-9_7
- Mandlik, V., Patil, S., Bopanna, R., Basu, S., and Singh, S. (2016). Biological activity of coumarin derivatives as anti-leishmanial agents. *PLoS One* 11 (10), e0164585. doi:10.1371/journal.pone.0164585
- Mandlik, V., and Singh, S. (2016). Molecular docking and molecular dynamics simulation study of inositol phosphorylceramide synthase-inhibitor complex in leishmaniasis: insight into the structure based drug design. *F1000Research* 5, 1610. doi:10.12688/f1000research.9151.2
- Maroli, M., Feliciangeli, M. D., Bichaud, L., Charrel, R. N., and Gradoni, L. (2013). Phlebotomine sandflies and the spreading of leishmaniasis and other diseases of public health concern. *Med. Vet. Entomol.* 27 (2), 123–147. doi:10.1111/j.1365-2915.2012.01034.x
- Martinez, S., and Marr, J. J. (1992). Allopurinol in the treatment of American cutaneous leishmaniasis. *N. Engl. J. Med.* 326 (11), 741–744. doi:10.1056/NEJM199203123261105
- Mateo, H., Marin, C., Perez-Cordon, G., and Sanchez-Moreno, M. (2008). Purification and biochemical characterization of four iron superoxide dismutases in *Trypanosoma cruzi*. *Mem. Inst. Oswaldo Cruz* 103 (3), 271–276. doi:10.1590/s0074-02762008000300008
- Matlashewski, G. (2001). *Leishmania* infection and virulence. *Med. Microbiol. Immunol.* 190 (1–2), 37–42. doi:10.1007/s004300100076
- Maya Arango, J., Orellana, M., Ferreira, J., Kemmerling Weis, U., López Muñoz, R., and Morello Casté, A. (2010). Chagas disease: present status of pathogenic mechanisms and chemotherapy. *Biol. Res.* 43, 323–331. doi:10.4067/S0716-97602010000300009
- Meyerhoff, A. (1999). US food and drug administration approval of AmBisome (liposomal amphotericin B) for treatment of visceral leishmaniasis. *Clin. Infect. Dis.* 28 (1), 42–48. doi:10.1086/51508510.1086/515086
- Modabber, F., Buffet, P. A., Torreale, E., Milon, G., and Croft, S. L. (2007). Consultative meeting to develop a strategy for treatment of cutaneous leishmaniasis. *Kinetoplastid Biol. Dis.* 6 (1), 3. doi:10.1186/1475-9292-6-3

- Moffat, J. G., Vincent, F., Lee, J. A., Eder, J., and Prunotto, M. (2017). Opportunities and challenges in phenotypic drug discovery: an industry perspective. *Nat. Rev. Drug Discov.* 16 (8), 531–543. doi:10.1038/nrd.2017.111
- Moreno-Viguri, E., Jimenez-Montes, C., Martin-Escobano, R., Santivanez-Veliz, M., Martin-Montes, A., Azqueta, A., et al. (2016). *In vitro* and *in vivo* anti-*Trypanosoma cruzi* activity of new arylamine mannich base-type derivatives. *J. Med. Chem.* 59 (24), 10929–10945. doi:10.1021/acs.jmedchem.6b00784
- Morillo, C. A., Marin-Neto, J. A., Avezum, A., Sosa-Estani, S., Rassi, A., Jr, Rosas, F., et al. (2015). Randomized trial of benznidazole for chronic Chagas' cardiomyopathy. *N. Engl. J. Med.* 373 (14), 1295–1306. doi:10.1056/NEJMoa1507574
- Mukherjee, A., Padmanabhan, P. K., Sahani, M. H., Barrett, M. P., and Madhubala, R. (2006). Roles for mitochondria in pentamidine susceptibility and resistance in *Leishmania donovani*. *Mol. Biochem. Parasitol.* 145 (1), 1–10. doi:10.1016/j.molbiopara.2005.08.016
- Muscia, G. C., Cazorla, S. I., Frank, F. M., Borosky, G. L., Buldain, G. Y., Asis, S. E., et al. (2011). Synthesis, trypanocidal activity and molecular modeling studies of 2-alkylaminomethylquinoline derivatives. *Eur. J. Med. Chem.* 46 (9), 3696–3703. doi:10.1016/j.ejmech.2011.05.035
- Nagle, A., Biggart, A., Be, C., Srinivas, H., Hein, A., Caridha, D., et al. (2020). Discovery and characterization of clinical candidate LXE408 as a kinetoplastid-selective proteasome inhibitor for the treatment of leishmaniasis. *J. Med. Chem.* 63 (19), 10773–10781. doi:10.1021/acs.jmedchem.0c00499
- Nagle, A. S., Khare, S., Kumar, A. B., Supek, F., Buchynskyy, A., Mathison, C. J., et al. (2014). Recent developments in drug discovery for leishmaniasis and human African trypanosomiasis. *Chem. Rev.* 114 (22), 11305–11347. doi:10.1021/cr500365f
- Ndao, M., Beaulieu, C., Black, W. C., Isabel, E., Vasquez-Camargo, F., Nath-Chowdhury, M., et al. (2014). Reversible cysteine protease inhibitors show promise for a Chagas disease cure. *Antimicrob. Agents Chemother.* 58 (2), 1167–1178. doi:10.1128/AAC.01855-13
- Neumann, A., Czub, J., and Baginski, M. (2009). On the possibility of the amphotericin B-sterol complex formation in cholesterol and ergosterol-containing lipid bilayers: a molecular dynamics study. *J. Phys. Chem. B.* 113 (48), 15875–15885. doi:10.1021/jp905133f
- Nogueira, N. P., Saraiva, F. M. S., Oliveira, M. P., Mendonca, A. P. M., Inacio, J. D. F., Almeida-Amaral, E. E., et al. (2017). Heme modulates *Trypanosoma cruzi* bioenergetics inducing mitochondrial ROS production. *Free Radic. Biol. Med.* 108, 183–191. doi:10.1016/j.freeradbiomed.2017.03.027
- Norcliffe, J. L., Mina, J. G., Alvarez, E., Cantizani, J., de Dios-Anton, F., Colmenarejo, G., et al. (2018). Identifying inhibitors of the *Leishmania* inositol phosphorylceramide synthase with antiprotozoal activity using a yeast-based assay and ultra-high throughput screening platform. *Sci. Rep.* 8 (1), 1–10. doi:10.1038/s41598-018-22063-9
- Ortiz, D., Forquer, I., Boitz, J., Soysa, R., Elya, C., Fulwiler, A., et al. (2016). Targeting the cytochrome bc1 complex of *Leishmania* parasites for discovery of novel drugs. *Antimicrob. Agents Chemother.* 60 (8), 4972–4982. doi:10.1128/AAC.00850-16
- Pal, B., Murti, K., Siddiqui, N. A., Das, P., Lal, C. S., Babu, R., et al. (2017). Assessment of quality of life in patients with post kalaazar dermal leishmaniasis. *Health Qual. Life Outcomes.* 15 (1), 148. doi:10.1186/s12955-017-0720-y
- Papanastasiou, I., Prousis, K. C., Georgikopoulou, K., Pavlidis, T., Scoulica, E., Kolocouris, N., et al. (2010). Design and synthesis of new adamantyl-substituted antileishmanial ether phospholipids. *Bioorg. Med. Chem. Lett.* 20 (18), 5484–5487. doi:10.1016/j.bmcl.2010.07.078
- Paris, C., Loiseau, P. M., Bories, C., and Breard, J. (2004). Miltefosine induces apoptosis-like death in *Leishmania donovani* promastigotes. *Antimicrob. Agents Chemother.* 48 (3), 852–859. doi:10.1128/aac.48.3.852-859.2004
- Pearson, R. D., and Sousa, A. Q. (1996). Clinical spectrum of leishmaniasis. *Clin. Infect. Dis.* 22 (1), 1–13. doi:10.1093/clinids/22.1.1
- Piacenza, L., Peluffo, G., Alvarez, M. N., Martinez, A., and Radi, R. (2013). *Trypanosoma cruzi* antioxidant enzymes as virulence factors in Chagas disease. *Antioxid. Redox Signal.* 19 (7), 723–734. doi:10.1089/ars.2012.4618
- Prates, F. V., Dourado, M. E., Silva, S. C., Schrieffer, A., Guimaraes, L. H., Brito, M. D., et al. (2017). Fluconazole in the treatment of cutaneous leishmaniasis caused by *leishmania braziliensis*: a randomized controlled trial. *Clin. Infect. Dis.* 64 (1), 67–71. doi:10.1093/cid/ciw662
- Punukollu, G., Gowda, R. M., Khan, I. A., Navarro, V. S., and Vasavada, B. C. (2007). Clinical aspects of the Chagas' heart disease. *Int. J. Cardiol.* 115 (3), 279–283. doi:10.1016/j.ijcard.2006.03.004
- Purkait, B., Kumar, A., Nandi, N., Sardar, A. H., Das, S., Kumar, S., et al. (2012). Mechanism of amphotericin B resistance in clinical isolates of *Leishmania donovani*. *Antimicrob. Agents Chemother.* 56 (2), 1031–1041. doi:10.1128/AAC.00030-11
- Rakotomanga, M., Blanc, S., Gaudin, K., Chaminade, P., and Loiseau, P. M. (2007). Miltefosine affects lipid metabolism in *Leishmania donovani* promastigotes. *Antimicrob. Agents Chemother.* 51 (4), 1425–1430. doi:10.1128/AAC.01123-06
- Rassi, A., Jr, Rassi, A., and Marin-Neto, J. A. (2010). Chagas disease. *Lancet* 375 (9723), 1388–1402. doi:10.1016/S0140-6736(10)60061-X
- Recher, M., Barboza, A. P., Li, Z.-H., Galizzi, M., Ferrer-Casal, M., Szajnman, S. H., et al. (2013). Design, synthesis and biological evaluation of sulfur-containing 1, 1-bisphosphonic acids as antiparasitic agents. *Eur. J. Med. Chem.* 60, 431–440. doi:10.1016/j.ejmech.2012.12.015
- Rodriguez-Poveda, C. A., González-Pacanosowska, D., Szajnman, S. H., and Rodríguez, J. B. (2012). 2-alkylaminoethyl-1, 1-bisphosphonic acids are potent inhibitors of the enzymatic activity of *Trypanosoma cruzi* squalene synthase. *Antimicrob. Agents Chemother.* 56 (8), 4483–4486. doi:10.1128/AAC.00796-12
- Sánchez, L. V., and Ramírez, J. D. (2013). Congenital and oral transmission of American trypanosomiasis: an overview of physiopathogenic aspects. *Parasitology* 140 (2), 147. doi:10.1017/S0031182012001394
- Scalise, M. L., Arrua, E. C., Rial, M. S., Esteve, M. I., Salomon, C. J., and Fichera, L. E. (2016). Promising efficacy of benznidazole nanoparticles in acute *Trypanosoma cruzi* murine model: *in-vitro* and *in-vivo* studies. *Am. J. Trop. Med. Hyg.* 95 (2), 388–393. doi:10.4269/ajtmh.15-0889
- Schijman, A. G. (2006). Congenital chagas disease. *Perspect. Med. Virol.* 13, 223–258. doi:10.1016/S0168-7069(06)13012-8
- Schmidt, A., and Krauth-Siegel, R. (2002). Enzymes of the trypanothione metabolism as targets for antitrypanosomal drug development. *Curr. Top. Med. Chem.* 2 (11), 1239–1259. doi:10.2174/1568026023393048
- Sen, R., Ganguly, S., Saha, P., and Chatterjee, M. (2010). Efficacy of artemisinin in experimental visceral leishmaniasis. *Int. J. Antimicrob. Agents.* 36 (1), 43–49. doi:10.1016/j.ijantimicag.2010.03.008
- Shaked-Mishan, P., Ulrich, N., Ephros, M., and Zilberstein, D. (2001). Novel intracellular SbV reducing activity correlates with antimony susceptibility in *Leishmania donovani*. *J. Biol. Chem.* 276 (6), 3971–3976. doi:10.1074/jbc.M005423200
- Shakibaie, M., Forootanfar, H., Golkari, Y., Mohammadi-Khorsand, T., and Shakibaie, M. R. (2015). Anti-biofilm activity of biogenic selenium nanoparticles and selenium dioxide against clinical isolates of *Staphylococcus aureus*, *Pseudomonas aeruginosa*, and *Proteus mirabilis*. *J. Trace Elem. Med. Biol.* 29, 235–241. doi:10.1016/j.jtemb.2014.07.020
- Shang, N., Li, Q., Ko, T.-P., Chan, H.-C., Li, J., Zheng, Y., et al. (2014). Squalene synthase as a target for Chagas disease therapeutics. *PLoS Pathog.* 10 (5), e1004114. doi:10.1371/journal.ppat.1004114
- Shikanai-Yasuda, M. A., and Carvalho, N. B. (2012). Oral transmission of Chagas disease. *Clin. Infect. Dis.* 54 (6), 845–852. doi:10.1093/cid/cir956
- Simitsopoulou, M., Roilides, E., Dotis, J., Dalakiouridou, M., Dudkova, F., Andreadou, E., et al. (2005). Differential expression of cytokines and chemokines in human monocytes induced by lipid formulations of amphotericin B. *Antimicrob. Agents Chemother.* 49 (4), 1397–1403. doi:10.1128/AAC.49.4.1397-1403.2005
- Soto-Mancipe, J., Grogil, M., and Berman, J. D. (1993). Evaluation of pentamidine for the treatment of cutaneous leishmaniasis in Colombia. *Clin. Infect. Dis.* 16 (3), 417–425. doi:10.1093/clind/16.3.417
- Soy, D., Aldasoro, E., Guerrero, L., Posada, E., Serret, N., Mejia, T., et al. (2015). Population pharmacokinetics of benznidazole in adult patients with Chagas disease. *Antimicrob. Agents Chemother.* 59 (6), 3342–3349. doi:10.1128/AAC.05018-14
- Stickles, A. M., De Almeida, M. J., Morrissey, J. M., Sheridan, K. A., Forquer, I. P., Nilsen, A., et al. (2015). Subtle changes in endocytosis-like quinoline structure alter the site of inhibition within the cytochrome bc1 complex of *Plasmodium falciparum*. *Antimicrob. Agents Chemother.* 59 (4), 1977–1982. doi:10.1128/AAC.04149-14
- Sundar, S., and Oliari, P. L. (2007). Miltefosine in the treatment of leishmaniasis: clinical evidence for informed clinical risk management. *Ther. Clin. Risk Manag.* 3 (5), 733–740.
- Swinney, D. C., and Anthony, J. (2011). How were new medicines discovered? *Nat. Rev. Drug Discov.* 10 (7), 507–519. doi:10.1038/nrd3480
- Swinney, D. C. (2013). Phenotypic vs. target-based drug discovery for first-in-class medicines. *Clin. Pharmacol. Ther.* 93 (4), 299–301. doi:10.1038/clpt.2012.236
- Tarleton, R. L., Gürtler, R. E., Urbina, J. A., Ramsey, J., and Viotti, R. (2014). Chagas disease and the London declaration on neglected tropical diseases. *PLoS Negl. Trop. Dis.* 8 (10), e3219. doi:10.1371/journal.pntd.0003219

- Tasbihi, M., Shekari, F., Hajjarian, H., Masoori, L., and Hadighi, R. (2019). Mitochondrial proteome profiling of *Leishmania tropica*. *Microb. Pathog.* 133, 103542. doi:10.1016/j.micpath.2019.103542
- Temperton, N. J., Wilkinson, S. R., Meyer, D. J., and Kelly, J. M. (1998). Overexpression of superoxide dismutase in *Trypanosoma cruzi* results in increased sensitivity to the trypanocidal agents gentian violet and benznidazole. *Mol. Biochem. Parasitol.* 96 (1–2), 167–176. doi:10.1016/s0166-6851(98)00127-3
- Tiwari, B., Pahuja, R., Kumar, P., Rath, S. K., Gupta, K. C., and Goyal, N. (2017). Nanotized curcumin and miltefosine, a potential combination for treatment of experimental visceral leishmaniasis. *Antimicrob. Agents Chemother.* 61 (3). doi:10.1128/AAC.01169-16
- Toledo, A. C. D. C., Jr, da Silva, R. E., Carmo, R. F., Amaral, T. A., Luz, Z. M. P., and Rabello, A. (2013). Assessment of the quality of life of patients with cutaneous leishmaniasis in Belo Horizonte, Brazil, 2009–2010. A pilot study. *Trans. R. Soc. Trop. Med. Hyg.* 107 (5), 335–336. doi:10.1093/trstmh/trt021
- Urbina, J. A., Concepcion, J. L., Rangel, S., Visbal, G., and Lira, R. (2002). Squalene synthase as a chemotherapeutic target in *Trypanosoma cruzi* and *Leishmania mexicana*. *Mol. Biochem. Parasitol.* 125 (1–2), 35–45. doi:10.1016/S0166-6851(02)00206-2
- Valle, I. V., Machado, M. E., Araujo, C., da Cunha-Junior, E. F., da Silva Pacheco, J., Torres-Santos, E. C., et al. (2019). Oral pentamidine-loaded poly(D,L-lactic-co-glycolic) acid nanoparticles: an alternative approach for leishmaniasis treatment. *Nanotechnology* 30 (45), 455102. doi:10.1088/1361-6528/ab373e
- Vasudevan, G., Carter, N. S., Drew, M. E., Beverley, S. M., Sanchez, M. A., Seyfang, A., et al. (1998). Cloning of *Leishmania* nucleoside transporter genes by rescue of a transport-deficient mutant. *Proc. Natl. Acad. Sci. U.S.A.* 95 (17), 9873–9878. doi:10.1073/pnas.95.17.9873
- Vázquez, K., Paulino, M., O Salas, C., J Zarate-Ramos, J., Vera, B., and Rivera, G. (2017). Trypanothione reductase: a target for the development of anti-*Trypanosoma cruzi* drugs. *Mini Rev. Med. Chem.* 17 (11), 939–946. doi:10.2174/1389557517666170315145410
- Vera, A. M., Casadiego, O. A., Mantilla, J. C., and Escobar, P. (2018). Evaluation of ketoconazole formulations for topical use in cutaneous leishmaniasis caused by *Leishmania (Viannia)*. *Rev. Peru Med. Exp. Salud Publica.* 35 (3), 476. doi:10.17843/rpmesp.2018.353.3531
- Verma, N. K., and Dey, C. S. (2004). Possible mechanism of miltefosine-mediated death of *Leishmania donovani*. *Antimicrob. Agents Chemother.* 48 (8), 3010–3015. doi:10.1128/AAC.48.8.3010-3015.2004
- Vieira, P. S., Souza, T., Honorato, R. V., Zanphorlin, L. M., Severiano, K. U., Rocco, S. A., et al. (2017). Pyrrole-indolinone SU11652 targets the nucleoside diphosphate kinase from *Leishmania* parasites. *Biochem. Biophys. Res. Commun.* 488 (3), 461–465. doi:10.1016/j.bbrc.2017.05.048
- Villa-Pulgarín, J. A., Gajate, C., Botet, J., Jimenez, A., Justies, N., Varela, -M, R. E., et al. (2017). Mitochondria and lipid raft-located FOF1-ATP synthase as major therapeutic targets in the antileishmanial and anticancer activities of ether lipid edelfosine. *PLoS Negl. Trop. Dis.* 11 (8), e0005805. doi:10.1371/journal.pntd.0005805
- Vinuesa, T., Herraiz, R., Oliver, L., Elizondo, E., Acarregui, A., Esquisabel, A., et al. (2017). Benznidazole nanoformulates: a chance to improve therapeutics for chagas disease. *Am. J. Trop. Med. Hyg.* 97 (5), 1469–1476. doi:10.4269/ajtmh.17-0044
- Wadhone, P., Maiti, M., Agarwal, R., Kamat, V., Martin, S., and Saha, B. (2009). Miltefosine promotes IFN- γ -dominated anti-leishmanial immune response. *J. Immunol.* 182 (11), 7146–7154. doi:10.4049/jimmunol.0803859
- Walker, J., and Saravia, N. G. (2004). Inhibition of *Leishmania donovani* promastigote DNA topoisomerase I and human monocyte DNA topoisomerases I and II by antimonial drugs and classical antitopoisomerase agents. *J. Parasitol.* 90 (5), 1155–1162. doi:10.1645/GE-3347
- Walsh, T. J., Goodman, J. L., Pappas, P., Bekersky, I., Buell, D. N., Roden, M., et al. (2001). Safety, tolerance, and pharmacokinetics of high-dose liposomal amphotericin B (AmBisome) in patients infected with *Aspergillus* species and other filamentous fungi: maximum tolerated dose study. *Antimicrob. Agents Chemother.* 45 (12), 3487–3496. doi:10.1128/AAC.45.12.3487-3496.2001
- Want, M. Y., Islammuddin, M., Chouhan, G., Ozbak, H. A., Hemeg, H. A., Chattopadhyay, A. P., et al. (2017). Nanoliposomal artemisinin for the treatment of murine visceral leishmaniasis. *Int. J. Nanomedicine* 12, 2189–2204. doi:10.2147/IJN.S106548
- Want, M. Y., Islammuddin, M., Chouhan, G., Dasgupta, A. K., Chattopadhyay, A. P., and Afrin, F. (2014). A new approach for the delivery of artemisinin: formulation, characterization, and *ex-vivo* antileishmanial studies. *J. Colloid Interf. Sci.* 432, 258–269. doi:10.1016/j.jcis.2014.06.035
- Want, M. Y., Islammuddin, M., Chouhan, G., Ozbak, H. A., Hemeg, H. A., Dasgupta, A. K., et al. (2015). Therapeutic efficacy of artemisinin-loaded nanoparticles in experimental visceral leishmaniasis. *Colloids Surf. B Biointerfaces* 130, 215–221. doi:10.1016/j.colsurfb.2015.04.013
- WHO (2020). Neglected tropical diseases: treating more than one billion people for the fifth consecutive year. Geneva, Switzerland: World Health Organization. Available at: https://www.who.int/neglected_diseases/news/treating-more-than-one-billion-people-fifth-consecutive-year/en/#:~:text=25%20September%202020%20%7C%20Geneva%20%E2%80%93%20%93%20large%20scale%20preventive%20treatment%20campaigns.
- WHO-Expert-Committee (2002). “Control of chagas disease,” in *World Health Organization Technical Report Series*. Vol. 905, 1–109. Available at: <https://pubmed.ncbi.nlm.nih.gov/12092045/>.
- Wijnant, G.-J., Van Bocxlaer, K., Yardley, V., Harris, A., Alavijeh, M., Silva-Pedrosa, R., et al. (2018). Comparative efficacy, toxicity and biodistribution of the liposomal amphotericin B formulations Fungisome® and AmBisome® in murine cutaneous leishmaniasis. *Int. J. Parasitol. Drugs Drug Resist.* 8 (2), 223–228. doi:10.1016/j.ijpddr.2018.04.001
- Wyllie, S., Brand, S., Thomas, M., De Rycker, M., Chung, C.-w., Pena, I., et al. (2019). Preclinical candidate for the treatment of visceral leishmaniasis that acts through proteasome inhibition. *Proc. Natl. Acad. Sci. U.S.A.* 116 (19), 9318–9323. doi:10.1073/pnas.1820175116
- Yanik, M., Gurel, M. S., Simsek, Z., and Kati, M. (2004). The psychological impact of cutaneous leishmaniasis. *Clin. Exp. Dermatol.* 29 (5), 464–467. doi:10.1111/j.1365-2230.2004.01605.x
- Yasur-Landau, D., Jaffe, C. L., David, L., and Baneth, G. (2016). Allopurinol resistance in *Leishmania infantum* from dogs with disease relapse. *PLoS Negl. Trop. Dis.* 10 (1), e0004341. doi:10.1371/journal.pntd.0004341
- Yeates, C. (2002). Sitamaquine (GlaxoSmithKline/Walter Reed army Institute). *Curr. Opin. Investig. Drugs* 3 (10), 1446–1452.
- Zhai, L., Blom, J., Chen, M., Christensen, S. B., and Kharazmi, A. (1995). The antileishmanial agent licochalcone A interferes with the function of parasite mitochondria. *Antimicrob. Agents Chemother.* 39 (12), 2742–2748. doi:10.1128/aac.39.12.2742
- Zhai, L., Chen, M., Blom, J., Theander, T. G., Christensen, S. B., and Kharazmi, A. (1999). The antileishmanial activity of novel oxygenated chalcones and their mechanism of action. *J. Antimicrob. Chemother.* 43 (6), 793–803. doi:10.1093/jac/43.6.793
- Zhou, Y., Messier, N., Ouellette, M., Rosen, B. P., and Mukhopadhyay, R. (2004). *Leishmania major* LmACR2 is a pentavalent antimony reductase that confers sensitivity to the drug pentostam. *J. Biol. Chem.* 279 (36), 37445–37451. doi:10.1074/jbc.M404383200

Conflict of Interest: The authors declare that the research was conducted in the absence of any commercial or financial relationships that could be construed as a potential conflict of interest.

Copyright © 2021 J, M and Chanda. This is an open-access article distributed under the terms of the Creative Commons Attribution License (CC BY). The use, distribution or reproduction in other forums is permitted, provided the original author(s) and the copyright owner(s) are credited and that the original publication in this journal is cited, in accordance with accepted academic practice. No use, distribution or reproduction is permitted which does not comply with these terms.



Structure Activity Relationship of *N*-Substituted Phenylhydrazolones Against *Trypanosoma cruzi* Amastigotes

Maarten Sijm¹, Louis Maes², Iwan J. P. de Esch¹, Guy Caljon², Geert Jan Sterk¹ and Rob Leurs^{1*}

¹Division of Medicinal Chemistry, Faculty of Sciences, The Amsterdam Institute of Molecular and Life Sciences (AIMMS), Vrije Universiteit Amsterdam, Amsterdam, Netherlands, ²Laboratory for Microbiology, Parasitology and Hygiene (LMPH), University of Antwerp, Antwerp, Belgium

OPEN ACCESS

Edited by:

Gildardo Rivera,
Instituto Politécnico Nacional (IPN),
Mexico

Reviewed by:

Gabriella Gabriella,
University of Florence, Italy
Guillermo R. Labadie,
National University of Rosario,
Argentina
Andrei I. Khlebnikov,
Tomsk Polytechnic University, Russia

*Correspondence:

Rob Leurs
r.leurs@vu.nl

Specialty section:

This article was submitted to
Medicinal and
Pharmaceutical Chemistry,
a section of the journal
Frontiers in Chemistry

Received: 20 September 2020

Accepted: 16 April 2021

Published: 30 April 2021

Citation:

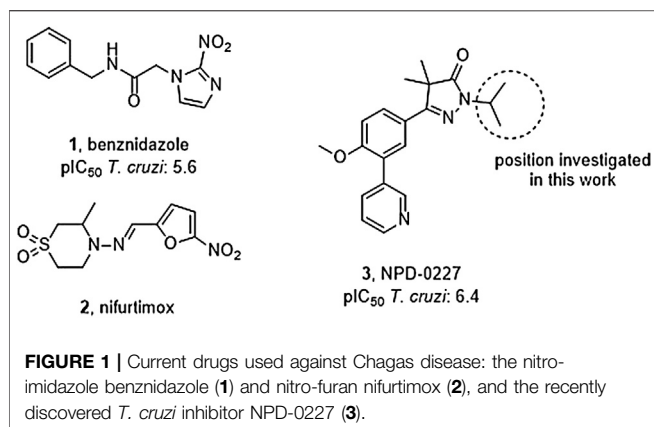
Sijm M, Maes L, de Esch IJP, Caljon G,
Sterk GJ and Leurs R (2021) Structure
Activity Relationship of *N*-Substituted
Phenylhydrazolones Against
Trypanosoma cruzi Amastigotes.
Front. Chem. 9:608438.
doi: 10.3389/fchem.2021.608438

Current drugs for Chagas disease have long treatment regimens with occurrence of adverse drug effects leading to poor treatment compliance. Novel and efficacious medications are therefore highly needed. We previously reported on the discovery of NPD-0227 (2-isopropyl-5-(4-methoxy-3-(pyridin-3-yl)phenyl)-4,4-dimethyl-2,4-dihydro-3H-pyrazol-3-one) as a potent *in vitro* inhibitor of *Trypanosoma cruzi* (pIC₅₀ = 6.4) with 100-fold selectivity over human MRC-5 cells. The present work describes a SAR study on the exploration of substituents on the phenylpyrazolone nitrogen. Modifications were either done directly onto this pyrazolone nitrogen or alternatively by introducing a piperidine linker. Attention was pointed toward the selection of substituents with a cLogP preferably below NPD-0227's cLogP of 3.5. Generally the more apolar compounds showed better activities than molecules with cLogPs <2.0. Several new compounds were identified with potencies that are in the same range as NPD-0227 (pIC₅₀ = 6.4) and promising selectivities. While the potency could not be improved, valuable SAR was obtained. Furthermore the introduction of a piperidine linker offers new opportunities for derivatization as valuable novel starting points for future *T. cruzi* drug discovery.

Keywords: structure activity relationship, chagas disease, phenotypic optimization, trypanosoma cruzi, phenylpyrazolones

INTRODUCTION

The protozoan parasite *Trypanosoma cruzi* is the causative agent of Chagas disease. It is estimated that over six million people are infected worldwide, the majority in Latin-America where the parasite is endemic. (Lidani et al., 2019; WHO, 2021). *T. cruzi* is spread by several insect vectors, most of which belong to the triatomine family (Kollien and Schaub, 2000; Martinez et al., 2019). Other ways of transmission are *via* blood transfusions, laboratory accidents or parental transmission from mother to infant (Schmunis, 1999; Torrico et al., 2004; Rassi et al., 2010). The life cycle of *T. cruzi* consists of several developmental stages in the mammalian host and insect vector (Rassi et al., 2010). While the vector appears unaffected by the parasite, infected humans can develop life-threatening symptoms and pathologies. The acute stage of the disease starts shortly after the parasite enters the body but a strong immune response will cause a large reduction of the initial peak of parasitemia, however, without full elimination of the parasite leading to persistent infection of certain tissues



(Dias, 1984). The acute symptoms are non-specific, such as fever, mild splenomegaly and edema, making diagnosis difficult (Prata, 2001). After 2 months, the disease enters the chronic phase in which the parasite becomes dormant and no symptoms are observed. This dormant phase can last for over 10 years up to lifelong (Prata, 2001). Estimates of further evolution of chronic infection toward clinical symptoms, such as cardiopathy or megaesophagus and megacolon, ranges between 10–60% of infected people and varies widely in different regions (Coura and Viñas, 2010; Coura and Borges-Pereira, 2011). Patients can become life-long asymptomatic carriers thus representing a parasite reservoir.

Vector control, early diagnosis and effective chemotherapy are essential to combat Chagas disease. Two drugs are currently marketed: the nitro-imidazole benznidazole (**1**, **Figure 1**) and the nitro-furan nifurtimox (**2**) (Rassi et al., 2010). Both drugs contain a nitro-aromatic functionality which is commonly associated with toxic side effects. Furthermore, the treatment regimens of both vary between 60–90 days and are known to cause various side effects which cause patients to discontinue

their treatment (Castro et al., 2006; Pinazo et al., 2013). Benznidazole (**1**) is currently used as first-line treatment as it has a better overall safety profile (Alpern et al., 2017). While the efficacy of both drugs is well established in the acute phase, much debate is ongoing on about their efficacy in the chronic phase (Sgambatti de Andrade et al., 1996; Zhang and Tarleton, 1999; Bern, 2011). The recent BENEFIT trial investigated the efficacy of Benznidazole (**1**) on chronic Chagas' heart disease. While reduced parasitemia was observed by PCR, this did not result in significant reduction of clinical deterioration of cardiac function after 5 years (Morillo et al., 2015). Afterward several concerns were raised in literature with regard to the PCR analysis and benznidazole dosage, precluding firm conclusions on the efficacy potential in the chronic phase of infection (Hamers et al., 2016).

The overall need for new and improved chemotherapies for Chagas disease is high, both for current and future patients. New medication is also needed as contingency measure for upcoming resistance against the available current drugs (Coura and Viñas, 2010; Mejia et al., 2012). Unfortunately, the pipeline toward new drugs is largely empty. Most research on *T. cruzi* is performed in academia though the last few years several public-private collaborations have been initiated. In this paper, we describe part of the research of the EU-funded, public-private consortium PDE4NPD, that focuses on 3'/5'-cyclic nucleotide phosphodiesterases (PDEs) as targets against several neglected tropical diseases. The present work further elaborates the SAR of the previously reported *T. cruzi* inhibitor NPD-0227 (**3**, **Figure 1**) and investigates the role of different substituents on the pyrazolone nitrogen (Sijm et al., 2019). Besides the SAR aiming at improving potency, compounds were also specifically designed to improve physicochemical properties, such as cLogP and solubility. As *T. cruzi* ultimately proceeds *via* a dormant intracellular form, a possible drug needs to pass several cell membranes before reaching the parasite. During this process the drug is transferred

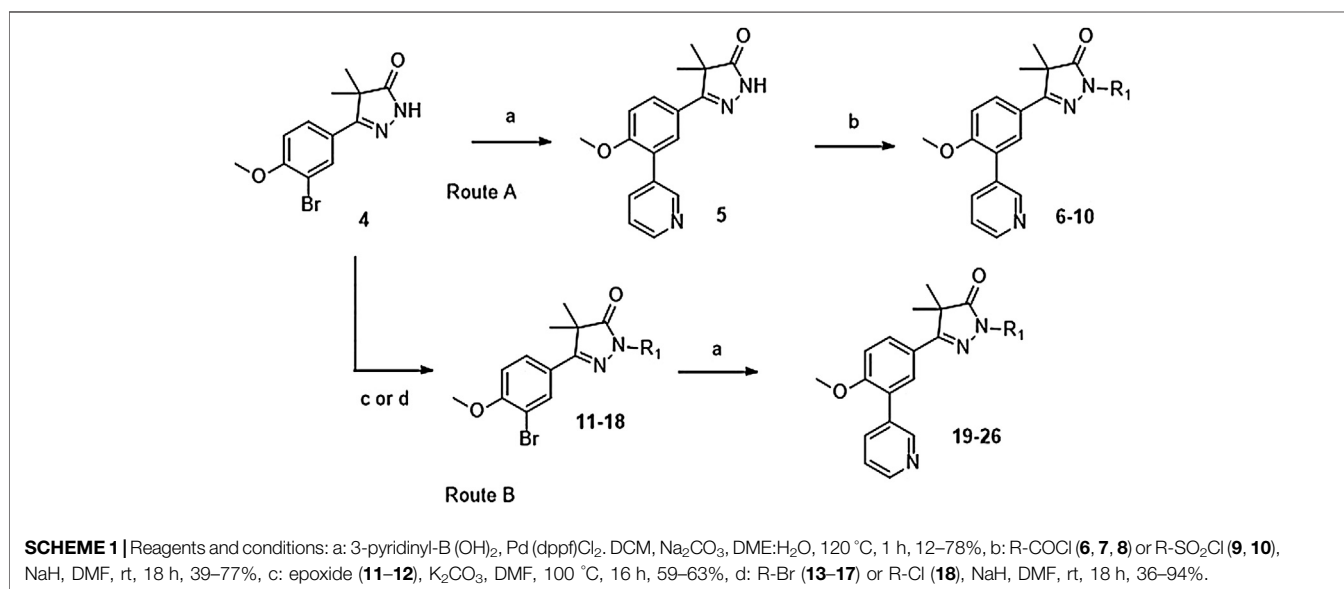
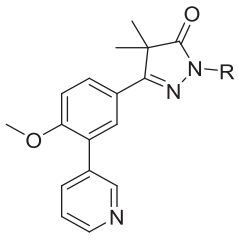
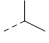
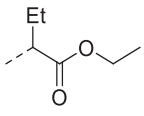
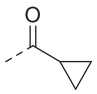
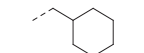
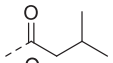
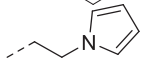
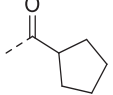
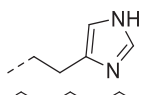
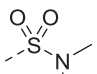
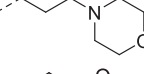
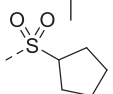
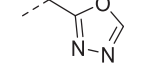
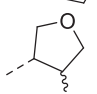
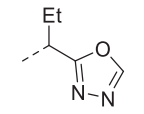
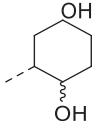
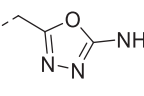
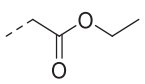
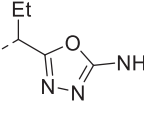


TABLE 1 | *In vitro* activity against intracellular amastigotes of *T. cruzi* (Tulahuen strain)^a and MRC-5 cells^a of phenylhydhydropyrazolones with modifications directly on the pyrazolone nitrogen.


Cpd	R	<i>T. cruzi</i> (pIC ₅₀)	MRC-5 (pIC ₅₀)	SI ^b	cLogP	Cpd	R	<i>T. cruzi</i> (pIC ₅₀)	MRC-5 (pIC ₅₀)	SI ^b	cLogP
3		6.4	4.4	100	3.5	22		5.2	<4.2	>10	3.4
6		4.4	<4.2	>2	3.2	23		5.6	4.9	5	4.8
7		4.5	<4.2	>2	3.9	24		5.5	4.5	10	3.8
8		4.4	<4.2	>2	4.1	25		4.5	<4.2	>2	2.3
9		4.4	<4.2	>2	1.9	26		<4.2	<4.2	N.D.	2.5
10		5.0	4.4	4	3.6	33		5.1	<4.2	>8	1.5
19		4.4	<4.2	>2	1.9	34		5.2	<4.2	>10	2.5
20		5.1	<4.2	>8	3.4	35		4.2	4.2	0	1.3
21		5.2	<4.2	10	2.6	36		4.4	<4.2	2	2.4

^aAll reported values are measured as duplicates and had a standard deviation less than ± 0.2 .^bSelectivity index was calculated as IC₅₀ MRC-5 cells divided by IC₅₀ *T. cruzi*.

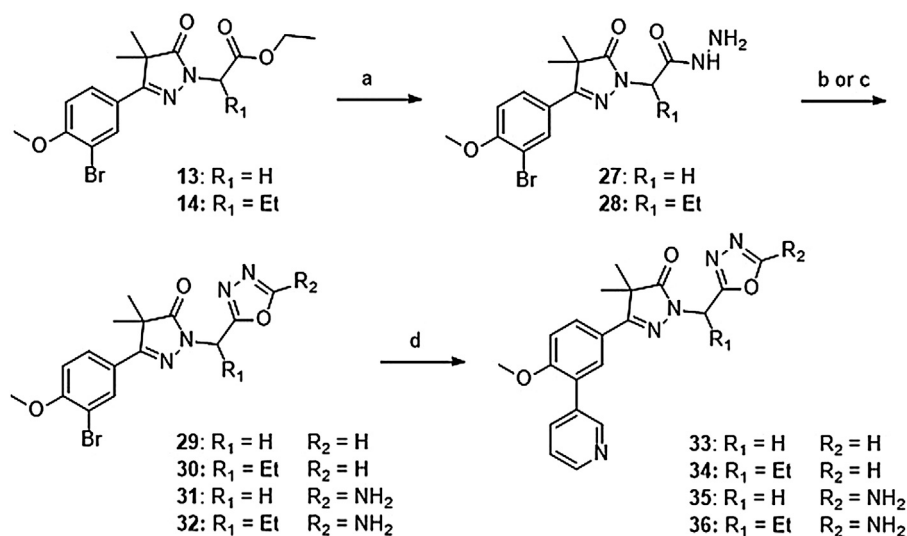
multiple times between hydrophobic and hydrophilic phases, as such an optimal cLogP is thought to be between 0 and 2 and the drug having no charges (Basore et al., 2015; Bennion et al., 2017).

Chemistry

Phenylpyrazolone analogues with a substituent directly on the pyrazolone nitrogen atom were synthesized using two different routes. The first route started with a Suzuki reaction to obtain dihydropyrazolone **5** (Route A, **Scheme 1**) which was then functionalized using sodium hydride and various acyl chlorides and sulfonyl chlorides to obtain compounds **6–10** (**Table 1**). The second route (Route B) started with alkylation

of the dihydropyrazolone **4**, either using potassium carbonate to yield intermediates **11–12**, or using sodium hydride to generate intermediates **13–18**. These intermediates were then converted to the 3-pyridinyl derivatives *via* a Suzuki cross coupling, yielding final compounds **20–26** (**Scheme 1**, **Table 1**).

Introduction of methylene-oxadiazoles on the pyrazolone head group started with the previously synthesized ester analogues **13** and **14** (**Scheme 2**). Subsequent hydrazination yielded the corresponding hydrazides (**27** and **28**) which were ring-closed with either triethylorthoformate or cyanuric bromide to deliver the unsubstituted oxadiazoles (**29** and **31**) and the amine substituted oxadiazoles (**30** and **32**) respectively. These oxadiazoles were then converted to the



SCHEME 2 | Reagents and conditions: a: N_2H_4 , EtOH, rt, 18 h, 90–94%; b: $(EtO)_3CH$, reflux, 18 h, 34–78% (**29–30**), c: $BrCN$, $NaHCO_3$, MeOH, H_2O , o. n., 22–46% (**31–32**), d: 3-pyridinyl-B (OH) $_2$, Pd (dppf) Cl_2 , DCM, Na_2CO_3 , DME: H_2O , 120 °C, 1 h 36–74%.

corresponding 3-pyridinyl analogues *via* a Suzuki cross-coupling to yield compounds **33–36**.

The synthesis of the piperidine substituted dihydropyrazolones started with keto-ester **37** (Scheme 3) which was prepared according to previously reported methodology (Sijm et al., 2019). This keto-ester was condensed with 4-hydrazinylpiperidine to yield piperidine substituted dihydropyrazolone **38**. The piperidine nitrogen atom was protected using boc-anhydride to give intermediate (**39**) which could be used in a Suzuki cross-coupling to install the 3-pyridine moiety. Subsequent deprotection of **40** with 4 M HCl in dioxane yielded the free amine building block (**41**) which was used to install the desired electrophiles (**42–83**, Tables 2,3) *via* various methodologies.

Pharmacology and Parasitology

All compounds were tested for their trypanocidal activity against intracellular forms of *T. cruzi* (Tulahuen CL2, β -galactosidase strain (drug sensitive strain (discrete typing units, DTU VI)) as well as for cytotoxicity on MRC-5_{SV2} cells (human lung fibroblasts). (Blaazer et al., 2014).

RESULTS AND DISCUSSION

In the previous work by Sijm et al., the pyrazolone nitrogen was substituted with various (cyclo)-alkyl moieties resulting in the identification of NPD-0227 (**3**) as a potent ($pIC_{50} = 6.4$) *T. cruzi* inhibitor with 100-fold selectivity over human MRC-5 cells (Table 1) (Sijm et al., 2019; Sijm et al., 2020). To further explore SAR and to investigate molecules with varying cLogPs, more polar and diverse substituents was explored.

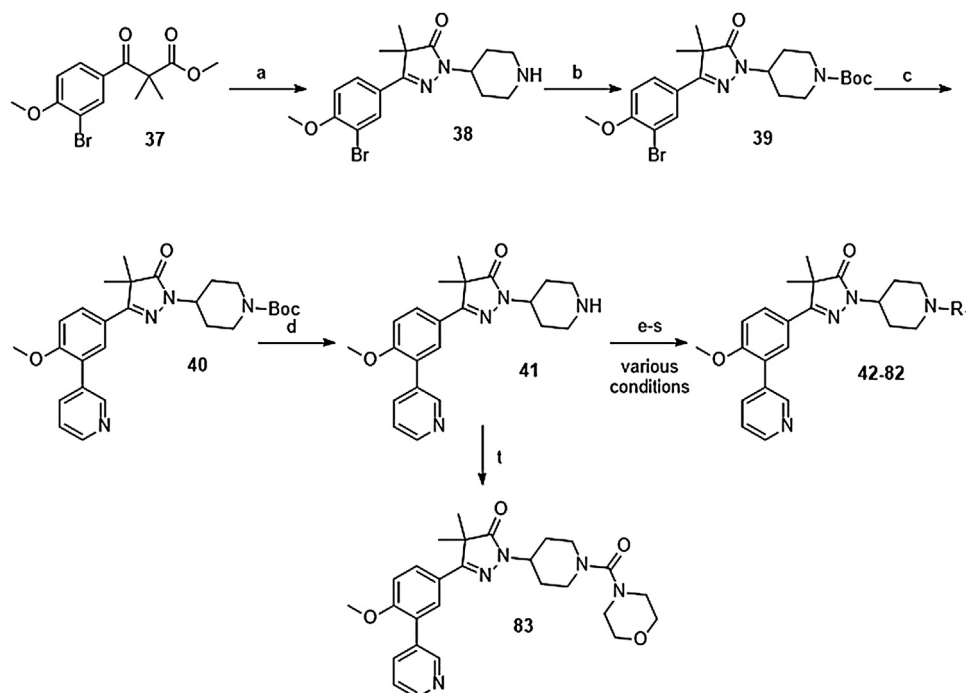
Introduction of a carbonyl-alkyl moieties directly onto the pyrazolone nitrogen (**6–8**, Table 1) resulted in weak inhibitors

with pIC_{50} 's around 4.5. Similarly, introduction of sulphonyl-alkyl moieties such as dimethylsulfonamide (**9**) or sulphonylcyclopentyl (**10**) did not lead to inhibitors with pIC_{50} values above 5.0. Epoxides were used to introduce β -alcohols on the pyrazolone ring resulting in compounds **19** and **20**. These alcohols also showed a large decrease in activity compared to NPD-0227 ($pIC_{50} = 6.4$) with pIC_{50} 's of 4.4 and 5.1, respectively. Similarly, the introduction of ethyl-esters (**21**, **22**) resulted in decreased potencies compared to NPD-0227 with both compounds showing pIC_{50} values of only 5.2.

While the substituents with a polar moiety (**6–10**, **19–22**, Table 1) showed decreased activities, as expected, introduction of more apolar moieties such as methyl-cyclohexyl (**23**) and pyrazole (**24**) showed moderate activity with pIC_{50} values of 5.5. Introduction of more polar substituents attached to an aliphatic linker, such as imidazole **25** and morpholine **26** with cLogPs around 2.3 resulted in lower potencies ($pIC_{50} < 4.6$). While the introduction of various oxadiazoles (**33–36**) on this position yielded compounds with a more desirable cLogP's, this did not lead to very active compounds, with 1-propan-oxazole (**34**) showed the highest potency ($pIC_{50} = 5.2$). As activities were generally close to the lower detection limit of the assay, selectivity indexes were quite low or defined as “bigger than”.

The initial attempts to introduce polar functional groups such as carbonyls, sulphonyls and alcohols close to the pyrazolone ring had a negative effect on their potency. One of the most potent compounds so far was methylcyclohexyl **23**, a bulky and apolar substituent. It was thought that introduction of a piperidine would introduce a similar sized moiety which would improve options to introduce polarity as a new handle to further modify.

This piperidine linker was first investigated by forming amides with corresponding acid chlorides or carboxylic acids, which led to analogues **42–47** (Table 2). These groups introduced some polarity but these modifications did not lead to potent ligands



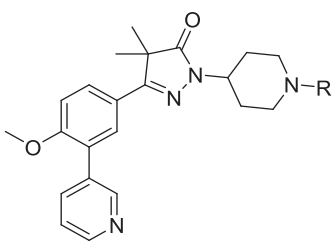
SCHEME 3 | Reagents and conditions: a: 4-hydrazinylpiperidine.2HCl, MeOH, H₂O, reflux, 3 days, 80%; b: Boc₂O, TEA, DCM, rt, 4 h, 89%; c: 3-pyridinyl-B(OH)₂, Pd(dppf)Cl₂, DCM, Na₂CO₃, DME:H₂O, 120 °C, 1 h, 86%; d: 4 M HCl in dioxane, rt, 18 h, 84%; e: R-COCl (**42**, **43**), R-SO₂Cl (**48**), NaH, DMF, rt, 2 h, 38–42%; f: EDCI, HOBT, RCOOH (**44**, **46**), DIPEA, DCM, 18–30 h, 23–31%; g: oxazole-5-carboxylic acid (**45**), T3P, DIPEA, EtOAc, 50 °C, 70 h, 7%; h: R-COCl (**47**) or R-SO₂Cl (**49–54**) or OCN-R (**55**, **57–59**, **61**) or Cl(CO)NR₁R₂ (**56**, **60**), TEA, DCM, rt, 2–42 h, 13–79%; i: epoxide (**62–66**), DMAP, i-PrOH, 50–100 °C, 2–120 h, 4–30%; j: formic acid (**67**), formaldehyde, 18 h, rt, 15%; k: R-CO-R (**68–69**, **71**, **74**), NaBH(OAc)₃, AcOH, DCE, 70 °C, 18–72 h, 10–53%; l: R-Br (**70**), K₂CO₃, DMF, rt, 48 h, 10%; m: methylacrylate (**72**), DBN, ACN, 90 h, rt, 45%; n: ClCH₂CO-R (**73**), K₂CO₃, ACN, 24 h, rt, 39%; o: HCO-R (**74–78**), NaBH(OAc)₃, AcOH, DCE, 22–72 h, 5–48%; q: Ar-Br (**79–80**), Pd₂(dba)₃, BINAP, NaOtBu, 80 °C, 7 days, 11–19%; r: Cl-Ar (**81**), Cs₂CO₃, DMF, 90 °C, 4 h, 24%; s: F-Ar (**82**), DMSO, K₂CO₃, 110 °C, 6 days, 16%; t: i: (**83**) NaHCO₃, 4-NO₂Ph-chloroformate, dioxane, rt, 22 h, ii: K₂CO₃, morpholine, DMF, rt, 4 days.

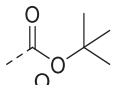
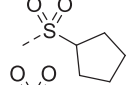
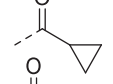
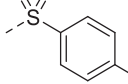
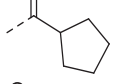
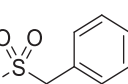
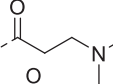
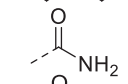
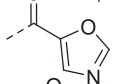
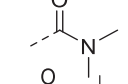
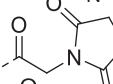
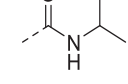
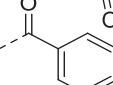
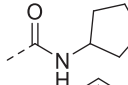
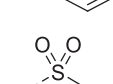
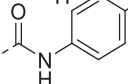
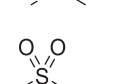
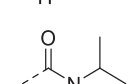

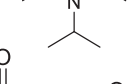
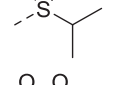
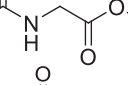
(pIC₅₀ < 5.3). Introducing sulphonamides instead of regular amides gave similar results as the majority showed moderately low activity (**48–54**). Alkyl-sulphonamides with a cyclopropyl (**49**), isopropyl (**50**), dimethylamino (**51**) and cyclopentyl (**52**) all showed pIC₅₀'s around 5.1, while the smaller methyl substituted sulphonamide (**48**) had a slightly lower activity (pIC₅₀ = 4.5). Introduction of an aromatic ring on to the sulphonamide did not have a positive effect. Tosylate **53** (cLogP = 4.4) was inactive with a pIC₅₀ below 4.2. Introduction of an extra carbon between the sulphonamide and the benzene ring was successful as methylbenzyl **54** (cLogP = 3.8) showed a similar potency as NPd-0227 (**3**, Table 1) with a pIC₅₀ value of 6.2 and >100-fold selectivity over human MRC-5.

The boc-protected analogue **40** (cLogP = 3.6; pIC₅₀ = 5.9, Table 2) which was obtained during the synthesis of the free-amine building block showed that relatively large substituents are allowed on the piperidine linker, which was confirmed by sulphonamide **54**. The preference for larger, bulky substituents is also apparent with the urea linked analogues (**55–59**). While the carbamide is inactive (**55**, cLogP = 1.6; pIC₅₀ = <4.2), introduction of larger apolar groups increased activity (**57–59**), with the most potent compound being the 4-fluorophenyl **59** (pIC₅₀ = 5.9; cLogP = 4.0, 25-fold selectivity). The even more bulky diisopropyl analogue (**60**),

however, was totally inactive (pIC₅₀ < 4.2). Introduction of more polar substituents attached to the urea linker did not improve activity with pIC₅₀ values of <4.2 for ethylacetate derivative **61** (cLogP = 1.8) and 4.9 for the morpholine analogue (**83**, cLogP = 1.8). Two types of epoxides were used to introduce β-alcohols. While the aliphatic analogues **62–64** (Table 3) showed low potencies (pIC₅₀ < 4.6), the aromatic derivatives (**65–66**) showed micromolar activities with pIC₅₀ values of 5.6 and 5.7. Selectivity of the unsubstituted phenyl ring (**65**) was however a lot better than the 4-fluorophenyl (**66**).

As shown in Table 1 and in previous work, aliphatic substituents on the dihydropyrazolone nitrogen led to the most potent compounds (Sijm et al., 2019). Introduction of aliphatic substituents on the piperidine nitrogen resulted in poor potencies, possibly caused by the introduction of a tertiary amine which can be protonated, as charged compounds are less likely to cross the cell membrane. The unsubstituted piperidine (**41**, cLogP = 2.3, Table 3) is totally inactive (pIC₅₀ < 4.2) and the alkylated analogues (**67–73**) are not very active inhibitors (pIC₅₀ < 5.0). Analogues with an aromatic ring showed higher activities: the 2-furanylmethyl (**74**, cLogP = 3.5) and the 3-pyridinylmethyl (**77**, cLogP = 4.4) showed pIC₅₀ values of 5.0 and 5.3, respectively. The benzyl substituted

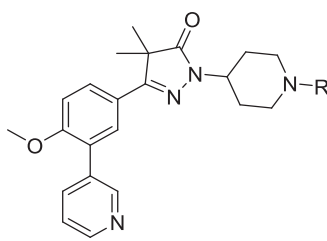
TABLE 2 | *In vitro* activity against intracellular amastigotes of *T. cruzi* (Tulahuen strain)^a and MRC-5 cells^a of phenylhydhydropyrazolones with a piperidine linker.


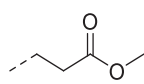
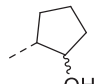
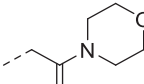
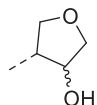
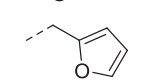
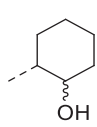
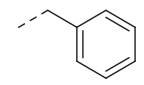
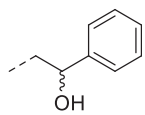
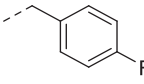
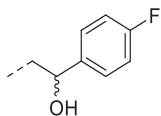
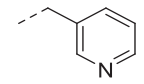
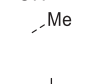
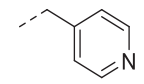
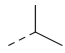
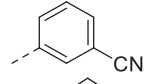

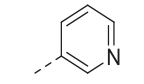
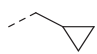
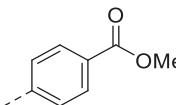
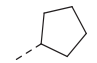
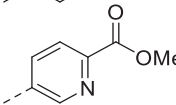
Cpd	R	<i>T. cruzi</i> (pIC ₅₀)	MRC-5 (pIC ₅₀)	SI ^b	cLogP	Cpd	R	<i>T. cruzi</i> (pIC ₅₀)	MRC-5 (pIC ₅₀)	SI ^b	cLogP
40		5.9	<4.2	>50	3.6	52		5.2	4.5	5	3.1
42		4.4	<4.2	>2	2.7	53		<4.2	<4.2	N.D.	4.4
43		5.2	4.5	5	3.6	54		6.2	<4.2	>100	3.8
44		4.5	<4.2	>2	2.1	55		<4.2	<4.2	N.D.	1.6
45		4.6	<4.2	>3	1.6	56		4.5	<4.2	>2	2.0
46		<4.2	<4.2	N.D.	0.9	57		4.9	<4.2	>5	2.6
47		<4.2	<4.2	N.D.	3.8	58		5.5	4.5	10	3.2
48		4.5	<4.2	>2	1.4	59		5.9	4.5	25	4.0
49		5.0	<4.2	>6	2.2	60		<4.2	<4.2	N.D.	3.6
50		5.1	<4.2	>8	2.5	61		<4.2	<4.2	N.D.	1.8
51		5.1	<4.2	>8	1.4	83		4.9	<4.2	>5	1.8

^aAll reported values are measured as duplicates and had a standard deviation less than ± 0.2 .^bSelectivity index was calculated as IC₅₀ MRC-5 cells divided by IC₅₀ *T. cruzi*.

piperidine **75** and the 4-pyridinemethyl **78** both showed pIC₅₀ values around 5.6, while 4-fluorobenzyl **76** (cLogP = 4.6) showed sub-micromolar potency with a pIC₅₀ of 6.1. Selectivity indexes of these compounds were moderate to poor, with the best compound, 4-pyridinemethyl **78** showing 16-fold selectivity toward *T. cruzi* over MRC-5 cells.

The final set of substituents on the piperidine linker were aromatic rings (Table 3, **79–82**). This sub-series showed moderate activities with the 3-cyanophenyl (**79**), 4-methylbenzoate (**81**) and methyl-5-picolinate (**82**) all having low micromolar activities (pIC₅₀ = 5.7). The 3-pyridinyl analogue (**80**) was less active with a pIC₅₀ of 5.2. Best

TABLE 3 | *In vitro* activity against intracellular amastigotes of *T. cruzi* (Tulahuen strain)^a and MRC-5 cells^a toxicity by phenyldihydropyrazolones with a piperidine linker.


Cpd	R	<i>T. cruzi</i> (pIC ₅₀)	MRC-5 (pIC ₅₀)	SI ^b	cLogP	Cpd	R	<i>T. cruzi</i> (pIC ₅₀)	MRC-5 (pIC ₅₀)	SI ^b	cLogP
41	H	<4.2	<4.2	N.D	2.3	72		<4.2	<4.2	N.D.	2.6
62		4.5	4.5	1	3.0	73		4.4	<4.2	>2	1.6
63		<4.2	<4.2	N.D	1.9	74		5.0	4.6	3	3.5
64		4.5	4.6	<1	3.4	75		5.6	4.6	10	4.4
65		5.6	<4.2	>25	3.8	76		6.1	5.1	10	4.6
66		5.7	5.2	3	3.9	77		5.3	4.5	6	3.2
67		4.4	<4.2	>2	2.7	78		5.7	4.5	16	3.2
68		4.5	<4.2	>2	3.5	79		5.7	<4.2	>32	4.4
69		4.9	4.5	3	3.6	80		5.2	4.5	5	3.4
70		4.8	4.5	2	3.5	81		5.7	5.0	5	4.6
71		4.6	4.5	1	4.1	82		5.7	<4.2	>32	4.0

^aAll reported values are measured as duplicates and had a standard deviation less than ± 0.2 .^bSelectivity index was calculated as IC₅₀ MRC-5 cells divided by IC₅₀ *T. cruzi*.

selectivity index was observed for 3-cyanophenyl **79** and methyl-5-picolinate **82**, which both had over 32-fold selectivity.

Overall, the introduction of polar moieties on the phenyldihydropyrazolones generally led to low activities against *T. cruzi*.

Especially the introduction of a polar moiety directly next to the pyrazolone nitrogen such as all carbonyl, sulphonyl and β -alcohol linked moieties (**6–10**, **19**, **20**) resulted in analogues with low potencies. Introduction of aliphatic substituents or aromatic

moieties resulted in interesting new anti-*T. cruzi* inhibitors with the best compounds **54** and **76** reaching sub micromolar potency. Installing a piperidine linker allowed for the introduction of a variety of substituents and it became apparent that aromatic moieties, either directly, with a methylene bridge or with a 2-atom linker performed best, showing pIC₅₀'s around 6.0.

CONCLUSION

Our study results in valuable SAR data that has been obtained by introducing a variety of substituents on the dihydropyrazolone nitrogen atom. While decorating this position is synthetically very efficient and a wide variety of chemical functionalities are allowed, our studies did not lead to compounds that have a better activity than NPD-0227. Especially the piperidine linker opens a whole new range of options to introduce substituents and analogues reached low micromolar inhibitory activities against *T. cruzi*. The most active compounds were obtained if the piperidine is substituted with apolar moieties such as aryl or benzyl rings. Introduction of more polar substituents, such as imidazole **25** (cLogP = 2.3), succinimide **46** (cLogP = 0.9) and morpholine **73** (cLogP = 1.6) generally lead to compounds with high micromolar activities. The structural moiety performing best is a 2-atom linker followed by an aromatic moiety, of which sulphonamide **54** (cLogP = 3.8), urea **59** (cLogP = 4.0) and β -alcohols **65** and **66** (cLogP = 3.8/3.9) performed best. These molecules all have activities around 6.0 (pIC₅₀) and especially sulphonamide **54** is promising with a pIC₅₀ of 6.2 and >100-fold selectivity over MRC-5 cells. Also other aromatic substituents performed well, such as 4-fluorobenzyl (**76**), 3-cyanophenyl (**79**) and 5-methylnicotinate (**82**) show promising activities around 6.0, with **79** and **82** showing best selectivities (>32-fold) toward *T. cruzi*. While these results of this study are important in the design of novel 'drug leads' for Chagas disease, the original goal, of identifying high potency molecules with a lower cLogP did not succeed. Most potent compounds with a cLogP below 2.0 were oxadiazole **33** and sulfamide **51**, which both showed a pIC₅₀ of 5.1.

Experimental Section Biology

Trypanosoma cruzi in vitro assay. Bloodstream trypomastigotes of the Y strain of *T. cruzi* were obtained by cardiac puncture of infected Swiss Webster mice on the parasitaemia peak (Meirelles et al., 1986; Batista et al., 2010). For the standard *in vitro* susceptibility assay on intracellular amastigotes, *T. cruzi* Tulahuen CL2, β -galactosidase strain (nifurtimox-sensitive) was used. The strain is maintained on MRC-5_{SV2} (human lung fibroblast) cells in MEM medium, supplemented with 200 mM L-glutamine, 16.5 mM NaHCO₃ and 5% inactivated fetal calf serum (FCSi). All cultures and assays were conducted at 37°C under an atmosphere of 5% CO₂. Benznidazole was included in the assays as a positive control.

MRC-5 cytotoxicity in vitro assay. MRC-5_{SV2} cells, originally from a human diploid lung cell line, were cultivated in MEM supplemented with L-glutamine (20 mM), 16.5 mM sodium hydrogen carbonate and 5% FCSi. For the assay, 10⁴ cells/well

were seeded onto the test plates containing the pre-diluted sample and incubated at 37°C and 5% CO₂ for 72 h. Cell viability was assessed fluorometrically 4 h after addition of resazurin (excitation 550 nm, emission 590 nm). The results are expressed as percentage reduction in cell viability compared to untreated controls. Tamoxifen was included in the assays as a positive control.

The use of laboratory rodents was carried out in strict accordance to all mandatory guidelines (EU directives, including the Revised Directive 2010/63/EU on the Protection of Animals used for Scientific Purposes that came into force on January 1, 2013, and the Declaration of Helsinki in its latest version).

Experimental Section Chemistry

Chemicals and reagents were obtained from commercial suppliers and were used without further purification. Anhydrous DMF, THF, and DCM were obtained by passing them through an activated alumina column prior to use. Microwave reactions were executed using a Biotage® Initiator microwave system. ¹H NMR spectra were recorded on a Bruker Avance 250 (250 MHz), Bruker Avance 400 (400 MHz), Bruker Avance 500 (500 MHz) or Bruker 600 Avance (600 MHz) spectrometer. Data are reported as follows: chemical shift, integration, multiplicity (s = singlet, d = doublet, dd = double doublet, t = triplet, dt = double triplet, q = quartet, p = pentet, h = heptet, bs = broad singlet, m = multiplet), and coupling constants (Hz). Chemical shifts are reported in ppm with the natural abundance of deuterium in the solvent as the internal reference [CDCl₃: δ 7.26, (CD₃)₂SO: δ 2.50]. ¹³C NMR spectra were recorded on a Bruker Avance 500 (126 MHz) or Bruker Avance 600 (150 MHz). Chemical shifts are reported in ppm with the solvent resonance resulting from incomplete deuteration as the internal reference [CDCl₃: δ 77.16 or (CD₃)₂SO: δ 39.52]. Systematic names for molecules according to IUPAC rules were generated using the Chemdraw AutoName program. LC-MS data was gathered using a Shimadzu HPLC/MS workstation with a LC-20AD pump system, SPD-M20A diode array detection, and a LCMS-2010 EV mass spectrometer. The column used is an Xbridge C18 5 μ m column (100 mm \times 4.6 mm). Solvents used were the following: solvent B = ACN, 0.1% formic Acid; solvent A = water, 0.1% formic acid. The analysis was conducted using a flow rate of 1.0 ml/min, start 5% B, linear gradient to 90% B in 4.5 min, then 1.5 min at 90% B, linear gradient to 5% B in 0.5 min and then 1.5 min at 5% B, total run time of 8 min. All reported compounds have purities >95%, measured at 254 nm, unless otherwise mentioned. All HRMS spectra were recorded on a Bruker microTOF mass spectrometer using ESI in positive-ion mode. In case of bromine containing molecules, the lowest peak of ⁷⁹Br was reported. Column purifications were either carried out automatically using Biotage equipment or manually, using 60–200 mesh silica. TLC analyses were performed with Merck F254 alumina silica plates using UV visualization. All reactions were done under N₂ atmosphere, unless

specifically mentioned. The cLogPs were calculated using CDD vault, CDD vault uses the ionic logP algorithm.

Experimental Data

Compound **5**, **6**, **15**, **23**, **27**, **29**, **33**, **38–42** and **83** are described below, other compounds can be found in the supporting information.

3-(4-Methoxy-3-(pyridin-3-yl)phenyl)-4,4-dimethyl-1H-pyrazol-5(4H)-one (**5**)

Pyrazolone **4** (1.0 g, 3.4 mmol) and pyridin-3-ylboronic acid (0.62 g, 5.1 mmol) were charged to a microwave tube after which DME (12 ml) and 1 M Na₂CO₃ (6.7 ml, 6.7 mmol) were added. The mixture was degassed with N₂ for 5 m after which Pd (dppf)Cl₂ (0.28 g, 34 mmol) was added. The reaction was heated at 120°C for 1 h in the microwave. The reaction mixture was diluted with EtOAc (30 ml) and filtered over Celite. The residue was washed with saturated NaHCO₃ (2 ml × 30 ml) and brine (1 ml × 30 ml). The organic phase was dried over Na₂SO₄, filtered and concentrated *in vacuo*. The remaining crude was purified over SiO₂ using a gradient of 50% EtOAc in heptane toward 5% MeOH in EtOAc to yield 700 mg (2.4 mmol, 70%) of the title compound as a white solid. ¹H NMR (500 MHz, CDCl₃) δ 11.50 (s, 1H), 8.69 (s, 1H), 8.55 (d, *J* = 3.8 Hz, 1H), 7.91 (apparent dt, *J* = 7.9, 1.9 Hz, 1H), 7.84 (dd, *J* = 8.7, 2.3 Hz, 1H), 7.73 (d, *J* = 2.3 Hz, 1H), 7.46 (dd, *J* = 7.9, 4.8 Hz, 1H), 7.22 (d, *J* = 8.8 Hz, 1H), 3.83 (s, 3H), 1.37 (s, 6H). ¹³C NMR (126 MHz, CDCl₃) δ 181.1, 161.6, 157.7, 150.0, 148.6, 137.1, 133.7, 128.1, 128.0, 127.4, 124.4, 123.8, 112.4, 56.3, 46.9, 22.5. LC-MS (ESI) *m/z* found: 296 (M + H)⁺; retention time: 2.67 min. HRMS-ESI (M + H)⁺ calculated for C₁₇H₁₈N₃O₂: 296.1394, found: 296.1391.

1-(cyclopropanecarbonyl)-3-(4-Methoxy-3-(Pyridin-3-Yl)phenyl)-4,4-Dimethyl-1h-Pyrazol-5(4H)-One (**6**)

Pyrazolone **5** (50 mg, 0.17 mmol) was dissolved in DMF (2 ml) and sodium hydride (60% in mineral oil) (10 mg, 0.25 mmol) was added. After stirring for 30 min cyclopropanecarbonyl chloride (20 mg, 0.19 mmol) was added and the mixture was stirred at rt for 18 h after which the reaction was quenched with water (25 ml) and extracted with EtOAc (25 ml). The organic layer was washed with sat. aq. NaHCO₃ (2 ml × 20 ml), brine (20 ml) and dried over MgSO₄ after which volatiles were evaporated yielding 24 mg (0.07 mmol, 39%) of the title compound as a white solid. ¹H NMR (500 MHz, CDCl₃) δ 8.76 (d, *J* = 2.0 Hz, 1H), 8.60 (dd, *J* = 4.8, 1.7 Hz, 1H), 7.95–7.84 (m, 3H), 7.38 (dd, *J* = 7.8, 4.8 Hz, 1H), 7.09–7.03 (m, 1H), 3.89 (s, 3H), 3.05–2.97 (m, 1H), 1.61 (s, 6H), 1.32–1.25 (m, 2H), 1.11–1.02 (m, 2H). ¹³C NMR (126 MHz, CDCl₃) δ 178.0, 171.9, 162.3, 158.7, 150.0, 148.3, 137.1, 133.3, 129.5, 128.7, 127.8, 123.1, 122.9, 111.2, 55.8, 49.9, 23.2, 13.5, 11.3. LC-MS (ESI) *m/z* found: 364 (M + H)⁺; retention time: 3.43 min. HRMS-ESI (M + H)⁺ calculated for C₂₁H₂₂N₃O₃: 364.1656, found: 364.1653.

Ethyl 2-(3-(3-bromo-4-methoxyphenyl)-4,4-dimethyl-5-oxo-4,5-dihydro-1H-pyrazol-1-yl)acetate (**13**)

Pyrazolone **4** (5.0 g, 16.8 mmol) was dissolved in DMF (35 ml) and sodium hydride (60% in mineral oil) (0.49 g, 20.2 mmol) was added. After stirring for 30 min ethyl 2-bromoacetate (2.23 ml,

20.2 mmol) was added and the mixture was heated to 50°C for 3 h after which the reaction was quenched with water (250 ml). Solids were filtered off and dried *in vacuo*, yielding 5.6 g (14.6 mmol, 87%) of the title compound as a white solid. ¹H NMR (500 MHz, CDCl₃) δ 8.05 (d, *J* = 2.2 Hz, 1H), 7.70 (dd, *J* = 8.6, 2.2 Hz, 1H), 6.93 (d, *J* = 8.7 Hz, 1H), 4.55 (s, 2H), 4.23 (q, *J* = 7.1 Hz, 2H), 3.95 (s, 3H), 1.53 (s, 6H), 1.29 (t, *J* = 7.1 Hz, 3H). ¹³C NMR (126 MHz, CDCl₃) δ 179.1, 167.8, 160.9, 157.2, 131.4, 126.7, 124.6, 112.3, 111.5, 61.7, 56.4, 48.1, 45.8, 22.5, 14.1. LC-MS (ESI) *m/z* found: 383 (M + H)⁺; retention time: 4.75 min. HRMS-ESI (M + H)⁺ calculated for C₁₆H₂₀BrN₂O₄: 383.0601, found: 383.0588.

3-(3-Bromo-4-methoxyphenyl)-1-(cyclohexylmethyl)-4,4-dimethyl-1H-pyrazol-5(4H)-one (**15**)

Pyrazolone **4** (100 mg, 0.30 mmol) was dissolved in DMF (3 ml) and sodium hydride (60% in mineral oil) (15 mg, 0.38 mmol) was added. After stirring for 30 min (bromomethyl)cyclohexane (63 mg, 0.67 mmol) was added and the mixture was stirred at rt for 18 h after which the reaction was quenched with water (25 ml) and extracted with EtOAc (25 ml). The organic layer was washed with brine (2 ml × 20 ml) and dried over MgSO₄ after which volatiles were evaporated yielding 105 mg (0.27 mmol, 91%) of the title compound as a transparent oil. ¹H NMR (500 MHz, CDCl₃) δ 8.03 (d, *J* = 2.2 Hz, 1H), 7.66 (dd, *J* = 8.6, 2.2 Hz, 1H), 6.90 (d, *J* = 8.7 Hz, 1H), 3.92 (s, 3H), 3.56 (d, *J* = 7.2 Hz, 2H), 1.89–1.80 (m, 1H), 1.74–1.68 (m, 2H), 1.67–1.61 (m, 3H), 1.45 (s, 6H), 1.28–1.13 (m, 5H), 1.08–0.89 (m, 2H). ¹³C NMR (126 MHz, CDCl₃) δ 178.6, 160.1, 156.9, 131.2, 126.5, 125.0, 112.3, 111.5, 56.4, 50.3, 48.3, 36.9, 30.5, 26.4, 25.7, 22.8. LC-MS (ESI) *m/z* found: 393 (M + H)⁺; retention time: 6.05 min. HRMS-ESI (M + H)⁺ calculated for C₁₉H₂₆BrN₂O₂: 393.1172, found: 393.1156.

1-(cyclohexylmethyl)-3-(4-Methoxy-3-(Pyridin-3-Yl)phenyl)-4,4-Dimethyl-1h-Pyrazol-5(4H)-One (**23**)

Pyrazolone **15** (100 mg, 0.16 mmol) and pyridin-3-ylboronic acid (47 mg, 0.38 mmol) were charged to a microwave tube after which DME (3 ml) and 1 M Na₂CO₃ (0.8 ml, 0.8 mmol) were added. The mixture was degassed with N₂ for 5 m after which Pd (dppf) Cl₂ (21 mg, 25 μmol) was added. The reaction was heated at 120°C for 1 h in the microwave. The reaction mixture was diluted with EtOAc (30 ml) and filtered over Celite. The residue was washed with saturated NaHCO₃ (2 ml × 30 ml) and brine (1 ml × 30 ml). The organic phase was dried over Na₂SO₄, filtered and concentrated *in vacuo*. The remaining crude was purified over SiO₂ using a gradient of 50% EtOAc in heptane toward 100% EtOAc to yield 64 mg (0.16 mmol, 64%) of the title compound as a white solid. ¹H NMR (500 MHz, CDCl₃) δ 8.78 (d, *J* = 2.1 Hz, 1H), 8.59 (d, *J* = 4.8 Hz, 1H), 7.88 (apparent dt, *J* = 7.8, 1.9 Hz, 1H), 7.82 (d, *J* = 2.2 Hz, 1H), 7.77 (dd, *J* = 8.6, 2.2 Hz, 1H), 7.37 (dd, *J* = 7.9, 4.9 Hz, 1H), 7.03 (d, *J* = 8.6 Hz, 1H), 3.87 (s, 3H), 3.58 (d, *J* = 7.2 Hz, 2H), 2.05–1.79 (m, 2H), 1.76–1.60 (m, 5H), 1.50 (s, 6H), 1.29–1.10 (m, 3H), 1.06–0.95 (m, 2H). ¹³C NMR (126 MHz, CDCl₃) δ 178.7, 161.0, 157.8, 150.1, 148.2, 137.0, 133.6, 128.7, 127.6, 127.5, 124.2, 123.1, 111.1, 55.8, 50.3, 48.4, 36.9, 30.5, 26.4, 25.7, 22.9. LC-MS (ESI) *m/z* found: 392 (M + H)⁺; retention time:

4.54 min. HRMS-ESI ($M + H$)⁺ calculated for $C_{24}H_{30}N_3O_2$: 392.2333, found: 392.2319.

2-(3-(3-bromo-4-methoxyphenyl)-4,4-dimethyl-5-oxo-4,5-dihydro-1H-pyrazol-1-yl) acetohydrazide (27)

Ester **13** (1.5 g, 3.91 mmol) was refluxed in hydrazine monohydrate (1.89 ml, 39.1 mmol) and ethanol (25 ml) for 18 h. After that the mixture was allowed to cool down, the mixture was concentrated and 20 ml of water was added. The solids were filtered off and dried *in vacuo* yielding 1.36 g (3.7 mmol, 94%) of the title compound as a white solid. ¹H NMR (500 MHz, DMSO-*d*₆) δ 9.29 (s, 1H), 7.96 (s, 1H), 7.79 (d, *J* = 8.6 Hz, 1H), 7.17 (d, *J* = 8.6 Hz, 1H), 4.29 (d, *J* = 13.2 Hz, 4H), 3.90 (s, 3H), 1.39 (s, 6H). ¹³C NMR (126 MHz, DMSO-*d*₆) δ 178.9, 166.4, 160.0, 157.0, 130.5, 127.6, 124.6, 113.1, 111.8, 56.9, 47.7, 45.9, 22.4. LC-MS (ESI) *m/z* found: 369 ($M + H$)⁺; retention time: 3.59 min.

1-((1,3,4-Oxadiazol-2-yl)methyl)-3-(3-bromo-4-methoxyphenyl)-4,4-dimethyl-1H-pyrazol-5(4H)-one (29)

Hydrazide **27** (200 mg, 0.54 mmol) was stirred in triethylorthoformate (0.9 ml, 5.4 mmol) and PTSA (10.30 mg, 0.054 mmol) was added. The mixture was heated at 80°C for 18 h after which the volatiles were evaporated and the resulting crude was purified over SiO₂ using a gradient of 20% EtOAc in heptane toward 80% EtOAc in heptane. This yielded 70 mg (0.19 mmol, 34%) of the title compound as a white solid. ¹H NMR (500 MHz, CDCl₃) δ 8.42 (s, 1H), 7.99 (d, *J* = 2.2 Hz, 1H), 7.66 (dd, *J* = 8.7, 2.2 Hz, 1H), 6.90 (d, *J* = 8.7 Hz, 1H), 5.22 (s, 2H), 3.92 (s, 3H), 1.52 (s, 6H). ¹³C NMR (126 MHz, CDCl₃) δ 178.5, 161.9, 161.6, 157.4, 153.6, 131.4, 126.9, 124.2, 112.3, 111.6, 56.4, 48.1, 39.0, 22.6. LC-MS (ESI) *m/z* found: 397 ($M + H$)⁺; retention time: 4.27 min. HRMS-ESI ($M + H$)⁺ calculated for $C_{15}H_{16}BrN_4O_3$: 379.0400, found: 379.0391.

1-((1,3,4-Oxadiazol-2-yl)methyl)-3-(4-methoxy-3-(pyridin-3-yl)phenyl)-4,4-dimethyl-1H-pyrazol-5(4H)-one (33)

Pyrazolone **29** (50 mg, 0.13 mmol) and pyridin-3-ylboronic acid (24 mg, 0.38 mmol) were charged to a microwave tube after which DME (3 ml) and 1 M Na₂CO₃ (0.5 ml, 0.5 mmol) were added. The mixture was degassed with N₂ for 5 m after which Pd (dppf) Cl₂ (11 mg, 13 μmol) was added. The reaction was heated at 120°C for 1 h in the microwave. The reaction mixture was diluted with EtOAc (30 ml) and filtered over Celite. The residue was washed with saturated NaHCO₃ (2 ml × 30 ml) and brine (1 ml × 30 ml). The organic phase was dried over Na₂SO₄, filtered and concentrated *in vacuo*. The remaining crude was purified over SiO₂ using a gradient of 50% EtOAc in heptane toward 100% EtOAc to yield 36 mg (0.10 mmol, 72%) of the title compound as a white solid. ¹H NMR (500 MHz, CDCl₃) δ 8.79 (s, 1H), 8.61 (s, 1H), 8.41 (s, 1H), 7.95–7.83 (m, 1H), 7.83–7.73 (m, 2H), 7.41 (s, 1H), 7.03 (d, *J* = 8.4 Hz, 1H), 5.23 (s, 2H), 3.87 (s, 3H), 1.56 (s, 6H). ¹³C NMR (126 MHz, CDCl₃) δ 178.6, 162.4, 162.0, 158.2, 153.6, 149.5, 147.6, 137.5, 133.9, 128.9, 128.0, 127.4, 123.4, 111.2,

55.9, 48.2, 39.0, 22.8. LC-MS (ESI) *m/z* found: 378 ($M + H$)⁺; retention time: 2.93 min. HRMS-ESI ($M + H$)⁺ calculated for $C_{20}H_{20}N_5O_3$: 378.1562, found: 378.1562.

3-(3-Bromo-4-methoxyphenyl)-4,4-dimethyl-1-(piperidin-4-yl)-1H-pyrazol-5(4H)-one (38)

Keto-ester **37** (32 g, 102 mmol) was dissolved in methanol (200 ml) and stirred. To this solution 4-hydrazinylpiperidine dihydrochloride (76 g, 406 mmol) dissolved in Water (80 ml) was added. The mixture was refluxed for 72 h after which 150 ml water was added and MeOH was removed *in vacuo*. To the remaining solution 10 M NaOH was added slowly until the pH was ~13. Solids were collected and washed with water (20 ml) to yield 31 g (82 mmol, 80%) of the title compound. ¹H NMR (500 MHz, CDCl₃) δ 8.00 (d, *J* = 2.2 Hz, 1H), 7.78 (dd, *J* = 8.6, 2.2 Hz, 1H), 7.16 (d, *J* = 8.8 Hz, 1H), 4.06–3.94 (m, 1H), 3.90 (s, 3H), 3.04–2.93 (m, 2H), 2.53–2.51 (m, 2H), 1.84–1.75 (m, 2H), 1.66–1.56 (m, 2H), 1.35 (s, 6H). ¹³C NMR (126 MHz, CDCl₃) δ 177.5, 159.7, 156.9, 130.4, 127.4, 124.8, 113.1, 111.9, 56.9, 51.5, 48.4, 45.6, 31.7, 22.4. LC-MS (ESI) *m/z* found: 380 ($M + H$)⁺; retention time: 3.19 min. HRMS-ESI ($M + H$)⁺ calculated for $C_{17}H_{23}BrN_3O_2$: 380.0968, found: 380.0968.

Tert-butyl 4-(3-(3-bromo-4-methoxyphenyl)-4,4-dimethyl-5-oxo-4,5-dihydro-1H-pyrazol-1-yl) piperidine-1-carboxylate (39)

Piperidine **38** (25 g, 65.7 mmol) was added to a round-bottom flask after which DCM (500 ml) was added, followed by di-tert-butyl dicarbonate (15.6 ml, 67.1 mmol) and triethylamine (9.4 ml, 67.1 mmol). The reaction mixture was extracted with water (2 ml × 400 ml) and brine (400 ml) and the organic layer was dried over Na₂SO₄. Solids were filtered off and volatiles were evaporated yielding 28 g (58 mmol, 89%) of the title compound as a light-brown solid. ¹H NMR (500 MHz, CDCl₃) δ 8.05 (d, *J* = 2.1 Hz, 1H), 7.70 (dd, *J* = 8.7, 2.2 Hz, 1H), 6.94 (d, *J* = 8.6 Hz, 1H), 4.31–4.20 (m, 3H), 3.96 (s, 3H), 2.87 (t, *J* = 12.9 Hz, 2H), 2.03 (apparent qd, *J* = 12.5, 4.5 Hz, 2H), 1.83–1.78 (m, 2H), 1.51 (s, 9H), 1.48 (s, 6H). LC-MS (ESI) *m/z* found: 424 ($M + H$, -t-Bu)⁺; retention time: 5.34 min. HRMS-ESI ($M + H$)⁺ calculated for $C_{22}H_{31}N_3O_4$: 480.1492, found: 480.1477.

Tert-butyl 4-(3-(4-methoxy-3-(pyridin-3-yl)phenyl)-4,4-dimethyl-5-oxo-4,5-dihydro-1H-pyrazol-1-yl) piperidine-1-carboxylate (40)

Boc-protected piperidine **39** (25.2 g, 52.5 mmol) and pyridin-3-ylboronic acid (9.0 g, 73 mmol) were charged to a round-bottom flask after which DME (400 ml) and 1 M Na₂CO₃ (210 ml, 210 mmol) were added. The mixture was degassed with N₂ for 15 m after which Pd (dppf) Cl₂ (2.1 g, 2.6 mmol) was added. The reaction was heated at 80°C for 16 h. The reaction mixture was diluted with MTBE (500 ml) and filtered over Celite. The residue was washed with saturated NaHCO₃ (2 ml × 600 ml) and brine (1 ml × 600 ml). The organic phase was dried over Na₂SO₄, filtered and concentrated *in vacuo* to yield 21.5 g (44.9 mmol, 86%) of the title compound. ¹H NMR (500 MHz, CDCl₃) δ 8.75

(s, 1H), 8.56 (d, $J = 4.0$ Hz, 1H), 7.84 (d, $J = 7.9$ Hz, 1H), 7.78 (d, $J = 2.0$ Hz, 1H), 7.75 (dd, $J = 8.6, 2.1$ Hz, 1H), 7.35 (dd, $J = 7.7, 4.9$ Hz, 1H), 7.01 (d, $J = 8.7$ Hz, 1H), 4.33–4.08 (m, 3H), 3.85 (s, 3H), 2.82 (s, 2H), 1.99 (apparent q, $J = 11.2$ Hz, 2H), 1.76 (d, $J = 11.6$ Hz, 2H), 1.47 (s, 7H), 1.45 (s, 9H). ^{13}C NMR (126 MHz, CDCl_3) δ 178.0, 161.2, 157.8, 154.7, 150.1, 148.3, 136.8, 133.5, 128.7, 127.7, 127.5, 124.0, 123.1, 111.1, 79.7, 55.8, 50.8, 48.8, 30.0, 28.4, 22.7. LC-MS (ESI) m/z found: 479 ($\text{M} + \text{H}$) $^+$; retention time: 4.03 min. HRMS-ESI ($\text{M} + \text{H}$) $^+$ calculated for $\text{C}_{27}\text{H}_{35}\text{N}_4\text{O}_4$: 479.2653, found: 479.2651.

3-(4-Methoxy-3-(pyridin-3-yl)phenyl)-4,4-dimethyl-1-(piperidin-4-yl)-1H-pyrazol-5(4H)-one Hydrochloride (41)

Boc-protected piperidine **40** (25.1 g, 52.4 mmol) was dissolved in dioxane (100 ml) and hydrogen chloride in dioxane (4 N) (131 ml, 524 mmol) was added in portions. The reaction was stirred for 40 h after which volatiles were evaporated. Attempts were made to recrystallize the resulting dark-oil from MTBE, *i*Pr-OH, *i*PrOH: H_2O to no avail. The crude was redissolved in EtOAc (800 ml) and extracted with aq. sat. Na_2CO_3 (2 ml \times 500 ml) and brine (500 ml). The organic layer was dried over Na_2SO_4 and volatiles were evaporated. Attempts to recrystallize from *i*-PrOH or *i*PrOH: H_2O were again unsuccessful. Evaporation of *i*-PrOH: H_2O ultimately yielded 16.7 g (44.1 mmol, 84%) of the title compound as a light brown powder. ^1H NMR (500 MHz, CDCl_3) δ 8.70–8.67 (m, 1H), 8.56 (dd, $J = 4.9, 1.6$ Hz, 1H), 7.91 (apparent dt, $J = 8.0, 1.9$ Hz, 1H), 7.85 (dd, $J = 8.7, 1.9$ Hz, 1H), 7.76 (d, $J = 1.8$ Hz, 1H), 7.47 (dd, $J = 7.7, 4.9$ Hz, 1H), 7.23 (d, $J = 8.8$ Hz, 1H), 4.08–3.96 (m, 1H), 3.84 (s, 3H), 3.00 (d, $J = 12.3$ Hz, 2H), 2.58–2.51 (m, 2H), 1.81 (apparent qd, $J = 12.3, 4.1$ Hz, 2H), 1.68–1.58 (m, 2H), 1.39 (s, 6H). ^{13}C NMR (126 MHz, CDCl_3) δ 177.2, 160.3, 157.5, 149.7, 149.6, 148.3, 148.2, 136.7, 133.2, 127.8, 127.2, 123.5, 123.4, 112.0, 55.9, 51.0, 48.0, 45.2, 31.2, 22.2. LC-MS (ESI) m/z found: 379 ($\text{M} + \text{H}$) $^+$; retention time: 2.40 min. HRMS-ESI ($\text{M} + \text{H}$) $^+$ calculated for $\text{C}_{22}\text{H}_{27}\text{N}_4\text{O}_2$: 379.2129, found: 379.2121.

1-(1-(cyclopropanecarbonyl)piperidin-4-yl)-3-(4-methoxy-3-(pyridin-3-yl)phenyl)-4,4-dimethyl-1H-pyrazol-5(4H)-one (42)

Amine **41** (100 mg, 0.26 mmol) was stirred with sodium hydride (60% in mineral oil) (16 mg, 0.40 mmol) in DMF (1 ml). After 30 min cyclopropanecarbonyl chloride (0.026 ml, 0.29 mmol) was added. The reaction was stirred for 2 h after which the reaction was quenched with water (20 ml) and extracted with EtOAc (20 ml). The organic layer was washed with sat. aq. NaHCO_3 solution (2 ml \times 20 ml), brine (20 ml) and dried over MgSO_4 . Volatiles were evaporated and the remaining crude was purified over SiO_2 using a gradient of 50% EtOAc in heptane toward 5% MeOH in EtOAc, yielding 45 mg (0.10 mmol, 38%) of the title compound as a white solid. ^1H NMR (500 MHz, CDCl_3) δ 8.78 (s, 1H), 8.60 (d, $J = 4.0$ Hz, 1H), 7.89 (d, $J = 7.9$ Hz, 1H), 7.80 (d, $J = 2.2$ Hz, 1H), 7.77 (dd, $J = 8.6, 2.2$ Hz, 1H), 7.41 (dd, $J = 7.7, 4.9$ Hz, 1H), 7.03 (d, $J = 8.7$ Hz, 1H), 4.75 (d, $J = 12.9$ Hz, 1H), 4.41–4.29 (m, 2H), 3.88 (s, 3H), 3.24 (t, $J = 12.7$ Hz, 1H), 2.72 (apparent t, $J = 12.4$ Hz, 1H), 2.14–1.74 (m, 7H), 1.50 (s, 6H), 1.05–0.95 (m, 2H), 0.77 (dd, $J = 7.9, 3.5$ Hz, 2H). ^{13}C NMR (126 MHz, CDCl_3) δ 178.0, 171.9, 161.3, 157.8, 149.8, 148.0, 137.2, 133.7, 128.7, 127.6, 127.5, 124.0, 123.3, 111.2, 55.8, 50.7, 48.8, 44.7, 41.4,

30.8, 29.7, 22.8, 11.1, 7.5, 7.4. LC-MS (ESI) m/z found: 447 ($\text{M} + \text{H}$) $^+$; retention time: 3.20 min. HRMS-ESI ($\text{M} + \text{H}$) $^+$ calculated for $\text{C}_{26}\text{H}_{31}\text{N}_4\text{O}_3$: 447.2391, found: 447.2390.

3-(4-Methoxy-3-(pyridin-3-yl)phenyl)-4,4-dimethyl-1-(1-(morpholine-4-carbonyl)piperidin-4-yl)-1H-pyrazol-5(4H)-one (83)

Amine **41** (400 mg, 1.1 mmol) was dissolved in dioxane (15 ml) and 25 ml of saturated NaHCO_3 was added followed by a dropwise addition of a 4-nitrophenyl chloroformate (639 mg, 3.2 mmol) in dioxane (10 ml) solution. The reaction mixture was stirred for 22 h, diluted with EtOAc and washed with a saturated sodium bicarbonate solution. The organic fraction was dried with brine, evaporated to dryness in the presence of SiO_2 and purified over the same medium using 1:3 EtOAc:hexane with 1% TEA toward 100% EtOAc with 1% TEA. After confirming identity of the product by semi-crude NMR it was used in the following step. K_2CO_3 (25 mg, 0.18 mmol) and morpholine (0.016 ml, 0.18 mmol) were dissolved in DMF (5 ml) to which the earlier isolated intermediate (50 mg, 0.092 mmol) was added. This reaction mixture was stirred at room temperature for 4 days and an additional equivalent morpholine (0.016 ml, 0.18 mmol) was added after 2 days. The reaction mixture was diluted with EtOAc (25 ml) and washed with sat. aq. Na_2CO_3 (25 ml). The aqueous layer was back extracted with EtOAc (25 ml) and the combined organic layers were washed with brine (25 ml), dried over Na_2SO_4 and concentrated *in vacuo*. The remaining crude was coated on SiO_2 and purified over SiO_2 using a gradient from EtOAc (1% TEA): cyclohexane 1:1 (v/v) toward 1% MeOH in EtOAc (1% TEA), evaporation of volatiles yielded a colourless oil which was redissolved in DCM and concentrated to afford 19 mg (0.039 mmol, 43%). ^1H NMR (600 MHz, CDCl_3) δ 8.83–8.78 (m, 1H), 8.62–8.59 (m, 1H), 8.04–7.98 (m, 1H), 7.82 (d, $J = 2.2$ Hz, 1H), 7.77 (dd, $J = 8.7, 2.2$ Hz, 1H), 7.49 (dd, $J = 7.8, 5.1$ Hz, 1H), 7.03 (d, $J = 8.7$ Hz, 1H), 4.29–4.23 (m, 1H), 3.87 (s, 3H), 3.85–3.80 (m, 2H), 3.70–3.63 (m, 4H), 3.31–3.25 (m, 4H), 2.94–2.83 (m, 2H), 2.10–2.02 (m, 2H), 1.85–1.78 (m, 2H), 1.49 (s, 6H). ^{13}C NMR (151 MHz, CDCl_3) δ 178.0, 163.9, 161.1, 157.8, 148.5, 146.5, 138.5, 134.4, 128.7, 128.0, 126.9, 124.2, 123.7, 111.2, 66.7, 55.8, 51.0, 48.8, 47.4, 46.1, 30.0, 22.7. LC-MS (ESI) m/z found: 492 ($\text{M} + \text{H}$) $^+$; retention time: 3.07 min. HRMS-ESI ($\text{M} + \text{H}$) $^+$ calculated for $\text{C}_{27}\text{H}_{34}\text{N}_5\text{O}_4$: 492.2605, found 492.2615.

DATA AVAILABILITY STATEMENT

The original contributions presented in the study are included in the article/Supplementary Material, further inquiries can be directed to the corresponding author.

AUTHOR CONTRIBUTIONS

MS contributed to the synthesis of the molecules, LM and GC did the parasitological screenings, MS, GS, IE, and RL were involved in the design of the molecules, LM, IE, and RL were responsible for obtaining the required funding, the manuscript was written by MS, GS, and RL and all authors made corrections and gave feedback to the manuscript.

FUNDING

The PDE4NPDP project was funded by the European Union under the FP-7-Health program, project ID: 602,666.

REFERENCES

- Alpern, J. D., Lopez-Velez, R., and Stauffer, W. M. (2017). Access to Benznidazole for Chagas Disease in the United States—Cautious Optimism? *PLoS Negl. Trop. Dis.* 11, e0005794. doi:10.1371/journal.pntd.0005794
- Basore, K., Cheng, Y., Kushwaha, A. K., Nguyen, S. T., and Desai, S. A. (2015). How Do Antimalarial Drugs Reach Their Intracellular Targets? *Front. Pharmacol.* 6. doi:10.3389/fphar.2015.00091
- Batista, D. d. G. J., Batista, M. M., Oliveira, G. M. d., Amaral, P. B. d., Lannes-Vieira, J., Britto, C. C., et al. (2010). Arylimidamide DB766, a Potential Chemotherapeutic Candidate for Chagas' Disease Treatment. *Antimicrob. Agents Chemother.* 54, 2940–2952. doi:10.1128/aac.01617-09
- Bennion, B. J., Be, N. A., McNERney, M. W., Lao, V., Carlson, E. M., Valdez, C. A., et al. (2017). Predicting a Drug's Membrane Permeability: A Computational Model Validated with *In Vitro* Permeability Assay Data. *J. Phys. Chem. B* 121, 5228–5237. doi:10.1021/acs.jpcc.7b02914
- Bern, C. (2011). Antitrypanosomal Therapy for Chronic Chagas' Disease. *N. Engl. J. Med.* 364, 2527–2534. doi:10.1056/nejmct1014204
- Blaazer, A. R., Orrling, K. M., Shanmugham, A., Jansen, C., Maes, L., Edink, E., et al. (2014). Fragment-Based Screening in Tandem with Phenotypic Screening Provides Novel Antiparasitic Hits. *J. Biomol. Screen.* 20, 10. doi:10.1177/1087057114549735
- Castro, J. A., deMecca, M. M., and Bartel, L. C. (2006). Toxic Side Effects of Drugs Used to Treat Chagas' Disease (American Trypanosomiasis). *Hum. Exp. Toxicol.* 25, 471–479. doi:10.1191/0960327106het653oa
- Coura, J. R., and Borges-Pereira, J. (2011). Chronic Phase of Chagas Disease: Why Should it Be Treated? A Comprehensive Review. *Mem. Inst. Oswaldo Cruz* 106, 641–645. doi:10.1590/s0074-02762011000600001
- Coura, J. R., and Viñas, P. A. (2010). Chagas Disease: a New Worldwide Challenge. *Nature* 465, S6–S7. doi:10.1038/nature09221
- Dias, J. C. P. (1984). Acute Chagas' Disease. *Mem. Inst. Oswaldo Cruz* 79, 85–91. doi:10.1590/s0074-02761984000500017
- Hamers, R. L., Gool, T. V., Goorhuis, A., Cordeiro, M. A. S., Urbina, J. A., Gascon, J., et al. (2016). Benznidazole for Chronic Chagas' Cardiomyopathy. *N. Engl. J. Med.* 374, 189–190. doi:10.1056/NEJMcl1514453
- Kollien, A., and Schaub, G. (2000). The Development of *Trypanosoma cruzi* in Triatominae. *Parasitol. Today* 16, 381–387. doi:10.1016/s0169-4758(00)01724-5
- Lidani, K. C. F., Andrade, F. A., Bavia, L., Damasceno, F. S., Beltrame, M. H., Messias-Reason, I. J., et al. (2019). Chagas Disease: From Discovery to a Worldwide Health Problem. *Front. Public Health* 7, 166. doi:10.3389/fpubh.2019.00166
- Martinez, F., Perna, E., Perrone, S. V., and Liprandi, A. S. (2019). Chagas Disease and Heart Failure: An Expanding Issue Worldwide. *Eur. Cardiol.* 14, 82–88. doi:10.15420/ecr.2018.30.2
- Meirelles, M. N., de Araujo-Jorge, T. C., Miranda, C. F., de Souza, W., and Barbosa, H. S. (1986). Interaction of *Trypanosoma cruzi* with Heart Muscle Cells: Ultrastructural and Cytochemical Analysis of Endocytic Vacuole Formation and Effect upon Myogenesis *In Vitro*. *Eur. J. Cell Biol* 41, 198–206.
- Mejia, A. M., Hall, B. S., Taylor, M. C., Gómez-Palacio, A., Wilkinson, S. R., Triana-Chávez, O., et al. (2012). Benznidazole-Resistance in *Trypanosoma cruzi* Is a Readily Acquired Trait that Can Arise Independently in a Single Population. *J. Infect. Dis.* 206, 220–228. doi:10.1093/infdis/jis331
- Morillo, C. A., Marin-Neto, J. A., Avezum, A., Sosa-Estani, S., Rassi, A., Rosas, F., et al. (2015). Randomized Trial of Benznidazole for Chronic Chagas' Cardiomyopathy. *N. Engl. J. Med.* 373, 1295–1306. doi:10.1056/nejmoa1507574
- Pinazo, M.-J., Guerrero, L., Posada, E., Rodríguez, E., Soy, D., and Gascon, J. (2013). Benznidazole-Related Adverse Drug Reactions and Their Relationship to Serum Drug Concentrations in Patients with Chronic Chagas Disease. *Antimicrob. Agents Chemother.* 57, 390–395. doi:10.1128/aac.01401-12
- Prata, A. (2001). Clinical and Epidemiological Aspects of Chagas Disease. *Lancet Infect. Dis.* 1, 92–100. doi:10.1016/s1473-3099(01)00065-2
- Rassi, A., Jr, Rassi, A., and Marin-Neto, J. A. (2010). Chagas Disease. *The Lancet* 375, 1388–1402. doi:10.1016/s0140-6736(10)60061-x
- Schmunis, G. A. (1999). Prevention of Transfusional *Trypanosoma cruzi* Infection in Latin America. *Mem. Inst. Oswaldo Cruz* 94, 93–101. doi:10.1590/s0074-02761999000700010
- Sgambatti de Andrade, A. L. S., Zicker, F., de Oliveira, R. M., Almeida e Silva, S., Luquetti, A., Travassos, L. R., et al. (1996). Randomised Trial of Efficacy of Benznidazole in Treatment of Early *Trypanosoma cruzi* Infection. *Lancet* 348, 1407–1413. doi:10.1016/s0140-6736(96)04128-1
- Sijm, M., Siciliano de Araújo, J., Kunz, S., Schroeder, S., Edink, E., Orrling, K. M., et al. (2019). Phenylidihydropyrazolones as Novel Lead Compounds against *Trypanosoma cruzi*. *ACS Omega* 4, 6585–6596. doi:10.1021/acsomega.8b02847
- Sijm, M., Sterk, G. J., Caljon, G., Maes, L., Esch, I. J. P., and Leurs, R. (2020). Structure-Activity Relationship of Phenylpyrazolones against *Trypanosoma cruzi*. *ChemMedChem* 15, 1310–1321. doi:10.1002/cmdc.202000136
- Torrico, F., Carlier, Y., Truyens, C., Suarez, E., Dramaix, M., Alonso-vega, C., et al. (2004). Maternal *Trypanosoma cruzi* Infection, Pregnancy Outcome, Morbidity, and Mortality of Congenitally Infected and Non-infected Newborns in Bolivia. *Am. J. Trop. Med. Hyg.* 70, 201–209. doi:10.4269/ajtmh.2004.70.201
- WHO (2021). Chagas Disease (American Trypanosomiasis). Available at: <http://www.who.int/mediacentre/factsheets/fs340/en/> (Accessed November 05, 2018).
- Zhang, L., and Tarleton, R. L. (1999). Parasite Persistence Correlates with Disease Severity and Localization in Chronic Chagas' Disease. *J. Infect. Dis.* 180, 480–486. doi:10.1086/314889

ACKNOWLEDGMENTS

Authors would like to thank D. Ahrens, A. Chen, M. Roseboom, J. Teeken H. Custers for technical assistance and M. Wijtmans for valuable advice.

Conflict of Interest: The authors declare that the research was conducted in the absence of any commercial or financial relationships that could be construed as a potential conflict of interest.

Copyright © 2021 Sijm, Maes, de Esch, Caljon, Sterk and Leurs. This is an open-access article distributed under the terms of the Creative Commons Attribution License (CC BY). The use, distribution or reproduction in other forums is permitted, provided the original author(s) and the copyright owner(s) are credited and that the original publication in this journal is cited, in accordance with accepted academic practice. No use, distribution or reproduction is permitted which does not comply with these terms.

GLOSSARY

ACN acetonitrile

AcOH acetic acid

BINAP 2,2'-bis(diphenylphosphino)-1,1'-binaphthyl

bs broad singlet

d days

d doublet

DBN 1,5-Diazabicyclo[4.3.0]non-5-ene

DCE dichloroethane

DCM dichloromethane

dd double doublet

DIPEA *N,N*-diisopropylethylamine

DMAP 4-dimethylaminopyridine

DME dimethoxyethane

DMF dimethylformamide

DMSO dimethylsulfoxide

dt double triplet

DTU discrete typing unit

EDCI 1-Ethyl-3-(3-dimethylaminopropyl)carbodiimide

ESI electron spray ionization

EtOAc ethylacetate

EtOH ethanol

FCS fetal calf serum

h heptethour

h heptethour

HOBt hydroxybenzotriazole

HPLC high pressure liquid chromatography

HRMS high resolution mass spectroscopy

Hz Hertz

i-PrOH isopropanol

LC-MS liquid chromatography mass spectroscopy

m minute

m multiplet

MeOH methanol

MRC-5 medical research council strain 5

MTBE methyl tertbutyl ether

NaOtBu sodium tert-butoxide

o.n. overnight

p pentet

PDE4NPD phosphodiesterase inhibitors for neglected parasitic disease

pIC₅₀ -log of the value at which 50% of growth is inhibited

rt room temperature

s singlet

SAR structure activity relationship

t triplet

T3P propylphosphonic anhydride

Tcr *Trypanosoma cruzi*

TEA triethylamine

q quartet

THF tetrahydrofuran

TLC thin layer chromatography

UV ultraviolet



Development and Characterization of PLGA Nanoparticles Containing 17-DMAG, an Hsp90 Inhibitor

Kercia P. Cruz¹, Beatriz F. C. Patricio², Vinícius C. Pires¹, Marina F. Amorim¹, Alan G. S. F. Pinho¹, Helenita C. Quadros³, Diana A. S. Dantas¹, Marcelo H. C. Chaves², Fabio R. Formiga^{4,5}, Helvécio V. A. Rocha² and Patrícia S. T. Veras^{1,6*}

¹ Laboratory of Parasite-Host Interaction and Epidemiology, Gonçalo Moniz Institute, Oswaldo Cruz Foundation (FIOCRUZ), Salvador, Brazil, ² Laboratory of Micro and Nanotechnology, Institute of Technology of Drugs (Farmanguinhos), Oswaldo Cruz Foundation (FIOCRUZ), Rio de Janeiro, Brazil, ³ Laboratory of Tissue Engineering and Immunopharmacology, Gonçalo Moniz Institute, Oswaldo Cruz Foundation (FIOCRUZ), Salvador, Brazil, ⁴ Department of Immunology, Aggeu Magalhães Institute (IAM), Oswaldo Cruz Foundation (FIOCRUZ), Recife, Brazil, ⁵ Graduate Program in Applied Cellular and Molecular Biology, University of Pernambuco (UPE), Recife, Brazil, ⁶ National Institute of Science and Technology of Tropical Diseases (INCT-DT), National Council for Scientific Research and Development (CNPq), Salvador, Brazil

OPEN ACCESS

Edited by:

Gildardo Rivera,
Instituto Politécnico Nacional
(IPN), Mexico

Reviewed by:

Andrei I. Khlebnikov,
Tomsk Polytechnic University, Russia
Edson Roberto Silva,
University of São Paulo, Brazil

*Correspondence:

Patrícia S. T. Veras
patricia.veras@fiocruz.br

Specialty section:

This article was submitted to
Medicinal and Pharmaceutical
Chemistry,
a section of the journal
Frontiers in Chemistry

Received: 21 December 2020

Accepted: 09 April 2021

Published: 13 May 2021

Citation:

Cruz KP, Patricio BFC, Pires VC, Amorim MF, Pinho AGSF, Quadros HC, Dantas DAS, Chaves MHC, Formiga FR, Rocha HVA and Veras PST (2021) Development and Characterization of PLGA Nanoparticles Containing 17-DMAG, an Hsp90 Inhibitor. *Front. Chem.* 9:644827. doi: 10.3389/fchem.2021.644827

Leishmaniasis is a spectrum of neglected tropical diseases and its cutaneous form (CL) is characterized by papillary or ulcerated skin lesions that negatively impact patients' quality of life. Current CL treatments suffer limitations, such as severe side effects and high cost, making the search for new therapeutic alternatives an imperative. In this context, heat shock protein 90 (Hsp90) could present a novel therapeutic target, as evidence suggests that Hsp90 inhibitors, such as 17-Dimethylaminoethylamino-17-Demethoxygeldanamycin (17-DMAG), may represent promising chemotherapeutic agents against CL. As innovative input for formulation development of 17-DMAG, nano-based drug delivery systems could provide controlled release, targeting properties, and reduced drug toxicity. In this work, a double emulsion method was used to develop poly (lactic-co-glycolic acid) (PLGA) nanoparticles containing 17-DMAG. The nanoparticle was developed using two distinct protocols: Protocol 1 (P1) and Protocol 2 (P2), which differed concerning the organic solvent (acetone or dichloromethane, respectively) and procedure used to form double-emulsions (Ultra-Turrax[®] homogenization or sonication, respectively). The nanoparticles produced by P2 were comparatively smaller (305.5 vs. 489.0 nm) and more homogeneous polydispersion index (Pdl) (0.129 vs. 0.33) than the ones made by P1. Afterward, the P2 was optimized and the best composition consisted of 2 mg of 17-DMAG, 100 mg of PLGA, 5% of polyethylene glycol (PEG 8000), 1.5 mL of the internal aqueous phase, 1% of polyvinyl alcohol (PVA), and 4 mL of the organic phase. Optimized P2 nanoparticles had a particle size of 297.2 nm (288.6–304.1) and encapsulation efficacy of 19.35% (15.42–42.18) by the supernatant method and 31.60% (19.9–48.79) by the filter/column method. Release kinetics performed at 37°C indicated that ~16% of the encapsulated 17-DMAG was released about to 72 h. In a separate set of experiments, a cell uptake assay employing confocal fluorescence microscopy revealed the internalization by macrophages of P2-optimized rhodamine B labeled nanoparticles at 30 min, 1, 2, 4, 6, 24, 48, and 72 h. Collectively, our results indicate

the superior performance of P2 concerning the parameters used to assess nanoparticle development. Therefore, these findings warrant further research to evaluate optimized 17-DMAG-loaded nanoparticles (NP2-17-DMAG) for toxicity and antileishmanial effects *in vitro* and *in vivo*.

Keywords: leishmaniasis, Hsp90, 17-DMAG, double emulsion, PLGA, nanoparticles

INTRODUCTION

Constituting a severe public health problem throughout the world, the spectrum of leishmaniasis consists of neglected tropical diseases caused by parasite species of the genus *Leishmania*, 20 of which are capable of infecting humans (Masmoudi et al., 2013; Akhoundi et al., 2016; WHO, 2020a). Although endemic in 97 countries, the disease is mainly concentrated in Africa, Asia, and the Americas (WHO, 2020b). It is currently estimated that around 12 million people are infected worldwide, with an annual incidence of more than one million new cases per year; one billion of the world's population lives in areas at risk of infection (Akhoundi et al., 2016; WHO, 2020a).

Leishmaniasis can be divided into two primary clinical forms: cutaneous and visceral, with varying presentations depending on the species and virulence of the infecting parasite, as well as the type of host immune response (Kaye and Scott, 2011; Akhoundi et al., 2016; Oryan and Akbari, 2016; Srivastava et al., 2016; Veras and De Menezes, 2016; WHO, 2020a). Among the cutaneous presentations, mucocutaneous leishmaniasis (MCL), caused mainly by *L. aethiopica* in the Old World and *L. braziliensis* in the New World, is the most debilitating form, with destructive lesions occurring on the palate, lips and nasal septum (Akhoundi et al., 2016; Burza et al., 2018; WHO, 2020a). The most common form, localized cutaneous leishmaniasis (LCL), is caused by a variety of parasite species, including *L. major*, *L. tropica*, and *L. aethiopica* in the Old World, in addition to *L. braziliensis*, *L. guyanensis*, *L. amazonensis*, and *L. mexicana* in the New World (Kaye and Scott, 2011; Masmoudi et al., 2013; Burza et al., 2018; Meira and Gedamu, 2019). Despite not being fatal, LCL can affect patients' quality of life according to the evolution and spread of skin lesions, social stigmatization, psychological effects, and absenteeism (Carvalho et al., 1994; Scorza et al., 2017; Burza et al., 2018).

Currently, chemotherapy is the recommended treatment for patients diagnosed with leishmaniasis, mainly pentavalent antimonials and Amphotericin B in a free or liposomal-encapsulated form (Croft et al., 2006; Frézard et al., 2009; Seifert, 2011; Brasil, 2015; De Menezes et al., 2015; Andrade-Neto et al., 2018). Alternatively, other drugs, such as pentamidine and paromomycin, can also be applied in leishmaniasis treatment (Santos et al., 2008; De Menezes et al., 2015). These therapies present several limitations, including high cost, invasive route of administration, prolonged cycle and systemic side effects, e.g., weakness, myalgia, rigors/chills, hemolysis and fever, as well as instability at high temperatures in some formulations (Sundar et al., 2004; Frézard et al., 2009; Chávez-Fumagalli et al., 2015; De Menezes et al., 2015). Additionally, drug accumulation in the

organs can lead to pancreatitis, nephrotoxicity, hepatotoxicity, myocarditis, and cardiotoxicity (Rath et al., 2003; Frézard et al., 2009; Seifert, 2011; Masmoudi et al., 2013; Chávez-Fumagalli et al., 2015; De Menezes et al., 2015). The only currently available non-invasive orally administered treatment for leishmaniasis, miltefosine, presents limitations including vomiting, diarrhea, kidney, and liver toxicity, as well as potential teratogenic effects and high cost in some regions (Rath et al., 2003; Seifert, 2011; Masmoudi et al., 2013; De Menezes et al., 2015; Andrade-Neto et al., 2018). This scenario highlights the need to discover new drugs that offer increased efficacy and less toxicity (De Menezes et al., 2015). So far, efforts to this end have focused on (i) increasing the safety and efficacy of treatments already in use; (ii) combined drug therapy via novel therapeutic protocols; (iii) the search for new therapeutic targets in parasites or host cells; (iv) repurposing drugs used to treat other diseases; (v) developing more effective delivery systems (Frézard et al., 2009; De Menezes et al., 2015; Andrade-Neto et al., 2018).

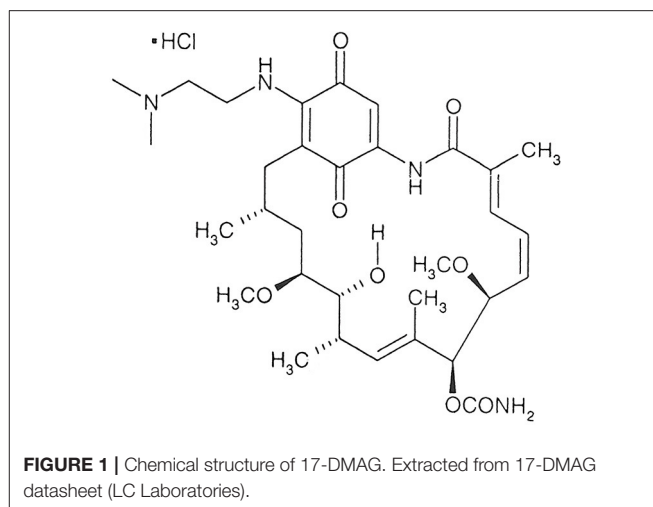
Heat Shock Protein 90 (Hsp90), a ubiquitous and highly conserved molecular chaperone, is responsible for performing the folding of other proteins, namely client proteins, subsequently preventing the post-translational formation of oligomeric complexes with incorrect, inactive and non-functional structures (Zhao and Houry, 2005; Erlejman et al., 2014). This chaperone has been described as a potential therapeutic target in treating cancer and infectious diseases caused by different parasite species, including those of the *Leishmania* genus (Solit and Chiosis, 2008; Pallavi et al., 2010; Roy et al., 2012; Whitesell and Lin, 2012; Schopf et al., 2017; Guswanto et al., 2018). Notably, in leishmaniasis, Hsp90 has been shown to aid in re-establishing the functional stability of proteins in response to environmental pressure, such as differences in pH and temperature, during parasite differentiation processes (Zilberstein and Shapira, 1994; Graefe et al., 2002; Solit and Chiosis, 2008; Pallavi et al., 2010; Roy et al., 2012; Hombach et al., 2014; Schopf et al., 2017).

Structurally, Hsp90 is comprised of three main domains: the intermediate central proteolytic domain, involved in the interface between Hsp90 and its client proteins; the C-terminal domain, which facilitates homodimerization; the N-terminal domain, responsible for interaction with and the hydrolysis of ATP (Pratt and Toft, 2003; Zhao and Houry, 2005; Brown et al., 2007). The family of benzoquinone ansamycins constitutes a class of Hsp90 inhibitors that compete with ATP for binding at the Hsp90 interaction site, thereby hindering chaperone activity (Zhao and Houry, 2005; Brown et al., 2007; Erlejman et al., 2014). Subsequently, truncated or malformed proteins become degraded by the ubiquitin-proteasome system (Chiosis et al.,

2004; Xiao et al., 2006; Sidera and Patsavoudi, 2013). In parasites of the genus *Leishmania*, this inhibition leads to parasite death, evidencing the importance of Hsp90 in the maintenance of cellular homeostasis (Wiesgigl et al., 2001; Li et al., 2009; Roy et al., 2012; Hombach et al., 2013).

Research by our group previously demonstrated that geldanamycin (GA), 17-AAG, and 17-DMAG, Hsp90 inhibitors of benzoquinone ansamycin family, were capable of eliminating promastigote forms of *L. amazonensis* at concentrations determined as non-toxic for human monocyte lineage cells (THP-1) (Palma et al., 2019). It was also demonstrated that the treatment of *L. amazonensis*-infected macrophages with 17-AAG reduced the percentage of infected macrophages and numbers of intracellular parasites in a time- and dose-dependent manner at concentrations deemed non-toxic to host cells (Petersen et al., 2012). Furthermore, 17-AAG was found to control, both *in vitro* and *in vivo*, *L. braziliensis* infection in BALB/c mouse macrophages (Santos et al., 2014). This study demonstrates that 17-AAG reduces the size of ear lesions and parasitic load at the lesion site, but not in the draining lymph nodes of infected mice, resulting in infection relapse (Santos et al., 2014). To overcome this described limitation, it will be tested a water-soluble analog of 17-AAG, 17-DMAG (Egorin et al., 2002; Sausville, 2004; Whitesell and Lin, 2012). Because it is a water-soluble molecule and has better pharmacokinetics than 17-AAG, 17-DMAG can achieve lymph nodes of treated animals, eliminating the parasites on this site. To optimize a formulation containing-Hsp90 inhibitor for leishmaniasis treatment, we propose the encapsulation of 17-DMAG in a nanoparticle, which can have controlled release of the drug, prolonging its action with fewer administrations. This delivery system can also help prevent toxicity occurrences in future tests for *L. braziliensis* infection control.

Nanoparticle-based controlled release systems offer several advantages: improved safety, efficacy, target specificity (drug targeting), biocompatibility, bioavailability, biodegradability, and reduced toxicity in comparison to traditional drug delivery systems (Zhang et al., 2008; Formiga et al., 2009; Yildirim et al., 2011; Lin, 2015; Utreja et al., 2020). By directing the active principle to specific tissues and releasing it gradually over time, the dose necessary to observe treatment efficacy becomes reduced, thereby contributing to a reduction in side effects (Yildirim et al., 2011; Wolfram et al., 2015). Synthetic polymers such as poly(lactic-co-glycolic acid) (PLGA), polylactic acid (PLA) and polycaprolactone (PCL) are commonly used in drug delivery systems because they do not offer a risk of inducing an unwanted immune response (Formiga et al., 2009; Zhang and Zhang, 2017; Utreja et al., 2020). The main application of these systems consists of cases in which the free form of a drug presents limitations, such as shortened half-life, requiring the need for multiple applications, and inadequate target specificity, which can lead to the occurrence of a range of side effects (Zhang et al., 2008; Formiga et al., 2009). Thus, the present work aimed to produce polymeric nanoparticles (NPs) containing the Hsp90 inhibitor, 17-DMAG, and perform morphological and physical-chemical characterization. The results obtained herein will enable, in the future, an evaluation of *in vitro* and



in vivo optimized 17-DMAG-loaded NPs (NP2-17-DMAG) as antileishmanial treatment.

MATERIALS AND METHODS

Reagents and Chemicals

The hydrochloride salt of alvespimycin, 17-DMAG (**Figure 1**), was purchased from LC Laboratories (Massachusetts, USA). Resomer® RG 503 H, Poly (D, L-lactide-co-glycolide) (50:50) (PLGA), Poly (vinyl alcohol) (87–90% hydrolyzed average mol wt 30,000–70,000, PVA) and poly(ethylene glycol) (PEG, MW = 8,000) were purchased from Sigma-Aldrich (Darmstadt, Germany). Alamar blue® was purchased from Invitrogen (Massachusetts, USA). Microcon-30 0.5ML microtubes were purchased from Merk Millipore (Darmstadt, Germany). A C18 HPLC column and C18 Supelguard Guard Cartridge were purchased from Sigma-Aldrich (Darmstadt, Germany).

Preparations of PLGA NPs

Two different double emulsion protocols were used to prepare PLGA NPs. In the first protocol (P1), PLGA NPs containing 17-DMAG (NP1-17-DMAG) were prepared using a modified double emulsion/solvent evaporation technique (Salvador et al., 2015). Briefly, 50 mg of PLGA was dissolved in 5 mL of acetone, and 2 mg of 17-DMAG was dissolved in 5% PEG solution (250 mg in 5 mL of distilled water). The 17-DMAG solution was then added to the pre-cooled PLGA solution and emulsified using a Q700 sonicator (QSonica, Newtown, Connecticut, USA) at 6% amplitude for 2 min. Subsequently, 10 mL of PVA 1% w/v was added to the mixture. The recipient was then covered with aluminum foil and then homogenized at 10,000 rpm for 5 min (Ultra-turrax® T-25, IKA, Germany) to form a double emulsion. Next, 10 mL of 2% isopropyl alcohol was added. Finally, the suspension was magnetically stirred for 30 min with a subsequent solvent evaporation step using a rotary evaporator (IKA) for 1 h at 56°C under 250 mBar.

In the second double emulsion protocol (P2), PLGA NPs (NP2-17-DMAG) were also produced using another double

emulsion/solvent evaporation technique (Mainardes et al., 2009). Initially, 100 mg of PLGA was dissolved in 4 mL of dichloromethane. Another solution containing 2 mg of 17-DMAG dissolved in 1.5 mL of PEG 5% w/v was then added to the pre-cooled PLGA solution to form a single emulsion using a Q700 sonicator (QSonica, Newtown, Connecticut, USA) at 40% amplitude for 1 min. To form the double emulsion, the single emulsion was incorporated in 10 mL of PVA 1% w/v, then sonicated. Finally, 30 mL of PVA 1% w/v was added to the recipient, covered with aluminum foil and magnetically stirred for 30 min. The solvent extraction step was performed using a rotary evaporator (IKA) for 1 h at 40°C under 200 mBar.

Following each nanoparticle protocol preparation, suspensions were washed in distilled water three times at $39,800 \times g$ for 15 min at 4°C (T-865, Thermo Fisher Scientific, Massachusetts, USA). Samples were frozen at -80°C, then lyophilized for 24 h at -48°C under 0.050 mBar (FreeZone 2.5 Liter Benchtop, Labconco, USA) and subsequently stored at 4°C. For blank nanoparticle preparation (NP1-Ø and NP2-Ø), these same protocols were followed in the absence of 17-DMAG.

To evaluate the influence of PLGA and PEG concentration on the encapsulation efficiency (%EE) of 17-DMAG and the size of the produced NPs, P2 was performed as described above using 100 or 200 mg of PLGA and 2.5% w/v or 5% w/v of PEG.

PLGA NPs Characterization

Dynamic Light Scattering

DLS was used to measure the particle size, polydispersion index (PdI) and zeta potential (ZP) of the obtained NPs. After washing, NP-17-DMAG or NP-Ø produced by the P1 or P2 double-emulsion protocols were resuspended in 5 mL of distilled water and diluted 1:125 in distilled water. DLS analysis was performed in triplicate using a ZetaSizer Nano ZS90 (Malvern Panalytical, UK) at 25°C.

Transmission Electron Microscopy

For imaging and size confirmation, NPs were washed as described in item 2.2 and analyzed by TEM. Aliquots of NP-17-DMAG or NP-Ø produced by the P1 or P2 double-emulsion protocols were diluted 1:10 in distilled water, then 10 µL of each sample was placed on a formvar film-coated grid and stained with 2% uranyl acetate for 2 min. TEM analysis was performed using a JEM-1230 transmission electron microscope (JEOL LTD, Japan).

Scanning Electron Microscopy

SEM was used to examine the shape and surface morphology of the NP-17-DMAG or NP-Ø produced by the P1 or P2 double-emulsion protocols. For SEM analysis, lyophilized NPs (1 mg) were placed on an adhesive stub and coated with gold-palladium under vacuum using an ion coater. All samples were analyzed and photographed at 15 kV using a JSM-6390LV microscope (JEOL LTD, Japan).

HPLC for 17-DMAG Quantification

To quantify 17-DMAG, HPLC was performed using a C18 HPLC column and C18 Supelguard Guard Cartridge following manufacturer protocols. First, the mobile phase was prepared

using HPLC grade acetonitrile (27%), HPLC grade methanol (27%), ultrapure water (46%), and trifluoroacetic acid (0.05%). In parallel, 17-DMAG was diluted in distilled water at an initial concentration of 500 µg/mL, then diluted from 50 to 1 µg/mL in the mobile phase to construct concentration curves in triplicate. Each sample was analyzed at a 2D wavelength of 254 nm for 8 min at 25°C. The mobile phase flow rate was 1 mL/min, with 10 µL of each sample injected. The observed retention time for 17-DMAG under these conditions was ~3.8 min. Nanoparticle concentrations of 17-DMAG were calculated using a free compound curve (Empower software, version 3).

Encapsulation Efficiency (%EE) of 17-DMAG in NPs

Encapsulation efficiency determination was performed using two indirect methods: filter/column or supernatant. After the solvent was evaporated using the filter/column method, 500 µL of nanoparticle suspension was centrifuged in a 1.5 mL microtube with a Microcon 30 filter under $14,000 \times g$ for 1 h at 4°C. As the free drug fraction (F) in each sample flowed through the filter, NPs were retained. In parallel, absolute ethanol was added to another 500 µL aliquot of total nanoparticle suspension at a proportion of 1:1 to determine the total amount of 17-DMAG. After centrifugation at $6,200 \times g$ for 15 min at 4°C, the supernatant was collected and the total quantity of 17-DMAG (T) was measured. %EE was evaluated by HPLC following the formula:

$$\%EE = \frac{(T - F)}{T} \times 100,$$

where T corresponds to the total mass of the drug in the sample, whether encapsulated or not, and F corresponds to the non-encapsulated fraction (free fraction).

For the supernatant method, the supernatants obtained from three washes of the produced NPs were collected and then diluted at 1:5 in the mobile phase. HPLC then evaluated the %EE according to the formula:

$$\%EE = \frac{S}{T} \times 100,$$

where S corresponds to the total mass of 17-DMAG in the supernatants and T is the total mass of the drug added for encapsulation.

Release of 17-DMAG From NP2-17-DMAG *in vitro*

The release of 17-DMAG from NP2-17-DMAG was assessed *in vitro* using a modified method to determine the release kinetic profile (Quadros et al., 2020). Briefly, 2 mg of NP2-17-DMAG were placed into 1.5 mL polypropylene microcentrifuge tubes and resuspended in 1 mL of Dulbecco's modified Eagle's medium (DMEM) (Gibco), supplemented with 20 mM of HEPES (Sigma), 42.14 mM of sodium bicarbonate (Sigma), 10% of inactivated fetal bovine serum (Gibco), 2 mM of glutamine (Sigma), and 20 µg/mL of ciprofloxacin (Isofarma, Precabura, CE, BR) (complete DMEM medium). Next, the sealed tubes were

placed in a rotating shaker and maintained at 37°C for 72 h. At each specific time point (1, 3, 6, 12, 24, 48, and 72 h), the sample tubes were removed from the incubator and centrifuged at $21,000 \times g$ for 15 min at 4°C. The supernatant was then collected, frozen and immediately replaced with an equal volume of fresh release medium. To determine the 17-DMAG concentration, collected supernatants were diluted in the mobile phase and quantified using HPLC Shimadzu LC20-A (São Paulo, Brazil). All assays were performed in triplicate.

Animal Manipulation and Ethics Statement

BALB/c mice, male or female, aged 6–12 weeks, were provided by the Gonçalo Moniz Institute (IGM/FIOCRUZ) Animal Care Facility. The animals were maintained under pathogen-free conditions, with food and water *ad libitum*. All procedures involving animals were conducted under the International Guiding Principles for Biomedical Research Involving Animals. The Institutional Review Board approved this study's experimental design (CEUA protocol no. 007/2020) of the Gonçalo Moniz Institute, Bahia-Brazil (IGM-FIOCRUZ/BA).

Obtainment of Bone Marrow-Derived Macrophages From BALB/c Mice

BALB/c mice were euthanized using thiopental intraperitoneal injection (50 mg/kg). Mouse femurs and tibias were aseptically removed and kept in cold 0.9% NaCl solution containing 0.01 mg/mL of ciprofloxacin. In a sterile environment, bone extremities were removed and marrow cells were extracted by washing the bone cavity with Roswell Park Memorial Institute (RPMI) 1640 medium (GIBCO) supplemented with 20 mM of HEPES (SIGMA), 23 mM of sodium bicarbonate (SIGMA), 10% of inactivated fetal bovine serum (Gibco), 2 mM of Glutamine (Sigma) and 20 µg/mL of ciprofloxacin (Isofarma, Precabura, CE, BR) (complete RPMI medium). Extracted marrow cells were centrifuged at $300 \times g$ at 4°C for 10 min, then resuspended and cultivated in Petri dishes (three plates per animal) containing 10 mL of complete RPMI medium with 30% supernatant from L929 cell culture containing granulocyte macrophage colony-stimulating factor (GM-CSF). The dishes were cultivated at 37°C under 5% CO₂ and 95% humidity for 24 h, after which the supernatant was transferred to new plates. After 72 h, an additional 5 mL of complete RPMI medium containing 30% L929 supernatant was added to each culture to re-stimulate cells for differentiation.

On the 7th day, BMDM were recovered from bacterial Petri dishes using 5 mL of 1 mM EDTA solution (pH 8.0) for 5 min at 37°C. Cells were centrifuged at $300 \times g$ for 10 min at 4°C, then resuspended in 1 mL of complete DMEM medium and counted in a Neubauer chamber.

Uptake of Fluorescent NPs by BMDM *in vitro*

NPs containing rhodamine B (Sigma) were produced using the P2 protocol (item 2.2). BMDM were obtained as described above and plated at 10^5 cells per well in 1 mL of complete DMEM medium on 24-well plates containing glass coverslips. For the *in vitro* uptake assay, rhodamine B-containing NPs were lyophilized and then incubated with BMDM for 30 min,

TABLE 1 | Particle size (Size), polydispersion index (Pdl), zeta potential (ZP) and encapsulation efficiency (%EE) by supernatant or filter/column methods of NPs produced by P1 or P2 double emulsion protocols.

Protocol	Size (nm)	Pdl	ZP (mV)	%EE (supernatant)	%EE (filter /column)
P1	489	0.33	−34.4	14.9%	14.02%
P2	305.5	0.129	−28.7	15.04%	17%

1, 2, 4, 6, 24, 48, and 72 h. Wells were washed at each time point, and cells were fixed with 4% paraformaldehyde (PFA) for 15 min at room temperature. Finally, coverslips were mounted on slides using ProLong Gold antifade with DAPI® (Invitrogen, Darmstadt, Germany). Images were obtained by confocal fluorescence microscopy using a Leica SP8 device (Leica Microsystems, Mannheim, Germany).

Statistical Analysis

Graphs were constructed and statistical analyses were performed using GraphPad Prism version 5.01 (GraphPad Software Inc). The Kolmogorov-Smirnov test was employed to verify normality. For data with Gaussian distribution, Student's *t*-test or one-way ANOVA were used to compare between two groups or among three or more groups, respectively, followed by Tukey's post-test. For non-gaussian distributions, the Mann-Whitney U test was applied for comparisons between two groups, while Kruskal-Wallis was used to compare three or more groups. Differences were considered statistically significant when $p < 0.05$.

RESULTS

DLS Characterization and %EE of NPs Produced by P1 or P2 Double Emulsion Protocols

The NP1-17-DMAG had a larger average size, size variation (Pdl), and ZP than the NP2-17-DMAG (Table 1). No differences were detected in %EE values regardless of the quantitation method (supernatant or filter/column) used to determine the amount of 17-DMAG encapsulated in NP1-17-DMAG or NP2-17-DMAG (Table 1).

Morphological Characterization of NP1 and NP2

Consistent with the obtained Pdl values, electron microscopy analysis revealed a more significant size variation in NP1 (Figures 2A,B) compared to NP2 (Figures 2C,D). Both protocols produced spherical, regular-shaped NPs (Figure 2). No morphological differences were observed between NP-Ø and NP-17-DMAG.

SEM morphological analysis confirmed the spherical shape and smooth surface of the NPs produced by both double emulsion protocols (Figure 3). Consistent with DLS and TEM results, SEM analysis also revealed that NP1-Ø and NP1-17-DMAG exhibited more considerable size variation (Figures 3A,B) compared to NP2-Ø and NP2-17-DMAG (Figures 3C,D). Again, no morphological differences were

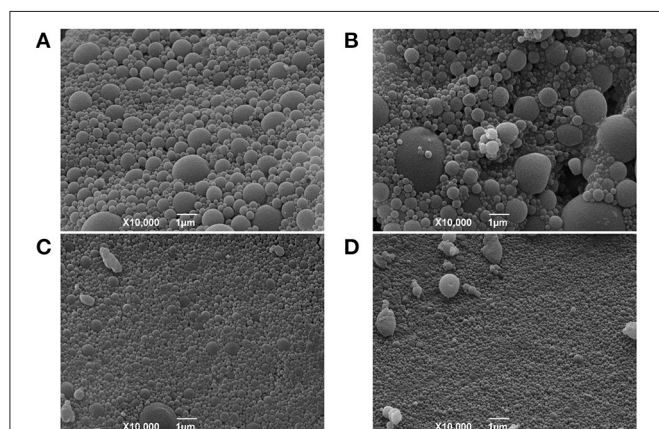
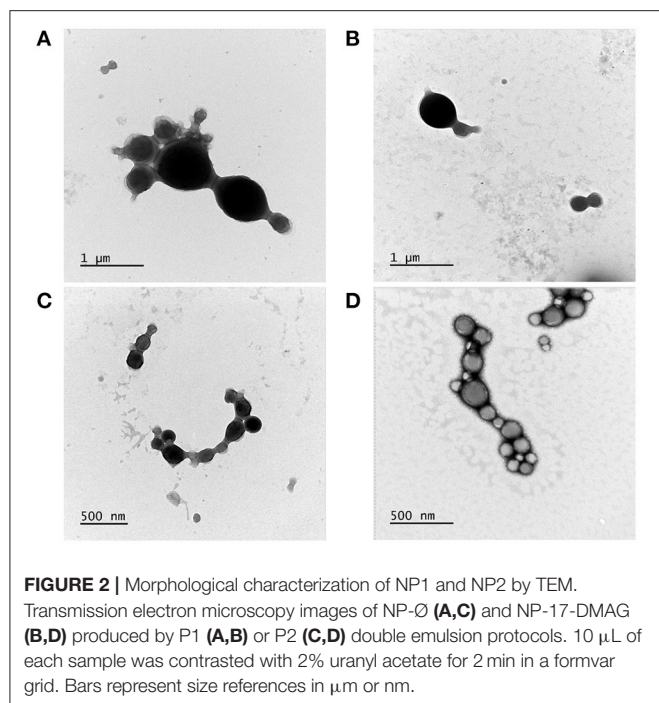
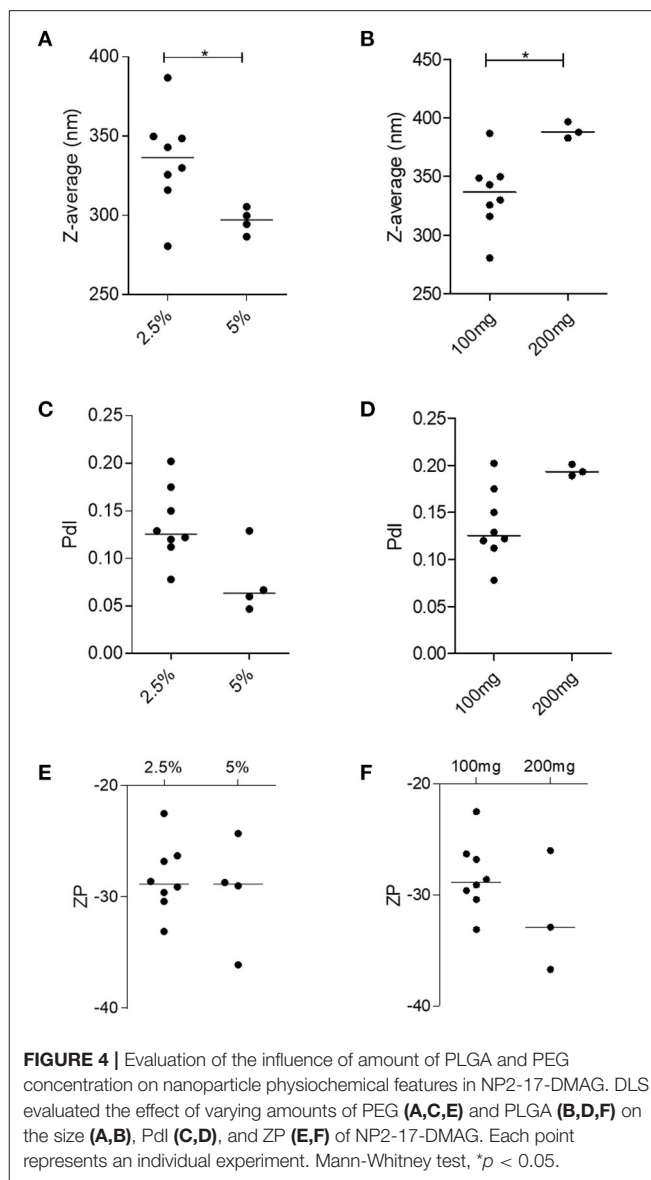


FIGURE 3 | SEM evaluations of NP1 and NP2. NP-Ø (**A,C**) or NP-17-DMAG (**B,D**) were produced by P1 (**A,B**) or P2 (**C,D**) double emulsion protocols. The produced NPs were frozen at -80°C and lyophilized for 24 h at -48°C under 0.050 mbar. Approximately 1 mg of each sample was vacuum-coated with gold-palladium using an ion coater and analyzed by SEM. All samples were analyzed and photographed at 15 kV. Bars represent 1 µm.

observed between NP-Ø (**Figures 3A,C**) and NP-17-DMAG (**Figures 3B,D**) regardless of the protocol used.

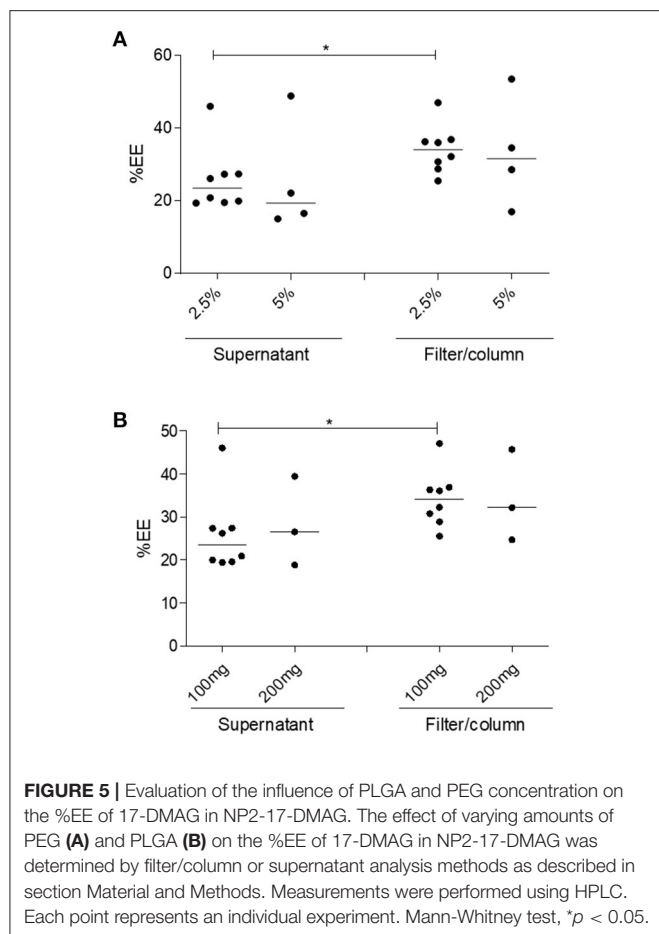
P2 Optimization Protocol

As NP2-17-DMAG exhibited superior physical-chemical and morphological characteristics compared to NP1-17-DMAG, we employed P2 to optimize the 17-DMAG encapsulation process with some variations. NPs produced using 5% PEG presented a smaller median size of 297.2 nm (Q1: 288.6; Q2: 304.1) compared to those made using 2.5% PEG (median size: 336.5 nm; Q1: 318.4;



Q2: 349.6) (**Figure 4A**). Similarly, NPs produced containing 100 mg of PLGA presented a smaller median size of 336.5 nm (Q1: 318.4; Q2: 349.6) in comparison to those containing 200 mg of PLGA (median size: 387.8 nm; Q1: 382.8; Q2: 396.7) (**Figure 4B**). No differences were detected concerning PDI and ZP values among NPs prepared using different PEG concentrations (**Figures 4C,E**), nor different PLGA masses (**Figures 4D,F**).

Similar %EE values were found for NP2-17-DMAG regardless of the amount of PEG used (2.5 or 5%) (**Figure 5A**). Median %EE values for 2.5 and 5% of PEG were 23.51% (Q1: 19.66; Q2: 27.38) and 19.35% (Q1: 15.42; Q2: 42.18), respectively, using the supernatant analysis method, vs. 34.12% (Q1: 29.31; Q2: 36.73) and 31.60% (Q1: 19.90; Q2: 48.79) using the filter/column method (**Figure 5A**). Furthermore, similar %EE results were seen in NPs produced with different amounts of PLGA (**Figure 5B**) using the supernatant quantitative analysis



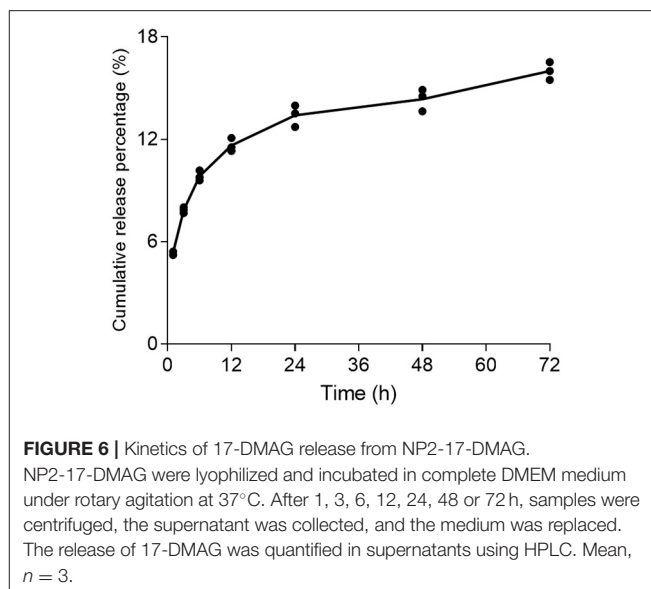
method, with respective median values of 23.51% (Q1: 19.66; Q2: 27.38) and 26.48% (Q1: 18.78; Q2: 39.39) for 100 and 200 mg of PLGA, respectively. The filter/column method yielded median %EE values of 34.12% (Q1: 29.31; Q2: 36.73) for 100 mg and 32.12% (Q1: 24.66; Q2: 44.63) for 200 mg of this polymer. It is worth noting that, in comparison to the supernatant analysis method, higher %EE results were obtained using the quantitative filter/column method regardless of NP2 protocol modifications (Figure 5).

In vitro Release of 17-DMAG From NP2-17-DMAG

At 1, 3, 6, 12, 24, 48, and 72 h of incubation, 5.36, 7.86, 9.85, 11.64, 13.41, 14.36, and 16% of 17-DMAG were cumulatively released from NP2-17-DMAG (Figure 6) *in vitro*, i.e., the amount of 17-DMAG was observed to continuously increase in complete DMEM medium for 72 h (Figure 6).

Uptake of Fluorescent NPs by BMDM *in vitro*

The rhodamine-encapsulated NPs produced by P2 (NP2-rhodamine) presented similar size, shape, and appearance (smooth surface) as the morphological characteristics of NPs produced with or without 17-DMAG (data not shown). The



uptake of NP2-rhodamine by BMDM was observed at an early incubation time of 30 min, 1, 2, 4, and 6 h (Figures 7A–E, respectively). After 24, 48 or 72 h (Figures 7F–H, respectively), greater numbers of NPs were observed in the cytoplasm of BMDM, indicating continued uptake by these cells.

DISCUSSION

The present work encapsulated 17-DMAG in PLGA NPs and investigated the resulting physical-chemical, morphological, and biological parameters. To standardize NP production, two double emulsion-solvent evaporation protocols (P1 and P2) were used (Astete and Sabliov, 2006; Mainardes et al., 2009). Analyses by DLS, TEM and SEM showed that NP1 presented larger sizes and higher PdI than NP2, which agrees with a previous report (Astete and Sabliov, 2006). We found that modifications in the PLGA-NP production protocol, such as the nature of the organic solvent used or the emulsion method, altered the characteristics of the produced NP. The larger sizes presented by NP1 may be due to laminar flow under stirring, such as that produced by the Ultra-Turrax® dispersing device. Accordingly, monodispersed drops may form in the emulsion, increasing the size of the produced NP, which is not observed under sonication (Astete and Sabliov, 2006). Concerning ZP, a measurement of the electrical behavior of NPs, both protocols produced NPs with values around -30 mV, indicating stability with minimal aggregate formation (Formiga et al., 2009). Furthermore, the observed similarity between %EE values in each protocol can be justified by using the same polymer and surfactant (PEG), as these parameters significantly influence the entrapment of hydrophilic drugs (Astete and Sabliov, 2006).

The morphological characterization of NP1 and NP2 by TEM and SEM confirmed differences in size and PdI between the two protocols, revealing a similarly regular, spherical shape and smooth surface appearance. These aspects are essential as

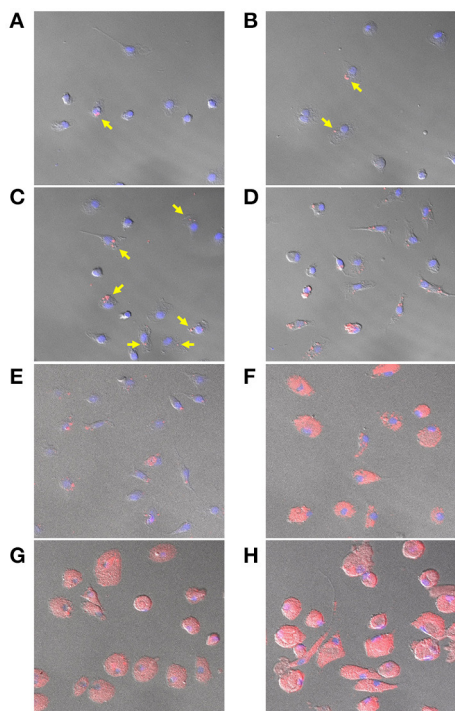


FIGURE 7 | Uptake of NP2-rhodamine by BMDM. BMDM were plated at 10^5 cells per well and incubated with NP2-rhodamine for 30 min (A), 1 h (B), 2 h (C), 4 h (D), 6 h (E), 24 h (F), 48 h (G) or 72 h (H). Following incubation, cells were fixed with 4% PFA and slides were mounted with DAPI. Cells were analyzed by confocal fluorescence microscopy (Leica SP8). Blue = DAPI; Red = rhodamine. Arrows indicate internalization of NP2-rhodamine by macrophages at early timepoints.

the morphological characteristics of NPs can predict possible interactions with living cells and uptake, intracellular localization and toxicity (Shang et al., 2014). Our results agree with previous studies (Cohen-Sela et al., 2009; McCall and Sirianni, 2013; Garbuzenko et al., 2014), demonstrating that PLGA particles produced by double emulsion presented spherical and regular shapes with smooth surfaces, regardless of modifications performed in the protocol. Following DLS, TEM and SEM characterization, P2 was selected as the better protocol for NP-17-DMAG production.

We then evaluated the effects of modifications to P2: NP2-17-DMAG produced with 100 mg of PLGA presented smaller sizes than 200 mg. This result stands in accordance with other authors who observed that increasing concentrations of PLGA generated larger particles (Astete and Sabliov, 2006; Rizkalla et al., 2006; Hernández-Giottonini et al., 2020). This has been observed to occur due to increased viscosity in the primary emulsion (w/o), which results in a less-efficient particle size reduction during the double emulsification process (w/o/w) (Iqbal et al., 2015). Similarly, using 5% PEG compared to 2.5% resulted in a smaller NP2-17-DMAG size. The decreased size was also observed at higher PEG concentrations in other studies (Zambaux et al., 1998; Rizkalla et al., 2006; Iqbal et al., 2015; Urbaniak and Musiał, 2019; Hernández-Giottonini et al., 2020).

Higher surfactant concentrations reduce surface tension and promote particle division during the homogenization process, thus decreasing the size of the particles formed (Keum et al., 2011; Fonte et al., 2012). This phenomenon is maintained until a saturation point is reached (Keum et al., 2011; Fonte et al., 2012; Iqbal et al., 2015; Urbaniak and Musiał, 2019).

Encapsulation efficiency (%EE) was measured indirectly in this study. Two methods, filter/column or supernatant, were employed to separate loaded NPs and the non-encapsulated drug. We identified higher %EE values using filter/column than the supernatant, which may be attributable to superior free drug separation by this first method. This finding is consistent with studies on nanoparticle purification efficiency (Akbulut et al., 2012; Robertson et al., 2016), demonstrating that nanoparticle separation by supernatant depends on nanoparticle size and shape, the molecular weight of the polymer, dispersion medium density, speed, and centrifugation time. The filter/column method has commonly been considered a more robust, more straightforward and efficient purification process (Robertson et al., 2016; Shah et al., 2020).

After characterizing NP2-17-DMAG, we evaluated the kinetics of drug release. We found that NP2-17-DMAG exhibited two release phases: a preliminary rapid release of 17-DMAG lasting up to 24 h, followed by a slow and sustained release from 24 to 72 h. This data is similar to results obtained by Rietscher et al. (2016) and Rafiei and Azita (2017), who analyzed the release of different compounds in PLGA or PLGA-PEG NPs. PLGA NPs containing paromomycin also presented a similar release profile (Afzal et al., 2019), which was expected for polymeric NPs encapsulating hydrophilic molecules. At the initial timepoints evaluated, the drug is rapidly released due to adsorbed molecules on the surface of NPs (Hirenkumar and Steven, 2012; Kapoor et al., 2015; Rietscher et al., 2016; Mir et al., 2017; Rafiei and Azita, 2017). In contrast, at subsequent time points, a sustained and slower release occurs due to gradual degradation of the polymeric matrix and slowly release of the drug contained there (Hirenkumar and Steven, 2012; Kapoor et al., 2015; Rietscher et al., 2016; Mir et al., 2017; Rafiei and Azita, 2017).

Nanoparticle uptake was evaluated through the incubation of BMDM with NP2-rhodamine. Fluorescence microscopy analysis revealed the internalization of NPs by macrophages beginning at early times of contact with NP2-rhodamine. At later timepoints, these particles continued to be internalized and accumulation was observed in these cells' cytoplasm. These results are in agreement with other studies of professional phagocytes, including RAW 264 and J774 macrophage cell-lines and primary resident and inflammatory macrophages, which have been shown to internalize NPs at early timepoints, such as at 30 min of incubation (Cohen-Sela et al., 2009; Nicolette et al., 2011; Petersen et al., 2018; Couto et al., 2020; Van Hees et al., 2020).

The present study revealed that PLGA NPs containing 17-DMAG prepared using a double emulsion protocol presents physical-chemical, morphological, and biological characteristics conducive to CLs treatment. Additional studies will be carried out to investigate biological and immunological effects of NP2-17-DMAG in *L. braziliensis* infection control both *in vitro* and *in vivo* in a future manuscript.

DATA AVAILABILITY STATEMENT

The raw data supporting the conclusions of this article will be made available by the authors, without undue reservation.

ETHICS STATEMENT

The animal study was reviewed and approved by BALB/c mice, male or female, aged 6–12 weeks, were provided by the Gonçalves Moniz Institute (IGM/FIOCRUZ) Animal Care Facility. The animals were maintained under pathogen-free conditions, with food and water *ad libitum*. All procedures involving animals were conducted under the International Guiding Principles for Biomedical Research Involving Animals. The Institutional Review Board approved this study's experimental design (CEUA protocol no. 007/2020) of the Gonçalves Moniz Institute, Fiocruz, Salvador, Brazil.

AUTHOR CONTRIBUTIONS

KC, BP, VP, FF, HR, and PV conceptualized and designed the experiments and analyzed and validated the data analysis. KC, BP, VP, MA, AP, DD, and MC performed the experiments. KC, VP, MA, AP, HQ, and PV wrote the paper. KC, BP, HR, FF, and PV reviewed and edited this paper. All authors contributed to the article and approved the submitted version.

REFERENCES

- Afzal, I., Sarwar, H. S., Sohail, M. F., Varikuti, S., Jahan, S., Akhtar, S., et al. (2019). Mannosylated thiolated paromomycin-loaded PLGA nanoparticles for the oral therapy of visceral leishmaniasis. *Nanomedicine* 14, 387–406. doi: 10.2217/nnm-2018-0038
- Akbulut, O., Mace, C. R., Martinez, R. V., Kumar, A. A., Nie, Z., Patton, M. R., et al. (2012). Separation of nanoparticles in aqueous multiphase systems through centrifugation. *Nano Lett.* 12, 4060–4064. doi: 10.1021/nl301452x
- Akhoundi, M., Kuhl, K., Cannel, A., Votýpka, J., Marty, P., Delaunay, P., et al. (2016). A historical overview of the classification, evolution, and dispersion of leishmania parasites and sandflies. *PLoS Negl. Trop. Dis.* 10:e0004349. doi: 10.1371/journal.pntd.0004349
- Andrade-Neto, V. V., Cunha-Junior, E. F., Dos Santos Faioes, V., Martins, T. P., Silva, R. L., Leon, L. L., et al. (2018). Leishmaniasis treatment: update of possibilities for drug repurposing. *Front. Biosci. Landmark* 23, 967–996. doi: 10.2741/4629
- Astete, C. E., and Sabliov, C. M. (2006). Synthesis and characterization of PLGA nanoparticles. *J. Biomater. Sci. Polym. Ed.* 17, 247–289. doi: 10.1163/156856206775997322
- Brasil (2015). *Manual de recomendações para diagnóstico, tratamento e acompanhamento de pacientes com a coinfeção Leishmania-HIV, 1st Edn.* Brasília: Ministério da Saúde.
- Brown, M. A., Zhu, L., Schmidt, C., and Tucker, P. W. (2007). Hsp90-From signal transduction to cell transformation. *Biochem. Biophys. Res. Commun.* 363, 241–246. doi: 10.1016/j.bbrc.2007.08.054
- Burza, S., Croft, S. L., and Boelaert, M. (2018). Leishmaniasis. *Lancet* 392, 951–970. doi: 10.1016/S0140-6736(18)31204-2
- Carvalho, E. M., Barral, A., Costa, J. M. L., Bittencourt, A., and Marsden, P. (1994). Clinical and immunopathological aspects of disseminated cutaneous leishmaniasis. *Acta Trop.* 56, 315–325. doi: 10.1016/0001-706X(94)90103-1
- Chávez-Fumagalli, M. A., Ribeiro, T. G., Castilho, R. O., Fernandes, S. O. A., Cardoso, V. N., Coelho, C. S. P., et al. (2015). New delivery systems for

FUNDING

This work was supported by grants from the Bahia State Research Support Foundation (PV-Universal 422867/2016-0 and SUS0019/2014), FIOCRUZ (INOVA-46700287000), and Gonçalves Moniz Institute (PV-PROEP 400898/2013-6). PV holds a grant from CNPq (305235/2019-2). The fellowship received by KC was financed by Coordination for the Improvement of Higher Education Personnel-Brazil (CAPES)-Finance Code 001. This study was partially supported by the Coordination for the Improvement of Higher Education Personnel (Coordenação de Aperfeiçoamento de Pessoal de Nível Superior - CAPES) - Finance Code 001. The funders had no role in study design, data collection or analysis, the decision to publish, or the manuscript's preparation.

ACKNOWLEDGMENTS

The authors would like to thank LAIPHE (FIOCRUZ-BA), LMN (Farmanguinhos-RJ), Electronic Microscopy Service (FIOCRUZ-BA), and Laboratory of Applied Chemistry Research (LIPAQ, SENAI CIMATEC-BA), for the support in the experiment's performance. The authors also would like to thank Carine S. A. Silva, Nathan A. A. Guiraud, and Gabriella B. Pita, for the realization of the initial experiments with polymeric nanoparticles, and Andris K. Walter, for English language revision and manuscript copyediting assistance.

- amphotericin B applied to the improvement of leishmaniasis treatment. *Rev. Soc. Bras. Med. Trop.* 48, 235–242. doi: 10.1590/0037-8682-0138-2015
- Chiosis, G., Vilenchik, M., Kim, J., and Solit, D. (2004). Hsp90: the vulnerable chaperone. *Drug Discov. Today* 9, 881–888. doi: 10.1016/S1359-6446(04)03245-3
- Cohen-Sela, E., Chorny, M., Koroukhov, N., Danenberg, H. D., and Golomb, G. (2009). A new double emulsion solvent diffusion technique for encapsulating hydrophilic molecules in PLGA nanoparticles. *J. Control. Release* 133, 90–95. doi: 10.1016/j.jconrel.2008.09.073
- Couto, P. V., Magalhães, C. P., Ferrante, M., Rebouças, J., de, S., Nguewa, P., et al. (2020). Solid lipid nanoparticles as a novel formulation approach for tanesipimycin (17-AAG) against leishmania infections: Preparation, characterization and macrophage uptake. *Acta Trop.* 211:105595. doi: 10.1016/j.actatropica.2020.105595
- Croft, S. L., Seifert, K., and Yardley, V. (2006). Current scenario of drug development for leishmaniasis. *Indian J. Med. Res.* 123, 399–410.
- De Menezes, J. P. B., Guedes, C. E. S., Petersen, A. L. O. A., Fraga, D. B. M., and Veras, P. S. T. (2015). Advances in development of new treatment for leishmaniasis. *Biomed. Res. Int.* 2015, 15–18. doi: 10.1155/2015/815023
- Egorin, M. J., Lagattuta, T. F., Hamburger, D. R., Covey, J. M., White, K. D., Musser, S. M., et al. (2002). Pharmacokinetics, tissue distribution, and metabolism of 17-(dimethylaminoethylamino)-17-demethoxygeldanamycin (NSC 707545) in CD 2f 1 mice and fischer 344 rats. *Cancer Chemother. Pharmacol.* 49, 7–19. doi: 10.1007/s00280-001-0380-8
- Erlejan, A. G., Lagadari, M., Toneatto, J., Piwien-Pilipuk, G., and Galigniana, M. D. (2014). Regulatory role of the 90-kDa-heat-shock protein (Hsp90) and associated factors on gene expression. *Biochim. Biophys. Acta Gene Regul. Mech.* 1839, 71–87. doi: 10.1016/j.bbagr.2013.12.006
- Fonte, P., Soares, S., Costa, A., Andrade, J. C., Seabra, V., Reis, S., et al. (2012). Effect of cryoprotectants on the porosity and stability of insulin-loaded PLGA nanoparticles after freeze-drying. *Biomater.* 2, 329–339. doi: 10.4161/biom.23246

- Formiga, F. R., Ansorena, E., De Mendonza, A. E., Imbuluzqueta, E., González, D., and Prieto, M. J. B. (2009). *Nanosistemas a base de poliésteres. Nanotecnología Farm. Real. y posibilidades Farmacoter.* Madrid: Real Academia Nacional de Farmacia, 41–101.
- Frézard, F., Demicheli, C., and Ribeiro, R. R. (2009). Pentavalent antimonials: new perspectives for old drugs. *Molecules* 14, 2317–2336. doi: 10.3390/molecules14072317
- Garbuzenko, O. B., Winkler, J., Tomassone, M. S., and Minko, T. (2014). Biodegradable Janus nanoparticles for local pulmonary delivery of hydrophilic and hydrophobic molecules to the lungs. *Langmuir* 30, 12941–12949. doi: 10.1021/la502144z
- Graefe, S. E. B., Wiesgigl, M., Gaworski, I., Macdonald, A., and Clos, J. (2002). Inhibition of HSP90 in *Trypanosoma cruzi* induces a stress response but no stage differentiation. *Eukaryot. Cell* 1, 936–943. doi: 10.1128/EC.1.6.936-943.2002
- Guswanto, A., Nugraha, A. B., Tuvshintulga, B., Tayebwa, D. S., Rizk, M. A., Batiha, G. E. S., et al. (2018). 17-DMAG inhibits the multiplication of several Babesia species and Theileria equi on *in vitro* cultures, and Babesia microti in mice. *Int. J. Parasitol. Drugs Drug Resist.* 8, 104–111. doi: 10.1016/j.ijpddr.2018.02.005
- Hernández-Giottonini, K. Y., Rodríguez-Córdova, R. J., Gutiérrez-Valenzuela, C. A., Peñuñuri-Miranda, O., Zavala-Rivera, P., Guerrero-Germán, P., et al. (2020). PLGA nanoparticle preparations by emulsification and nanoprecipitation techniques: effects of formulation parameters. *RSC Adv.* 10, 4218–4231. doi: 10.1039/C9RA10857B
- Hirenkumar, M., and Steven, S. (2012). Poly Lactic-co-Glycolic Acid (PLGA) as biodegradable controlled drug delivery carrier. *Polymers (Basel)* 3, 1377–1397. doi: 10.3390/polym3031377
- Hombach, A., Ommen, G., Chrobak, M., and Clos, J. (2013). The Hsp90-Sti1 interaction is critical for Leishmania donovani proliferation in both life cycle stages. *Cell. Microbiol.* 15, 585–600. doi: 10.1111/cmi.12057
- Hombach, A., Ommen, G., MacDonald, A., and Clos, J. (2014). A small heat shock protein is essential for thermotolerance and intracellular survival of Leishmania donovani. *J. Cell Sci.* 127, 4762–4773. doi: 10.1242/jcs.157297
- Iqbal, M., Valour, J. P., Fessi, H., and Elaissari, A. (2015). Preparation of biodegradable PCL particles via double emulsion evaporation method using ultrasound technique. *Colloid Polym. Sci.* 293, 861–873. doi: 10.1007/s00396-014-3464-9
- Kapoor, D. N., Bhatia, A., Kaur, R., Sharma, R., Kaur, G., and Dhawan, S. (2015). PLGA: a unique polymer for drug delivery. *Ther. Deliv.* 6, 41–58. doi: 10.4155/tde.14.91
- Kaye, P., and Scott, P. (2011). Leishmaniasis: complexity at the host-pathogen interface. *Nat. Rev. Microbiol.* 9, 604–615. doi: 10.1038/nrmicro2608
- Keum, C. G., Noh, Y. W., Baek, J. S., Lim, J. H., Hwang, C. J., Na, Y. G., et al. (2011). Practical preparation procedures for docetaxel-loaded nanoparticles using polylactic acid-co-glycolic acid. *Int. J. Nanomedicine* 6, 2225–2234. doi: 10.2147/ijn.s24547
- Li, Q., Zhou, Y., Yao, C., Ma, X., Wang, L., Xu, W., et al. (2009). Apoptosis caused by Hsp90 inhibitor geldanamycin in Leishmania donovani during promastigote-to-amastigote transformation stage. *Parasitol. Res.* 105, 1539–1548. doi: 10.1007/s00436-009-1582-y
- Lin, W. (2015). Introduction: nanoparticles in medicine. *Chem. Rev.* 115, 10407–10409. doi: 10.1021/acs.chemrev.5b00534
- Mainardes, R. M., Gremião, M. P. D., Brunetti, I. L., Fonseca, L. M., and Khalil, N. M. (2009). Zidovudine-loaded PLA and PLA-PEG blend nanoparticles: influence of polymer type on phagocytic uptake by polymorphonuclear cells. *Pharm. Nanotechnol.* 98, 257–267. doi: 10.1002/jps.21406
- Masmoudi, A., Hariz, W., Marrekchi, S., Amouri, M., and Turki, H. (2013). Old world cutaneous leishmaniasis: diagnosis and treatment. *J. Dermatol. Case Rep.* 7, 31–41. doi: 10.3315/jdcrr.2013.1135
- McCall, R. L., and Sirianni, R. W. (2013). PLGA nanoparticles formed by single- or double-emulsion with vitamin E-TPGS. *J. Vis. Exp.* e51015. doi: 10.3791/51015
- Meira, C. S., and Gedamu, L. (2019). Protective or detrimental? understanding the role of host immunity in leishmaniasis. *Microorganisms* 7:695. doi: 10.3390/microorganisms7120695
- Mir, M., Ahmed, N., and Rehman, A., ur (2017). Recent applications of PLGA based nanostructures in drug delivery. *Colloids Surf. B Biointerfaces* 159, 217–231. doi: 10.1016/j.colsurfb.2017.07.038
- Nicolette, R., Santos, D. F. D., and Faccioli, L. H. (2011). The uptake of PLGA micro or nanoparticles by macrophages provokes distinct *in vitro* inflammatory response. *Int. Immunopharmacol.* 11, 1557–1563. doi: 10.1016/j.intimp.2011.05.014
- Oryan, A., and Akbari, M. (2016). Worldwide risk factors in leishmaniasis. *Asian Pac. J. Trop. Med.* 9, 925–932. doi: 10.1016/j.apjtm.2016.06.021
- Pallavi, R., Roy, N., Nageshan, R. K., Talukdar, P., Pavithra, S. R., Reddy, R., et al. (2010). Heat shock protein 90 as a drug target against protozoan infections: biochemical characterization of HSP90 from plasmodium falciparum and Trypanosoma evansi and evaluation of its inhibitor as a candidate drug. *J. Biol. Chem.* 285, 37964–37975. doi: 10.1074/jbc.M110.155317
- Palma, L. C., Ferreira, L. F. G. R., Petersen, A. L., de, O. A., Dias, B. R. S., Menezes, J. P. B. de, Moreira, D. R., et al. (2019). A docking-based structural analysis of geldanamycin-derived inhibitor binding to human or Leishmania Hsp90. *Sci. Rep.* 9:14756. doi: 10.1038/s41598-019-51239-0
- Petersen, A. L., de, O. A., Campos, T. A., Santos Dantas, D. A. dos, Rebouças, J., de, S., da Silva, J. C., et al. (2018). Encapsulation of the HSP-90 chaperone inhibitor 17-AAG in stable liposome allow increasing the therapeutic index as assessed, *in vitro*, on Leishmania (L) amazonensis amastigotes-hosted in mouse CBA macrophages. *Front. Cell. Infect. Microbiol.* 8, 1–14. doi: 10.3389/fcimb.2018.00303
- Petersen, A. L., de, O. A., Guedes, C. E. S., Versoza, C. L., Lima, J. G. B., de Freitas, L. A. R., et al. (2012). 17-AAG Kills intracellular Leishmania amazonensis while reducing inflammatory responses in infected macrophages. *PLoS ONE* 7:e49496. doi: 10.1371/journal.pone.0049496
- Pratt, W. B., and Toft, D. O. (2003). Regulation of signaling protein function and trafficking by the hsp90/hsp70-based chaperone machinery. *Exp. Biol. Med.* 228, 111–133. doi: 10.1177/153537020322800201
- Quadros, H. C., Santos, L., de, M. F., Meira, C. S., Khouri, M. I., Mattei, B., et al. (2020). Development and *in vitro* characterization of polymeric nanoparticles containing recombinant adrenomedullin-2 intended for therapeutic angiogenesis. *Int. J. Pharm.* 576:118997. doi: 10.1016/j.ijpharm.2019.118997
- Rafiei, P., and Azita, H. (2017). Docetaxel-loaded Plga and Plga-Peg nanoparticles for intravenous application: pharmacokinetics and biodistribution profile. *Int. J. Nanomed.* 12, 935–947. doi: 10.2147/IJN.S121881
- Rath, S., Augusto Trivelin, L., Imbrunito, T. R., Tomazela, D. M., De Jesús, M. N., Calvo Marzal, P., et al. (2003). Antimoniais empregados no tratamento da leishmaniose: Estado da arte. *Quim. Nova* 26, 550–555. doi: 10.1590/S0100-40422003000400018
- Rietscher, R., Czaplowska, J. A., Majdanski, T. C., Gottschaldt, M., Schubert, U. S., Schneider, M., et al. (2016). Impact of PEG and PEG-b-PAGE modified PLGA on nanoparticle formation, protein loading and release. *Int. J. Pharm.* 500, 187–195. doi: 10.1016/j.ijpharm.2016.01.021
- Rizkalla, N., Range, C., Lacasse, F. X., and Hildgen, P. (2006). Effect of various formulation parameters on the properties of polymeric nanoparticles prepared by multiple emulsion method. *J. Microencapsul.* 23, 39–57. doi: 10.1080/02652040500286185
- Robertson, J. D., Rizzello, L., Avila-Olias, M., Gaitzsch, J., Contini, C., Magoń, M. S., et al. (2016). Purification of Nanoparticles by Size and Shape. *Sci. Rep.* 6, 1–9. doi: 10.1038/srep27494
- Roy, N., Nageshan, R. K., Ranade, S., and Tatu, U. (2012). Heat shock protein 90 from neglected protozoan parasites. *Biochim. Biophys. Acta Mol. Cell Res.* 1823, 707–711. doi: 10.1016/j.bbamcr.2011.12.003
- Salvador, A., Sandgren, K. J., Liang, F., Thompson, E. A., Koup, R. A., Pedraz, J. L., et al. (2015). Design and evaluation of surface and adjuvant modified PLGA microspheres for uptake by dendritic cells to improve vaccine responses. *Int. J. Pharm.* 496, 371–381. doi: 10.1016/j.ijpharm.2015.10.037
- Santos, D. M., Petersen, A. L. O. A., Celes, F. S., Borges, V. M., Veras, P. S. T., and de Oliveira, C. I. (2014). Chemotherapeutic potential of 17-AAG against cutaneous Leishmaniasis caused by Leishmania (Viannia) braziliensis. *PLoS Negl. Trop. Dis.* 8:e3275. doi: 10.1371/journal.pntd.003275
- Santos, D. O., Coutinho, C. E. R., Madeira, M. F., Bottino, C. G., Vieira, R. T., Nascimento, S. B., et al. (2008). Leishmaniasis treatment—a challenge that remains: a review. *Parasitol. Res.* 103, 1–10. doi: 10.1007/s00436-008-0943-2

- Sausville, E. A. (2004). Geldanamycin analogs. *J. Chemother.* 16, 68–69. doi: 10.1179/joc.2004.16.Supplement-1.68
- Schopf, F. H., Biebl, M. M., and Buchner, J. (2017). The HSP90 chaperone machinery. *Nat. Rev. Mol. Cell Biol.* 18, 345–360. doi: 10.1038/nrm.2017.20
- Scorza, B. M., Carvalho, E. M., and Wilson, M. E. (2017). Cutaneous manifestations of human and murine leishmaniasis. *Int. J. Mol. Sci.* 18:1296. doi: 10.3390/ijms18061296
- Seifert, K. (2011). Structures, targets, and recent approaches in anti-leishmanial drug discovery and development. *Open Med. Chem. J.* 5, 31–39. doi: 10.2174/1874104501105010031
- Shah, N. K., Ivone, R., Shen, J., and Meenach, S. A. (2020). A comparison of centrifugation and tangential flow filtration for nanoparticle purification: a case study on acetalated dextran nanoparticles. *Particuology* 50, 189–196. doi: 10.1016/j.partic.2019.06.004
- Shang, L., Nienhaus, K., and Nienhaus, G. U. (2014). Engineered nanoparticles interacting with cells: size matters. *J. Nanobiotechnol.* 12, 1–11. doi: 10.1186/1477-3155-12-5
- Sidera, K., and Patsavoudi, E. (2013). HSP90 inhibitors: current development and potential in cancer therapy. *Recent Pat. Anticancer. Drug Discov.* 9, 1–20. doi: 10.2174/15748928113089990031
- Solit, D. B., and Chiosis, G. (2008). Development and application of Hsp90 inhibitors. *Drug Discov. Today* 13, 38–43. doi: 10.1016/j.drudis.2007.10.007
- Srivastava, S., Shankar, P., Mishra, J., and Singh, S. (2016). Possibilities and challenges for developing a successful vaccine for leishmaniasis. *Parasit. Vectors* 9:277. doi: 10.1186/s13071-016-1553-y
- Sundar, S., Mehta, H., Suresh, A. V., Singh, S. P., Rai, M., and Murray, H. W. (2004). Amphotericin B treatment for Indian visceral leishmaniasis: conventional versus lipid formulations. *Clin. Infect. Dis.* 38, 377–383. doi: 10.1086/380971
- Urbaniak, T., and Musiał, W. (2019). Influence of solvent evaporation technique parameters on diameter of submicron lamivudine-poly-ε-caprolactone conjugate particles. *Nanomaterials* 9:1240. doi: 10.3390/nano9091240
- Utreja, P., Verma, S., Rahman, M., and Kumar, L. (2020). Use of nanoparticles in medicine. *Curr. Biochem. Eng.* 6, 7–24. doi: 10.2174/2212711906666190724145101
- Van Hees, S., Elbrink, K., De Schryver, M., Delputte, P. L., and Kiekens, F. (2020). Improving cellular uptake and cytotoxicity of chitosan-coated poly(lactic-co-glycolic acid) nanoparticles in macrophages. *Nanomedicine* 15, 2671–2688. doi: 10.2217/nnm-2020-0317
- Veras, P. S. T., and De Menezes, J. P. B. (2016). Using proteomics to understand how Leishmania parasites survive inside the host and establish infection. *Int. J. Mol. Sci.* 17:1270. doi: 10.3390/ijms17081270
- Whitesell, L., and Lin, N. U. (2012). HSP90 as a platform for the assembly of more effective cancer chemotherapy. *Biochim. Biophys. Acta Mol. Cell Res.* 1823, 756–766. doi: 10.1016/j.bbamcr.2011.12.006
- WHO (2020a). *Leishmaniasis*. Available online at: https://www.who.int/health-topics/leishmaniasis#tab=tab_1 (accessed October 14, 2020).
- WHO (2020b). *Weekly Epidemiological Record*. Geneva: WHO, 265–280.
- Wiesig, M., Clos, J., and Schekman, R. W. (2001). Heat shock protein 90 homeostasis controls stage differentiation in *Leishmania donovani*. *Mol. Biol. Cell* 12, 3307–3316. doi: 10.1091/mbc.12.11.3307
- Wolfram, J., Zhu, M., Yang, Y., Shen, J., Gentile, E., Paolino, D., et al. (2015). Safety of nanoparticles in medicine. *Curr. Drug Targets* 16, 1671–1681. doi: 10.2174/1389450115666140804124808
- Xiao, L., Lu, X., and Ruden, D. (2006). Effectiveness of Hsp90 inhibitors as anti-cancer drugs. *Mini Rev. Med. Chem.* 6, 1137–1143. doi: 10.2174/138955706778560166
- Yildirimer, L., Thanh, N. T. K., Loizidou, M., and Seifalian, A. M. (2011). Toxicological considerations of clinically applicable nanoparticles. *Nano Today* 6, 585–607. doi: 10.1016/j.nantod.2011.10.001
- Zambaux, M. F., Bonneaux, F., Gref, R., Maincent, P., Dellacherie, E., Alonso, M. J., et al. (1998). Influence of experimental parameters on the characteristics of poly(lactic acid) nanoparticles prepared by a double emulsion method. *J. Control. Release* 50, 31–40. doi: 10.1016/S0168-3659(97)00106-5
- Zhang, L., Gu, F. X., Chan, J. M., Wang, A. Z., Langer, R. S., and Farokhzad, O. C. (2008). Nanoparticles in medicine: therapeutic applications and developments. *Clin. Pharmacol. Ther.* 83, 761–769. doi: 10.1038/sj.clpt.6100400
- Zhang, X., and Zhang, P. (2017). Polymersomes in nanomedicine—a review. *Curr. Nanosci.* 13, 124–129. doi: 10.2174/1573413712666161018144519
- Zhao, R., and Houry, W. A. (2005). Hsp90: a chaperone for protein folding and gene regulation. *Biochem. Cell Biol.* 83, 703–710. doi: 10.1139/o05-158
- Zilberstein, D., and Shapira, M. (1994). The role of pH and temperature in the development of leishmania parasites. *Annu. Rev. Microbiol.* 48, 449–470. doi: 10.1146/annurev.mi.48.100194.002313

Conflict of Interest: The authors declare that the research was conducted in the absence of any commercial or financial relationships that could be construed as a potential conflict of interest.

Copyright © 2021 Cruz, Patricio, Pires, Amorim, Pinho, Quadros, Dantas, Chaves, Formiga, Rocha and Veras. This is an open-access article distributed under the terms of the Creative Commons Attribution License (CC BY). The use, distribution or reproduction in other forums is permitted, provided the original author(s) and the copyright owner(s) are credited and that the original publication in this journal is cited, in accordance with accepted academic practice. No use, distribution or reproduction is permitted which does not comply with these terms.



Benzopyrazine-Based Small Molecule Inhibitors As Trypanocidal and Leishmanicidal Agents: Green Synthesis, *In Vitro*, and *In Silico* Evaluations

Jonathan Rock¹, Daniel Garcia¹, Omar Espino¹, Shaila A. Shetu¹, Manuel J. Chan-Bacab², Rosa Moo-Puc³, Navin B. Patel⁴, Gildardo Rivera^{5*} and Debasish Bandyopadhyay^{1,6*}

¹Department of Chemistry, University of Texas Rio Grande Valley, Edinburg, TX, United States, ²Departamento de Microbiología Ambiental y Biotecnología, Universidad Autónoma de Campeche, Campeche, México, ³Unidad Médica de Alta Especialidad, Instituto Mexicano Del Seguro Social, Mérida, México, ⁴Department of Chemistry, Veer Narmad South Gujarat University, Gujrat, India, ⁵Laboratorio de Biotecnología Farmacéutica, Centro de Biotecnología Genómica, Instituto Politécnico Nacional, Reynosa, México, ⁶School of Earth Environment and Marine Sciences (SEEMS), University of Texas Rio Grande Valley, Edinburg, TX, United States

OPEN ACCESS

Edited by:

Tara Louise Pukala,
University of Adelaide, Australia

Reviewed by:

Marcus Scotti,
Federal University of Paraíba, Brazil
Guillermo R. Labadie,
National University of Rosario,
Argentina

*Correspondence:

Debasish Bandyopadhyay,
debasish.bandyopadhyay@utrgv.edu
Gildardo Rivera
gildardors@hotmail.com

Specialty section:

This article was submitted to
Medicinal and Pharmaceutical
Chemistry,
a section of the journal
Frontiers in Chemistry

Received: 16 June 2021

Accepted: 01 September 2021

Published: 17 September 2021

Citation:

Rock J, Garcia D, Espino O, Shetu SA,
Chan-Bacab MJ, Moo-Puc R,
Patel NB, Rivera G and
Bandyopadhyay D (2021)
Benzopyrazine-Based Small Molecule
Inhibitors As Trypanocidal and
Leishmanicidal Agents: Green
Synthesis, *In Vitro*, and *In Silico*
Evaluations.
Front. Chem. 9:725892.
doi: 10.3389/fchem.2021.725892

World Health Organization (WHO) identified twenty tropical disease categories as neglected tropical diseases (NTDs)¹. Chagas' disease (also known as American trypanosomiasis) and leishmaniasis are two major classes of NTDs. The total number of mortality, morbidity, and disability attributed each year due to these two categories of diseases in magnitudes is much higher than the so-called elite diseases like cancer, diabetes, AIDS, cardiovascular and neurodegenerative diseases. Impoverished communities around the world are the major victim of NTDs. The development of new and novel drugs in the battle against Chagas' disease and leishmaniasis is highly anticipated. An easy and straightforward on-water green access to synthesize benzopyrazines is reported. This ultrasound-assisted procedure does not require any catalyst/support/additive/hazardous solvents and maintains a high atom economy. A series of eleven benzopyrazines has been synthesized, and most of the synthesized compounds possess the drug-likeness following Lipinski's "Rule of 5". Benzopyrazines **3** and **4** demonstrated moderate leishmanicidal activity against *L. mexicana* (M378) strain. The selective lead compound **1** showed good leishmanicidal, and trypanocidal activities (*in vitro*) against both *L. mexicana* (M378) and *T. cruzi* (NINOA) strains compared to the standard controls. The *in vitro* trypanocidal and leishmanicidal activities of the lead compound **1** have been validated by molecular docking studies against four biomolecular drug targets viz. *T. cruzi* histidyl-tRNA synthetase, *T. cruzi* trans-sialidase, leishmanial rRNA A-site, and leishmania major *N*-myristoyl transferase.

Keywords: trypanocidal¹, leishmanicidal², trypanosoma cruzi³, small molecule inhibitors⁴, quinoxalines⁵, ecofriendly⁶, on-water⁷

¹Respectfully dedicated to Professor (Dr.) Julie Banerji and Professor (Dr.) Avijit Banerji on the occasion of their 75th birth anniversaries.

INTRODUCTION

Heterocycles play a significant role in drug discovery research. A considerable number of the small molecule inhibitors are heterocyclic compounds. Among various classes of heterocycles, for example, aza-, oxo-, phospho-, thioheterocycles; aza- or nitrogen heterocycles are found in many pharmacologically relevant compounds natural and synthetic. Benzopyrazine (also known as quinoxaline) is a fused bicyclic scaffold in which benzene is fused with pyrazine (Bandyopadhyay and Banik, 2021). A few naturally occurring antibiotics and nutrients like vitamin B2 contain benzopyrazine moiety as a core in their structures (Figure 1). This scaffold is present as the key structural motif in many biologically active compounds, which includes anticancer (Lee et al., 2012; Bandyopadhyay et al., 2013; Qi et al., 2018), antibacterial (El-Attar et al., 2018), antitubercular (Achutha et al., 2013), anti-ebola (Loughran et al., 2016), antifungal (Carta et al., 2001) among many others. Consequently, several procedures of synthesizing benzopyrazines have been reported in the literature. A few synthetic procedures, reported in the immediate past, include the synthesis of benzopyrazines under the catalytic influence of Co_3O_4 nanocages based nickel catalyst (Sharma et al., 2021), iron-catalyzed transfer hydrogenative condensation (Putta et al., 2021), sodium hydroxide-mediated hydrogen-transfer (Wang et al., 2021), as well as the uses of tungstophosphoric acid-support (Kumaresan et al., 2020), and Co-based nanocatalyst (Panja et al., 2020).

On the other hand, the World Health Organization (WHO) identified twenty tropical disease categories as neglected tropical diseases (NTDs). In general, the population below the poverty

line are the primary sufferers of NTDs. Every year millions of people from 149 countries worldwide are being infected by NTDs that cause the waste of billions of dollars and a loss of thousands of lives. Based on the mortality and morbidity rates, Chagas' disease (named after the Latin American physician Carlos Chagas, also known as American trypanosomiasis) and leishmaniasis are two major categories of NTDs that demand immediate attention from the global community (Maheshwari and Bandyopadhyay, 2021). We report herein an ultrasound-assisted on-water green synthesis of diversely substituted benzopyrazine derivatives (Scheme 1) and subsequent *in vitro* trypanocidal and leishmanicidal evaluation of these compounds. Further, we hypothesize that the biological (trypanocidal and leishmanicidal) activity is due to the interaction and subsequent inhibition of the protozoal proteins responsible for these diseases. In addition, we validated our hypothesis through *in silico* docking study.

MATERIALS AND METHODS

General

We determined the melting points of the final products by a digital melting point apparatus (DigiMelt MPA 160 by SRS). Elemental (CHN) analyses were carried out by a PerkinElmer 2,400 Series II elemental analyzer, their results were found to be in good agreement ($\pm 0.5\%$) with the calculated values. Sonication was performed with the UP200St (200W, 26kHz) ultra-sonicator (Hielscher Ultrasonics GmbH, Germany). FT-IR spectra were recorded on a Bruker Alpha modular Platinum-ATR FT-IR spectrometer with OPUS software, using the samples directly

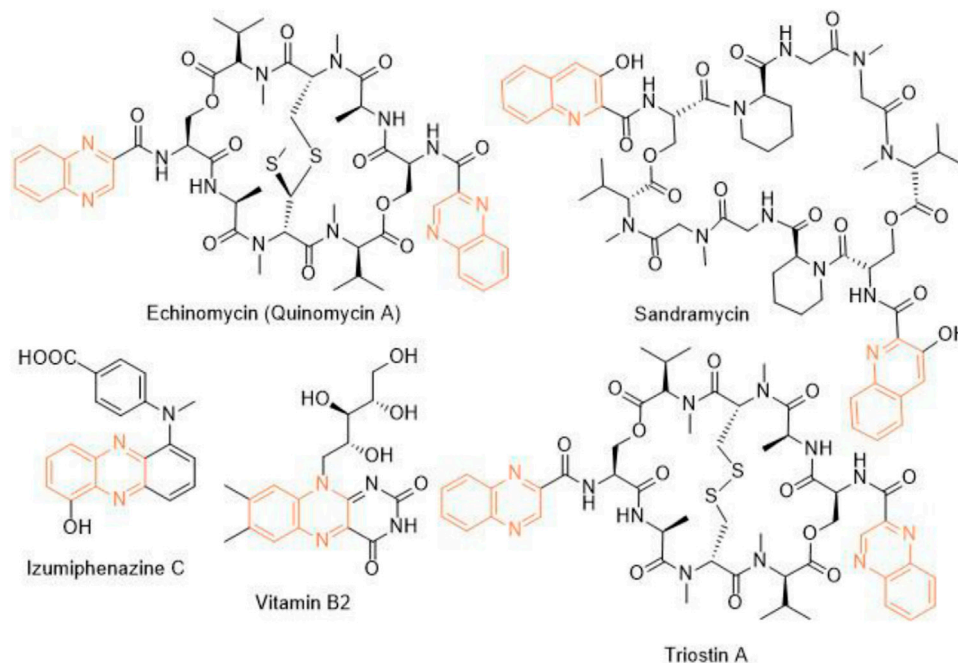
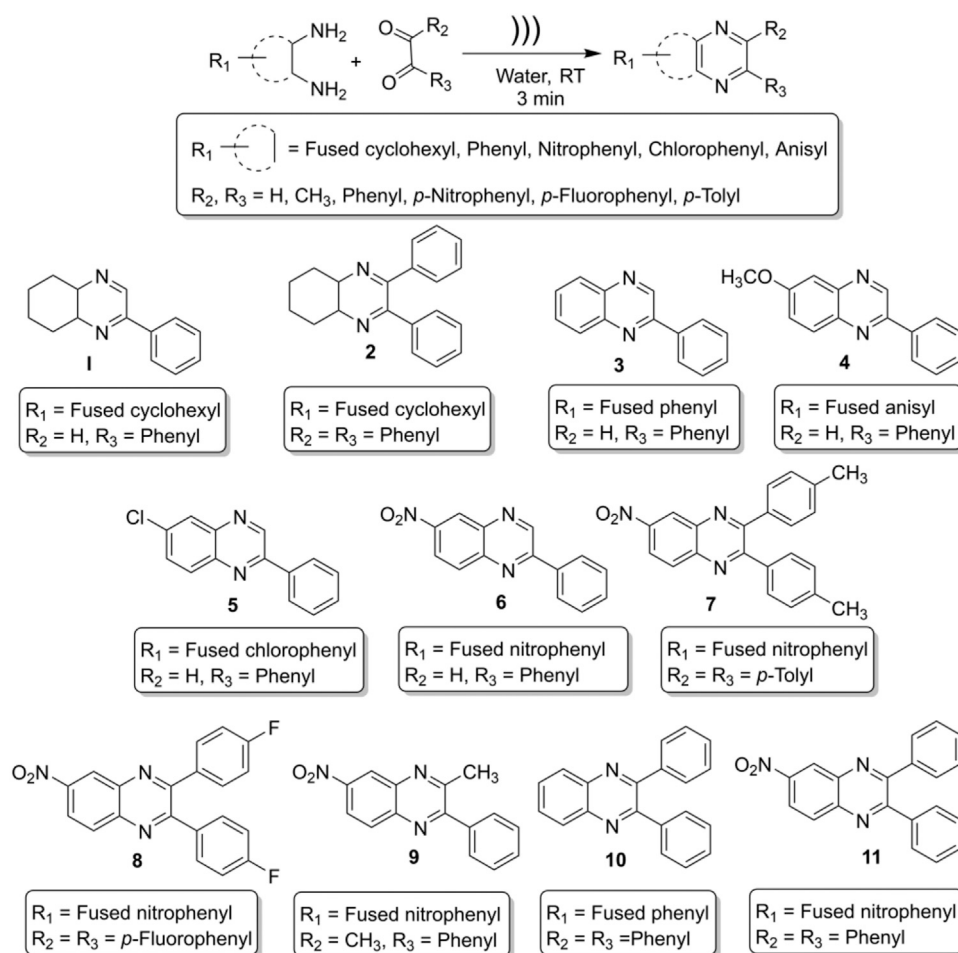


FIGURE 1 | Representative examples of naturally occurring bioactive benzopyrazines.



SCHEME 1 | Ultrasound-assisted on-water green synthesis of diverse benzopyrazines.

(neat) without making pallets. ¹H NMR (600 MHz) and ¹³C NMR (150 MHz) spectra were obtained at room temperature with Bruker superconducting Ultrashield Plus 600 MHz NMR spectrometer with central field 14.09 T, coil inductance 89.1 Hz, and magnetic energy 1,127.2 kJ using CDCl₃ or d₆-DMSO as solvent. Chemicals were purchased from Sigma-Aldrich, Inc. (St. Louis, MO) and VWR International (Missouri, TX). Solvents were purchased from Fisher Scientific International Inc. (Pittsburgh, PA) throughout the investigation.

General Procedure for the Synthesis of Benzopyrazines

In a general procedure of this on-water reaction, *ortho*-diamine and dicarbonyl compounds were mixed (1:1 M ratio) in a hard glass test tube, and 1 ml tap water was added to the reaction mixture. In a model reaction, 1 ml water was taken in a hard glass test tube, and 1 mmol of *o*-phenylene diamine (108 mg) and 1 mmol of phenylglyoxal hydrate (134 mg) were added into the test tube. The ultrasonic probe was inserted into the test tube (reaction mixture), and the mixture was sonicated. The reaction was monitored by thin-layer chromatography (TLC) every after 1 minute. The most intense TLC

spot was seen after 3 minutes. Further sonication did not increase the intensity of the product spot; rather, it reduced the product and generated gummy material. Initially, the reaction was carried out in deionized water, but no significant change in yield was observed compared to tap water. At the end of the reaction, the product looked like a chunk, and it was not soluble in water. Consequently, the product was extracted with 9 ml (3 × 3 mL) of ethyl acetate. The organic layer was dried over sodium sulfate and concentrated by reduced pressure distillation by a rotary evaporator. The crude mass was passed quickly through a purification column with ethyl acetate to get highly pure (>98%) and crystalline compounds. The spectral data of the compounds are given below:

2-phenyl-4a,5,6,7,8,8a-hexahydroquinoxaline (1, Scheme 1). Brownish-yellow amorphous solid (206 mg, 97%); m. p. 135–136°C; IR (KBr) 3,415, 1,660, 1,536, 1,448, 1,294, 764 cm⁻¹; ¹H NMR (600 MHz, CDCl₃) δ 1.46–2.18 (m, 8H), 3.66 (br s, 1H), 3.77 (d, *J* = 3.60 Hz, 1H), 7.42 (s, 1H), 7.48–7.50 (m, 2H), 7.86 (dd, *J* = 7.56, 1.38 Hz, 2H), 8.39 (d, *J* = 2.10 Hz, 1H); ¹³C NMR (150 MHz, CDCl₃) 22.35, 22.66, 27.75, 28.07, 54.11, 54.21, 126.59, 128.77, 130.55, 136.12, 151.62, 155.44. Anal. Calcd for C₁₄H₁₆N₂: C, 79.21; H, 7.60; N, 13.20. Found: C, 79.09; H, 7.52; N, 13.11.

TABLE 1 | The yield, and atom economy in the synthesis of benzopyrazines (**1–11**).

Compound	Yield (%) ^a	Atom economy
1	97	85.48
2	96	88.89
3	94	76.92
4	92	80.00
5	95	76.92
6	98	78.57
7	99	86.36
8	93	84.21
9	97	80.00
10	96	83.33
11	98	84.21

^aIsolated yield.

2,3-diphenyl-4a,5,6,7,8,8a-hexahydroquinoxaline (2, Scheme 1). Greenish-yellow crystalline solid (276 mg, 96%); m. p. 94–95°C; IR (KBr) 3,312, 3,061, 2,930, 2,851, 1,665, 1,560, 1,489, 1,446, 1,240, 1,184, 1,077, 1,012, 758, 698 cm⁻¹; ¹H NMR (600 MHz, CDCl₃) δ 1.48–1.85 (m, 8H), 3.84 (br s, 2H), 7.24–7.39 (m, 10H); ¹³C NMR (150 MHz, CDCl₃) δ 22.51, 27.42, 55.01, 127.92, 128.01, 129.26, 138.29, 159.49. Anal. Calcd for C₂₀H₂₀N₂: C, 83.30; H, 6.99; N, 9.71. Found: C, 83.18; H, 6.87; N, 9.58.

2-Phenylquinoxaline (3, Scheme 1). Light brown crystalline solid (194 mg, 94%); m. p. 77–79°C; IR (v in cm⁻¹): 1727, 1,538, 1,482, 1,303, 1,124, 1,027, 951, 760, 682, 550; ¹H NMR (600 MHz, CDCl₃) δ 7.52–7.59 (m, 3H), 7.74–7.80 (m, 2H), 8.14 (d, *J* = 8.16 Hz, 1H), 8.17 (d, *J* = 8.22 Hz, 1H), 8.21 (d, *J* = 7.62 Hz, 2H), 9.34 (s, 1H); ¹³C NMR (150 MHz, CDCl₃) δ 127.57, 129.14, 129.16, 129.54, 129.65, 130.20, 130.28, 136.80, 141.60, 142.32, 143.37, 151.85. Anal. Calcd for C₁₄H₁₀N₂: C, 81.53; H, 4.89; N, 13.58. Found: C, 81.18; H, 4.87; N, 14.06.

6-Methoxy-2-phenylquinoxaline (4, Scheme 1): White crystalline solid (217 mg, 92%); m. p. 75–77°C; IR (v in cm⁻¹): 1,616, 1,541, 1,508, 1,489, 1,456, 1,374, 1,314, 1,212, 1,117, 1,019, 827, 754, 687; ¹H NMR (600 MHz, CDCl₃) δ 3.90 (s, 3H), 7.30 (dd, *J* = 8.95, 2.76 Hz, 1H), 7.35 (d, *J* = 2.70 Hz, 1H), 7.43–7.49 (m, 3H), 7.90 (d, *J* = 9.06 Hz, 1H), 8.07 (s, 1H), 8.08 (m, 1H), 9.08 (s, 1H); ¹³C NMR (150 MHz, CDCl₃) δ 55.84, 106.91, 122.89, 127.52, 129.10, 129.12, 130.05, 137.02, 137.80, 140.76, 143.98, 151.95, 161.08. Anal. Calcd for C₁₅H₁₂N₂O: C, 76.25; H, 5.12; N, 11.86. Found: C, 77.01; H, 4.91; N, 12.13.

6-Chloro-2-phenylquinoxaline (5, Scheme 1): Light brown crystalline solid (215 mg, 95%); m. p. 146–147°C; IR (v in cm⁻¹): 1,699, 1,540, 1,481, 1,449, 1,315, 1,223, 1,132, 1,073, 958, 829, 756, 711, 687; ¹H NMR (600 MHz, CDCl₃) δ 7.47–7.51 (m, 3H), 7.61 (dd, *J* = 8.85, 2.22 Hz, 1H), 7.98 (d, *J* = 8.82 Hz, 1H), 8.01–8.04 (m, 1H), 8.08 (d, *J* = 2.16 Hz, 1H), 8.10–8.12 (m, 1H), 9.24 (s, 1H); ¹³C NMR (150 MHz, CDCl₃) δ 127.54, 127.63, 129.24, 130.37, 130.46, 130.54, 130.57, 136.34, 140.12, 142.68, 143.44, 152.59. Anal. Calcd for C₁₄H₉ClN₂: C, 69.86; H, 3.77; N, 11.64. Found: C, 70.23; H, 4.06; N, 10.88.

6-Nitro-2-phenylquinoxaline (6, Scheme 1): Pale yellow crystalline solid (246 mg, 98%); m. p. 210–211°C; IR (v in cm⁻¹): 1,616, 1,556, 1,522, 1,348, 1,316, 1,077, 851, 832, 791, 764, 691; ¹H NMR (600 MHz, CDCl₃) δ 7.52–7.55 (m, 3H),

8.16–8.21 (m, 3H), 8.47 (dd, *J* = 9.12, 2.52 Hz, 1H), 8.95 (d, *J* = 2.46 Hz, 1H), 9.42 (s, 1H); ¹³C NMR (150 MHz, CDCl₃) δ 123.79, 125.67, 127.95, 129.43, 131.19, 131.41, 135.64, 140.36, 144.93, 145.50, 147.47, 154.33. Anal. Calcd for C₁₄H₉ClN₂: C, 69.86; H, 3.77; N, 11.64. Found: C, 70.23; H, 4.06; N, 10.88.

6-Nitro-2,3-di-*p*-tolylquinoxaline (7, Scheme 1): Yellow crystalline solid (352 mg, 99%); m. p. 162–163°C; IR (v in cm⁻¹): 1,521, 1,339, 1,182, 1,050, 978, 818, 723, 601, 545, 530; ¹H NMR (600 MHz, CDCl₃) δ 2.41 (s, 6H), 7.21 (d, *J* = 7.86 Hz, 4H), 7.49 (t, *J* = 7.80 Hz, 4H), 8.27 (d, *J* = 9.12 Hz, 1H), 8.50–8.52 (m, 1H), 9.05 (d, *J* = 2.46 Hz, 1H); ¹³C NMR (150 MHz, CDCl₃) δ 21.42, 21.43, 123.02, 125.54, 129.19, 129.74, 129.84, 130.61, 135.38, 135.43, 139.83, 139.87, 140.03, 143.56, 147.70, 155.70, 156.32. Anal. Calcd for C₂₂H₁₇N₃O₂: C, 74.35; H, 4.82; N, 11.82. Found: C, 73.98; H, 4.53; N, 12.01.

2,3-Bis(4-fluorophenyl)-6-nitroquinoxaline (8, Scheme 1): Yellowish solid (337 mg, 93%); m. p. 157–159°C; IR (v in cm⁻¹): 1,599, 1,528, 1,512, 1,397, 1,341, 1,230, 1,163, 1,050, 978, 846, 726, 564; ¹H NMR (600 MHz, CDCl₃) δ 7.11 (t, *J* = 8.46 Hz, 4H), 7.56–7.60 (m, 4H), 8.29 (d, *J* = 9.12 Hz, 1H), 8.55 (dd, *J* = 9.12, 2.46 Hz, 1H), 9.06 (d, *J* = 2.46 Hz, 1H); ¹³C NMR (150 MHz, CDCl₃) δ 115.74, 115.89, 123.51, 125.54, 130.72, 131.81, 131.91, 131.97, 132.02, 133.95, 133.98, 134.02, 134.04, 139.92, 143.48, 148.01, 154.37, 154.97, 162.86, 164.61. Anal. Calcd for C₂₀H₁₁F₂N₃O₂: C, 66.12; H, 3.05; N, 11.57. Found: C, 66.58; H, 3.07; N, 11.33.

3-Methyl-6-nitro-2-phenylquinoxaline (9, Scheme 1): Light yellow crystalline solid (257 mg, 97%); m. p. 131–133°C; IR (v in cm⁻¹): 1,519, 1,398, 1,328, 1,071, 1,003, 897, 818, 764, 741, 693, 588; ¹H NMR (600 MHz, CDCl₃) δ 2.78 (s, 3H), 7.49 (t, *J* = 1.56 Hz, 3H), 7.61 (d, *J* = 5.58 Hz, 2H), 8.10–8.17 (m, 1H), 8.40–8.44 (m, 1H), 8.94 (s, 1H); ¹³C NMR (150 MHz, CDCl₃) δ 23.85, 12,211, 124.67, 127.73, 127.91, 127.93, 128.72, 128.99, 136.88, 138.82, 142.64, 155.32, 156.15. Anal. Calcd for C₁₅H₁₁N₃O₂: C, 67.92; H, 4.18; N, 15.84. Found: C, 68.05; H, 4.10; N, 15.79.

2,3-Diphenylquinoxaline (10, Scheme 1): Colorless crystals (271 mg, 96%); m. p. 118–121°C; IR (v in cm⁻¹): 1,665, 1,560, 1,489, 1,240, 1,184, 1,077, 1,012, 877, 807, 758, 698; ¹H NMR (600 MHz, CDCl₃) δ 7.36–7.40 (m, 6H), 7.55 (m, 4H), 7.79 (dd, *J* = 4.86, 3.00 Hz, 2H), 8.21 (dd, *J* = 4.86, 2.88 Hz, 2H); ¹³C NMR (150 MHz, CDCl₃) δ 128.30, 128.83, 129.24, 129.89, 129.98, 139.13, 141.27, 153.49. Anal. Calcd for C₂₀H₁₄N₂: C, 85.08; H, 5.00; N, 9.92. Found: C, 84.97; H, 5.11; N, 10.02.

6-Nitro-2,3-diphenylquinoxaline (11, Scheme 1): Deep yellow solid (321 mg, 98%); m. p. 182–184°C; IR (v in cm⁻¹): 1,520, 1,341, 1,188, 1,063, 1,024, 979, 698; ¹H NMR (600 MHz, CDCl₃) δ 7.38–7.46 (m, 6H), 7.57–7.60 (m, 4H), 8.31 (d, *J* = 9.18 Hz, 1H), 8.54 (dd, *J* = 2.46, 9.12 Hz, 1H), 9.09 (d, *J* = 2.52 Hz, 1H); ¹³C NMR (150 MHz, CDCl₃) δ 123.30, 125.64, 128.47, 129.65, 129.84, 129.92, 130.77, 138.05, 138.12, 139.99, 143.59, 147.90, 155.70, 156.32. Anal. Calcd for C₂₀H₁₃N₃O₂: C, 73.38; H, 4.00; N, 12.84. Found: C, 73.69; H, 4.06; N, 12.71.

Trypanocidal and Leishmanicidal (*in vitro*) Evaluations

We used the promastigotes of *L. mexicana* (MHOM/MX/ ISETGS) clinical strain for the leishmanicidal growth

TABLE 2 | IC₅₀ (μM ± SD) of the benzopyrazine (**1–11**) against epimastigotes from *T. cruzi* and promastigote from *L. mexicana*.

Compound	<i>L. mexicana</i> (M378)	<i>T. cruzi</i> (NINOA)
1	12.46 ± 0.62	37.85 ± 0.52
2	>100	>100
3	50.86 ± 1.02	>100
4	39.83 ± 0.29	>100
5	>100	>100
6	>100	>100
7	>100	>100
8	>100	>100
9	>100	>100
10	>100	>100
11	>100	>100
Miltefosine	—	19.56 ± 0.61
Nifurtimox	9.32 ± 0.31	—

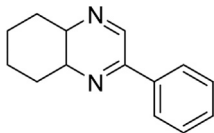
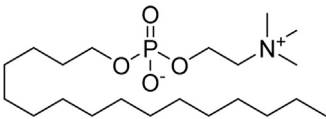
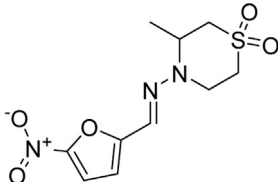
inhibition assay. The clinical strain was initially isolated from a patient suffering from diffuse cutaneous leishmaniasis. We carried out the trypanocidal assay with the epimastigotes of *T. cruzi* (MHOM/MX/1994/NINOA). The clinical strain was originally isolated from a patient with the disease in the acute phase for this assay. Schneider's *Drosophila* medium, supplemented with 10% fetal bovine serum, penicillin (100 IU/ml), and streptomycin (100 μg/ml), was used to culture the parasites at 26°C. The antiprotozoal assays were carried out in 96-well plates using dimethyl sulfoxide (DMSO) as the

carrier. The standard controls and the testing compounds were solubilized in DMSO and diluted as required. All the antiprotozoal assays were performed in duplicate. Aliquots of 100 μL of compound solution and 100 μL of culture medium containing 10,000 *Leishmania* promastigotes or 20,000 *T. cruzi* epimastigotes were combined to obtain concentrations of 50, 25, 12.5, 6.25, 3.125 μg/ml, and so on. Two first-line commercial drugs nifurtimox (antichagasic drug) and miltefosine (leishmanicidal drug), were used as positive controls. Only the parasite-containing culture was used as the negative control. The plates were incubated for 72 h at a temperature of 26°C, and the antiprotozoal activity of the compounds was determined by direct count of parasites in a Neubauer chamber (Chan-Bacab et al., 2009). The IC₅₀ values (the concentration required to inhibit 50% of parasite growth were calculated (in μg/mL) by probit analysis (Hernández-Núñez et al., 2009).

In Silico Molecular Docking Studies

We conducted the *in silico* molecular docking study following our previously published procedure (Laskar et al., 2019). In brief, the ligands were prepared with their corresponding assigned atoms types and charges using ChemOffice 2015 as MOL files and converted to PDB and PDBQT sequentially following a few steps utilizing open-source and well-known graphic user interface software. We imported the control drugs (positive controls) from ChemSpider as MOL format; if not, control ligands were manually prepared from scratch. Crystal structures of the four proteins 4YPF, 1S0J, 4K32,

TABLE 3 | Molecular docking scores of the compound **1** and the standard controls with the biomolecular targets.

Compound	Structure	Docking score ^a (PDB ID: 4YPF)	Docking score ^a (PDB ID: 1S0J)	Docking score ^a (PDB ID: 4K32)	Docking score ^a (PDB ID: 6QDA)
1		-6.7	-7.3	-6.3	-7.4
Miltefosine		-4.7	-5.4	-4.9	-6.0
Nifurtimox		-7.0	-7.8	-6.6	-7.5

^aBinding affinity [kcal/mol].

4YPF: Crystal structure of *T. cruzi* Histidyl-tRNA synthetase in complex with quinolin-3-amine.

1S0J: Trypanosoma cruzi trans-sialidase in complex with MuNANA (Michaelis complex).

4K32: Crystal structure of geneticin bound to the leishmanial rRNA A-site.

6QDA: *Leishmania major* N-myristoyltransferase in complex with quinazoline inhibitor IMP-0000811.

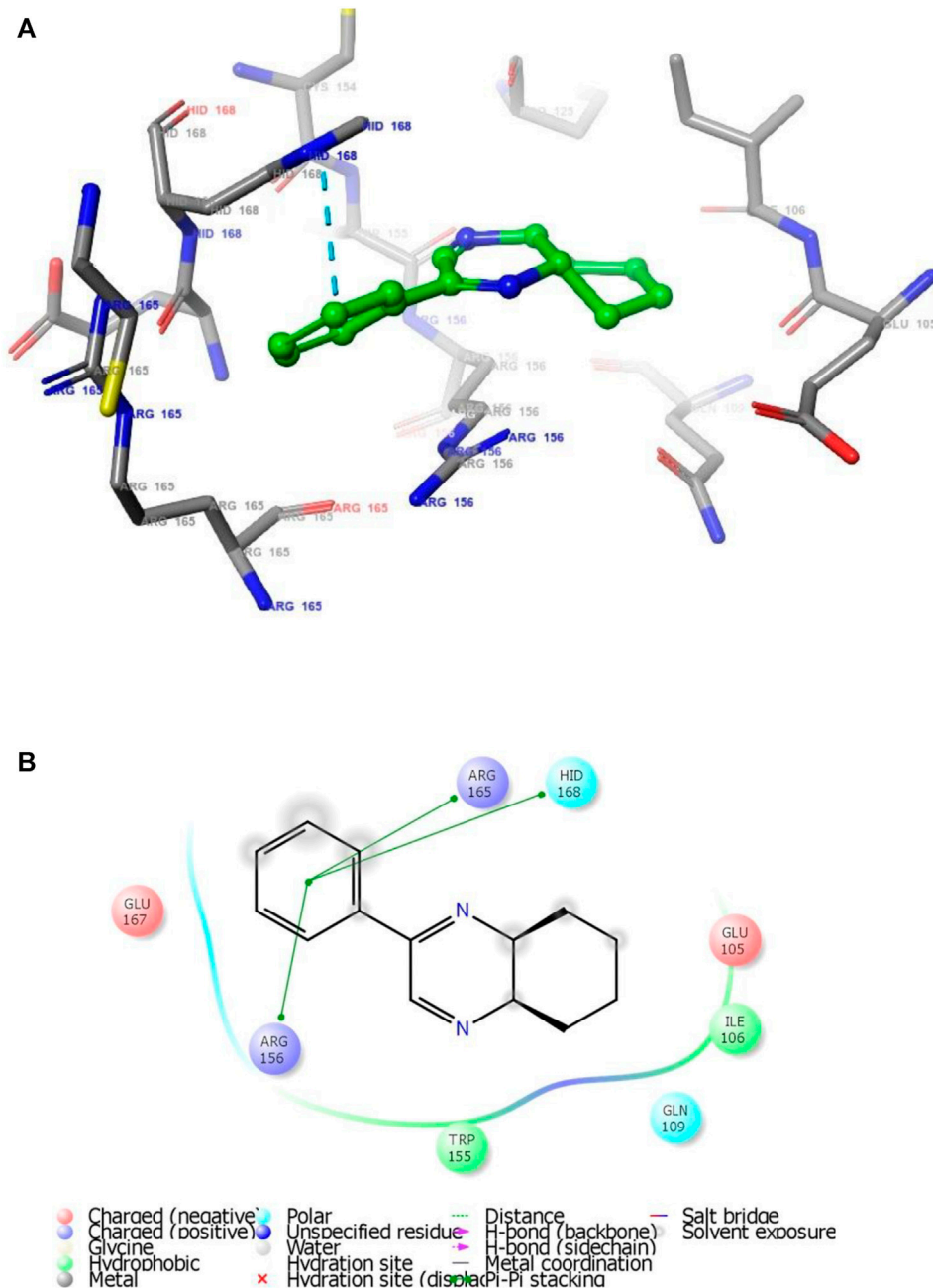


FIGURE 2 | (A) The binding mode of the interactions between **1** with *T. cruzi* Histidyl-tRNA synthetase (PDB ID: 4YPF). **(B)** Results of the validation of **1** inside the *T. cruzi* histidyl-tRNA synthetase active sites.

6QDA (biological targets in this study) were imported from RCSB (Rose et al., 2011) (<http://www.rcsb.org>), a member of Worldwide Protein Data Bank (wwPDB). The MOL formats of the ligands were changed to PDB format by Avogadro software (Hanwell et al., 2012). The ligands were saved in .pdb format and AutoDock4. AutoDockTools 1.5.6, part of AutoDock4 (AD4), were used to alter the ligands and receptors (proteins) from PDB to PDBQT formats. PDBQT format provides the molecular structure coordinate files, including atomic partial charges, atom types,

torsional flexibility information, etc. The ligand files (in.pdb form) were loaded onto the AutoDockTools dashboard to detect torsion root, rotatable bonds and add gasteiger charges for atomic charges, if necessary. The receptor-binding sites were localized using the Adaptive Poisson-Boltzmann Solver (APBS) plugin for surface electrostatic calculation and Computed Atlas Surface Topology of proteins (CASTp) for a pocket that void detection on the protein surface (Liang et al., 1998). Binding site visualization was made feasible by Schrödinger Maestro, AutoDock4, PyMOL, and other

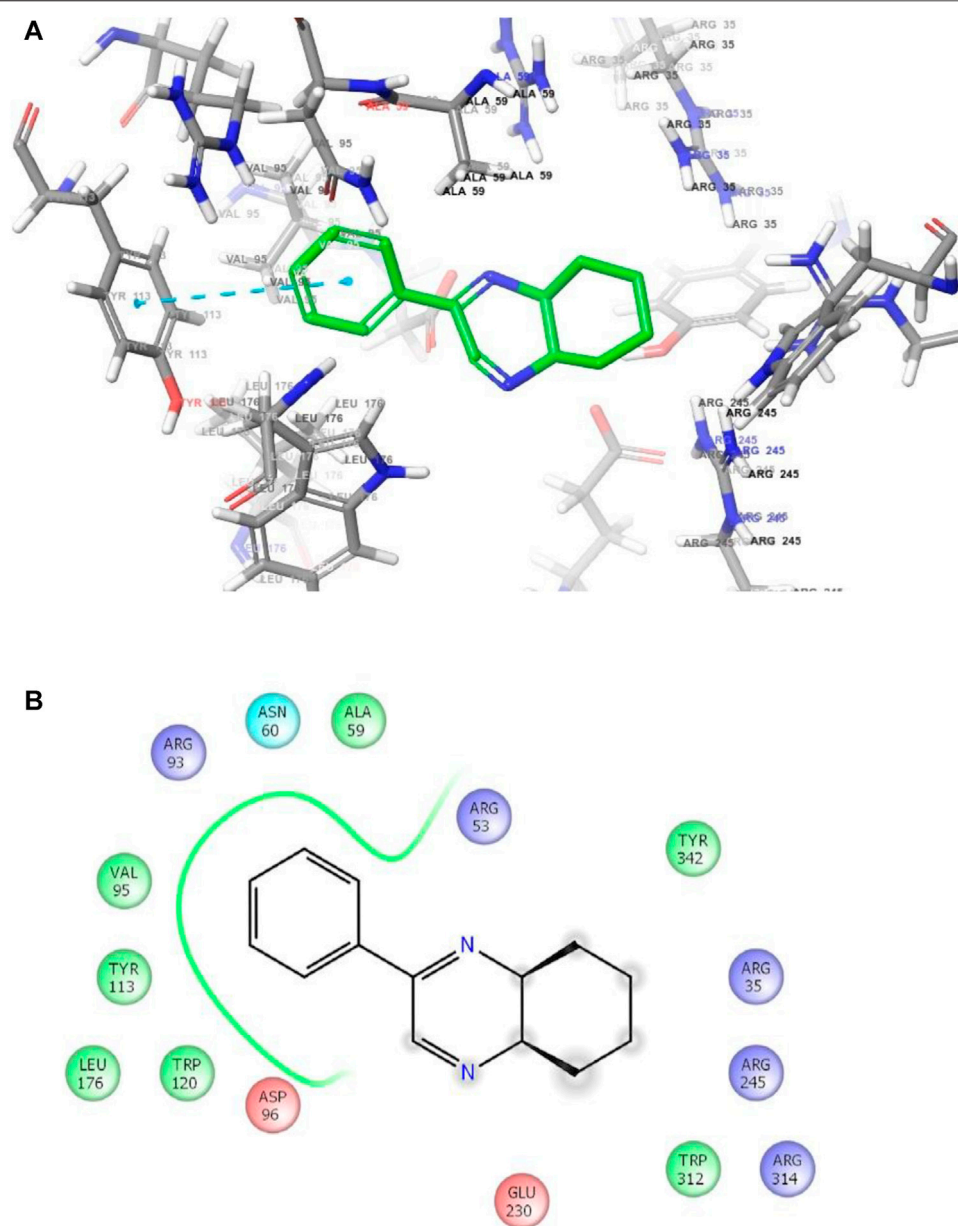


FIGURE 3 | (A) The binding mode of the interactions between **1** with *T. cruzi* trans-sialidase (PDB ID: 1SQJ). **(B)** Results of the validation of **1** inside the *T. cruzi* trans-sialidase active sites.

software. (Morris et al., 2009; Seeliger and de Groot, 2010; Schrödinger Release 2016-4, 2016; PyMOL Molecular Graphics System, 2015; Pettersen et al., 2004). These software packages offer a complete molecular viewer and graphic user interface, which are essential for structure-based drug design and discovery. PDBQT structure formats are compatible with AutoDock Vina (Trott and Olson, 2010), a complementary AD4 molecular docking program, and are required to run the docking simulations. We used the Schrödinger Maestro to visualizing and preparing the PDB receptor and ligand conformation

files for docking. We uploaded the receptor files to the Maestro workspace, and the binding site surface area was calculated using the Task Tree search bar and selecting Binding Surface Area Analysis. The resulting free energy binding affinities (in kcal/mol) were recorded as docking scores. These scores were considered to evaluate the strength of non-covalent interaction between different receptor-ligand conformations. A conformer with the lowest energy and highest cluster counts was regarded as the best ligand conformation that fits the binding site. The structural analysis was effectuated in Schrödinger

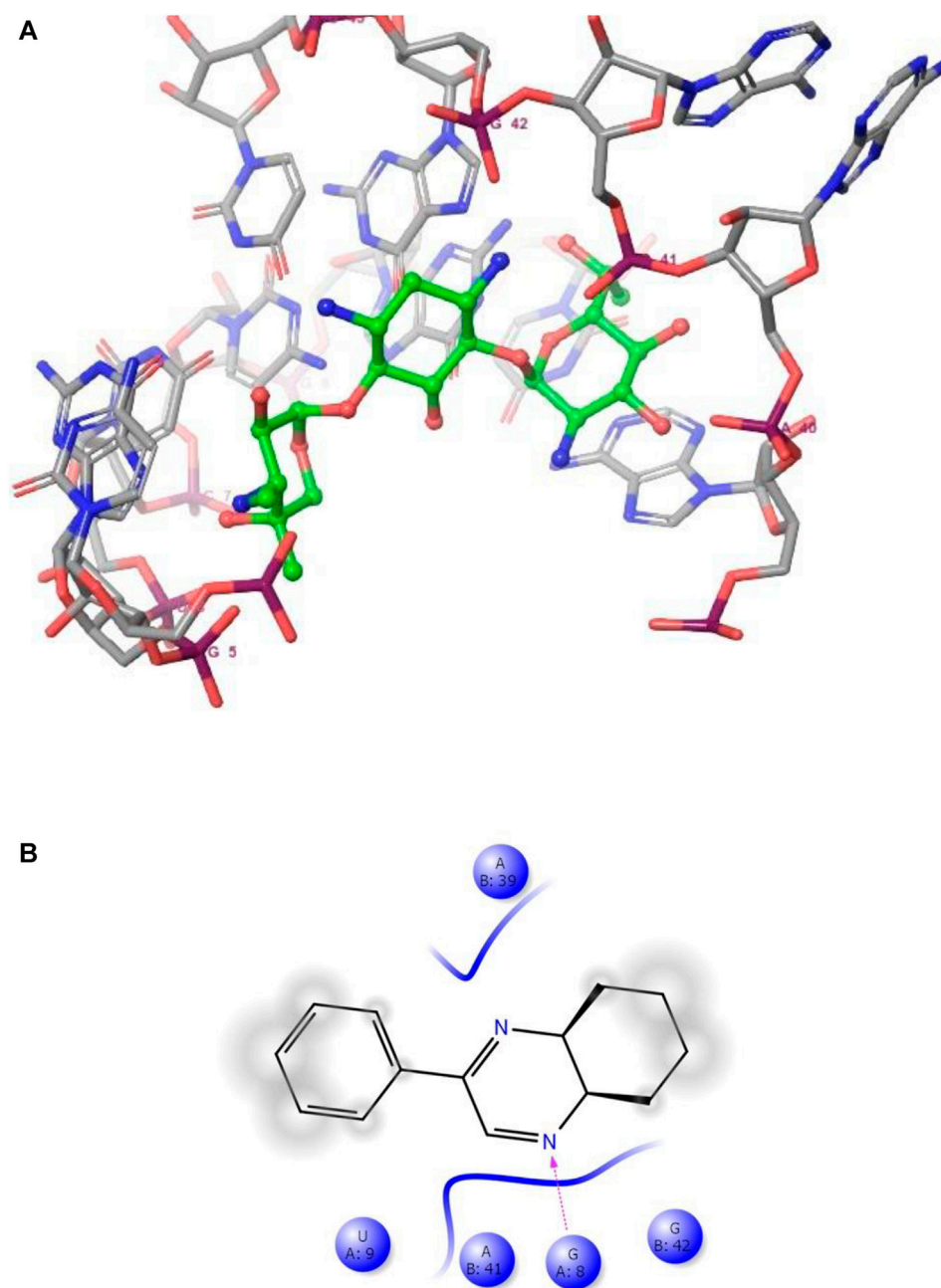


FIGURE 4 | (A) The binding mode of the interactions between **1** with Leishmanial rRNA A-site (PDB ID: 4K32). **(B)** Results of the validation of **1** inside the Leishmanial rRNA A-site active sites.

Maestro was set to 1) visualize the formation and quantify distances of H-bonds, π - π stacking interactions, and close contacts of each ligand to the receptor of interest; 2) obtain images of ligand-receptor residue interactions within the vicinity of the binding site, and 3) observe the receptor surface homology through molecular dynamics simulation (Haile, 1992). The *in silico* docking study evaluated miltefosine and nifurtimox, leishmanicidal, and trypanocidal control drugs, respectively.

RESULTS

Green Synthesis of Diverse Benzopyrazines

Ultrasound-assisted diversely substituted benzopyrazines were synthesized, inserting a powerful sonicator probe into the reaction mixture. For the diamine and dicarbonyl compounds, various substituents based on electron-withdrawing or electron-donating ability were tested to generalize the reaction. The nitro, chloro, on

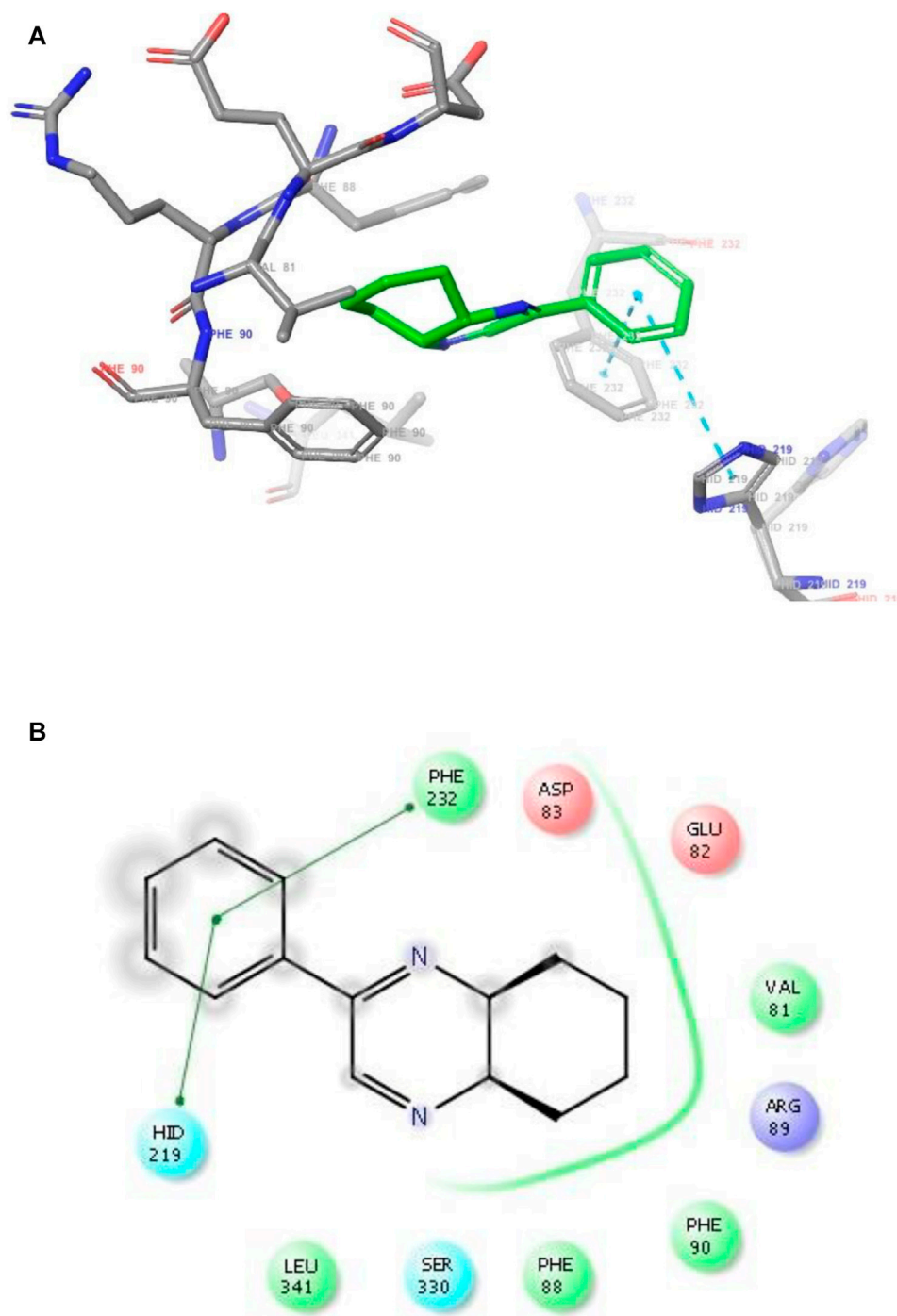


FIGURE 5 | (A) The binding mode of the interactions between **1** with Leishmania major *N*-myristoyltransferase (PDB ID: 6QDA). **(B)** Results of the validation of **1** inside the Leishmania major *N*-myristoyltransferase active sites.

the diamine represent strong and weak electron-withdrawing groups (EWG), whereas the fused cyclohexyl and methoxy groups represent mild and strong electron-donating groups (EDG). The ultimate goal was to evaluate whether the presence of these functional groups influences the nucleophilicity of the diamines. Similarly, the dicarbonyls' electrophilicity was varied by introducing *p*-nitro,

p-fluoro (EWG) or methyl (EDG) in the dicarbonyl system. The overall yield of the products indicates that the presence of EWG or EDG does not influence the reaction significantly, which in turn supports the universality of this synthetic method. Based on the available literature, this is the first example of synthesizing benzopyrazines under this condition. Our method produced

TABLE 4 | Interactions between compound **1** with the four biomolecular targets (PDB IDs: 4YPF, 1S0J, 4K32 and 6QDA).

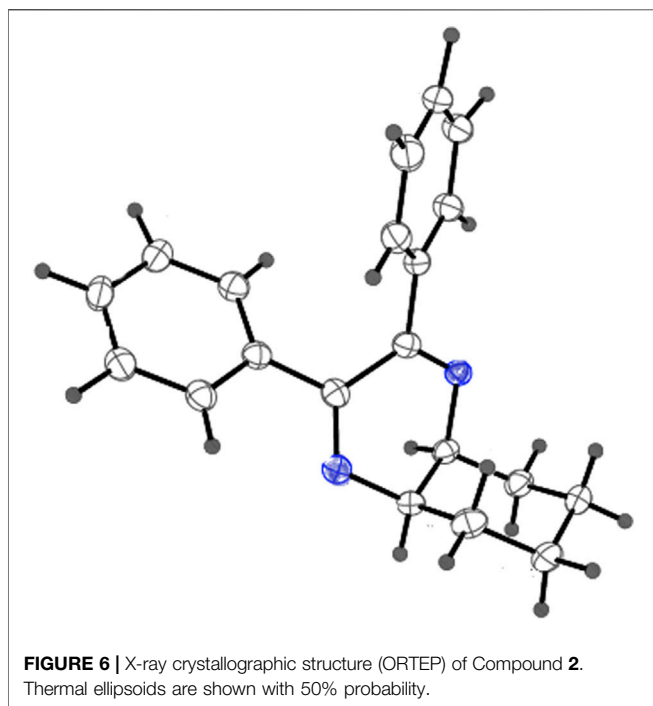
Receptor	Binding site residue(s)	Type of interactions	Hydrophobic residues	Docking score ^a
4YPF	HID168	π - π stacking	GLU105, ILE106, GLN109, PRO125, TRP155, ARG165, GLU167, CYS365	-6.7
1S0J	N/A	Hydrophobic interaction	ARG35, ARG53, ASN60, ARG93, ASP96, TYR113, TRP120, LEU176, GLU230, TRP312, ARG314, TYR342	-7.3
4K32	Guanine 8	H-Bond	U9, A39, A40, A41, G43	-6.3
6QDA	HID 219, PHE232	π - π stacking	VAL81, GLU82, ASP83, PHE88, ARG89, PHE90, SER330, LEU341	-7.4

^aBinding affinity [kcal/mol].4YPF: Crystal structure of *T. cruzi* Histidyl-tRNA synthetase in complex with quinolin-3-amine.

1S0J: Trypanosoma cruzi trans-sialidase in complex with MuNANA (Michaelis complex).

4K32: Crystal structure of geneticin bound to the leishmanial rRNA A-site.

6QDA: Leishmania major N-myristoyltransferase in complex with quinazoline inhibitor IMP-0000811.



excellent yields of the corresponding products (overall yield 92% or more) in a very short period. The yield of the products and the atom economy of the reactions are shown in **Table 1**. The range of atom economy in the series varies from 76.92 to 88.89%, which undoubtedly supports the greenness of the synthetic method.

Trypanocidal and Leishmanicidal Evaluations (*in vitro*) of the Benzopyrazines (1–11)

We used the promastigotes of *L. mexicana* (MHOM/MX/ISSETGS) clinical strain for the leishmanicidal growth inhibition assay. The clinical strain was initially isolated from a patient suffering from diffuse cutaneous leishmaniasis. We carried out the trypanocidal assay with the epimastigotes of *T. cruzi* (MHOM/MX/1994/NINOA). The clinical strain was originally isolated from a patient with the disease in the acute phase for this assay. Schneider's *Drosophila*

medium, supplemented with 10% fetal bovine serum, penicillin (100 IU/ml), and streptomycin (100 μ g/ml), was used to culture the parasites at 26°C. Two commercial drugs, miltefosine, and nifurtimox were used as standard controls. Compound **1** demonstrated good *in vitro* activity against both the strains with comparable IC₅₀ values with both the controls: miltefosine and nifurtimox. Compounds **3** and **4** showed moderate IC₅₀ values against the *L. mexicana* (M378) strain (**Table 2**). The standard biosecurity and institutional procedure were followed during the experiment.

In Silico Molecular Docking of the Compound 1

T. cruzi Histidyl-tRNA synthetase (PDB ID: 4YPF; Koh et al., 2015) and *T. cruzi* trans-sialidase (PDB ID: 1S0J; Amaya et al., 2004) are considered as two major biological drug targets for American trypanosomiasis whereas Leishmanial rRNA A-site (PDB ID: 4K32; Shalev et al., 2013) and Leishmania major N-myristoyltransferase (PDB ID: 6QDA; Bell et al., 2020) are considered as the major biomolecular drug targets for leishmaniasis (Kelly et al., 2020). As shown in **Table 2**, compound **1** showed comparable *in vitro* trypanocidal and leishmanicidal activities with two standard commercial drugs; therefore, we hypothesized the inhibition of the proteins as mentioned earlier with compound **1**. To validate our hypothesis, we carried out extensive molecular docking studies of compound **1** against the four proteins. The docking scores are presented in **Table 3**. Docking interactions between compound **1** with the four proteins are shown in **Figures 2–5**.

In Silico Drug-likeness Determination

Drug-likeness indicates the possibility of a molecule becoming a drug. Accordingly, a drug molecule should have a balance of various physicochemical properties like molecular weight, hydrogen bond donor, hydrogen bond acceptor, total polar surface area, rotatable bond, hydrophilicity, lipophilicity, hydrophobicity, lipophilicity, bioavailability, half-life, etc. The druggability assessment of all the eleven benzopyrazines was performed in compliance with Lipinski's rule of five (RO5) (Lipinski et al., 1997; Lipinski et al., 2001; Lipinski, 2004). The druggability parameters of the eleven benzopyrazines are shown in

TABLE 5 | Validation[†] of drug-likeness of the benzopyrazines (1–11).

Compound	miLogP ^a	HBA ^b	HBD ^c	TPSA ^d	RB ^e	MW ^f	Violation
1	2.96	2	0	24.73	1	212.30	0
2	4.62	2	0	24.73	2	288.39	0
3	3.41	2	0	25.78	1	206.25	0
4	3.44	3	0	35.02	2	236.27	0
5	4.06	2	0	25.78	1	240.69	0
6	3.34	5	0	71.61	2	251.25	0
7	5.91	5	0	71.61	3	355.40	1
8	5.34	5	0	71.61	3	363.32	1
9	3.56	5	0	71.61	2	265.27	0
10	5.08	2	0	25.78	2	282.35	1
11	5.01	5	0	71.61	3	327.34	1

[†]Molinspiration property engine v2018.10.

^amiLogP: Moriguchi octanol-water partition coefficient, is based on quantitative structure-LogP relationships, by using topological indexes.

^bHydrogen bond acceptor.

^cHydrogen bond donor.

^dTotal polar surface area.

^eNumber of rotatable bonds.

Table 4. Compound 1 shows the minimum miLogP value (2.96) out of all the eleven analogs without having any significant violations of druggability.

DISCUSSION

We have carried out an expeditious green synthesis of a series of diversely substituted benzopyrazines with a high atom economy using an ultrasonic probe. No catalyst and/or additive was used during the reaction. The reaction was conducted in the greenest solvent water and extracted with a recommended green solvent ethyl acetate (McElroy et al., 2015). The reaction comprises a nucleophilic addition of the 1,2-dicarbonyl compounds to the diamines. A plausible mechanism may involve ultrasound-assisted activation of the carbonyl groups and subsequent attack of the lone pair of electrons of the amine groups due to a negative electromeric (-E) effect. Eventually, the elimination of two water molecules and subsequent ring-closure lead to the formation of benzopyrazines with a high atom economy. Our method, as described herein, complies with most of the green chemistry principles by removing the use of hazardous solvent/catalyst/additive/procedure (Bandyopadhyay and Banik, 2021). All the reactions were carried out for 3 minutes to remove/reduce the possibility of by-product formation as the reaction mixtures became hot after sonication for an average of 3 minutes, and undesired by-products might form.

Up-/downregulation of a specific enzyme(s) (proteins) is associated with almost all diseases. Subsequently, appropriate inhibition of upregulating disease-causing enzyme(s) (direct or indirect) through enzyme-ligand interactions is considered an effective strategy for treating the specific disease. The enzyme *T. cruzi* histidyl-tRNA helps the parasite to incorporate histidine during its protein synthesis through aminoacylation reaction in a two-step process. Accordingly, inhibition of this enzyme will stop the required protein synthesis, which will kill the parasite (Pham et al., 2014). Then again, *T. cruzi* trans-sialidase is a membrane-anchored enzyme that helps the parasite to transfer sialic acids from the cellular surface

of the host to that of the parasite. As no known human analog of this enzyme exists, *T. cruzi* trans-sialidase is considered a safe drug target for Chagas' disease (Miller and Roitberg, 2013). On the other hand, the leishmanial ribosomal-RNA A-site is considered a suspected binding site for the small molecule inhibitors, which can interfere with translation processes in the course of protozoal protein synthesis (Shalev et al., 2013). In addition, another enzyme leishmania major *N*-myristoyltransferase has been reported as a validated drug target in the treatment of leishmaniasis. This enzyme acts as a biocatalyst in the co-translational N-terminal myristoylation reaction, which is essential in synthesizing a wide range of pathogenic proteins (Bell et al., 2020). Based on these published reports, the four proteins mentioned earlier were chosen as the biological targets in the present study.

Developing new therapeutic agents to counter eukaryotic pathogens is exceedingly challenging. Apart from the drug discovery-related regular hassles, this particular effort needs to balance two additional crucial factors: 1) the evolutionary conservation of drug targets between the animal or insect (host) and the microorganism and 2) the development of strain-dependent drug resistance in the human body. Chagas' disease was mainly originated and confined to the Latin American countries until a few decades ago; however, the epidemiology of this life-threatening disease has been changing with time. An increased number of cases have been identified in the United States of America, Canada, and many other countries from Europe, some parts of Africa, the Eastern Mediterranean, and the Western Pacific regions. Currently, an estimated 75 million people are in the risk zone of this disease (Maheshwari and Bandyopadhyay, 2021; World Health Organization, 2021).

In contrast, infection due to the protozoa *Trypanosoma cruzi* is curable if appropriate treatment can be started soon after the infection. Leishmaniasis, another major vector-borne protozoal disease, has three major types: visceral, cutaneous, and mucocutaneous. An estimated 700,000 to 1 million people become infected each year (Maheshwari and Bandyopadhyay, 2021; World Health Organization, 2021). Accordingly, there is a strong need for new drugs with higher potency and far-ranging efficacy against trypanosome parasites

such as *Leishmania* and *Trypanosoma*. Our benzopyrazine **1** showed comparable *in vitro* activity against both the protozoa (*L. Mexicana* and *T. cruzi*) with IC_{50} values 12.46 and 37.85 μ M respectively, whereas the standard commercial drugs nifurtimox and miltefosine have IC_{50} values 9.32 and 19.56 μ M against *L. Mexicana* and *T. cruzi*. Based on the observed similarities in the IC_{50} values, we hypothesized the inhibitory activity of benzopyrazine **1**, which has been validated through subsequent *in silico* protein-ligand interactions study. Two other benzopyrazines **3** and **4** showed moderate to high IC_{50} values (against the *L. mexicana* (M378) strain (50.86 and 39.83 μ M, respectively) (**Table 2**).

As has been mentioned earlier, the proteins *T. cruzi* Histidyl-tRNA synthetase (PDB ID: 4YPF) and *T. cruzi* trans-sialidase (PDB ID: 1S0J) are considered as two major biological drug targets for Chagas' disease, whereas Leishmanial rRNA A-site (PDB ID: 4K32) and *Leishmania* major *N*-myristoyltransferase (PDB ID: 6QDA) are considered as the major biomolecular drug targets for leishmaniasis (Kelly et al., 2020). Benzopyrazine **1** demonstrated better binding affinity towards all the four proteins than the standard control drug miltefosine and comparable docking scores with another control drug nifurtimox (**Table 3**). Benzopyrazine **1** binds the ARG156, ARG165, and HID158 residues of *T. cruzi* Histidyl-tRNA synthetase, ALA59, VAL95, LEU176, and ASP96 residues of *T. cruzi* trans-sialidase, forms salt-bridge with Leishmanial rRNA A-site, and binds the PHE 232, HID 219, GLU82, SER330 residues of the *Leishmania* major *N*-myristoyltransferase (**Figures 2–5**). The binding sites, type of interactions, hydrophobic residues, and docking scores of compound **1** with the four biomolecular targets (PDB IDs: 4YPF, 1S0J, 4K32 and 6QDA) have been summarized in **Table 4**. Compound **1** showed a higher binding affinity with the proteins with PDB IDs 6QDA and 1S0J (−7.4 and −7.3 kcal/mol, respectively) than the biomolecular targets with PDB IDs 4K32 and 4YPF (−6.3 and −6.7, respectively). The protein-ligand docking interactions of the co-crystallized ligands as described in the protein data bank (PDB) have also been conducted, and the results have been summarized in **Supplementary Table S1** (see Supplementary material). Notably, for the protein with PDB ID 4YPF, compound **1** has a higher binding affinity (−6.7 kcal/mol) than the co-crystallized ligand quinoline-3-amine (−5.8 kcal/mol). It is worthy of mentioning that the *cis*-stereochemistry of the 5,6,7,8-tetrahydroquinoxaline ring-juncture (Compounds **1** and **2**) was confirmed by X-ray crystallographic analysis of compound **2**. The X-ray crystallographic structure (ORTEP) of Compound **2** is shown in **Figure 6**. The thermal ellipsoids are shown with 50% probability. The asymmetric unit comprises one molecule of compound **2** situated in a general position. The X-ray parameters can be found in **Supplementary Table S2** (see Supplementary material). Here it is essential to mention that the benzopyrazines **3** and **4** demonstrated moderate leishmanicidal activity against *L. mexicana* (M378) strain. In addition, the lead compound **1** showed good leishmanicidal and trypanocidal activities (*in vitro*) against both *L.*

mexicana (M378) and *T. cruzi* (NINOA) strains compared to the standard controls. The other eight analogs did not demonstrate notable biological activity against any of the tested strains. This observation indirectly supports the selective toxicity of **1**, **3**, and **4** against the pathogenic strains. If all compounds showed activity against the parasites, this effect could be considered a toxic effect.

Finally, the drug-likeness of all the eleven benzopyrazine derivatives has been determined following the RO5 (Lipinski et al., 2001). Seven out of eleven compounds did not show any violations which support the drug-likeness of these molecules. Benzopyrazines **1**, **3**, and **4** are in good agreement with the RO5 (**Table 5**). Based on the promising druglike-ness as shown in **Table 5**, it is expected that the molecules should have good pharmacokinetics and pharmacodynamics properties.

CONCLUSION

An expeditious green ultrasound-assisted one-pot procedure of synthesizing benzopyrazines is reported. This newly developed method satisfies many aspects of green chemistry and maintains a high atom economy. No catalyst/support/additive/hazardous solvents were used to accomplish the synthesis. Most of the synthesized compounds possess drug-likeness and follow RO5. A minor violation of RO5 was noticed for four out of eleven products. Benzopyrazines **3** and **4** demonstrated moderate leishmanicidal activity against *L. mexicana* (M378) strain. The selective lead compound **1** showed good leishmanicidal, and trypanocidal activities (*in vitro*) against both *L. mexicana* (M378) and *T. cruzi* (NINOA) strains compared to the standard controls. The hypothesis of binding of the lead benzopyrazine **1** to the active sites of the four proteins (*T. cruzi* Histidyl-tRNA synthetase, *T. cruzi* trans-sialidase, leishmanial rRNA A-site, and leishmania major *N*-myristoyltransferase) responsible for Chagas' disease and leishmaniasis disease. As mentioned earlier, the inhibition of the proteins with the compounds **1** has been validated by *in silico* molecular docking studies. Accordingly, benzopyrazine **1**, as reported herein, may find its application in the future drug development process against two major neglected tropical diseases: Chagas' disease and leishmaniasis.

DATA AVAILABILITY STATEMENT

The original contributions presented in the study are included in the article/**Supplementary Material**, further inquiries can be directed to the corresponding authors.

AUTHOR CONTRIBUTIONS

DB conceptualized, and DB and GR designed the experiments and validated the data analysis. JR, DG, OE, SS, MC-B, and RM-P performed the experiments and collected the data, and analyzed. DB wrote the manuscript, and NP and GR reviewed and edited the manuscript. All authors contributed to the article and approved the submitted version.

FUNDING

The authors are grateful to the Department of Chemistry and the School of Earth Environment and Marine Sciences (SEEMS) of the University of Texas Rio Grande Valley for start-up funding (to DB) and extending facilities for this study. The Department of Chemistry at the University of Texas Rio Grande Valley is grateful for the generous support provided by a Departmental Grant from the Robert A. Welch Foundation (Grant No. BX-0048). This research was partially funded by Secretaria de Investigación y Posgrado-Instituto Politécnico Nacional, grant number (GR: SIP-SIP-20200491 and 20210050).

REFERENCES

- Achutha, L., Parameshwar, R., Reddy, B. M., and Babu, H. V. (2013). Microwave-assisted Synthesis of Some Quinoxaline-Incorporated Schiff Bases and Their Biological Evaluation. *J. Chem.* 2013, 578438. doi:10.1155/2013/578438
- Amaya, M. F., Watts, A. G., Damager, I., Wehenkel, A., Nguyen, T., Buschiazio, A., et al. (2004). Structural Insights into the Catalytic Mechanism of *Trypanosoma Cruzi* Trans-sialidase. *Structure* 12, 775–784. doi:10.1016/j.str.2004.02.036
- Bandyopadhyay, D., and Banik, B. K. (2021). "Microwave-assisted Synthesis of Medicinally Privileged Heterocycles" in *Advanced Synthetic Techniques*, ed. G. Brahmachari. Oxford, United Kingdom: Elsevier, 49–110.
- Bandyopadhyay, D., Cruz, J., Morales, L. D., Arman, H. D., Cuate, E., Lee, Y. S., et al. (2013). A green Approach toward Quinoxalines Andbis-Quinoxalines and Their Biological Evaluation against A431, Human Skin Cancer Cell Lines. *Future Med. Chem.* 5, 1377–1390. doi:10.4155/fmc.13.101
- Bell, A. S., Yu, Z., Hutton, J. A., Wright, M. H., Brannigan, J. A., Paape, D., et al. (2020). Novel Thienopyrimidine Inhibitors of Leishmania N-Myristoyltransferase with On-Target Activity in Intracellular Amastigotes. *J. Med. Chem.* 63, 7740–7765. doi:10.1021/acs.jmedchem.0c00570
- Carta, A., Sanna, P., Gherardini, L., Usai, D., and Zanetti, S. (2001). Novel Functionalized Pyrido[2,3-G]quinoxalinones as Antibacterial, Antifungal and Anticancer Agents. *Il Farmaco* 56, 933–938. doi:10.1016/s0014-827x(01)01161-2
- Chan-Bacab, M. J., Hernández-Núñez, E., and Navarrete-Vázquez, G. (2009). Nitazoxanide, Tizoxanide and a New Analogue [4-nitro-N-(5-nitro-1,3-thiazol-2-yl)benzamide; NTB] Inhibit the Growth of Kinetoplastid Parasites (*Trypanosoma Cruzi* and *Leishmania Mexicana*) *In Vitro*. *J. Antimicrob. Chemother.* 63, 1292–1293. doi:10.1093/jac/dkp117
- El-Attar, M. A. Z., Elbayaa, R. Y., Shaaban, O. G., Habib, N. S., Abdel Wahab, A. E., Abdelwahab, I. A., et al. (2018). Design, Synthesis, Antibacterial Evaluation and Molecular Docking Studies of Some New Quinoxaline Derivatives Targeting Dihydropterotate Synthase Enzyme. *Bioorg. Chem.* 76, 437–448. doi:10.1016/j.bioorg.2017.12.017
- Haile, J. M. (1992). *Molecular Dynamics Simulation*, 18. New York, USA: Wiley.
- Hanwell, M. D., Curtis, D. E., Lonie, D. C., Vandermeersch, T., Zurek, E., and Hutchison, G. R. (2012). Avogadro: an Advanced Semantic Chemical Editor, Visualization, and Analysis Platform. *J. Cheminform.* 4, 17. doi:10.1186/1758-2946-4-17
- Hernández-Núñez, E., Tlahuext, H., Moo-Puc, R., Torres-Gómez, H., Reyes-Martínez, R., Cedillo-Rivera, R., et al. (2009). Synthesis and *In Vitro* Trichomonocidal, Giardicidal and Amebicidal Activity of N-acetamide(sulfonamide)-2-methyl-4-nitro-1H-imidazoles. *Eur. J. Med. Chem.* 44, 2975–2984. doi:10.1016/j.ejmech.2009.01.005
- Kelly, P., Hadi-Nezhad, F., Liu, D. Y., Lawrence, T. J., Lington, R. G., Ibba, M., et al. (2020). Targeting tRNA-Synthetase Interactions towards Novel Therapeutic Discovery against Eukaryotic Pathogens. *Plos Negl. Trop. Dis.* 14, e0007983. doi:10.1371/journal.pntd.0007983
- Koh, C. Y., Kallur Siddaramaiah, L., Ranade, R. M., Nguyen, J., Jian, T., Zhang, Z., et al. (2015). A Binding Hotspot in *Trypanosoma Cruzi* histidyl-tRNA Synthetase Revealed by Fragment-Based Crystallographic Cocktail Screens. *Acta Cryst. D Biol. Crystallogr.* 71, 1684–1698. doi:10.1107/s1399004715007683

ACKNOWLEDGMENTS

DB and SS are thankful to the Office of Sustainability (UTRGV) for a Graduate Sustainability Research Fellowship to SS.

SUPPLEMENTARY MATERIAL

The Supplementary Material for this article can be found online at: <https://www.frontiersin.org/articles/10.3389/fchem.2021.725892/full#supplementary-material>

- Kumaresan, M., Saravanan, V., Sami, P., and Swaminathan, M. (2020). A green Solid Acid Catalyst 12-tungstophosphoric Acid H₃[PW₁₂O₄₀] Supported on G-C₃N₄ for Synthesis of Quinoxalines. *Res. Chem. Intermed.* 46, 4193–4209. doi:10.1007/s11164-020-04200-0
- Laskar, S., Espino, O., and Bandyopadhyay, D. (2019). Isolation, Solid-State Structure Determination, *In Silico* and *In Vitro* Anticancer Evaluation of an Indole Amino Acid Alkaloid L-Abrine. *Ccdd* 19, 707–715. doi:10.2174/156800961966619011111937
- Lee, Y. B., Gong, Y.-D., Kim, D. J., Ahn, C.-H., Kong, J.-Y., and Kang, N.-S. (2012). Synthesis, Anticancer Activity and Pharmacokinetic Analysis of 1-[(substituted 2-Alkoxyquinoxalin-3-yl)aminocarbonyl]-4-(hetero)arylpiperazine Derivatives. *Bioorg. Med. Chem.* 20, 1303–1309. doi:10.1016/j.bmc.2011.12.026
- Liang, J., Woodward, C., and Edelsbrunner, H. (1998). Anatomy of Protein Pockets and Cavities: Measurement of Binding Site Geometry and Implications for Ligand Design. *Protein Sci.* 7, 1884–1897. doi:10.1002/pro.5560070905
- Lipinski, C. A., Lombardo, F., Dominy, B. W., and Feeney, P. J. (2001). Experimental and Computational Approaches to Estimate Solubility and Permeability in Drug Discovery and Development Settings. *Adv. Drug Deliv. Rev.* 46 (1–3), 3–26. doi:10.1016/s0169-409x(00)00129-0
- Lipinski, C. A. (2004). Lead- and Drug-like Compounds: the Rule-Of-Five Revolution. *Drug Discov. Today Tech.* 1, 337–341. doi:10.1016/j.ddtec.2004.11.007
- Lipinski, C. A., Lombardo, F., Dominy, B. W., and Feeney, P. J. (1997). Experimental and Computational Approaches to Estimate Solubility and Permeability in Drug Discovery and Development Settings. *Adv. Drug Deliv. Rev.* 23, 3–25. doi:10.1016/s0169-409x(96)00423-1
- Loughran, H. M., Han, Z., Wrobel, J. E., Decker, S. E., Ruthel, G., Freedman, B. D., et al. (2016). Quinoxaline-based Inhibitors of Ebola and Marburg VP40 Egress. *Bioorg. Med. Chem. Lett.* 26, 3429–3435. doi:10.1016/j.bmcl.2016.06.053
- Maheshwari, K. K., and Bandyopadhyay, D. (2021). Heterocycles in the Treatment of Neglected Tropical Diseases. *Cmc* 28, 472–495. doi:10.2174/0929867327666200219141652
- McElroy, C. R., Constantinou, A., Jones, L. C., Summerton, L., and Clark, J. H. (2015). Towards a Holistic Approach to Metrics for the 21st century Pharmaceutical Industry. *Green. Chem.* 17, 3111–3121. doi:10.1039/c5gc00340g
- Miller III, B. R., and Roitberg, A. E. (2013). *Trypanosoma Cruzi* Trans-sialidase as a Drug Target against Chagas Disease (American Trypanosomiasis). *Future Med. Chem.* 5, 1889–1900. doi:10.4155/fmc.13.129
- Morris, G. M., Huey, R., Lindstrom, W., Sanner, M. F., Belew, R. K., Goodsell, D. S., et al. (2009). AutoDock4 and AutoDockTools4: Automated Docking with Selective Receptor Flexibility. *J. Comput. Chem.* 30, 2785–2791. doi:10.1002/jcc.21256
- Panja, D., Paul, B., Balasubramanian, B., Gupta, R. K., and Kundu, S. (2020). Application of a Reusable Co-based Nanocatalyst in Alcohol Dehydrogenative Coupling Strategy: Synthesis of Quinoxaline and Imine Scaffolds. *Catal. Commun.* 137, 105927. doi:10.1016/j.catcom.2020.105927
- Pettersen, E. F., Goddard, T. D., Huang, C. C., Couch, G. S., Greenblatt, D. M., Meng, E. C., et al. (2004). UCSF Chimera?A Visualization System for Exploratory Research and Analysis. *J. Comput. Chem.* 25, 1605–1612. doi:10.1002/jcc.20084
- Pham, J. S., Dawson, K. L., Jackson, K. E., Lim, E. E., Pasaje, C. F. A., Turner, K. E. C., et al. (2014). Aminoacyl-tRNA Synthetases as Drug Targets in Eukaryotic Parasites. *Int. J. Parasitol. Drugs Drug Resist.* 4 (1), 1–13. doi:10.1016/j.ijpddr.2013.10.001

- Putta, R. R., Chun, S., Lee, S. B., Hong, J., Oh, D.-C., and Hong, S. (2021). Iron-catalyzed One-Pot Synthesis of Quinoxalines: Transfer Hydrogenative Condensation of 2-nitroanilines with Vicinal Diols. *RSC Adv.* 11, 18225–18230. doi:10.1039/d1ra02532e
- Qi, J., Dong, H., Huang, J., Zhang, S., Niu, L., Zhang, Y., et al. (2018). Synthesis and Biological Evaluation of N-Substituted 3-Oxo-1,2,3,4-Tetrahydro-Quinoxaline-6-Carboxylic Acid Derivatives as Tubulin Polymerization Inhibitors. *Eur. J. Med. Chem.* 143, 8–20. doi:10.1016/j.ejmech.2017.08.018
- Rose, P. W., Beran, B., Bi, C., Bluhm, W. F., Dimitropoulos, D., Goodsell, D. S., et al. (2011). The RCSB Protein Data Bank: Redesigned Web Site and Web Services. *Nucleic Acids Res.* 39 (Suppl. 1), D392–D401. doi:10.1093/nar/gkq1021
- Schrödinger Release 2016-4 (2016). *MS Jaguar*, Schrödinger. New York, USA: LLC.
- Seeliger, D., and de Groot, B. L. (2010). Ligand Docking and Binding Site Analysis with PyMOL and Autodock/Vina. *J. Comput. Aided Mol. Des.* 24, 417–422. doi:10.1007/s10822-010-9352-6
- Shalev, M., Kondo, J., Kopelyanskiy, D., Jaffe, C. L., Adir, N., and Baasov, T. (2013). Identification of the Molecular Attributes Required for Aminoglycoside Activity against *Leishmania*. *Proc. Natl. Acad. Sci.* 110, 13333–13338. doi:10.1073/pnas.1307365110
- Sharma, A., Dixit, R., Sharma, S., Dutta, S., Yadav, S., Arora, B., et al. (2021). Efficient and Sustainable Co3O4 Nanocages Based Nickel Catalyst: A Suitable Platform for the Synthesis of Quinoxaline Derivatives. *Mol. Catal.* 504, 111454. doi:10.1016/j.mcat.2021.111454
- The PyMOL Molecular Graphics System (2015). *Version 1.8* Schrödinger. New York, USA: LLC.
- Trott, O., and Olson, A. J. (2010). AutoDock Vina: Improving the Speed and Accuracy of Docking with a New Scoring Function, Efficient Optimization, and Multithreading. *J. Comput. Chem.* 31, 455–461. doi:10.1002/jcc.21334
- Wang, Y.-B., Shi, L., Zhang, X., FuHu, L.-R. W., Hu, W., Zhang, W., et al. (2021). NaOH-mediated Direct Synthesis of Quinoxalines from O-Nitroanilines and Alcohols via a Hydrogen-Transfer Strategy. *J. Org. Chem.* 86, 947–958. doi:10.1021/acs.joc.0c02453
- World Health Organization (2021). Chagas Disease (Also Known as American Trypanosomiasis). available at: [https://www.who.int/news-room/fact-sheets/detail/chagas-disease-\(american-trypanosomiasis\)](https://www.who.int/news-room/fact-sheets/detail/chagas-disease-(american-trypanosomiasis)) (Accessed June 14, 2021).
- World Health Organization (2021). Leishmaniasis. available at: <https://www.who.int/news-room/fact-sheets/detail/leishmaniasis> (Accessed June 14, 2021).
- Conflict of Interest:** The authors declare that the research was conducted in the absence of any commercial or financial relationships that could be construed as a potential conflict of interest.
- Publisher's Note:** All claims expressed in this article are solely those of the authors and do not necessarily represent those of their affiliated organizations, or those of the publisher, the editors and the reviewers. Any product that may be evaluated in this article, or claim that may be made by its manufacturer, is not guaranteed or endorsed by the publisher.

Copyright © 2021 Rock, Garcia, Espino, Shetu, Chan-Bacab, Moo-Puc, Patel, Rivera and Bandyopadhyay. This is an open-access article distributed under the terms of the Creative Commons Attribution License (CC BY). The use, distribution or reproduction in other forums is permitted, provided the original author(s) and the copyright owner(s) are credited and that the original publication in this journal is cited, in accordance with accepted academic practice. No use, distribution or reproduction is permitted which does not comply with these terms.

Advantages of publishing in Frontiers



OPEN ACCESS

Articles are free to read
for greatest visibility
and readership



FAST PUBLICATION

Around 90 days
from submission
to decision



HIGH QUALITY PEER-REVIEW

Rigorous, collaborative,
and constructive
peer-review



TRANSPARENT PEER-REVIEW

Editors and reviewers
acknowledged by name
on published articles

Frontiers

Avenue du Tribunal-Fédéral 34
1005 Lausanne | Switzerland

Visit us: www.frontiersin.org

Contact us: frontiersin.org/about/contact



REPRODUCIBILITY OF RESEARCH

Support open data
and methods to enhance
research reproducibility



DIGITAL PUBLISHING

Articles designed
for optimal readership
across devices



FOLLOW US

@frontiersin



IMPACT METRICS

Advanced article metrics
track visibility across
digital media



EXTENSIVE PROMOTION

Marketing
and promotion
of impactful research



LOOP RESEARCH NETWORK

Our network
increases your
article's readership